# MOLECULAR
# PHYSICS

VOLUME 4

1961

# CONTENTS OF VOLUME 4

# CONTENTS OF VOLUME 4

# CONTENTS OF VOLUME 4

# On the magnetically dilute Heisenberg and Ising ferromagnetics

by G. S. RUSHBROOKE and D. J. MORGAN†

Physics Department, King's College, Newcastle upon Tyne,
University of Durham

The lowering of the Curie temperature of a ferromagnetic substance by random dilution with non-magnetic elements is studied on the basis of Heisenberg and Ising models having nearest-neighbour interactions between magnetic elements only. It is proved that the limiting concentration, $p_{\rm C}$, of magnetic elements, below which there is no Curie temperature, is the same for all such models, whether Heisenberg or Ising and regardless of the spin value concerned: it depends only on the lattice structure. Numerical estimates of $p_{\rm C}$ are given for various lattices. Successive approximations are developed to the full Curie temperature curve, and it is found that whereas for the Ising model $T_{\rm C}(p)$ approximates to $p T_{\rm C}(1)$ near $p=1$, $T_{\rm C}(p) < p T_{\rm C}(1)$ for the Heisenberg model.

## 1. INTRODUCTION

We are concerned with the lowering of the Curie temperature of a ferromagnetic substance by admixture of non-magnetic material and the eventual elimination of ferromagnetic behaviour. We shall restrict attention to a purely random arrangement of magnetic and non-magnetic elements on the sites of a crystal lattice, as might obtain in quenched material, and shall treat the problem on the basis of short-range, localized, interactions between the magnetic elements only. More precisely, we suppose that the effective Hamiltonian for the complete system, in an external magnetic field $H$, has the form either

$$\mathscr{H} = -2J \sum_{\langle i,j \rangle} S^{(i)} S^{(j)} - g\beta H \sum_{(i)} S_3^{(i)} \tag{1 H}$$

or

$$\mathscr{H} = -2J \sum_{\langle i,j \rangle} S_3^{(i)} S_3^{(j)} - g\beta H \sum_{(i)} S_3^{(i)}. \tag{1 I}$$

The symbol $\sum_{i,j}$ denotes summation over all pairs of neighbouring magnetic elements, and $S^{(i)} = (S_1^{(i)}, S_2^{(i)}, S_3^{(i)})$ is a spin variable located at the $i$th magnetic element. $J$ measures the magnitude of the 'exchange interaction'‡, while $g$ and $\beta$ denote the gyromagnetic ratio and Bohr magneton respectively.

With the Hamiltonian (1 H) we speak of the Heisenberg problem, with (1 I) of the Ising problem. We shall denote the proportion of magnetic elements by $p$. When $p=1$ we have the fully magnetic Heisenberg and Ising problems, which have been extensively studied, particularly when the spin variables pertain to spin $\frac{1}{2}$, i.e. for the problems which can be denoted by H($\frac{1}{2}$) and I($\frac{1}{2}$). Although we shall in fact deal, for general $p$, with these particular problems we shall not restrict attention to them but discuss the generalizations H($s$) and I($s$), where $s$ is the maximum value of $S_3^{(i)}$.

---

† Present address: Department of Applied Mathematics, University College, Cardiff.
‡ Some workers on the Ising problem for spin $\frac{1}{2}$ have used $J$ where we use $2J$.

Granted the assumption of random mixing, and the nature of the Hamiltonian, the model also demands a specific lattice structure. Although we have worked very generally, so as to include all possible lattices, we shall largely restrict attention to the face-centred cubic (f.c.c.), body-centred cubic (b.c.c.) and simple cubic (s.c.) lattices, making some comment on the plane square array (p.s.).

We shall be concerned primarily with estimating the critical value, $p_c$, of $p$ below which there is no ferromagnetic behaviour, i.e. no Curie temperature. Denoting $kT/J$ by $\theta$, the Curie temperature, $\theta_c$, will, in general, be a function of $p$, i.e. $\theta_c(p)$; we shall find that $\theta_c(p)$ decreases as $p$ decreases from unity, and eventually vanishes when $p = p_c$. Since we shall find that $p_c$ is of the order 0·2–0·3, a power-series expansion in powers of $p$ is appropriate, certainly for fixing $p_c$. For very small $p$ the magnetic elements in a random array will be effectively isolated, producing purely paramagnetic behaviour: for rather larger $p$ we must consider physical clusters of small numbers of neighbouring magnetic elements. In order to have an expression for $\chi$, the total magnetic susceptibility, valid up to and including terms in $p^n$ we must consider explicitly clusters involving $n$, or fewer, sites. And for estimating $p_c$ we have taken the calculations as far as $n = 5$, performing subsequent extrapolations.

## 2. General theory

Each of the Hamiltonians (1) may be written

$$\mathscr{H} = -2J\mathscr{P} - g\beta HQ$$

where $\mathscr{P}$ and $Q$ commute. The zero-field susceptibility, $\chi$, deriving from the equations

$$\chi = -\left(\frac{\partial^2 F}{\partial H^2}\right)_{H=0}, \quad F = -kT \ln \langle \exp(-\mathscr{H}/kT)\rangle$$

is given by

$$\frac{\chi kT}{g^2\beta^2} = \frac{\langle Q^2 \exp(2\mathscr{P}/\theta)\rangle}{\langle \exp(2\mathscr{P}/\theta)\rangle} \tag{2}$$

where $\langle\ \rangle$ denotes trace in any matrix representation.

For a randomly magnetically dilute substance, suppose that there are†

$N_1$      isolated magnetic elements;

$N_2$      isolated neighbouring magnetic pairs;

$N_{3,t_3}$    isolated neighbouring magnetic triplets (of two types, corresponding to $t_3 = 1, 2$, say);

$N_{n,t_n}$    isolated 'connected'-clusters of $n$ magnetic elements, of various types denoted by the suffix $t_n$.

Let $\mathscr{P}(n, t_n)$ denote $\sum_{\langle i,j\rangle} S^{(i)} . S^{(j)}$ or $\sum_{\langle i,j\rangle} S_3^{(i)} S_3^{(j)}$, where $i, j$ are neighbouring sites within the cluster $(n, t_n)$, and $Q(n)$ denote $\sum_i S_3^{(i)}$, where $i$ runs over the $n$ sites of the cluster. Then, on account of the factorization property of partition-functions, (2) may be written

$$\frac{\chi kT}{g^2\beta^2} = \sum_{n,t_n} N_{n,t_n} \frac{\langle Q(n)^2 \exp(2\mathscr{P}(n,t_n)/\theta)\rangle}{\langle \exp(2\mathscr{P}(n,t_n)/\theta)\rangle}. \tag{3}$$

Here $N_{1,t_1} = N_1$, $N_{2,t_2} = N_2$. We shall, in fact, always denote $\sum_{t_n} N_{n,t_n}$ by $N_n$, so

† The various clusters possible for $n \leqslant 5$ are illustrated in Appendix I.

that $N_n$ is the number of clusters of $n$ magnetic elements, irrespective of their geometry.

For large $\theta$ the magnetic elements are essentially uncoupled, and we have a paramagnetic substance. When $\theta$ decreases to the Curie temperature $\chi kT$ becomes infinite, i.e. the right-hand side of (3) diverges. For a given value of $p$, this divergence determines $\theta_c(p)$. When $p = 1$ we have the Curie temperature of the pure magnetic substance, and we shall see that as $p$ decreases $\theta_c(p)$ also decreases. Eventually $\theta_c(p) = 0$, when $p = p_c$. But, in any one term of (3), as we approach $\theta = 0$ only the largest exponential, corresponding to the ground state of $-2J\mathscr{P}(n, t_n)$, has any significance. Consequently $p_c$ is determined by the condition

$$\sum_{n,t_n} N_{n,t_n} \langle Q(n)^2 \rangle_{t_n}^{(0)} \quad \text{divergent,} \tag{4}$$

where $\langle Q(n)^2 \rangle_{t_n}^{(0)}$ is the expectation value of $Q(n)^2$ for the ground state of $-2J\mathscr{P}(n, t_n)$, i.e. of the zero-field Hamiltonian for the magnetic cluster concerned. For ferromagnetic problems $J$ is, of course, positive.

We shall see below that $\langle Q(n)^2 \rangle_{t_n}^{(0)}$ is independent of the type of cluster concerned, depending only on the number of sites involved, so that (4) may be written

$$\sum_n N_n \langle Q(n)^2 \rangle^{(0)} \quad \text{divergent.} \tag{5}$$

In fact we shall prove that for the Heisenberg problem

$$\langle Q(n)^2 \rangle_{t_n}^{(0)} = \tfrac{1}{3}ns(ns+1), \quad n \geqslant 1, \tag{6 H}$$

while for the Ising problem

$$\langle Q(n)^2 \rangle_{t_n}^{(0)} = n^2 s^2, \quad n \geqslant 2, \tag{6 I}$$

so that the condition (5) becomes either

$$\tfrac{1}{3} \sum_n N_n(ns + n^2 s^2) \quad \text{divergent} \tag{7 H}$$

or

$$\sum_n N_n n^2 s^2 \quad \text{divergent.} \tag{7 I}$$

Now the numbers $N_{n,t_n}$ have, in themselves, nothing to do with either Heisenberg or Ising problems: they are properties only of the lattice concerned and functions of the probability, $p$, that a given site is occupied by a magnetic element. In fact

$$N_{n,t_n} = Np^n \text{ (polynomial in } p) $$

and, in particular,

$$N_1 = Np(1-p)^z \tag{8}$$

where $z$ is the lattice coordination number. Also, accounting for all the magnetic elements

$$\sum_n nN_n = Np. \tag{9}$$

Thus, by (8) and (9),

$$\tfrac{1}{3} \sum_n N_n (ns + n^2 s^2) = \tfrac{1}{3}Nps + \tfrac{1}{3}Ns^2(p + a_2 p^2 + a_3 p^3 + \ldots) \tag{10 H}$$

and

$$\sum_n N_n n^2 s^2 = Ns^2(p + a_2 p^2 + a_3 p^3 + \ldots) \tag{10 I}$$

where $a_2$, $a_3$, ... are numbers depending only on the topology of the lattice concerned. Reverting to (3), we have

$$\frac{\chi \boldsymbol{k} T}{g^2 \beta^2} = \tfrac{1}{3} N s^2 \left[ \frac{s+1}{s} p + a_2 p^2 + a_3 p^3 + \dots \right] \qquad (11\,\text{H})$$

or

$$\frac{\chi \boldsymbol{k} T}{g^2 \beta^2} = N s^2 \left[ \frac{1-2s}{3s} p\,(1-p)^z + p + a_2 p^2 + a_3 p^3 + \dots \right] \qquad (11\,\text{I})$$

according as we are dealing with the Heisenberg or Ising problem, since $\langle Q(1)^2 \rangle^{(0)} = s(s+1)/3$ in either case. It is evident that these series diverge for the same value, $p_c$, of $p$, the magnitude of $s$ being irrelevant.

We have thus proved that the critical concentration $p_c$ is the same for both Heisenberg and Ising problems, and, moreover, that the magnitude of the spin $s$ in these problems is irrelevant to this value†. In fact $p_c$ is simply that value of $p$ for which $\sum_n N_n n^2$ diverges for a random mixture of A's and B's, $N_n$ being the number of 'connected'-clusters of A's. It is simply a characteristic of the lattice concerned, and its computation is conceivably amenable to Monte-Carlo methods.

## 3. The ground state of a cluster

Before discussing the above equations further we must justify equations (6 H) and (6 I). We consider the two problems separately.

### 3.1. Heisenberg problem

By writing $S^{(i)} \cdot S^{(j)}$ as $\tfrac{1}{2}(S_+{}^{(i)} S_-{}^{(j)} + S_-{}^{(i)} S_+{}^{(j)}) + S_3{}^{(i)} S_3{}^{(j)}$, where

$$S_\pm{}^{(i)} = S_1{}^{(i)} \pm i S_2{}^{(i)},$$

it is easily verified, from a direct-product representation in which each $S_3{}^{(i)}$ is diagonal, that the state corresponding to each $S_3{}^{(i)}$ having its maximum eigenvalue $s$ is an eigenstate of $\mathscr{P}(n, t_n)$ with eigenvalue $ls^2$, where $l$ is the number of lines in a diagram corresponding to the cluster $(n, t_n)$. For this state $Q(n)$, which commutes with $\mathscr{P}(n, t_n)$ has eigenvalue $ns$; and since $\mathscr{P}(n, t_n)$ is invariant under rotation of spin axes it follows‡ that this eigenvalue $ls^2$ of $\mathscr{P}$ has degeneracy $2ns + 1$, $Q(n)$ taking the values $ns$, $ns - 1$, ... $- ns$. This is, in fact§, the greatest eigenvalue of $\mathscr{P}$ and so corresponds to the ground state of $-2J\mathscr{P}$. That there are no other ground-states (with this same energy) follows explicitly for 'stars' i.e. pair, triangle, tetrahedron and further, fictitious, clusters in which every pair of sites is a pair of neighbours from the analysis of Rushbrooke and Wood [8] (Appendix III). We can therefore exclude any additional degeneracy in all other, less symmetrical, cases.

† We have since learnt that Elliott and Heap, at Oxford, have independently proved this theorem. A short joint communicaton has been sent to *Phys. Rev. Letters*. It is, moreover, evident from the nature of the proof that the theorem (as stated here) is equally true for longer-range interactions, of ferromagnetic type, not restricted to nearest neighbours. But, since the coefficients $a_n$ will change, the value of $p_c$ will depend on the range of interaction, and may be expected to decrease as this range increases.

‡ Alternatively, we may observe that, for any diagram $(n, t_n)$, $\mathscr{P}$ commutes not only with $Q$ but with $S^2$, where $S = \Sigma\, S^{(i)}$, and with $S_+$ and $S_-$, where $S_+ = \Sigma_i\, S_+{}^{(i)}$. We can thus generate the other eigenvectors of $\mathscr{P}$ by using these shift operators on the state for which $Q$ has eigenvalue $ns$.

§ This may be regarded as physically obvious, but follows mathematically from Wittmeyer's Theorem VI as quoted in E. Bodewig, *Matrix Calcvlus*, Amsterdam (1959), p. 76.

Consequently

$$\langle Q(n)^2 \rangle_{t_n}{}^{(0)} = \langle Q(n)^2 \rangle^{(0)} = \frac{2}{2ns+1} \sum_{k=0}^{ns} (ns-k)^2 = \tfrac{1}{3}ns(ns+1)$$

as stated in (6 H). For the Heisenberg problem, in fact, at sufficiently low temperatures any cluster of $n$ magnetic elements behaves as a single paramagnetic system having spin $ns$: as would be expected from a simple physical picture of coupled spins.

### 3.2. *Ising problem*

Since all symbols now commute, we can pass straight to the partition function and write, for any cluster

$$\frac{\chi kT}{g^2\beta^2} = \frac{\sum\limits_{(r)} (r_1+r_2+\ldots+r_n)^2 \exp\left[+2\sum\limits_{\langle i,j \rangle} r_i r_j/\theta\right]}{\sum\limits_{(r)} \exp\left[+2\sum\limits_{\langle i,j \rangle} r_i r_j/\theta\right]} \tag{12}$$

where $\sum\limits_{(r)}$ implies $\sum\limits_{r_1=-s,-s+1,\ldots}^{s}$ , $\sum\limits_{r_2=-s,-s+1,\ldots}^{s}$ , $\ldots$ $\sum\limits_{r_n=-s,-s+1,\ldots}^{s}$ . The maximum value of $\sum\limits_{i,j} r_i r_j$ occurs when $r_i=s$, all $i$, and when $r_i=-s$, all $i$. Thus the ground state of $-2J\mathscr{P}(n,t_n)$ is again $ls^2$, but now the degeneracy is 2. For each of these states $Q(n)=ns$, and hence when $n \geqslant 2$

$$\langle Q(n)^2 \rangle_{t_n}{}^{(0)} = \langle Q(n)^2 \rangle^{(0)} = n^2 s^2$$

as stated in (6 I). In pictorial language, at sufficiently low temperatures the Ising coupling (when $n \geqslant 2$) produces, in the $z$-direction, a spin component $ns$ which can point only up or down.

### 4. NUMERICAL ESTIMATION OF $p_c$

Having thus completed the justification of (11) we pass next to the numerical estimation of $p_c$ for various lattices. First, of course, we must compute, for any lattice, the coefficients $a_2, a_3 \ldots$, which demands knowledge of $N(n,t_n)$ as a function of $p$. For $n \leqslant 3$ the required expressions have been found by Behringer [2]; we have confirmed these calculations in extending them to $n \leqslant 5$, but have ourselves confined attention to powers of $p$ up to and including $p^5$ only. This is all that is needed for determining $a_2, a_3, a_4$ and $a_5$. Even so, the computations are very extensive, and can hardly be reported in detail. In Appendix II we give the resulting expressions for $a_2, a_3, a_4$ and $a_5$ in terms of parameters whereby they may be evaluated for any lattice, and in table 1 list their values for the four lattices of chief interest to us.

| Lattice | $a_2$ | $a_3$ | $a_4$ | $a_5$ |
|---|---|---|---|---|
| Face-centred cubic | 12 | 84 | 504 | 3012 |
| Body-centred cubic | 8 | 56 | 248 | 1232 |
| Simple cubic | 6 | 30 | 114 | 438 |
| Plane square | 4 | 12 | 24 | 52 |

Table 1.

This is not very adequate information on which to estimate the radius of convergence of (11), but a possible method is from the sequence $a_n{}^{1/n}$, and for

this purpose we have plotted $a_n^{-1/n}$ against $1/n$ to observe its trend.    For large $n$, of course, it must tend to $p_c$.

Alternatively, we may invert the series (11), first dividing by the leading term, obtaining an equation of the form

$$1 + b_2 p + b_3 p^2 + b_4 p^3 + b_5 p^4 + \ldots = 0. \tag{13}$$

In (13) the $b$'s vary with $s$ and differ for the Heisenberg and Ising problems.    A sequence of approximations to $p_c$ can now be found from the roots of the equations

$$1 + b_2 p = 0, \quad 1 + b_2 p + b_3 p^2 = 0, \quad 1 + b_2 p + b_3 p^2 + b_4 p^3 = 0$$

and

$$1 + b_2 p + b_3 p^2 + b_4 p^3 + b_5 p^4 = 0.$$

We have done this, for the lattices already specified, for the problems $I(\frac{1}{2})$, $H(\frac{1}{2})$ and $H(1)$.    This provides three other sequences of estimates of $p_c$, which have also been plotted against $1/n$ (where now $n$ is the highest suffix of $b$ retained in (13)).    Figure 1 shows all these results graphically for the body-centred cubic lattice.        The final conclusions about $p_c$ which we have, perhaps optimistically, reached in this way are tabulated in table 2.

We must, however, emphasize that in no case would we ascribe more than about 10 per cent accuracy to the result.
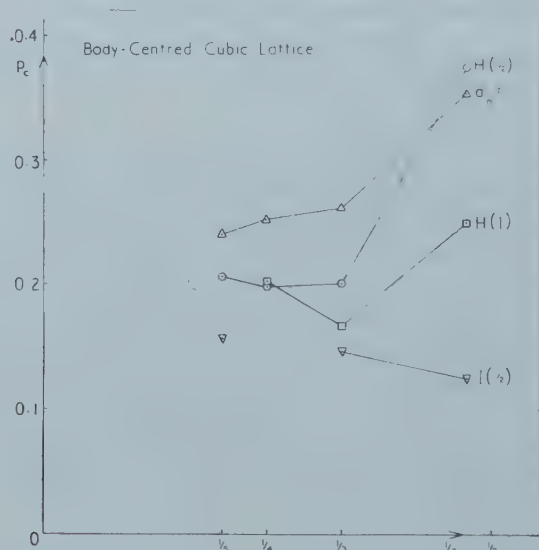


Figure 1.    Sequences leading to an estimate of $p_c$ for the body-centred cubic lattice.    For fuller explanation see § 4 of text.

| Lattice | $p_c$ |
|---|---|
| Face-centred cubic | 0·18 |
| Body-centred cubic | 0·22 |
| Simple cubic | 0·28 |
| Plane square | 0·48 |

Table 2.

## 5. CURIE TEMPERATURE AS A FUNCTION OF CONCENTRATION

So far we have concentrated on finding $p_c$, the proportion of magnetic elements at which the Curie temperature is zero. To find the Curie temperature, $\theta_c(p)$, when $p > p_c$ we must return to equation (3) and evaluate explicitly the susceptibility of each small cluster. If these cluster-susceptibilities are known for clusters of $n$, and fewer sites, then (3) gives the coefficients up to and including $a_n(\theta)$ in the series

$$\frac{\chi \mathbf{k} T}{N g^2 \beta^2} = a_1 p + a_2(\theta) p^2 + a_3(\theta) p^3 + \ldots \tag{14}$$

where $a_1 = s(s+1)/3$ for both Heisenberg and Ising problems. Inverting this series, we have

$$\frac{N g^2 \beta^2 s(s+1) p}{3 \chi \mathbf{k} T} = 1 + b_2(\theta) p + b_3(\theta) p^2 + \ldots, \tag{15}$$

the last coefficient known exactly being $b_n(\theta)$. Of course, the coefficients $a_n(\theta)$ as well as $b_n(\theta)$ now depend on $s$ and differ for the Heisenberg and Ising problems. Since we have taken the calculations in detail only as far as $n = 4$, rather than choosing a value of $\theta$ and then asking at what value of $p$ (14) diverges, we have preferred to base successive approximations to $\theta_c(p)$ on the vanishing of the right-hand side of (15). In this scheme we shall refer to the connection between $\theta_c$ and $p$ provided by the equation $1 + b_2(\theta) p = 0$ as the *second* approximation, so that the order of the approximation gives the size of the largest clusters considered explicitly. A *first* approximation, though lying outside the present formulism, may be regarded as provided by the Curie–Weiss theory which yields

$$\theta_c(p) = p \theta_c(1).$$

The $n$th approximation in our present scheme, $n \geqslant 2$, is furnished by the equation

$$1 + b_2(\theta) p + b_3(\theta) p^2 + \ldots + b_n(\theta) p^{n-1} = 0. \tag{16}$$

The second approximation for $H(\frac{1}{2})$ and $I(\frac{1}{2})$ has been discussed recently by Brout [3], and is easily generalized to any spin. But we confine attention now to the problems $H(\frac{1}{2})$ and $I(\frac{1}{2})$, for which we have proceeded fully as far as $n = 4$. In the case of $I(\frac{1}{2})$ we have gone one stage further for the plane square and simple cubic lattices.

The crux of the calculation is the evaluation of the susceptibility of a cluster. The required expressions, for $n \leqslant 4$, are collected in Appendix I.

For the Heisenberg problem perhaps the most straightforward procedure is to express $\mathcal{P}(n, t_n)$ and $Q(n)$ as $2^n$th order square matrices which are the direct products of $n$ 2nd order matrices in a representation in which $S_3^{(i)}$ is diagonal. There is then little difficulty in finding their simultaneous eigenvectors and corresponding eigenvalues (especially so with the facility of electronic computers). We have, however, used this method only for the 'chain' of four sites. We generally used an indirect method illustrated for the triangle of three sites in Appendix III.

For the Ising problem the most straightforward method, which we have used for all clusters with $n \leqslant 4$, is simply the direct evaluation of the right-hand side of (12). An alternative method is provided by use of the theory of Oguchi [6] and

Katsura [5] which employs the variable $u$, equal to $\tanh 1/(2\theta)$.   The basic equation† is

$$\frac{4\chi \boldsymbol{k} T}{Ng^2\beta^2} = 1 + 2 \sum_{m=1}^{\infty} \Omega_{2,m} u^m$$

where $\Omega_{2,m}$ is the coefficient of $N$ in the number of ways in which diagrams of $m$ lines can be put on the lattice, these diagrams, which are not necessarily connected, satisfying the requirements that only 'single bonds' are allowed and that there are just two points at which an odd number of lines end.   Without giving the full theory, which is essentially straightforward, here, we quote our final results for the simple cubic and plane square lattices:

*Simple cubic lattice*:

$$\frac{Ng^2\beta^2 p}{4\chi \boldsymbol{k} T} = 1 - 6up + 6u^2p^2 - \left[ 6u^3 - 24\frac{u^5 + u^6 + u^7}{1 + u^4} \right] p^3$$
$$+ \left[ 30u^4 - 96\frac{u^6 + u^7 + u^8}{1 + u^4} \right] p^4 + \ldots \qquad (17)$$

*Plane square lattice*:

$$\frac{Ng^2\beta^2 p}{4\chi \boldsymbol{k} T} = 1 - 4up + 4u^2p^2 - \left[ 4u^3 - 8\frac{u^5 + u^6 + u^7}{1 + u^4} \right] p^3$$
$$+ \left[ 12u^4 - 32\frac{u^6 + u^7 + u^8}{1 + u^4} \right] p^4 + \ldots \quad .$$
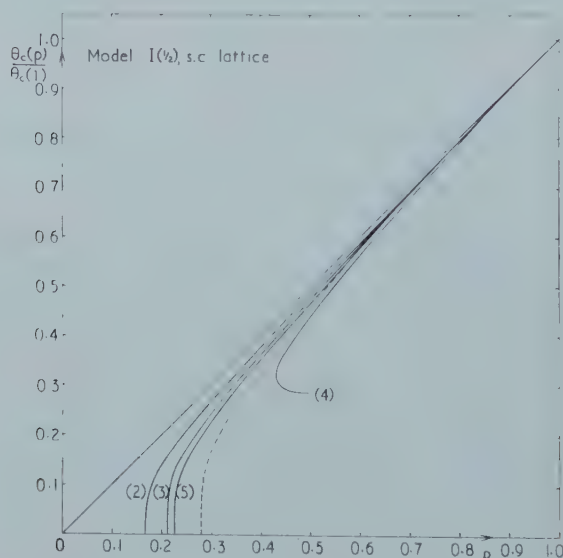


Figure 2.   Successive approximations to $\theta_c(p)/\theta_c(1)$ for the Ising spin $\frac{1}{2}$ problem, simple cubic lattice.   The approximations are based on equation (17).   The broken curve indicates our final conclusions for this model.

Our expressions for $\chi$ or $\chi^{-1}$ from equations (14) and (15) for $n = 4$ have been checked by expanding the right-hand sides in powers of $\theta^{-1}$ and comparing the

† This is not stated quite correctly by Katsura, and was not given by Oguchi.

resulting series with high-temperature expansions obtained quite independently by the present authors (to be published).

Figure 2 shows the approximations 2, 3, 4 and 5 obtained by equating to zero successive truncations of the right-hand side of equation (17), i.e. these approximations to $\theta_c(p)$ for the problem $I(\frac{1}{2})$, simple cubic lattice. Figure 3 shows approximations 2, 3 and 4 for the problem $H(\frac{1}{2})$, body centred cubic lattice. In both cases we have plotted the ratio $\theta_c(p)/\theta_c(1)$, as found from the approximation concerned. This not only reveals the trend of the approximations more clearly than simply plotting $\theta_c(p)$ would do, but also partly compensates for the inadequate assessment of $\theta_c(1)$ from a low-order approximation of this type. In point of fact, however, the last approximation plotted in each case does give a reasonably good value for $\theta_c(1)$: thus the 5th approximation of figure 2 gives $\theta_c(1) = 2\cdot315$, while the 4th approximation of figure 3 gives $\theta_c(1) = 2\cdot665$, estimates within about 3 per cent of the values ($2\cdot25$ and $2\cdot60$, respectively) usually accepted in these cases. We have carried through similar calculations for other lattices, and the results shown here are quite typical.
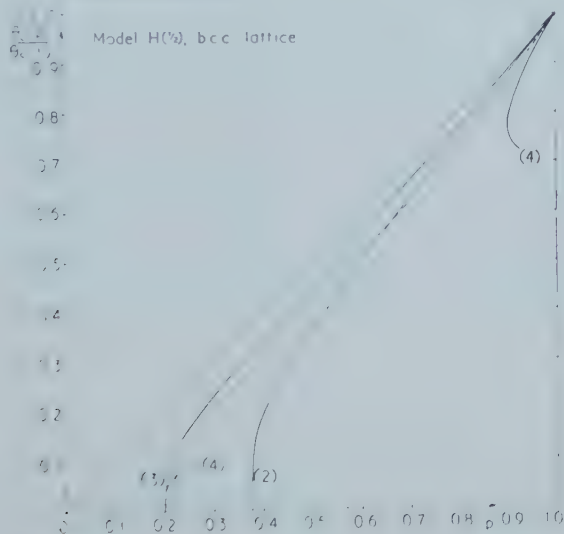


Figure 3.  Successive approximations to $\theta_c(p)/\theta_c(1)$ for the Heisenberg spin $\frac{1}{2}$ problem, body-centred cubic lattice. The approximations are based on equation (16). The broken curve indicates our final conclusions for this model.

## 6. DISCUSSION AND CONCLUSIONS

It is unfortunate that for both problems the 4th approximation illustrated, based on a cubic equation for $p$, fails over a significant part of the range. In the Ising case, of course, we have a 5th approximation to restore the balance. Such behaviour is not uncommon when Curie temperatures are sought from the vanishing of successive power-series approximations to $\chi^{-1}$. When the expansion is in powers of $\theta^{-1}$ this is the method originally used, in the case $p = 1$, by Opechowski [7], and more recently used by Behringer [2] in some high-temperature work for $p < 1$. We would much prefer to estimate $\theta_c(p)$ from the radius of convergence of the series in powers of $p$ for $\chi$ itself, but judge that we have insufficient terms in the expansion to do this convincingly.

Nevertheless, one feature of interest does emerge from these full $\theta_c(p)$ curves. For the Ising problem, figure 2, it is evident that

$$\frac{d}{dp}\left(\frac{\theta_c(p)}{\theta_c(1)}\right) = 1 \quad \text{when} \quad p = 1, \tag{18}$$

whereas for the Heisenberg problem, figure 3, it seems likely that

$$\frac{d}{dp}\left(\frac{\theta_c(p)}{\theta_c(1)}\right) > 1 \quad \text{when} \quad p = 1.$$

Application to other lattices produces the same conclusion. Further, and perhaps more convincing, support is provided by our high-temperature expansion work to which reference has already been made. This latter work, for the three cubic lattices, suggests indeed that (18) holds for $I(\frac{1}{2})$ and $I(1)$, whereas for $H(\frac{1}{2})$ and $H(1)$ the slope at $p = 1$ is in the range $1\cdot25$–$1\cdot40$. With this and the estimates of table 2 in mind, we have attempted to indicate, by the broken curves in figures 2 and 3, a final conclusion regarding $\theta_c(p)$ for the two problems concerned.

In this paper we have investigated the consequences of a model, or set of models, of a randomly dilute ferromagnetic: whether any physical ferromagnetic can be described by such a model is a different matter. It is not impossible that the Fe–Cr alloy could be described by the model $H(1)$, body-centred cubic lattice, and theoretically we should expect the $\theta_c(p)$ curve for this model to be very like that shown for $H(\frac{1}{2})$ in figure 3. The limiting value, $p_c$, is reported by Arrott and Sato [1] as 20 atomic per cent Fe, in fairly close accord with our theoretical predictions for the model. But since our theoretical prediction of $p_c$ is the same for all such models (involving nearest-neighbour interactions only) it would be of interest to have accurate experimental results on the lowering of the Curie temperature of iron by the random admixture of a little chromium: for the limiting slope of $\theta_c(p)$ at $p = 1$ is apparently more sensitive to the details of the interaction mechanism.

Finally, it is perhaps significant that $p_c$ is the same for Heisenberg and Ising models even in two dimensions. Earlier work of Rushbrooke and Wood [8], on high-temperature series for $p = 1$, failed to support the earlier spin-wave conclusion that $\theta_c(1) = 0$ for a two-dimensional $H(\frac{1}{2})$ problem. The present result likewise suggests qualitatively similar behaviour for Heisenberg and Ising two-dimensional problems. Further work is in progress on this issue, in view of the importance of its bearing on spin-wave theory.

## Appendix I

The susceptibilities of small clusters for the Heisenberg and Ising spin $\frac{1}{2}$ problems: $\theta = \boldsymbol{k}T/J$, $\kappa = 1/(2\theta)$

$$\text{Susceptibility, i.e. } \chi \boldsymbol{k}T/\beta^2$$

| Cluster | H($\tfrac{1}{2}$) | I($\tfrac{1}{2}$) |
|---|---|---|
| $\bullet$ | $1$ | $1$ |
| $\bullet\!-\!\bullet$ | $\dfrac{8e^\kappa}{3e^\kappa + e^{-3\kappa}}$ | $\dfrac{4e^\kappa}{e^\kappa + e^{-\kappa}}$ |
| $\bullet\!-\!\bullet\!-\!\bullet$ | $\dfrac{10e^{2\kappa}+1+e^{-4\kappa}}{2e^{2\kappa}+1+e^{-4\kappa}}$ | $\dfrac{9e^{2\kappa}+2+e^{-2\kappa}}{e^{2\kappa}+2+e^{-2\kappa}}$ |
| triangle | $\dfrac{5e^{3\kappa}+e^{-3\kappa}}{e^{3\kappa}+e^{-3\kappa}}$ | $\dfrac{9e^{3\kappa}+3e^{-\kappa}}{e^{3\kappa}+3e^{-\kappa}}$ |
| chain of 4 | $\dfrac{40e^{3\kappa}+8e^{-\kappa}+16e^{-\kappa}\cosh 2\sqrt{2}\kappa}{5e^{3\kappa}+3e^{-\kappa}+6e^{-\kappa}\cosh 2\sqrt{2}\kappa + 2e^{-3\kappa}\cosh 2\sqrt{3}\kappa}$ | $\dfrac{16e^{3\kappa}+8e^\kappa+8e^{-\kappa}}{e^{3\kappa}+3e^\kappa+3e^{-\kappa}+e^{-3\kappa}}$ |
| star (Y) | $\dfrac{40e^{3\kappa}+16e^\kappa+8e^{-5\kappa}}{5e^{3\kappa}+6e^\kappa+2e^{-3\kappa}+3e^{-5\kappa}}$ | $\dfrac{16e^{3\kappa}+12e^\kappa+4e^{-3\kappa}}{e^{3\kappa}+3e^\kappa+3e^{-\kappa}+e^{-3\kappa}}$ |
| triangle with tail | $\dfrac{40e^{4\kappa}+8e^{2\kappa}+8e^{-2\kappa}+8e^{-4\kappa}}{5e^{4\kappa}+3e^{2\kappa}+4e^{-2\kappa}+3e^{-4\kappa}+e^{-6\kappa}}$ | $\dfrac{16e^{4\kappa}+4e^{2\kappa}+8+4e^{-2\kappa}}{e^{4\kappa}+e^{2\kappa}+3+3e^{-2\kappa}}$ |
| square | $\dfrac{40e^{4\kappa}+16+8e^{-4\kappa}}{5e^{4\kappa}+7+3e^{-4\kappa}+e^{-8\kappa}}$ | $\dfrac{16e^{4\kappa}+16}{e^{4\kappa}+6+e^{-4\kappa}}$ |
| square with diagonal | $\dfrac{40e^{5\kappa}+8e^\kappa+16e^{-3\kappa}}{5e^{5\kappa}+3e^\kappa+7e^{-3\kappa}+e^{-7\kappa}}$ | $\dfrac{16e^{5\kappa}+8e^\kappa+8e^{-\kappa}}{e^{5\kappa}+2e^\kappa+4e^{-\kappa}+e^{-3\kappa}}$ |
| tetrahedron | $\dfrac{40e^{6\kappa}+24e^{-2\kappa}}{5e^{6\kappa}+9e^{-2\kappa}+2e^{-6\kappa}}$ | $\dfrac{16e^{6\kappa}+16}{e^{6\kappa}+4+3e^{-2\kappa}}$ |

5-point clusters: we record the susceptibilities of two of these, although we have made no explicit use of these expressions:

| | | |
|---|---|---|
| cross (star) | $\dfrac{35e^{4\kappa}+30e^{2\kappa}+2+3e^{-4\kappa}+10e^{-6\kappa}}{3e^{4\kappa}+6e^{2\kappa}+2+3e^{-4\kappa}+2e^{-8\kappa}}$ | $\dfrac{25e^{4\kappa}+36e^{2\kappa}+6+4e^{-2\kappa}+9e^{-4\kappa}}{e^{4\kappa}+4e^{2\kappa}+6+4e^{-2\kappa}+e^{-4\kappa}}$ |
| bowtie/diamond | $\dfrac{35e^{6\kappa}+20e^{2\kappa}+12+12e^{-4\kappa}+e^{-10\kappa}}{3e^{6\kappa}+4e^{2\kappa}+4+4e^{-4\kappa}+e^{-10\kappa}}$ | $\dfrac{25e^{6\kappa}+27e^{2\kappa}+24+3e^{-2\kappa}+e^{-6\kappa}}{e^{6\kappa}+3e^{2\kappa}+8+3e^{-2\kappa}+e^{-6\kappa}}$ |
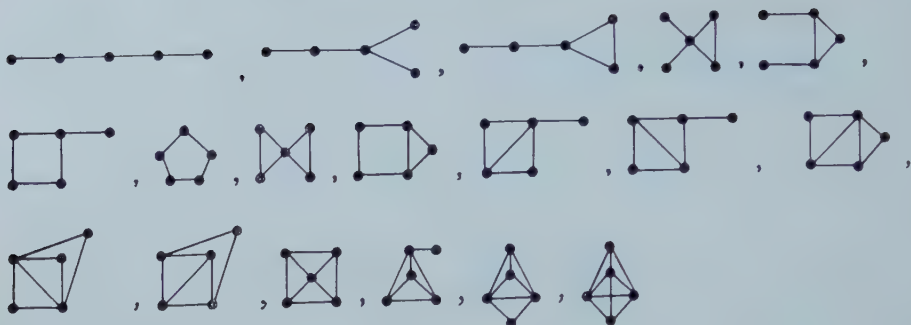
Note: the last of these clusters occurs only on the hexagonal close-packed lattice.

Finally, we add expressions, in terms of the lattice parameters defined in Appendix II, for the occurrences of clusters (i) to (x) above. When multiplied by $N$, these expressions give the number of corresponding clusters obtaining on a lattice of $N$ sites, in powers of $p$ (the proportion of magnetic elements) up to and including terms in $p^4$:

$$\text{(i)} \quad p - zp^2 + \tfrac{1}{2}z(z-1)p^3 - \tfrac{1}{6}z(z-1)(z-2)p^4 \ldots;$$

$$\text{(ii)} \quad \tfrac{1}{2}zp^2[1 - \{2z - 2 - r_3\}p + \tfrac{1}{2}\{2z - 2 - r_3\}\{2z - 3 - r_3\}p^2 \ldots];$$

$$\text{(iii)} \quad \tfrac{1}{2}z(z-1)p^3 - \tfrac{1}{2}zr_3p^3 - z\{(z-1)^2 - r_3\}p^4 - 2zr_3(r_3 - 1)p^4$$
$$+ \tfrac{1}{2}zq_1p^4 + \tfrac{1}{2}zr_4p^4 + \tfrac{5}{2}zr_3(z-2)p^4 - \tfrac{1}{2}z(z-1)(z-2)p^4 \ldots;$$

$$\text{(iv)} \quad \tfrac{1}{6}zr_3p^3 - \tfrac{1}{2}zr_3(z-2)p^4 + \tfrac{1}{2}zr_3(r_3 - 1)p^4 - \tfrac{1}{6}zq_1p^4 \ldots;$$

$$\text{(v)} \quad \tfrac{1}{2}z\{(z-1)^2 - r_3\}p^4 + \tfrac{3}{2}zr_3(r_3 - 1)p^4 - \tfrac{1}{2}zq_1p^4 - \tfrac{1}{2}zr_4p^4 - zr_3(z-2)p^4 \ldots;$$

$$\text{(vi)} \quad \tfrac{1}{6}z(z-1)(z-2)p^4 - \tfrac{1}{2}zr_3(z-2)p^4 + \tfrac{1}{2}zr_3(r_3 - 1)p^4 - \tfrac{1}{6}zq_1p^4 \ldots;$$

$$\text{(vii)} \quad \tfrac{1}{2}zr_3(z-2)p^4 - zr_3(r_3 - 1)p^4 + \tfrac{1}{2}zq_1p^4 \ldots;$$

$$\text{(viii)} \quad \tfrac{1}{8}zr_4p^4 - \tfrac{1}{4}zr_3(r_3 - 1)p^4 + \tfrac{1}{8}zq_1p^4 \ldots;$$

$$\text{(ix)} \quad \tfrac{1}{4}zr_3(r_3 - 1)p^4 - \tfrac{1}{4}zq_1p^4 \ldots;$$

$$\text{(x)} \quad \tfrac{1}{24}zq_1p^4 \ldots .$$

## Appendix II

We give here expressions, appropriate to any lattice, for the coefficients $a_2$, $a_3$, $a_4$, $a_5$ of equation (11). They involve parameters of the type already introduced in lattice-statistics problems by Rushbrooke and Wood [8] and Domb and Sykes [4], but with some changes in notation. These parameters are most conveniently defined as enumerating certain line-, or link- diagrams on a lattice. Precisely,

$\tfrac{1}{2}Nz$      = number of ways a link can be placed on the lattice (of $N$ points), i.e. $z$ = lattice coordination number;

$(1/2n)Nzr_n$ = number of (unlabelled) closed, non-crossing, circuits of $n$ points on the lattice (i.e. placings of a 'ring' of size $n$);

and the numbers of ways in which unlabelled link-diagrams having the topologies

     (a)      (b)      (c)      (d)      (e)
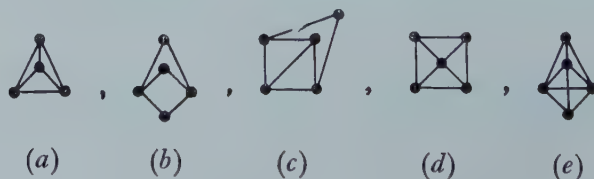
can be placed on the lattice are denoted by

$$(a)\ \tfrac{1}{24}Nzq_1,\ (b)\ \tfrac{1}{12}Nzq_2,\ (c)\ \tfrac{1}{4}Nzq_3,\ (d)\ \tfrac{1}{8}Nzq_4\ \text{and}\ (e)\ \tfrac{1}{12}Nzq_5.$$

The values of the parameters required for the coefficients $a_2 \ldots a_5$ are listed, for various lattices, below:

| | $z$ | $r_3$ | $r_4$ | $r_5$ | $q_1$ | $q_2$ | $q_3$ | $q_4$ | $q_5$ |
|---|---|---|---|---|---|---|---|---|---|
| Linear | 2 | 0 | 0 | 0 | 0 | 0 | 0 | 0 | 0 |
| Honeycomb | 3 | 0 | 0 | 0 | 0 | 0 | 0 | 0 | 0 |
| Plane square | 4 | 0 | 2 | 0 | 0 | 0 | 0 | 0 | 0 |
| Plane triangular | 6 | 2 | 4 | 10 | 0 | 0 | 0 | 0 | 0 |
| Diamond | 4 | 0 | 0 | 0 | 0 | 0 | 0 | 0 | 0 |
| Simple cubic | 6 | 0 | 4 | 0 | 0 | 0 | 0 | 0 | 0 |
| Body-centred cubic | 8 | 0 | 12 | 0 | 0 | 18 | 0 | 0 | 0 |
| Face-centred cubic | 12 | 4 | 22 | 140 | 4 | 36 | 16 | 4 | 0 |
| Hexagonal close-packed | 12 | 4 | 22 | 140 | 4 | 37 | 17 | 6 | 1 |

It is important, in the present context, to emphasize that these lattice parameters are only indirectly related to the occurrences of the point clusters depicted in Appendix I. For example, with the *point-cluster* drawn as



it is essential that sites with no bond between them should *not* be neighbours. On the other hand, with the link-diagram, similarly illustrated as (*d*) above, although vertices must not coincide, there is no such restriction against their being nearest neighbours.

In terms of these parameters, then, we have

$$a_2 = z,$$
$$a_3 = z\,[z-1-r_3],$$
$$a_4 = (z/2)[2(z-1)^2 + r_3(7r_3 - 1 - 4z) - 3r_4 - 2q_1],$$

and

$$a_5 = (z/6)[6(z-1)^3 + r_3(70 + 6z - 18z^2 - 15r_3 + 48zr_3 - 97r_3{}^2 + 72r_4 + 72q_1)$$
$$+ 30r_4 - 18zr_4 - 12r_5 - 48q_1 - 12zq_1 + 13q_2 - 66q_3 + 48q_4 - 42q_5].$$

It is immediately apparent that whereas $a_2$, $a_3$ and $a_4$ are the same for face-centred and hexagonal close-packed lattices, $a_5$ is different. But the change is negligible (of course): $a_5$ equals 3012 and 3014 for these two lattices, respectively.

The coefficients $b_2$, $b_3$, $b_4$, $b_5$ of equation (13) vary from problem to problem, but are particularly simple in the case $\mathrm{I}(\tfrac{1}{2})$. They then are

$$b_2 = -z,$$
$$b_3 = z[1 + r_3],$$
$$b_4 = -(z/2)[2 + 7r_3{}^2 - r_3 - 3r_4 - 2q_1],$$
$$b_5 = (z/6)[6 + 97r_3{}^3 + 15r_3{}^2 - 70r_3 - 72r_3 r_4 - 30r_4 + 12r_5$$
$$- 72r_3 q_1 + 48q_1 - 13q_2 + 66q_3 - 48q_4 + 42q_5].$$

In either case it is evident that for a $z$-branch tree, i.e., a lattice of coordination number $z$ on which there are no closed circuits, the critical concentration, $p_c$, determined by the radius of convergence of (11) or the vanishing of (12), is given

by $p_c = 1/(z-1)$.   This result is not unexpected; for it is known that when $p = 1$ the cluster-variational, or quasi-chemical, treatment of the $I(\frac{1}{2})$ model is exact for such a tree: and Sato, *et al.* [9] have shown that the corresponding cluster-variational treatment of the magnetically dilute $I(\frac{1}{2})$ model leads to $p_c = 1/(z-1)$. We notice, table 1, that the true value of $p_c$ seems to be appreciably greater than that of the corresponding tree.

### APPENDIX III

We illustrate the method which we generally used for calculating the $H(\frac{1}{2})$ susceptibilities tabulated in Appendix I by considering the cluster comprising a triangle of sites.   Calling these $a$, $b$ and $c$, introducing the Pauli matrices $\sigma^{(i)} = 2S^{(i)}$, and abbreviating $\sigma^{(i)} \cdot \sigma^{(j)}$ to $(ij)$ we have, in the notation of the text and of Appendix I,

$$\exp(2\mathscr{P}/\theta) = 1 + \sum_{n \geqslant 1} \frac{[(ab) + (bc) + (ca)]^n \kappa^n}{n!}.$$

Now suppose

$$[(ab) + (bc) + (ca)]^n = A_n + B_n [(ab) + (bc) + (ca)], \tag{1}$$

as is justified, *a posteriori*, by induction.   Then since, from the commutation rules for $\sigma$ matrices

$$[(ab) + (bc) + (ca)]^2 = 9$$

(see Rushbrooke and Wood [8] for a collection of basic formulae of this type), we have

$$A_{n+1} = 9B_n, \quad B_{n+1} = A_n$$

whence

$$A_n = \tfrac{1}{2}[3^n + (-3)^n], \quad B_n = \tfrac{1}{6}[3^n - (-3)^n].$$

Hence

$$\langle \exp(2\mathscr{P}/\theta) \rangle = 8\left[1 + \sum_{n \geqslant 1} A_n \kappa^n\right] = 4[\exp(3\kappa) + \exp(-3\kappa)]$$

and

$$\langle Q^2 \exp(2\mathscr{P}/\theta) \rangle = 8\left[3 + 3\sum_{n \geqslant 1} A_n \kappa^n + 6\sum_{n \geqslant 1} B_n \kappa^n\right]$$
$$= 4[5\exp(3\kappa) + \exp(-3\kappa)].$$

The generalization of (1) for the ring $\begin{array}{c} b \quad\quad c \\ \square \\ a \quad\quad d \end{array}$ is

$$[(ab) + (bc) + (cd) + (da)]^n = A_n + B_n [(ab) + (bc) + (cd) + (da)]$$
$$+ C_n [(ac) + (cd)]$$
$$+ D_n [(ab)(cd) + (bc)(da)]$$
$$+ E_n [(ac)(bd)],$$

an expression embodying the symmetry of the cluster.   For the small clusters dealt with there is little difficulty in choosing the independent spin combinations on the right-hand side.   In this particular example, of course,

$$\langle \exp(\mathscr{P}/\theta) \rangle = 16\left[1 + \sum_{n \geqslant 1} A_n \kappa^n\right]$$

and

$$\langle Q^2 \exp(2\mathscr{P}/\theta) \rangle = 16\left[4 + 4\sum_{n \geqslant 1} A_n \kappa^n + 8\sum_{n \geqslant 1} B_n \kappa^n + 4\sum_{n \geqslant 1} C_n \kappa^n\right].$$

## References

[1] Arrott, A., and Sato, H., 1958, *Bull. Amer. phys. Soc.*, **3**, 42.

[2] Behringer, R. E., 1957, *J. chem. Phys.*, **26**, 1504; 1958, *Ibid.*, **29**, 537.

[3] Brout, R., 1959, *Phys. Rev.*, **115**, 824.

[4] Domb, C., and Sykes, M. F., 1957, *Proc. roy. Soc.* A, **240**, 214.

[5] Katsura, S., 1958, *Prog. theor. Phys.*, **20**, 192.

[6] Oguchi, T., 1951, *J. phys. Soc., Japan*, **6**, 31.

[7] Opechowski, W., 1937, *Physica*, **4**, 181.

[8] Rushbrooke, G. S., and Wood, P. J., 1955, *Proc. phys. Soc. Lond.*, A, **68**, 1161; 1958, *Mol. Phys.*, **1**, 257.

[9] Sato, H., Arrott, A., and Kikuchi, R., 1959, *J. Phys. Chem. Solids*, **10**, 19.

# Molecular two-centre hybrid and exchange integrals between $2p\pi$ and $3p\pi$ atomic orbitals

by ALF LOFTHUS

Department of Physics, University of Oslo, Blindern, Oslo, Norway

All possible two-centre hybrid and exchange integrals between $2p\pi$ and $3p\pi$ atomic orbitals with equal orbital exponent $\alpha$ have been calculated and tabulated for $\alpha = 1\cdot00$ $(0\cdot25)$ $9\cdot00$.

## 1. Introduction

Most of the existing tables and expressions for molecular integrals are restricted to orbitals of principal quantum numbers 1 and 2. It is obvious that extensions of available integrals to higher orbitals would be very important for the quantum-mechanical discussion of molecular electronic structure. The greatly increasing complexity of the evaluation of such integrals makes it probably more practical to base further developments on electronic computer programming rather than giving explicit formulae and tables. However, for the special but very important case of equal exponent for the orbitals involved, it is still feasible and practical to evaluate closed expressions for integrals between orbitals of quantum numbers 2 and 3, for which tables can be made.

The purpose of the present work is to give formulae and tables of all possible two-centre integrals between $2p\pi$ and $3p\pi$ Slater atomic orbitals with equal exponent, of the following types:

*Hybrid integrals:*

$$L = (\psi_a \psi_a' | \psi_a'' \psi_b''') = \int \int \psi_a(1) \psi_a'(1) (e^2/r_{12}) \psi_a''(2) \psi_b'''(2) \, d\tau_1 \, d\tau_2; \qquad (1a)$$

*Exchange integrals:*

$$A = (\psi_a \psi_b' | \psi_a'' \psi_b''') = \int \int \psi_a(1) \psi_b'(1) (e^2/r_{12}) \psi_a''(2) \psi_b'''(2) \, d\tau_1 \, d\tau_2; \qquad (1b)$$

where $\psi$, $\psi'$, $\psi''$ and $\psi'''$ denote various Slater atomic orbitals of the form

$$\psi(2p\pi) = (2p) = (k^5/\pi)^{1/2} \exp(-kr) r \sin\vartheta \cos\varphi, \qquad (2a)$$

$$\psi(3p\pi) = (3p) = (2k^7/\pi)^{1/2} \exp(-kr) r^2 \sin\vartheta \cos\varphi. \qquad (2b)$$

Here $k = Z/2a_0$, $Z$ is the effective nuclear charge, and $a_0 = 0\cdot5292$ Å the Bohr radius.

The different angles and distances involved in these expressions are shown in the figure.

These hybrid and exchange integrals can be expressed in terms of tabulated auxiliary functions [2] of the types†

$$H_\tau^j(m, \alpha; n, \beta) = \int_1^\infty \int_1^\infty Q_\tau^j(\mu_>) P_\tau^j(\mu_<) \exp\left[-(\alpha\mu_1 + \beta\mu_2)\right] \times \{(\mu_1^2 - 1)(\mu_2^2 - 1)\}^{j/2} \mu_1^m \mu_2^n \, d\mu_1 \, d\mu_2 \qquad (3)$$

† The $H_\tau^j$ functions are sometimes designated $W_\tau^j$.

and

$$G_\tau^j(m, \alpha) = \int_{-1}^{+1} \exp(-\alpha\nu) P_\tau^j(\nu)(1-\nu^2)^{j/2}\nu^m \, d\nu \qquad (4)$$

where $\alpha = kR = ZR/2a_0$. (In the present case $\alpha = \beta$.)

The integrations were performed in elliptical coordinates; the general methods used are outlined elsewhere [3].
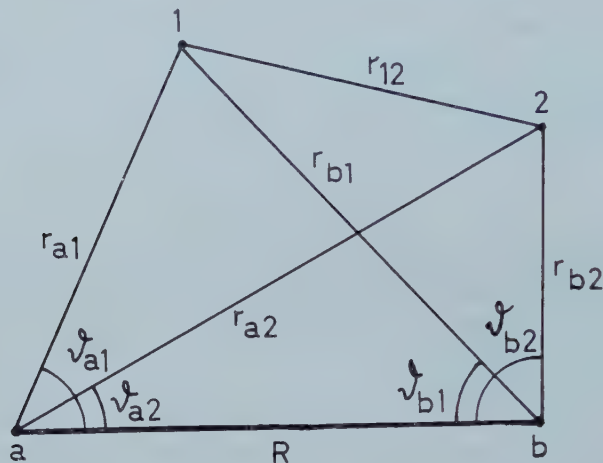


Polar coordinates for two variables points (1 and 2) around centres $a$ and $b$.

## 2. RESULTS

There are altogether twelve different hybrid integrals which can be constructed from $2p\pi$ and $3p\pi$ orbitals:

$$
\begin{aligned}
L_0 &= (2p_a 2p_a | 2p_a 2p_b) & L_6 &= (2p_a 3p_a | 2p_a 3p_b) \\
L_1 &= (2p_a 2p_a | 3p_a 3p_b) & L_7 &= (2p_a 3p_a | 2p_a 2p_b) \\
L_2 &= (2p_a 2p_a | 3p_a 2p_b) & L_8 &= (2p_a 3p_a | 3p_a 3p_b) \\
L_3 &= (2p_a 3p_a | 3p_a 2p_b) & L_9 &= (3p_a 3p_a | 2p_a 3p_b) \\
L_4 &= (3p_a 3p_a | 2p_a 2p_b) & L_{10} &= (3p_a 3p_a | 3p_a 2p_b) \\
L_5 &= (2p_a 2p_a | 2p_a 3p_b) & L_{11} &= (3p_a 3p_a | 3p_a 3p_b)
\end{aligned}
\right\} . \qquad (5)
$$

These integrals were reduced to finite expressions involving the functions $H_\tau^j$ and $G_\tau^j$, and from these expressions numerical values of the integrals were computed, the results of which are given in table 1.

There are seven exchange integrals between $2p\pi$ and $3p\pi$ orbitals:

$$
\begin{aligned}
A_0 &= (2p_a 2p_b | 2p_a 2p_b) & A_4 &= (2p_a 2p_b | 2p_a 3p_b) \\
A_1 &= (2p_a 2p_b | 3p_a 3p_b) & A_5 &= (2p_a 3p_b | 3p_a 3p_b) \\
A_2 &= (2p_a 3p_b | 2p_a 3p_b) & A_6 &= (3p_a 3p_b | 3p_a 3p_b) \\
A_3 &= (2p_a 3p_b | 3p_a 2p_b)
\end{aligned}
\right\} . \qquad (6)
$$

These integrals were reduced to finite expressions involving $H_\tau^j$ functions only. The numerical results are given in table 2.

| $\alpha$ | $L_0 = (2p_a2p_a\|2p_a2p_b)$ | $L_1 = (2p_a2p_a\|3p_a3p_b)$ | $L_2 = (2p_a2p_a\|3p_a2p_b)$ | $L_3 = (2p_a3p_a\|3p_a2p_b)$ |
|---|---|---|---|---|
| 1·00 | 1·7313 (−1) | 1·4869 (−1) | 1·4787 (−1) | 1·2551 (−1) |
| 1·25 | 1·6210 (−1) | 1·4390 (−1) | 1·4116 (−1) | 1·2009 (−1) |
| 1·50 | 1·4995 (−1) | 1·3829 (−1) | 1·3348 (−1) | 1·1385 (−1) |
| 1·75 | 1·3718 (−1) | 1·3198 (−1) | 1·2506 (−1) | 1·0697 (−1) |
| 2·00 | 1·2424 (−1) | 1·2512 (−1) | 1·1616 (−1) | 9·9657 (−2) |
| 2·25 | 1·1150 (−1) | 1·1784 (−1) | 1·0702 (−1) | 9·2093 (−2) |
| 2·50 | 9·9232 (−2) | 1·1029 (−1) | 9·7844 (−2) | 8·4454 (−2) |
| 2·75 | 8·7649 (−2) | 1·0259 (−1) | 8·8815 (−2) | 7·6892 (−2) |
| 3·00 | 7·6889 (−2) | 9·4873 (−2) | 8·0081 (−2) | 6·9534 (−2) |
| 3·25 | 6·7029 (−2) | 8·7241 (−2) | 7·1757 (−2) | 6·2483 (−2) |
| 3·50 | 5·8102 (−2) | 7·9790 (−2) | 6·3925 (−2) | 5·5815 (−2) |
| 3·75 | 5·0101 (−2) | 7·2599 (−2) | 5·6640 (−2) | 4·9582 (−2) |
| 4·00 | 4·2997 (−2) | 6·5732 (−2) | 4·9933 (−2) | 4·3817 (−2) |
| 4·25 | 3·6739 (−2) | 5·9234 (−2) | 4·3813 (−2) | 3·8536 (−2) |
| 4·50 | 3·1265 (−2) | 5·3141 (−2) | 3·8275 (−2) | 3·3737 (−2) |
| 4·75 | 2·6509 (−2) | 4·7471 (−2) | 3·3300 (−2) | 2·9411 (−2) |
| 5·00 | 2·2399 (−2) | 4·2235 (−2) | 2·8861 (−2) | 2·5539 (−2) |
| 5·25 | 1·8867 (−2) | 3·7431 (−2) | 2·4924 (−2) | 2·2094 (−2) |
| 5·50 | 1·5844 (−2) | 3·3052 (−2) | 2·1452 (−2) | 1·9047 (−2) |
| 5·75 | 1·3270 (−2) | 2·9083 (−2) | 1·8404 (−2) | 1·6366 (−2) |
| 6·00 | 1·1085 (−2) | 2·5506 (−2) | 1·5743 (−2) | 1·4019 (−2) |
| 6·25 | 9·2383 (−3) | 2·2297 (−2) | 1·3429 (−2) | 1·1974 (−2) |
| 6·50 | 7·6819 (−3) | 1·9434 (−2) | 1·1425 (−2) | 1·0200 (−2) |
| 6·75 | 6·3744 (−3) | 1·6889 (−2) | 9·6954 (−3) | 8·6656 (−3) |
| 7·00 | 5·2790 (−3) | 1·4637 (−2) | 8·2084 (−3) | 7·3443 (−3) |
| 7·25 | 4·3638 (−3) | 1·2652 (−2) | 6·9339 (−3) | 6·2100 (−3) |
| 7·50 | 3·6010 (−3) | 1·0909 (−2) | 5·8448 (−3) | 5·2395 (−3) |
| 7·75 | 2·9667 (−3) | 9·3834 (−3) | 4·9169 (−3) | 4·4114 (−3) |
| 8·00 | 2·4403 (−3) | 8·0527 (−3) | 4·1284 (−3) | 3·7069 (−3) |
| 8·25 | 2·0043 (−3) | 6·8955 (−3) | 3·4600 (−3) | 3·1091 (−3) |
| 8·50 | 1·6440 (−3) | 5·8921 (−3) | 2·8948 (−3) | 2·6030 (−3) |
| 8·75 | 1·3466 (−3) | 5·0246 (−3) | 2·4178 (−3) | 2·1756 (−3) |
| 9·00 | 1·1017 (−3) | 4·2765 (−3) | 2·0163 (−3) | 1·8154 (−3) |

Table 1.

| $\alpha$ | $L_4 = (3p_a 3p_a\|2p_a 2p_b)$ | $L_5 = (2p_a 2p_a\|2p_a 3p_b)$ | $L_6 = (2p_a 3p_a\|2p_a 3p_b)$ | $L_7 = (2p_a 3p_a\|2p_a 2p_b)$ |
|---|---|---|---|---|
| 1·00 | 1·4110 (−1) | 1·4982 (−1) | 1·2678 (−1) | 1·4314 (−1) |
| 1·25 | 1·3287 (−1) | 1·4399 (−1) | 1·2195 (−1) | 1·3444 (−1) |
| 1·50 | 1·2369 (−1) | 1·3719 (−1) | 1·1633 (−1) | 1·2479 (−1) |
| 1·75 | 1·1393 (−1) | 1·2963 (−1) | 1·1005 (−1) | 1·1458 (−1) |
| 2·00 | 1·0392 (−1) | 1·2148 (−1) | 1·0329 (−1) | 1·0417 (−1) |
| 2·25 | 9·3941 (−2) | 1·1296 (−1) | 9·6201 (−2) | 9·3837 (−2) |
| 2·50 | 8·4215 (−2) | 1·0425 (−1) | 8·8943 (−2) | 8·3829 (−2) |
| 2·75 | 7·4920 (−2) | 9·5538 (−2) | 8·1658 (−2) | 7·4318 (−2) |
| 3·00 | 6·6185 (−2) | 8·6964 (−2) | 7·4472 (−2) | 6·5427 (−2) |
| 3·25 | 5·8091 (−2) | 7·8660 (−2) | 6·7491 (−2) | 5·7233 (−2) |
| 3·50 | 5·0684 (−2) | 7·0723 (−2) | 6·0800 (−2) | 4·9773 (−2) |
| 3·75 | 4·3980 (−2) | 6·3230 (−2) | 5·4465 (−2) | 4·3054 (−2) |
| 4·00 | 3·7970 (−2) | 5·6233 (−2) | 4·8532 (−2) | 3·7058 (−2) |
| 4 25 | 3·2629 (−2) | 4·9761 (−2) | 4·3028 (−2) | 3·1753 (−2) |
| 4·50 | 2·7918 (−2) | 4·3829 (−2) | 3·7969 (−2) | 2·7093 (−2) |
| 4·75 | 2·3792 (−2) | 3·8435 (−2) | 3·3357 (−2) | 2·3029 (−2) |
| 5·00 | 2·0201 (−2) | 3·3566 (−2) | 2·9182 (−2) | 1·9504 (−2) |
| 5·25 | 1·7093 (−2) | 2·9199 (−2) | 2·5429 (−2) | 1·6464 (−2) |
| 5·50 | 1·4416 (−2) | 2·5308 (−2) | 2·2076 (−2) | 1·3855 (−2) |
| 5·75 | 1·2123 (−2) | 2·1860 (−2) | 1·9098 (−2) | 1·1626 (−2) |
| 6·00 | 1·0166 (−2) | 1·8820 (−2) | 1·6468 (−2) | 9·7296 (−3) |
| 6·25 | 8·5028 (−3) | 1·6153 (−2) | 1·4155 (−2) | 8·1223 (−3) |
| 6·50 | 7·0944 (−3) | 1·3824 (−2) | 1·2130 (−2) | 6·7647 (−3) |
| 6·75 | 5·9058 (−3) | 1·1798 (−2) | 1·0367 (−2) | 5·6217 (−3) |
| 7·00 | 4·9058 (−3) | 1·0043 (−2) | 8·8357 (−3) | 4·6623 (−3) |
| 7·25 | 4·0669 (−3) | 8·5277 (−3) | 7·5118 (−3) | 3·8591 (−3) |
| 7·50 | 3·3650 (−3) | 7·2243 (−3) | 6·3711 (−3) | 3·1885 (−3) |
| 7·75 | 2·7794 (−3) | 6·1064 (−3) | 5·3913 (−3) | 2·6300 (−3) |
| 8·00 | 2·2917 (−3) | 5·1507 (−3) | 4·5523 (−3) | 2·1657 (−3) |
| 8·25 | 1·8866 (−3) | 4·3357 (−3) | 3·8360 (−3) | 1·7807 (−3) |
| 8·50 | 1·5507 (−3) | 3·6428 (−3) | 3·2260 (−3) | 1·4620 (−3) |
| 8·75 | 1·2729 (−3) | 3·0549 (−3) | 2·7080 (−3) | 1·1987 (−3) |
| 9·00 | 1·0433 (−3) | 2·5575 (−3) | 2·2691 (−3) | 9·8152 (−4) |

Table 1.—*Continued.*

| α | $L_8 = (2p_a3p_a\|3p_a3p_b)$ | $L_9 = (3p_a3p_a\|2p_a3p_b)$ | $L_{10} = (3p_a3p_a\|3p_a2p_b)$ | $L_{11} = (3p_a3p_a\|3p_a3p_b)$ |
|---|---|---|---|---|
| 1·00 | 1·2882 (−1) | 1·2751 (−1) | 1·2653 (−1) | 1·3238 (−1) |
| 1·25 | 1·2477 (−1) | 1·2276 (−1) | 1·2132 (−1) | 1·2832 (−1) |
| 1·50 | 1·2002 (−1) | 1·1723 (−1) | 1·1529 (−1) | 1·2356 (−1) |
| 1·75 | 1·1467 (−1) | 1·1105 (−1) | 1·0862 (−1) | 1·1820 (−1) |
| 2·00 | 1·0884 (−1) | 1·0437 (−1) | 1·0148 (−1) | 1·1233 (−1) |
| 2·25 | 1·0265 (−1) | 9·7366 (−2) | 9·4061 (−2) | 1·0609 (−1) |
| 2·50 | 9·6206 (−2) | 9·0175 (−2) | 8·6523 (−2) | 9·9587 (−2) |
| 2·75 | 8·9624 (−2) | 8·2939 (−2) | 7·9020 (−2) | 9·2923 (−2) |
| 3·00 | 8·3007 (−2) | 7·5783 (−2) | 7·1679 (−2) | 8·6206 (−2) |
| 3·25 | 7·6447 (−2) | 6·8811 (−2) | 6·4605 (−2) | 7·9530 (−2) |
| 3·50 | 7·0027 (−2) | 6·2111 (−2) | 5·7881 (−2) | 7·2977 (−2) |
| 3·75 | 6·3815 (−2) | 5·5748 (−2) | 5·1565 (−2) | 6·6620 (−2) |
| 4·00 | 5·7867 (−2) | 4·9771 (−2) | 4·5696 (−2) | 6·0515 (−2) |
| 4·25 | 5·2226 (−2) | 4·4213 (−2) | 4·0294 (−2) | 5·4709 (−2) |
| 4·50 | 4·6922 (−2) | 3·9088 (−2) | 3·5366 (−2) | 4·9236 (−2) |
| 4·75 | 4·1975 (−2) | 3·4403 (−2) | 3·0906 (−2) | 4·4119 (−2) |
| 5·00 | 3·7396 (−2) | 3·0151 (−2) | 2·6898 (−2) | 3·9369 (−2) |
| 5·25 | 3·3186 (−2) | 2·6320 (−2) | 2·3320 (−2) | 3·4992 (−2) |
| 5·50 | 2·9341 (−2) | 2·2888 (−2) | 2·0146 (−2) | 3·0984 (−2) |
| 5·75 | 2·5849 (−2) | 1·9833 (−2) | 1·7344 (−2) | 2·7336 (−2) |
| 6·00 | 2·2695 (−2) | 1·7127 (−2) | 1·4885 (−2) | 2·4035 (−2) |
| 6·25 | 1·9862 (−2) | 1·4743 (−2) | 1·2736 (−2) | 2·1063 (−2) |
| 6·50 | 1·7329 (−2) | 1·2653 (−2) | 1·0867 (−2) | 1·8401 (−2) |
| 6·75 | 1·5075 (−2) | 1·0828 (−2) | 9·2472 (−3) | 1·6027 (−2) |
| 7·00 | 1·3078 (−2) | 9·2407 (−3) | 7·8491 (−3) | 1·3919 (−2) |
| 7·25 | 1·1314 (−2) | 7·8658 (−3) | 6·6465 (−3) | 1·2056 (−2) |
| 7·50 | 9·7637 (−3) | 6·6791 (−3) | 5·6154 (−3) | 1·0415 (−2) |
| 7·75 | 8·4049 (−3) | 5·6582 (−3) | 4·7342 (−3) | 8·9748 (−3) |
| 8·00 | 7·2185 (−3) | 4·7826 (−3) | 3·9831 (−3) | 7·7154 (−3) |
| 8·25 | 6·1856 (−3) | 4·0340 (−3) | 3·3448 (−3) | 6·6175 (−3) |
| 8·50 | 5·2891 (−3) | 3·3957 (−3) | 2·8036 (−3) | 5·6635 (−3) |
| 8·75 | 4·5132 (−3) | 2·8529 (−3) | 2·3458 (−3) | 4·8368 (−3) |
| 9·00 | 3·8437 (−3) | 2·3925 (−3) | 1·9596 (−3) | 4·1225 (−3) |

Table 1.—*Continued.*

Two-centre hybrid integrals, in units of $Z(e^2/a_0)$. $(\alpha = \tfrac{1}{2}Z\,R/a_0$; $Z$ = effective nuclear charge, $R$ = internuclear distance (Å), $a_0 = 0.5292$ Å, $e^2/a_0 = 27.206$ ev.)

| $\alpha$ | $A_0 = (2p_a2p_b\|2p_a2p_b)$ | $A_1 = (2p_a2p_b\|3p_a3p_b)$ | $A_2 = (2p_a3p_b\|2p_a3p_b)$ | $A_3 = (2p_a3p_b\|3p_a2p_b)$ |
|---|---|---|---|---|
| 1·00 | 1·5786 (−1) | 1·3554 (−1) | 1·1966 (−1) | 1·1932 (−1) |
| 1·25 | 1·4063 (−1) | 1·2478 (−1) | 1·1143 (−1) | 1·1096 (−1) |
| 1·50 | 1·2263 (−1) | 1·1300 (−1) | 1·0217 (−1) | 1·0158 (−1) |
| 1·75 | 1·0484 (−1) | 1·0075 (−1) | 9·2275 (−2) | 9·1586 (−2) |
| 2·00 | 8·8023 (−2) | 8·8519 (−2) | 8·2125 (−2) | 8·1366 (−2) |
| 2·25 | 7·2686 (−2) | 7·6692 (−2) | 7·2066 (−2) | 7·1267 (−2) |
| 2·50 | 5·9114 (−2) | 6·5575 (−2) | 6·2385 (−2) | 6·1580 (−2) |
| 2·75 | 4·7408 (−2) | 5·5375 (−2) | 5·3309 (−2) | 5·2523 (−2) |
| 3·00 | 3·7536 (−2) | 4·6214 (−2) | 4·4994 (−2) | 4·4249 (−2) |
| 3·25 | 2·9370 (−2) | 3·8142 (−2) | 3·7532 (−2) | 3·6845 (−2) |
| 3·50 | 2·2731 (−2) | 3·1151 (−2) | 3·0960 (−2) | 3·0340 (−2) |
| 3·75 | 1·7416 (−2) | 2·5189 (−2) | 2·5270 (−2) | 2·4722 (−2) |
| 4·00 | 1·3220 (−2) | 2·0178 (−2) | 2·0420 (−2) | 1·9945 (−2) |
| 4·25 | 9·9484 (−3) | 1·6021 (−2) | 1·6346 (−2) | 1·5940 (−2) |
| 4·50 | 7·4263 (−3) | 1·2613 (−2) | 1·2967 (−2) | 1·2626 (−2) |
| 4·75 | 5·5022 (−3) | 9·8517 (−3) | 1·0200 (−2) | 9·9169 (−3) |
| 5·00 | 4·0481 (−3) | 7·6367 (−3) | 7·9587 (−3) | 7·7271 (−3) |
| 5·25 | 2·9588 (−3) | 5·8773 (−3) | 6·1628 (−3) | 5·9754 (−3) |
| 5·50 | 2·1495 (−3) | 4·4926 (−3) | 4·7378 (−3) | 4·5878 (−3) |
| 5·75 | 1·5525 (−3) | 3·4119 (−3) | 3·6174 (−3) | 3·4985 (−3) |
| 6·00 | 1·1153 (−3) | 2·5753 (−3) | 2·7440 (−3) | 2·6506 (−3) |
| 6·25 | 7·9709 (−4) | 1·9325 (−3) | 2·0687 (−3) | 1·9960 (−3) |
| 6·50 | 5·6695 (−4) | 1·4420 (−3) | 1·5504 (−3) | 1·4942 (−3) |
| 6·75 | 4·0143 (−4) | 1·0704 (−3) | 1·1555 (−3) | 1·1124 (−3) |
| 7·00 | 2·8301 (−4) | 7·9045 (−4) | 8·5656 (−4) | 8·2382 (−4) |
| 7·25 | 1·9871 (−4) | 5·8092 (−4) | 6·3177 (−4) | 6·0701 (−4) |
| 7·50 | 1·3898 (−4) | 4·2497 (−4) | 4·6371 (−4) | 4·4512 (−4) |
| 7·75 | 9·6852 (−5) | 3·0950 (−4) | 3·3879 (−4) | 3·2491 (−4) |
| 8·00 | 6·7257 (−5) | 2·2446 (−4) | 2·4643 (−4) | 2·3612 (−4) |
| 8·25 | 4·6550 (−5) | 1·6213 (−4) | 1·7849 (−4) | 1·7088 (−4) |
| 8·50 | 3·2117 (−5) | 1·1665 (−4) | 1·2876 (−4) | 1·2317 (−4) |
| 8·75 | 2·2092 (−5) | 8·3615 (−5) | 9·2529 (−5) | 8·8439 (−5) |
| 9·00 | 1·5152 (−5) | 5·9723 (−5) | 6·6245 (−5) | 6·3268 (−5) |

Table 2.

| $\alpha$ | $A_4 = (2p_a 2p_b \| 2p_a 3p_b)$ | $A_5 = (2p_a 3p_b \| 3p_a 3p_b)$ | $A_6 = (3p_a 3p_b \| 3p_a 3p_b)$ |
|---|---|---|---|
| 1·00 | 1·3570 (−1) | 1·2194 (−1) | 1·2701 (−1) |
| 1·25 | 1·2367 (−1) | 1·1451 (−1) | 1·2029 (−1) |
| 1·50 | 1·1063 (−1) | 1·0609 (−1) | 1·1260 (−1) |
| 1·75 | 9·7259 (−2) | 9·6978 (−2) | 1·0419 (−1) |
| 2·00 | 8·4107 (−2) | 8·7505 (−2) | 9·5315 (−2) |
| 2·25 | 7·1618 (−2) | 7·7963 (−2) | 8·6223 (−2) |
| 2·50 | 6·0108 (−2) | 6·8616 (−2) | 7·7149 (−2) |
| 2·75 | 4·9769 (−2) | 5·9679 (−2) | 6·8295 (−2) |
| 3·00 | 4·0690 (−2) | 5·1317 (−2) | 5·9830 (−2) |
| 3·25 | 3·2876 (−2) | 4·3646 (−2) | 5·1885 (−2) |
| 3·50 | 2·6269 (−2) | 3·6735 (−2) | 4·4556 (−2) |
| 3·75 | 2·0774 (−2) | 3·0608 (−2) | 3·7900 (−2) |
| 4·00 | 1·6270 (−2) | 2·5259 (−2) | 3·1943 (−2) |
| 4·25 | 1·2627 (−2) | 2·0655 (−2) | 2·6685 (−2) |
| 4·50 | 9·7160 (−3) | 1·6742 (−2) | 2·2103 (−2) |
| 4·75 | 7·4166 (−3) | 1·3457 (−2) | 1·8157 (−2) |
| 5·00 | 5·6188 (−3) | 1·0731 (−2) | 1·4798 (−2) |
| 5·25 | 4·2267 (−3) | 8·4916 (−3) | 1·1969 (−2) |
| 5·50 | 3·1583 (−3) | 6·6709 (−3) | 9·6107 (−3) |
| 5·75 | 2·3451 (−3) | 5·2044 (−3) | 7·6627 (−3) |
| 6·00 | 1·7309 (−3) | 4·0333 (−3) | 6·0684 (−3) |
| 6·25 | 1·2703 (−3) | 3·1060 (−3) | 4·7748 (−3) |
| 6·50 | 9·2737 (−4) | 2·3775 (−3) | 3·7336 (−3) |
| 6·75 | 6·7356 (−4) | 1·8093 (−3) | 2·9020 (−3) |
| 7·00 | 4·8687 (−4) | 1·3693 (−3) | 2·2427 (−3) |
| 7·25 | 3·5032 (−4) | 1·0308 (−3) | 1·7237 (−3) |
| 7·50 | 2·5097 (−4) | 7·7205 (−4) | 1·3177 (−3) |
| 7·75 | 1·7905 (−4) | 5·7545 (−4) | 1·0022 (−3) |
| 8·00 | 1·2723 (−4) | 4·2691 (−4) | 7·5856 (−4) |
| 8·25 | 9·0074 (−5) | 3·1530 (−4) | 5·7142 (−4) |
| 8·50 | 6·3538 (−5) | 2·3187 (−4) | 4·2850 (−4) |
| 8·75 | 4·4665 (−5) | 1·6982 (−4) | 3·1991 (−4) |
| 9·00 | 3·1294 (−5) | 1·2388 (−4) | 2·3784 (−4) |

Table 2.—*Continued.*

Two-centre exchange integrals, in units of $Z(e^2/a_0)$. $(\alpha = \frac{1}{2} Z R/a_0$; $Z =$ effective nuclear charge, $R =$ internuclear distance (Å), $a_0 = 0·5292$ Å, $e^2/a_0 = 27·206$ ev.)

## 3. Accuracy of the Calculations

The evaluation of molecular integrals is usually very complicated, and the utmost care must always be taken to avoid mistakes and computational errors.

In the present calculations all hybrid integrals were recalculated for $\alpha = 4 \cdot 00$ by means of the Barnett–Coulson method [1], and agreement between the two methods was found. It was not practical to recalculate the exchange integrals in this way, but in this case the formulae are simpler in structure and much easier to check.

Formulae and some numerical values for $L_0$ and $A_0$ did already exist in the literature [3], but were repeated here as a means of checking the methods. Complete agreement was found.

The significance of the figures given in the tables was assured by studying the ratio between successive entries in the tables. This ratio gives slowly varying functions of $\alpha$, and obvious computational errors and large rounding-off errors were easily revealed as erratic fluctuations in these functions.

## References

[1] Barnett, M. P., and Coulson, C. A., 1951, *Phil. Trans.* A, **243**, 221.
[2] Miller, J., Gerhauser, J. M., and Matsen, F. A., 1959, *Quantum Chemistry Integrals and Tables* (Austin : University of Texas Press).
[3] Preuss, H., 1956, *Integraltafeln zur Quantenchemie* (Berlin: Spinger-Verlag).

# Ground–state properties of some heterocyclics

by A. T. AMOS and G. G. HALL

Department of Mathematics, Imperial College, London S.W.7

The self-consistent bond orders for the ground states of a number of heterocyclic molecules are calculated by a steepest descents method. The parameters used are those of McWeeny and Peacock whose value of the electronegativity parameter is much smaller than has been customary. The dipole moments are deduced and found to be in as good agreement with experiment as those calculated with larger electronegativity parameters. The CC bond lengths are also calculated for acridine and found to be in excellent agreement with experiment.

## 1. Introduction

The molecular orbital theory of heterocyclic molecules, unlike the theory of conjugated hydrocarbons, has not yet become standardized. The difficulty is that the nitrogen nucleus requires different parameters from the carbon nucleus and so raises the problem of the magnitude of these parameters. This problem can be largely avoided in a homonuclear molecule since the parameters can often be removed by a transformation. The variety of values for these parameters, used by different authors, makes it very difficult to compare their results. An assessment of the situation is made even more difficult by the wide range of theoretical assumptions employed.

The prime purpose of this paper is to show that the self-consistent version of molecular orbital theory, which has proved most successful for hydrocarbons, can be applied to a variety of heterocyclics with one choice of parameter values and will give agreement with experiment for a variety of properties. To make comparisons easier, the parameter values suggested by McWeeny and Peacock [1] are adopted here. This particular choice has been made, partly because the theory used is also the same, so that the results can be accumulated, and partly because their criterion, namely comparison with the observed spectra of several molecules, seems more sensitive to changes in the parameters than those previously used. A consequence of this choice is that no adjustment of the parameters to improve the agreement with experiment is possible later.

## 2. The method of calculation

Molecular orbital theory, in the form in which it is applied to conjugated molecules (see e.g. [2]), is based on orthonormal orbitals, antisymmetrical in the molecular plane and localized around each nucleus. The effective single-electron Hamiltonian has matrix elements, relative to these orbitals, which are the sum of terms, some dependent on the electronic structure through the charge and bond order matrix $p_{rs}$ and some independent. With the approximations to the

interelectronic integrals introduced by Pariser and Parr [3], these matrix elements can be written as

$$H_{rr} = \omega_r - \tfrac{1}{2}\gamma_{rr} - \tfrac{1}{2}p_{rr}\gamma_{rr} - \sum_{s \neq r} Z_s \gamma_{rs} + \sum_s p_{ss}\gamma_{rs},$$

$$H_{rs} = \beta_{rs} - \tfrac{1}{2}p_{rs}\gamma_{rs},$$

where $\omega_r$ is the energy of an electron in a localized orbital $\chi_r$ in the standard excited state, $\beta_{rs}$ is the interaction energy between two such orbitals, $Z_s$ is here unity and

$$\gamma_{rs} = \int |\chi_r(1)|^2 \, 1/r_{12} |\chi_s(2)|^2 \, dV_{12}.$$

The coefficients which define the molecular orbitals are the eigenvectors of this $H_{rs}$ matrix and from these the matrix $p_{rs}$ can be defined. It is possible, however, to calculate the $p_{rs}$ directly without first finding the eigenvectors.

The method of calculation uses two facts. The first is that the single-electron density matrix, which is just $\tfrac{1}{2}p_{rs}$, is idempotent. The second is that the total energy is a minimum for the correct $p_{rs}$. An initial $p_{rs}$, usually based on the corresponding Hückel-type matrix for the unsubstituted hydrocarbon, is brought closer to satisfying the equations for the correct $p_{rs}$ by a steepest descent method but has then to be readjusted to restore idempotency. The calculation proceeds by iteration so as to satisfy both requirements. Equations and further details are given by McWeeny [4].

The calculation has been programmed for the University of London 'Mercury' computer so that the calculation for one molecule is completed in one operation. About ten iterations were necessary for consistency to within 0·0001 for the larger molecules and took about 25 min. For quinoline, the use of the Hückel-type naphthalene values for the initial matrix did not lead to convergence but the use of the self-consistent naphthalene values with an adjustment of the charges was sufficient to give a satisfactory initial matrix.

### 3. VALUES OF THE PARAMETERS

The values of the parameters $\gamma_{rs}$ are taken from Pariser [5] and Pariser and Parr [3] where possible and the inverse distance approximation is used for the remaining more distant nuclei. These values were assumed to be independent of whether the nuclei were carbon or nitrogen.

The $\beta_{rs}$ parameters for CC bonds are all taken to be equal. A larger value is theoretically justified for a CN bond and $\beta_{\text{CN}}$ is taken as $1·076\beta_{\text{CC}}$ [3] although the results are not very sensitive to this increase.

The most important parameter is the value of $\omega_r$ which is a measure of the electronegativity of the atom relative to that of carbon. McWeeny and Peacock [1] have investigated different values of $\omega_r$ and find that the agreement between the calculated and observed spectra of the heterobenzenes is best for

$$\omega_r = 0·35\beta.$$

If the diagonal matrix element $H_{rr}$ is expressed in the conventional Hückel form as

$$\alpha_{\text{N}} = \alpha_{\text{C}} + \beta\delta,$$

this value of $\omega_r$ corresponds approximately to

$$\delta = 0·20.$$

This value is much lower than has been used earlier. In the first Hückel-type calculations (e.g. [6, 7]) δ has been taken as large as 2 but this is now generally considered to be too large. Orgel *et al.* [8] suggest the value 1 on the ground that it leads to the correct dipole moment of pyridine. The value 0·6 has also been supported [9, 10, 11] on the same basis. This criterion is not decisive, however, for it depends on the value assigned to the dipole moment of the σ electrons. By estimating this σ contribution more accurately, Hameka and Liquori [12] find good agreement with the dipole moments of a number of heterocyclics using δ = 0·4. The use of the bond-order bond-length relation to fix δ has been proposed by Lofthus [13] and he suggests δ = 0·9–1·0. These calculations have all been of the Hückel type, though with differing conventions as to overlap integrals, and so are not exactly comparable with the self-consistent ones.

## 4. Bond orders

The bond orders for a variety of molecules, obtained by this calculation, are shown in figure 1. The parent hydrocarbons were also calculated and are included in figure 1 for comparison. It is clear that, while substitution does not produce large changes, its effect is more pronounced on the charges on and close to the nitrogen atoms.

As can be seen in figure 1 the atomic charges are more nearly uniform than those predicted in previous calculations. This is due in part to the smaller
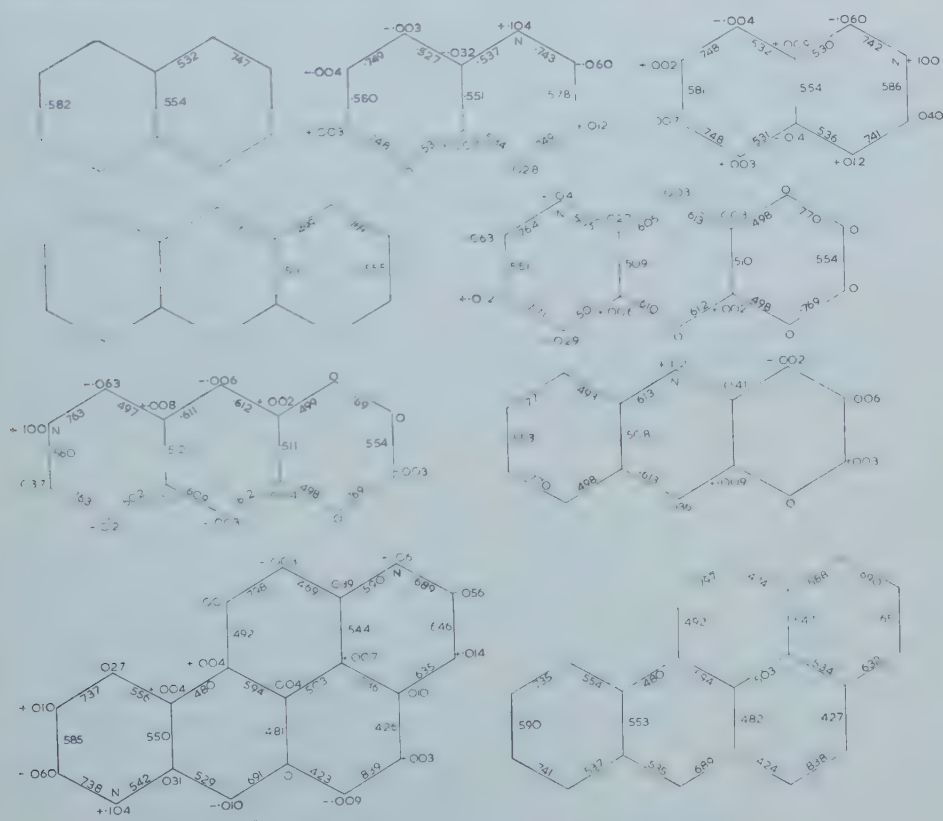


Figure 1. Calculated charges and bond orders.

value of δ and in part to the self-consistent equations which penalize any large accumulation of charge. The charge on the nitrogen atoms is always about 1·10, as it is also in the examples quoted by McWeeny, whereas other calculations, e.g. [7, 12], give larger and more varied values. The C atoms nearest to an N atom have charges of 0·96 and 0·94, the latter being assigned to the atom whose bond to the nitrogen has the larger order. The charges of the atoms in the purely carbon rings depart very little from unity and do not always give the signs of the net charge suggested by the law of alternating polarity.

Perturbation theory [14, 15, 16] suggests that the bond orders should be little changed by substitution and this is borne out in figure 1. There are small changes, however, and these seem to follow a pattern. Of the two bonds to the nitrogen the larger bond order is reduced and the smaller increased by about 0·005. The next nearest bonds all decrease in order but by amounts which vary from 0·006 to 0·002.
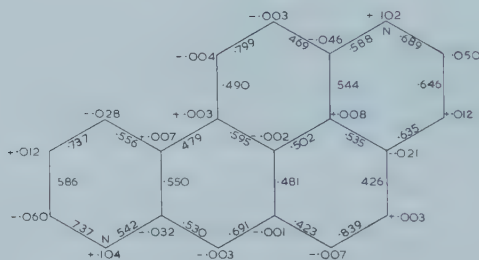


Figure 2.   Approximate charges and bond orders.

The reality of this pattern can be demonstrated more clearly by using the quinoline and iso-quinoline results to predict the results for other molecules. This is done by superimposing the differences due to substitution of the simpler molecules on to the results for the parent hydrocarbon of the larger as the position of the nitrogen dictates and if there is any overlap the results are averaged. The results obtained in this way for one molecule are shown in figure 2. The bond orders are in very good agreement with the accurate ones given in figure 1 though the charges are not quite so accurate. This procedure is useful in improving the initial matrices required for the iteration calculation.

## 5. DIPOLE MOMENTS

The contribution to the dipole moment of these molecules due to their mobile electrons is readily calculated. It must be supplemented, however, by the dipole moment due to the σ electrons. Hameka and Liquori [12] have shown that the contribution is due, very largely, to the lone pairs of the nitrogen atoms. By considering approximate analytical forms for the orbitals they estimate that the lone pair dipole moment is about 1·33$D$ greater than that of a CH bond. Such calculations are, necessarily, approximate and the results are quite sensitive to the parameters employed. For this reason it seems better to use the experimental dipole moment of one molecule to fix the σ moment and to use this value in the remaining calculations. Pyridine has been selected since its dipole moment is most accurately known [17, 18].

The dipole moments calculated in this way using the charges in figure 1 and in [1] are shown in table 1, together with the observed values and those

| | $\mu_\sigma$ | $\mu_\pi^{\parallel}$ | $\mu_\pi^{\perp}$ | $\mu$ | $\mu_{exp}$ | $\mu_{HL}$ |
|---|---|---|---|---|---|---|
| Pyridine | (1·74) | 0·41 | | (2·15) | 2·15 ± 0·05 [17, 18] | 2·20 |
| Pyrimidine | 1·74 | 0·39 | | 2·13 | 2·10 ± 0·10 [19] | 2·19 |
| Pyridazine | 3·01 | 0·78 | | 3·79 | 3·94 [20] | 3·80 |
| Quinoline | 1·74 | 0·46 | 0·05 | 2·20 | 2·16 [21] | 2·22 |
| Isoquinoline | 1·74 | 0·42 | 0·20 | 2·17 | 2·54 [21] | 2·38 |
| Benzquinoline | 1·74 | 0·49 | 0·03 | 2·23 | | |
| Benzisoquinoline | 1·74 | 0·47 | 0·31 | 2·23 | | |
| Acridine | 1·74 | 0·55 | | 2·29 | 1·95 [22] | |

Table 1. Calculated and observed dipole moments (in Debyes).

calculated by Hameka and Liquori. The agreement with experiment is within the probable error of the experimental values. The agreement with the Hameka and Liquori calculations is also good and shows that the dipole moment is not a very sensitive criterion for δ. The lone pair moment of 1·74 D is not so much larger than that of Hameka and Liquori as to contradict their calculations.

## 6. BOND LENGTHS

The theory of the relation between bond order and bond length developed by Coulson [23] and Deas [24] applies only to alternant hydrocarbons. It is based on the equality, at the equilibrium internuclear distance, of the attractive force due to the mobile electrons and the repulsive force due to the compression of the σ electrons. For alternant hydrocarbons there are no other forces but for other conjugated molecules there is the attractive force of electrostatic type due to the net charges on the atoms. This force is the product of the net charges and the force between the corresponding orbitals, i.e.

$$\nabla(\gamma_{rs}).$$

When this force is compared with the first two, for molecules of the type considered here, it is found to be only about 1 per cent of their magnitude, largely because the net charges are only 0·1 at most. Thus the alternant theory applies also to bonds whose net charges are as small as this.

| $p$ | $r$ | $r_{exp}$ (acridine II) [25] | $r_{exp}$ (acridine III) [26] |
|---|---|---|---|
| 0·493 | 1·433$_0$ | 1·429 | 1·433 |
| 0·771 | 1·361$_6$ | 1·360 | 1·366 |
| 0·553 | 1·415$_9$ | 1·428 | 1·419 |
| 0·770 | 1·362$_2$ | 1·359 | 1·366 |
| 0·498 | 1·431$_5$ | 1·434 | 1·433 |
| 0·508 | 1·429$_1$ | 1·434 | 1·436 |
| 0·613 | 1·398$_1$ | 1·398 | 1·399 |

Table 2. CC bond lengths of acridine

Since the bond orders calculated here are the self-consistent ones and not the Coulson ones the Deas relation for bond lengths should, in principle, be revised but a graph of the experimental lengths for naphthalene and anthracene follows the Deas graph fairly closely except that the high bond orders should have slightly longer lengths. This suggests that the Deas relation should still be accurate enough.

The CC bond lengths for acridine, calculated from the Deas relation, are given in table 2 along with the experimental results obtained by refined calculations on the x-ray diffraction data for two different crystalline forms of acridine. The agreement with experiment is surprisingly good. This agreement also helps to confirm that $\delta$ need not be as large as 1 to give acceptable bond lengths.

## 7. ISOMERIC ENERGY DIFFERENCES

In addition to the quantities already mentioned, these calculations also give the contribution of the mobile electrons to the total energy. This is not, unfortunately, a quantity susceptible of experimental measurement. One quantity which can be deduced from it and is capable of measurement is the energy difference between isomeric molecules. The values calculated are vertical energy differences since no allowances are made for any changes in bond length between isomers. It seems likely that these changes will be small.

From these calculations, iso-quinoline should be more stable than quinoline by $0.00322|\beta|$ or 356 cal/mole. Similarly benzisoquinoline is more stable than benzquinoline by 398 cal/mole and more stable than acridine by 685 cal/mole. There does not seem to be any experimental estimate to compare with these predictions.

## REFERENCES

[1] McWEENY, R., and PEACOCK, T. E., 1957, *Proc. phys. Soc. Lond.*, A, **70**, 41.
[2] HALL, G. G., 1959, *Rep. Prog. Phys.*, **22**, 1.
[3] PARISER, R., and PARR, R. G., 1953, *J. chem. Phys.*, **21**, 466, 767.
[4] McWEENY, R., 1956, *Proc. roy. Soc.* A, **235**, 496.
[5] PARISER, R., 1956, *J. chem. Phys.*, **24**, 250.
[6] WHELAND, G. W., and PAULING, L., 1935, *J. Amer. chem. Soc.*, **57**, 2086.
[7] COULSON, C. A., and LONGUET-HIGGINS H. C., 1947, *Trans. Faraday Soc.*, **43**, 87.
[8] ORGEL, L. E., COTTRELL, T., DICK, W., and SUTTON, L. E., 1951 *Trans. Faraday Soc.*, **47**, 113.
[9] CHALVET O., and SANDORFY, C., 1949, *C.R. Acad. Sci., Paris.*, **228**, 566.
[10] LÖWDIN, P. O., 1951, *J. chem Phys.*, **19**, 1323.
[11] DAVIES, D. W., 1955, *Trans Faraday Soc.*, **51**, 449.
[12] HAMEKA, H. F , and LIQUORI, A. M., 1958, *Mol. Phys.*, **1**, 9.
[13] LOFTHUS, A., 1959, *Mol. Phys.*, **2**, 367.
[14] COULSON, C. A., and LONGUET-HIGGINS, H. C., 1947, *Proc. roy. Soc.* A, **191**, 39; **192**, 16
[15] POPLE, J. A., 1955, *Proc. roy. Soc* A, **233**, 233.
[16] McWEENY, R., 1956, *Proc. roy. Soc.* A **237**, 355.

[17] DE MORE, B. B., WILCOX, W. S., and GOLDSTEIN, J. H., 1954, *J. chem. Phys.*, **22**, 876.
[18] JANNELLI, L., and OTSINI, P. G., 1956, *Gazz. chim. ital.*, **86**, 1104.
[19] HÜCKEL, W., and SALINGER, C. M., 1944, *Ber. dtsch. chem. Ges.*, **77**, 810.
[20] SCHNEIDER, W. C., 1948, *J. Amer. chem. Soc.*, **70**, 627.
[21] RAU, G., and NARAYANASWAMY, B. N., 1934, *Z. phys. Chem.* B, **26**, 23.
[22] BERGMANN, E., ENGEL, L., and MAYER, H., 1932, *Ber. dtsch. chem. Ges.*, **65**, 446.
[23] COULSON, C. A., 1939, *Proc. roy. Soc.* A, **169**, 413.
[24] DEAS, H. D., 1955, *Phil. Mag.*, **46**, 670.
[25] PHILLIPS, D. C., AHMED, F. R., and BARNES, W. H., 1960, *Acta cryst.*, *Camb.*, **13**, 365.
[26] PHILLIPS, D. C., 1956, *Acta cryst.*, *Camb.*, **9**, 237.

# Bond length alternation in pentalene

by P. C. DEN BOER-VEENENDAAL and D. H. W. DEN BOER
Organisch Chemisch Laboratorium, University of Utrecht

According to LCAO-MO calculations lower $\pi$-electron and total electron energy values result if the molecular symmetry group for pentalene is taken to be $C_{2h}$ instead of $D_{2h}$. Though a considerable reduction in $\pi$-electron energy is obtained, the gain in total electron energy is much smaller. Nevertheless it may be stated that in the ground state the twofold axes $C_2^x$ and $C_2^y$ are not present.

## 1. INTRODUCTION

The calculated properties of the unknown hydrocarbon pentalene are of interest because of its supposed simple molecular structure (figure 1 (*a*)). Energies, bond orders, charges and other available quantitites [1–8] have been tabulated by Coulson and Daudel [9].
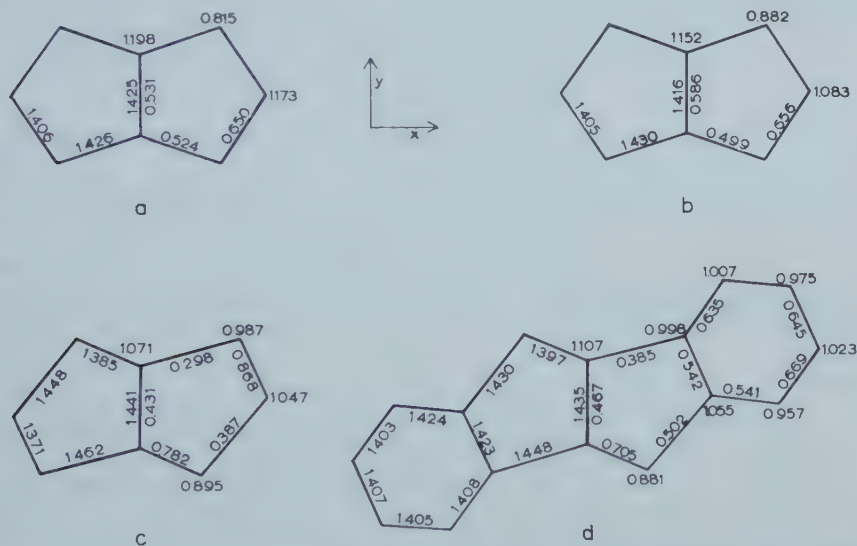


Figure 1. Bond orders, charges (right-hand side of formulae) and calculated bond lengths (left hand side) for: (*a*) pentalene [9], (*b*) symmetrical pentalene (self-consistent values), (*c*) asymmetrical pentalene (id.), (*d*) dibenzpentalene [6].

Craig and Maccoll [4] discussed the disagreement between the molecular and the orbital valence bond treatment of pentalene and in a later paper [5] classified moleculeslike pentalene as pseudoaromatics. This classification was based on symmetry considerations.

Coulson [10] quoting the work of Shida [11] showed that the lowest energy structure of the pseudoaromatic compound cyclobutadiene should be a rectangle. Here the degeneracy of the partly occupied molecular orbitals evidently leads to a structure where bond lengths alternate. The resulting rectangle, however— representing a Kékulé structure—is apparently unstable too.

Longuet-Higgins [12] stated that vibrational instability might result from the mixing of electronic states in such a way that ultimately dissociation into two molecules of acetylene occurs. A similar consideration applies to pentalene if the conjugation across the central bond is neglected.

If in pentalene this bond is omitted, cyclooctatetraene results, a well-known cyclic compound, where a sequence of single and double bonds—with out-of-plane distortion—has been found experimentally [13]. The phenomenon of alternating bond lengths—in many cases confirmed experimentally—in conjugated molecules of the chain type as well as in conjugated polyene radicals has been discussed extensively [14, 15]. The calculations given in this paper support the view that even in pentalene this tendency for alternating bond lengths persists.

So far the molecular symmetry $D_{2h}$ (figure 1 (a)) has been accepted for pentalene, but the possibility of bond length alternation is ruled out by this hypothesis, which entails the presence of two-fold axes $C_2^x$ and $C_2^y$. In view of this the symmetry of pentalene was reduced to $C_{2h}$ in the following calculations, leaving only a two-fold axis perpendicular to the plane of the molecule (figure 1 (c)).

## 2. Bond lengths and charges in the $D_{2h}$ model

It was decided to improve the $\pi$-electron energy values, bond orders and charges as obtained for symmetrical pentalene using the molecular orbital method. An iterative process was applied for the calculation of self-consistent data [16].

From the coulomb integral $\alpha_i^0$, $\alpha_i'$ was calculated using the equation

$$\alpha_i' = \alpha_i^0 + \omega(1 - q_i)\beta^0 \tag{1}$$

in which $\beta^0$ is the standard resonance integral, $q_i$ the charges and $\omega$ a proportionality coefficient, here taken to be unity [17, 18].

Similarly the resonance integral was corrected [14] using:

$$\beta = \beta^0 \exp\left(\frac{-1\cdot40 + l}{0\cdot3106}\right). \tag{2}$$

Bond lengths $l$ resulted from the bond orders with the aid of the expression (3):

$$l = 1\cdot51 - 0\cdot16p \tag{3}$$

which gives a slightly better agreement with the experimental $l$–$p$ curve than the one given by Longuet-Higgins and Salem [14].

The solution of a new set of secular equations, in which the corrected coulomb and resonance integrals are inserted, leads to new bond orders and charges. This process can be repeated indefinitely but in this case rapid convergence appeared. The values obtained after four cycles were considered to be final and are given in figure 1 (b). Further iterations lead only to small changes of bond lengths (less than 0·005 Å) and charges (less than 0·01 e).

## 3. Bond lengths and charges in the $C_{2h}$ model

In this case the calculations leading to improved data for $\pi$-electron energies and molecular orbital coefficients have to be performed in two steps. The reason for this is that before the iterative process outlined above can be applied, it has to be decided at what degree of skewness self-consistency can be expected. A parameter $k$ for the skewness was introduced by assigning alternating values $\beta$ and $k\beta$ to the resonance integrals in pentalene round the perimeter of the molecular structure (figure 2). The range of $k$ values was taken between 1·0 and 1·4.
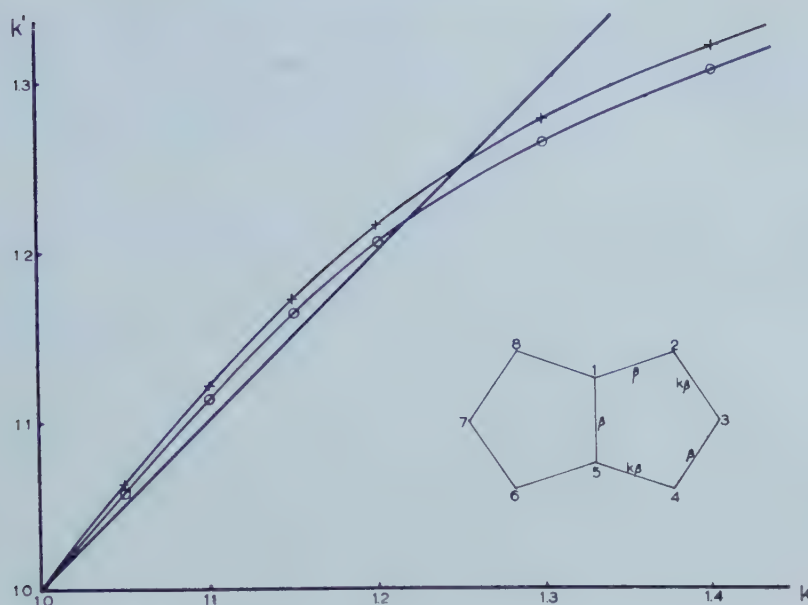
Figure 2. Curved lines show the relation between the introduced parameter $k$ and $k'=\beta_{ij}/\beta_{kl}$; $(+ \ + \ + \ \beta_{23}/\beta_{34};$ ○ ○ ○ $\beta_{45}/\beta_{12})$. The straight line would result in case of self-consistency.

Using a specific value of $k$, the usual Hückel-type equations were written down and solved. The solution leads to bond orders, and hence from (3) to bond lengths. These bond lengths now provide new resonance integrals according to (2) for two bonds now differing by the loss of symmetry. The new ratio $k'$ will not in general be identical with the starting value $k$. The relation between a series of $k$ values and the calculated corresponding $k'$ values is shown in figure 2 from which it can be seen that when $k$ is near to 1·2 self-consistency for the skew structure is to be expected. The exact point of intersection is not very important because the variation of one parameter can lead only to a rough approximation. For this reason the point $k=1·2$ was taken as the starting point for the iterative process outlined in the above section. The improvement of bond orders and charges was obtained in a convergent series; the final values were taken as given in figure 1 $(c)$.

From a comparison of figure 1 $(b)$ and 1 $(c)$ it appears that in the asymmetrical structure the charges are more nearly equal to unity. Such a charge distribution is evidently more favourable from electrostatic considerations. However, the lowering of the energy found can by no means be attributed to this simple effect only.

An analogous skew pentalene skeleton is found in ' trans ' dibenzpentalene where the two six-membered rings bring down the symmetry to $C_{2h}$ automatically. In figure 1 $(d)$ the charges and bond orders as obtained by Pullman *et al.* [6] are given as well as the calculated bond lengths.

### 4. π-ELECTRON ENERGIES

In the ground state the four lowest molecular orbitals are all doubly occupied (figure 3). The total π-electron energy for each structure can be obtained by the usual simple addition of molecular orbital energies and is given by:

$$E = \sum q_i \alpha_i + 2 \sum_{i<j} p_{ij} \beta_{ij}. \tag{4}$$

This results in $(8\alpha^0 + 10\cdot094\beta^0)$ for the $C_{2h}$ model and in $(8\alpha^0 + 9\cdot772\beta^0)$ for the symmetrical one.

$b_{3g}$ ———— $-1.912$　　　　　$b_g$ ———— $-1.864$
$b_{1u}$ ———— $-1.724$　　　　　$a_u$ ———— $-1.750$

$b_{3g}$ ———— $-1.385$　　　　　$b_g$ ———— $-1.395$

$a_u$ ════ $-0.041$

$a_{1u}$ ———— $+0.137$
$b_{1u}$ —⊖—⊖— $+0.359$

$a_u$ —⊖—⊖— $+0.485$

$b_{3g}$ —⊖—⊖— $+0.945$　　　　$b_g$ —⊖—⊖— $+0.985$

$b_{2g}$ —⊖—⊖— $+1.407$　　　　$b_g$ —⊖—⊖— $+1.393$

$b_{1u}$ —⊖—⊖— $+2.175$　　　　$a_u$ —⊖—⊖— $+2.185$

a　　　　　　　　　　　　　　b
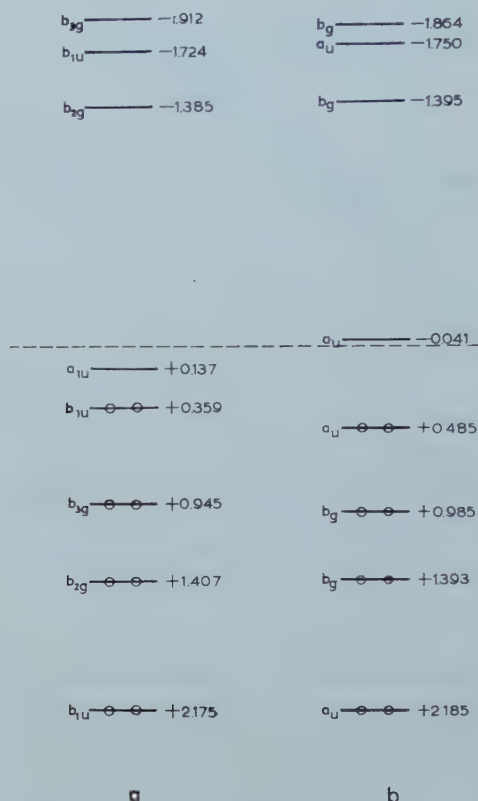
Figure 3.　Molecular orbital energies in units $\beta^0$ and symmetries for symmetrical pentalene (a) and asymmetrical pentalene (b).

In fact this energy is not defined very well, because the self-consistent $\alpha$'s are determined by the empirical expression (1). In other words, the operator used to obtain this energy cannot be given in simple terms.

A better defined energy value $E'$ results if use is made of equation (5):

$$E' = \sum_i q_i \alpha_i^0 + 2 \sum_{i<j} p_{ij} \beta_{ij}. \tag{5}$$

This is the sum of the one-electron energies for electrons moving in the field of equally charged positive carbon ions. Preference was given to the energy values obtained by the use of expression (4) because then allowance is made for the uneven charge distribution in the molecule.

It can be stated that the minimum $\pi$-electron energy belongs to an asymmetrically distorted molecule to be described as a structure somewhere between one of the Kékulé structures and a conventional delocalized model.

## 5. TOTAL ELECTRON ENERGY

A conclusion on the stability of a structure, however, cannot be based on $\pi$-electron calculations only. In fact some allowance for the effect of $\sigma$-electrons has been made already in the iterative process used, through equation (3) which

gives zero bond strain. It is obvious that in a comparison of the two structures the total electron energy has to be considered. The stabilization energy which may favour the deformation of pentalene can be estimated using equation (6) given by Longuet-Higgins and Salem [14]. The total energy $v$ of a bond in equilibrium is given by

$$v = -2aP'\beta + \text{const} \qquad (6)$$

where $P' = -(0{\cdot}16)^{-1}$ as is found from equation (3) by differentiating with respect to length. The value $0{\cdot}3106$ Å is taken for $a$ as has been done before (2).

A summation over all bonds leads to the desired energy difference between the symmetrical (s) and asymmetrical (a) structure:

$$V_{(s)} - V_{(a)} = -2aP' \sum_{i<j} [\beta_{ij(s)} - \beta_{ij(a)}] + \left(\sum_i q_i \alpha_i\right)_{(s)} - \left(\sum_i q_i \alpha_i\right)_{(a)} \qquad (7)$$

from which a deformation energy of $-0{\cdot}14\beta^0$—several kcal/mole—results. This figure—if significant—is lower than the difference in $\pi$-electron energies found. It illustrates clearly the significance of the compressional energy which counteracts strongly a distortion favoured by the $\pi$-electrons. It should be emphasized that the value given may be much in error because it is obtained from the very small differences in the corresponding $\beta$'s for the two structures.

## 6. Spectrum

Brown [3] concluded from his calculations on the probable spectrum of pentalene that the compound should absorb in the visible. Using group-theoretical considerations similar allowed transitions are found for the distorted structure. As could be anticipated a minor change in the direction of polarization of the absorbed light appears.

Some interesting conclusions may be drawn from a comparison of the separate orbital energies (figure 3). The lowest three are only very slightly changed by the deformation, whereas the energy of the top occupied (i.e. the fourth) orbital is lowered appreciably. As the full symmetry is broken, the fourth and fifth levels, which are originally $b_{1u}$ and $a_{1u}$, both become $a_u$ and so are able to interact. This can be seen from the lowering by $0{\cdot}12\beta^0$ of the fourth and the rising by $0{\cdot}18\beta^0$ of the fifth level. It is as if the allowed interaction provides additional stabilization.

The lowest electronic transition—not an allowed one—is calculated to be $0{\cdot}11\beta^0$ in the symmetrical and $0{\cdot}52\beta^0$ in the unsymmetrical case. This is a large change, representing a huge shift to the blue. Reference should be made here to the rather general principle that in passing from symmetrical structures (with equal bond lengths) to unsymmetrical ones (alternating bond lengths) the difference between the top occupied and the lowest unoccupied energy level is much increased [19].

A similar situation does not appear in the ground state of the anions $C_8H_6$, where two $\pi$-electrons have to be placed in the fifth molecular orbital. A simple calculation makes clear that here the symmetrical molecule possesses the lowest energy.

## 7. Discussion

In this paper it is shown that even in a small molecule, such as pentalene, the effect of bond alternation has to be considered. Consequently the concept

of pseudoaromaticity [5] in its original form does not apply to the lowest energy state of this hydrocarbon.

Alternating bond lengths in the rectangular cyclobutadiene model as well as in pentalene, if it is treated as slightly perturbed cyclooctatetraene, may be related to the degeneracy of the highest occupied $\pi$-electron levels. This effect has been called a pseudo Jahn–Teller effect [10].

In pentalene, however, using the LCAO–MO method no such degeneracy is found. Nevertheless the possible occurrence of a less symmetrical configuration could be made plausible from simple energy calculations. In contrast to the view that an asymmetrical distortion of the structure may lead to dissociation one has to consider the, perhaps only metastable, energy minima of the skew structures.

REFERENCES

[1] COULSON, C. A., and RUSHBROOKE, G. S., 1940, *Proc. Camb. phil. Soc.*, **36**, 193.
[2] SYRKIN, Y. K., and DYATKINA, M., 1946, *Acta phys.-chim. URSS*, **21**, 641.
[3] BROWN, R. D., 1949, *Trans. Faraday Soc.*, **45**, 296; 1950, *Ibid.*, **46**, 146.
[4] CRAIG, D. P., and MACCOLL, A., 1949, *J. chem. Soc.*, p. 964.
[5] CRAIG, D. P., 1951, *J. chem. Soc.*, p. 3175.
[6] PULLMAN, B., PULLMAN, A., BERGMANN, E. A., BERTHIER, G., FISCHER, E., HIRSHBERG, Y., and PONTIS, J., 1952, *J. Chim. phys.*, **49**, 24.
[7] ESTELLES, J., and FERNÁNDEZ ALONZO, J. I., 1953, *Chem. Abstr.*, **47**, 10291.
[8] BERGMANN, E., 1959, *Non-benzenoid Aromatic Compounds* (New York: Interscience Publishers), p. 142.
[9] COULSON, C. A., and DAUDEL, R., 1955, *Dictionary of Values of Molecular Constants, Wave Mechanical Methods*.
[10] COULSON, C. A., 1958, Chemical Society Special Publication, No. 12, p. 85.
[11] SHIDA, S., 1954, *Bull. chem. Soc. Japan*, p. 27.
[12] LONGUET-HIGGINS, H. C., 1959, *Theoretical Organic Chemistry*; *Kékulé Symposium* (London: Butterworth), p. 9.
[13] KARLE, I. L., 1952, *J. chem. Phys.*, **20**, 65.
[14] LONGUET-HIGGINS, H. C., and SALEM, L., 1959, *Proc. roy. Soc.* A, **251**, 172; 1960, *Ibid.*, **255**, 435.
[15] OOSHIKA, Y., 1957, *J. phys. Soc. Japan*, **12**, 1238.
[16] DAUDEL, R., LEFEBVRE, R., and MOSER, C., 1959, *Quantum Chemistry* (New York: Interscience Publishers), p. 78.
[17] MULLER, N., PICKETT, L. W., and MULLIKEN, R. S., 1954, *J. Amer. chem. Soc.*, **76**, 4770.
[18] WHELAND, G. W., and MANN, D. E., 1949, *J. chem. Phys.*, **17**, 264.
[19] PLATT, J. R., 1956, *J. chem. Phys.*, **25**, 80.

# The influence of molecular shape on solvent shifts in the proton magnetic resonance spectra of polar solutes

by P. DIEHL† and R. FREEMAN

National Physical Laboratory, Teddington, Middlesex

The variation of the position of high resolution proton magnetic resonance lines of a polar solute with dielectric constant of the solvent may be calculated on the assumption that the dipole polarizes the surrounding medium, setting up an electrostatic 'reaction field' which alters the distribution of the electrons responsible for magnetic shielding. The theory predicts that the shape of the solute molecule should be important in determining the magnitude of this reaction field. The magnetic shielding values measured in a range of solutions of acetonitrile, representing a rod-like molecule, and of paraldehyde, a disc-like molecule, are shown to support the 'shape theory' rather than the simpler treatment which assumes that all solutes are spheres. Evidence is obtained that paraldehyde is essentially only one of the many possible stereoisomers, the 'chair' form with all the methyl groups in equatorial positions.

## 1. Introduction

Of the organic substances which are of interest to the nuclear magnetic resonance spectroscopist, the majority are solids at room temperature and must therefore be studied in solution when high resolution spectra are required. It is therefore important to understand exactly how an environment of solvent molecules affects the nuclear resonance spectrum of the solute, especially where measurements made in one solvent are to be compared with data obtained in another.

Recently Buckingham [1] has discussed the several contributions to proton screening constants arising from interactions with a solvent, in terms of simple theoretical models, and in particular has proposed the 'reaction field' theory to explain the chemical shifts observed when the solute is polar. This is an adaptation of the theoretical model [2] used to explain the dipole moment measurements on solutions of polar solute molecules, and success in accounting for the observed nuclear shielding effects would tend to justify the validity of the original model and thus lend some support to the theory of dipole moments in solution.

The aim of the present investigation is to determine the influence of the shape of the solute molecule on the magnitude of the reaction field and the consequent shielding effects.

† Present address: Physikalisches Institut der Universität Basel, Klingelbergstrasse 82, Basel, Switzerland.

## 2. The reaction field theory

In his paper on " Chemical shifts in the nuclear magnetic resonance spectra of molecules containing polar groups ", Buckingham [3] has developed a theory of polar solvent effects using the Onsager model. A dissolved polar molecule polarizes the surrounding medium giving rise to an electric field, the reaction field $E$, at the solute. The component of this field acting along the axis of the X–H bonds tends to move the electrons along the bond and thus shifts the nuclear resonance line of the proton. An approximate calculation of this contribution to the shielding leads to the equation,

$$\sigma_E = -2 \times 10^{-12} E \cos \theta - 10^{-18} E^2 \tag{1}$$

where $E \cos \theta$ is the component of $E$ in the bond direction and

$$E = \frac{2(\epsilon-1)(n^2-1)}{3(2\epsilon+n^2)} \frac{\mu}{\alpha} \tag{2}$$

where $\epsilon$ is the dielectric constant of the medium, $n$ the refractive index of the solute as a liquid, $\mu$ the dipole moment of the solute in the gas phase and $\alpha$ the polarizability of the solute.

For this simple theory of the reaction field, the solute molecule is represented as a polarizable dipole at the centre of a spherical cavity in the solvent. As measurements of dipole moments in solution have shown, this theory is an oversimplification, and only a more elaborate model is likely to give a quantitative result. More complex models for the reaction field calculation have been developed by Scholte [4] and Dekker [5].

The first author gives the reaction field of a non-polarizable, evenly distributed dipole in a non-spherical cavity; the second gives the reaction field of a polarizable, eccentrically-placed dipole in a spherical cavity. In this paper a non-spherical cavity will be considered and the calculation extended to a polarizable dipole.

The reaction field in a non-spherical cavity with a non-polarizable dipole is given by

$$E' = 3 \frac{m}{abc} \frac{\xi_a(1-\xi_a)(\epsilon-1)}{\epsilon+(1-\epsilon)\xi_a} \tag{3}$$

where

$$\xi_a = \tfrac{1}{2}abc \int_0^\infty \frac{d\lambda}{(a^2+\lambda)^{3/2}(b^2+\lambda)^{1/2}(c^2+\lambda)^{1/2}} \tag{4}$$

and $a$, $b$, $c$ are the axes of the cavity ellipsoid. The reaction field itself polarizes the dipole and so $m$, which represents the total dipole moment, must be put equal to $\mu + \alpha_1 E'$, where $\alpha_1$ is the polarizability along the dipole axis. Thus

$$E' = \frac{\mu}{abc} \frac{3\xi_a(1-\xi_a)(\epsilon-1)}{\left[\epsilon+\xi_a(1-\epsilon)-\dfrac{3\alpha_1}{abc}\xi_a(1-\xi_a)(\epsilon-1)\right]}. \tag{5}$$

Now the polarizability along the dipole axis [4] is given by

$$\alpha_1 = \frac{n^2-1}{3[1+(n^2-1)\xi_a]} abc. \tag{6}$$

Substitution of (6) in (5) and simplification gives

$$E' = \frac{3\mu}{abc} \frac{\xi_a(1-\xi_a)(\epsilon-1)(1+(n^2-1)\xi_a)}{\epsilon-\epsilon\xi_a+n^2\xi_a}. \tag{7}$$

This may be rewritten in the form

$$E' = \frac{\mu}{abc} 3\xi_a [1 + (n^2 - 1)\xi_a] \frac{\epsilon-1}{\epsilon+\dfrac{n^2\xi_a}{1-\xi_a}}. \tag{8}$$

For a molecule which is spherical, $abc = r^3$ and $\xi_a = \frac{1}{3}$ and equation (8) degenerates to equation (2) which may be written

$$E = \frac{\mu}{r^3} \frac{n^2 + 2}{3} \frac{\epsilon - 1}{\epsilon + \frac{1}{2}n^2} \tag{9}$$

since

$$\alpha = \frac{n^2 - 1}{n^2 + 2} r^3.$$

These expressions may be used to calculate the reaction field for either a spherical or spheroidal solute if the refractive index, dipole moment and geometry are known.

## 3. EXPERIMENTAL

In order to verify the predictions of the theory the chemical shift of a suitable polar solute must be measured in a series of solvents covering a range of dielectric constant, and at a concentration low enough to approximate infinite dilution. In the present investigation a molecule has been chosen which contains two groups of protons differently oriented with respect to the reaction field. The chemical shift between these two groups may then be related to the dielectric constant of the solvent without involving the sometimes uncertain bulk susceptibility correction, while solvent interactions of the van der Waals type would be expected to influence both groups of protons about equally, so that the reaction field effect may be separated out.

To illustrate the influence of molecular shape, two cases have been considered, a prolate and an oblate spheroid, referred to for the sake of simplicity as the rod and the disc. The measurements of Buckingham *et al.* [1] on solutions of acetonitrile provide an excellent example of a rod-like solute with the dipole along the axis of the rod and for which the approximation of a uniform reaction field seems reasonable because of the small size of the molecule.

Paraldehyde has been chosen as an example of a disc-like solute. It is known from dielectric measurements on this molecule that the dipole is normal to the plane of the disc [6]. Measurements of the dipole moment of paraldehyde in solution give anomalously high values and this has been ascribed to its disc-like shape [7]. The main polar bonds are fairly evenly spread over the molecule so that to a good approximation the reaction field may be regarded as uniform. The nuclear magnetic resonance measurements reported below indicate that the two groups of protons are differently affected by the reaction field, which suggests that the molecule is rather rigid and the two groups held at different orientations with respect to the dipole axis. The structure of the molecule is considered in more detail in § 4.

The reaction field effect is small enough to be masked by strong solvent interactions such as the anomalous shielding effects of aromatic ring currents or the formation of intermolecular hydrogen bonds. For this reason all aromatic solvents and all solvents which would be expected to associate through hydrogen bonding, have been intentionally excluded from the investigation.

The solutions were made up by volume from British Drug Houses laboratory reagent grade paraldehyde to be approximately 3 mole per cent, which is a good approximation to infinite dilution for the present purpose. Spectra were recorded at about 24°C on a Varian high resolution spectrometer operating at 60 Mc/s. The centre of each multiplet pattern arising from the solute was measured with respect to an external benzene reference by the modulation sideband method, the audio-frequency being measured by a frequency counter.

Table 1 gives the list of solvents used and their dielectric constants together with the measured line positions relative to benzene and corrected for bulk diamagnetic susceptibility. The susceptibility data were taken from the *International Critical Tables* or estimated from Pascal's constants. The $CH_3$–CH frequency differences, which do not involve the magnetic susceptibility correction, are probably accurate to better than $\pm 0.5$ c.p.s.

| Number | Solvent | Dielectric constant[a] | Chemical shift in c.p.s.[d] | | |
|--------|---------|------------------------|------|--------|------------|
|        |         |                        | CH   | $CH_3$ | Difference |
| 1  | n–Hexane            | 1·89    | 113·1      | 330·3 | 217·2 |
| 2  | Cyclohexane         | 2·02    | 113·5      | 330·3 | 216·8 |
| 3  | Carbon tetrachloride | 2·24   | 103·6      | 319·2 | 215·6 |
| 4  | Triethylamine       | 2·42    | 111·0[c]   | 330·0 | 219·0 |
| 5  | Carbon disulphide   | 2·64    | 97·5       | 314·1 | 216·6 |
| 6  | Ether               | 4·34    | 108·7      | 330·4 | 221·7 |
| 7  | Chloroform          | 4·81    | 96·2       | 315·5 | 219·3 |
| 8  | Ethyl acetate       | 6·02    | 104·2      | 328·5 | 224·3 |
| 9  | Methyl acetate      | 6·68    | 105·5      | 331·3 | 225·8 |
| 10 | Methyl formate      | 8·5     | 104·4      | 329·9 | 225·5 |
| 11 | Bromocyclopentane   | 9·4[b]  | 106·2[c]   | 328·9 | 222·7 |
| 12 | Paraldehyde         | 13·9    | 102·1      | 328·2 | 226·1 |
| 13 | Cyclohexanone       | 18·3    | 105·7      | 333·6 | 227·9 |
| 14 | Acetone             | 20·7    | 102·5      | 331·1 | 228·6 |
| 15 | Acetaldehyde        | 21·1    | 104·5      | 332·3 | 227·8 |
| 16 | Acetonitrile        | 37·5    | 90·1[c]    | 316·3 | 226·2 |

(a) U.S. National Bureau of Standards Table of dielectric constants, U.S. Government Printing office, Washington 25, D.C. (1951).

(b) Measured by Mr. E. Rushton, Standards Division, National Physical Laboratory.

(c) Magnetic susceptibility estimated from Pascal's constants.

(d) Measured with respect to an external benzene reference and corrected for bulk susceptibility.

Table 1.

## 4. The structure of paraldehyde

Paraldehyde is known to be a trimer of acetaldehyde [8] and has been shown to have the form of a puckered six-membered ring of alternate carbon and oxygen atoms with tetrahedral bond angles [9]. This means that several stereo-isomers are possible as in the somewhat analogous cyclohexane derivatives. Unfortunately the evidence in the literature about the stereoisomerism of this substance is not altogether consistent. The vapour has been studied by electron diffraction by Carpenter and Brockway [9] who were able to show that the molecule almost certainly has the structure shown in figure 1 (D). However the structure (A) could not be entirely excluded owing to the similarity of the theoretical intensity curves for these two configurations. The experimental technique of these authors appears to have been more refined than that of Ackermann and Mayer [10], whose electron diffraction measurements on paraldehyde, though not in conflict, were much less conclusive. More recently Aoki [11] has remeasured the diffraction pattern but has been unable to fit experimental and theoretical intensity curves on the assumption that only one isomer is present.

The derivative of paraldehyde which has the three methyl groups fully chlorinated may be prepared in two stereoisomeric forms, α-parachloral (m.p. 116°c) and β-parachloral (m.p. 152°c). Using dipole moment measurements, infra-red spectroscopy and high-resolution nuclear magnetic resonance, Novak and Whalley [12] have shown convincingly that the α-isomer corresponds to structure (A) and the β-isomer to structure (D). Moreover the infra-red spectrum of β-parachloral was found to contain bands analogous to those observed by the same authors in the paraldehyde spectrum, suggesting that paraldehyde also has the structure (D).

The evidence quoted above does not exclude the possibility that more than one isomer of paraldehyde exists, but suggests that if only one form is present then it is almost certainly the one illustrated in figure 1 (D).
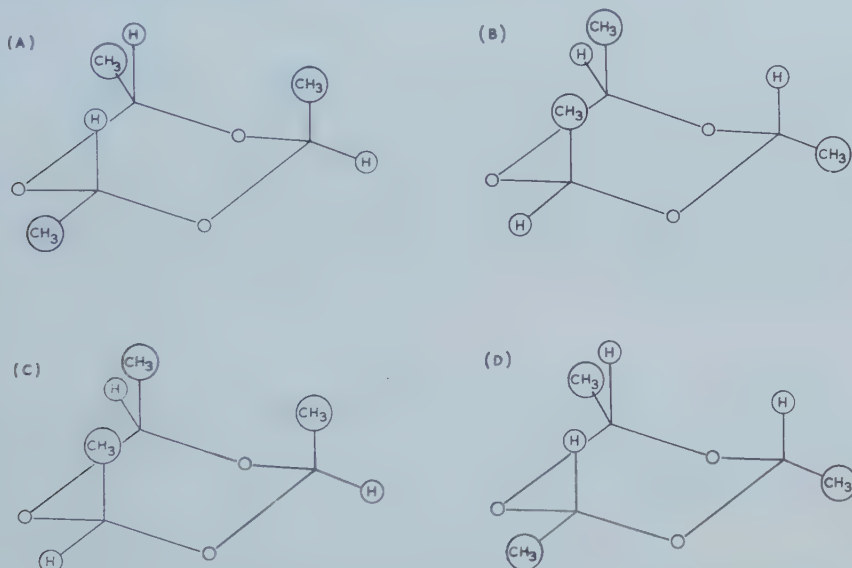


Figure 1.   The possible stereoisomers of the 'chair' form of paraldehyde.

Certain experimental observations of the high resolution proton magnetic resonance spectrum throw some new light on this problem. There is a strong doublet resonance assigned to the $CH_3$ groups $(J = 5.25 \pm 0.1$ c.p.s.) and a weaker quadruplet from the CH groups, with no other chemically shifted lines detectable either in the pure liquid or the several solutions studied. When paraldehyde is mixed with acetaldehyde, the spectra of the two components are quite distinct, so there is no chemical exchange between the two species, which suggests that the paraldehyde ring is quite stable at room temperature, as indeed Bell *et al.* [13] have found experimentally.

If two or more isomers were present, this would involve either the superposition of the spectrum of each isomer or rapid exchange between isomers, and in the latter case the $J$ multiplets would not be observed. Therefore the nuclear resonance evidence is that paraldehyde is essentially a single stereoisomer; if any other forms are present the concentrations are very low, since the practical limit of detection of weak signals is certainly less than 2 mole per cent. The essential point is that the solvent effect measurements reported in §3 have been made on just one stereoisomer.

The next step is to decide which isomer this is. For the whole of this class of isomerism it is known that the 'chair' form is more stable than the 'boat' configuration. Two molecules which have structures very similar to paraldehyde, namely sym-trioxane and trithioformaldehyde have been shown to exist in the chair form by x-ray diffraction [14, 15] and infra-red measurements [16]. Therefore only the four 'chair' isomers of paraldehyde have been considered. The methyl groups may be permuted between axial and equatorial positions as shown in figure 1. The two unsymmetrical structures (A) and (B) may be rejected on the grounds that they would give rise to an $A_2B$ type spectrum for the proton resonance of both CH and $CH_3$. An accidental degeneracy to an $A_3$ spectrum would seem unlikely, and would certainly be lifted by the solvent effects. Structure (C) must be excluded for reasons of steric repulsion, a point which may be readily appreciated if a suitable molecular model is constructed. This leaves only isomer (D) where all three methyl groups are equatorial.

This model has been used to calculate the average component of the reaction field along the bonds in the CH and $CH_3$ groups, assuming free rotation of the methyl groups but an otherwise rigid molecule. The CH groups have almost the full reaction field along the bond, whereas the average projected value for the $CH_3$ groups is very small, about one-ninth of the total and in the opposite sense. The experimental results are a strong confirmation of this model, since the CH resonance is strongly affected by the reaction field, while the $CH_3$ lines are only slightly shifted, if at all.

## 5. DISCUSSION

The expression (8) for the reaction field component along the carbon–hydrogen bond reduces to

$$E' \cos \theta = 0.78 \frac{\mu}{abc} \cos \theta \; \frac{\epsilon - 1}{\epsilon + 0.51} \quad \text{for acetonitrile} \tag{10}$$

and

$$E' \cos \theta = 2.8 \frac{\mu}{abc} \cos \theta \; \frac{\epsilon - 1}{\epsilon + 2.86} \quad \text{for paraldehyde.} \tag{11}$$

The chemical shifts should therefore vary linearly with $(\epsilon - 1)/(\epsilon + \beta)$ for the solvent where $\beta = 0.51$ for acetonitrile and 2.86 for paraldehyde. Figure 2 shows the chemical shift measurements on paraldehyde. The graph of the frequency difference between the CH and the $CH_3$ resonances gives a good fit to a straight line as predicted, but the graphs (A) and (B) in figure 2 can only be regarded as fitting a linear relation if certain solvents, carbon tetrachloride, carbon disulphide, chloroform and acetonitrile, are regarded as exceptions. In these solvents the lines appear at a magnetic field which seems too low by about 20 parts per hundred million. In a similar way, the measurements of Buckingham et al. [1] on solutions of methane in various solvents gave shielding value anomalies of about the same magnitude in a series of solvents which included those mentioned above. The effect is not understood but it seems to influence both groups of protons almost equally for it is not apparent in figure 2 (C).

The chemical shift measurements reported by Buckingham et al. [1] for acetonitrile in a range of solvents have been used here to provide a comparison with paraldehyde and thus illustrate the influence of molecular shape. These

authors used $\beta = 1\cdot25$ when plotting the results, and found a reasonably good fit to a straight line. The fit is however equally good with $\beta = 0\cdot51$ (equation (10)) except that the slope is altered (it is shown below that the precise value of the theoretical slope is not very meaningful).
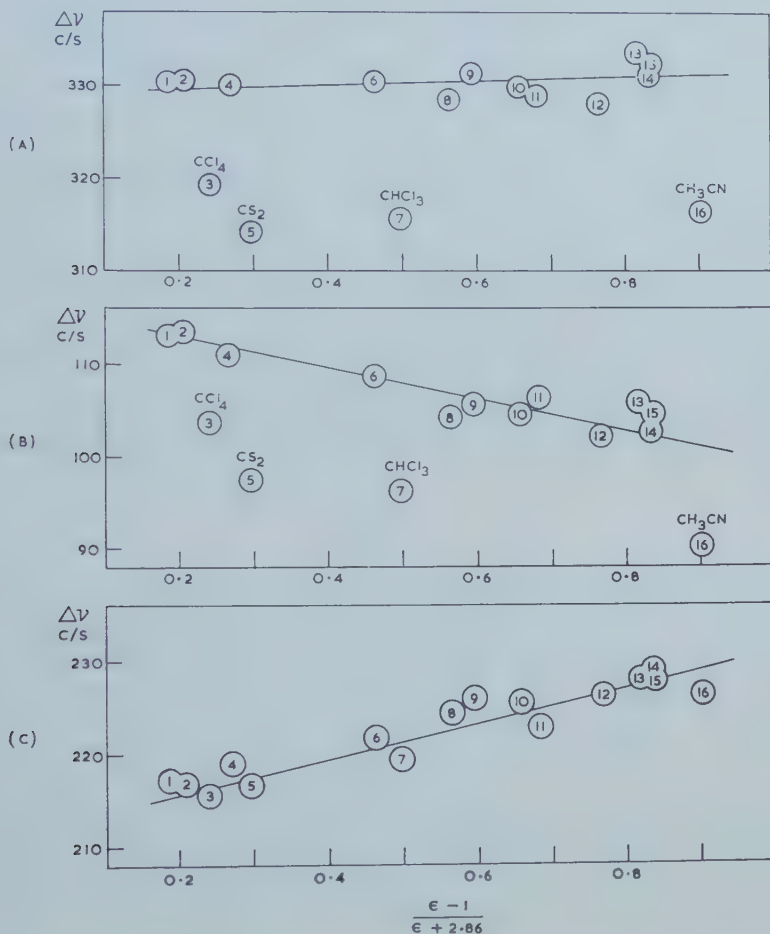


Figure 2. The chemical shift (in c.p.s.) of the proton magnetic resonance lines of paraldehyde in various solvents plotted against $(\epsilon-1)/(\epsilon+2\cdot86)$ for the solvent. (A) CH₃ groups. (B) CH groups. (C) the frequency difference between CH₃ and CH groups. Solvents are numbered as in table 1.

Apart from the shape function $\xi_a$, several factors contribute to the difference in reaction field between acetonitrile and paraldehyde, the refractive index of the solute as a liquid, the dipole moment of the vapour and the molecular dimensions. These physical constants of the two molecules have been tabulated by Buckingham and Le Fèvre [17], together with values of $\xi_a$ evaluated by the method of Ross and Sack [18]. The interplay of these various factors is most easily appreciated by means of table 2.

| Data | Acetonitrile | Paraldehyde | |
|---|---|---|---|
| | | CH groups | CH$_3$ groups |
| $n_D{}^2$ at 25°c | 1·800 | 1·989 | |
| Dipole moment $\mu$ | 3·96 D | 1·44 D | |
| $a$ | 2·98 Å | 1·90 Å | |
| $b$ | 1·90 Å | 4·75 Å | |
| $c$ | 1·90 Å | 4·75 Å | |
| $\xi_a$ | 0·22 | 0·59 | |
| $\cos \theta$ (mean) | $+\frac{1}{3}$ | $+1$ | $-\frac{1}{9}$ |
| $\dfrac{\mu \cos \theta}{abc}$ | $+1\cdot23 \times 10^5$ | $+3\cdot36 \times 10^4$ | $-3\cdot73 \times 10^3$ |
| $\Delta \left\{ \dfrac{\epsilon-1}{\epsilon+\beta} \right\}$ | 0·527 | 0·628 | 0·628 |
| $\Delta E' \cos \theta$ | $+5\cdot02 \times 10^4$ | $+5\cdot93 \times 10^4$ | $-6\cdot59 \times 10^3$ |
| $\Delta \sigma$ (observed) | $-17 \times 10^{-8}$ | $-18 \times 10^{-6}$ | $+2 \times 10^{-6}$ |
| $x$ (shape theory) | 3·4 | 3·0 | |
| Simple spherical approximation | | | |
| $\Delta E \cos \theta$ | $+8\cdot73 \times 10^4$ | $+2\cdot55 \times 10^4$ | $-2\cdot83 \times 10^3$ |
| $x$ (sphere) | 1·9 | 7·1 | |

Table 2.

The constant of proportionality between the reaction field component along a bond and the consequent chemical shift $\sigma_E$ has been shown [3] to be determined by $\lambda/R^2$, where $\lambda$ is an appropriate effective charge and $R$ is a distance which is typical of a CH bond. Reasonable approximate values of $\lambda$ and $R$ would be $10^{-10}$ e.s.u. and 1 Å, but it will be seen that an accurate estimate of $\lambda/R^2$ is not possible. If one puts

$$\sigma_E = -x\, 10^{-12} E' \cos \theta, \qquad (12)$$

then $x$ becomes a parameter of order of magnitude unity, to be determined from the experimental results. It would seem reasonable to expect $x$ to be the same for CH bonds in different molecules. The test of the 'shape theory' will be to account for the observed chemical shifts of acetonitrile and paraldehyde with a unique value of $x$.

The parameter $x$ may be evaluated from the expression

$$\Delta \sigma_E = -x\, 10^{-12} \frac{\mu}{abc} \cos \theta\, 3\xi_a [1+(n^2-1)\xi_a]\, \Delta \left( \frac{\epsilon-1}{\epsilon+\beta} \right) \qquad (13)$$

where $\Delta$ signifies the change in a quantity when the solvent is changed from cyclohexane to acetone, thus

$$\frac{6 \times 10^7 \Delta \sigma_E}{\Delta \left\{ \dfrac{\epsilon-1}{\epsilon+\beta} \right\}}$$

is the slope of the graphs of figure 2. From table 2 it can be seen that the new theory, which takes into account the shape of the molecule, accounts for the experimental results with an almost constant value of $x$ (3·4, 3·0), whereas the simple spherical cavity theory would require $x=1\cdot9$ for acetonitrile and $x=7\cdot1$ for paraldehyde.

It must be concluded that the shape of the molecule is an important factor in determining the magnitude of the reaction field and the consequent chemical shifts. For these two solutes it is in fact a reasonably good approximation to assume a uniform reaction field over the whole molecule. In acetonitrile this is because the molecule is small and contains only one group of protons, in paraldehyde because the polar bonds are spread over the molecule. This may not be generally true, and preliminary investigations of some other solutes tend to suggest that localization of the dipole moment in one part of the molecule leads to a reaction field which is not uniform, and this adds a further important complication to the calculation of the reaction field chemical shifts.

## References

[1] BUCKINGHAM, A. D., SCHAEFER, T., and SCHNEIDER, W. G., 1960, *J. chem. Phys.*, **32**, 1227.
[2] ONSAGER, L., 1936, *J. Amer. chem. Soc.*, **58**, 1486.
[3] BUCKINGHAM, A. D., 1960, *Canad. J. Chem.*, **38**, 300.
[4] SCHOLTE, T. H., 1949, *Physica*, **15**, 437, 450.
[5] DEKKER, A. J., 1946, *Physica*, **12**, 209.
[6] MILLER, R. C., and SMYTHE, C. P., 1956, *J. phys. Chem.*, **60**, 1354.
[7] LE FÈVRE, R. J. W., MULLEY, J. W., and SYMTHE, B. M., 1950, *J. chem. Soc.*, p. 290.
[8] BURSTYN, W., 1902, *Sitzber. Wiener Akad.*, 511.
[9] CARPENTER, D. C., and BROCKWAY, L. O., 1936, *J. Amer. chem. Soc.*, **58**, 1270.
[10] ACKERMANN, P. G., and MAYER, J. E., 1936, *J. chem. Phys.*, **4**, 377.
[11] AOKI, K., 1953, *J. chem. Soc. Japan*, **74**, 110.
[12] NOVAK, A., and WHALLEY, E., 1958, *Canad. J. Chem.*, **36**, 116.
[13] BELL, R. P., LIDWELL, O. M., and VAUGHAN-JACKSON, M. W., 1936, *J. chem. Soc.*, p. 1792.
[14] MOERMAN, N. F., 1937, *Rec. Trav. chim. Pays-Bas.*, **56**, 161.
[15] MOERMAN, N. F., and WIEBENGA, E. H., 1937, *Z. Kristogr.*, **97**, 323.
[16] RAMSAY, D. A., 1948, *Trans. Faraday Soc.*, **44**, 289.
[17] BUCKINGHAM, A. D., and LE FÈVRE, R. J. W., 1952, *J. chem. Soc.*, p. 1932.
[18] ROSS, I. G., and SACK, R. A., 1950, *Proc. phys. Soc. Lond. B*, **63**, 893.

# Electrons and holes in alternant hydrocarbons

by A. D. McLACHLAN†

Conant Chemical Laboratory, Harvard University, Cambridge,
Massachusetts

This paper uses the theory of creation and destruction operators to give a
new simpler proof of the well-known pairing relation between electronic states
of alternant hydrocarbon positive and negative ions. The method is like
one that Heisenberg used to explain why the atomic spectra of elements
such as C (with two electrons in the $2p$ shell), and O (with two holes) are so
similar. It depends on the analogy between electrons in an orbital $\psi$ and
holes in the paired antibonding orbital $\psi'$ of the $\pi$-electron shell. A modified
pairing relation holds also in a magnetic field. Applications of the operators
to other problems are suggested.

## 1. INTRODUCTION

The idea that the holes in an almost filled shell of electrons behave like a
kind of particle has a long history in solid state physics, where it helps to explain
the properties of semiconductors and the anomalous Hall effect, but one of its
first successes was in the theory of atomic spectra. The elements carbon and
oxygen, for example, have the same electronic structure, except that oxygen
has two holes in the $2p$ shell, while carbon has two $2p$ electrons. Or again,
nickel has two holes in the $3d$ shell compared with titanium which has two
electrons. In these pairs of elements, there is, as Heisenberg [1] showed in
1931, a very precise analogy between the motions of electrons and holes, so
that the low-lying atomic states of each pair correspond very closely, with similar
angular momenta, total spins, and energies. To prove that this correspondence
was a general rule Heisenberg wrote the Hamiltonian of the valence electrons
in terms of creation and destruction operators [2, 3], and then demonstrated
how this Hamiltonian could also be written in terms of creation and destruction
operators for holes. As a result he could define a precise wave function for
holes in the oxygen atom, which corresponded to the one for $2p$ electrons in
carbon. Provided that orbits outside the $2p$ shell were not involved and that
the occupied orbits were alike in the two atoms, Heisenberg proved that the
two sets of atomic energy levels should be identical because the Hamiltonians
for the two electrons in one atom and the two holes in the other were identical.
Recently there has been strong evidence for an even more striking correspondence
between electrons and holes in alternant hydrocarbons and their ions. Hoijtink
and Weijland [4, 5] found almost indistinguishable electronic absorption
spectra in positive and negative ions derived from the same parent conjugated
hydrocarbon; Weissman and de Boer [6, 7], and Carrington [8], found very
similar ring proton hyperfine structure in the electron spin resonance spectra
of the pairs of ions formed by anthracene, tetracene, and perylene. At first
these effects were attributed to the 'pairing' of the molecular orbitals for the

D

$\pi$ electrons [9, 10], but soon Weijland [5] proved that the electronic states of positive and negative ions were much more closely connected, even when he made some allowance for correlation among these electrons. McLachlan then took the final step [11] of showing that the pairing relations held in a theory which allowed completely for correlation of the $\pi$ electrons among the ring carbon atoms. Under the restrictions of Pariser and Parr's theory [12, 13] the corresponding wave functions of electrons and holes in the $\pi$-electron shell match exactly in the positive and negative ions, and lead to identical energy levels and electronic spectra. In this paper a new derivation of the pairing theorem is given, using creation and destruction operators. The new proof has several advantages: instead of calculating energy matrix elements between all types of configuration one now only has to derive a Hamiltonian; the relative signs of matrix elements are taken care of by the commutation laws of the operators, and the transition from electrons to holes is very simple. There is one important difference between the alternant hydrocarbons and atoms or semiconductors which is brought out very clearly; an electron in an orbital $\psi$ corresponds not to a hole in $\psi$ but to a 'paired hole' which occupies the paired orbital $\psi'$.

## 2. CREATION AND DESTRUCTION OPERATORS

Suppose that $a$, $b$, $c$,... are an arbitrary complete orthonormal set of spin orbitals for some electrons, and that $|xy\ldots z\rangle$ stands for the normalized antisymmetric wave function (Slater determinant) $\|x(1)y(2)\ldots z(N)\|$ in which $N$ electrons occupy the orbitals $x, y, \ldots z$. This notation implies that $|xy\ldots z\rangle = -|yx\ldots z\rangle$ because of antisymmetry, and that $|xy\ldots z\rangle = 0$ if the same orbital occurs more than once. For example $|xxy\rangle = 0$. The creation operators $\eta_a$, $\eta_b$, $\eta_c$,... and destruction operators $\bar{\eta}_a$, $\bar{\eta}_b$, $\bar{\eta}_c$,... are then completely defined by two equations:

$$\eta_a|xy\ldots z\rangle = |axy\ldots z\rangle \tag{1}$$

for every choice of $x, y, \ldots z$; and $\bar{\eta}_a$ is the adjoint operator to $\eta_a$, such that

$$\langle xy\ldots z|\bar{\eta}_a|pq\ldots r\rangle = \langle pq\ldots r|\eta_a|xy\ldots z\rangle^* \tag{2}$$

for all pairs of configurations $|pq\ldots r\rangle$ and $|xy\ldots z\rangle$. From (1) and (2) we deduce that

$$\bar{\eta}_a|axy\ldots z\rangle = |xy\ldots z\rangle, \tag{3}$$

so that $\eta_a$ and $\bar{\eta}_a$ respectively create and destroy electrons in spin orbital $a$. One may therefore use $\eta$ and $\bar{\eta}$ to generate every electron configuration from the state $|\rangle$ in which there are no electrons at all;

$$|ab\ldots c\rangle = \eta_a\eta_b\ldots\eta_c|\rangle, \tag{4}$$

$$\langle|\bar{\eta}_c\ldots\bar{\eta}_b\bar{\eta}_a = \langle ab\ldots c|. \tag{5}$$

The antisymmetry of the wave functions requires that $\eta_a$, $\eta_b$ anticommute, for

$$\eta_a\eta_b|xy\ldots z\rangle = |abxy\ldots z\rangle = -|baxy\ldots z\rangle = -\eta_b\eta_a|xy\ldots z\rangle. \tag{6}$$

Hence $\eta$ and $\bar{\eta}$ obey the rules

$$\eta_a\eta_b + \eta_b\eta_a = 0, \tag{7}$$

$$\bar{\eta}_a\bar{\eta}_b + \bar{\eta}_b\bar{\eta}_a = 0. \tag{8}$$

They also obey a third commutation law

$$\eta_a \bar{\eta}_b + \bar{\eta}_b \eta_a = 1 \quad (a=b) \atop = 0 \quad (a \neq b). \Bigg\} \tag{9}$$

In the standard textbooks on quantum mechanics [2, 3] it is proved that equations (4)–(9) are equivalent to the definition of $\eta$ and $\bar{\eta}$ in terms of antisymmetric wave functions according to equations (1) and (2). Also the many-electron Hamiltonian

$$\mathscr{H} = \sum_\mu U(\mathbf{r}_\mu) + \sum_{\mu < \nu} \frac{e^2}{r_{\mu\nu}} \tag{10}$$

can be written

$$\mathscr{H} = \sum_{a,b} \eta_a \langle a|U|b \rangle \bar{\eta}_b + \tfrac{1}{2} \sum_{a,b:\,c,d} \eta_a \eta_b \left\langle ab \left| \frac{e^2}{r_{12}} \right| cd \right\rangle \bar{\eta}_d \bar{\eta}_c. \tag{11}$$

(note the order of $\bar{\eta}_d$ and $\bar{\eta}_c$).

We shall assume that the $\pi$ electrons in an alternant hydrocarbon move over $n$ orthonormal $2p_z$ orbitals $\phi_1 \ldots \phi_n$, one from each carbon atom. The operators $\eta_{r\sigma}$ and $\bar{\eta}_{r\sigma}$ will then create or destroy a $\pi$ electron of spin $\sigma(\sigma = \alpha, \beta)$ in the orbital $\phi_r$. It is also useful to define operators for the electron densities $(\mathbf{q}_r)$ and bond orders $(\mathbf{p}_{rs})$ for electrons of $\alpha$ and $\beta$ spins,

$$\mathbf{q}_r^\alpha = \eta_{r\alpha} \bar{\eta}_{r\alpha}, \qquad \mathbf{q}_r^\beta = \eta_{r\beta} \bar{\eta}_{r\beta}; \tag{12}$$

$$\mathbf{p}_{rs}^\alpha = \eta_{r\alpha} \bar{\eta}_{s\alpha}, \qquad \mathbf{p}_{rs}^\beta = \eta_{r\beta} \bar{\eta}_{s\beta}; \tag{13}$$

and for total bond orders and electron densities.

$$\mathbf{q}_r = \mathbf{q}_r^\alpha + \mathbf{q}_r^\beta, \tag{14}$$

$$\mathbf{p}_{rs} = \mathbf{p}_{rs}^\alpha + \mathbf{p}_{rs}^\beta. \tag{15}$$

## 3. The $\pi$-electron Hamiltonian

To prove the pairing theorem we have first to express the general Hamiltonian of equation (11) in terms of integrals over the carbon $2p_z$ orbitals. The two-electron part of $\mathscr{H}$ involves electron repulsion integrals

$$\langle rs|tu \rangle = \int \int \phi_r^*(1)\phi_t(1)\frac{e^2}{r_{12}}\phi_s^*(2)\phi_u(2)\,d\tau_1\,d\tau_2, \atop \langle rs|rs \rangle = \gamma_{rs}; \Bigg\} \tag{16}$$

and one-electron integrals of several types. We shall divide the operator $U$ which represents the kinetic and potential energy of an electron in the field of the screened carbon nuclei into two kinds of term. $U_r$, for an electron on atom $r$, is its total energy in the field of the screened nucleus $r$, while $U_t(r \neq t)$ is the potential energy of the electron on $r$ in the field of another nucleus $t$. This serves to define the integrals

$$\beta_{rs} = \int \phi_r^* U \phi_s \, d\tau \quad (r \neq s),$$

$$E_r = \int \phi_r^* U_r \phi_r \, d\tau,$$

$$g_{rt} = -\int \phi_r^* U_t \phi_r \, d\tau \quad (r \neq t), \Bigg\} \tag{17}$$

$$\alpha_r = E_r - \sum_t{}' g_{rt}.$$

Substitution of these integrals into (11) leads to the Hamiltonian

$$\mathscr{H} = \sum_r \mathbf{q}_r \alpha_r + \sum_{r,s} \mathbf{P}_{rs}\beta_{rs} + \tfrac{1}{2}\sum_{rs,tu}\sum_{\sigma,\tau}\eta_{r\sigma}\eta_{s\tau}\langle rs|tu\rangle\bar{\eta}_{u\tau}\bar{\eta}_{t\sigma}. \tag{18}$$

We now use the familiar assumptions of Pariser, Parr [12], and Pople [13], which are all necessary to derive our result. These are:

(1) The orbitals $\phi_1 \ldots \phi_n$ are exactly orthogonal†.

(2) We neglect all electron repulsion integrals which arise from the overlap of two orbitals, keeping only $\langle rs|rs\rangle = \gamma_{rs}$.

(3) An electron on atom $r$ is perfectly shielded from the nuclear charge of another atom $t$ when atom $t$ bears a $\pi$ electron;

$$g_{rt} = \gamma_{rt} \quad \text{when} \quad r \ne t. \tag{19}$$

(4) The effective potential energy of a $\pi$ electron is the same on each carbon atom;

$$E_r + \tfrac{1}{2}\gamma_{rr} = \text{const.} = K \text{ for all atoms.} \tag{20}$$

(5) The resonance integral $\beta_{rs}$ vanishes unless $r$ and $s$ are next neighbours. In an alternant hydrocarbon with even-numbered rings of carbon atoms alternate atoms belong to the starred and unstarred sets, so that $\beta_{rs}$ vanishes when two atoms belong to the same set.

With these assumptions the electron repulsion part of the energy becomes

$$\tfrac{1}{2}\sum_r \gamma_{rr}\left[\sum_{\sigma,\tau}\eta_{r\sigma}\eta_{r\tau}\bar{\eta}_{r\tau}\bar{\eta}_{r\sigma}\right] + \sum_{r<s}\gamma_{rs}\left[\sum_{\sigma,\tau}\eta_{r\sigma}\eta_{s\tau}\bar{\eta}_{s\tau}\bar{\eta}_{r\sigma}\right], \tag{21}$$

and by using the commutation rules (7)–(9) we rearrange it in the form

$$\sum_r \gamma_{rr}\mathbf{q}_r{}^\alpha\mathbf{q}_r{}^\beta + \sum_{\alpha_r<s}\gamma_{rs}\mathbf{q}_r\mathbf{q}_s. \tag{22}$$

Eliminating $\alpha_r$ by means of equations (17), (19), and (20),

$$\alpha_r = K - \tfrac{1}{2}\gamma_{rr} - \sum_{r \ne t}\gamma_{rt}, \tag{23}$$

we note that $\sum_r \mathbf{q}_r = \mathbf{N}$, the operator for the total number of electrons, and finally obtain

$$\mathscr{H} = \mathbf{N}K + \sum_{r,s}\mathbf{P}_{rs}\beta_{rs} + \sum_{r<s}\gamma_{rs}[(\mathbf{q}_r - 1)(\mathbf{q}_s - 1) - 1]$$
$$+ \sum_r \gamma_{rr}[(\mathbf{q}_r{}^\alpha - \tfrac{1}{2})(\mathbf{q}_r{}^\beta - \tfrac{1}{2}) - \tfrac{1}{4}]. \tag{24}$$

Equation (24) is very like equation (3.17) of reference [11], and is the crucial stage in our argument, for we will show in the next section that the motion of holes is governed by a very similar Hamiltonian.

## 4. HOLES AND ' PAIRED ' HOLES

If $|-\rangle$ is the closed shell state $\|(\phi_1)^2(\phi_2)^2\ldots(\phi_n)^2\|$ in which each atom bears two $\pi$ electrons, we can form basic electronic states $|\bar{a}\bar{b}\ldots\bar{c}\rangle$ by destroying electrons or creating holes in the closed shell;

$$|\bar{a}\bar{b}\ldots\bar{c}\rangle = \bar{\eta}_a\bar{\eta}_b\ldots\bar{\eta}_c|-\rangle. \tag{25}$$

One may also interpret $|\bar{a}\bar{b}\ldots\bar{c}\rangle$ as a state in which holes occupy the spin-orbitals

---

† Alternatively we may assume that $\phi_1 \ldots \phi_n$ are orthogonalized linear combinations of the true atomic orbitals, and each $\phi_r$ is localized on atom $r$ and its near neighbours.

$a, b, c, \ldots$. Then $|-\rangle$ is the state with no holes, and $\bar{\eta}_a$ and $\eta_a$ can be renamed $\zeta_a$ and $\bar{\zeta}_a$, the creation and destruction operators for holes.

$$\zeta_a = \bar{\eta}_a, \quad \bar{\zeta}_a = \eta_a; \tag{26}$$

$$|\bar{a}\bar{b}\ldots\bar{c}\rangle = \zeta_a\zeta_b\ldots\zeta_c|-\rangle. \tag{27}$$

We shall also define bond order and electron density operators $\bar{\mathbf{p}}_{rs}{}^x = \zeta_{rx}\bar{\zeta}_{sx}$ and $\bar{\mathbf{q}}_r{}^\alpha = \zeta_{rx}\bar{\zeta}_{rx}$ for holes. They are connected with the corresponding operators for electrons by the relations

$$\bar{\mathbf{p}}_{rs}{}^\alpha = -\mathbf{p}_{sr}{}^\alpha, \quad \bar{\mathbf{q}}_r{}^\alpha = 1 - \mathbf{q}_r{}^\alpha, \quad \bar{\mathbf{q}}_r = 2 - \mathbf{q}_r. \tag{28}$$

Since the energy is a Hermitian operator

$$\beta_{rs} = \beta_{sr}{}^* \tag{29}$$

and the Hamiltonian for the holes, derived from (24) is

$$\mathcal{H} = (2n - \mathbf{N})K - \sum_{r,s}\bar{\mathbf{p}}_{rs}\beta_{rs}{}^* + \sum_{r < s}\gamma_{rs}[(\bar{\mathbf{q}}_r - 1)(\bar{\mathbf{q}}_s - 1) - 1]$$

$$+ \sum_r \gamma_{rr}[(\bar{\mathbf{q}}_r{}^\alpha - \tfrac{1}{2})(\bar{\mathbf{q}}_r{}^\beta - \tfrac{1}{2}) - \tfrac{1}{4}]. \tag{30}$$

This is identical with (24) except for the constant $(2n - \mathbf{N})$ and the replacement of $\beta_{rs}$ by $-\beta_{rs}{}^*$. We now exploit the division of atoms into starred and unstarred sets to define operators $\theta$ and $\bar{\theta}$ which create and destroy 'paired' holes in the $\pi$-electron shell of an alternant hydrocarbon:

$$\left.\begin{array}{l}\theta_{r\alpha} = \pm \check{\zeta}_{r\beta} \\ \bar{\theta}_{r\alpha} = \pm \bar{\zeta}_{r\beta}\end{array}\right\} \quad +\text{ on starred atoms,} \quad -\text{ on unstarred atoms.} \tag{31}$$

Thus if the operator $\psi_{i\alpha} = \sum_r C_{ri}\eta_{r\alpha}$ (see Dirac [2], page 229) creates an electron of spin $\alpha$ in the bonding molecular orbital $\psi_i = \sum_r C_{ri}\phi_r$, then $\theta_{i\alpha} = \sum_r C_{ri}{}^*\theta_{r\alpha}$ creates a hole of spin $\beta$ in the paired antibonding orbital $\psi_i'$ which has the coefficients $C_{ri}' = \pm C_{ri}$ on starred and unstarred atoms respectively.

We can define the configuration which is the pair of $ab\ldots c$ to be

$$|a'b'\ldots c'\rangle = \theta_a\theta_b\ldots\theta_c|-\rangle. \tag{32}$$

The electron density and bond-order operators for paired holes are

$$\mathbf{q}_r'{}^\alpha = \theta_{r\alpha}\bar{\theta}_{r\alpha} = 1 - \mathbf{q}_r{}^\beta, \tag{33}$$

and

$$\mathbf{p}_{rs}'{}^\alpha = \theta_{r\alpha}\bar{\theta}_{s\alpha} = \pm \mathbf{p}_{sr}{}^\beta \tag{34}$$

when atoms $r$ and $s$ are in different or the same sets respectively. (We have chosen to reverse the spins so that the unpaired spin density operator $\rho_r = (\mathbf{q}_r{}^\alpha - \mathbf{q}_r{}^\beta) = (\mathbf{q}_r'{}^\alpha - \mathbf{q}_r'{}^\beta)$ on atom $r$ has the same value in a state and its pair.) Since all bonds are between atoms of different sets, the Hamiltonian for 'paired' holes is

$$\mathcal{H}' = (2n - \mathbf{N}')K + \sum_{r,s}\mathbf{p}_{rs}'\beta_{rs}{}^* + \sum_{r < s}\gamma_{rs}[(\mathbf{q}_r' - 1)(\mathbf{q}_s' - 1) - 1]$$

$$+ \sum_r \gamma_{rr}[(\mathbf{q}_r'{}^\alpha - \tfrac{1}{2})(\mathbf{q}_r'{}^\beta - \tfrac{1}{2}) - \tfrac{1}{4}]. \tag{35}$$

The main difference between $\mathscr{H}$ and $\mathscr{H}'$ is that $\beta_{rs}{}^*$ replaces $\beta_{rs}$.  When there is no magnetic field $\beta_{rs}$ is real and

$$\mathscr{H}' = \mathscr{H} + 2(n - \mathbf{N})K. \tag{36}$$

Thus the corresponding states

$$\Psi = \sum C_{ab\ldots c} |ab\ldots c\rangle,$$
$$\Psi' = \sum C_{ab\ldots c} |a'b'\ldots c'\rangle, \tag{37}$$

have the same energy, but for a constant;

$$W' = W + 2(n - N)K \tag{38}$$

where $N$ is the number of electrons in $\Psi$.  Hence, if $\Psi_i$ is a wave function for an electronic state of a hydrocarbon with $N$ $\pi$ electrons, $\Psi_i'$ is the wave function of a corresponding state in the hydrocarbon with $(2n - N)$ electrons, or $N$ holes. All the properties deduced previously [11], such as the uniform charge distribution and 'odd' and 'even' states of neutral alternant hydrocarbons follow as before.

## 5. PAIRING IN A MAGNETIC FIELD

In a magnetic field it is appropriate to define the states $|ab\ldots c\rangle$ and $|a'b'\ldots c'\rangle$ in terms of the modified atomic orbitals [14, 15]

$$\chi_r(\mathbf{r}) = \phi_r(\mathbf{r}) \exp[(e/i\hbar c)\mathbf{r}.\mathbf{A}_r]. \tag{39}$$

In equation (39) $\mathbf{A}_r$ is the vector potential of the magnetic field at nucleus $r$, and $\mathbf{r}$ the position of the electron relative to this nucleus.  In a weak magnetic field London showed that the motion of the electrons over these modified orbitals is governed by the same Hamiltonian as before, except that $\beta_{rs}$ becomes $\beta_{rs}(1 + if_{rs})$, where

$$f_{rs} = (e/\hbar c)(\mathbf{A}_r - \mathbf{A}_s).\mathbf{R}_{rs}, \tag{40}$$

and $\mathbf{R}_{rs} = \frac{1}{2}(\mathbf{r}_r + \mathbf{r}_s)$ is the position of the midpoint of the bond.  Since $\beta$ is no longer real the state corresponding to $\Psi$ is now

$$\Psi' = \sum C^*_{ab\ldots c} |a'b'\ldots c'\rangle. \tag{41}$$

In deriving equation (41) we have neglected spin–orbit coupling and the interaction of the electron spin with the external field.  However, when the last of these is included, $\Psi'$ only corresponds to $\Psi$ in a magnetic field of uniform direcuon along the $z$-axis.  We should also note, in equation (41), that the complex conjugate coefficient $C^*_{ab\ldots c}$ arises from the different transformation properties of the operators $\eta$ and $\theta$ when one changes from atomic to molecular orbitals; so that the paired holes still occupy the paired orbitals $\Psi_i'$, and not their complex conjugates $\Psi_i'^*$.  In a non-uniform field the interaction

$$\mathscr{V} = g\beta \sum_{r,s} \sum_{\sigma,\tau} \eta_{r\sigma} \langle r|\mathbf{H}|s\rangle . \langle \sigma|\mathbf{S}|\tau\rangle \bar{\eta}_{s\tau} \tag{42}$$

between electron spin and the field does not have the same form when expressed in terms of operators for paired holes, even when one neglects the overlap terms

$$\langle r|\mathbf{H}|s\rangle = \int \chi_r{}^*(\mathbf{r})\mathbf{H}(\mathbf{r})\chi_s(r)\,d\mathbf{r}.$$

As a result, the pairing theorem no longer holds.

## 6. Discussion

Creation and destruction operators are a natural choice in the problem of electrons and holes, but they may also have other useful applications. For example, in problems involving the interaction of two separated groups of electrons, such as the $\sigma$ and $\pi$ electrons of aromatic hydrocarbons [16, 17], the Hamiltonian at once divides up into $\sigma$–$\sigma$, $\pi$–$\pi$, and $\sigma$–$\pi$ portions, and Coulomb and exchange terms are clearly separated. Atom and bond populations, and electron density matrices [17], are also very easily defined as expectation values of operators like $\mathbf{q}_r$ and $\mathbf{p}_{rs}$ in the electronic state concerned. Finally, since the operator

$$\lambda . \eta_{A\alpha}\eta_{A\beta} + \mu . \eta_{B\alpha}\eta_{B\beta} + \nu[\eta_{A\alpha}\eta_{B\beta} - \eta_{A\beta}\eta_{B\alpha}] 2^{-1,2} \tag{43}$$

generates the partially ionic and covalent bond wave function

$$\lambda . \psi_{A-B+} + \mu . \psi_{A+B-} + \nu . \psi_{A:B} \tag{44}$$

for a bond between atoms A and B, a product of such operators may be useful in treating the theory [18] of 'separated electron pairs'.

## Appendix

### *The effects of overlap*

We shall conclude this paper with a comment about the effects of overlap and 'differential overlap'. To neglect overlap is such a drastic step that one is surprised that real molecules have the pairing properties predicted by the simplified theory. Yet the agreement between, say, the electron spin resonance spectra of a positive and a negative alternant hydrocarbon ion is exceedingly good, and suggests that some of the effects of overlap may cancel one another. Let us then express the electronic wave functions of these molecules in terms of a new basic set of *orthogonalized* atomic $\pi$ orbitals $\phi_R$, $\phi_S$, ... localized near the atoms $r$, $s$, ... and derived from $\phi_1 \ldots \phi_n$ by the transformation [19]

$$\phi_R = \sum_s [(1+\mathbf{S})^{-1/2}]_{rs}\phi_s, \tag{45}$$

$$= \phi_r - \tfrac{1}{2}\sum_s S_{rs}\phi_s + \tfrac{3}{8}\sum_{s,t} S_{rs}S_{st}\phi_t - \cdots, \tag{46}$$

where $S_{rs}$, $(r \neq s)$, is the overlap integral. New one-electron integrals $\alpha_R$, $\beta_{RS}$, and electron repulsion integrals $\langle RS|TU \rangle$ are now calculated from $\alpha_r$, $\beta_{rs}$, and $\langle rs|tu \rangle$. The transformed one-electron integrals

$$\left.\begin{aligned}
\alpha_R &= \alpha_r - \sum_s S_{rs}\beta_{rs} + \cdots, \\
\beta_{RS} &= \beta_{rs} - \tfrac{1}{2}S_{rs}(\alpha_r + \alpha_s) + \cdots, \qquad & r, s \text{ neighbours,} \\
\beta_{RT} &= \tfrac{1}{2}\sum_s (S_{rs}\beta_{st} + \beta_{rs}S_{st}) - \cdots, \qquad & rs, st \text{ neighbours,}
\end{aligned}\right\} \tag{47}$$

will no longer satisfy the assumptions of Hückel theory, since $\alpha_R$ depends on the number of neighbours an atom has, and $\beta_{RT}$ does not vanish for second neighbours, which must be in the same set. However, the new two-electron integrals have a very interesting property, first noted by McWeeny [20]. $\langle RS|TU \rangle$ is the Coulomb repulsion energy between the charge distributions $-e\phi_R\phi_T$ and $-e\phi_S\phi_U$, so that when $R$ and $T$ are neighbours

$$\phi_R\phi_T = \phi_r\phi_t - \tfrac{1}{2}S_{rt}(\phi_r^2 + \phi_t^2) + \cdots. \tag{48}$$

But Mulliken's well-known approximation [21] for electron repulsion integrals, which is often very accurate, states that

$$\langle rs|tu\rangle \simeq \tfrac{1}{4}S_{rt}S_{su}(\gamma_{rs}+\gamma_{ru}+\gamma_{ts}+\gamma_{tu}),\tag{49}$$

and depends on replacing $\phi_r\phi_s$ by $\tfrac{1}{2}S_{rs}(\phi_r^2+\phi_s^2)$. Combining equations (48) and (49), we conclude that if Mulliken's approximation holds for the integrals involving the original atomic orbitals $\phi_r$, $\phi_s$, ..., then the orthogonal orbitals $\phi_R$, $\phi_S$, .... obey the assumption of 'zero differential overlap':

$$\langle RS|TU\rangle = \delta_{RT}\delta_{SU}\gamma_{ST}.\tag{50}$$

(This result only holds exactly if we neglect terms involving $S^2$ and higher powers in the expansion (46).)

We now believe that the pairing theorem should refer to a wave function formed from the orthogonal combinations of atomic orbitals, instead of the ordinary ones, and the assumption that Mulliken's approximation is exact for the non-orthogonal orbitals $\phi_1...\phi_n$ should replace Pariser and Parr's assumptions of 'zero differential overlap'. This reinterpretation of the theory makes it depend on more reasonable assumptions, and makes its explanation of the intensities of electronic transitions more convincing. According to equation (48) the electronic transition moment $\mathbf{M}_{RS}$ of a bond should be extremely small, and justify the neglect of these bond terms in intensity calculations.

## REFERENCES

[1] HEISENBERG, W., 1931 *Ann. Phys., Lpz.,* **10**, 888.
[2] DIRAC, P. A. M., 1958, *Quantum Mechanics,* 4th edition (Oxford: University Press), p. 248.
[3] LANDAU, L. D., and LIFSCHITZ, E. M., 1958, *Quantum Mechanics* (London: Pergamon Press), p. 215.
[4] HOIJTINK, G. J., and WEIJLAND, W. P., 1957, *Rec. Trav. chim. Pays-Bas,* **76**, 836.
[5] WEIJLAND, W. P., 1958, Thesis, Free University of Amsterdam.
[6] DE BOER, E., and WEISSMAN, S. I., 1957, *J. chem. Phys.,* **26**, 963.
[7] DE BOER, E., and WEISSMAN, S. I., 1958, *J. Amer. chem. Soc.,* **80**, 4549.
[8] CARRINGTON, A., 1959, *J. chem. Soc.,* p. 947.
[9] HÜCKEL, E., 1932, *Z. Phys.,* **76**, 628.
[10] COULSON, C. A., and RUSHBROOKE, G. S., 1940, *Proc. Camb. phil. Soc.,* **36**, 193.
[11] McLACHLAN, A. D., 1959, *Mol. Phys.,* **2**, 271.
[12] PARISER, R., and PARR, R. G., 1953, *J. chem. Phys.,* **21**, 466, 767.
[13] POPLE, J. A., 1953, *Trans. Faraday Soc.,* **49**, 1375.
[14] LONDON, F., 1937, *J. phys. Radium,* **8**, 397.
[15] POPLE, J. A., 1958, *Mol. Phys.,* **1**, 175.
[16] McLACHLAN, A. D., DEARMAN, H. H., and LEFEBVRE, R., 1960, *J. chem. Phys.,* **33**, 65.
[17] McWEENY, R., 1960, *Rev. mod. Phys.,* **32**, 335.
[18] PARKS, J. M., and PARR, R. G., 1958, *J. chem. Phys.,* **28**, 335.
[19] LÖWDIN, P. O., 1955, *Phys. Rev.,* **97**, 1490.
[20] McWEENY, R., 1954, *Proc. roy. Soc.* A, **227**, 288.
[21] MULLIKEN, R. S., 1949, *J. Chim. phys.,* **46**, 497.

# Errors in "Wave functions for the methane molecule"

by I. M. MILLS

Department of Chemistry, University of Reading

Two errors in my paper " Wave functions for the methane molecule " [1] are corrected. They concern my f-harmonic approximation to the wave-function in the equilibrium configuration, for which the final expression for the wave function, the energy lowering, and the density function were all in error.

As a result of more recent work on the spherical approximation to the electronic wave function of the methane molecule [2, 3], two important errors in the author's paper " Wave functions for the methane molecule " [1] have come to light. They lie in the improved wave function which I obtained by including terms representing f-type harmonics in my calculations. With the current interest in one-centre wave functions, it seems worth while correcting these errors in order to obtain both the true energy lowering and the non-spherical contribution to the electron density function.

The treatment in §3 of reference [1] was based on an improved form for the wave function of the type

$$\Psi = \Psi_0 \left[ 1 + \sum_{\mu} q(\mathbf{r}_{\mu}) \right] \tag{1}$$

the function $q$ being varied so as to minimize the total energy under the influence of the perturbed Hamiltonian

$$H = H_0 + \sum_{\mu} v(\mathbf{r}_{\mu}). \tag{2}$$

The function $v$ consisted of the $f_{xyz}$ harmonic term from the potential field of the protons, this being regarded as the most important non-spherical term missing from the original Hamiltonian (see [1]). The expression obtained for the energy lowering, correct to the second order (since the first-order lowering is zero) was :

$$E = \tfrac{1}{2} \int \rho_1^{\,0} [\mathrm{grad}\, q]^2 \, d\mathbf{r} + 2 \int \rho_1^{\,0} v\, q\, d\mathbf{r} \tag{3}$$

and minimizing this with respect to $q$ gave the differential equation

$$\mathrm{div}\, [\rho_1^{\,0}\, \mathrm{grad}\, q] = 2\rho_1^{\,0}\, v. \tag{4}$$

This differential equation was solved for the function $q(\mathbf{r})$ and the results were tabulated in reference [1]; the energy lowering obtained, as given by equation (3), was

$$E = -0 \cdot 28 \text{ atomic units.} \tag{5}$$

The energy lowering given by (3) was based on second-order perturbation theory, and since the modification to the original wave function which I found necessary was large compared to $\Psi_0$, I then went on to try a function of the form

$$\Psi = \Psi_0 \left[ a + b \sum_{\mu} q(\mathbf{r}_{\mu}) \right] \tag{6}$$

retaining the function $q$ obtained by solution of (4) and varying $a$ and $b$ so as to normalize (6) and further lower the energy. Unfortunately I made a numerical error in solving the secular equation for $a$ and $b$, obtaining:

$$a = 0 \cdot 985, \quad b = 0 \cdot 411, \quad E = -0 \cdot 68 \text{ atomic units,}$$

whereas on eliminating the error we find :

$$a = 0 \cdot 941, \quad b = 0 \cdot 818, \quad E = -0 \cdot 24 \text{ atomic units.} \tag{7}$$

Thus table 3 of reference [1], p. 103, should be amended to read as follows:

> *Calculated* total energy of methane, $R_0 = 2$:
> (2) Improved model:
> Electronic energy    $-53\cdot22$     $-0\cdot24$
> Nuclear repulsion     $+13\cdot84$    Total:  $-39\cdot62$
>       (energy values in atomic units)

This final value for the energy lowering ,$0\cdot24$ a.u., is much more in accord with the results of Saturno and Parr's work [2], for they used a more elaborate final wave function and still only succeeded in lowering the calculated energy by $0\cdot30$ a.u. below the value obtained using a spherical wave function.    At first glance it is surprising that the energy given by (7) is not as low as that given by (5), despite the introduction of the parameters $a$ and $b$; the answer lies in the fact that equation (3), from which the result (5) was derived, is only an approximate expression whereas the result (7) is the exact energy appropriate to the wave function (6).    In this particular case the main effect of including the parameters $a$ and $b$ is quite simply to normalize the wave function (6), and if this normalization error is removed from the original wave function (1) and from the derived energy expression (3) the final result is almost identical with (7) above, as has been shown by Marshall [3].

The other serious error in my original paper is that one term is missing from the expression given for the modified one-electron density function, equation (9), p. 104 in [1].    This equation should read:

$$\rho_1(\mathbf{r}) = a^2\rho_1{}^0 + 2ab\rho_1{}^0 q(\mathbf{r}) + b^2\rho_1{}^0 q^2(\mathbf{r}) + b^2 \int \rho_2{}^0(\mathbf{rr}')q^2(\mathbf{r}')\, d\mathbf{r}' \qquad (8)$$

as may be verified by integrating $\Psi^2$, given by (6), over the coordinates of all but one electron.    The last term involving the two-electron density function $\rho_2{}^0(\mathbf{rr}')$ was omitted in reference [1].    When this last term is expanded in terms of one-electron functions, equation (8) can be re-written (by combining part of the last term with the first term on the right-hand side of (8)):

$$\rho_1(\mathbf{r}) = \rho_1{}^0 + 2ab\rho_1{}^0 q(\mathbf{r}) + b^2\rho_1{}^0 q^2(\mathbf{r})$$
$$- 2b^2[(1s)^2 \int (1s)^2 q^2\, d\mathbf{r} + (2s)^2 \int (2s)^2 q^2\, d\mathbf{r}$$
$$+ \{(2px)^2 + (2py)^2 + (2pz)^2\} \int (2p)^2 q^2\, d\mathbf{r} + (1s)(2s) \int (1s)(2s)\, q^2\, d\mathbf{r}]. \qquad (9)$$

The orbital functions have been abbreviated by writing 1s for $\psi_{1s}(\mathbf{r})$, etc., in this equation.    The values of the various integrals in equation (9) are listed in the table below; the whole of the term in square brackets proves to be very small, and since it is spherically symmetric in the coordinates its effect is to make a very small modification to the main spherical term $\rho_1{}^0(\mathbf{r})$ in equation (9).    The biggest modification to the density function $\rho_1(\mathbf{r})$ resulting from the revisions discussed here follow from the new values of $a$ and $b$: the effect is to increase the importance of the second and third terms in equation (9) and hence to increase the 'pile-up' of electrons around each proton.    The effect is illustrated in the figure below which should replace the lower half (*b*) of figure 1 in Mills [1].

$$\int (1s)^2 q^2\, d\mathbf{r} = 0\cdot000_0 \qquad\qquad \int (1s)(2s) q^2\, d\mathbf{r} = 0\cdot000_1$$

$$\int (2s)^2 q^2\, d\mathbf{r} = 0\cdot019_6 \qquad\qquad \int (2p)^2 q^2\, d\mathbf{r} = 0\cdot022_7$$

Values of integrals appearing as coefficients in equation (9) calculated from functions tabulated by Mills [1], in atomic units.
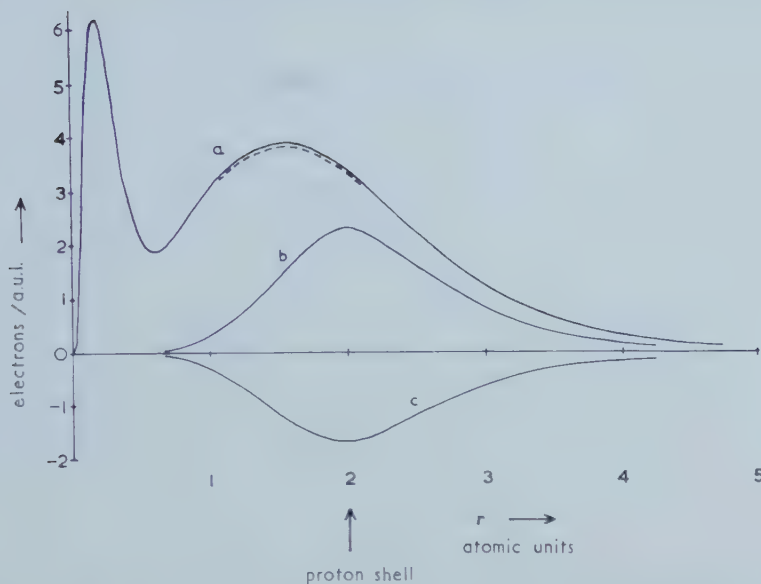
Radical density functions in electrons per atomic unit of length.

The curve (*a*), full line, shows the radial electron density under the spherical approximation. The curves (*b*) and (*c*) show the corrections that should be added to the curve (*a*) to obtain the radial electron density along a radius through one of the protons (curve (*b*)) or along a radius exactly between three protons (curve (*c*)). The dotted curve close to (*a*) shows the correction which should be made to curve (*a*) before adding (*b*) or (*c*) due to the last term in equation (8) enclosed in square brackets.

Saturno and Parr discuss my paper [1] in an appendix to their paper [2], and apart from their comments concerning the errors discussed above, they remark that the total energy which I calculated for the spherical model of methane appears to be somewhat in error since they obtain a slightly lower total energy using analytical functions than I obtained using the full Hartree–Fock self-consistent field treatment. I have re-examined the original work and cannot find any numerical error to explain this discrepancy; however, as Saturno and Parr observe the discrepancy is mainly associated with the (1s) orbital to which the total energy is very sensitive, and it is perhaps possible that numerical uncertainties in solving the Hartree–Fock equations caused this error. Otherwise it remains a mystery. In any case a small change in the (1s) orbital comparable to the difference between my results and those of Saturno and Parr would not affect any of the later deductions to a significant extent, with the single exception of changing the total energy; in particular nothing in my second paper [4] is affected by any of the errors discussed here.

I should like to express my thanks to Professor R. G. Parr who originally drew my attention to these discrepancies, and to Dr. Trevor Marshall who is considering them in more detail in his thesis [3] and to whom I am indebted for discussion of this problem. I should also like to apologize for the original errors and for any trouble that they may have caused other workers.

REFERENCES

[1] Mills, I. M., 1958, *Mol. Phys.*, **1**, 99.
[2] Saturno, A. F., and Parr, R. G., 1960, *J. chem. Phys.*, **33**, 22.
[3] Marshall, T., 1960, Ph.D. Thesis, University of Cambridge.
[4] Mills, I. M., 1958, *Mol. Phys.*, **1**, 107.

# Isotope shifts in the NMR spectra of $H_2$, HD and $D_2$ due to zero-point vibration

by T. W. MARSHALL†

National Physical Laboratory, Teddington, Middlesex

The variation with interatomic separation of the nuclear magnetic screening constant for $H_2$ has been studied in a previous paper. Here an estimate is made of the difference in screening which is a consequence of the different zero-point vibrational functions in $H_2$, HD and $D_2$. The results are in good agreement with the observed values.

## 1. Introduction

Isotope shifts have been observed in a number of NMR spectra [1] and it was pointed out by Ramsey [2] that these were due mainly to the difference in zero-point vibrational functions which result from the different isotopic masses. A complete calculation of this effect is possible only if we possess values for the screening constant $\sigma$ for all values of the interatomic separation $R$, in addition to the wave-function representing the nuclear vibration. A series of such values was obtained recently for the hydrogen molecule [3] using the method of gauge-invariant atomic orbitals. This method gave excellent agreement with more accurate calculations of $\sigma$ when $R$ was put equal to the equilibrium distance in $H_2$ and to zero (corresponding to the helium atom), and therefore we use the values of $\sigma(R)$ in the neighbourhood of the equilibrium position to calculate the isotope shifts in $H_2$, HD and $D_2$.

## 2. Theory

We assume that all the molecules are in the ground vibrational state and that the Born–Oppenheimer approximation is valid. If the potential field in which the nuclei move is $V(R)$ and the nuclear wave-function is $\Psi(R)$, then the 'centre of gravity' of the line will correspond to the value of $\sigma$ averaged over the nuclear motion, that is

$$\sigma_{\text{obs}} = \int_0^\infty \Psi'^2 \sigma \, dR. \tag{1}$$

We obtain a quadratic fit for $\sigma$ in the neighbourhood of $R_e$ the equilibrium position,

$$\sigma(R) = \sigma(R_e) + (R - R_e)\sigma'(R_e) + \tfrac{1}{2}(R - R_e)^2\sigma''(R_e) \tag{2}$$

and assume that $\Psi'^2$ is sufficiently small outside this neighbourhood to add no higher terms to the integral. With this approximation

$$\sigma_{\text{obs}} = \sigma(R_e) + \overline{(R - R_e)}\sigma'(R_e) + \overline{\tfrac{1}{2}(R - R_e)^2}\sigma''(R_e) \tag{3}$$

---

† Guest worker, National Physical Laboratory, 1959–60. Present address: University College of the West Indies, Mona, Jamaica.

where

$$\overline{R-R_e} = \int \Psi^2 (R-R_e)\, dR$$

and

$$\overline{(R-R_e)^2} = \int \Psi^2 (R-R_e)^2\, dR. \tag{4}$$

The values of $\sigma'$ and $\sigma''$ which fit the values obtained by Marshall and Pople [3] most closely in the neighbourhood of $R_e$ are

$$\left.\begin{aligned} \sigma'(R_e) &= -11\cdot30 \times 10^{-6}, \\ \sigma''(R_e) &= 11\cdot06 \times 10^{-6}. \end{aligned}\right\} \tag{5}$$

(Distances are in units of the Bohr radius.)

According to equation (3) there are two distinct effects. The second term is non-vanishing only if the potential energy $V(R)$ has an anharmonic part, whereas the third term, which depends on the amplitude of vibration, is non-vanishing even for a harmonic potential well. A function which represents $V(R)$ adequately over the whole range of $R$ is the Morse function, but since we are concerned here only with the lowest vibrational state, it is preferable to represent $V$ as the sum of a harmonic and a cubic term

$$V(R) = f(R-R_e)^2 - g(R-R_e)^3. \tag{6}$$

This potential gives a ground-state eigenfunction to first order in $g$ of

$$\Psi = \Psi_0 + g\hbar^{1/2}\mu^{-1/4}f^{-5/4}\left(\frac{3}{2\sqrt{2}}\Psi_1 + \frac{1}{2\sqrt{3}}\Psi_3\right) \tag{7}$$

where $\Psi_0$, $\Psi_1$ and $\Psi_3$ are the ground and first and third excited states of the corresponding harmonic oscillator for which $g$ is zero. We have put $\mu$ for the 'reduced mass' of the molecule. If $M$ is the mass of a proton, this has the following values for the three molecules $H_2$, HD and $D_2$

$$\left.\begin{aligned} \mu_{H_2} &= \tfrac{1}{2}M, \\ \mu_{HD} &= \tfrac{2}{3}M, \\ \mu_{D_2} &= M. \end{aligned}\right\} \tag{8}$$

Substituting (7) in (4) one obtains

$$\overline{R-R_e} = \tfrac{3}{8}g\hbar\mu^{-1/2}f^{-3/2}, \tag{9}$$

$$\overline{(R-R_e)^2} = \tfrac{1}{2}\hbar\mu^{-1/2}f^{-1/2}. \tag{10}$$

The values of $f$ and $g$ are obtainable from the vibrational spectra of these molecules [4] and in fact within the limits of the Born–Oppenheimer approximation, we should obtain the same values for all three molecules. The most accurate spectra so far obtained [5, 6] confirm this conclusion and it is these values for $f$ and $g$ which we use here. Substituting numerical values in (9) and (10), we obtain for the mean and mean-square displacements (in atomic units):

$$\left.\begin{array}{lll} \text{for } H_2 & \overline{R-R_e} = 0\cdot029\,99, & \overline{(R-R_e)^2} = 0\cdot027\,14, \\ \text{for } HD & \overline{R-R_e} = 0\cdot025\,98, & \overline{(R-R_e)^2} = 0\cdot023\,52, \\ \text{for } D_2 & \overline{R-R_e} = 0\cdot021\,20, & \overline{(R-R_e)^2} = 0\cdot019\,19. \end{array}\right\} \tag{11}$$

If these values are substituted in (3), the predicted values of shielding differences are

$$\left.\begin{array}{l} \sigma(D_2) - \sigma(H_2) = 0\cdot55 \times 10^{-7}, \\ \sigma(D_2) - \sigma(HD) = 0\cdot30 \times 10^{-7}. \end{array}\right\} \tag{12}$$

## 3. Discussion

The above screening differences are for the proton or the deuteron—whichever is appropriate—and refer in each case to the centre of the multiplet caused by indirect spin–spin coupling. No such direct calculation of this effect has been previously reported, but Ramsey [2] assumed the dependence

$$\sigma(R) = \sigma(R_e)(R/R_e)^n \tag{13}$$

and showed how an approximate value for $n$ could be obtained.

There exist no accurate experimental data for these shifts but the values obtained above agree within the quoted probable error with the values obtained by Wimett [7]

$$\left.\begin{array}{l} \sigma(D_2) - \sigma(H_2) = (0\cdot65 \pm 0\cdot59) \times 10^{-7}, \\ \sigma(D_2) - \sigma(HD) = (0\cdot48 \pm 0\cdot32) \times 10^{-7}. \end{array}\right\} \tag{14}$$

The work described above has been carried out as part of the research programme of the National Physical Laboratory, and this paper is published by permission of the Director of the Laboratory.

## References

[1] Gutowsky, H. S., 1959, *J. chem. Phys.*, **31**, 1683.
[2] Ramsey, N. F., 1952, *Phys. Rev.*, **87**, 1075.
[3] Marshall, T. W., and Pople, J. A., 1960, *Mol. Phys.*, **3**, 339.
[4] Herzberg, G., 1950, *Spectra of Diatomic Molecules* (Van Nostrand), p. 93.
[5] Stoicheff, B. P., 1954, *Canad. J. Phys.*, **32**, 630.
[6] Stoicheff, B. P., 1957, *Canad. J. Phys.*, **35**, 730.
[7] Wimett, T. F., 1953, *Phys. Rev.*, **91**, 476.

# Properties of Hafner's new heptalene and pentalene derivatives

by M. ASGAR ALI† and C. A. COULSON

Mathematical Institute, Oxford

A critical study has been made of Hafner's new heptalene and pentalene derivatives I and II. Conventional valence-bond, molecular-orbital and free-electron approximations have been used. All agree that I should be genuinely aromatic, and II should not be. The valence-bond method suggests that II should be pseudo-aromatic, the other methods suggest that it should possess cyclo-olefinic character. All methods confirm the very long wavelength absorption of I, but the agreement in the case of II is less satisfactory. Charge distributions, bond orders and lengths are calculated by the molecular-orbital method, and compared with heptalene, pentalene, azulene and acenaphthylene. The relevance of the aromatic sextet rule is pointed out in discussing charge distribution in these odd-numbered ring compounds. Localization energies are also calculated, and are used to predict the positions of greatest reactivity for electrophilic, nucleophilic and radical reactions.

---

## 1. INTRODUCTION

Recently Hafner [1] has reported the synthesis of $1:10$ penteno $2:4$ dimethyl heptalene (I) and $1:8$ penteno $4:6$ dimethyl azulene (II). These are interesting compounds because they are members of the relatively small number of molecules containing heptalene or pentalene skeletons. The important properties of these molecules, which any satisfactory theory must explain, are as follows:
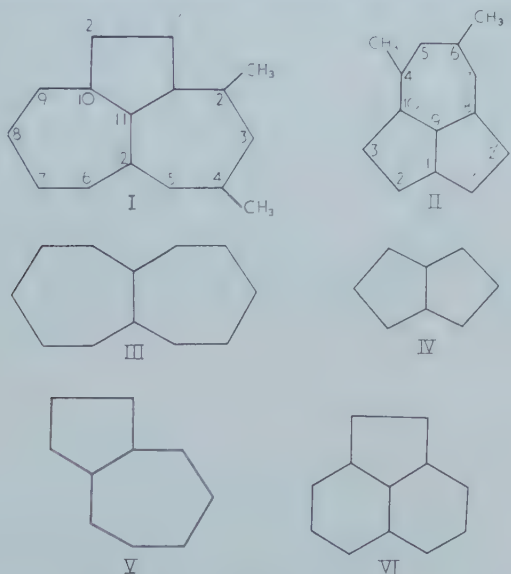


### 1.1. *Molecule I*

Its colour is deep red. The spectrum in the visible region resembles that of azulene, but is displaced to even longer wavelengths. Thus $\lambda_{max} = 1073, 1027,$

897, 793, 746 m$\mu$, compared with the azulene values $\lambda_{max} = 697$, 661, 632, 603 580 m$\mu$.   It is soluble in 50 per cent sulphuric acid, with a red colour, but is precipitated by addition of water.   It undergoes acylation by a Friedel Crafts reaction.   These and other observations led Hafner [1] to conclude that I is aromatic.

### 1.2. *Molecule II*

By contrast, this molecule lacks the stability and aromaticity of I, undergoes dimerization and shows reactions reminiscent of those of dibenzopentalene synthesized by Blood and Linstead [2, 3].   Its light absorption shows a strong maximum at $\lambda = 475$ m$\mu$ and three other maxima between 350 m$\mu$ and 400 m$\mu$.

These differences between I and II raise an interesting problem because both molecules satisfy the criterion which Craig empirically attributes to pseudo-aromatic compounds [4].   Therefore it is difficult to understand their difference in behaviour and stability.   This present paper will be concerned with these differences, and with similar types of similarity and difference between I and II and heptalene (III), pentalene (IV), Azulene (V) and acenaphthylene (VI). Molecules III and IV have not yet been synthesized, but V and VI are well known.

## 2. AROMATIC AND PSEUDO-AROMATIC

In view of the fundamental distinction between aromatic and pseudo-aromatic molecules, a brief review of Craig's analysis is desirable.   In the case of normal aromatic alternant hydrocarbons such as benzene and naphthalene, we know that the semi-empirical LCAO MO method and the semi-empirical valence-bond method are in complete agreement as to the symmetry of the ground state, and its resonance stability.   When this situation arises, there is no further problem.   But for non-alternant molecules such as pentalene and heptalene it has been shown by Craig and Maccoll [5] that the two methods disagree even as regards the symmetry of the ground state, despite the fact that their resonance energies per electron are high, and comparable with that of benzene.   Thus in pentalene, for example, if we suppose that the valence-bond ground state is built by linear combination of the Kekulé structures A and B of VII, its wave function is $\psi = A + B$.   But a rotation of 180° around the long horizontal axis of symmetry converts A into $-B$ and B into $-A$.   (Craig gives simple rules for determining whether the sign is $+$ or $-$ in rotations of this kind.)   This means that the function $\psi$ becomes $-\psi$, showing that it does not possess the full symmetry of the framework.   Indeed, Craig and Maccoll [5] show that the symmetry of $\psi$ is actually $B_{1g}$.   An exactly similar situation exists in heptalene III.



(A)        VII        (B)

Such molecules, whose ground-state wave functions are not fully symmetrical, are called pseudo-aromatic.   In these molecules Craig [6] has put forward arguments to show that the valence-bond resonance integral $\alpha$ should have a smaller value than for the more familiar aromatics.   When this happens, their resonance stabilization will be smaller; they will show typical unsaturation characteristics; and finally, since the gain in resonance energy, small as it is, can only be achieved

by an effective equalization of all the C—C bonds, it may not be sufficient to overcome the compressional energy associated with the deformation of the $\sigma$-bonds. Pseudo-aromatics will then tend to lose their approximate equality of bond lengths, and behave more like polyolefines, in the manner of butadiene or hexatriene. Thus all pseudo-aromatics will show a tendency to behave as polyolefins; but of course a polyolefine need not be a pseudo-aromatic.

It is not immediately clear whether this argument will differentiate between I and II, and we have therefore felt that a semi-empirical valence-bond calculation would be justified. There is a further important point in connection with pseudo-aromatics such as these. This point has already been emphasized by Longuet-Higgins [7]. In a simple MO treatment in which all the orbital energies are distinct, the lowest energy configuration with $2n$ electrons will be one in which the lowest $n$ orbitals are each doubly-occupied, and all the others are empty. This inevitably leads to a wave function of maximum possible symmetry. The only ways in which the ground state could have less than maximum symmetry would be that the $n$th and $(n+1)$th orbitals were degenerate, or that there were other low-lying orbitals leading to configurations which, by mutual interaction, led to a lowering of the energy below the lowest symmetrical configuration. The first possibility normally arises when, as in benzene, there is at least a three-fold axis of symmetry, and so is irrelevant in our present discussion. In order to consider the second possibility we have made conventional Hückel-type calculations for I and II, supposing that the Coulomb terms $\alpha$ are the same for each carbon atom, and the resonance integrals $\beta$ are the same for each carbon–carbon bond. As a further check upon these results we have also used the free-electron MO method. Here the only disposable parameter is the carbon–carbon distance, taken to be constant and labelled $a$. One of us [8] has already shown that this method should give results very similar to the LCAO approximation. We shall use it to determine the details of the charge distribution due to the $\pi$-electrons, and also the energies of the various occupied and unoccupied orbitals. We have throughout neglected the influence of the two attached methyl groups. There is no reason to suppose that this is large. Some detailed calculations, reported near the end of the present paper, show that in fact this influence is so small as not significantly to alter the charge distribution or ultra-violet spectrum.

Finally, with a view to predicting the reactive sites on the molecules I and II, we have calculated both the $\pi$-electron charge distributions and localization energies. For the purposes of our calculations we have everywhere supposed that both molecules are planar.

## 3. Valence-bond calculations

The numbers of canonical structures for I and II are very large, and a full valence-bond calculation would not be justified. We have therefore only included the three Kekulé structures (A–C and A′–C′ respectively) drawn in figure 1. In these diagrams we have drawn arrows along the double bonds, in order to define the phase of the corresponding wave functions. Each function is completely determined once one single term is written down. Our convention is that the leading diagonal of the first contributing Slater determinant will be such that spin $\alpha$ is assigned to the head, and spin $\beta$ to the tail, of each arrow; and the spin factor of the leading diagonal term is $\beta(1)\alpha(2)\beta(3)\alpha(4)\ldots\alpha(2n)$.

E 2
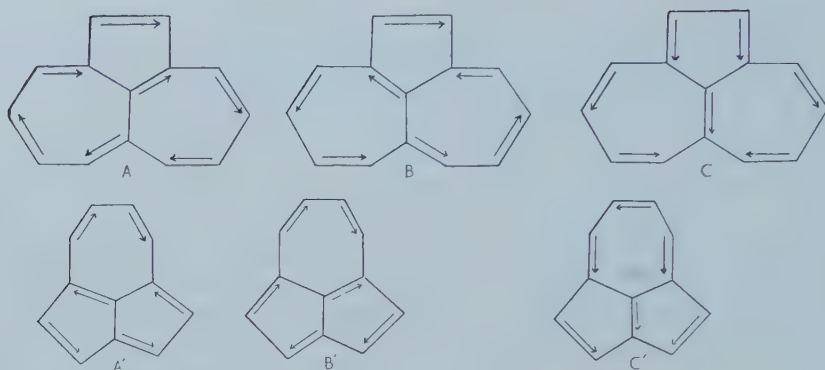
Figure 1.

The structures A ... C′ are the only Kekulé structures for the two molecules: but they do not belong to any canonical set, as defined by the usual technique of Rümer diagrams. If we arrange the atoms in such a diagram so that A and B both obey the non-crossing rule, then C will show crossing. If this crossing is resolved in the usual way, it will be found that C is the sum of at least two excited canonical structures from the set containing A and B. This makes no fundamental difference either to the calculations or to their interpretation, for the Rümer diagram is only a very convenient technique for obtaining a complete set of linearly independent singlet structures, and it has no chemical significance whatever. In the case of the heptalene compound I, structure C is important because it is only in this structure that the bonds 1—1′, 2′—10 and 11—12 are double bonds. A similar role is played by structure C′ in molecule II. The extent of complete conjugation will therefore be revealed by the weight of this structure C (or C′). Now C can be shown to have equal and opposite matrix components with the two Kekulé structures, so that it will have no interaction with A + B, but will have strong interaction with A − B. If this interaction is sufficiently strong it may succeed in lowering A − B below A + B and hence affecting the symmetry of the ground and excited states. (We are indebted to Professor H. C. Longuet-Higgins for pointing out the importance of this third structure.) These molecules belong to the space group $C_{2v}$. The symmetry operations of this group are E, $C_2$, $\sigma_v$ (reflection in the symmetry plane perpendicular to the plane of the molecule) and $\sigma_v'$ (reflection in the plane of the molecule). The transformations of A, B, C under the operations of this group are shown in the table:

|   | E | $C_2$ | $\sigma_v$ | $\sigma_v'$ |
|---|---|---|---|---|
| A | A | − B | − B | A |
| B | B | − A | − A | B |
| C | C | C | C | C |
| $\chi$ | 3 | 1 | 1 | 3 |

Thus the group is resolved according to the rule
$$\Gamma = 2A_1 + B_2$$
and the bases of the corresponding irreducible representations are
$$\Gamma (A_1); \quad A - B \text{ and } C$$
$$\Gamma (B_2); \quad A + B.$$

Matrix elements between A, B, C may be found using Pauling's rule [9]. The table below shows the three eigenvalues (in terms of the Coulomb integral $Q$ and exchange integral $\alpha$), together with the corresponding normalized wave functions, for both molecules.

<div align="center">

Molecule I

| Eigenvalue | Normalized wave function | Symmetry |
|---|---|---|
| $E_1 = Q + 2.897\alpha$ | $\psi = 0.426(A - B) - 0.753\,C$ | $A_1$ |
| $E_2 = Q + 2.727\alpha$ | $\psi = 0.696(A + B)$ | $B_2$ |
| $E_3 = Q + 1.762\alpha$ | $\psi = 0.582(A - B) + 0.664\,C$ | $A_1$ |

Molecule II

| | | |
|---|---|---|
| $E_1 = Q + 2.50\alpha$ | $\psi = 0.667(A + B)$ | $B_2$ |
| $E_2 = Q + 2.305\alpha$ | $\psi = 0.359(A - B) + 0.836\,C$ | $A_1$ |
| $E_3 = Q + 0.938\alpha$ | $\psi = 0.669(A - B) - 0.556\,C$ | $A_1$ |

</div>

Thus according to these calculations I is genuinely aromatic, with a totally symmetric ground state. But II is pseudo-aromatic, with a $B_2$ ground state. Part of the explanation for this lies in the fact that the coefficient of the exchange integral in the matrix component between A and C is almost twice as large as between A and B. Thus C interacts strongly with $A - B$. In the case of molecule II, $C'$ interacts less strongly with $A' - B'$, the coefficient of the same exchange integral in the matrix component between $A'$ and $C'$ now being actually smaller than between $A'$ and $B'$. In the case of the heptalene derivative I we could represent the successive introduction of A, B, C schematically as follows, figure 2:
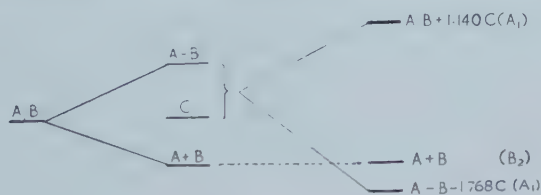


Figure 2.

It is gratifying that this simple theory should so nicely illustrate Hafner's experimental results.

The argument just given would have been more convincing if the calculated energy differences between the two ground states and the corresponding first-excited states, had been rather larger. In fact they are small, and we know from Craig's work on benzene that in that case the inclusion of ionic structures lowers the $B_{2u}$ state $0.46\alpha$ more than it lowers the $A_{1u}$ state. This difference is greater than the differences between the $A_1$ and $B_2$ states in I and II. But the following comments may be made in partial justification for our conclusions.

The charge distributions obtained later by molecular-orbital calculations do not indicate any marked difference between the role of ionic structures in I and II. So far as I is concerned, the agreement of our calculations both with its observed stability and with the MO calculations strongly suggests that here the $B_2$ energy is not lowered through ionic and other additional resonance as much as $0.17\alpha$ more than the $A_1$ energy is lowered. For if it were, the order of $A_1$ and $B_2$ would be interchanged. Such a change would then leave $B_2$ in molecule II between $0.2\alpha$ and $0.4\alpha$ lower than $A_1$. In fact, in order to alter the sequence for molecule II we

should need to suppose that ionic and other additional resonance operated in the same relative way for the A and B symmetries of benzene but in an opposite way for II.   This would seem unlikely, and may be regarded as partial justification for our conclusions that I is almost certainly aromatic, and II may possibly be pseudo-aromatic.

### 4. Semi-empirical lcao mo calculations

There is a difficulty in applying the simple Hückel-type mo treatment to I and II.   These molecules are non-alternants, for which the starring process of Coulson and Rushbrooke [10] cannot be carried through.   In such a case there are non-uniform distributions of charge on the various carbon atoms, with the result [10] that the simple treatment is not self-consistent.   But the charge displacements (see later) are not large, and we may therefore hope to get qualitatively reliable results in this approach.   In the case of I, where both mo and vb approximations lead to a totally symmetric ground state, we may accept the mo results with more confidence than in the case of II, where the two theories predict different symmetries.

Before coming to these mo calculations there is one suggestive (but not rigorous) way of looking at the difference between I and II, to which our attention has been drawn by Dr. S. L. Altmann.   We have shown below (VIII and IX) the perimeter-model diagrams of I and II, in the spirit of recent work by Moffitt and others. Let us first put all the $\pi$-electrons into orbitals associated with the perimeter, and then allow them to move on to the isolated central carbon atom.   The advantage of this is that the perimeter is a cyclic polyene, with 13 and 11 carbon atoms respectively.   The corresponding energies are as shown in the diagram below, in which all the levels, except the lowest in each case, are doubly-degenerate.



VIII                                          IX



VIII                    IX
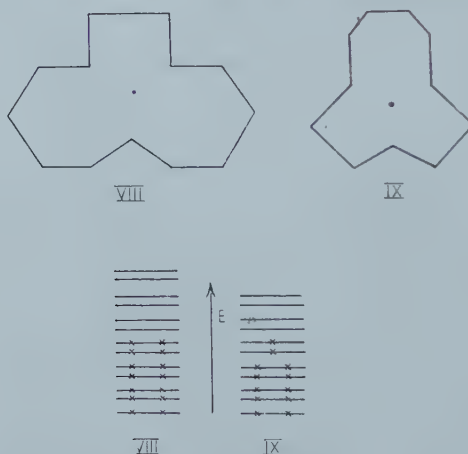
We have 14 and 12 electrons respectively.    These will just fill a complete shell in VIII, as shown by the crosses, but in IX they will half-fill the degenerate fourth level.    Thus VIII belongs to the $4n+2$ class (with $n=3$) and IX to the $4n$ class (also with $n=3$).    So VIII would be expected to be aromatic, but not IX.    Now we allow electrons to flow on to the centre atom.    This will disturb the neat energy relationship just described, but it seems very probable that it would leave the first molecule still aromatic and the second non-aromatic.    Indeed, before the second stage, a Jahn–Teller effect would set in, as in cyclo-octatetraene ($4n$, with

$n=2$) leading to a polyolefinic type of molecule. It is interesting that such a simple account as this can lead to predictions in agreement with experiment. There is one further point about this argument. It may be asked why in the case of VIII, for example, we chose to start with all 14 $\pi$-electrons in the perimeter and none on the internal carbon atom in the centre, in preference to 12 $\pi$-electrons in the perimeter and 2 in the centre. It is true that either of these could be regarded as starting points. But since the second description differs from the first in that two electrons are taken from a bonding orbital (one of the top degenerate ones in the diagram) and are placed in a non-bonding orbital, the energy of the second description is much higher than that of the first. It is therefore a worse starting point. In addition, if we were to take into account electron repulsion terms, this would be even more true, since the mutual Coulomb interaction of two electrons on the central carbon atom would raise the energy of this structure by several electron volts. It is for this reason that our original description is to be preferred.

As for the MO calculations themselves, they follow entirely standard methods. There is no need therefore to describe them in detail. On account of the $C_{2v}$ symmetry the secular determinant factors into two parts, one corresponding to symmetrical ($b_1$) and the other antisymmetrical ($a_2$) molecular orbitals. The secular determinant gives the individual orbital energies. When the overlap integral $S \equiv \int \phi_i \phi_j d\tau$ is neglected, as in the simple Hückel treatment, these energies are all of the form $E = \alpha + k\beta$, where $\alpha$ is the Coulomb term for a carbon atom, $\beta$ is the C—C resonance integral, and $k$ is a constant for each level, found from the secular determinant. But when the overlap integral between adjacent $\pi$-orbitals is included (actually given the numerical value $\frac{1}{4}$), Wheland [11] has shown that the energies take the equally simple form $E = \alpha + m\gamma$, where $\gamma$ is a new resonance integral defined by $\gamma = \beta - S\alpha$, and $m$ is given in terms of $k$ by the relation $m = k/(1 + kS)$. A knowledge of these energies now leads to a calculation of the LCAO coefficients, and hence the charges and $\pi$-bond orders [12]. The bond orders $p$ may now be converted into bond lengths $x$ by using the standard formula derived by one of us [12]

$$x = s - \frac{s-d}{1 + K(1-p)/p} \tag{1}$$

in which $s$, $d$, $t$ are the carbon–carbon single, double and triple bond lengths, here taken to be 1·540, 1·340 and 1·204 Å respectively, and $K$ is a constant (0·8095) chosen so that the lengths $x$ are correct when $p = 0$, 1 and 2. It is probable that, since we are dealing with $sp^2$ trigonally hybridized carbon atoms, the effective single bond length should be about 1·51 Å instead of 1·54 Å, which refers to $sp^3$ tetrahedral hybrids. But since the larger value has almost universally been used in earlier estimations of the lengths of carbon–carbon bonds, we have adhered to it ourselves. This makes no difference, of course, to the sequence of lengths, but it does imply that the last figure in the quoted lengths is of no significance except for purposes of comparison. Table 1 gives the energies of the molecular orbitals for both molecules, and table 2 gives the bond lengths.

The numbers quoted are the values of $m$ in the energy relation $E = \alpha + m\gamma$[†]. Orbitals with label A are antisymmetric with respect to the reflection $\sigma_v$, the others

---

[†] Most of these energies have previously been calculated by M. E. Dyatkina and E. M. Shustorovitsch (*Doklady Akad. Nauk SSRS*, 1957, **117**, 1021) in terms of $\beta$ (i.e. with neglect of overlap). They agree with our own values to the accuracy quoted by Dyatkina and Shustorovitsch.

| Molecule I | | | | | | | |
|---|---|---|---|---|---|---|---|
| Bonding | 1·518 | 1·232 | 1·227(A) | 0·993 | 0·885(A) | 0·637 | 0·227(A) |
| Anti-bonding | −0·359 | −0·862(A) | −1·004 | −2·392(A) | −3·741 | −3·774(A) | −5·103 |
| Molecule II | | | | | | | |
| Bonding | 1·531 | | 1·197 | 1·184(A) | 0·800 | 0·688(A) | 0·429 |
| Anti-bonding | −0·306(A) | | −0·697 | −1·947(A) | −3·623 | −3·689(A) | −4·765 |

Table 1.    Energies of molecular orbitals.

| Molecule I | | | | | | | | | |
|---|---|---|---|---|---|---|---|---|---|
| Bond | 1–2 | 2–3 | 3–4 | 4–5 | 5–12 | 11–12 | 11–1 | 1–1′ | 1–2′ |
| Length | 1·425 | 1·388 | 1·416 | 1·388 | 1·426 | 1·419 | 1·434 | 1·414 | 1·395 |
| Molecule II | | | | | | | | | |
| Bond | 1–2 | 2–3 | 3–10 | 10–9 | 1–9 | 10–4 | 4–5 | 5–6 | |
| Length | 1·429 | 1·383 | 1·427 | 1·436 | 1·414 | 1·410 | 1·400 | 1·403 | |

Table 2.    Bond lengths (Å) calculated by MO method.
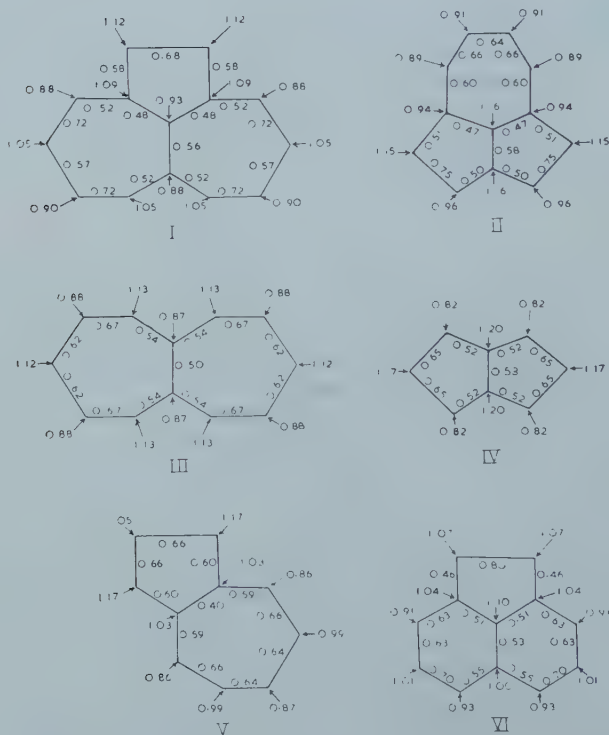


Figure 3.

are symmetric. The correct group theory designations are $a_2$ for the antisymmetric (A) orbitals, and $b_1$ for the symmetric (S) orbitals. In the lowest configuration all the bonding orbitals are doubly occupied, all the anti-bonding ones are empty. Table 2 gives the bond lengths calculated by the use of equation (1). The bonds not listed in this table may be found by symmetry from those that are. Table 3 shows a few significant comparisons between molecules I and II and pentalene [5, 10], heptalene [13], azulene [14] and acenaphthylene [15]. Finally figure 3 gives the molecular diagrams (charges on atoms and $\pi$-bond orders) for all six molecules.

| Molecule | I | II | Heptalene | Pentalene | Azulene | Acenaphthylene |
|---|---|---|---|---|---|---|
| Resonance energy | 2·241 | 2·059 | 1·464 | 1·087 | 1·597 | 2·273 |
| Resonance energy per carbon atom | 0·160 | 0·172 | 0·122 | 0·136 | 0·160 | 0·189 |
| Lowest excitation energy | 0·586 | 0·735 | 0·337 | 0·421 | 0·871 | 0·856 |

Table 3. Calculated resonance energies (units of $\gamma$).

Several deductions may be drawn from an inspection of figure 3. Thus

(i) Wherever, as in I, II, V and VI, there is a five-membered ring which can draw electrons away from an adjacent six- or seven-membered ring, it does so, tending to establish a local 'aromatic sextet'. Similarly whenever, as in I, II and V, there is a seven-membered ring which can give electrons to an adjacent five- or six-membered ring, it does so, tending again to establish a local aromatic sextet. A comparison of I with III, or II with IV, shows how the bridge can either accept or donate superfluous electrons for this purpose.

(ii) The olefinic bridge in acenaphthylene VI has a very high bond order, suggesting that in the ground state there is little conjugation with the naphthalene region. But just the opposite is true with the heptalene derivative I, which thus appears to be genuinely aromatic throughout.

(iii) In the case of II the bond order of the 2—3 and 1'—2' bonds is high (0·75) and compares with the olefinic bond (0·80) in acenaphthylene. This suggests that there really is less conjugation here than in I, and that, if a more self-consistent calculation were made, allowing for the variation of $\beta$ with bond length, even greater bond orders would be found. It is a plausible conclusion that, in such a case, one of the five-rings would act as a reactive olefinic bridge joining the 1 : 8 positions in azulene. There is a much smaller tendency for this to happen in I. Something of this kind may be responsible for the great experimental differences found by Hafner for these two molecules.

(iv) It is possible to use the charge distribution in figure 3 to estimate the contribution $\mu_\pi$ which the $\pi$-electrons make to the molecular dipole moment (the resonance moment). Our results are that $\mu_\pi$(molecule)/$\mu_\pi$(azulene) is about $\frac{2}{3}$ for I and about $\frac{3}{4}$ for II. We do not give the exact values of $\mu_\pi$ but have preferred to give the ratio relative to azulene because, as Wheland and Mann [16] showed for the case of azulene, $\mu_\pi$ is very sensitive to any allowance that may be made in the Coulomb terms, as a result of charge migrations. It seems likely, however, that $\mu_\pi$ would be modified to about the same extent in I, II and azulene. If so, our estimated $\mu_\pi$ for I is 0·7D and for II 0·8D. But we do not claim very great reliability for these estimates.

It is worth while to refer briefly to the lower electronic transitions predicted by our simple MO treatment.  Now on account of its failure to take adequate account of varying spin multiplicity, these calculations strictly refer to the centre of the associated singlet and triplet 0–0 transitions, and should therefore be interpreted as locating the appropriate bands in only an approximate manner.  In addition, no account has been taken of configuration interaction, sometimes known to be important in affecting the order of the transitions [17].  Table 4 shows the energies of the lowest two states, for molecules I, II and azulene, together with their appropriate symmetries.  This table shows that the observed displacement of the first absorption maximum of I to longer wavelengths as compared with azulene can be very easily accounted for from these calculations.

|  | Molecule I | Molecule II | Azulene |
|---|---|---|---|
| Lowest state | $14\alpha+13\cdot441\gamma$ (A$_1$) | $12\alpha+11\cdot659\gamma$ (A$_1$) | $10\alpha+9\cdot596\gamma$ |
| First excited state | $14\alpha+12\cdot855\gamma$ (B$_2$) | $12\alpha+10\cdot923\gamma$ (B$_2$) | $10\alpha+8\cdot725\gamma$ |
| Difference | $0\cdot586\gamma$ | $0\cdot735\gamma$ | $0\cdot871\gamma$ |

Table 4.   Total energies of lowest two states.

The lowest two transitions in I, II and azulene are shown in table 5.   In the last column of this table we have converted from excitation energies computed in terms of the resonance integral $\gamma$ to wavelengths $\lambda$ in m$\mu$ by taking $\gamma = -2\cdot041$ ev.  This value—which lies in the region of acceptable $\gamma$—gives approximately the correct excitation energy for azulene, and would lead us to expect roughly the

| Transition | Description of electron jump | | Excitation energy | $\lambda$(m$\mu$) calc. | $\lambda$(m$\mu$) obs. |
|---|---|---|---|---|---|
| | | Molecule I | | | |
| $N_1 \rightarrow V_1$ | $a_2 \rightarrow b_1$ | Allowed | $0\cdot586\gamma$ | 1037 | 1073 |
| $N_2 \rightarrow V_1$ | $b_1 \rightarrow b_1$ | Forbidden | $0\cdot996\gamma$ | 610 | — |
| $N_1 \rightarrow V_2$ | $a_2 \rightarrow a_2$ | Forbidden | $1\cdot089\gamma$ | 558 | — |
| $N_1 \rightarrow V_3$ | $a_2 \rightarrow b_1$ | Allowed | $1\cdot232\gamma$ | 493 | — |
| | | Molecule II | | | |
| $N_1 \rightarrow V_1$ | $b_1 \rightarrow a_2$ | Allowed | $0\cdot735\gamma$ | 826 | 475 |
| $N_2 \rightarrow V_1$ | $a_2 \rightarrow a_2$ | Forbidden | $0\cdot994\gamma$ | 611 | — |
| $N_1 \rightarrow V_2$ | $b_1 \rightarrow b_1$ | Forbidden | $1\cdot126\gamma$ | 539 | — |
| $N_1 \rightarrow V_3$ | $b_1 \rightarrow a_2$ | Allowed | $2\cdot374\gamma$ | 256 | — |
| | | Azulene | | | |
| $N_1 \rightarrow V_1$ | $a_2 \rightarrow b_1$ | Allowed | $0\cdot871\gamma$ | 697 | (697) |
| $N_2 \rightarrow V_1$ | $b_1 \rightarrow b_1$ | Forbidden | $1\cdot171\gamma$ | 519 | 353 |
| $N_1 \rightarrow V_2$ | $a_2 \rightarrow a_2$ | Forbidden | $1\cdot331\gamma$ | 456 | — |
| $N_1 \rightarrow V_3$ | $a_2 \rightarrow b_1$ | Allowed | $3\cdot036\gamma$ | 200 | — |

All these are calculated with $\gamma = -2\cdot041$ ev$= -47$ kcal/mole, which gives correctly the longest wavelength transition for azulene.

Table 5.   $N \rightarrow V$ transitions.

correct values for I and II. The situation so far as I is concerned is very satis-
factory. But for II, where our agreement with experiment is less satisfactory,
our conclusions are provisional until the true nature of the ground state has been
settled. In both I and II no account has been taken of the hyperconjugative
effect of the two methyl substituents. This (see later) is quite small compared
with the other energy differences in this table. But the observed deep red colour
of molecule I finds a ready explanation from these figures.

It is convenient at this stage to refer back to a possibility previously mentioned.
If there had been several low-lying configurations of molecule II with symmetry $B_2$
it might have been possible, by mutual interaction of these configurations, to
lower the lowest $B_2$ state below the lowest $A_1$ state, and so get agreement with the
valence bond calculations. But tables 1 and 5 show that there are no such low-
lying configurations. Hence the disagreement between the VB and MO con-
clusions for molecule II cannot be resolved in this way. Nor have we any
alternative suggestion to propose.

## 5. REACTIVITIES

Two chief methods are used to predict the reactivity of conjugated molecules
for electrophilic, nucleophilic and radical substitution reactions. In the first
we use the charge densities (see figure 3) and free valences. In the second we
compute localization energies ($A_e$, $A_n$, $A_r$ respectively). It has been found that in
most alternant hydrocarbons these two methods are in complete agreement as to
the positions at which these three types of reaction occur. But in non-alternants
this situation is not always found. We have therefore calculated the three
types of localization energies. They are shown in table 6, in units of the resonance
integral $\gamma$. The lowest values in each column are shown in italics. These show
the predicted points of substitution.

| Position | Molecule I | | | Position | Molecule II | | |
|---|---|---|---|---|---|---|---|
| | $A_e$ | $A_n$ | $A_r$ | | $A_e$ | $A_n$ | $A_r$ |
| 1' | 1·419 | 1·927 | 1·673 | 1' | 1·695 | 1·330 | *1·512* |
| 2 | 1·508 | *1·246* | *1·377* | 2' | *1·391* | 1·823 | 1·607 |
| 3 | 1·394 | 1·817 | 1·606 | 7 | 1·824 | *1·296* | 1·560 |
| 4 | 1·712 | 1·353 | 1·533 | 6 | 1·897 | 1·373 | 1·635 |
| 5 | *1·295* | 1·589 | 1·442 | | | | |

Table 6. Localization energies (in units of $-\gamma$).

In the case of I position 5 is the most reactive site for electrophilic reactions,
although, according to figure 3, the olefinic bridge atoms 1' and 2' carry distinctly
more charge. But position 2 is the best for nucleophilic reactions, in agreement
with the charges in figure 3. Agreement is also obtained for radical reactions,
where positions 2 and 5 have the same free valence and almost the same $A_r$.
In molecule II the agreement between localization energies, charges and free
valences is perfect for all three types of reaction. Thus the only point of diver-
gence concerns positions 5 and 1' in, I for electrophilic reactions. There is some
evidence that in this case the charge distribution is the more correct, since Hafner
reports that I undergoes formylation by the Vilismeier reaction at the bridge atom 1'.
But further comparisons must wait until more experimental results are available.

In particular, if II is pseudo-aromatic, as we believe, it will probably show little substitutional reactivity at all. In this connection we may refer to some recent work of Peters [18], who has suggested that a $\pi$-electron molecule may be expected to show aromatic behaviour if all the localization energies are greater than approximately 80 per cent of the value found for benzene. In units of $\beta$, this implies values greater than about $2 \cdot 0\beta$. If we work in terms of the resonance integral $\gamma$, as in this paper, the critical value would be

$$0 \cdot 80 \times 1 \cdot 850\gamma = 1 \cdot 48\gamma.$$

A glance at table 6 shows that with only one exception ($A_r$ for molecule II) the smallest localization energies are considerably less than $1 \cdot 48\gamma$. So we may conclude that, according to this criterion, neither molecule should show characteristic aromatic reaction properties.

Finally we discuss the dienophile character of I and II. It has been shown by R. D. Brown [19] that the paralocalization energy associated with a given pair of suitably oriented carbon centres bears a good correlation with the ease of Diels–Alder addition of maleic anhydride. Further, it is possible to calculate relative rates of addition if we may suppose that the entropy factor is constant. We have therefore calculated the rates for such Diels–Alder reactions with I and II. The results are in the table below.

| Compound | Para-localization energy | Rate constant for compound relative to Rate constant for 9 : 10 positions in anthracene | |
|---|---|---|---|
| | | (a) $\gamma = -34$ kcal/mole | (b) $\gamma = -47$ kcal/mole |
| I | $-2 \cdot 24\gamma$ | $4 \cdot 5 \times 10^{-5}$ | $1 \cdot 64 \times 10^{-6}$ |
| II | $-2 \cdot 57\gamma$ | $2 \cdot 54 \times 10^{-13}$ | $1 \cdot 15 \times 10^{-17}$ |

Since we have no guarantee that the value of $\gamma$ appropriate to these reactions is the same as that required for ultra-violet spectra, we have calculated these rates both (a) with $\gamma = -34$ kcal/mole, a value which has often been used for this purpose in the past, and (b) with $\gamma = -47$ kcal/mole, the value we have already found suitable for the electronic transitions of table 5. It is clear from the table that I and II should differ considerably in this reaction. With I the reaction should be slow, but with II it should be quite unobservable. It is gratifying to report that Hafner, in a private communication, has informed us that the heptalene derivative I does undergo Diels–Alder addition at the positions 2 and 5 for which our calculations were made. For all other geometrically possible positions the rate would be far slower. The dienophilic activity of 2 and 5 in I is very reasonable when it is realized that (i) the sum of the free valences is a maximum for these two positions, and (ii) the residual molecule consists of azulene + a double bond: this is the most stable residual molecule that can be obtained, starting from I.

## 6. FREE-ELECTRON MO CALCULATIONS

In the FE method the $\pi$ electrons are supposed to move with no mutual interaction other than that implied by the Exclusion Principle, along the lines joining adjacent nuclei. Thus the electrons move on a network of linear segments, in each of which the wave function satisfies the one-dimensional Schrödinger

equation (in atomic units)

$$-\tfrac{1}{2}\frac{d^2\psi_i(x_i)}{dx_i{}^2} = E\psi_i(x_i).$$

The conditions of finiteness, single-valuedness, continuity and the Hermitian character of the Hamiltonian prescribe all that is needed to determine the allowed $E$ values (see e.g. [20, 21]). If we put $E = \tfrac{1}{2}\lambda^2$, then along each segment $\psi$ takes the form

$$\psi_i = A_i \cos \lambda x_i + B_i \sin \lambda x_i.$$

Ruedenberg and Scherr [21] have given a matrix formulation which determines the $\lambda$ easily; and from this, with the conditions for normalization, each $A_i$ and $B_i$ is obtained. The charge density at a point whose coordinate is $x_i$ is now defined as

$$\rho(x_i) = 2 \sum_i |\psi_i(x_i)|^2$$

where the summation extends over all the occupied molecular orbitals. Table 7 below shows the calculated energies for all the occupied and the two lowest unoccupied orbitals, together with their symmetry assignments, as in table 1.

| Molecule I | | | | | | | |
|---|---|---|---|---|---|---|---|
| Bonding | 0 | 0·595(A) | 0·814 | 1·741 | 2·131(A) | 2·907 | 4·152(A) |
| Anti-bonding | 5·704 | 7·141 | | | | | |

| Molecule II | | | | | | |
|---|---|---|---|---|---|---|
| Bonding | 0 | 0·770 | 1·079(A) | 2·565(A) | 2·617 | 3·668 |
| Anti-bonding | 5·581(A) | 6·675 | | | | |

Table 7. Free-electron energies of molecular orbitals (ev).

In this table the C—C distance $a$ has been taken equal to 1·40 Å.

The charge densities at the positions of the nuclei, calculated from the previous formula for $\rho(x_i)$ are shown below. These are in units of $1/a$ for all except the 'internal' carbon atoms, where, as Griffiths and others have shown, it is more appropriate to express them in units of $\tfrac{2}{3}a$.

| Molecule I | | | | | | | | |
|---|---|---|---|---|---|---|---|---|
| Atom | 1 | 2 | 3 | 4 | 5 | 11 | 12 | 1' |
| Charge | 1·109 | 0·903 | 1·046 | 0·915 | 1·044 | 0·907 | 0·861 | 1·100 |

| Molecule II | | | | | | | |
|---|---|---|---|---|---|---|---|
| Atom | 1 | 2 | 3 | 4 | 5 | 9 | 10 |
| Charge | 1·183 | 0·960 | 1·118 | 0·902 | 0·920 | 1·180 | 0·918 |

The close agreement between these sets of charges and those shown in figure 3 is astonishing.

It is possible to use the energies of table 7 to calculate the possible electronic transitions, assuming that these arise from a one-electron jump from an occupied orbital to one or other unoccupied level. The results are shown in the following

table, from which it will be seen that the FE method also predicts an absorption at very long wavelengths. With a highly simplified treatment of this kind, it would be unreasonable to expect anything like exact agreement, particularly if it is remembered that there are no disposable parameters whatever involved in table 8.

| Transition | Description of electron jump | | $\lambda(m\mu)$ calc. | $\lambda(m\mu)$ obs. |
|---|---|---|---|---|
| | | Molecule I | | |
| $N_1 \to V_1$ | $a_2 \to b_1$ | Allowed | 799 | 1073 |
| $N_2 \to V_1$ | $b_1 \to b_1$ | Forbidden | 443 | — |
| $N_1 \to V_2$ | $a_2 \to b_1$ | Allowed | 415 | — |
| | | Molecule II | | |
| $N_1 \to V_1$ | $b_1 \to a_2$ | Allowed | 648 | 475 |
| $N_2 \to V_1$ | $b_1 \to a_2$ | Allowed | 418 | — |
| $N_1 \to V_2$ | $b_1 \to b_1$ | Forbidden | 412 | — |

Table 8. Calculated $N \to V$ transitions (FE method).

## 7. INCLUSION OF HYPERCONJUGATION

We have repeated the molecular-orbital calculations reported earlier in this paper by allowing for the hyperconjugative interaction of the two methyl groups with the $\pi$-electrons of the rings. The following parameters were used

$$\alpha_{(H_3)} = \alpha_C - 0.5\beta_{CC}, \quad \alpha_{(C \text{ in } CH_3)} = \alpha_C - 0.1\beta_{CC},$$

$$\beta_{C-CH_3} = \beta_{CC}\exp{-5.686(1.54-1.39)} = 0.43\beta_{CC},$$

$$\beta_{C=H_3} = 2.5\beta_{CC},$$

where $\alpha_C$ and $\beta_{CC}$ refer to the appropriate values for benzene. This inclusion of hyperconjugation changes the $\pi$-electron densities and bond orders in the rings by only a few units in the third place of decimals. Thus the maximum changes in charge distribution are $0.005$ electrons in position 5 of I and $0.004$ electrons in position 5 of II. The maximum changes in bond orders are $0.007$ for the bond 6—7 of I and $0.006$ for the bond 4—10 of II. This confirms that the methyl groups do not play any decisive role in the equilibrium structures of these molecules and can therefore be safely left out of consideration.

## 8. CONCLUSION

In summary, we can say that all three treatments—i.e. valence bond, molecular orbital and free electron—agree in predicting that the heptalene derivative I should be aromatic. All treatments agree that the pentalene derivative II should differ substantially from I, but whereas the VB method suggests that the molecule is pseudo-aromatic, the other methods suggest that it should have characteristics of a cyclic polyolefin. One likely possibility would be that it should resemble a normal azulene molecule bridged by a near-double bond at positions 1 and 8.

This view is in accord with Hafner's observation [3] that in the presence of tetra-cyanoethylene molecule II gives a violet addition product whose structure is almost certainly X.



$\underline{\Sigma}$
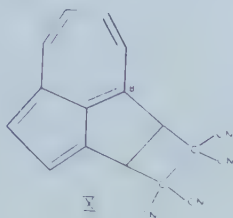
We would like to express our sincere thanks to Professor J. D. Roberts for drawing our attention to this problem, to Dr. K. Hafner for providing us with certain information before publication, to Professors H. C. Longuet-Higgins, F.R.S. and D. P. Craig and to Dr. S. L. Altmann for valuable discussion and criticism, to a referee for suggesting the calculation of localization energies and certain other improvements in presentation, and to Dr. J. S. Rollett for help in computing eigenvalues and eigenvectors of the matrix on the Oxford University Mercury computer. One of us (M.A.A.) would also like to acknowledge the award of the Lytton Moslem scholarship from the Government of West Bengal, during the tenure of which this study was undertaken.

## REFERENCES

[1] HAFNER, K., and SCHNEIDER, J., 1958, *Angew. Chem.*, **70**, 702; 1959, *Liebigs Ann. Chem.*, 624, 37.
[2] BLOOD, C. T., and LINSTEAD, R. P., 1952, *J. chem. Soc.*, p. 2263.
[3] Private communication to the authors.
[4] CRAIG, D. P., 1952, *J. Chim. phys.*, **49**, 143.
[5] CRAIG, D. P., and MACCOLL, A., 1949, *J. chem. Soc.*, p. 964.
[6] CRAIG, D. P., 1951, *J. chem. Soc.*, p. 3175.
[7] LONGUET-HIGGINS, H. C., 1958, Chem. Soc. Special Publication No. 12, the ' Kekule Symposium ' at London, p. 17.
[8] COULSON, C. A., 1953, *Proc. Phys. Soc. Lond.*, A, **116**, 652.
[9] PAULING, L., 1933, *J. chem. Phys.*, **1**, 280.
[10] COULSON, C. A., and RUSHBROOKE, G. S., 1940, *Proc. Camb. phil. Soc.*, **36**, 193.
[11] WHELAND, G. W., 1941, *J. Amer. chem. Soc.*, **63**, 2025.
[12] COULSON, C. A., 1939, *Proc. roy. Soc. A*, **169**, 413.
[13] *Dictionary of values of Molecular Constants*, edited by C. A. COULSON and R. DAUDEL, Vol. 3, p. 22.
[14] COULSON, C. A., and LONGUET-HIGGINS, H. C., 1947, *Rev. Sci.*, Paris, **85**, 929.
[15] CRAWFORD, V. A., and COULSON, C. A., 1948, *J. chem. Soc.*, p. 1990.
[16] WHELAND, G. W., and MANN, D. E., 1949, *J. chem. Phys.*, **17**, 264.
[17] DEWAR, M. J. S., and LONGUET-HIGGINS, H. C., 1954, *Proc. phys. Soc. Lond. A*, **67**, 795, and later papers by one or both authors.
[18] PETERS, D., 1960, *J. chem. Soc.*, p. 1274.
[19] BROWN, R. D., 1950, *J. chem. Soc.*, p. 2730.
[20] GRIFFITH, J. S., 1953, *Trans. Faraday Soc.*, **49**, 345; *Proc. Camb. phil. Soc.*, **49**, 650.
[21] RUEDENBERG, K., and SCHERR, C. S., 1953, *J. chem. Phys.*, **21**, 1565.

# Electron spin resonance of $(CO_2H)CH_2$–$\dot{C}H(CO_2H)$ in succinic acid

by D. POOLEY and D. H. WHIFFEN

The Chemistry Department, The University, Birmingham 15
and The Basic Physics Division, National Physical Laboratory, Teddington

Electron spin resonance investigations on a $\gamma$-irradiated single crystal of succinic acid have confirmed and extended the findings of Heller and McConnell on the hyperfine couplings in the radical $(CO_2H)\dot{C}H$–$CH_2(CO_2H)$. Complete coupling tensors, and the g tensor, are given in the table. These confirm that the radical has almost the same orientation as the unchanged molecules. The plane of the free radical carbon is twisted $5°$ from the original carbon skeleton plane and this leads to appreciable non-equivalence of the hydrogen atoms of the $CH_2$ group.

## 1. Introduction

It is of interest to measure the hyperfine coupling constants in free radicals by means of their electron resonance spectra. The anisotropic couplings between the unpaired electron and a hydrogen attached to the free radical carbon centre, commonly designated an $\alpha$ hydrogen, have been studied in a number of cases, notably radicals derived from glycine [1], glycollic acid [2] and its ion [3], malonic acid [4], and $\alpha$-alanine [5]. The hydrogen atoms on the next carbon, $\beta$ hydrogens, are less well known and preliminary studies showed that the radical formed on irradiation of succinic acid with $\gamma$-rays gave a relatively simple spectrum and showed large $\beta$ hydrogen couplings. Independently Heller and McConnell obtained the same radical with x-irradiation and have published [6] an interpretation of the spectra for a limited number of crystal orientations. The present investigation confirms all their observations and their interpretation is accepted. However, it has been possible to interpret the spectra of further crystal orientations which were not studied in detail by Heller and McConnell and the complete intramolecular coupling tensors are now available for discussion.

## 2. Experimental

The measurements were made with a spectrometer working at 9200 Mc/s [7] which has been modified to work with 100 kc/s field modulation [8] to give improved sensitivity. The crystals of succinic acid were grown from water by slow cooling and were irradiated with $^{60}$Co $\gamma$-rays to the extent of several M rad at room temperature and were studied at room temperature. Other experimental details are to be found in earlier publications [1, 2].

The crystal structure has been studied by Robertson and co-workers [9, 10] and the present results are discussed in relation to right-handed Cartesian axes, $X'$, $Y$ and $Z'$ introduced by these authors. The crystal was rotated about these axes in turn and spectra observed at $10$ intervals; also the two skew positions corresponding to the steady magnetic field parallel to the directions with cosines $(3^{-1/2}, \pm 3^{-1/2}, 3^{-1/2})$ and $(3^{-1/2}, \pm 3^{-1/2}, -3^{-1/2})$ were studied. As

expected for a monoclinic crystal with the b-axis coinciding with $Y$, spectra for the magnetic field along $(l, m, n)$ and $(l, -m, n)$ were identical. As observed by Heller and McConnell [6], the spectra obtained with the magnetic field parallel or perpendicular to the b-axis could be interpreted in terms of one magnetically distinguishable radical with the structure $(CO_2H)CH_2-\dot{C}H(CO_2H)$; in agreement with the crystal structure other orientations gave spectra which were a superposition of two chemically equivalent radicals in distinguishable orientations.

The spectra were interpreted in terms of a spin Hamiltonian [2]

$$\mathscr{H} = -\beta \mathbf{S} \cdot g \cdot \mathbf{H}_0 + h \sum_j \mathbf{S} \cdot T^j \cdot \mathbf{I}^j.$$

The tensors were assumed to be symmetrical [11] as $g$ variations are small. The direct coupling of the nucleus to the magnetic field was omitted since it has little effect on the observed spectra at 9200 Mc/s when all the coupling constants, except those discussed in §3.4, are as large as they are in the present case. Its omission greatly simplifies the calculation of spectra from trial coupling tensors.

The results are given in the table. Throughout this table there is a complete linking of upper and lower signs which refer to the magnetically distinguishable radicals. It is believed that all tensor elements are accurate to $\pm 2$ Mc/s and that the direction cosines of principal axes associated with strong anisotropy are correct to $\pm 6°$. However, where cylindrical or spherical symmetry is approached the axes are less accurately determined.

| Tensor in relation to $X'YZ'$ axes | | | | Principal values | Iso-tropic com-ponent | Anisotropic component | |
|---|---|---|---|---|---|---|---|
| | | | | | | Principal values | Direction cosines |
| H($\alpha$) | $+60$ | $\mp 21$ | $-14$ | $(-)$ 92 | | $(-)31$ | $(-0\cdot58, \pm0\cdot38, +0\cdot72)$ |
| ($-$) | $\mp 21$ | $+45$ | $\pm 8$ | $(-)$ 59 | $(-)$ 60 | $(+)$ 1 | $(+0\cdot57, \mp0\cdot44, +0\cdot69)$ |
| | $-14$ | $\pm 8$ | $+76$ | $(-)$ 30 | | $(+)30$ | $(+0\cdot59, \pm0\cdot81, +0\cdot04)$ |
| H$_1$($\beta$) | $+96$ | $\mp 4$ | $+ 2$ | $(+)108$ | | $(+)$ 8 | $(+0\cdot30, \mp0\cdot94, -0\cdot12)$ |
| ($+$) | $\mp 4$ | $+106$ | $\pm 2$ | $(+)$ 98 | $(+)100$ | $(-)$ 1 | $(+0\cdot55, \pm0\cdot07, +0\cdot83)$ |
| | $+ 2$ | $\pm 2$ | $+97$ | $(+)$ 93 | | $(-)$ 7 | $(+0\cdot78, \pm0\cdot32, -0\cdot54)$ |
| H$_2$($\beta$) | $+78$ | $\pm 4$ | $0$ | $(+)$ 89 | | $(+)$ 9 | $(+0\cdot27, \pm0\cdot72, +0\cdot65)$ |
| ($+$) | $\mp 4$ | $+81$ | $\pm 7$ | $(+)$ 79 | $(+)$ 80 | $(-)$ 1 | $(+0\cdot83, \pm0\cdot17, -0\cdot53)$ |
| | $0$ | $\pm 7$ | $+81$ | $(+)$ 72 | | $(-)$ 8 | $(+0\cdot49, \mp0\cdot68, +0\cdot55)$ |
| $g$ | $+2\cdot0037$ | $\pm0\cdot0004$ | $-0\cdot0011$ | $2\cdot0045$ | | | $(+0\cdot83, \pm0\cdot18, -0\cdot52)$ |
| ($-$) | $\pm0\cdot0004$ | $+2\cdot0026$ | $\pm0\cdot0000$ | $2\cdot0026$ | $2\cdot0030$ | | $(+0\cdot03, \pm0\cdot93, +0\cdot37)$ |
| | $-0\cdot0011$ | $\pm0\cdot0000$ | $+2\cdot0027$ | $2\cdot0019$ | | | $(+0\cdot55, \mp0\cdot32, +0\cdot77)$ |

Coupling tensors in Mc/s. Upper and lower signs linked throughout table (see text).

Space limitations do not permit the reproduction of all the spectra and the figure merely exemplifies the type of derivative spectrum observed and the positions of equal intensity absorption centres deduced from the tensors of the table. Spectra for two other orientations have been depicted by Heller and McConnell [6]. Quantitative agreement between their work and the present is within experimental errors in all orientations studied by them.
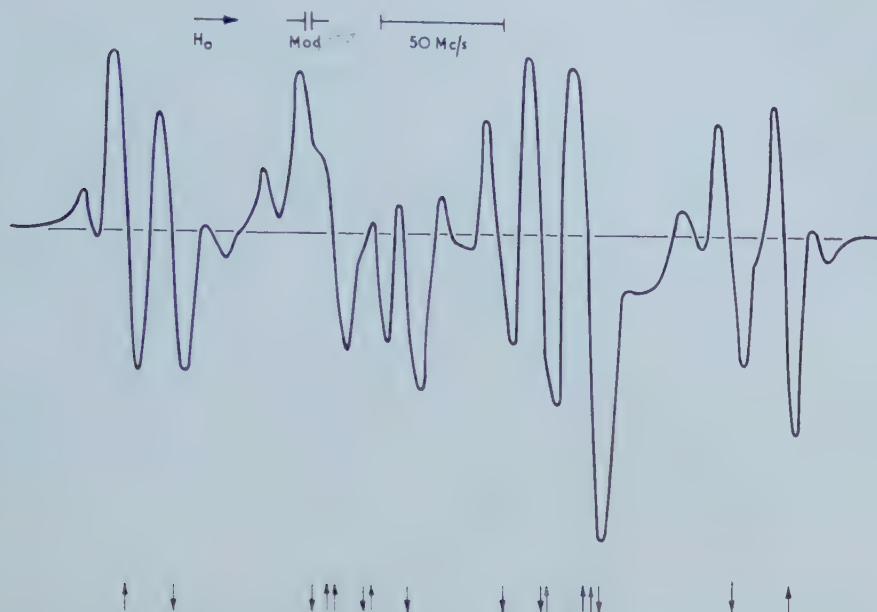
Derivative spectrum for magnetic field parallel to $(-3^{-1/2}, 3^{-1/2}, 3^{-1/2})$. Below are shown individual line positions computed from the table. Arrow heads upwards refer to radicals with the upper signs of the table and arrow heads downwards to the lower signs.

## 3. Discussion

All the evidence confirms the nature of the radical formed to be $(CO_2H)\dot{C}HCH_2(CO_2H)$. Since the undamaged molecule has a centre of symmetry [9, 10], removal of an H atom from either end of the molecule gives magnetically equivalent radicals of which there are two types identified by the upper or lower signs of the table. For the sake of definiteness these tensors, and in particular the directions of their principal axes, can be compared with those to be expected for a radical formed by the removal of an H atom from $C_1'$ in a molecule whose centre is situated at the origin of the unit cell. Full coordinates for this molecule are given in table 4 of reference [10] in terms of the $X'YZ'$ axes used also in the present paper.

### 3.1. *The H($\alpha$) couplings*

Although the two H atoms attached to $C_1'$ are not fully equivalent in the crystal structure it is to be expected that the reorganization which occurs when one is removed is such that the same radical geometry is formed whichever H atom is ejected. The results confirm this view as only one pair of H($\alpha$) tensors is distinguished. The principal values 92, 59 and 30 Mc/s are in close agreement with those observed in related radicals [1, 2, 3, 4] and calculated theoretically [12]. There can be little doubt that these couplings should be given a negative sign and that the C–H bond lies parallel to the axis showing a 30 Mc/s coupling and that the 59 Mc/s axis lies perpendicular to the plane of the carbon radical centre.

F 2

It is reasonable to suppose that the C–H in the radical lies approximately along the internal bisector of the $CH_2$ group from which it is derived and the $sp^2$ plane of the radical centre is approximately that of the carbon chain of the molecule. Cartesian axes parallel to the median line of the carbon chain, $L$, perpendicular to the plane of the carbon atoms, $N$, and the perpendicular direction, $M$, have been introduced by Morrison and Robertson [9]. Taking the exact values of reference [10] the angles between the tensor axes of 92, 59 and 30 Mc/s with $L$, $N$, $M$ respectively are $4°$, $10°$ and $10°$ provided the upper signs of the table are associated with the molecule situated at the unit cell origin as selected by the x-ray workers [9, 10]. The alternative sign choice would give $44°$, $45°$, $64°$ and these values do not accord with the expected parallelism; this second sign association may be rejected for the remainder of this discussion.

It is clear that the $H(\alpha)$ coupling is therefore observed to be in good agreement as regards magnitude and direction with expectations and this gives confidence that such $H(\alpha)$ tensors may be used to orient the radicals in substances where the crystal structure has not been determined.

### 3.2. *The g tensor*

In related radicals [2, 3, 4] it has been found that the minimum value of $g$ lies perpendicular to the radical plane and this is again observed. The axis for which $g = 2 \cdot 0019$ being $8°$ from the $H(\alpha)$ tensor axis of coupling 59 Mc/s and $10°$ from the $N$ axis of the undamaged molecule. The average value of $g$, $2 \cdot 0030$, is slightly greater than the free spin value, $2 \cdot 0023$ in agreement with theoretical expectations [13]. The anisotropy is sufficiently small that the electron is accurately aligned along the magnetic field, as assumed in the calculation of spectra from the hyperfine coupling tensors.

### 3.3. *The $H(\beta)$ tensors*

Both theory [14], and such experimental evidence as exists [1, 15], suggest that the coupling to $\beta$ hydrogen atoms is positive. Heller and McConnell [6] state that the spin density on the carbon 2p orbital provides the greater part of the anisotropic contribution to the $\beta H$ atoms and this is in accord with the size of the anisotropy, $\pm 8$ Mc/s and the $C_1'$ to $\beta H$ distances of $2 \cdot 14$ Å. The most positive coupling should occur when the spins are aligned approximately along the $C_1'$ to H direction and would indeed be exactly along this direction if the odd electron were located exactly at $C_1'$ instead of being distributed in a p orbital. Numbering the H atoms in the same way as in reference [10] it is found that $H_1C_1'$ makes an angle of $2°$ with the principal axis associated with the 108 Mc/s coupling in the second tensor of the table. The $H_2-C_1'$ direction makes an angle of $3°$ with the 89 Mc/s axis of the third tensor. This therefore provides evidence that the tensor labelled $H_1(\beta)$ refers to $H_1$ of reference [10] and $H_2(\beta)$ to $H_2$ and also that the positive sign of the isotropic coupling is correct.

These axes of largest coupling for $H_1$ and $H_2$ make angles of $59°$ and $74°$ respectively with the 59 Mc/s axis of $H(\alpha)$ which is believed to be perpendicular to the plane of the free radical carbon. This means that $H_2$ lies nearer the plane than $H_1$ which is consistent with its reduced isotropic coupling. It is probably unjustified with the present experimental accuracy, to determine the angle of twist of the radical carbon plane relative to the $CH_2$ group from the tensor axes.

But if the coupling is of the form $B \cos^2 \theta$ as suggested by Heller and McConnell [6] and the angle of twist is $\psi$ then the observed coupling constants lead to the two equations

$$B \cos^2 (30 - \psi) = 100$$

and

$$B \cos^2 (30 + \psi) = 80,$$

whose solution is $B = 120$ Mc/s, $\psi = 5°$. These values are reasonable and agree sufficiently with the value $B = 112$ Mc/s derived [6] from the $CH_3$ coupling in $(CH_3)_2 \dot{C}OH$. The direction of twist about $C_1'-C_1$ is such that the plane of the radical lies more nearly parallel to the plane of the adjacent $-COOH$ group than does the carbon plane of the undamaged molecule. The $-COOH$ group is bonded through its hydrogen atoms to neighbouring molecules and is assumed to be unchanged in direction. The principal axes of $H(\alpha)$ make angles of $2°$, $4°$ and $4°$ with the directions to be expected if the radical plane is twisted $5°$ as indicated above. These angles are to be compared with $4°$, $10°$ and $10°$ calculated in §3.1 at which stage in the argument the twist was ignored.

The directions of the remaining axes of the $H(\beta)$ tensor are less accurately known and no clear conclusion can be obtained from them.

### 3.4. *Other hydrogen couplings*

In agreement with reference [13] a number of weak lines was observed in addition to the strong lines interpreted above. Some of these are explained by the couplings already given if the full theory [2, 4, 16] including the Hamiltonian term representing the direct coupling of the proton to the magnetic field is employed to calculate the spectra. However, for many crystal orientations two prominent, if weak, satellites separated by 14 Mc/s from the outside lines of the spectra can be plainly observed. The weak lines at the extreme outsides of the spectra can be seen in the figure. The fuller theory will not explain lines in these positions using only the couplings of the table. They can be explained [16] if there is anisotropic coupling between the electron and other hydrogen atoms provided this coupling is less than the width of individual lines, 9 Mc/s, so that no further splitting of the strong lines is apparent. The lines are too regular in position with respect to their strong neighbours to be due to $^{13}C$ containing radicals [17].

These outer lines were entirely absent from the spectra from a crystal grown from heavy water. Otherwise the spectra showed the normal spectra overlaid in the centre by lines arising from radicals formed from $CO_2D-CH_2-CHD-CO_2D$; the partial exchange of hydrogen attached to carbon was confirmed by the infra-red spectrum. Weak lines from anisotropic coupling to a D atom would be separated from the main lines by only 2 Mc/s and would therefore be unobservable. This experiment shows that the extra coupling of the normal spectra is to H atoms in a carboxylic acid group and not in a $CH_2$ group of a neighbouring molecule.

References

[1] GHOSH, D. K., and WHIFFEN, D. H., 1959, *Mol. Phys.*, **2**, 285.
[2] ATHERTON, N. M., and WHIFFEN, D. H., 1960, *Mol. Phys.*, **3**, 1.
[3] ATHERTON, N. M., and WHIFFEN, D. H., 1960, *Mol. Phys.*, **3**, 103.
[4] MCCONNELL, H. M., HELLER, C., COLE, T., and FESSENDEN, R. W., 1960, *J. Amer. chem. Soc.*, **82**, 766.
[5] MIYAGAWA, I., and GORDY, W., 1960, *J. chem. Phys.*, **32**, 255.
[6] HELLER, C., and MCCONNELL, H. M., 1960, *J. chem. Phys.*, **32**, 1535.
[7] ABRAHAM, R. J., OVENALL, D. W., and WHIFFEN, D. H., 1958, *Trans. Faraday Soc.*, **54**, 1128.
[8] INGRAM, D. J. E., 1958, *Free Radicals* (London : Butterworths).
[9] MORRISON, J. D., and ROBERTSON, J. M., 1949, *J. chem. Soc.*, p. 980.
[10] BROADLEY, J. S., CRUICKSHANK, D. W. J., MORRISON, J. D., ROBERTSON, J. M., and SHEARER, H. M. M., 1959, *Proc. roy. Soc.* A, **251**, 441.
[11] MCCONNELL, H. M., 1958, *Proc. nat. Acad. Sci., Wash.*, **44**, 766.
[12] MCCONNELL, H. M., and STRATHDEE, J., 1959, *Mol. Phys.*, **2**, 159.
[13] MCCONNELL, H. M., and ROBERTSON, R. E., 1957, *J. phys. Chem.*, **61**, 1018.
[14] MCLACHLAN, A. D., 1958, *Mol. Phys.*, **1**, 233.
[15] FORMAN, A., MURRELL, J. N., and ORGEL, L. E., 1959, *J. chem. Phys.*, **31**, 1129.
[16] TRAMMELL, G. T., ZELDES, H., and LIVINGSTON, R., 1958, *Phys. Rev.*, **110**, 630.
[17] MCCONNELL, H. M., and FESSENDEN, R. W., 1959, *J. chem. Phys.*, **31**, 1688.

# The principle of congruence for mixtures of n-alkanes

by M. L. McGLASHAN

Chemistry Department, The University, Reading

Brønsted and Koefoed's principle of congruence for mixtures of n-alkanes is given a general analytical form. It is shown that the volumes of mixing of n-pentane + n-hexadecane, determined experimentally by Desmyter and van der Waals, may be used in conjunction with the principle of congruence to predict correctly the volumes of mixing of the five other pairs of n-alkanes which have been studied by the same authors.

---

According to Brønsted and Koefoed's [1] principle of congruence there exists a single valued function $f(n)$ of $n$ such that at given temperature and pressure any excess mixing function $X_m^E$ such as the excess Gibbs function $G_m^E$, or the excess enthalpy $H_m^E$, or the excess volume $V_m^E$, is given for any values of the chain lengths $n_A$, $n_B$ of two normal alkanes A, B, and for any value of the mole fraction $x$ of B, by the relation

$$X_m^E(n_A, n_B, x) = f([1-x]n_A + xn_B) - (1-x)f(n_A) - xf(n_B). \qquad (1)$$

It is the object of this note to study the expansion of the function $f(n)$ in powers of $n$. If such a function $f_1(n)$ exists then any function $f_2(n)$ of the form

$$f_2(n) = f_1(n) + a + bn, \quad (a, b \text{ const.}), \qquad (2)$$

will serve equally well, since the terms containing $a$ and $b$ contribute nothing to $X_m^E$. We therefore write

$$f(n) = \sum_{r=0}^{s} A_r n^{r+2}, \quad (A_r \text{ const.}), \qquad (3)$$

where we have arbitrarily terminated the series after $s+1$ terms. Substituting (3) into (1) we obtain after some algebra

$$X_m^E(n_A, n_B, x) = -(n_B - n_A)^2 x(1-x)$$
$$\times \sum_{r=0}^{s} A_r \sum_{t=0}^{r} ([1-x]n_A + xn_B)^t (n_B^{r-t+1} - n_A^{r-t+1})/(n_B - n_A). \qquad (4)$$

In the simplest case when

$$f(n) = A_0 n^2, \qquad (5)$$

equation (4) reduces to

$$X_m^E(n_A, n_B, x) = -A_0(n_B - n_A)^2 x(1-x), \qquad (6)$$

which is the form used by Brønsted and Koefoed [1] to fit the values of the excess Gibbs function $G_m^E$ obtained from their vapour pressure measurements at 20°c for three pairs of n-alkanes, and by van der Waals [2] to fit his measurements of the heat of mixing $H_m^E$ at 20°c for five pairs of n-alkanes.

The volumes of mixing $V_m^E$ of pairs of n-alkanes [3] are, however, far from parabolic in $x$ and so cannot conform with the principle of congruence in the restricted form implied by (6). They nevertheless do conform with the

principle when it is expressed in the general form (1).   This has been shown by Hijmans [4] using a geometrical method, and will be shown again here as an example of an analytical method based on equation (4).

We use the experimental volumes of mixing of Desmyter and van der Waals [3] for the pair n-pentane + n-hexadecane, together with the principle of congruence in the form of equation (4), to predict volumes of mixing for the five other pairs of n-alkanes which have been studied by the same authors. We begin with the pair n-pentane + n-hexadecane rather than with one of the other pairs so as to use (4) for interpolation only, since for the other pairs the average chain length $(1-x)n_A + xn_B$ is always between 5 and 16.   The experimental values of $V_m^E(5, 16, x)$ can be fitted within the experimental accuracy when we put $X = V$ and retain only terms up to $r = 3$, that is to say when we put $s = 3$, in equation (4), with $A_0 = 0.94635$, $A_1 = -0.080410$, $A_2 = 0.0034967$ and $A_3 = -0.00006116 \text{ cm}^3 \text{ mole}^{-1}$.   If the principle of congruence is valid the volumes of mixing for the other pairs should then also be given by equation (4) with $X = V$, $s = 3$, and with the same values of the coefficients $A_r$.   Volumes of mixing calculated in this way are compared with the experimental results in the figure.   We see that there is agreement everywhere within $\pm 0.03 \text{ cm}^3 \text{ mole}^{-1}$ in $V_m^E$.
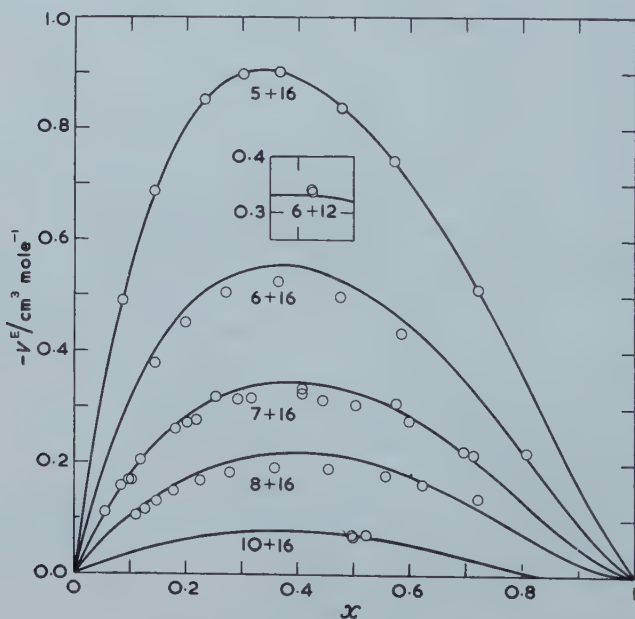


Figure 1.   Volumes of mixing $V^E$ of six pairs of n-alkanes plotted in each case against the mole fraction $x$ of the n-alkane with the greater number of carbon atoms.   The curves are those calculated as described in the text.   The circles are the experimental points of Desmyter and van der Waals [3].   So as to avoid confusing the diagram the results for 6 + 12 are shown as an insert with the vertical scale displaced.

Since experimental results for $X_m^E$ are often fitted to equations of the form

$$X_m^E = x(1-x) \sum_{q=0}^{s} B_q(1-2x)^q, \qquad (7)$$

may be useful to conclude this note by giving the relation between the

coefficients $B_q$ which of course depend on $n_A$, $n_B$, and the coefficients $A_r$ of equation (4) which according to the principle of congruence do not depend on $n_A$, $n_B$. The required relation is

$$B_q = - \sum_{r=q}^{s} A_r \sum_{p=q}^{r} (n_B^{r-p+1} - n_A^{r-p+1}) 2^{-p} \binom{p}{q} (n_A + n_B)^{p-q} (-1)^q (n_B - n_A)^{q+1}. \quad (8)$$

## REFERENCES

[1] BRONSTED, J. N., and KOEFOED, J., 1946, *Kgl. Danske Videnskab. Selskab., Mat.-fys. Medd.*, **22**, 1.
[2] VAN DER WAALS, J. H., 1950, *Thesis*, University of Groningen. See also VAN DER WAALS, J. H., and HERMANS, J. J., 1950, *Rec. Trav. chim. Pays-Bas*, **69**, 949, 971; 1951, *Ibid.*, **70**, 101
[3] DESMYTER, A., and VAN DER WAALS, J. H., 1958, *Rec. Trav. chim. Pays-Bas*, **77**, 53.
[4] HIJMANS, J., 1958, *Mol. Phys.*, **1**, 307.

# Note on McGlashan's paper, "the principle of congruence for mixtures of n-alkanes"

by J. HIJMANS and TH. HOLLEMAN

Koninklijke/Shell-Laboratorium, Amsterdam

(Shell Internationale Research Maatschappij N.V.)

In a recent paper, McGlashan [1] has analysed the experimental volumes of mixing of normal alkanes by means of Brønsted's principle of congruence [2]. According to this principle the excess volume of a mixture of two n-alkanes with chain-lengths $n_A$ and $n_B$ and concentrations $x_A$ and $x_B$, can be written as

$$V^e(n_A,\ n_B,\ x_A,\ x_B) = V(n_A x_A + n_B x_B) - x_A V(n_A) - x_B V(n_B), \qquad (1)$$

where the function $V(n)$ describes the dependence on chain-length of the molar volumes of pure n-alkanes. In this equation, the average chain-length,

$$n_A x_A + n_B x_B = n \qquad (2)$$

can assume fractional as well as integral values.

The validity of equation (1) may be verified either graphically, as described by one of us [3], or by assuming a definite analytical form for the function $V(n)$ and comparing the values obtained from (1) by means of this expression, with the experimental excess-volumes. The latter comparison was made by McGlashan [1], who used for $V(n)$ a series in ascending powers of the chain-length,

$$V(n) = \sum_{i=0}^{8} A_i n^i. \qquad (3)\dagger$$

In the present note we want to draw attention to the fact that the series (3) does not show the asymptotic behaviour which is to be expected for a homologous series such as the n-alkanes. The principle of congruence implies that the molar volumes of liquid n-alkanes and their mixtures are determined by the concentrations of $CH_2$- and $CH_2$-groups, irrespective of the way in which these groups are linked together into molecules. As the concentration of end groups tends to zero for large values of $n$, all these liquids will ultimately behave as assemblies of $CH_2$-groups, and molar quantities such as $V(n)$ will become proportional to the number of $CH_2$-groups in a mole of liquid, i.e. to $n-2$. Therefore

$$V(n) \sim a_0 + a_1 (n-2). \qquad (4)$$

In view of this asymptotic behaviour it seems natural to use —rather than the series (3)—a series in *descending* powers of $n-2$,

$$V(n) = a_1(n-2) + a_0 + \frac{a_{-1}}{n-2} + \frac{a_{-2}}{(n-2)^2} + \cdots . \qquad (5)$$

In order to test the usefulness of this series we have substituted it into (1) and fitted the resulting expression for $V^e$ to the experimental data of the mixture $C_5/C_{16}$. The first two terms in (5) (as in (3)) do not contribute to $V^e$. Of the remaining terms only two are needed to represent the data to within the experimental accuracy.

† The coefficients $A_i$ in equation (3) correspond to the coefficients $A_{r-2}$ in McGlashan's paper.

The values of the coefficients of these terms, obtained by the method of least squares, are

$$a_{-1} = -13 \cdot 58 \text{ cm}^3/\text{mole} \quad \text{and} \quad a_{-2} = +7 \cdot 55 \text{ cm}^3/\text{mole}.$$

The excess volumes of the mixtures $C_6/C_{16}$, $C_7/C_{16}$, $C_8/C_{16}$, $C_{10}/C_{16}$ and $C_6/C_{12}$, calculated by means of the same two coefficients, all agree with the experimental data to within $0 \cdot 03 \text{ cm}^3/\text{mole}$, i.e. the two relevant terms of (5) give as good a fit as the four terms of McGlashan's series (3).

To obtain an impression of the convergence of the series (3) and (5) we have calculated the contributions from successive terms in these series to the $V^e$ of a $C_5/C_{16}$mixture with a composition corresponding to $n = n_A x_A + n_B x_B = 10$ or $x_A = 6/11$, $x_B = 5/11$. As seen from the table, the absolute values of the contributions from the first four terms of McGlashan's series are considerably greater than $V^e$ itself. Therefore the coefficients $A_i$ must strongly depend on the—physically irrelevant—number of terms taken into account. In this respect the behaviour of the series (5) is much more satisfactory.

---

(*a*) Series (3):

| | | |
|---|---|---|
| $A_2 (n_B - n)(n - n_A)$ | $=$ | $-28 \cdot 391$ |
| $A_3 (n_B - n)(n - n_A)[n + n_A + n_B]$ | $=$ | $+74 \cdot 781$ |
| $A_4 (n_B - n)(n - n_A)[n^2 + {}_A nn + nn_B + n_A{}^2 + n_A n_B + n_B{}^2]$ | $=$ | $-70 \cdot 389$ |
| $A_5 (n_B - n)(n - n_A)[n^3 + n^2 n_A + \dots \quad\quad + n_B{}^3]$ | $=$ | $+23 \cdot 139$ |
| $V^e(5, 16, 6/11, 5/11)$ | $=$ | $-\ 0 \cdot 860$ |

(*b*) Series (5):

| | | |
|---|---|---|
| $a_{-1} \dfrac{(n_B - n)(n - n_A)}{(n - 2)(n_A - 2)(n_B - 2)}$ | $=$ | $-\ 1 \cdot 213$ |
| $a_{-2} \dfrac{(n_B - n)(n - n_A)}{(n - 2)(n_A - 2)(n_B - 2)} \left[ \dfrac{1}{n - 2} + \dfrac{1}{n_A - 2} + \dfrac{1}{n_B - 2} \right]$ | $=$ | $+\ 0 \cdot 357$ |
| $V^e(5, 16, 6/11, 5/11)$ | $=$ | $-\ 0 \cdot 856$ |

Contributions of individual terms in the series expansion of $V^e$ for $n_A = 5$, $n_B = 16$, $n = 10$.

---

Furthermore the curvature of the expression for $V^e$ obtained from McGlashan's first four coefficients, changes sign at a composition corresponding roughly to $n = 13$. This means that mixtures of molecules with chain-length $> 13$ would show a volume dilatation instead of a contraction, for which there is no experimental evidence. The excess volumes found by means of (5) remain negative for all values of $n$.

We are indebted to Dr. McGlashan for sending us his manuscript prior to publication.

REFERENCES

[1] McGlashan, M. L., 1961, *Mol. Phys.*, **4**, 87.
[2] Brønsted, J. N., and Koefoed, J., 1946, *Kgl. Danske Videnskab. Selskab., Mat.-fys. Medd.*, **22**, 1.
[3] Hijmans, J., 1958, *Mol. Phys.*, **1**, 307.

# Electronic structure and spectra of $[Cr(C_6H_6)_2]^+$ and $[Fe(C_5H_5)_2]^+$

by D. A. LEVY and L. E. ORGEL

Department of Theoretical Chemistry, University Chemical Laboratory,
Lensfield Road, Cambridge

The molecular-orbital treatment of the energy levels of sandwich molecules leads to the conclusion that of the different orbitals available for $d$ electrons the $e_{1g}(d_{xz}, d_{yz})$ orbital is least stable, but it does not establish the relative stability of the remaining orbitals, $a_{1g}(d_{z^2})$ and $e_{2g}(d_{x^2-y^2}, d_{xy})$ [1, 2, 3]. Magnetic susceptibility data on $[Cr(C_6H_6)_2]^-$ and the observation of a paramagnetic resonance spectrum with well-resolved hyperfine structure from solutions at room temperature show that the ground state is $^2A_{1g}(e_{2g})^4(a_{1g})^1$ [1]. The susceptibility of $[Fe(C_5H_5)_2]^-$ is sufficiently different from the spin-only value to indicate that the ground state must be the $^2E_{2g}$ state of the configuration $(a_{1g})^2(e_{2g})^3$ [3]. Here we discuss the energies of these two states, $^2A_{1g}$ and $^2E_{2g}$, in the light of the published absorption spectra [4, 5, 6].

We assume:

(1) That the separation between the $e_{1g}d$ orbital and the other $d$ orbitals is sufficiently large to justify our neglecting excited $d$ electron configurations involving $e_{1g}$ electrons when discussing the two lowest states.

(2) That Slater Condon parameters may be used to determine the electron repulsion energies of states of sandwich molecules in the same way as for octahedral complexes, etc.

Then the energies of the two relevant states are

$$^2E_{2g} = 10F_0 - 20F_2 - 40F_4,$$
$$^2A_{1g} = 10F_0 - 140F_4.$$

If we take $F_2 = 1600$ cm$^{-1}$, $F_4 = 100$ cm$^{-1}$ for Fe⁺ and $F_2 = 1075$ cm$^{-1}$, $F_4 = 70$ cm$^{-1}$ for Cr⁺ we find [7]

$$\left.\begin{aligned} E(A_{1g}) &= 10F_0 - 1{\cdot}74\,\text{ev}, \\ E(E_{2g}) &= 10F_0 - 4{\cdot}46\,\text{ev}, \end{aligned}\right\} \text{ for } [Fe(C_5H_5)_2]^+,$$

$$\left.\begin{aligned} E(A_{1g}) &= 10F_0 - 1{\cdot}21\,\text{ev}, \\ E(E_{2g}) &= 10F_0 - 3{\cdot}01\,\text{ev}, \end{aligned}\right\} \text{ for } [Cr(C_6H_6)_2]^+.$$

We see that the intra-atomic correlation energy favours the $^2E_{2g}$ state by 2·72 ev in $[Fe(C_5H_5)_2]^+$ and by 1·79 ev in $[Cr(C_6H_6)_2]^-$. The fact that $[Cr(C_6H_6)_2]^+$, has a $^2A_{1g}$ ground state shows that the $e_{2g}$ orbital is substantially below the $a_{1g}$ level in $[Cr(C_6H_6)_2]^+$, while the fact that the ground state of $[Fe(C_5H_5)_2]^+$ is a $^2E_{2g}$ state shows only that the $e_{2g}$ level is not more than 2·72 ev above the $a_{1g}$ level.

More precise information on the levels is obtained by interpreting the visible and near-ultra-violet absorption spectra. The first absorption band of

$[\mathrm{Cr(C_6H_6)_2}]^+$ occurs at $1 \cdot 07$ ev and has $\epsilon_{max} = 9 \cdot 8$.   There is one other very weak band, at $2 \cdot 14$ ev, before the strong ultra-violet absorption sets in.   We must assign the longest wavelength band to the $^2A_{1g} \rightarrow ^2E_{2g}$ transition.   We then deduce that the $e_{2g}$ level lies $2.9$ ev below the $a_{1g}$ level in $[\mathrm{Cr(C_6H_6)_2}]^+$.   The very weak band at $2 \cdot 14$ ev is presumably the lowest energy doublet-quartet transition.

In the spectrum of the $[\mathrm{Fe(C_5H_5)_2}]^+$ ion the first band is at $2 \cdot 02$ ev.   From this we may deduce that the $e_{2g}$ level lies about $0 \cdot 7$ ev below the $a_{1g}$ level.   This result presumes that no further band will be found in the infra-red beyond $10\,000$ å.

These results are not likely to be very accurate since we have neglected many important factors.   In addition to the assumptions already noted we have supposed that the $F_2$ and $F_4$ integrals are the same in the molecule ions as in the free atoms.   Almost certainly this is not the case and we have over-estimated the absolute magnitudes of the energy differences between the two orbitals. However, the conclusion that the $e_{2g}$ level is relatively much more stable in $[\mathrm{Cr(C_6H_6)_2}]^+$ than in $[\mathrm{Fe(C_5H_5)_2}]^+$ seems inevitable.   This suggests that back donation into the $e_{2g}$ orbital is far more important in benzene complexes than in dicyclopentadienyls, a conclusion which is consistent with much chemical evidence and with theoretical arguments [3].

## REFERENCES

[1] MOFFITT, W., 1954, *J. Amer. chem. Soc.*, **76**, 3386.
[2] DUNITZ, J., and ORGEL, L. E., 1955, *J. chem. Phys.*, **23**, 954.
[3] ROBERTSON, R. E., and McCONNELL, H. M., 1960, *J. phys. Chem.*, **64**, 70.
[4] YAMADA, S., YAMAZAKI, H., NISHIKAWA, H., and TSUCHIDA, R., 1960, *Bull. chem. Soc. Japan*, **33**, 481.
[5] WILKINSON, G., ROSENBLUM, M., WHITING, M. C., and WOODWARD, R. B., 1952, *J. Amer. chem. Soc.*, **74**, 2125.
[6] HARIU, P. H., and PETERSON, N. C., 1957, *Proc. N. Dak. Acad. Sci.*, **11**, 31.
[7] ORGEL, L. E., 1955, *J. chem. Phys.*, **23**, 1819.

# On the carbon–chlorine bond angles in
# 1, 2, 3, 4-tetrachlorobenzene

by C. DEAN†, C. RICHARDSON and T. SAKURAI
University of Pittsburgh, Pittsburgh 13, Pa., U.S.A.

For halogen-substituted benzene, if the halogen atoms exist at ortho positions on the benzene ring, deformation of the bond angle due to the repulsion between the halogens is expected. However, various authors have obtained different results as to the nature of this strain. From the electron diffraction study of the gas molecule, Bastiansen and Hassel concluded [1] that the deformation is mainly out-of-plane bending and of magnitude from 12 to 18 degrees for many chloro and bromo benzenes. But in a recent x-ray study of 1, 2, 4, 5-tetra-bromobenzene, Gafner and Herbstein [2, 3] showed that the molecule is planar in the crystal within the accuracy of their measurements. The infra-red spectrum of hexachlorobenzene measured by Kopelman and Schnepp [4] suggests that the molecule is planar, while the ultra-violet spectrum measured by the same authors [5] gave evidence of a puckered structure. On the other hand, steric forces between halogen atoms were calculated theoretically by Coulson and Stocker [6] who concluded that for ortho-substituted molecules, the mole-cule is planar but that angular displacement occurs in the plane.

A method which yields bond angles directly with good accuracy is the Zeeman splitting of nuclear quadrupole resonance (n.q.r.) in a single crystal. This method was applied to 1, 2, 4, 5-tetrachlorobenzene by Dean *et al.* [7] but no definite conclusion about the planarity of the molecule could be drawn since the direction of the benzene ring is not obtained by n.q.r.

We have applied the n.q.r. method to 1, 2, 3, 4-tetrachlorobenzene, using a recording spectrograph described elsewhere [8]. A single crystal about 1 cm in diameter was grown by the Bridgman technique using material which was purified by zone refining. The space group of the crystal is monoclinic P2₁/C, 4 molecules in a unit cell. The pure n.q.r. spectrum of $^{35}Cl$ consists of two doublets: the higher of frequencies 36·76 and 36·64 Mc/s at room temperature assigned to chlorines at the 2, 3 positions on the benzene ring; the lower of frequencies 36·33 and 36·30 assigned to chlorines at the 1, 4 positions. From the symmetry of the crystal two different bond directions related by a screw axis were expected for each frequency. For one molecule, two bonds, to chlorines at the 1 and 4 positions, were not detected. This was because these bonds were nearly parallel to the axis of the high-frequency coil, which rules that the chlorine signal is weak. For the other molecule all four σ bond directions were observed. If the molecule has the puckered form as is obtained by Bastiansen and Hassel, the plane of the benzene ring will be obtained as a best fit plane through these four σ bonds. This plane was obtained by the least-squares method and the

angle the $\sigma$ bond makes with the benzene plane was calculated. Angles between $\sigma$ bonds were also calculated. Results are shown in the table. The estimated error for these angles is $\pm 1°$.

| Angle between | | Molecule A | Molecule B |
|---|---|---|---|
| Benzene plane and $Cl_1$ $\sigma$ bond | | $-3/4°$ | |
| $Cl_2$ | ,, | $2/4°$ | |
| $Cl_3$ | ,, | $-2/4°$ | |
| $Cl_4$ | ,, | $-1/4°$ | |
| $Cl_1$ $\sigma$ bond and $Cl_2$ $\sigma$ bond | | $60 \quad 3/4°$ | |
| $Cl_2$ ,, ,, $Cl_3$ | ,, | $61 \quad 1/4°$ | $60 \quad 3/4°$ |
| $Cl_3$ ,, ,, $Cl_4$ | ,, | $61 \quad 2/4°$ | |

Thus the present results support that the molecule is almost planar in the crystal. If puckered molecules exist at random in the crystal, the average structure obtained by x-rays might give the planar molecule. But this possibility is rejected by the present experiment, because in such a case the observed n.q.r. signal would give both directions, not the average. A puckered molecule with rapid conversion between the two steric isomers might look planar in n.q.r., but this seems to be rejected too by the normal appearance of the resonance spectrum. The angular distortion within the plane is smaller than the theoretically anticipated value of 4 degrees [6]. In this respect our results are consistent with those of Gafner and Herbstein.

Two other related compounds, tetrachloro-paraquinone and tetrachloro-hydroquinone have been investigated too. For these molecules the out of plane bending of the C–Cl bonds is only about one degree and the angular distortions are small. The molecular orientation obtained by n.q.r. was combined with the x-ray diffraction, and complete crystal structure analyses for all these crystals have been performed. A further discussion will be given elsewhere with results of the crystal structure analyses.

## REFERENCES

[1] BASTIANSEN, O., and HASSEL, O., 1947, *Acta chem. Scand.*, **1**, 489.
[2] GAFNER, G., and HERBSTEIN, F. H., 1958, *Mol. Phys.*, **1**, 412.
[3] GAFNER, G., and HERBSTEIN, F. H., 1960, *Acta cryst., Camb.*, **13**, 702.
[4] KOPELMAN, R., and SCHNEPP, O., 1959, *J. chem. Phys.*, **30**, 597.
[5] SCHNEPP, O., and KOPELMAN, R., 1959, *J. chem. Phys.*, **30**, 868.
[6] COULSON, C. A., and STOCKER, D., 1959, *Mol. Phys.*, **2**, 397.
[7] DEAN, C., POLLAK, M., CRAVEN, B. M., and JEFFREY, G. A., 1958, *Acta cryst., Camb.*, **11**, 710.
[8] DEAN, C., 1960, *Rev. sci. Instrum.*, **31**, 934.

# The crystal spectra of very weak transitions
# I. Measurements of the naphthalene 3200 Å system at 4°K

by D. P. CRAIG

William Ramsay and Ralph Forster Laboratories,
University College London

L. E. LYONS and J. R. WALSH

Department of Physical Chemistry, University of Sydney

The weak absorption system of crystalline naphthalene at 3200 Å has been measured at 4°K in polarized light. Previous work at 20°K is supplemented by a number of newly recorded absorption lines, and by re-measurement of the frequencies of all lines at the lower temperature.

The spectrum is compared with the vapour spectrum and corresponding bands identified so far as possible. Exciton resonance effects are analysed and discussed. The analysis discloses that the important $b_{3g}$ vibrations of upper state frequencies 438 and 911 cm$^{-1}$ are both reduced by 5 per cent in the crystal, and smaller changes are identified in other vibrations. Comparison with the vapour spectrum shows that vibrationally induced bands, even when relatively strong, are little influenced by intermolecular forces, whereas very weak pure electronic bands give evidence of much greater effects.

## 1. INTRODUCTION

The weak absorption system of naphthalene near 3200 Å is one of the best studied of the aromatic band systems. It thus provides a favourable case for investigating the changes that take place to the free molecule spectrum, as observed in the vapour, due to intermolecular forces in the crystal. As has already been briefly reported [1] the study of such changes in very weak systems is of special interest. Crystal effects are different in pure electronic, and in vibrationally induced bands, which occur side-by-side in very weak absorption systems in complex molecules. In this paper we shall describe the observed crystal spectrum and its relation to the vapour spectrum, and in a following paper deal with the theory of the vapour-crystal relationships.

## 2. EXPERIMENTAL

The new experimental studies at 4°K supplement the work of Prikhotjko [2], McClure and Schnepp [3] (both at 20°K), Zmerli [4] (20 K) and Griessbach *et al.* [5] (at 100°K). Agreement between the several sets of measurements is generally good, and our discussion is therefore confined mainly to some new points concerning the relation of vapour and crystal spectra.

Cryoscopic grade naphthalene was treated with Raney nickel, recrystallized several times from aqueous alcohol and finally sublimed. Thin crystals were grown by sublimation. Thicker ones were cut from a large crystalline sample with

a jeweller's saw and polished with cotton wool moistened with alcohol. The thickness of the crystals was measured with an Ehringhaus Compensator and orientations determined with a polarizing microscope.

The absorption spectra of the crystals were recorded in a Hilger Large Quartz spectrograph E492 on Kodak orthochromatic plates using hydrogen arc illumination. Light from the source passed through the crystal in the helium-cooled cell, and was then analysed into two plane-polarized beams by a Wollaston prism and focused in two images one above the other on to the spectrograph slit. Exposures of up to three hours were required; each gave the absorption in the two polarizations simultaneously, and a reference iron-arc spectrum was then photographed in the gap between the two absorption spectra. Wavelengths were measured by quadratic interpolation from prints and converted to wavenumber units *in vacuo*. The sharper bands are accurate to $\pm 2\,\mathrm{cm}^{-1}$. The crystal samples used were *ab* sections, and were oriented with *a* and *b* axes coinciding with the polarization directions of the Wollaston prism. The two records are therefore of absorption of plane-polarized light with electric vector parallel and perpendicular to the *b* monoclinic axis in the *ab* plane.

## 3. Results and analysis

The frequencies of all the observed lines are listed in the Appendix and compared with those of Prikhotjko [2] and Schnepp and McClure [3]. The lower frequency lines beginning at $29\,944\,\mathrm{cm}^{-1}$ are seen only in crystals of millimetre

| Vapour frequency and intensity (cm$^{-1}$) | Polarization† | Assignment‡ | Crystal analogues | |
|---|---|---|---|---|
| | | | *a* pol. | *b* pol. |
| 32020 (M) | L | 0–0 | 31475 (5) | 31626 (10) |
| 32458 (VS) | S | 0+438 | 31961 (8) | 31960 (9) |
| 32509 (W) | L | 0+489 | 32031 (2) | Not obs. |
| 32521 (MW) | L | 0+501 | — | |
| 32722 (W) | L | 0+702 | 32231 (7) | 32259 (8) |
| 32931 (MS) | S | 0+911 | 32411 (6) | 32414 (8) |
| 33159 (MS) | S | 0+438+702 | 32675 (9) | 32678 (8) |
| 33410 (W) | L | 0+1390 | 32931 (2) | — |
| 33445 (M) | S | 0+438+987 | 32948 (8) | 32952 (8) |
| 33455 (MW) | L | 0+1435 | 32956 (7) | 32952 (8) |
| 33869 (MW) | S | | 33390 (8)⎫ | Obscured |
| 33892 (MW) | S | 0+438+1435 | 33390 (8)⎬ | Obscured |
| 33918 (W) | S | 0+911+987 | 33390 (8)⎭ | Obscured |
| 33955 (W) | L | 0+501+1435 | — | — |

† L means long-axis polarized, species $B_{2u}\!\leftarrow\!A_g$; S means short-axis polarized, species $B_{1u}\!\leftarrow\!A_g$.

‡ Frequencies quoted in this table are the vapour values.

Table 1. The stronger principal bandheads of naphthalene vapour, and crystal analogues.

thicknesses, and we have no satisfactory analysis of them. They may be due to an impurity, as has recently been proposed [6], or to another and very weak electronic transition of naphthalene itself. Our analysis of the remaining lines is as follows.

We have considered first the vapour absorption bands recently recorded at high resolution [7] and have identified so far as possible the crystal bands which can be unambiguously related to the strongest of them (table 1). This leaves a number of crystal absorptions unassigned; these are included in table 2, giving all the stronger crystal lines with assignments where possible. No assignments are proposed for the very numerous weaker lines included in the Appendix. These would be too uncertain to have real value. By concentrating on the strong crystal lines we can bring out more clearly the relation between vapour and crystal energy levels and so define what has to be explained theoretically. The assignment of the vapour bands given in table 1 is taken from the fuller compilation [7] in which the polarizations are deduced from the rotational contours of vapour bands. The assignments are based on the finding that the stronger bands may be related, by using a small number of totally symmetrical vibration frequencies, either to the origin of the pure electronic transitions at $32\,020\ cm^{-1}$ or to false origins separated from the electronic origin by $b_{3g}$ vibration frequencies. The most important such vibration has values $506\ cm^{-1}$ and $438\ cm^{-1}$ in the ground and excited states respectively and another, with values $936\ cm^{-1}$ and $911\ cm^{-1}$, is prominent. Each of these true and false origins is extended in progressions of the same totally symmetrical intervals, the best established being, in the upper state, 501, 702, 987, 1147, 1390 and $1435\ cm^{-1}$.

The key to the analysis of the crystal spectrum and its correlation with the vapour spectrum is the frequency of the electronic origin. This is not immediately identifiable, because crystal forces split the pure electronic 0–0 transition into two oppositely polarized absorption bands, neither of which appears at the pure electronic frequency. The two components in naphthalene are at $31\,626\ cm^{-1}$ ($b$ polarized) and $31\,475\ cm^{-1}$ ($a$ polarized). It is still useful however to locate the frequency at which the pure electronic absorption would appear in the absence of exciton resonance effects, because this frequency is one of the origins to which a number of lines in the spectrum may be referred using vibration frequencies identified in the vapour spectrum. We shall designate this the *virtual* electronic origin.

In the vapour spectrum the 0–0 bandhead is at $32\,020\ cm^{-1}$ and the principal false origin in absorption is at $32\,458\ cm^{-1}$, corresponding to a transition induced through vibrational perturbation by the upper state $b_{3g}$ vibration $438\ cm^{-1}$. The corresponding vibration-induced hot band, due to the ground state $b_{3g}$ frequency $506\ cm^{-1}$, is at $31\,514\ cm^{-1}$, separated by $506+438=944\ cm^{-1}$ from the principal false origin. In the vapour fluorescence spectrum, and in the radiofrequency induced emission [8] the roles are reversed, and the band at $31\,514\ cm^{-1}$ is the principal origin. The search for the electronic origin in the crystal involves identifying the corresponding false origins. In absorption the lines at $31\,960$–$1\ cm^{-1}$ correspond to the false origin $0+438$ of the vapour spectrum. In fluorescence the strongest origin has been taken to be the line at $31\,062\ cm^{-1}$ [9], but this has not generally been accepted as the analogue of the vapour band $31\,514\ cm^{-1}$, mainly for two reasons. Firstly, it lies $900\ cm^{-1}$ instead of $944\ cm^{-1}$ from the analogue of $0+438\ cm^{-1}$, and secondly the Boltzmann factor for an initial state 0–506 is too small at the temperature used to allow the transition to be seen. These arguments have now been powerfully reinforced by Prikhotjko and Shpak [6] who show that the line at $31\,062\ cm^{-1}$ is an emission by $\beta$-methyl-naphthalene present as an impurity, and that it vanishes in pure naphthalene.

| *a* pol. | *b* pol. | Assignment | Comments |
|---|---|---|---|
| 31063 (3) | 31063 (5) | 0 − 482 | Corresponds to vapour 0 − 506 |
|  | 31310 (5) |  |  |
| 31475 (5) | 31626 (10) | 0—0 | Electronic origin split by 151 cm$^{-1}$ |
| 31961 (8) | 31960 (9) | 0 + 416 | Strongest false origin.    Vapour 0 + 438 |
| 32231 (7) | 32259 (8) | 0 + 701 | Splitting 28 cm$^{-1}$ |
| 32411 (6) | 32414 (8) | 0 + 869 | False origin.   Vapour 0 + 911 |
| 32463 (8) | 32463 (7) | 0 + 416 + 503 |  |
| 32620 (6) | 32621 (6) | 0 + 1076 ($\Delta = -2$) | Weak false origin.   Vapour 0 + 1107 |
| 32657 (9) | 32678 (8) | 0 + 416 + 715 |  |
| 32748 (7) | 32749 (6) |  | Vapour 0 + 1200 |
| 32769 (8) | 32770 (6) |  |  |
| 32832 (6) | 32832 (5) |  |  |
| { 32869 (3) | { 32869 (5) |  |  |
| { 32874 (5) | { 32873 (5) |  |  |
| { 32948 (8) | 32952 (8) | ($\Delta = -5$) |  |
| { 32956 (7) |  | 0 + 416 + 987 |  |
| 33058 (6) | { 33056 (5) |  |  |
|  | { 33060 (5) |  |  |
| 33091 (6) | 33093 (4) |  |  |
| 33103 (7) | 33105 (8) | 0 + 416 + 1144 | Vapour 0 + 438 + 1147 |
| 33130 (6) | 33131 (5) | 0 + 868 + 716 ($\Delta + 8$) |  |
| 33150 (7) | 33152 (8) | 0 + 1607 | Weak false origin.   Vapour 0 + 1610 |
| 33177 (3) | 33178 (5) | 0 + 416 + 503 + 716 ($\Delta + 2$) |  |
| 33238 (3) | 33243 (8) |  |  |
| 33255 (5) | 33255 (4) | 0 + 416 + 503 + 788 ($\Delta − 4$) |  |
| 33302 (7) | 33302 (6) |  |  |
| 33350 (8) | 33352 (7) | 0 + 416 + 1390 ($\Delta − 2$) |  |
| ⎡ 33387 (8) |  | 0 + 416 + 1430 ($\Delta + 2$) |  |
| { 33390 (8) | Continuum | 0 + 416 + 2 × 716 ($\Delta + 2$) |  |
| ⎣ 33427 (7) |  |  |  |
| 33433 (7) |  |  |  |
| 33442 (8) |  | 0 + 416 + 503 + 987 ($\Delta + 7$) |  |
| 33499 (3) | 33500 (6) |  |  |
| 33509 (2) | 33510 (6) |  |  |
| 33535 (4) | 33535 (6) |  |  |
| 33560 (4) | 33561 (6) |  |  |
| 33648 (6) |  |  |  |
| 33658 (6) |  |  |  |
| 33666 (6) |  | 0 + 416 + 716 + 987 ($\Delta − 3$) |  |
| 33856 (6) |  |  |  |
| 33965 (8) |  |  |  |

Table 2.    List of strongest crystal absorption lines and assignments.

Thus, almost all the fluorescence lines recorded in the literature are due to β-methyl naphthalene.

As Schnepp and McClure first proposed [10], the electronic origin appears in the split components at 31 475 cm⁻¹ and 31 636 cm⁻¹. These lines, and others in the important region near the origin, are reproduced in the figure.
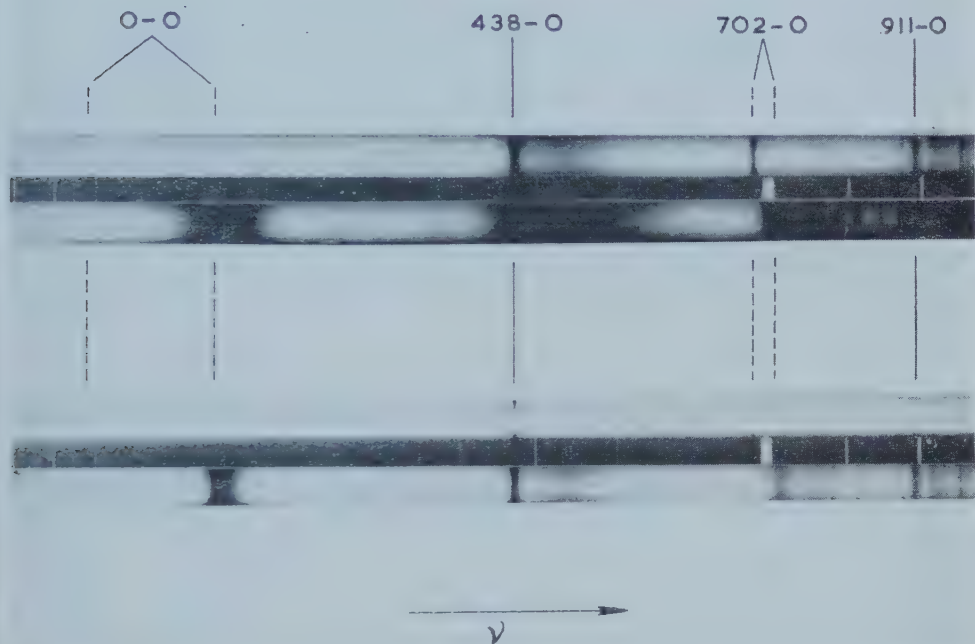


The absorption spectra near the electronic origin of two naphthalene crystals, of thicknesses 1·6 microns (upper) and 0·4 microns (lower). Each shows the *ac* polarized component above the reference iron spectrum and the *b* component below. The pure electronic transition and the transition ending on the one quantum totally symmetrical 702 cm⁻¹ upper state vibrational level are split (dotted lines). The false origins involving one quantum upper state vibrations of 438 cm⁻¹ and 911 cm⁻¹ (vapour values) are not split (full lines).

Important evidence is provided in Bolotnikova's work [11] on the fluorescence of naphthalene in crystalline paraffin solutions, following the methods of Shpolsky [12]. This spectrum is shifted by some 170 cm⁻¹ to high frequencies of the pure crystal and is sharp enough to permit accurate measurement of vibrational intervals. In particular, it shows that the vapour $b_{3g}$ frequency of 506 cm⁻¹ is reduced to about 495 cm⁻¹, while totally symmetrical intervals are unaltered or even somewhat increased. The sensitivity of the $b_{3g}$ frequency 506 cm⁻¹ to change of environment is a significant pointer to the interpretation we shall give. Similar measurements have recently been made by Pesteil [13]. Another important clue to the location of the 0–0 frequency is in the work of Pesteil and Ciais [14] who studied the fluorescence emission of a crystalline solution of $C_{10}H_8$ in $C_{10}D_8$,

the two species being present in equal amount.    Since the first excited level of $C_{10}H_8$ is the lower, the fluorescence emission originates largely from it; moreover, since the two are virtually identical in their external fields, they will form a mixed crystal with the same lattice constants as those of pure naphthalene.    The composition of the mixed crystal must be variable from point to point; from regions of equimolecular microscopic composition the emission spectrum will be the same as that of a pure naphthalene crystal, except for exciton resonance effects. These will be less than in pure naphthalene, because the energy levels of $C_{10}H_8$ and $C_{10}D_8$ differ by about $100\ cm^{-1}$, and the conditions for resonance exciton transfer are less favourable.    The observed spectrum confirms these expectations. The impurity line $31\,062\ cm^{-1}$ is present strongly in the spectrum and is at the same frequency as in pure crystalline naphthalene, but a number of intrinsic fluorescence lines are also observed.    The two components of the pure electronic transition now appear at $31\,561\ cm^{-1}$ and $31\,526\ cm^{-1}$, with a splitting of $35\ cm^{-1}$, instead of at $31\,626$ and $31\,475\ cm^{-1}$ (splitting $151\ cm^{-1}$) in pure naphthalene. The mean of the first pair is at $31\,544\ cm^{-1}$ and of the second at $31\,550\ cm^{-1}$. The first is likely to be the better estimate of the virtual origin, because the exciton shift will be smaller in the mixed crystal.    We shall therefore adopt the value $31\,544\ cm^{-1}$; its approximate correctness will be confirmed subsequently.    The value agrees exactly with McClure and Schnepp's conclusion [3], based on comparison of the pure crystal spectrum with that of the mixed crystal of naphthalene in durene.

It is necessary to consider the relation of the value for the virtual electronic origin to the positions of the false origin in absorption at $31\,960\ cm^{-1}$.    The separation is $416\ cm^{-1}$, a reduction by a factor $0 \cdot 952$ from the vapour interval of $437\ cm^{-1}$.    A second series of bands in the vapour is produced by a $b_{3g}$ vibration which has the frequencies $936$ and $911\ cm^{-1}$ in ground and excited states respectively.    Corresponding to negative and positive frequency displacements by the first and second of these frequencies respectively, there are two additional false origins in the vapour spectrum, which should have analogues in the crystal. The absorption false origin is readily identified by its intensity and polarization property as a pair of slightly split bands at $32\,411$ ($a$ polarized) and $32\,414\ cm^{-1}$ ($b$ polarized), with a mean displacement of $868\ cm^{-1}$ from the electronic origin. This interval is $0 \cdot 953$ times the vapour value of $911\ cm^{-1}$.    There is thus a pattern of consistency in the comparison of vapour and crystal spectra which supports the view that the main crystal fluorescence and absorption origins are simply related to those in the vapour.    The principal effect is a 5 per cent reduction in both the main perturbing $b_{3g}$ vibrations in the solid state.

A second important feature of the crystal spectrum is that the intensities are greater towards higher frequencies than is observed in the vapour spectrum.    The reason for this is the mixing of the upper states of the 3200 Å system with that of the next electronic system at 2750 Å induced by crystal forces.    As explained in an analogous case of second-order effects in anthracene [15] the mixing increases as the separation of the states concerned goes down.    Accordingly, we find that many of the prominent higher combination bands in the crystal appear only very weakly in the vapour spectrum, or have not been seen at all.    Thus at higher frequencies the crystal and vapour spectra are less and less alike, although the same fundamental vibration frequencies continue to appear in the combinations concerned.

## 4. ACTIVITY OF TOTALLY SYMMETRICAL VIBRATIONS

The vapour spectrum leads to the values 501, 702, 987, 1147, 1390 and 1435 cm$^{-1}$ for totally symmetrical fundamentals of the upper electronic state. In the crystal spectrum these vibrations appear, changed in frequency in some cases, added to the strong false origin 31 960 cm$^{-1}$. The 501 cm$^{-1}$ vibration appears once only in combination with strong bands in the vapour, but owing to the intensification of higher frequency lines in the crystal two-quantum combinations are sometimes observed. Thus

$$32\,463 = 31\,960 + 503, \quad \text{and} \quad 32\,969 = 31\,960 + 2 \times 503 \; (\Delta = -3).$$

A number of other combinations are observed, and it appears that 503 cm$^{-1}$ gives somewhat better agreement in the crystal than 501 cm$^{-1}$. As in the vapour, the totally symmetrical frequency 702 cm$^{-1}$ (vapour value) appears strongly. The line at 32 675 must be assigned 31 960 + 716, and the overtone 31 960 + 2 × 716 is probably one of the strong pair of lines near 33 387 − 90. The frequency 716 recurs in 33 177 − 8 = 31 960 + 503 + 716 and in several other totally symmetrical combinations built on to the false origin 31 960 cm$^{-1}$; the frequency thus appears to have been increased in the crystal from 702 to 716 cm$^{-1}$. In combinations built on to true electronic origin, however, the position is less clear, as will be subsequently mentioned.

The upper state fundamental 987 cm$^{-1}$ (vapour value) appears in the strong line 32 948 = 31 960 + 988 and probably in 33 666 = 31 960 + 716 + 988 ($\Delta = -2$). Its value is thus not significantly altered from the vapour. The assignments 33 104 = 31 960 + 1147 ($\Delta = -3$), 33 601 = 31 960 + 503 + 1147 ($\Delta = 3$), and for the poorly resolved line 33 826 = 31 960 + 716 + 1147 ($\Delta = 4$) suggest that the frequency 1147 cm$^{-1}$ of the vapour is also essentially unchanged. The vapour 1390 cm$^{-1}$ occurs unchanged in the strong 33 350 = 31 960 + 1390 and probably in 34 064 = 31 960 + 716 + 1390. For the vapour 1435 cm$^{-1}$ we have a near equality with 2 × 716. The potential Fermi resonance does not appear strongly however; one of the pair of lines near 33 390 can be assigned 31 960 + 1430 and the rather strong 34 105 = 31 960 + 716 + 1430. The interval 1430 is not as intensely developed in the crystal as 1435 cm$^{-1}$ is in the vapour, and its slightly reduced value of 1430 cm$^{-1}$ is not well established. In combination with the weaker false origin 32 411 − 4 cm$^{-1}$ only the frequencies 716, 1147 and 1390 are clearly observed, and with the still weaker 32 620 only 503 and 716.

The false origins and lines involving totally symmetrical separations from them are not expected to show factor group splittings [1], and in none of the cases already cited is there evidence of such splittings, within experimental error. The pure electronic origin, however, is split, and splittings are expected to occur in lines separated by totally symmetrical vibrational intervals, roughly in proportion to the intensity of the line concerned. Moreover, other manifestations of intermolecular resonance, such as intensity transfers and disturbances to vibrational intervals are expected in these lines more than in vibrationally induced ones. The interpretation of this part of the spectrum is in fact much more difficult. The only band aside from the origin which is intense enough to give a splitting definitely outside the experimental uncertainty corresponds to the vapour 0 + 702, the two components of which fall at 32 231 (*a* pol.) and 32 259 (*b* pol.). This splitting of 28 cm$^{-1}$ is in the same sense as that of the origin (*a* component at lower frequency) and is less by a factor 1/5·5 in magnitude. This ratio is roughly that of the intensities of the corresponding bands in the vapour, as expected. The (weak) line

expected at $0+503$ cm$^{-1}$ falls in the region too close to the strong false origin 31 960 cm$^{-1}$ to be definitely identifiable: the pair 32 008–32 010 ($\Delta = -2$) is a possibility. $0+987$ falls at 32 531 cm$^{-1}$: the most likely lines are 32 525–32 527 cm$^{-1}$, but again the identification is doubtful. The frequency 1390 is uncertain in combination with the origin; and 1430 is represented by the weak pair 32 979–32 980. The weakness of these lines is not unexpected, because they are notably weak in the vapour; however, the combination corresponding to the vapour $0+702$, which is stronger, is somewhat anomalous. The mean of the split components is 32 245 cm$^{-1}$, which is separated from the origin 31 544 by 701 cm$^{-1}$, a value very close to the vapour 702 cm$^{-1}$, and different from the value of 716 cm$^{-1}$ which fits several intervals in the series of lines originating in the false origin 31 960 cm$^{-1}$. The occurrence of two frequencies for the same vibrational mode, one in progressions of vibrationally induced bands, and the other in pure electronic bands showing factor group splitting is novel and at first sight improbable. However, we think it is the correct interpretation of the experimental results in the absorption spectrum already discussed. Values of excited fundamentals observed in the vapour and crystal spectra are collected and compared in table 3.

| Excited state Vapour frequency (cm$^{-1}$) | Species | Crystal frequency (cm$^{-1}$) | Change crystal-vapour |
|---|---|---|---|
| 501 | $a_g$ | 503 | $+2(+0{\cdot}4$ per cent) |
| 702 | $a_g$ | 716† | $+14(+2$ per cent) |
| 987 | $a_g$ | $\sim 987$ | 0 |
| 1390 | $a_y$ | $\sim 1390$ | 0 |
| 1435 | $a_g$ | $\sim 1430$ | $-5$ |
| 438 | $b_{3g}$ | 416 | $-22(-5$ per cent) |
| 911 | $b_{3g}$ | 868 | $-43(-4{\cdot}7$ per cent) |

† Except in combination with the electronic origin, when the value is 702 cm$^{-1}$.

Table 3. Some fundamental vibration frequencies observed in the crystal, and vapour analogues.

Although, as already discussed, measurements of the supposed crystal fluorescence of naphthalene mainly record emission by $\beta$-methylnaphthalene impurity, it is useful to consider briefly the interpretation of some fluorescence lines intrinsic to naphthalene itself. In the recorded spectra [4, 9, 10] these lines are much weaker than the impurity lines, but may be identified in favourable cases.

At low enough temperature the initial state for fluorescence emission is the lowest excited electronic level of the crystal, namely the level recorded in the very weak absorption line 31 475 cm$^{-1}$. In spite of its low oscillator strength, however, this line should appear *relatively* strong in emission, because of the high population of its initial state. Additionally, from the same initial state, progressions in ground state totally symmetrical vibrations should be observed. The totality of such bands constitutes the electronically allowed fluorescence series, corresponding to the split electronic origin, and progression numbers, seen in absorption by the pure crystal. Then, corresponding to the vibrationally induced series in absorption, there will be downward transitions from the upper

state to ground state non-totally symmetrical $b_{3g}$ vibrational levels. Application of symmetry arguments shows, however, that these transitions will be confined to one direction of polarization, while the analogous absorption lines appear in both polarizations. Thus, the 'mirror symmetry' of vapour absorption and fluorescence spectra is lost in pure crystals. Shpak and Sheka [6] observed the pure electronic line at 31 480 cm $^{-1}$; and Zmerli [4] reports bands near to the expected false origins 31 475–506, and 31 475–936, together with bands built on them with totally symmetrical frequencies. A number of the same fluoresence lines were reported also by Obreimov and Shabaldas [9]. Thus it seems indicated in fluorescence, and rather definite in absorption, that the crystal spectra conform to expectation for an exciton model, of which some features will be treated theoretically in a following paper.

## 5. ASSIGNMENT

The assignment of the electronic transition to its symmetry species was established some time ago by McClure [16], from studies of naphthalene in crystals of durene. The assignment is $B_{2u} \leftarrow A_g$, polarized along the longer in-plane axis. It has since been confirmed from studies of band contours in the vapour spectrum [7]. The observations in the present paper may also be used to confirm the assignment, as already briefly reported [1]. The detailed arguments on this point will, however, be reserved for a following paper on the theory of crystal exciton effects in weak transitions.

## APPENDIX

*Band frequencies (cm⁻¹) and intensities for crystalline naphthalene*

(Estimated intensities in brackets)†

| McClure and Schnepp [3] $a$ polarized | Present work $a$ polarized | Prokhotjko [2] unpolarized | Present work $b$ polarized | McClure and Schnepp $b$ polarized |
|---|---|---|---|---|
| 29945 | 29944(3) | 29945(5) | 29944(8) | 29945 |
| | | | 30059(1) | |
| | | | 30067(1) | |
| | | | 30087(6) | |
| | | | 30105(1) | |
| | | | 30118(1) | |
| | | | 30243(3) | |
| | | | 30255(3) | |
| | | | 30263(3) | |
| | | | 30350(6) | |

† Our intensities are visual estimates. They refer only to the comparison of bands in one polarization, and not to the comparison of $a$ bands with $b$ bands. Also the bands down to an including 31 367 cm$^{-1}$ were measured in crystals of millimetre thicknesses, and their intensity ratings refer to appearance under these conditions. All later bands were measured in crystals of micron thicknesses.

D. P. Craig *et al.*

| McClure and Schnepp [3] *a* polarized | Present work *a* polarized | Prikhotjko [2] unpolarized | Present work *b* polarized | McClure and Schnepp *b* polarized |
|---|---|---|---|---|
| | | | 30368(5) | |
| | | | 30385(3) | |
| | | | 30392(4) | |
| | | | 30405(2) | |
| | | | 30413(2) | |
| | | | 30446(6) | |
| | | | 30493(3) | |
| | | | 30631(2) | |
| | | | 30647(1) | |
| | | | 30659(2) | |
| | | | 30669(6) | |
| | | | 30693(1) | |
| | | | 30708(1) | |
| | | | 30791(1) | |
| | | | 30801(3) | |
| | | | 30815(2) | |
| | | | 30866(1) | |
| | | | 30885(1) | |
| | | | 30931(1) | |
| 31062(w) | 31063(3) | 31059(10) | 31063(5) | 31062(m) |
| | | | 31073(1) | |
| | | 31082(10) | 31084(3) | |
| | 33103(2) | 31102(3) | 31097(2) | |
| | 31116(2) | 31127(3) | 31114(1) | |
| | | 31162(2) | | |
| | | 31213–22(3) | | |
| | | | 31235(3) | |
| | | | 31245(2) | |
| | | | 31278(3) | |
| | | | 31310(5) | |
| | | 31319(3) | 31319(3) | |
| | | | 31356(1) | |
| | | | 31367(1) | |
| | | | 31441(1) | |
| | | 31449(6) | | |
| | | | 31458(1) | |
| | 31471(4) | | 31469(1) | |
| 31475(w) | 31475(5) | 31476(8) | | |
| | | | 31493(1) | |
| | | | 31501(1) | |
| | | 31534(−) | | |
| | | 31545(3) | | |
| | | 31570(3) | | |
| | | | 31583(2) | |
| | | | 31597(2) | |
| | | 31636(12) | 31626(10) | 31642(vs) |
| | | 31674(3) | | |
| | | 31706(−) | | |
| | | 31748(3) | | |
| | | | 31773(1) | |
| | | 31786(6) | 31784(1) | |
| | | | 31791(1) | |
| | | 31822(2) | | |

| McClure and Schnepp [3] a polarized | Present work a polarized | Prikhotjko [2] unpolarized | Present work b polarized | McClure and Schnepp b polarized |
|---|---|---|---|---|
| | | | 31840(1) | |
| | | | 31850(1) | |
| | | 31857(3) | 31858(1) | |
| | | | 31869(3) | |
| | | 31878(3) | | |
| | | | 31888(3) | 31889(m) |
| | | | 31905(2) | |
| | | | 31911(2) | |
| 31921(m) | 31920(4) | 31924(2) | | 31921(?) |
| | 31942(3) | | | |
| 31976(s) | 31961(8) | 31960(20) | 31960(9) | 31976(vs) |
| | 31977(1) | | | |
| | 31989(1) | | | |
| | 31997(2) | 31999(10) | | |
| | 32008(3) | | 31010(3) | |
| | 32022(2) | | 32023(3) | |
| | | 32026(10) | | |
| | 32031(2) | | | |
| | | 32054(10) | | |
| | | | 32079(2) | |
| | | 32083(1) | | |
| | | | 32093(1) | |
| | | | 32105(2) | |
| | 32119(2) | 32118(2) | 32119(2) | |
| 32122(w) | | | | 32122(s) |
| | 32125(2) | | 32128(2) | |
| | | | 32143(2) | |
| | 32150(2) | | 32149(2) | |
| | | 32154(2) | 32155(2) | 32154(w) |
| | 32172(3) | 32174(2) | 32173(2) | 32170(w) |
| | | | 32183(2) | |
| | 32188(4) | 32187(2) | | |
| | | | 32196(1) | |
| | 32213(1) | | 32215(1) | |
| | 32220(1) | | | |
| | | | 32226(1) | |
| 32236(s) | 32231(7) | 32229(3) | | |
| | 32242(1) | | | |
| | 32254(1) | 32255(1·5) | | |
| | | | 32259(8) | |
| | | 32274(1·5) | | 32275(m) |
| | | 32293(2) | | |
| 32298(w) | 32299(4) | | 32300(4) | 32298(m) |
| | | 32303(2) | | |
| | | | 32306(4) | |
| | | | 32312(1) | |
| | 32317(3) | 32319(2) | 32320(6) | |
| | | | 32327(1) | |
| | | 32331(1) | 32333(1) | |
| | | 32346(3·5) | 32348(6) | 32353(w) |
| | 32357(2) | | | |
| | | | 32368(1) | |
| 32375(m) | 32376(4) | 32373(1) | 32376(3) | 32375(?) |

| McClure and Schnepp [3] *a* polarized | Present work *a* polarized | Prikhotjko [2] unpolarized | Present work *b* polarized | McClure and Schnepp *b* polarized |
|---|---|---|---|---|
|  | 32387(4) | 32385(2) | 32384(1) ⎫<br>32388(1) ⎭ |  |
| 32397(s) | 32397(4) | 32396(3·5) | 32398(5) |  |
| 32420(s) | 32411(6) | 32412(5) | 32414(8) | 32420(m) |
| 32432(w) | 32433(1) | 32430(3·5) |  | 32432(s) |
|  | 32444(1) |  | ⎧ 32444(1) |  |
|  |  | 32448(2) | ⎨ |  |
|  |  |  | ⎩ 32450(1) |  |
|  | 32455(2) |  | 32454(1) |  |
| 32466(w) | 32463(8) | 32462(4) | 32463(7) | 32466 |
|  | 32472(1) |  |  |  |
|  |  |  | 32481(1) |  |
|  | 32492(1) |  | 32490(1) |  |
|  |  | 32492(2) |  |  |
| 32495(w) | 32497(1) |  | 32495(4) | 32495(s) |
|  | 32504(1) |  |  |  |
|  |  |  | 32507(1) |  |
|  | 32510(1) |  |  |  |
|  |  |  | 32516(1) |  |
|  | 32527(3) |  | 32525(4) |  |
| 32535(w) | 32537(2) | 32537(2) | 32537(4) | 32535(m) |
|  |  |  | 32548(1) |  |
|  | 32551(1) |  |  |  |
|  |  |  | 32555(1) |  |
|  | 32564(4) |  | 32565(4) |  |
|  | 32574(4) | 32574(1·5) | 32575(4) |  |
|  |  |  | 32585(2) |  |
|  |  | 32595(1) | 32594(2) |  |
|  |  |  | 32601(2) |  |
|  |  |  | 32614(3) |  |
| 32621(m) | 32620(6) | 32619(4) | 32621(6) | 32621(?) |
|  |  |  | 32633(2) |  |
| 32640(m) | 32641(5) ⎫ |  | ⎧ 32643(4) | 32640(w) |
|  |  | 32649(1·5) | ⎨ |  |
|  | 32652(2) ⎭ |  | ⎩ 32653(3) |  |
|  | 32664(1) |  | 32663(2) |  |
|  | 32675(9) | 32676(10) | 32678(8) |  |
| 32690(m) | 32693(2) |  | 32692(1) | 32690(vs) |
|  |  |  | 32697(1) |  |
| 32710? | 32707(2) | 32701(1) | 32707(3) | 32710(m) |
|  | 32713(2) |  |  |  |
|  |  | 32718(1·5) |  |  |
|  |  |  | 32721(3) |  |
|  | 32725(4) |  | 32727(3) |  |
|  | 32737(2) |  | 32735(1) |  |
| 32750(s) | 32748(7) | 32747(2) | 32749(6) | 32750(w) |
|  | 32763(2) |  | 32759(3) |  |
|  |  | 32767(3·5) |  |  |
| 32772(s) | 32769(8) |  | 32770(6) | 32772(w) |
|  |  |  | 32777(2) |  |
|  | 32780(3) |  |  |  |
|  |  | 32786(2) | 32784(1) |  |
| 32794(w) | 32791(3) | 32792(1) | 32792(3) | 32792(?) |
|  | 32801(1) |  | 32799(1) |  |

| McClure and Schnepp [3] a polarized | Present work a polarized | Prikhotjko [2] unpolarized | Present work b polarized | McClure and Schnepp b polarized |
|---|---|---|---|---|
| | 32806(1) | 32807(1·5) | 32805(1) | |
| | | | 32813(2) | |
| | 32816(2) | | | |
| | | | 32819(2) | |
| 32835(w) | 32832(6) | 32831(3) | 32832(5) | 32835(vw) |
| | | | 32840(2) | |
| | 32847(2) | | 32846(2) | |
| | 32853(1) | | | |
| | 32861(1) | 32862(1) | 32858(1) | |
| | 32869(3) | | 32869(5) | |
| 32880(w) | 32874(5) | 32876(2) | 32873(5) | |
| | 32880(3) | | | |
| | | | 32885(2) | |
| | 32890(2) | | | |
| | | | 32896(2) | |
| | | | 32903(2) | |
| | 32910(2) | 32909(1) | 32910(6) | |
| | | 32918(1) | | |
| | 32922(3) | 32922(1) | 32924(6) | |
| | 32931(2) | | | |
| | 32940(1) | 32938(1) | | |
| | 32948(8) | 32948(10) | | |
| 32962(m) | | | 32952(8) | 32962(vs) |
| | 32956(7) | 32958(5) | | |
| | 32969(4) | 32971(2) | 32972(2) | |
| | 32979(4) | 32983 | 32980(2) | |
| 32990(w) | | | 32990(2) | 32990(vs) |
| | 32995(3) | | 32998(2) | |
| | | 33000(1) | | |
| | 33005(3) | | 33006(2) | |
| 33015(vs) | 33014(3) | 33013(1) | 33013(2) | 33015(s) |
| | 33029(3) | 33029(1) | | |
| | | | 33033(5) | |
| 33043(vw) | 33038(3) | 33035(4) | 33041(2) | 33043(s) |
| | 33054(1) | | | |
| | | | 33056(5) | |
| 33060(vw) | 33058(6) | 33055(4·5) | | 33060(m) |
| | | | 33060(5) | |
| | 33065(2) | | | |
| | | 33070(3·5) | 33069(3) | |
| | 33073(2) | | | |
| | 33082(3) | | | |
| 33080(w) | 33091(6) | 33089(3·5) | 33093(4) | 33080(w) |
| 33105(m) | 33103(7) | 33103(9) | 33105(8) | 33105(m) |
| 33118(m) | | | 33117(3) | 33118(m) |
| | 33123(3) | | 33124(2) | |
| 33127(m) | | | | 33127(s) |
| | 33130(6) | 33130(4) | 33131(5) | |
| 33149(m) | 33150(7) | 33151(9) | 33152(8) | 33149(s) |
| | 33159(1) | | | |
| 33163(m) | 33167(2) | 33167(3) | 33169(4) | 33163(s) |
| 33179(m) | 33177(3) | 33177(4) | 33178(5) | 33179(s) |
| | 33186(1) | | | |

| McClure and Schnepp [3] *a* polarized | Present work *a* polarized | Prikhotjko [2] unpolarized | Present work *b* polarized | McClure and Schnepp *b* polarized |
|---|---|---|---|---|
| | 33193(2) | | ⌈ 33194(3) | |
| | | 33200(1) | { | |
| 33204(w) | | | ⌊ 33205(3) | 33204(w) |
| | ⌈ 33218(3) ⌉ | | | |
| 33220(w) | { } | 33221(1) | 33221(5) | 33220(w) |
| | ⌊ 33222(3) ⌋ | | | |
| | 33233(3) | | 33234(3) | |
| 33243(vw) | 33238(3) | 33240(3·5) | 33243(8) | 33243(2) |
| 33257(vw) | 33255(5) | | 33255(4) | 33257(w) |
| | 33265(5) | 33264(2) | 33265(4) | |
| | | | 33269(2) | |
| | 33276(1) | | | |
| | 33284(3) ⌉ | | ⌈ 33282(3) | |
| | { | 33289(2) | { | |
| | 33291(3) ⌋ | | ⌊ 33292(3) | |
| | 33302(7) | 33301 | 33302(6) | |
| 33310(vvw) | 33313(2) | | 33313(3) | 33310(vw) |
| | 33319(2) | | | |
| | | | 33322(3) | |
| | 33324(2) | 33325(1) | | |
| | 33336(3) | 33337(1) | 33338(4) | |
| | 33343(3) | 33341(2) | 33344(3) | |
| | 33350(8) | 33351(6) | 33352(7) | |
| | ⌈ 33361(3) ⌉ | | ⌈ 33363(4) ⌉ | |
| 33366(w) | { } | 33369(1) | { } | 33366(m) |
| | ⌊ 33369(2) ⌋ | | ⌊ 33370(3) ⌋ | |
| | 33379(2) | | | |
| | 33387(8) | | | |
| | 33390(8) | 33390(8) | | |
| 33412(m) | 33412(5) | 33413(2) | | |
| 33428(m) | 33427(7) | 33428(9) | | |
| | 33433(7) | | | |
| 33441(m) | 33442(8) | 33445(10) | | |
| 33456(vs) | 33459(1) | | | |
| | 33467(3) | | | |
| | 33471(3) | 33471(3) | | |
| 33481(s) | | | | |
| | 33489(2) | | | |
| | 33499(3) | 33500(6) | 33500(6) | |
| | 33509(2) | | 33510(6) | |
| 33518(w) | | | | |
| | 33535(4) | 33536(6) | 33535(6) ⌉ | |
| | | | | 33542(w) |
| | 33547(3) | | | |
| | 33560(4) | 33560(4·5) | 33561(6) ⌋ | |
| | 33572(3) ⌉ | | | |
| | { | 33576(4) | | |
| | 33580(2) ⌋ | | | |
| | 33585(2) | 33586(4) | | |
| | 33595(2) | | | |
| | 33601(4) | 33599(5) | | |
| | 33611(2) | 33615(5) | | |
| | 33625(2) | 33623(7) | | |
| | 33632(3) | | | |

| McClure and Schnepp [3] *a* polarized | Present work *a* polarized | Prikhotjko [2] unpolarized | Present work *b* polarized | McClure and Schnepp *b* polarized |
|---|---|---|---|---|
| | 33648(6) | 33646(10) | | |
| | 33658(6) ⎫ | | | |
| | | 33662(10) | | |
| | 33666(6) ⎬ | | | |
| | 33683(3) ⎭ | 33682(7) | | |
| | | 33700(9) | | |
| | | 33715(–) | | |
| | | 33736(20) | | |
| | | 33763(15) | | |
| | | 33784(15) | | |
| | 33796(2) | | | |
| | 33804(2) | | | |
| | 33826(4) | 33826(8) | | |
| | 33856(6) | 33855(10) | | |
| | 33872(5) | 33873(9) | | |
| | 33889(3) | 33887(6) | | |
| | 33899(3) | 33898(6) | | |
| | 33916(2) | | | |
| | 33927(2) | 33926(8) | | |
| | 33935(4) | 33936(9) | | |
| | 33946(4) | 33945(8·5) | | |
| | 33965(8) | 33966(10) | | |
| | 33979(7) | 33980(9) | | |
| | 33985(6) | | | |
| | 33995(7) | 33995(9) | | |
| | 34002(3) | | | |
| | 34015(3) | 34017(2) | | |
| | 34021(2) | | | |
| | 34038(3) | 34038(7) | | |
| | 34064(3) | 34063(4) | | |
| | | ⎡ 34078(5) | | |
| | 34082(3) ⎨ | | | |
| | | ⎣ 34088(5) | | |
| | 34105(6) | 34104(9) | | |
| | 34119(2) | | | |
| | 34131(2) | 34134(1) | | |
| | 34149(7) | 34149(8) | | |
| | 34168(3) ⎫ | | | |
| | | 34172(7) | | |
| | 34176(3) ⎭ | | | |

REFERENCES

[1] Craig, D. P., Lyons, L. E., Walmsley, S. H., and Walsh, J. R., 1959, *Proc. chem. Soc.*, p. 389.
[2] Prikhotjko, A. F., 1944, *J. Phys., Moscow*, **8**, 257.
[3] McClure, D. S., and Schnepp, O., 1955, *J. chem. Phys.*, **23**, 1575.
[4] Zmerli, A., 1959, *J. Chim. phys.*, p. 357.
[5] Griessbach, von D., Will, G., and Wolf, H. C., 1956, *Z. Naturf.* A, **11**, 791.
[6] Prikhotjko, A., and Shpak, M. T., 1959, *Optics & Spectrosc.*, **6**, 73; Shpak, M. T., and Sheka, E. F., 1960, *Optics & Spectrosc.*, **8**, 32.
[7] Craig, D. P., Hollas, J. M., Redies, M. F., and Wait, S. C., 1959, *Proc. chem. Soc.* p. 361 (and in press).

[8] FREEMAN, D. E., 1961, *J. mol. Spectrosc.*, **6**, 305.

[9] OBREIMOV, I., and SHABALDAS, C., 1943, *J. Phys., Moscow*, **7**, 168.

[10] SCHNEPP, O., and MCCLURE, D. S., 1953, *J. chem. Phys.*, **21**, 959.

[11] BOLOTNIKOVA, T. N., 1959, *Bull. Akad. Sci. U.R.S.S.*, **23**, 29.

[12] SHPOLSKY, E. V., 1956, *Bull. Akad. Sci. U.R.S.S.*, **20**, 471.

[13] PESTEIL, P., 1960, *C. R. Acad. Sci., Paris*, **250**, 497.

[14] PESTEIL, P., and CIAIS, A., 1960, *C. R. Acad. Sci., Paris*, **250**, 494.

[15] CRAIG, D. P., 1955, *J. chem. Soc.*, p. 2302.

[16] MCCLURE, D. S., 1954, *J. chem. Phys.*, **22**, 1668.

# The crystal spectra of very weak transitions
## II. Theoretical

by D. P. CRAIG and S. H. WALMSLEY†

William Ramsay and Ralph Forster Laboratories, University
College London

The theory of intermolecular resonance effects in the spectra of molecular
crystals is extended to very weak systems in which the pure electronic transi-
tions are either forbidden (as in the benzene 2600 Å system) or comparable
in intensity with accompanying vibrationally induced transitions (as in the
naphthalene 3200 Å system). For the pure electronic transitions the inter-
molecular coupling is through transition octupole moments, giving splittings
and intensity transfers of the same type, though smaller, as those familiar in
the stronger, dipole-coupled, systems. Values of octupole–octupole and
octupole–dipole interactions sums are reported for naphthalene and the crystal
spectrum calculated. For vibration-induced transitions it is shown that the
intermolecular effects are due only to the small component of ' stolen '
character, thus allowing the lack of splitting and intensity transfer to be
understood. The nature of such bands as arising from localized excitation
can thus be explained in the framework of the simple rigid-lattice exciton
theory.

---

## 1. Introduction

Applications of the weak-coupling model [1] to the excited states of molecular
crystals have been made to interpret several ultra-violet spectra, including among
many examples particular band systems of benzene [2], naphthalene [3], anthra-
cene [4], phenanthrene [5] and coronene [6]. The phenomena which have been
understood, at least approximately, as the result of these studies, may be sum-
marized under two heads:

(i) In intense molecular transitions with oscillator strengths in the order
$f = 1.0$, two or more absorption maxima appear in the crystal for each vapour maxi-
mum according to the number of molecules in the unit cell, separated by *Davydov
splitting intervals*. The several maxima record absorption of light with particular
directions of polarization in relation to the crystal axes, and their intensities agree
approximately with expectation based on the squares of projections of the lengths
of the active molecular absorption direction on the crystal axes. First-order
perturbation theory on free molecule wave functions applies fairly well in this
case, and allows the splittings to be calculated.

(ii) In weaker transitions with oscillator strengths of about $f = 0.1$ changes due
to mixing with stronger transitions are superimposed on first-order effects that
are smaller than those in (i) in proportion to the ratio of intensities. An example
of this in anthracene has been discussed in detail [4]; the ratio of polarized in-
tensities is altered from the oriented gas value 7 : 1 to about 3 : 1 by second-order

---

† Present address: Division of Basic Physics, National Physical Laboratories, Teddington.

effects.    In systems of this class, the first-order energy changes are usually less than the energy intervals separating the maxima of members of a vibrational progression in the unperturbed molecule absorption system and each such vibrational maximum must be treated as a separate energy state in calculating crystal interactions.

In this paper we shall discuss the class of still weaker transitions, with oscillator strengths of about $f = 0.002$, which are either electronically forbidden in the free molecule, as is the 2600 Å system of benzene assigned $B_{2u} \leftarrow A_{1g}$, or are electronically allowed but extremely weak, as in the 3200 Å system of naphthalene, assigned to the long axis polarized species $B_{2u} \leftarrow A_g$ in the symmetry convention recommended by the International Commission [7].    In these cases all or most of the intensity observed is induced by vibrational disturbance of the electronic upper state concerned.    As we shall show, examples in this class can be understood by straight-forward development of the first and second-order theory already mentioned, without the need to invoke special doctrines of interaction with lattice motion, as has sometimes been thought necessary.    This theory, based as before on the rigid-lattice model and zero excitation wave vector, accounts very well for the principal observed features of the naphthalene 3200 Å system as already briefly noted [8].

Following the presentation of Craig and Walsh (loc. cit.) we suppose that each of the molecules constituting the crystal has a ground state wave function $\phi$ and a set of excited states $\varphi^r$.    The transitions in the free molecule from the ground state have energies $\Delta w^r$ measured in the equivalent wave numbers.    Their oscillator strengths $f$ measured in the vapour or solution spectrum lead to values of the transition dipole moments $\mathbf{M}^r$ according to the formula (1), the moment being measured in electronic charge times the atomic unit of length, and the energy $\mathscr{E}$ in Rydbergs,

$$f = (\tfrac{1}{3}) \mathbf{M}^2 \mathscr{E}. \tag{1}$$

The crystal ground-state wave function is taken to be the simple product of free molecule functions (2)

$$\Phi_G = \varphi_1 \varphi_2 \cdots \varphi_N \tag{2}$$

for the $N$ molecules constituting the finite crystal.    The ground state energy is given by (3), $\mathbf{V}_{lk}$ being the intermolecular potential energy and $w$ the molecular energy in the ground state:

$$E_G = Nw + \sum\sum \int \varphi_l \varphi_k \, \mathbf{V}_{lk} \, \varphi_l \varphi_k \, d\tau. \tag{3}$$

Wave functions for excited states of the crystal are built from localized excitation functions (4)

$$\phi^r_{ip} = \varphi_{11} \varphi_{12} \cdots \varphi^r_{ip} \cdots \varphi_{h, N/h} \tag{4}$$

in which one of the molecules is in its $r$th excited state, shown in (4) as the molecule occupying the $i$th site in the $p$th unit cell, in a crystal in which each of the unit cells has $h$ molecules.    Combinations of the functions (4) for translationally equivalent molecules can be set up according to representations of the translation group. For zero wave vector we have

$$\Phi^r_i = \sqrt{\left(\frac{h}{N}\right)} \sum_p \phi^r_{ip}. \tag{5}$$

Finally, it is necessary to combine the functions (5) appropriate to the several unit cell sites to get excited state crystal wave functions. In some cases the appropriate combinations are fully specified by symmetry, and in others it is necessary to solve a secular equation of low degree. In the special case of two crystallographically equivalent molecules in the unit cell, as in the monoclinic crystal of naphthalene which we shall use as an example, the wave functions are given by expression (6)

$$\Psi^r_{a,b} = 2^{-1/2} (\Phi^r_1 \pm \Phi^r_2).\tag{6}$$

Optical transitions are allowed from the ground state to upper states of $u$ character. In crystalline naphthalene molecules lie on inversion centres of the crystal, leading to the conclusion that allowed molecular transitions alone are permitted in the crystal; straight-forward application of symmetry arguments show that transitions to the state $\Psi^r_a$ with the upper sign in (6) are polarized in the $ac$ crystal plane, and to $\Psi^r_b$ with the lower sign along the $b$ crystal axis†.

Again, by applying the general argument (Craig and Walsh loc. cit.) to the naphthalene crystal it can be shown that the transition energies in the crystal spectrum are given by solutions of two secular equations, one for each of the crystal symmetry species to which transitions are allowed. Expression (7) is the secular equation for the $ac$ polarized absorption:

$$\det\{(\Psi^r_a \,|\, \sum_k \mathbf{H}_k + \sum\sum_{l<k} \mathbf{V}_{kl} - E_G \,|\, \Psi^s_a) - (\Psi^r_a \,|\, 1 \,|\, \Psi^s_a)E\} = 0.\tag{7}$$

$\mathbf{H}_k$ is the free molecule Hamiltonian of the $k$th molecule and the superscripts $r$ and $s$ refer to the $u$ *vibronic* excited states. The degree of the equation (7) equals the number of excited states that have to be included to give a result of the desired accuracy. Usually, as in naphthalene, not more than three electronic upper states are known well enough to be included. The diagonal elements of (7) give the first-order values of transition energies which, in intense systems, are not much altered by interactions with other states. Therefore the secular equation (7) only has to be solved for weaker systems, in which the off-diagonal elements become relatively more important.

Reduction of the matrix elements in (7) to primitive terms is effected as described for anthracene [4]. The matrix components in the diagonal elements reduce to

$$\Delta w^r + D^r + \sum_p{}' I^r_{lp} \pm \sum_q I^r_{lm}\tag{8}$$

the upper sign referring to $a$ components, and the lower to $b$, where

$$I^r_{lk} = (\varphi_l \varphi_l^r \,|\, \mathbf{V}_{lk} \,|\, \varphi_k \varphi^r_k)$$

and

$$D^r = \sum_q{}' \{(\varphi^r_p \varphi_q \,|\, \mathbf{V}_{pq} \,|\, \varphi_p^r \varphi_q) - (\varphi_p \varphi_q \,|\, \mathbf{V}_{pq} \,|\, \varphi_p \varphi_q)\}.$$

† The molecular axes are signed according to the following convention. A right-handed set of axes is located in the molecule at the origin. The axes in other molecules in the crystal are generated from this one by translation or by reflection in the $ac$ plane followed by translation.

The summations in (8) are over equivalent molecules (subscript $p$) and inequivalent (subscript $m$) respectively.    The non-diagonal elements reduce to expression (9)

$$\sum_{p}' K^{rs}{}_{lp} + \sum_{m} K^{rs}{}_{lm} + \sum_{p}' J^{rs}{}_{lp} \pm \sum_{m} J^{rs}{}_{lm} \tag{9}$$

where

$$K^{rs}{}_{lp} = (\varphi^r_l \varphi^s_l \,|\, \mathbf{V}_{lp} \,|\, \varphi_p \varphi_p)$$

$$J^{rs}{}_{lp} = \tfrac{1}{2}\{(\varphi_l \varphi^r_l \,|\, \mathbf{V}_{lp} \,|\, \varphi_p \varphi_p{}^s) + (\varphi_l \varphi_l{}^s \,|\, \mathbf{V}_{lp} \,|\, \varphi_p \varphi^r_p)\}.$$

The integrals may be given values in a convenient way if the interaction potential $\mathbf{V}_{kl}$ is first expanded as a series of multipole interaction terms as, for example, summarized by Hirschfelder et al. [9].    The first term in the expansion is then the interaction energy of two point dipoles of moments equal to the *transition* dipole moments leading to the free molecule excited states concerned. Since these transition dipole moments can be deduced from the measured transition intensities according to formula (1) the dipole–dipole interaction at least can be directly related to experimental quantities.    The interaction is in fact determined by sums of the dipole–dipole interaction over the crystal lattice, a number of which have now been reported in the papers already cited.    Investigation of magnitudes shows that, if a transition is of oscillator strength $f = 0\cdot1$ or more, the dipole terms will usually dominate, and this explains why it has not been necessary in dealing with intense systems to go beyond the dipole–dipole interaction in the expansion of $\mathbf{V}_{kl}$.    It should be mentioned that the integrals $D$ and $K$ appear in the expressions for the two polarized components with the same sign and are not important in the splitting of the absorption bands but only in the shift of the average absorption frequency from its vapour value.    Certain of the integrals $I$ and $J$ appear with opposite signs in the $a$ and $b$ components and are responsible for the splitting and also for a contribution to the shift.

## 2. Application to very weak transitions

In successively weaker transitions, having smaller and smaller dipole transition moments, the effects described in the last section should die away, leaving the spectrum of an oriented gas.    This is not observed in practice.    Such spectra show two main features which require separate treatment [8].    One is that pure electronic transitions appear unexpectedly strongly in the crystal compared with the vapour spectrum, and may show splittings up to one or two hundreds of wave numbers, and the other is that, in contrast, transitions which appear through the action of non-totally symmetrical vibrations are little changed in the crystal in intensity, and show only small splittings, in the order of 1 cm⁻¹.    We shall deal first with the calculation of changes in pure electronic transitions.

The effects in those bands of weak systems which record pure electronic transitions may be dealt with by taking higher terms in the expansion of the intermolecular potential $\mathbf{V}_{kl}$.    In the development, the following definitions of the tesseral harmonics (unnormalized) will be used :

$$Y_l^{m(c)} = (\tfrac{1}{2})(Y_l^m + Y_l^{-m}) = P_l^m (\cos\theta) \cos m\phi,$$

$$Y_l^{m(s)} = (\tfrac{1}{2i})(Y_l^m - Y_l^{-m}) = P_l^m (\cos\theta) \sin m\phi. \tag{10}$$

We then have, in expressions (11), the definitions of the corresponding multipole moments

$$Q_l^0 = r^l P_l^0 (\cos\theta) \qquad\qquad\qquad = r^l Y_l^0,$$
$$Q_l^{m(c)} = r^l P_l^m (\cos\theta) \cos m\phi \qquad = r^l Y_l^{m(c)}, \qquad\quad (11)$$
$$Q_l^{m(s)} = r^l P_l^m (\cos\theta) \sin m\phi \qquad = r^l Y_l^{m(s)}.$$

In relation to the axes shown for the naphthalene molecule the polar angles $\theta$ and $\phi$ are measured respectively downward from the $N$ axis, and anticlockwise from $L$ in the $LM$ plane.
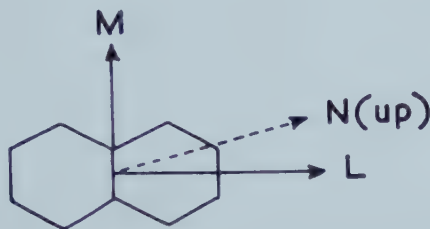


The first few terms in the expansion of the intermolecular potential between two neutral molecules $k$ and $l$ are given in (12)

$$\mathbf{V}_{kl} = e^2 R_{kl}^{-3} \sum_i \sum_j a_{ij} Q_1^i Q_1^j + e^2 R_{kl}^{-4} \sum_i \sum_j \{b_{ij} Q_1^i Q_2^j + b_{ij}' Q_2^i Q_1^j\}$$
$$+ e^2 R_{kl}^{-5} \sum_i \sum_j c_{ij} Q_2^i Q_2^j + \text{terms in } R^{-6}, R^{-7}, \dots . \qquad (12)$$

In each of the terms of expression (12) the first of the $Q$'s refers to molecule $k$ and the second to $l$. The coefficients $a_{ij}$, $b_{ij}$ and $c_{ij}$ depend on the orientations of the molecules to one another in the lattice, through the so-called Wigner coefficients, given in full by Curtiss *et al.* [9]. Finally the indices $i$ and $j$ run over all the values 0, 1 (c), 1(s), 2(c), 2(s), up to the order of the harmonics concerned. The first term of (12) is the dipole–dipole interaction, the second the dipole–quadrupole, and the third the quadrupole–quadrupole interaction. Since each of the $eQ$'s in a component of an electric multipole moment operator referred to a system of *molecular* axes, successive terms in the integrals $J$ in expression (9) are proportional to the products of *transition* multipole moments for the transitions of $\phi^k \leftarrow \phi$ and $\phi^s \leftarrow \phi$. Thus it follows that an integral $J$ will have a contribution from a chosen term of $\mathbf{V}_{lk}$ in (12) only if the relevant transition multipole moments are both non-zero. For example, in a $u \leftarrow g$ transition of naphthalene the odd-order multipoles alone contribute, successively dipole–dipole ($R^{-3}$), dipole–octupole ($R^{-5}$), octupole–octupole ($R^{-7}$), dipole-32-pole ($R^{-7}$) and higher terms. On account of the rising inverse powers of $R$ along the series it turns out that if a transition is dipole allowed its transition dipole moment is the only one that needs to be considered, unless it happens to be very small in spite of the allowed character of the transitions. In general only the terms of the lowest non-vanishing multipole moment have to be included, which cuts down the number of important terms in the expansion (12) to one or two. In any weak system the transition dipole moment is zero or very small, and the important interaction terms are the octupole–octupole for first-order effects, and dipole–octupole for second-order effects concerned in the crystal induced mixing of the weak transition with strong transitions near it in frequency.

In naphthalene the symmetry species of upper states, and active directions for allowed transitions from an $A_g$ ground state, are $B_{1u}(M)$, $B_{2u}(L)$, and $B_{3u}(N)$, in a

notation following the recommendations of the Joint Commission on Spectro-scopy [7]. In each of the transitions of species $B_{2u} \leftarrow A_g$ (long-axis polarized) and $B_{1u} \leftarrow A_g$ (short-axis polarized) there are two active components of the octupole transition moment, given in formulae (13). The first two refer to $L$ polarized, and the second two to $M$ polarized transitions.

$$
\begin{aligned}
Q_3{}^{1c} &= (3/2) L(5N^2 - R^2), \\
Q_3{}^{3c} &= 15 L(L^2 - 3M^2), \\
Q_3{}^{1s} &= (3/2) M(5N^2 - R^2), \\
Q_3{}^{3s} &= 15 M(3L^2 - M^2).
\end{aligned}
\qquad (13)
$$

| Set† | $(L,\ L)$ | $(M,\ M)$ | $(N,\ N)$ | $(L,\ M)$ | $(L,\ N)$ | $(M,\ N)$ |
|---|---|---|---|---|---|---|
| 1 | $+575$ | $-778$ | $+202$ | $+323$ | $-213$ | $+656$ |
| 2 | $+1361$ | $+80$ | $-1489$ | $+1164$ | $+1622$ | $-351$ |

† Set 1: sums over translationally equivalent molecules.
  Set 2: sums over inequivalent molecules.

Table 1.   Dipole–dipole sums for crystalline naphthalene (cm$^{-1}$ Å$^{-2}$).

| Set† | $Q_1{}^{1c} - Q_3{}^{1c}$ | $Q_1{}^{1c} - Q_3{}^{3c}$ | $Q_1{}^{1s} - Q_3{}^{1s}$ | $Q_1{}^{1s} - Q_1{}^{3s}$ |
|---|---|---|---|---|
| 1 | $-3.8$ | $-1.8$ | $-11.0$ | $+1.5$ |
| 2 | $+15.9$ | $+2.8$ | $+72.8$ | $+0.3$ |

| Set† | $Q_1{}^{1c} - Q_3{}^{1s}$ | $Q_1{}^{1c} - Q_3{}^{3s}$ | $Q_1{}^{1s} - Q_3{}^{1c}$ | $Q_1{}^{1s} - Q_3{}^{3c}$ |
|---|---|---|---|---|
| 1 | $+2.5$ | $-2.5$ | $+2.5$ | $-2.3$ |
| 2 | $+45.7$ | $-6.4$ | $-28.9$ | $-0.8$ |

† Set 1: sums over translationally equivalent molecules.
  Set 2: sums over inequivalent molecules.

Table 2.   Dipole–octupole sums for crystalline naphthalene (cm$^{-1}$ Å$^{-4}$).

## 3. First-order calculations

We can now state what data are necessary to calculate the splittings and other crystal effects in pure electronic transitions according to the secular equations (7). These are, first, the values of the dipole transition moment and the two components of the transition octupole moment for the molecular transition concerned and, second, the values of lattice-interaction sums for dipole–dipole, dipole–octupole, and octupole–octupole interactions. The dipole transitions moments

$$(\varphi \,|\, r\, Y_1{}^0 \,|\, \varphi^r),$$

etc. are known from absorption intensities according to (1); the octupole moments such as $(\varphi \,|\, r^3\, Y_3{}^{1c} \,|\, \varphi^r)$ and $(\varphi \,|\, r^3\, Y_3{}^{3c} \,|\, \varphi^r)$ are not known, and we must discuss the whole range of their permissible values. The lattice sums can be found by high-speed computation. The values for the naphthalene lattice are given in tables 1, 2 and 3. Table 1 (dipole–dipole sums) is taken from Craig and Walsh [3].

| Set | $Q_3^{1c}-Q_3^{1c}$ | $Q_3^{3c}-Q_3^{3c}$ | $Q_3^{1c}-Q_3^{3c}$ | |
|---|---|---|---|---|
| 1 | $-0\cdot34$ | $+0\cdot0020$ | $+0\cdot012$ | |
| 2 | $+0\cdot26$ | $-0\cdot0038$ | $+0\cdot467$ | |
| | $Q_3^{1s}-Q_3^{1s}$ | $Q_3^{3s}-Q_3^{3s}$ | $Q_3^{1s}-Q_3^{3s}$ | |
| 1 | $+1\cdot49$ | $-0\cdot0007$ | $+0\cdot049$ | |
| 2 | $+5\cdot00$ | $-0\cdot0061$ | $+0\cdot017$ | |
| | $Q_3^{1c}-Q_3^{1s}$ | $Q_3^{3c}-Q_3^{3s}$ | $Q_3^{1c}-Q_3^{3s}$ | $Q_3^{3c}-Q_3^{1s}$ |
| 1 | $-0\cdot26$ | $+0\cdot0162$ | $-0\cdot049$ | $-0\cdot066$ |
| 2 | $-3\cdot50$ | $-0\cdot0079$ | $-0\cdot427$ | $-0\cdot037$ |

**Table 3.** Octupole–octupole sums for crystalline naphthalene ($cm^{-1}$ $Å^{-6}$).

The form of the octupole moment expression given in (13) allows an estimate to be made of the limits within which actual values of the components can fall. The $\pi$-electrons in naphthalene are mostly confined within a rectangular box of dimensions approximately $4\cdot85 \times 2\cdot8 \times 2\cdot8$ in Ångstrom units. For physically possible electron distributions within this box the upper limits to the matrix components of $Q_3^{1c}$ and $Q_3^{3c}$ are $O_1^c = 22\,Å^3$ and $O_3^c = 215\,Å^3$ and to $Q_1^{1s}$ and $Q_3^{3s}$ are $O_1^s = 17\,Å^3$ and $O_3^s = 332\,Å^3$. The lower limits are in each case zero. The procedure adopted in making calculations is the following. The splitting observed in systems of any intensity is principally a first-order effect, and the
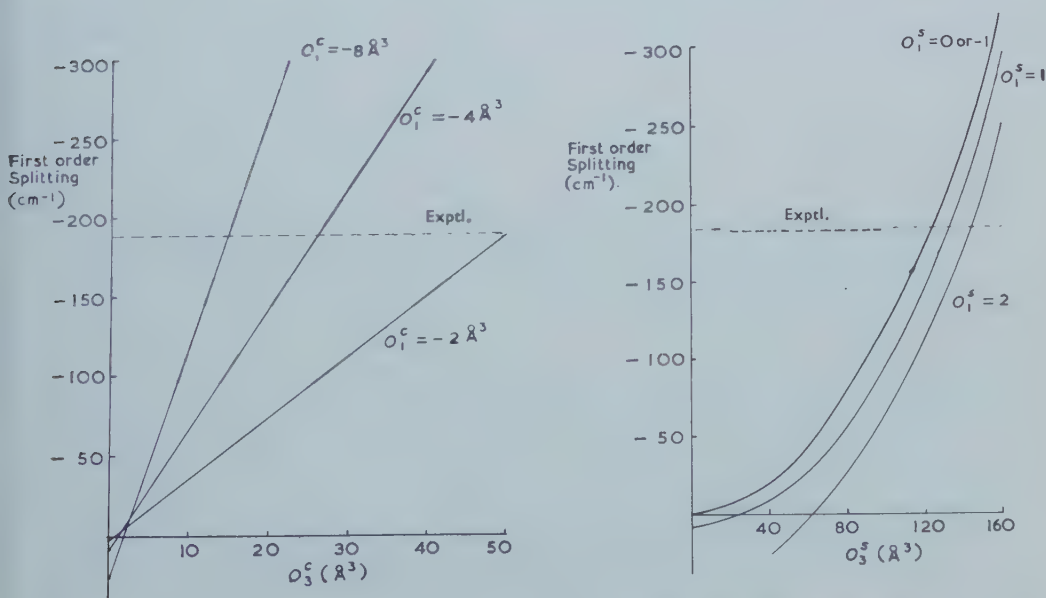


**Figure 1.** Calculated values of the splitting of the pure electronic origin band in the naphthalene crystal spectrum, the molecular transition being assumed (i) to belong to the long-axis polarized species $B_{2u} \leftarrow A_g$ (left-hand diagram) and (ii) to the short axis species $B_{1u} \leftarrow A_g$ (right-hand diagram).

intensity changes from the oriented gas values are second-order effects.    First-order calculations of the splitting are made for representative values of octupole moment components within the physically possible ranges.    Pairs of values, one of each of the components, are chosen to give splittings equal to the experimental ones ; second-order calculations of intensities are made for each pair and compared with the spectrum.    Finally, according to the indications so given, the calculations are refined iteratively.    If, as here, two different polarization directions are possible calculations are made for both.

Figure 1 shows the first-order splitting for transitions of species $B_{2u} \leftarrow A_g$ and $B_{1u} \leftarrow A_g$.    The range of octupole moments is limited to those reproducing the experimental fact that the $a$ component of the split doublet is at lower frequency [10, 11].

For the experimental value of the splitting, we use the values at liquid helium temperature [11].    Reduced to essential features, the changes between vapour and crystal spectra are those shown in figure 2.    The splitting of the origin band is
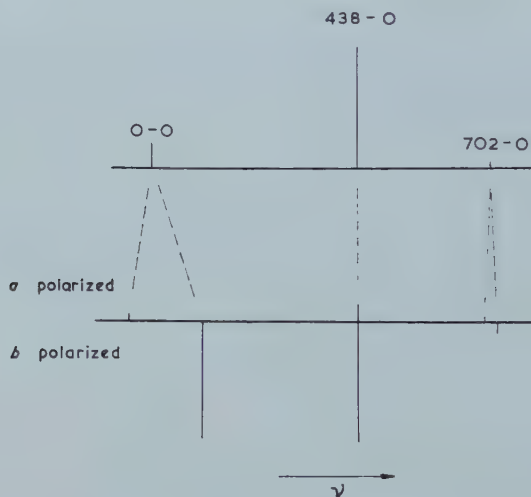


Figure 2.    The relation of the crystal spectrum (lower) to the vapour spectrum (upper) of naphthalene near the origin of the 3200 Å system, showing splittings and intensity changes.    The bands shown are the origin, the strongest false origin 438–0 and the totally symmetrical progression member 702–0.    The origin, and 702–0, are the only bands showing splittings greater than the experimental limit of 3–4 cm$^{-1}$.

151 cm$^{-1}$, but to get a value for comparison with first-order theory we must add to this the splittings observed in all bands separated from the origin by totally symmetrical vibrational intervals [4].    The total obtained by adding these weaker band splittings is 35 cm$^{-1}$, giving a total of 186 cm$^{-1}$.

Figure 1 allows the inference that if the transition is short-axis polarized the value of the octupole component $O_3{}^s = (|Q_3{}^{3s}|)$ must be at least 120 Å$^3$.    A number of pairs of values are chosen for second-order calculations from the rather small range of possible octupole moments, and discussed in the next section.    If, on the other hand, the transition is long-axis polarized, the splitting is compatible in the first order with a wide selection of values of the octupole transition moment components.    Table 3 shows that the biggest term in the first-order octupole splitting

is the cross term $Q_3{}^{1c} - Q_3{}^{3c}$, and in consequence we find that octupole components multiplying to give $O_1{}^c \times O_3{}^c \sim 105$ Å$^6$ will have about the correct splitting. It remains to choose several such pairs as the basis for the second-order calculations.

## 4. SECOND-ORDER CALCULATIONS

Second-order terms affect mainly the intensities of the lines in the spectrum of the crystal, by bringing about a mixing of the weak transition with stronger ones. What is observed is 'stealing' of intensity from intense transitions, so that intensity relationships are changed from the vapour spectrum.

An important feature of the mixing is that its extent is different in the two directions. As a result the intensity ratio of the two components of a chosen free molecule transition is not the same as the squared ratio of the projections of the active molecular axis on the two crystal axes. As well of course the total intensity changes. The observed crystal spectrum of naphthalene shows clear evidence, illustrated in figure 2, of both of these phenomena. In the first place the weak band system as a whole has an intensity four or five times stronger in $b$ polarization than in $a$ [12]. Also McClure and Schnepp [9] found, and it has been since confirmed [11] that in the origin (pure electronic) band the polarization ratio was very much higher than the average over the band system, showing that the ratio in the pure electronic transitions is higher than in the vibrationally induced ones. Moreover the $b$ component of the pure electronic band is as intense, or slightly more intense, than the $b$ component of the $0 + 438$ vibrationally induced transition, whereas if the vapour values of these intensities were unmodified the ratio would be $1 : 40$ in favour of the $0 + 438$ band, because of the smaller projections of the long molecular axis than the short.

As starting data for the second order calculations we require to know the properties of all those molecular transitions which are close enough in energy, and strong enough in intensity, to interact with the chosen transition under the influence of crystal forces. In naphthalene two such perturbing systems are known. The 2750 Å system has an oscillator strength $f \sim 0.1$, and is short-axis polarized. The 2200 Å system has $f \sim 1.7$ and is long-axis polarized. Each splits into $a$ and $b$ components in the crystal, and mixing occurs within the two sets of similarly polarized bands.

For a short axis assignment, the modified results given by the second-order calculation indicate that the best fit with experiment is given by octupole moments of approximate value $O_1{}^s = 0$ and $O_3{}^s = 95$ Å$^3$. The predicted intensity ratios, however, show that for all bands in the system the $a$ component is the more intense. In the experimentally observed spectrum, the $b$ component is always more intense, with the ratio in the 0–0 band greater than $10 : 1$. The short-axis assignment can therefore be rejected. The results of the calculation are given in table 4.

The position in the long-axis assignment is quite different. Here, as shown in figure 1, there is a wide range of pairs of octupole moment components which give about the observed splitting in the first order. In the second order only a few of these give even roughly correct intensities, and the agreement is not perfect for any. The best choice is $O_1{}^c = -9$ Å$^3$ and $O_3{}^c = 12$ Å$^3$†.

---

† In the brief report of this work [8] the values $-7$ Å$^3$ and $15$ Å$^3$ were selected. The present values give slightly better agreements.

Using these we get for the splitting $-170\,\mathrm{cm^{-1}}$ (expt. $-186$), for the polariza-
tion ratio in the origin band $a/b = 1/12$ (expt. $< 1/10$) and for the absolute oscillator
strength in the $b$ component of the pure electronic band $f = 0\cdot0006$.    The latter
increase is certainly too small, but the precise value is not known experimentally.
The agreement, however, is acceptable for the long axis assignment, the main
feature of the changes occurring between vapour and crystal being correctly
accounted for.    The results are given in table 4, which includes values for the
vibrationally induced 438–0 band.    The theory for this case is given in the following
section.

|  | Calculated for short-axis assignment, $O_1=0$, $O_3=95\,\mathrm{\AA^3}$ | Calculated for long-axis assignment $O_1=-9\,\mathrm{\AA^3}$, $O_3=12\,\mathrm{\AA^3}$ | Experiment |
|---|---|---|---|
| Splitting of 0–0 transition (cm$^{-1}$) | $-179$ | $-170$ | $-186$ |
| Splitting of 0+438 transition (cm$^{-1}$) | 11 | $0\cdot9$ | $<1$ |
| Polarization ratio $(a/b)$ of 0–0 | $1\cdot2/1$ | $1/12$ | $<1/10$ |
| Polarization ratio $(a/b)$ of 0+438 | $2\cdot1/1$ | $1/3\cdot5$ | $\sim1/4$ |
| $f$ value of $b$ component of 0–0 | $0\cdot0025$ | $0\cdot0006$ | Not known |
| $f$ value of $b$ component of 0+438 | $0\cdot0002$ | $0\cdot0035$ | Not known |

Table 4.    Calculated 3200 Å spectrum of crystalline naphthalene.

## 5. Crystal spectra of vibrationally perturbed transitions

We must consider the quite different changes in vibrationally induced transi-
tions under the influence of crystal forces and give an account of the lack of splitting
in the vibrationally induced bands.    The best known example of a vibrationally
induced electronic band system is the benzene system of electronic species
$B_{2u} \leftarrow A_{1g}$.    This is forbidden, and absorption bands appear recording transitions
to upper states in which excitation of a quantum of an $e_{2g}$ vibration is superposed
on the electronic excitation; in vibronic species the transition is of the allowed
type $E_{1u} \leftarrow A_{1g}$.    A similar mechanism is found in many weak aromatic absorption
systems, including the system in naphthalene at 3200 Å.

In the approximation of non-interacting vibrational and electronic motion the
vibronic wave function is a simple product of the electronic wave function $\varphi^r$ times
vibrational wave functions $\sigma^{r(n)}$ in each of the normal coordinates appropriate to
the symmetry and force system of the electronic state.    Thus, a single vibrational
mode being specified for simplicity, the product $\varphi^r \sigma^{r(n)}$ stands for the state in which
$n$ quanta of the vibration $\sigma$ are superposed on the electronic state $\varphi^r$, all the other
normal vibrations being in their zero quantum states.    If $\sigma$ is a totally symmetrical
vibration we have a situation which has already been analysed [13].

The intermolecular resonance integrals then contain Franck–Condon overlap integrals as factors, for example,

$$\int \sigma^{r(n)} \sigma^{0(0)} d\tau = \xi^{r(n)}.\tag{14}$$

If $\sigma$ is totally symmetrical the wave functions for all quantum levels have the same symmetry species and the factors (14) are in general non-zero.

The case is quite different for excitation of a non-totally symmetrical vibration. We take a one quantum vibration $\sigma^{r(1)}$ in a non-totally symmetrical mode and represent its effect on the electronic wave function as a mixing of this electronic wave function with another with the electronic symmetry possessed by the product $\varphi^r \sigma^{r(1)}$. Formally, the perturbed wave function is

$$c_1 \phi^r \sigma^{r(1)} + c_2 \phi^s \sigma^{s(0)};\tag{15}$$

$\varphi^r$ and $\varphi^s$ being independent of nuclear motion, i.e. specified for the equilibrium nuclear configuration. $c_1$ and $c_2$ are coefficients, $c_1$ being near unity and $c_2$ small. In practical cases we can show from the intensity of vibration-induced bands that $c_2$ is about $10^{-1}$ to $10^{-2}$. The treatment of intermolecular resonance effects introduces matrix elements of the type (16).

$$c_1^2 \left( \varphi_l^r \sigma_l^{r(1)} \varphi_l \sigma_l^{0(0)} \,|\, \mathbf{V}_{kl} \,|\, \varphi_k^r \sigma_k^{r(1)} \varphi_k \sigma_k^{0(0)} \right)$$
$$+ 2c_1 c_2 \left( \varphi_l^r \sigma_l^{r(1)} \varphi_l \sigma_l^{0(0)} \,|\, \mathbf{V}_{kl} \,|\, \varphi_k^s \sigma_k^{s(0)} \varphi_k \sigma_k^{0(0)} \right)$$
$$+ c_2^2 \left( \varphi_l^s \sigma_l^{s(0)} \varphi_l \sigma_l^{0(0)} \,|\, \mathbf{V}_{kl} \,|\, \varphi_k^s \sigma_k^{s(0)} \varphi_k \sigma_k^{0(0)} \right).\tag{16}$$

Since $\mathbf{V}_{kl}$ is a sum of interaction terms each of which is a product of a function of the positional co-ordinates of one particle only (nucleus or electron) in the $k$th molecule and one in the $l$th the first two terms of (16) will vanish, leaving the third as sole contributor. For example, in the first of the three expressions in (16) a term of $\mathbf{V}_{kl}$ involving an electron in molecule $k$ gives an integral containing the vibrational factor $\int \sigma^{r(1)} \sigma^{q(0)} d\tau$ which vanishes on account of symmetry, $\sigma$ being non-totally symmetrical; also a term involving a nuclear coordinate of molecule $k$ gives a zero contribution due to the electronic 'overlap' factor $\int \varphi_l^r \varphi_l d\tau = 0$. Thus, in the crystal spectrum of a transition induced by a non-totally symmetrical vibration only the mixed-in electronic state contributes to intermolecular resonance effects. We shall see that this enables many puzzling features of the spectra to be explained. It is at once obvious that resonance effects in such bands depending only on the small third term of expression (16) will be very small indeed, roughly in proportion to their small dipole intensities. Moreover the effects of higher multipole moments contributing to the splitting of the origin band will not appear in the accompanying vibrationally induced bands, and this is the reason for the characteristic differences that appear in crystal spectra between 'exciton' bands and 'localized excitation' bands, which show virtually no effect of crystal interactions. The latter have sometimes been discussed as if the essential feature was that the lattice structure was distorted, trapping the excitation on a particular site and so eliminating resonance effects. However, the important thing is the difficulty of resonance transfer of vibrational motion, which gives localization without the need to invoke interaction with the lattice. One can see that the same considerations, leading to very weak resonance effects, will apply to bands forming progressions and sequences for which a vibration-induced band is the apparent origin, i.e. bands separated from it by totally symmetrical intervals. Since the weak intermolecular resonance limits second as well as first order crystal effects, intensity transfers to and from vibration induced bands will be small, giving them in all respects a character approaching

expectation from the oriented gas model. On the other hand, pure electronic bands will show splitting and intensity transfer corresponding to the full operation of the higher-order moments, and this will be true of bands built on to the origin band by totally symmetrical intervals in proportion to their share of the total intensity. We anticipate therefore a clear division of the observed bands into (i) the origin band and progression members showing splitting and intensity transfer and (ii) vibrationally induced band and progression members showing very small splitting and intensity transfer. It is to be noted that even if the origin band is forbidden as in benzene it may appear under the reduced local symmetry of the crystal on account of resonance forces causing mixing with one of the allowed transitions. The two classes of crystal bands should thus be present even where only one class (the vibrationally induced) appears in the vapour.

For the calculation of the changes in the vibrationally induced bands of naphthalene first-order effects are entirely dipole–dipole in type, as has been explained. Given the intensity in the vibrationally induced bands ($f \sim 0 \cdot 0016$) we calculate the transition dipole length ($\mathbf{M} \sim 0 \cdot 067 \,\text{Å}$). Then, using the sums given in table 1, we find that, for a short-axis *vibronic* polarization the splitting is

$$(0 \cdot 067)^2 \times 2 \times 80 = 0 \cdot 7 \,\text{cm}^{-1},$$

and for a long-axis vibronic polarization it is $(0 \cdot 067)^2 \times 2 \times 1361 = 12 \cdot 2 \,\text{cm}^{-1}$, with the $b$ component lower in both cases. Experimentally the splitting is less than $1 \,\text{cm}^{-1}$, and the $b$ component is at the lower frequency. The agreement for short-axis polarization is thus satisfactory, and confirms the assignment of the vibrationally induced bands of the system to the short-axis polarized species.

In the second order we have to allow for the crystal induced mixing of the $0 + 438$ band with other electronic band systems, and this takes place once again through the dipole-dipole coupling terms in the potential. Straightforward calculation of the coupling with the $2750 \,\text{Å}$ and $2200 \,\text{Å}$ systems leads to an increase in the splitting to $0 \cdot 9 \,\text{cm}^{-1}$, and a reduction in the polarization ratio $b/a$ from the oriented gas value of $7 : 1$ to $3 \cdot 5 : 1$, which agrees satisfactorily with experiment.

## References

[1] DAVYDOV, A. S., 1948, *J. exp. theor. phys.*, **18**, 210.
[2] FOX, D., and SCHNEPP, O., 1955, *J. chem. Phys.*, **23**, 767.
[3] CRAIG, D. P., and WALSH, J. R., 1958, *J. chem. Soc.*, p. 1613.
[4] CRAIG, D. P., and HOBBINS, P. C., 1955, *J. chem. Soc.*, pp. 539 and 2309.
[5] McCLURE, D. S., 1956, *J. chem. Phys.*, **25**, 481.
[6] LYONS, L. E., and WALSH, J. R., 1959, *J. chem. Soc.*, p. 3447.
[7] INTERNATIONAL COMMISSION, 1955, *J. chem. Phys.*, **23**, 1997.
[8] CRAIG, D. P., LYONS, L. E., WALMSLEY, S. H., and WALSH, J. R., 1959, *Proc. chem. Soc.*, p. 389.
[9] HIRSCHFELDER, J. O., CURTISS, C. F., and BIRD, R. B., 1954, *Molecular Theory of Gases and Liquids* (New York: John Wiley), p. 843.
[10] McCLURE, D. S., and SCHNEPP, O., 1955, *J. chem. Phys.*, **23**, 1575.
[11] CRAIG, D. P., LYONS, L. E., and WALSH, J. R., 1961, *Mol. Phys.*, **4**, 97.
[12] CRAIG, D. P., and LYONS, L. E., 1952, *J. chem. Phys.*, **20**, 1499.
[13] CRAIG, D. P., 1955, *J. chem. Soc.*, p. 2302.

# Nuclear magnetic resonance studies of urea and thiourea adducts

by D. F. R. GILSON and C. A. McDOWELL

Department of Chemistry, University of British Columbia,
Vancouver 8, B.C., Canada

The 'wide-line' proton magnetic resonance spectra of *n*-tridecane
and *n*-hexadecane and their urea adducts have been examined from 77°K to
298°K. The results show that the enclosed component is capable of a con-
siderable degree of molecular motion. Estimates of the energy barriers
involved support the idea that the interaction between the urea cage and the
adducted hydrocarbon is only slight.

The thiourea adducts of some cyclic hydrocarbons have also been
examined.

## 1. Introduction

Adducts of urea [1] and thiourea [2] can be prepared from a variety of organic
molecules bearing various functional groups. In general urea forms adducts
with straight chain compounds, and thiourea forms adducts with branched and
cyclic compounds. The interest shown in these complexes has largely been
confined to their technological applications in the petroleum industry. Apart
from the x-ray structural investigations of Smith [3], Schlenk [4], and Lenne [5],
the only physical measurements which appear to have been made are the infra-red
studies of Fischer and McDowell [6], Stuart [7], and Barlow and Corish [8],
and the dielectric absorption measurements of Meakins [9]. From these
investigations information can be obtained concerning the changes in the urea
lattice resulting from the formation of the complexes. The bands assigned to
the urea molecules in the infra-red spectra of the complexes show marked shifts
in frequency compared with the spectrum of pure urea. These shifts are
attributed to the changes in hydrogen bonding which occur when the complexes
are formed. Little information can be obtained from any of these studies
regarding the behaviour of the enclathrated hydrocarbons. Dielectric absorption
studies [9] on long chain esters, ethers, ketones and alkyl bromides yield
interesting results in that they indicate only a slight interaction between the
urea lattice and the enclosed component. The high frequency of the absorption,
and low values of the energy barriers, indicate that the enclosed compounds are
only loosely held. The dielectric absorption of the 1 : 10-dibromodecane adduct,
which should possess zero dipole moment, was interpreted in terms of a
reorientation of the C–Br dipoles independently of the molecular chain. Buckling
and twisting of the carbon chain adjacent to the dipole was suggested to account
for the dielectric absorption in long chain ketones and secondary bromides.

'Wide-line' nuclear magnetic resonance provides an excellent means of
investigating molecular motion and we have used this technique to study
*n*-tridecane and *n*-hexadecane and their urea adducts, and also the thiourea

adducts of some cyclic hydrocarbons. To study the behaviour of the hydrocarbon itself, unobscured by resonance from the protons of the lattice, adducts were prepared using fully deuterated urea and thiourea.

## 2. Experimental

Chemicals were obtained from the following sources:

| | | |
|---|---|---|
| *n*-Tridecane | Phillips Petroleum Co. | 99 mole per cent pure |
| *n*-Hexadecane | Humphrey Wilkinson Inc. | 99 mole per cent pure |
| Cyclohexane | Eastman Kodak | SpectroGrade |
| Methyl cyclohexane | Eastman Kodak | SpectroGrade |
| Cyclohexane | Phillips Petroleum Co. | 99·98 mole per cent pure |
| Cyclopentane | Phillips Petroleum Co. | 99·98 mole per cent pure |
| Methyl cyclopentane | Phillips Petroleum Co. | 99 mole per cent pure |

Urea-$d_4$ and thiourea-$d_4$ were prepared by repeated recrystallization of reagent grade chemicals from pure $D_2O$. In preparing the adducts the calculated amount of hydrocarbon was added to a saturated solution of urea in deuterated methanol (prepared by decomposing magnesium methylate with $D_2O$). The solution was warmed until the precipitated adduct had dissolved, and then allowed to cool in a preheated, lagged Dewar. The larger crystals, *c*. 35 mm long, were crushed into 5 mm o.d. Pyrex tubes of which the bottom 3 cm were thinned to improve the 'filling factor' when the tubes were inserted in the n.m.r. probe.

The proton magnetic resonance spectra were obtained in a Varian V4200/4300B dual purpose spectrometer operating at 40 Mc/s. Temperature control was achieved by passing a stream of cooled nitrogen gas through a Dewar lead around the sample. The gas flow was obtained either by boiling liquid nitrogen directly with a heater, or by passing a stream of dry nitrogen through a copper coil immersed in refrigerant (liquid $N_2$, or a $CO_2$–acetone mixture). Temperatures were measured with a copper/constantan thermocouple connected to a ' Rubicon ' potentiometer. Second moments were obtained from the derivative curves by integration using the Van Vleck formulae [10]; the mean of four values being taken. The standard deviations were 0·35 gauss² for the adducts and 0·25 gauss² for the hydrocarbons. Line widths were measured between points of maximum slope of the absorption curve, as given by the maximum and minimum values of the derivative.

## 3. Results and discussion

### 3.1. *n-Paraffins*

#### 3.1.1. *Tridecane*

The temperature dependence of the line width and second moment of the proton resonance absorption are shown in figure 2. At 77°K the lowest temperature of measurement, the line width was 15·6 gauss and the second moment 21·5 gauss². At about 200°K a narrower line of 5 gauss width appeared and fine structure was present at the centre of the resonance line. This fine structure became more pronounced as the temperature was increased. At 256°K the second moment fell from 16·3 gauss² to 4·0 gauss². The broader line narrowed

to 12·7 gauss² at 256°K and then disappeared.   The line width and second moment then remained constant until the melting point at 268°K.   Proton magnetic resonance derivative curves are shown in figure 1.
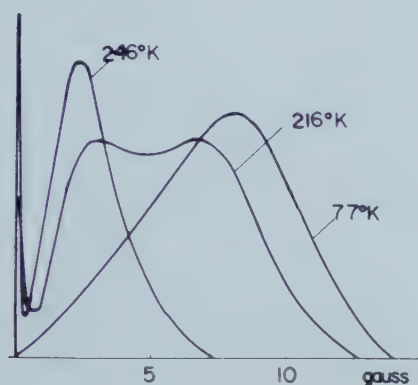


Figure 1.    Proton magnetic resonance line shape derivative curves for *n*-tridecane at various temperatures.
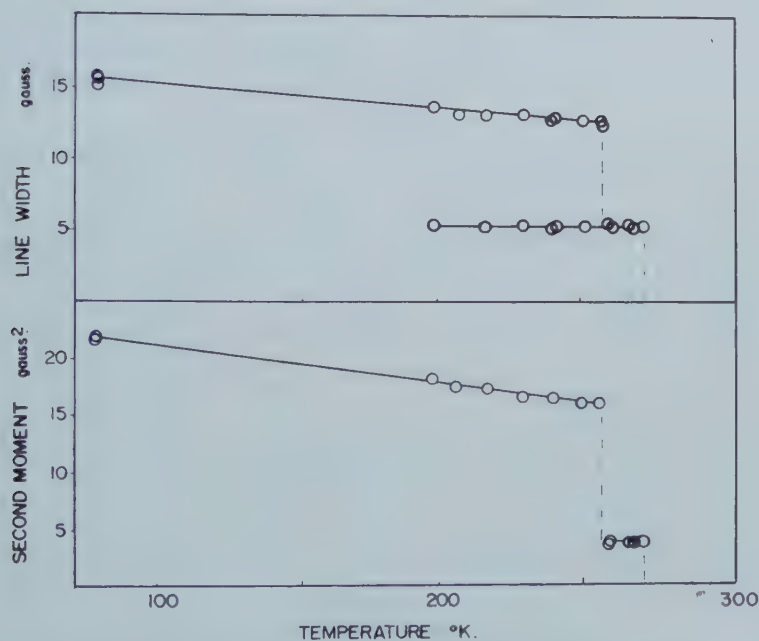


Figure 2.    Proton magnetic resonance line widths and second moments for *n*-tridecane at various temperatures.

### 3.1.2. *Hexadecane*

At 77°K the second moment of the proton magnetic resonance absorption was 23·5 gauss² and decreased smoothly to 15·4 gauss² at the melting point 289°K.   The line width decreased from 15·4 gauss to 12·3 gauss over this

temperature range.   Fine structure of the type observed in tridecane was also
present in the resonance signal from hexadecane.   The temperature dependence
of line width and second moment is shown in figure 3.
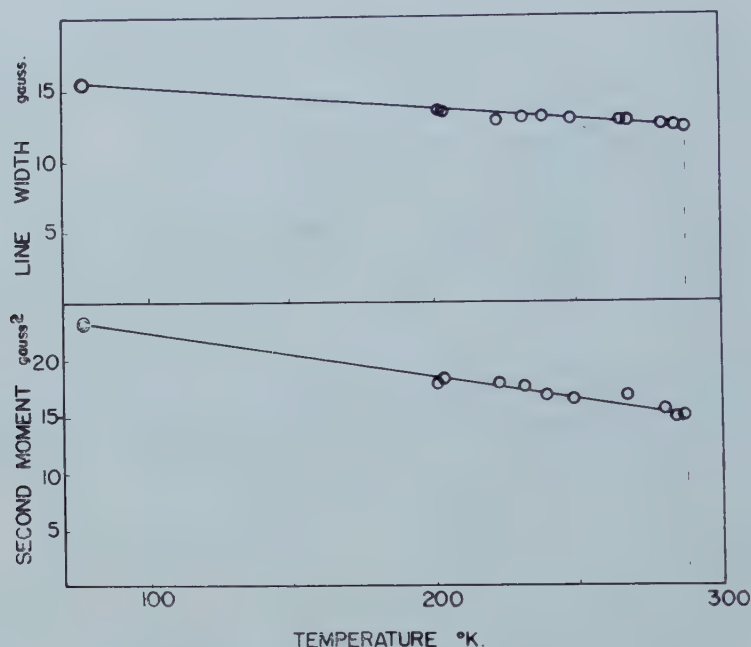


Figure 3.   Proton magnetic resonance line widths and second moments for *n*-hexadecane at
various temperatures.

The behaviour of tridecane and hexadecane is essentially similar to that
observed by Andrew [11] for octadecane, octacosane and dotriacontane.   The
theoretical intra- and inter-molecular second moments for a hydrocarbon chain
have been calculated by Andrew on the basis of Müller's x-ray structures of
*n*-paraffins [12].   In tridecane and hexadecane the experimental values of
21·5 gauss$^2$ and 23·5 gauss$^2$ at 77°K are well below the calculated rigid lattice
second moments of 27·7 and 27·3 gauss$^2$ respectively.   The hydrocarbons,
therefore, cannot be rigid at this temperature.   The gradual decrease in
second moment from the rigid lattice value to the value at a temperature just
below the melting points and transition points, was explained by Andrew in
terms of either rotatory oscillation or a form of cooperative motion in which the
hydrocarbon chains behaved as a set of meshing gears.   Pake [13] has shown that
the second moment should not be reduced by motion but remain constant at
the rigid lattice value, and therefore the Gutowsky–Pake treatment [14] is
invalid.   Nevertheless this method may still be applied provided the rate of
reorientation is sufficiently rapid [15].   Thus only the limiting values of second
moment have any real significance.   The second moments for the completely
rotating case, from the Gutowsky–Pake approach, are 8·5 and 8·7 gauss$^2$ for
tridecane and hexadecane respectively, and therefore complete rotation of the
hydrocarbon chain cannot have commenced in hexadecane at the melting point.
The large change in second moment in tridecane at 256°K corresponds to the

transition at 255°K reported by Finke *et al.* [16] from heat capacity measurements. The phase changes which occur in *n*-paraffins a few degrees below their melting points are attributed to the onset of rotation about the long axis of the molecule. The experimental second moment of 4·0 gauss² is lower than the calculated value of 8·5 gauss² for complete rotation. To account for the fine structure of the resonance curve Andrew [11] suggested that methyl group rotation was responsible. The intramolecular second moment for a rigid hydrocarbon chain is reduced by 3·8 gauss² if the terminal methyl groups rotate. The reduction in the inter-molecular contribution is about 2 gauss². The calculated second moments at low temperature are therefore 21·8 gauss² for tridecane and 21·4 gauss² for hexadecane on this model. Thus there is no satisfactory agreement between the experimental and theoretical second moments for any of the proposed forms of motion except possibly rotational oscillation.

If the appearance of fine structure is taken as an indication of methyl group rotation then this structure is present to a marked extent at temperatures where the experimental second moments are still much higher than the calculated values. It is possible that the fine structure results from a high degree of local molecular motion occurring at impurity sites caused by neighbouring homologues of the paraffin and at dislocations in the paraffin crystals. When full-scale molecular rotation occurs above the transition temperature even greater freedom of motion is possible at such sites and too low a value of the second moment results. Recently Richards [17] has suggested that the narrow line in the resonance spectrum of 1-oleodistearin results from the increased reorientational freedom caused by irregularities in the packing of the chains in the region of the double bonds.

## 3.2. *Urea adducts*

The urea adducts of *n*-hydrocarbons $C_7$–$C_{13}$ and $C_{16}$ were examined at 298°K. All the adducts showed similar spectra, a broad line of 7·1–7·3 gauss due to the protons of the urea cage, and a narrow line of modulation width due to the protons of the hydrocarbon chain. The adducts of tridecane and hexadecane were examined in more detail.

### 3.2.1. *Tridecane adduct*

The variations of the second moment and line width are given in figure 5. At 77°K the resonance curve consisted of two components, a broad line of 10·8 gauss and a narrower line of 3·3 gauss, see figure 4. The two lines narrowed until at 119°K they merged and a single line was obtained. At 140°K the signal separated into two components of widths 6·8 gauss and 1·8 gauss. At higher temperatures the broad line decreased in intensity disappearing at 230°K. The narrow line decreased slowly in width to 1 gauss at 270°K when it disappeared. The resonance line now consisted of a sharp line of modulation width. The second moment decreased from 12·6 gauss² at 77°K to 2·8 gauss² at 160°K and then decreased only slowly to 2·1 gauss² at 225°K when it fell to 0·7 gauss².

### 3.2.2. *Hexadecane*

The behaviour of the line width and second moment of the hexadecane adduct was very similar. Two components were again observed in the line shape, a narrow line of 2·2 gauss at 77°K decreasing to 0·9 gauss at 289°K and

a broad line of 11·9 gauss at 77°K which decreased to 5·5 gauss at 217°K and vanished in the range 220–230°K.  The second moment at 77°K was 15·5 gauss² decreasing to 2·6 gauss² at 160°K and then to 1·3 gauss² at 220°K.
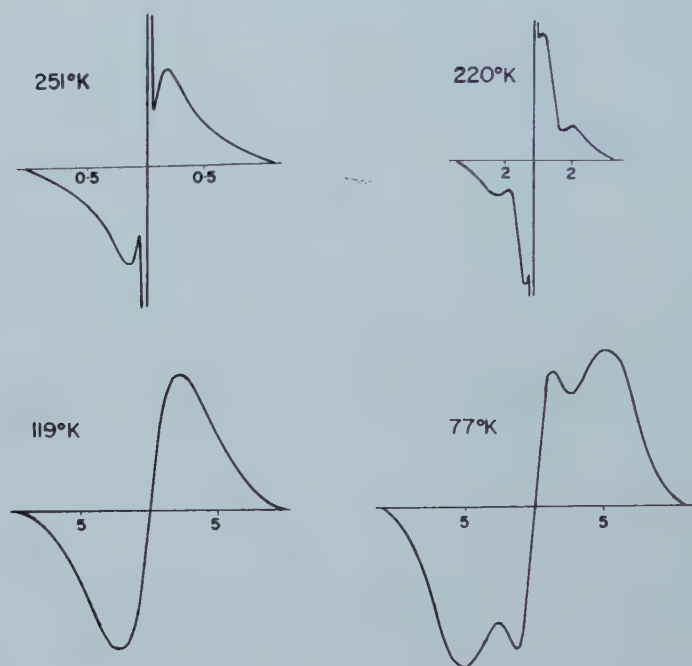


Figure 4.   Proton magnetic resonance line shape derivative curves for the *n*-tridecane urea-d$_4$ adduct at various temperatures.
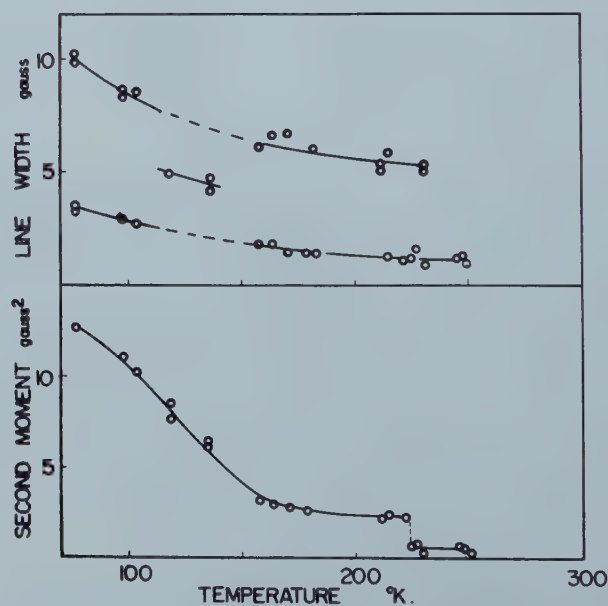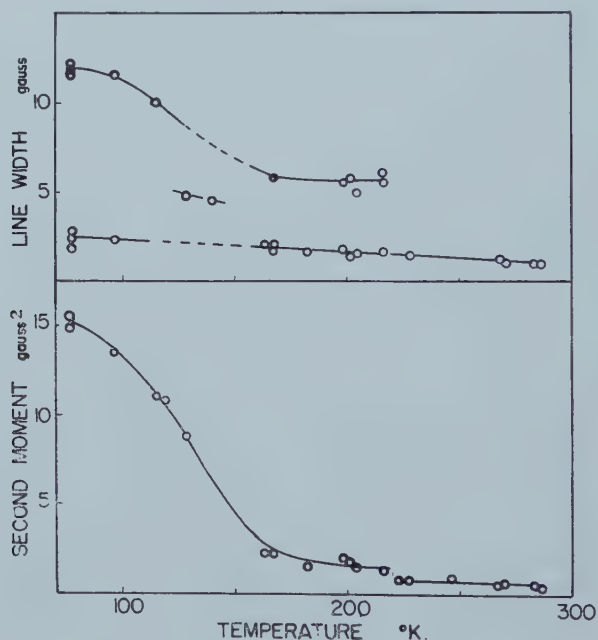


Figure 5.   Proton magnetic resonance line widths and second moments for the *n*-Tridecane-urea-d$_4$ adduct at various temperatures.

The x-ray structural investigations by Smith [3] showed that the unit cell of the urea adduct is hexagonal, $a_0 = 8.24$ Å, $c_0 = 11.01$ Å, with six urea molecules per unit cell. The urea molecules form a hollow hexagonal spiral in which the hydrocarbon is enclosed. The hydrocarbon chain is in an extended planar configuration with the long axis parallel to the *c* axis of the crystal. The time average position of the plane of the molecule is randomly oriented perpendicular to the *a* axis and at multiples of 120° to this position.

At room temperature both adducts exhibit a single narrow proton magnetic resonance absorption line. The hydrocarbon chain must be capable of a high degree of molecular motion in the channel. The motion cannot be purely rotational since, as has already been discussed, the intra-molecular second moment for a rotating chain is of the order of 8 to 9 gauss². A combination of rotation, torsional oscillation, flexing, and longitudinal and lateral motion must occur in the channel.

Parsonage and Staveley [18] in their work on the heat capacities of clathrates have found that in methane quinol clathrates the methane molecules are virtually rotating freely in their cells above about 150°K. Though the rotational contribution to the heat capacity cannot be accurately evaluated at lower temperatures they have deduced that even at 20°K the restriction on the freedom of rotation of the methane molecules is relatively small. Evidence is available from the work of Van der Waals and Platteeuw [19] on the vapour pressures of clathrates that the rotation of relatively large, oblong molecules in the cavities of clathrates may be hindered. In their studies on gas hydrates they showed that in the case of the hydrates of ethylene and ethane, the calculated equilibrium dissociation pressures were too low if the assumption were made that the enclathrated molecules could rotate freely. The discrepancies were attributed to the hindered rotation of the ethane and ethylene molecules in the cavities. Pure quadrupole resonance of $^{14}N_2$ molecules in $\beta$ quinol clathrates has been observed at temperatures below 25 K by Meyer and Scott [21]. Studies of the Zeeman splitting of the resonance line were made and these showed that at the temperatures studied, the axes of the trapped molecules oscillate around the trigonal crystalline axis of the $\beta$-quinol host. In this connection we may here recall that the absence of electron spin resonance of the oxygen molecule in a hydroquinone clathrate has been ascribed to hindered rotation of the oxygen molecule [20]†.

The second moment of the resonance line will consist of the following contributions:

    (i) Intra-molecular from the hydrocarbon chain.

    (ii) Inter-molecular from terminal methyl groups of adjacent chains in the same channel.

    (iii) Inter-molecular, from chains in different channels.

    (iv) Contribution due to the presence of other nuclei possessing spin.

    (v) Contributions from unexchanged protons in the urea lattice; unadducted hydrocarbon, and occluded solvent molecules.

---

† Meyer and Scott have recently studied the electron spin resonance of oxygen-quinol clathrates and have concluded that the hindering potential is quite small, and only interferes with the free rotation of the oxygen molecule at temperatures below that of liquid nitrogen —(personal communication from Dr. J. H. van der Waals).

Of the above possible contributions to the second moment only (i) and (ii) are of importance. No evidence for occluded solvent was found during the infra-red investigations [6]. The inter-molecular second moment due to adjacent terminal methyl groups cannot be calculated exactly since it depends on the relative juxtaposition of the methyl groups in the channel and this is not known with certainty. If the methyl groups approach to their Van der Waals radii and the protons in one group assume a staggered position with respect to those on the other group, then the second moment will be of the order of 1 gauss$^2$. The rigid lattice values of the second moment are thus 20·9 gauss$^2$ and 20·6 gauss$^2$ for the tridecane and hexadecane adducts respectively. The chains are therefore not rigid at 77°K. An angular amplitude of oscillation of 45° would be necessary to account for the observed reduction of second moment in the tridecane adduct. For the hexadecane adduct an amplitude of 30° is required.



Figure 6. Proton magnetic resonance line widths and second moments for the $n$-Hexadecane-urea-d$_4$ adduct at various temperatures.

Rotation of the terminal methyl groups about the C–C bonds will reduce the intra-molecular second moment by 3·8 gauss$^2$, and the inter-molecular contribution effectively to zero. The calculated values now become 16·1 gauss$^2$ for the tridecane adduct and 15·8 gauss$^2$ for the hexadecane adduct. The chain length of hexadecane is 22·84 Å which is slightly greater than twice the urea unit cell repeat distance of 11·01 Å. According to Smith [3] the chain is shortened slightly in order to fit into two unit cells. This will restrict the rotational oscillation of the chain. There is no shortening of the chain in tridecane, of course, and the molecule has a random $z$ coordinate in the channel. The decrease

in second moment of both adducts over the temperature range 77°–160°K could be due to an increasing amplitude of rotational oscillation until an amplitude of 60° is reached when of course the motion becomes fully rotational. The disappearance of the broad line and discontinuity in second moment for both adducts in the range 225°–230°K may result from an expansion of the urea lattice which allows the adducted hydrocarbon a greater freedom of motion.

Following the work of Gutowsky and Pake [14] an estimate of the barrier to rotation can be obtained from line-width data by using an expression of the type:

$$2\pi v_c = \alpha\gamma\delta H/\tan\left[(\pi/2)(\delta H^2 - B^2)/C^2\right] \tag{1}$$

in conjunction with

$$v_c = v_0 \exp\left(-E/RT\right) \tag{2}$$

where $v_c$ is the correlation frequency responsible for the line narrowing, $\delta H$ is the line width in the transition region, $B$ is the line width at a temperature above the transition region, and $C$ is the line width below this region. The constant $\alpha$ may be taken as $0\cdot18$ (ref. [21]), $\gamma$ is the gyromagnetic ratio. The disadvantages of this approach are the errors involved in choosing values for $B$ and $C$, and the assumption of a single correlation time, which is not necessarily justifiable. The values of the energy barriers involved are $1\cdot0$ kcal/mole for the tridecane adduct, and $1\cdot6$ kcal/mole for the hexadecane adduct. These values may be compared with those obtained by Meakins [9] from the temperature variation of the frequency of dielectric absorption. In the adducts of various long chain ethers, ketones and alkyl bromides the barriers ranged from $1\cdot0$ kcal/mole for didodecyl ether to $2\cdot4$ kcal/mole for *n*-octadecyl bromide. The values derived from the n.m.r. data therefore seem quite reasonable.

The line of about 3 gauss wide present in the resonance curve of both adducts at 77°K and narrowing to about 1 gauss at or near the melting point of the hydrocarbon is probably due to free or only partially adducted hydrocarbon. Mechanical degradation of adducts was observed during the preparation of KBr discs for the infra-red studies [6] and may have occurred during the packing of the adduct into the sample tube in these experiments.

### 3.3. *Thiourea adducts*

The line width and second moment of the cyclohexane thiourea-$d_4$ adduct at 77°K were 4·6 gauss and 2·7 gauss² decreasing to 1·6 gauss and 0·3 gauss² respectively at 298°K. The line width remained constant from 298°K to 400°K but began to decrease in intensity above about 340°K. The line widths of other thiourea adducts are given in the table. A broad line of 8·5–8·7 gauss was observed in each case and attributed to the protons of the thiourea lattice.

| | |
|---|---|
| Methyl cyclohexane | 1·0 gauss |
| Methyl cyclopentane | 1·4 gauss |
| Cyclopentane | — |
| Cyclohexene | 0·7 gauss |

Line widths of thiourea adducts at 25°C.

The structures of the thiourea adducts are similar to those of the urea adducts except that the channels are much larger with $a_0 = 15\cdot8$ Å, $c_0 = 12\cdot5$ Å. Straight chain compounds are thus too small to maintain the thiourea spiral and only

highly branched, or large cyclic molecules will adduct. The x-ray structure of the cyclohexane adduct has been studied by Lenne [5]. The cyclohexane rings are situated near the sulphur atoms and perpendicular to the $c$ axis. Rotation or oscillation of the cyclohexane rings is apparent from the x-ray results. The intra-molecular second moment of a rigid cyclohexane molecule is $17 \cdot 3$ gauss$^2$. Reorientation about the triad axis will reduce this to $3 \cdot 6$ gauss$^2$. Since the experimental values are much lower, the second moment must be inter-molecular in origin and isotropic reorientation must occur. The larger size of the sulphur atom and the greater dimensions of the channel leads to a periodicity of the Van der Waals forces along the length of the channel. The n.m.r. evidence supports the idea that in thiourea adducts the enclosed component is trapped at some potential minimum such that, while rotational or oscillatory motion may be quite unrestricted, translation motion is hindered. The narrow line of modulation width found for the cyclopentane–thiourea-d$_4$ adducts infer that the cyclopentane ring is also capable of translational motion in the channel presumably due to its smaller size.

The decrease in intensity of the resonance line in the cyclohexane adduct above $340°$K is obviously due to decomposition of the adduct.

## References

[1] BENGEN, F., 1940, Ger. Pat. Appl. O.Z. 12438, March.
[2] ANGLA, B., 1947, *Comptes Rend.*, **224**, 402.
    FETTERLY, L. C., 1950, U.S. Pat. 2,499,820.
[3] SMITH, A. E., 1952, *Acta cryst., Camb.*, **5**, 224.
[4] SCHLENK, W. JR., 1949, *Liebigs Ann.*, **565**, 204; 1951, *Ibid.*, **573**, 142.
[5] LENNE, H.-U., 1954, *Acta cryst., Camb.*, **7**, 1.
[6] FISCHER, P. H. H., and McDOWELL, C. A., 1960, *Canad. J. Chem.*, **38**, 187.
[7] STUART, A. V., 1956, *Rec. Trav. chim. Pays-Bas*, **75**, 906.
[8] BARLOW, G. B., and CORISH, P. J., 1959, *J. chem. Soc.*, p. 1706.
[9] MEAKINS, R. J., 1955, *Trans. Faraday Soc.*, **51**, 953.
[10] VAN VLECK, J. H., 1948, *Phys. Rev.*, **74**, 1168.
[11] ANDREW, E. R., 1950, *J. chem. Phys.*, **18**, 607.
[12] MULLER, A., 1932, *Proc. roy. Soc.* A, **138**, 514.
[13] PAKE, G. E., 1956, *Solid State Physics*, **2**, 1.
[14] GUTOWSKY, H. S., and PAKE, G. E., 1950, *J. chem. Phys.*, **18**, 163.
[15] ANDREW, E. R., and NEWING, R. A., 1958, *Proc. phys. Soc. Lond.*, **72**, 959.
[16] FINKE, H. L., GROSS, M. E., WADDINGTON, C., and HUFFMAN, H. M., 1954, *J. Amer. chem. Soc.*, **76**, 333.
[17] CHAPMAN, D., RICHARDS, R. E., and YORKE, R. W., 1960, *J. chem. Soc.*, p. 436.
[18] PARSONAGE, N. G., and STAVELEY, L. A. K., 1960, *Mol. Phys.*, **3**, 59.
[19] VAN DER WALLS, J. H., and PLATTEEUW, J. C., 1959, *Advanc. chem. Phys.*, II, 1.
[20] MEYER, H., O'BRIEN, M. C., and VAN VLECK, J. H., 1957, *Proc. roy. Soc.* A, **243**, 414.
[21] KUBO, R., and TOMITA, K., 1954, *J. phys. Soc. Japan*, **9**, 888.
[22] MEYER, H., and SCOTT, T. A., 1959, *J. Phys. Chem. Solids*, **11**, 215.

# Electron spin resonance and structure of the $CO_2^-$ radical ion

by D. W. OVENALL and D. H. WHIFFEN

Basic Physics Division, National Physical Laboratory, Teddington,
Middlesex

Analysis of the electron spin resonance spectrum shows that $CO_2^-$
radical ions are trapped in sodium formate at room temperature after
irradiation of the crystal with high energy $\gamma$-rays. This radical is bent with
an angle of about 134° and has a $^2A_1$ ground state. From the experimental
values of the $^{13}$C coupling coefficients and the $g$ values, coefficients are derived
for the mixing of atomic orbitals in the half-filled $4a_1$ molecular orbital which
appears to be 14 per cent carbon 2s, 66 per cent carbon $2p_z$ and 11 per cent
of each oxygen $2p_z$. There is also coupling to the sodium nucleus in an
adjacent cation.

## 1. INTRODUCTION

Preliminary work [1] showed that irradiation of solid sodium formate with
high energy $\gamma$-radiation led to the formation of $CO_2^-$ radical ions which remain
trapped in a specific orientation in the crystal. The dimer, $C_2O_4^=$, is the oxalate
ion and nitrogen dioxide, $NO_2$, is an isoelectronic molecule. Both of these
are very well known and it seemed of interest to make a full study of $CO_2^-$
including its $^{13}$C coupling coefficients.

$NO_2$ is the only well-known triatomic species with 17 valency electrons and
its electronic spectra [2, 3, 4] have proved difficult to interpret. Consequently
the electronic structure proposed for such 17 electron systems by Mulliken
[5, 6, 7] has not been fully verified experimentally, except for the prediction
that the molecule is bent.

## 2. EXPERIMENTAL

The crystal structure of sodium formate has been investigated with x-rays
by Zachariasen [8]. The unit cell is monoclinic with dimensions $a = 6·19$,
$b = 6·72$ and $c = 6·49$ Å with $\beta = 121·7°$. The space group is C2/c ($C_{2h}^6$ No. 15
Int. Tab.). The cell contains four molecules and all the formate planes lie
parallel to each other. The H, C and Na lie in chains parallel to the unique axis.
Crystals grown from aqueous solutions are elongated in the $c$ direction with
(010), (110) and (001) as the prominent faces. (001) is also a common twinning
plane.

Crystals were grown from aqueous solution and their appearance corresponded
in all respects to Zachariasen's description [8]. The crystals were irradiated
by the Spent Fuel Irradiation Unit, Harwell, with $\gamma$-rays of mean energy
1·0 MeV.

Electron resonance spectra were obtained with a superheterodyne spectrometer operating at 9000 Mc/s with derivative presentation on a chart recorder. Proton resonance signals were used to calibrate the magnetic field sweep. $g$ factors were obtained by comparison with $\alpha$, $\alpha$-diphenyl $\beta$-picryl hydrazyl placed inside the cavity on the same post as the crystal. This material has been recrystallized from carbon disulphide to avoid solvent retention and its $g$ value was taken [9] as 2·0036. The mounted crystal could be rotated from outside the cavity about a vertical axis perpendicular to the magnetic field. Spectra were taken at closely spaced intervals with the $b$ axis, the $c$ axis and the mutually perpendicular axis successively in the vertical direction.

The original spectra were observed on crystals of a few millimetres dimension after a dose of $10^6$ rad. The radicals appeared to be stably trapped and no evidence was obtained of appreciable decay. This accords with measurements by Gordy and Luck [10] who showed radicals to be formed in good yield. Four lines of equal intensity and equal spacing dominate the spectra for all crystal orientations and can be attributed to coupling with a $^{23}$Na nucleus of spin 3/2. No splitting of the simple pattern was observed, except on one occasion when it was demonstrated that the crystal employed was twinned.

Examination of the spectra at high gain disclosed two weak sets of four lines of equal intensity symmetrically disposed on either side of the main pattern with the same spacing. These are attributed to $^{13}$C coupling (spin 1/2) in the radical species, identified as $CO_2^-$, present in natural abundance. These were further studied on a large crystal weighing 140 mg irradiated with $5 \times 10^6$ rad. Approximate intensity measurements showed these outside lines to be 200 times weaker than the central pattern in agreement with the factor 180 to be expected from the 1·1 per cent abundance of $^{13}$C.
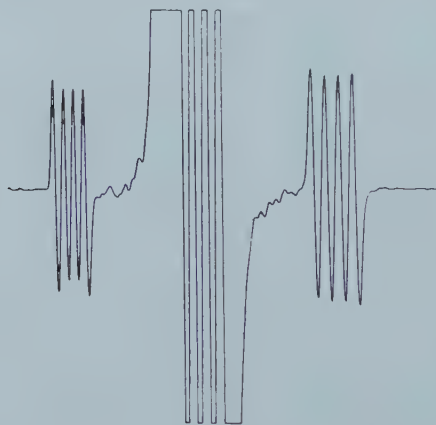


Figure 1.   Derivative record showing main spectrum of four lines (overloading recorder) from $^{23}$Na coupling flanked by similar patterns from $^{13}CO_2^-$. Low field to left; field sweep not strictly linear.

Figure 1 shows a full spectrum with the central pattern many times off scale. The apparent unequal sodium coupling is due to a non-linearity in the field sweep. The noise level should be judged against the extreme wings of the spectrum,

since the extremely weak features inside the $^{13}$C pattern are essentially repro-ducible and must be attributed to another radical or to $^{17}$O in the $CO_2^-$.

Figure 2 shows the results obtained rotating the crystal about the $b$ axis so that the magnetic field lies in the $a\,c$ plane. It can be seen that the minima of the $^{13}$C coupling and of the $g$ value coincide within experimental error with the projection of the formate plane which lies at a setting of 77·0 ·, being 18·7° from the $a$ axis which is parallel to the magnetic field at a setting of 58·3 ·.
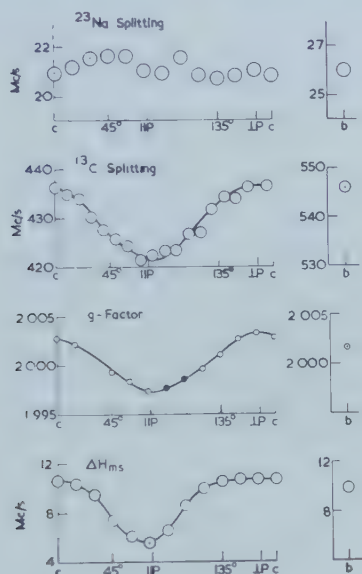


Figure 2. Variation of $^{23}$Na coupling, $^{13}$C coupling, $g$ value and $\Delta H_{\text{m.s.}}$ for rotation about $b$. Values for field parallel to $b$ shown on right. $\|P$ and $\perp P$ indicate the orientations for which the field is parallel and perpendicular to the formate plane.

The set of spectra obtained on rotation about axes perpendicular to $b$ are symmetrical with respect to this axis as required for a monoclinic crystal. The values when the magnetic field is parallel to $b$ are the only new quantitative information from these crystal settings and the hyperfine couplings and $g$ value for this arrangement are indicated on the right of figure 2.

| | Parallel to $b$ axis | Perpendicular to formate plane | Perpendicular to $b$ and parallel to formate plane | Isotropic or average value |
|---|---|---|---|---|
| $^{13}$C coupling (Mc/s) | 546 | 436 | 422 | 468 |
| $^{23}$Na coupling (Mc/s) | 26 | 21 | 21 | 23 |
| $g$ | 2·0014 | 2·0032 | 1·9975 | 2·0006 |
| $\Delta H_{\text{m.s.}}$ (Mc/s) | 9·8 | 10·6 | 5·5 | — |

Table 1. Summary of observations.

No splitting was observed which might indicate a change of sign [11] of a principal coupling coefficient although this might be difficult to detect when

the line widths are larger than the direct coupling of the nuclei to the magnetic field. The interpretation requires all principal couplings to be positive.

There was a marked change of line width with orientation, and $\Delta H_{\text{m.s.}}$, the maximum slope width, is also plotted in figure 2. The principal values, which lie along the symmetry axis and the perpendiculars to the symmetry planes of the formate ion, are collected together in table 1. The $^{13}C$ couplings are thought to be accurate to $\pm 2$ Mc/s, the $^{23}Na$ couplings to $\pm 1$ Mc/s, the $g$ values to $\pm 0.0002$ from experimental errors, plus any systematic error which arises from the assumption of $g = 2.0036$ for $\alpha$, $\alpha$-diphenyl $\beta$-picryl hydrazyl. $\Delta H_{\text{m.s.}}$ are accurate to $\pm 0.5$ Mc/s.

## 3. Discussion

### 3.1. Chemical nature of the radical

It is clear from the experimental results that the free electron resides in a radical which contains carbon but not hydrogen, since the $^{13}C$ coupling is very large and $^1H$ coupling is not observed. Although dominating the appearance of the spectrum, the sodium hyperfine coupling is in fact quite small (see §3.5) and consistent with a weak bond between the sodium ion and the free radical. These features, and the nature of the starting material, very strongly suggest that $CO_2^-$, formed by loss of hydrogen from the formate ion, is trapped in the crystal.
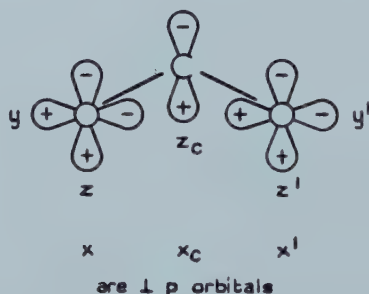


Figure 3.   Designation and phase of atomic p orbitals chosen as basis.   2s orbitals are $s_C$ on carbon, s and s' on the oxygens.   The crystallographic b axis is parallel to z. The plane of the paper is the plane of the $CO_2^-$ radical ion which is the nodal plane of the true $\pi$ system formed from $x$, $x'$ and $x_C$.

### 3.2. Expected electronic structure

The description of the presumed electronic structure of $NO_2$ given by Mulliken [5, 6] is expected to be applicable. The bent structure has $C_{2v}$ symmetry. The valency atomic orbitals may be labelled as indicated in figure 3. The molecular orbitals may be classified according to the symmetry classes of $C_{2v}$. The $b_1$ and $a_2$ orbitals have a node in the plane of the radicals and are therefore $\pi$ orbitals. The $a_2$ and $b_2$ orbitals have a node in the symmetry plane perpendicular to the O–O direction. Table 2 lists the molecular orbitals in the probable order of stability. An approximate description of each is given; the pseudo $\pi$ orbitals are those which correlate with $\pi$ orbitals in linear $CO_2$, but have lost their nodal plane in the bent structure.

Greatest interest attaches to the half-filled $4a_1$ orbital which is chiefly responsible for the magnetic resonance properties. With the atomic orbitals indicated in figure 3 the form of the $4a_1$ orbital may be written

$$l_1 s_C + l_2 z_C + l_3(z+z') + l_4(y-y') + l_5(s+s').$$

Since most of the two-centre integrals relating to hyperfine couplings and spin–orbit interactions are as yet unknown, it is necessary to neglect these and likewise all overlap integrals. As will be seen in §§ 3.3 and 3.4, the electron resonance results lead to estimates of $l_1$, $l_2$ and $l_3$. The oxygen s and s′ orbitals correlate to the $\sigma$ orbitals of linear $CO_2$ and will contribute principally to the $1a_1$, $2a_1$ and $5a_1$ molecular orbitals; consequently $l_5$ is expected to be small. Fischer-Hjalmers [12] finds a value of 0·078 for essentially this quantity in a self-consistent field treatment of ozone. $l_4$ is also likely to be fairly small.

| Symmetry | Number of electrons | Approximate description |
|---|---|---|
| $4b_2$ | 0 | $\sigma$ anti-bonding |
| $5a_1$ | 0 | $\sigma$ anti-bonding |
| $2b_1$ | 0 | $\pi$ anti-bonding |
| $4a_1$ | 1 | Mainly pseudo $\pi$ anti-bonding |
| $1a_2$ | 2 | $\pi$ non-bonding |
| $3b_2$ | 2 | Pseudo $\pi$ non-bonding |
| $1b_1$ | 2 | $\pi$ bonding |
| $3a_1$ | 2 | Pseudo $\pi$ bonding |
| $2b_2$ | 2 | Lone pair on O |
| $2a_1$ | 2 | Lone pair on O |
| $1b_2$ | 2 | $\sigma$ bonding |
| $1a_1$ | 2 | $\sigma$ bonding |
| lower | 6 | Inner 1s electrons |

(There is doubt as to the relative order of $1a_2$ and $3b_2$.)

Table 2. Molecular orbitals of bent $CO_2^-$.

The $4a_1$ orbital correlates with the $\pi$ antibonding orbital of the linear state and $l_2$ and $l_3$ are expected to have opposite signs. The coefficients of $s_C$ and $z_C$ are expected to have the same sign in the bonding orbital $1a_1$ and opposite signs in $4a_1$, so that the odd electron projects along the external bisector of the OCO angle. These signs match those of the analogous $4a_1$ orbital of ozone [12].

### 3.3. *The* $^{13}C$ *coupling*

The isotropic $^{13}C$ coupling is a measure of the contribution of $s_C$ to $4a_1$. It derives from the Fermi or contact term and is given by

$$g g_I \mu_0 \mu_N (8\pi/3) |\psi^2(0)|.$$

With the experimental value 468 Mc/s one finds

$$(8\pi/3)|\psi^2(0)| = 23 \cdot 6 \, \text{Å}^{-3}.$$

This is very much larger than any value that could be accepted for a linear structure with the odd electron in a $\pi$ orbital. Using Hartree atomic orbitals Smith *et al.* [13] have calculated this quantity to be 166 Å$^{-3}$ for a pure carbon 2s orbital. The ratio, 0·142, is therefore $l_1^2$ giving $l_1 = -0 \cdot 38$.

The anisotropic part of the coupling is given by

$$gg_I \mu_0 \mu_N \langle (3\cos^2\theta - 1)r^{-3} \rangle_{AV.}$$

where $\theta$ is the angle between the radius vector of the electron with the nucleus as origin and the magnetic field direction.

Table 1 shows the $^{13}C$ anisotropy almost to possess cylindrical symmetry about the $b$ axis. This symmetry is to be expected for the electron in a carbon orbital aligned in this direction and confirms that the bisector of the OCO angle is parallel to the same feature of the formate ions. There can be little doubt that the $CO_2^-$ takes up the orientation of the formate it replaces.

There is a slight difference between the principal values for directions perpendicular to $b$, namely 436 Mc/s perpendicular to the $CO_2^-$ plane and 422 Mc/s in it. This is in the wrong sense to be due to the spreading of the spin density to the oxygen atoms represented by $l_3$. It represents positive spin density in $x_C$. If this has cylindrical symmetry about $x$ then the net contribution is $+10$ Mc/s perpendicular to the $CO_2^-$ plane and $-5$ Mc/s in the plane, including the $b$ direction. The $4a_1$ orbital then contributes 83 Mc/s anisotropic $^{13}C$ coupling, after allowance also for the isotropic contribution.

This arises entirely from the density in $z_C$, since neither $s_C$ nor the $s_C - z_C$ overlap terms provide any anisotropy. Numerically 83 Mc/s corresponds to

$$\langle (z^2 - x^2/2 - y^2/2)r^{-5} \rangle_{Av.} = 2 \cdot 1\, \text{Å}^{-3}$$

in which expression $x$, $y$, $z$ are electron coordinates. The contribution for a fully occupied carbon 2p orbital has been calculated [13] to be $3 \cdot 2\, \text{Å}^{-3}$. The ratio $0 \cdot 66$ is then $l_2^2$ and $l_2 = +0 \cdot 81$.

Although it is only strictly necessary that $1a_1$ and $4a_1$ be orthogonal, it is interesting to make a more restrictive assumption to obtain an estimate of the OCO angle. It is to be expected that the carbon contribution to the $\sigma$ bonding orbitals, $1a_1$ and $1b_2$, can be rearranged to form two bonds hybridized along the O–C directions. The contributions of the carbon to other orbitals (except the antibonding $4b_2$ and $5a_1$) is expected to be orthogonal to these bond-forming orbitals. The relationship between angle and hybridization has been discussed by Coulson [14].

With $l_2/l_1 = -2 \cdot 13$ as above, Coulson's treatment leads to an OCO angle of $134°$ if $4a_1$ is required to be orthogonal to carbon orbitals in the C–O directions. The value $134°$ for the angle in $NO_2$ is well established [15, 16].

A mechanism by which spin density could be obtained in $x_C$ is similar to that for spin polarization of C–H bonds in planar aromatic free radicals. The value of 10 Mc/s as the principal anisotropic contribution represents a spin density of $+0 \cdot 08$ in $x_C$. An estimate by first-order perturbation theory of the contribution arising from the mixing under the influence of exchange terms of the three excited $A_1$ states arising from the excitation $2b_1 \leftarrow 1b_1$ gives a density $+4 \times 10^3/\Delta E$ where $\Delta E$ is the vertical excitation energy in cm$^{-1}$ (see Appendix). Since $\Delta E$ may be $\sim 10^5$ cm$^{-1}$, the estimated spin density in $x_C$ is $\sim +0 \cdot 04$ which is of the correct sign and about half the observed value. This is reasonable agreement considering the approximations made in the theory and in deducing the experimental value.

### 3.4. *The spectroscopic splitting factors, g*

The structure of strictly $A_1$ symmetry discussed above corresponds to fully quenched orbital angular momentum. In this approximation $g = (-)2 \cdot 0023$, the free electron value; the negative sign corresponding to the negative moment of the electron is usually omitted. Spin–orbit coupling can mix excited states of other symmetries with an imaginary mixing coefficient and this leads to departures of $g$ from the free spin value. As discussed by McConnell and Robertson [17] the departures may be of either sign and for pure p orbitals they are given by $2\zeta \Delta E$ where $\zeta$ is the one electron spin–orbit coupling constant and $\Delta E$ is the excitation energy. Admixture of configurations differing from the ground state by one electron promotion leads to $g$ less than the free spin value if the unpaired electron is promoted to an empty perpendicular orbital. If an electron of reversed spin is promoted from a doubly filled orbital to share the half-filled orbital then $g$ is increased.

For $g$ for the field direction perpendicular to the radical plane it is mixing of $B_2$ states which results in the partial unquenching of the $x$ axis orbital momentum. The lowest $B_2$ state arises from the promotion $4a_1 \leftarrow 3b_2$ and $g$ is expected to lie above the free spin value in agreement with the observed $2 \cdot 0032$.

When the magnetic field is along the symmetry axis admixture of $A_2$ states is important in determining $g$. The lowest $A_2$ state probably corresponds to $4a_1 \leftarrow 1a_2$ which should lead to an increase of $g$. However, the magnitude is expected to be proportional to $l_1{}^2$ which is believed to be very small.

Further $A_2$ states, two doublets and a quartet, correspond to the excitation $2b_1 \leftarrow 3b_2$. The sign of the net contribution to $g$ is uncertain. It would need to be negative to agree with the observed $g = 2 \cdot 0014$.

The greatest change of $g$ is observed when the field is in the O–O direction and the $y$ axis orbital momentum is partly unquenched by admixture of $B_1$ states. The lowest $B_1$ state arises from the promotion $2b_1 \leftarrow 4a_1$ and a large reduction of $g$ is expected, in agreement with the observed $1 \cdot 9975$.

For quantitative calculations it is necessary to know the coefficients in the $2b_1$ orbital. They are not expected to be very different from those in the corresponding $2\pi_u$ orbital in $CO_2$ calculated by Mulligan [18]. For the present purposes, when overlap is neglected, the coefficients must be renormalized and so the $2b_1$ orbital is best taken as

$$l_6 x_c + l_7 (x + x')$$

with $l_6 = +0 \cdot 75$ and $l_7 = -0 \cdot 47$. The departure from the free spin $g$ value is given by

$$-2(l_2 l_6 \zeta_C + 2 l_3 l_7 \zeta_O)(l_2 l_6 + 2 l_3 l_7)/\Delta E.$$

Here $\zeta_C$ and $\zeta_O$ are the one electron spin–orbit coupling parameters for carbon and oxygen and have the values $28 \, \text{cm}^{-1}$ and $152 \, \text{cm}^{-1}$ respectively [17]. The value of the first bracket governs the amount of admixture of the excited state and the second is a correction which expresses the fact that even with optimum mixing it would not be possible to obtain unit orbital angular momentum from $4a_1$ and $2b_1$ only. The unknowns in this expression are $l_3$ and $\Delta E$, the vertical excitation energy to the $B_1$ state. $\Delta E = 24\,000 \, \text{cm}^{-1}$ is a reasonable estimate, being the sort of value suggested [6, 4] for $NO_2$. Admittedly the irradiated crystals were not visibly coloured but the optical transition is expected to be weak [6]. Using the experimental value of $\Delta g = -0 \cdot 0048$ the quadratic may be

solved to give $l_3 = -0.33$. The alternative solution $l_3 = +1.1$ is entirely unacceptable. $l_3^2 = 0.11$ which indicates each oxygen to contribute 11 per cent of $p_z$ to the orbital. It is interesting to note that the negative sign expected for $l_3$ is confirmed and also that over 70 per cent of $\Delta g$ arises from the oxygen contributions.

Using the values of $l_1$ and $l_2$ from § 3.3 and the normalization condition

$$l_1^2 + l_2^2 + 2l_3^2 + 2l_4^2 + 2l_5^2 = 1,$$

one obtains $l_4^2 + l_5^2 = -0.01$. This is obtained as the difference of large quantities and is zero within the errors involved. This result confirms that $l_4$ and $l_5$ are small.

### 3.5. The $^{23}Na$ coupling

The sodium ions lie on the symmetry axis of the formate ion and likewise they must be on the symmetry axis of the $CO_2^-$. The anisotropy of the sodium coupling is small but the largest coupling appears for this axis which suggests that the positive anisotropic contribution is adding to a positive isotropic component.

The coupling for a sodium atom in the $^2S$ ground state is well known from atomic beam and related experiments [19, 20] and is half the zero field splitting of 1772 Mc/s between the $F = 1$ and 2 states. Consequently in the present case the occupancy of the 3s sodium orbital amounts to only 2.6 per cent as deduced from the isotropic coupling of 23 Mc/s.

In all crystal orientations the sodium coupling gives four equal intensity, equally spaced, lines and the sodium electrical quadrupole coupling must be virtually zero. The situation could be described as a deformation of the $CO_2^-$ orbital by the cation or by a very weak, one electron covalent bond. Each $CO_2^-$ would be expected to have two adjacent sodium ions, one on each side. There is no evidence to indicate which is the one which couples. In the undamaged formate crystal the sodium adjacent to the oxygen atoms is the closer.

### 3.6. Line widths

As shown in figure 2 there is a marked change of line width with crystal orientation. The line width appeared to be independent of dose up to $5 \times 10^6$ rad and so is not thought to be due to neighbouring free radicals. It may be due to unresolved coupling to other sodium ions or to the hydrogen atoms in neighbouring formate ions. Under high sensitivity, weak hydrogen 'spin flip' lines were observed 13 Mc/s outside the sodium pattern, indicating slight interaction with such hydrogens [21].

### 3.7. Comparison with other work

Very recently, Kemp [22] has observed electron resonance spectra of neutron irradiated calcite. A variety of radicals are formed, one of which, designated A, has $g$ values predominantly below the free spin value. This could be $CO_2^-$; Kemp refers briefly to this possibility but he presumes the $CO_2$ to be linear.

Various authors [23–26] have observed resonance from $NO_2$ and Bleaney et al. [27] have obtained orientation dependent $^{14}N$ couplings and $g$ values. These are similar to the present findings and in particular there is a low $g$ value, 1.994, which is associated in direction with the lowest coupling There was considerable overlapping of spectra from $NO_2$ in different orientations and the figures are not accurate enough for a strict comparison and discussion of the changes consequent on the differing electronegativities of nitrogen and carbon.

We wish to acknowledge helpful discussions with Dr. J. A. Pople. This work forms part of the research programme of the Basic Physics Division of the National Physical Laboratory and is published by permission of the Director.

## Appendix

The calculation of the spin density in $x_C$ is of some interest. Two doublet and a quartet $A_1$ states arise from the excitation $2b_1 \leftarrow 1b_1$. Only the components of the same resolved spin are involved and one may discuss the ground state, $G$, and the excited configurations, $P$, $Q$, $R$, represented by the specific spin schemes.

$$
\begin{array}{llll}
G & 1b_1 & 1\bar{b}_1 & 4a_1 \\
P & 1\bar{b}_1 & 2b_1 & 4a_1 \\
Q & 1b_1 & 2\bar{b}_1 & 4a_1 \\
R & 1b_1 & 2b_1 & 4\bar{a}_1
\end{array}
$$

where a bar indicates reversed spin. $(|P\rangle + |Q\rangle + |R\rangle)$ belongs to the quartet state which is not mixed with $G$. The true doublet states must be compounded from $(|P\rangle - |Q\rangle)$ and $(|P\rangle + |Q\rangle - 2|R\rangle)$ but it is unnecessary to assess this mixing provided their energy separation is small compared with their excitation energy from the ground state. That is, one may treat the doublet states as if they were degenerate.

The programme consists of two parts; firstly to obtain the spin density in $x_C$ arising from admixture of these configurations and secondly to obtain the mixing coefficients. For the spin density in $x_C$ one requires the expectation value of an operator $\sum_j \rho_j(x_C)$ which is the sum over all electrons of a one electron operator $\rho(x_C)$ which has only two non-zero matrix elements between atomic orbitals. These are

$$\langle x_C|\rho(x_C)|x_C\rangle = -\langle \bar{x}_C|\rho(x_C)|\bar{x}_C\rangle = 1.$$

Now
$$\langle G|\sum_j \rho_j(x_C)|G\rangle = \langle G|\sum_j \rho_j(x_C)|R\rangle = 0$$

and
$$\langle P|\sum_j \rho_j(x_C)|G\rangle = \langle Q|\sum_j \rho_j(x_C)|G\rangle$$
$$= -\langle 2b_1|\rho(x_C)|1b_1\rangle = -\rho_x$$

where the last expression defines $\rho_x$. Thus

$$(\langle P| - \langle Q|)\sum_j \rho_j(x_C)|G\rangle = 0$$

and admixture of $(\langle P| - \langle Q|)$ may be neglected. If the normalized doublet component which is important is written

$$|D\rangle = 6^{-1/2}(|P\rangle + |Q\rangle - 2|R\rangle)$$

then
$$\langle D|\sum_j \rho_j(x_C)|G\rangle = -2^{1/2}\cdot 3^{-1/2}\rho_x.$$

Inspection of the Hamiltonian matrix elements connecting $D$ and $G$ shows that $\langle D|\mathscr{H}|G\rangle = 3^{1/2}\cdot 2^{-1/2}K$, where
$$K = \langle 2b_1(j)4a_1(k)|l^2/r_{jk}|4a_1(j)1b_1(k)\rangle.$$

Using first-order perturbation theory the spin density in $x_C$ is found to be $+2K\rho_x/\Delta E$ where $\Delta F$ is the vertical excitation energy to $D$. This theory is analogous to the molecular orbital treatment of spin density at a $\sigma$ hydrogen

derived from an unpaired $\pi$ electron given by McConnell and Chesnut [28] and the final result is the analogue of their equation (32).

The $2b_1$ and $4a_1$ orbital coefficients are given in the main text. $1b_1$ has the form

$$l_8 x_C + l_9(x + x')$$

where $l_8$ and $l_9$ must be chosen to preserve orthogonality with $2b_1$. Then

$$\rho_x = l_6 l_8$$

and
$$K = l_1{}^2 l_6 l_8 (s_C x_C : s_C x_C)$$
$$+ l_2{}^2 l_6 l_8 (x_C z_C : x_C z_C) + 2 l_3{}^2 l_7 l_9 (xz : xz).$$

Terms in $l_4{}^2$ and $l_5{}^2$ are neglected but could readily be included if $l_4$ and $l_5$ were known. The nomenclature for Coulomb one-centre exchange integrals follows Mulligan [18] and numerical values were taken from his table XI to obtain the density $+4 \times 10^3 / \Delta E \, \mathrm{cm}^{-1}$ quoted in the text. It would be interesting to have a SCF treatment which did not require the space coordinates of $1b_1$ and $1\bar{b}_1$ to be identical, when the spin density in $x_C$ would appear as a direct property of the ground configuration.

## REFERENCES

[1] OVENALL, D. W., and WHIFFEN, D. H., 1960, *Proc. chem. Soc.*, p. 420.
[2] HARRIS, L., KING, G. W., BENEDICT, W. S., and PEARCE, R. W. B., 1940, *J. chem. Phys.*, **8**, 765.
[3] ROBINSON, G. W., MCCARTHY, M., and KEELTY, M. C., 1957, *J. chem. Phys.*, **27**, 972.
[4] NEUBERGER, D., and DUNCAN, A. B. F., 1954, *J. chem. Phys.*, **22**, 1693.
[5] MULLIKEN, R. S., 1942, *Rev. mod. Phys.*, **14**, 204.
[6] MULLIKEN, R. S., 1958, *Canad. J. Chem.*, **36**, 10.
[7] WALSH, A. D., 1953, *J. chem. Soc.*, p. 2266.
[8] ZACHARIASEN, W. H., 1940, *J. Amer. chem. Soc.*, **62**, 1011.
[9] HOLDEN, A. N., KITTEL, C., MERRITT, F. R., and YAGER, W. A., 1950, *Phys. Rev.*, **77**, 147.
[10] GORDY, W., and LUCK, C. F. (personal communication).
[11] ATHERTON, N. M., and WHIFFEN, D. H., 1960, *Mol. Phys.*, **3**, 1.
[12] FISCHER-HJALMARS, I, 1957, *Ark. Fys.*, **11**, 529.
[13] SMITH, W. V., SOROKIN, P. P., GELLES, I. L., and LASHER, G. J., 1959, *Phys. Rev.*, **115**, 1546.
[14] COULSON, C. A., 1948, *Victor Henri Volume Commemoratif*, Contribution à l'étude de la Structure Moléculaire, p. 15.
[15] BIRD, G. R., 1956, *J. chem. Phys.*, **25**, 1040.
[16] MOORE, G. E., 1953, *J. opt. Soc. Amer.*, **43**, 1045.
[17] MCCONNELL, H. M., and ROBERTSON, R. E., 1957, *J. phys. Chem.*, **61**, 1018.
[18] MULLIGAN, J. F., 1951, *J. chem. Phys.*, **19**, 347.
[19] KUSCH, P., and TAUB, H., 1949, *Phys. Rev.*, **75**, 1477.
[20] SHIMODA, and NISHIKANA, K., 1952, *J. phys. Soc., Japan*, **6**, 512.
[21] TRAMMELL, G. T., ZELDES, H., and LIVINGSTON, R., 1958, *Phys. Rev.*, **110**, 630.
[22] KEMP, J. C., 1960, *J. chem. Phys.*, **33**, 1269.
[23] BIRD, G. R., BAIRD, J. C., and WILLIAMS, R. B., 1958, *J. chem. Phys.*, **28**, 738.
[24] JEN, C. K., FONER, S. N., COCHRAN, E. L., and BOWERS, V. A., 1958, *Phys. Rev.*, **112**, 1169.
[25] ARD, W. B., 1955, *J. chem. Phys.*, **23**, 1967.
[26] MOLIN, YU. N., SHARPATYI, V. A., and BUBEN, N. YA., 1959, *Dokl. Akad. Nauk SSSR.*, **128**, 1224.
[27] BLEANEY, B., HAYES, W., and LLEWELLYN, P. M., 1957, *Nature, Lond.*, **179**, 140.
[28] MCCONNELL, H. M., and CHESNUT, D. B., 1958, *J. chem. Phys.*, **28**, 107.

# The proton magnetic resonance spectra of porphyrins
## Part II. Ring current effects in the porphyrins

by R. J. ABRAHAM

National Physical Laboratory, Teddington, Middlesex

A calculation of the field due to the ring current in the porphyrin system is given and shown to account for the observed chemical shifts of the protons in porphyrins. Also variations of the ring current are shown to account for the observed variations in the proton chemical shifts of different porphyrin molecules.

## 1. Introduction

The concept of an aromatic ring current was first used by Pauling [1] to explain the diamagnetic anisotropy of crystalline benzene. In this model, the six $\pi$ electrons in benzene under the influence of an applied magnetic field perpendicular to the molecular plane undergo Larmor precession along the carbon–carbon bonds in the molecule. This effect gives rise to the large diamagneti-susceptibility in this direction.

This concept was extended by Pople [2] to explain the difference between the proton chemical shifts of benzene and ethylene. The magnetic effect of the ring current was calculated by replacing the current loop by an equivalent dipole at the centre of the benzene hexagon, and averaging over all orientations of the molecule with respect to the external field.

Instead of the magnetic dipole approximation Waugh and Fessenden [3] and Johnson and Bovey [4] have calculated the actual magnetic field due to six $\pi$ electrons in benzene circulating in two current loops one above and one below the molecular plane. They have shown that whilst the protons in benzene experience a field due to the ring current in the same direction as the applied field, which gives rise to a decrease in the shielding constant (i.e. a low field shift) of these protons compared to those in ethylene, the field due to the ring current opposes the applied field immediately above or inside the current loop, and any proton situated in these positions will have a high field shift due to the ring current.

These conclusions have been verified experimentally in a number of ways, in particular by the experiments of Waugh and Fessenden [3] on 1 : 4-hexamethylene benzene. In this compound the chemical shifts of the methylene protons varied with the orientation of the particular methylene group with respect to the benzene ring, in the manner predicted by the above theories.

Pauling [1] extended his original ring current hypothesis to calculate the diamagnetic anisotropy in polycyclic aromatic systems, by treating the carbon skeleton of these systems as a conducting electrical network, in any current loop of which the e.m.f. is proportional to the area enclosed and the resistance proportional to the number of bonds. London [5] and later McWeeny [6] replaced this classical picture of Pauling, which gave too large values, by molecular orbital

calculations. These showed that essentially the same current, equal to the benzene ring current is induced in each benzene hexagon in a polycyclic system. This gave values of the diamagnetic anisotropy in good agreement with experiment. Bernstein, Schneider and Pople [7] used this result together with the equivalent dipole approximation, to calculate the proton chemical shifts in some polycyclic aromatic hydrocarbons and obtained reasonable agreement with experiment. However, in non-benzenoid conjugated rings, the ring current is not a simple function of the benzene ring current, as Pople [8] has shown, by extending the calculations of London to the azulene molecule.

The proton magnetic resonance spectra of the porphyrins have been given by Becker and Bradley [9] and Ellis *et al.* [10], and a more comprehensive study of these spectra in Part I of this series [11]. These spectra show very clearly the presence of a large ring current. The meso-proton chemical shifts are about 5 p.p.m. to low field of the normal value for an olefinic proton, whilst the N—H chemical shifts are about 11 p.p.m. to high field of the normal N—H value. However, calculations based on a current loop of $18\pi$ electrons with a radius of 3·3 Å give results too large by a factor of two [9, 10]. Also this simple model cannot explain the observed difference in the chemical shifts of the meso and beta protons in the molecule [11].

It will be shown that the observed chemical shifts of all the protons in the porphyrin molecule can be given a satisfactory explanation by extending the arguments which Pauling used to calculate the diamagnetic anisotropy of poly-cyclic compounds. From these calculations it is possible to predict how the proton chemical shifts in the porphyrins will change with changes in the ring current. It is shown that the observed differences in the proton resonance spectra of a neutral porphyrin molecule and the corresponding porphyrin di-cation can be explained as due to variations in the ring current, and an explanation of these variations is given.

## 2. THEORY

We wish to calculate the magnetic field at the various protons in the porphyrin molecule arising from the currents $i_1$ and $i_2$ (figure).

We first need to calculate these currents in terms of the known ring current in the benzene molecule.
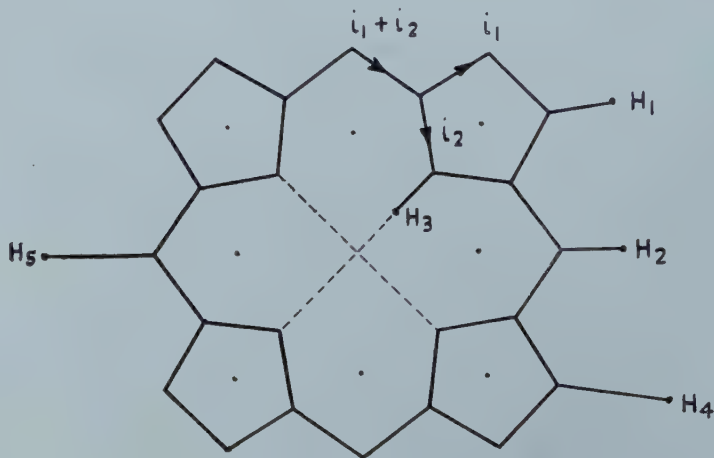


The porphyrin skeleton (drawn to scale).

We make the same assumptions as Pauling [1], i.e. that the e.m.f. round any loop is proportional to the area enclosed and that the resistance is proportional to the number of bonds. We also assume, for simplicity, that the resistances of the C—C and C—N bonds are equal. This gives for

(a) the pyrrole rings      e.m.f. $= kT = R(3i_1 - 2i_2)$,                          (1)

(b) the inner large ring   e.m.f. $= kS = R[8(i_1 + i_2) + 8i_2]$           (2)

and

(c) for benzene           e.m.f. $= kS_B = R(6i_B)$                         (3)

where $T$, $S$ and $S_B$ are the areas of the three rings concerned and $i_B$ is the benzene ring current. From these three equations, we obtain

$$i_1/i_B = 3(S/8 + T)/2S_B, \qquad (4)$$

$$i_2/i_B = 3(3S/8 - T)/4S_B. \qquad (5)$$

Taking the porphyrin dimensions given by Crute for nickel aetioporphyrin [12] and considering benzene as a hexagon of side $1.39$ Å gives $T = 3.31$ Å$^2$, $S/4 = 6.18$ Å$^2$ and $S_B = 5.02$ Å$^2$.

Substituting these in equations (4) and (5) gives

$$i_1 = 1.91 i_B; \quad i_2 = 0.89 i_B. \qquad (6)$$

We now need to calculate the magnetic effects of these currents. Following the treatment given by Bernstein *et al.* [7] for polycyclic aromatic hydrocarbons, we divide the prophyrin network into the four pyrrole rings and four hexagons (as shown in the figure) with an equivalent dipole at the centre of each segment. This gives for the pyrrole rings (area $T$, current $i_1$) an equivalent dipole $i_1 T/c$, and for each hexagon (area $S/4$, current $i_1 + i_2$) an equivalent dipole $(i_1 + i_2)S/4 c$. The field at any point in the plane of the molecule distant $R$ from an equivalent dipole of moment $M$, averaging over all orientations, is $10^6 \, M/3HR^3$ (p.p.m.), i.e. the field due to the pyrrole ring current at any point in the molecular plane distant $R$ from the pyrrole ring centre is given by

$$\lambda_1 = 10^6 \times 1.91 T i_B/3HcR^3 \text{ p.p.m.}$$

From reference [7]

$$\frac{10^6 i_B}{3Hc} = \frac{10^6}{3Hc} \times \frac{3e^2H}{2\pi mc} = \frac{10^6 e^2}{2\pi mc^2} = 4.49 \text{ Å},$$

i.e. $\lambda_1 = 28.4/R^3$ p.p.m.

Similarly the field due to the ring current in each hexagon at a point in the molecular plane distance $R$ from the centre of the hexagon is $77.8/R^3$ p.p.m. The total field due to the ring current at any point in the molecular plane outside the current loop is merely the sum of the contributions from each segment. This is shown in the table. The labelling of the protons in the table ($H_{1.5}$) corresponds to that in the figure. The distances $R$ were measured graphically by drawing the porphyrin skeleton following the measurements of Crute [12] taking the C—H distance for the meso and beta protons as $1.08$ Å and the N—H distance as $0.99$ Å [13]. The equivalent dipoles of the pyrrole rings were placed at the intersection of the lines from the apices of the pentagons to the mid-points of the opposite sides, and those of the hexagons at the intersection of the diagonals— these are shown as dots in the figure. In order to calculate the field at the beta

| | Beta protons (H₁) | | Meso protons (H₂) | | N–H protons (H₃) | | Beta methyls (H₄) | | Meso methyls (H₅) | |
|---|---|---|---|---|---|---|---|---|---|---|
| | $R$ (Å) | δ (p.p.m.) | $R$ (Å) | δ (p.p.m.) | $R$ (Å) | δ (p.p.m.) | $R$ (Å) | δ (p.p.m.) | $R$ (Å) | δ (p.p.m.) |
| Contributions from pyrrole rings | 2·30<br>5·24<br>6·70<br>8·16 | 2·33<br>0·20<br>0·09<br>0·05 | 3·25<br>3·25<br>7·15<br>7·15 | 0·83<br>0·83<br>0·08<br>0·08 | 2·16<br>3·25<br>3·25<br>4·06 | 2·81<br>0·83<br>0·83<br>0·43 | 3·15<br>5·74<br>7·55<br>8·95 | 0·91<br>0·15<br>0·07<br>0·04 | 3·90<br>3·90<br>7·96<br>7·96 | 0·48<br>0·48<br>0·06<br>0·06 |
| Contributions from hexagons | 3·46<br>4·50<br>6·43<br>7·04 | 1·88<br>0·85<br>0·30<br>0·21 | 2·50<br>5·05<br>5·05<br>6·70 | 4·97<br>0·60<br>0·60<br>0·26 | | | 4·15<br>5·32<br>7·10<br>7·85 | 1·09<br>0·51<br>0·22<br>0·16 | 3·35<br>5·85<br>5·85<br>7·57 | 2·07<br>0·39<br>0·39<br>0·19 |
| Contribution from large ring | | | | | | −21·2 | | | | |
| Total shift | | 5·91 | | 8·25 | | −16·3 | | 3·15 | | 4·31 |
| Calculated shift × 2/3 | | 3·9 | | 5·5 | | −10·9 | | 2·1 | | 2·9 |
| Observed shifts | | 4·2 | | 5·5 | | −11·0 | | 1·8 | | 2·9 |

Ring current contributions to the porphyrin proton chemical shifts.

and meso methyl protons the distance $R$ was taken as the average distance of the methyl protons, i.e. these protons ($H_1$ and $H_5$, figure) were considered to be at a distance $1.90$ Å from the ring carbon atom along the $C-C$ bond. The distances obtained ($R$) and the contributions from each segment ($\delta$) are given in the table, as well as the total field at the protons considered. All the fields considered so far are in the same direction as the main field, i.e. the positive values in the table represent a low field shift of these protons compared with the chemical shifts of similar protons.

In order to calculate the field at the N—H protons ($H_3$, figure) we break the porphyrin network down into the four pyrrole rings as before and now one large ring of area $S$, current $i_1 + i_2$ (figure). The fields at the N—H protons due to the pyrrole ring currents are calculated as above, but the field due to the large ring current cannot be calculated using the equivalent dipole approximation as this is not valid for points within the current loop. We now make use of the calculations of Johnson and Bovey [4] of the actual magnetic field due to the two current loops in benzene, as follows. As they calculated the field due to circular current loops, we consider the inner large ring as two circular current loops of radius $r$ defined by $\pi r^2 = S$. This gives $r = 2.81$ Å. The actual field at a point in the molecular plane at a distance $p$ from the ring centre is now given by looking up the appropriate value of $p\,r$ in Johnson and Bovey's tables and correcting for the different size of the current loops in the two cases. The field of the ring current is proportional to the current in the loop and inversely proportional to the radius. The result of this calculation is given in the table, for $p$, the distance of the N—H protons from the ring centre, equal to $0.96$ Å.

The effect of the large ring current is now to produce a high field shift of the N—H protons, shown by the negative sign in the table.

## 3. EXPERIMENTAL

The $\tau$ values for the meso, beta and N—H protons in the porphin di-cation are $-1.22$, $0.08$ and $14.40$ [11]. The magnitude of the field due to the ring current at the meso and beta protons can be estimated by comparing the above values with that of the protons in benzene ($\tau = 2.73$ [14]), assuming a low field shift in benzene due to the ring current of $1.50$ p.p.m. [4]. Thus in the porphyrin di-cation the meso and beta protons have a low field shift due to the ring current of $5.5$ and $4.2$ respectively.

The field of the ring current at the methyl protons can be obtained simply by comparing the meso methyl and beta methyl chemical shifts ($5.14$ and $6.22$ respectively [11]) with those of the side chain methyl group of $\beta$ carotene ($8.06$) [14]. This gives low field shifts at these two positions of $2.92$ and $1.84$ p.p.m. respectively.

To determine the field due to the ring current at the N—H protons, we compare the porphyrin N—H shifts with those of similarly constituted N—H protons. Examples are (a) Coproporphyrin I methyl ester in $CDCl_3$ ($13.89$) [9] against pyrrole N—H ($3.0$). The latter was estimated from the data of reference [15] using the $\tau$ value of cyclohexane ($8.56$) [14], i.e. there is a high field shift due to the ring current of $10.9$ p.p.m. (b) Porphin in trifluoracetic acid ($14.40$) against the $N^+$—H in $2:2:5$-trimethyl isopyrrole in TFA ($3.5$). The spectrum of this compound was not completely analysed by the N—H peak was readily assigned by its characteristic broad appearance. This gives a high field shift of $10.9$ p.p.m.

(c) Octamethyl porphyrin in TFA (14·8) with the N—H in 2-(2:3:4-trimethyl pyrryl)-Δ'pyrroline (1·5). This gives a high field shift of 13·3 p.p.m.

The above measurements are subject to some uncertainty, as the N—H protons may well be hydrogen-bonded in many cases. We have selected as the most probable value of the ring current shift at the N—H protons the value of 11·0 p.p.m.

## 4. Discussion

The observed values of the field of the ring currents at the five positions concerned are given in the table. It can be seen that the calculated values are all too large by a factor of about 1·5; in fact, multiplying the calculated values by two-thirds gives very good agreement for all the positions considered. The factor of 1·5 is not surprising in view of all the approximations made in the calculations. We have assumed in this semi-classical treatment that the C—C and C—N bonds have equal resistances to the precessing electrons. The C—N bonds will probably have a larger resistance, as this bond is more polar, and it would have been possible to obtain the observed shifts merely by inserting an extra resistance of the appropriate amount to take into account the effect of the nitrogen atoms. However, in view of the other approximations made in these calculations, this rather arbitrary step was not performed. The calculation of the field at the N—H protons assumed a circular current loop. This is not the case (see figure), though it is not clear whether actually considering the current moving in the molecular bonds would give a larger or smaller value. Also as has been mentioned earlier, the Pauling model is only approximately true for polycyclic compounds; e.g. the calculated diamagnetic anisotropy perpendicular to the molecule plane in pyrene, which is about the same size as the porphyrin skeleton, from Pauling's calculations is 6·92 times the value for benzene, whereas the observed value, and the value which London obtains by quantum-mechanical calculations, is 4·4 [16]. Again the Pauling model gives results about 1·5 time too large. In order to obtain a more exact calculation of the field due to the ring current in the porphyrins, it would be necessary to extend the quantum-mechanical calculations of Pople [8] to these much more complex molecules. This is beyond the scope of the present paper. However what this simple model does show conclusively is that the ring current hypothesis can account satisfactorily for the observed chemical shifts of the protons in these molecules: not only does it give reasonable values for the chemical shifts of both the ring and the N—H protons but it also predicts that the meso protons and meso methyl groups will lie to low field of the corresponding beta protons and beta methyl groups. The extent of the agreement between the observed and calculated values provides enough confidence in these calculations to enable us to extend them to the effects of substituent groups on the porphyrin ring currents. If a substituent group decreases the ring current in the porphyrin, this will lead to a high field shift of the meso, beta and side chain protons and a low field shift of the N—H protons; and further, the differences between the chemical shifts of corresponding protons in the substituted and parent compounds will be proportional to the actual fields due to the ring currents at these protons. For example, a decrease in the ring current which will give a high field shift at the meso protons of 1 p.p.m. will give at the same time high field shifts of 0·75 p.p.m. at the beta protons and 0·33 and 0·53 p.p.m. at the beta and meso methyl or methylene protons. Also the N—H protons will experience a low field shift of

2 p.p.m.    An example illustrating the effect of variations in the ring current will now be considered.

### The proton resonance spectra of neutral porphyrins and the porphyrin cation

The chemical shifts of the protons in a neutral porphyrin molecule are quite different from the chemical shifts of the same protons in the porphyrin di-cation; e.g. the $\tau$ values of the meso protons, beta methyl protons, methyl propionate methylene protons and the N—H protons in coproporphyrin I tetramethyl ester dissolved in $CDCl_3$ are 0·04, 6·45, 5·68, 6·80 and 13·89 respectively [9]. The values of the corresponding protons in coproporphyrin III tetramethyl ester dissolved in trifluoracetic acid are $-1·11$, 6·17, 5·33, 6·68 and 14·26 [11]. The difference between the proton chemical shifts in the I and III isomers is negligible [9]. Thus on forming the di-cation the side chain protons are all moved to low field and the N—H protons to high field. It has been suggested that the low field shift of the meso protons is due to the introduction of the positive charge on the nitrogen atom [10]. However, if this were the only effect, the N—H protons would be expected to have a much bigger low field shift, as these are much closer to the positive charge. In fact they are shifted to high field in the di-cation.

The meso proton low field shift of 1·15 and the beta methyl shift of 0·28 are in approximately the same ratio as the magnitudes of the fields due to the ring currents at these two positions ($1 : 0·33$ from above). This is very strong evidence for the presence of an increased ring current in the di-cation as compared to the neutral molecule. Further away from the porphyrin skeleton the effect decreases markedly, e.g. the chemical shift of the $\alpha$ methylene groups in the methyl propionate side chains only differ by 0·1 p.p.m. in the two cases, again what one would expect on this picture. This increase in the ring current would shift the N—H protons to high field by about 2·3 p.p.m. The observed high field shift of the N—H protons of only 0·4 p.p.m. would appear to be due to the superposition of two effects. A high field shift due to the increased ring current and a low field shift due to the introduction of a positive charge on the nitrogen atoms. This latter mechanism would need to produce a low field shift at the N—H protons of about 2 p.p.m. to explain the observed result. No experimental values of this effect are known, but this would appear to be a not unreasonable figure. However, any change in the hydrogen bonding of the N—H protons in the two cases would alter this figure somewhat.

The calculated increase in the ring current is about 20 per cent of the ring current in the neutral molecule. This increase could be discussed in terms of the lower resistance to the electron precession of the C—N⁺ bond compared with the C—N bond. However a more meaningful description of the mechanism responsible for this increase is to consider it as due to the greater resonance stabilization of the di-cation. In the di-cation all four nitrogen atoms are equivalent, whilst in the neutral molecule this is not so, as only two of them are bonded to protons. This reduces the number of Kekulé structures for any tautomer of the neutral molecule by a factor of two compared with the di-cation. This large change in the resonance energy, which accounts for the observed high basicity of the porphyrins [17] could well produce the observed increase in the ring current.

The samples of 2:2:5-trimethyl isopyrrole and 2-(2:3:4-trimethyl pyrryl)-$\Delta'$pyrroline were kindly supplied by Dr. E. Bullock of the University of Nottingham.

I would like to acknowledge the many helpful discussions I have had with Professor G. W. Kenner and Dr. A. H. Jackson.    Also it is a pleasure to acknowledge the considerable assistance I have received throughout this research from Dr. J. A. Pople.

The work described above has been carried out as part of the research programme of the National Physical Laboratory and this paper is published by permission of the Director of the Laboratory.

## REFERENCES

[1] PAULING, L., 1936, *J. chem. Phys.*, **4**, 673.
[2] POPLE, J. A., 1956, *J. chem. Phys.*, **24**, 1111.
[3] WAUGH, J. S., and FESSENDEN, R. W., 1957, *J. Amer. chem. Soc.*, **79**, 846.
[4] JOHNSON, C. E., and BOVEY, F. A., 1958, *J. chem. Phys.*, **29**, 1012.
[5] LONDON, F., 1937, *J. Phys. Radium*, **8**, 397.
[6] McWEENY, R., 1951, *Proc. phys. Soc. Lond.* A, **64**, 261, 291.
[7] BERNSTEIN, H. J., SCHNEIDER, W. G., and POPLE, J. A., 1956, *Proc. roy. Soc.* A, **236**, 515.
[8] POPLE, J. A., 1958, *Mol. Phys.*, **1**, 3.
[9] BECKER, E. D., and BRADLEY, R. B., 1959, *J. chem. Phys.*, **31**, 1413.
[10] ELLIS, J., JACKSON, A. H., KENNER, G. W., and LEE, J., 1960, Tetrahedron Letters, No. 2, 23.
[11] ABRAHAM, R. J., JACKSON, A. H., and KENNER, G. W., 1961, *J. chem. Soc.* (in the press).
[12] CRUTE, M. B., 1959, *Acta cryst., Camb.*, **12**, 24.
[13] BAK, B., CHRISTENSEN, D., HANSEN, L., and ANDERSEN, J. RASTRUP, 1956, *J. chem. Phys.*, **24**, 720.
[14] JACKMAN, L. M., 1959, *Applications of Nuclear Magnetic Resonance Spectroscopy in Organic Chemistry* (London : Pergamon Press).
[15] ABRAHAM, A. J., and BERNSTEIN, H. J., 1959, *Canad. J. Chem.*, **37**, 1056.
[16] LONDON, F., 1937, *J. chem. Phys.*, **5**, 837.
[17] NEUBERGER, A., and SCOTT, J. J., 1952, *Proc. roy. Soc.* A, **213**, 307.

# Thermodynamic properties of clathrates
## III. The heat capacity and entropy of krypton in the krypton quinol clathrates

by N. R. GREY, N. G. PARSONAGE and L. A. K. STAVELEY

Inorganic Chemistry Laboratory, Oxford

Measurements have been made of the heat capacity $C_p$ from $\sim 14$ to $300°$K of three clathrates of krypton and $\beta$-quinol, in which 24·2, 47·9 and 79·5 per cent of the cavities were occupied by krypton. $C_p$ was found to be a linear function of composition. These results together with those previously obtained for the argon clathrate make it possible to fix within comparatively narrow limits a distance parameter characteristic of the quinol lattice (in effect a measure of the thickness of the wall of the cavity). This should make it possible to carry out a reliable analysis of the contribution made to the heat capacity of quinol clathrates by diatomic and polyatomic molecules.

---

## 1. INTRODUCTION

This paper is the third of a series dealing with heat capacity measurements carried out to elucidate the motion of small molecules trapped in the cavities of the $\beta$-quinol clathrates. The two previous papers have been concerned with the argon clathrate [1] and the methane clathrate [2], and we describe here measurements on the krypton clathrate. There were two reasons for studying another clathrate with monatomic molecules in the holes. Firstly, such molecules undergo one type of motion only, the contribution of which to the heat capacity can be estimated from the theory due to van der Waals [3]. The comparison between observed and calculated heat capacity values provides one of the best tests of this theory. In the argon clathrate this comparison in certain temperature regions was complicated by slight anomalies in the thermal properties of some of the clathrates studied. Secondly, it is of obvious interest to examine the extent to which diatomic and polyatomic molecules in the cavities can rotate freely. This has already been done for methane and it is hoped to carry out experiments on diatomic molecules. Here it is necessary to deduct from the gross contribution of the trapped molecules to the heat capacity that part due to their vibration (or 'rattling') which must be estimated from the van der Waals theory. Therefore to put the heat capacity analysis of such clathrates on as sound a basis as possible it was clearly desirable to make measurements on more than one clathrate with monatomic molecules.

## 2. EXPERIMENTAL

Heat capacity measurements were made on three clathrates prepared by slow crystallization from hot solutions of quinol in *n*-propanol in the presence of krypton under pressure. Krypton of not less than 99 per cent purity was supplied by British Oxygen Co. Ltd. in cylinders filled to 30 atmospheres, and to achieve the higher pressures for the preparation of krypton-rich clathrates it was necessary

to liquefy the krypton and allow it to evaporate into the crystallization vessel. The values of $x$ for the three samples studied, $x$ being the number of moles of krypton per 3 moles of quinol, were 0·242, 0·479 and 0·795. $C_p$ measurements were made with the calorimeter used for the argon and methane clathrates. These measurements were made from $\sim 14$ to $300°$K on the clathrates with $x = 0·242$ and 0·795. For the other sample, no measurements were carried out above $265°$K owing to a defect in the calorimeter. Plots of $C_p$ against $x$ ($C_p$ being referred to the quantity $3C_6H_4(OH)_2 . xKr$) were linear, and on extrapolation to $x = 0$ gave values (table 2) for the heat capacity of pure $\beta$-quinol (i.e. with all the holes empty) in agreement with those obtained from measurements on methane clathrates to about 0·5 per cent.

Only one of the krypton clathrates (that with $x = 0·479$) lost any krypton in the course of the measurements. Here the loss was small, being about 0·34 per cent of the krypton originally present in the crystals, and a suitable correction was made to the $C_p$ values as described in the paper on the argon clathrates [1].

## 3. Discussion

The experimental $C_p$ results are given in table 1. Their precision expressed as the root mean square deviation from the smooth curve is 0·6 per cent from 14 to 90°K and 0·12 per cent from 90 to 300°K. Within these limits, $C_p$ at any one temperature over the whole temperature range is a linear function of $x$, the fraction of holes filled. In table 2 are recorded at regular temperature intervals the derived values of $C_{Kr}$, the molar heat capacity of krypton in the clathrate, and $C_p^Q$, the heat capacity of three moles of pure $\beta$-quinol.

In order to calculate $C_{Kr}$ from the equations which follow from van der Waals theory [3] it is necessary to assign values to two quantities $\bar{\epsilon}$ and $\bar{\sigma}$ characteristic of the quinol lattice. $\bar{\epsilon}$ may be said to represent the strength of the intermolecular attraction which the wall of the cavity is capable of exerting and $\bar{\sigma}$ is a measure

| K1. $3C_6H_4(OH)_2 . 0·795$ Kr (0·04327 moles in the calorimeter) |
|---|---|---|---|---|---|
| $T(°K)$ | $C_p$ | $T(°K)$ | $C_p$ | $T(°K)$ | $C_p$ |
| 13·45 | 3·65 | 85·18 | 36·41 | 170·64 | 60·99 |
| 15·90 | 5·30 | 90·29 | 37·75 | 176·52 | 62·74 |
| 18·80 | 7·31 | 95·66 | 39·09 | 183·14 | 64·83 |
| 22·48 | 9·88 | 101·05 | 40·52 | 190·24 | 66·98 |
| 26·86 | 12·73 | 106·24 | 41·99 | 197·18 | 69·29 |
| 31·36 | 15·40 | 111·27 | 43·46 | 204·74 | 71·39 |
| 36·32 | 18·14 | 116·45 | 44·99 | 211·04 | 73·54 |
| 41·06 | 20·59 | 121·77 | 46·55 | 218·78 | 75·98 |
| 41·75 | 20·94 | 126·95 | 47·93 | 226·35 | 78·55 |
| 47·74 | 23·76 | 131·99 | 49·43 | 234·22 | 81·10 |
| 53·91 | 26·35 | 137·18 | 50·87 | 242·37 | 83·71 |
| 58·69 | 28·25 | 142·49 | 52·44 | 250·78 | 86·38 |
| 65·05 | 30·38 | 147·96 | 54·08 | 259·43 | 89·39 |
| 69·66 | 31·69 | 153·68 | 55·74 | 268·30 | 92·64 |
| 74·41 | 33·09 | 159·21 | 57·48 | 276·56 | 95·06 |
| 79·80 | 34·69 | 164·87 | 59·29 | | |

| K2.  $3C_6H_4(OH)_2 . 0\cdot242$ Kr ($0\cdot03946$ moles in the calorimeter) |

| $T(°K)$ | $C_p$ | $T(°K)$ | $C_p$ | $T(°K)$ | $C_p$ |
|---|---|---|---|---|---|
| 13·65 | 2·76 | 90·74 | 35·23 | 177·63 | 60·50 |
| 16·76 | 4·65 | 95·63 | 36·51 | 183·95 | 62·45 |
| 19·90 | 6·60 | 98·73 | 37·31 | 191·03 | 64·57 |
| 23·68 | 8·96 | 103·66 | 38·64 | 198·36 | 66·96 |
| 28·24 | 11·75 | 108·77 | 40·14 | 205·52 | 69·16 |
| 32·75 | 14·25 | 114·05 | 41·70 | 213·01 | 71·54 |
| 37·47 | 16·53 | 119·16 | 43·06 | 220·79 | 74·13 |
| 42·62 | 19·15 | 124·43 | 44·58 | 227·35 | 75·91 |
| 48·11 | 21·56 | 129·87 | 46·14 | 235·15 | 78·47 |
| 53·81 | 24·24 | 135·16 | 47·65 | 243·24 | 81·20 |
| 59·54 | 26·17 | 144·10 | 50·35 | 251·61 | 84·07 |
| 65·76 | 28·13 | 149·65 | 52·04 | 260·24 | 86·89 |
| 70·69 | 29·51 | 155·07 | 53·60 | 269·10 | 89·91 |
| 75·74 | 30·90 | 160·63 | 55·41 | 277·70 | 92·73 |
| 80·92 | 32·49 | 166·34 | 57·20 | 286·14 | 95·70 |
| 85·95 | 34·04 | 171·92 | 58·73 | | |

K3.   $3C_6H_4(OH)_2 . 0\cdot479$ Kr ($0\cdot03895$ moles in the calorimeter)

| $T(°K)$ | $C_p$ | $T(°K)$ | $C_p$ | $T(°K)$ | $C_p$ |
|---|---|---|---|---|---|
| 17·00 | 5·21 | †85·60 | 34·62 | 150·16 | 53·39 |
| 18·33 | 6·16 | †88·32 | 35·62 | 152·54 | 53·82 |
| 20·81 | 7·75 | †90·28 | 36·23 | 156·05 | 55·10 |
| 24·71 | 10·33 | †90·56 | 36·06 | 158·19 | 55·66 |
| 29·44 | 13·27 | †94·29 | 37·24 | 162·05 | 56·96 |
| 34·64 | 16·13 | 98·61 | 38·34 | 168·16 | 58·58 |
| 39·60 | 18·61 | 104·02 | 39·94 | 174·38 | 60·77 |
| 44·56 | 21·04 | 110·67 | 41·79 | 180·68 | 61·92 |
| 49·84 | 23·34 | 115·16 | 42·95 | 185·69 | 63·96 |
| 56·00 | 25·66 | 117·14 | 43·48 | 193·66 | 66·69 |
| 61·67 | 28·79 | 120·81 | 44·40 | 202·11 | 68·84 |
| 65·60 | 29·19 | 123·23 | 45·25 | 210·18 | 71·53 |
| 66·51 | 29·21 | 126·29 | 46·25 | 217·77 | 74·19 |
| 70·98 | 30·68 | 131·74 | 48·30 | 225·64 | 76·89 |
| 71·02 | 30·72 | 134·98 | 48·77 | 235·78 | 79·82 |
| 76·63 | 32·28 | 139·63 | 50·42 | 244·50 | 82·65 |
| 79·31 | 33·30 | 140·85 | 50·41 | 253·28 | 85·19 |
| †82·76 | 34·01 | 144·40 | 51·47 | 262·07 | 88·55 |
| †85·06 | 34·58 | 146·50 | 52·29 | | |

† Corrected for loss of krypton from the clathrate.

Table 1.   Experimental values of the heat capacities of the samples of krypton clathrate in cal deg$^{-1}$ mole$^{-1}$.

of the effective thickness of this wall.    The theoretical estimate of the heat capacity contribution of the molecules in the holes is much more sensitive to the value of $\bar{\sigma}$ than to $\bar{\epsilon}$.    In the calculations on the argon and methane clathrate we took $\bar{\sigma} = 3\cdot3$ Å, the value originally used by van der Waals, and for argon obtained values

for its molar heat capacity in the clathrate which at high temperatures were about
0·5 cal deg$^{-1}$ mole$^{-1}$ higher than the experimental values.   Meanwhile, van der
Waals and Platteuw had concluded from a reconsideration of the lattice dimensions
of clathrates that a lower value of $\bar{\sigma} = 2·9$ Å was to be preferred. Later, Dr. van
der Waals pointed out to us privately that by taking $\bar{\sigma} = 3·0$, the agreement between
the experimental and theoretical heat capacities of argon in its clathrate was much

| $T(°\text{K})$ | $C_p^Q$ | $T(°\text{K})$ | $C_p^Q$ | $T(°\text{K})$ | $C_p^Q$ |
|---|---|---|---|---|---|
| 15 | 3·13 | 80 | 31·03 | 200 | 66·32 |
| 20 | 5·93 | 90 | 33·83 | 210 | 69·44 |
| 25 | 9·00 | 100 | 36·53 | 220 | 72·57 |
| 30 | 11·90 | 110 | 39·32 | 230 | 75·75 |
| 35 | 14·59 | 120 | 42·10 | 240 | 79·05 |
| 40 | 16·86 | 130 | 45·00 | 250 | 82·34 |
| 45 | 19·19 | 140 | 47·94 | 260 | 85·64 |
| 50 | 21·46 | 150 | 51·00 | 270 | 88·97 |
| 55 | 23·56 | 160 | 54·02 | 280 | 92·41 |
| 60 | 25·31 | 170 | 57·06 | 290 | 95·81 |
| 65 | 26·83 | 180 | 60·15 | 298·16 | 98·57 |
| 70 | 28·20 | 190 | 63·25 | 300 | 99·23 |

Table 2.   The heat capacity of three moles of β-quinol at regular temperature intervals
in cal deg$^{-1}$.

| $T(°\text{K})$ | $C_{\text{Kr}}$ (experimental) | $C_{\text{Kr}}$ (theoretical) | | |
|---|---|---|---|---|
| | | $\bar{\sigma} = 2·9$ | $\bar{\sigma} = 3·0$ | $\bar{\sigma} = 3·3$ Å |
| 25 | 3·25 | 5·3779 | 5·5474 | 5·8001 |
| 45 | 4·00 | 5·1827 | 5·3696 | 5·6999 |
| 70 | 4·44 | 5·0327 | 5·2132 | 5·5960 |
| 120 | 4·81 | 4·8505 | 5·0275 | 5·4390 |
| 200 | 4·80 | 4·6894 | 4·8479 | 5·2610 |
| 298·16 | 4·72 | 4·5723 | 4·7148 | 5·1139 |

Table 3.   Experimental and theoretical values of $C_{\text{Kr}}$, the krypton contribution to $C_p$, in
cal deg$^{-1}$ mole$^{-1}$ Kr.

improved.   $C_{\text{Kr}}$ has therefore been calculated using $\bar{\sigma} = 2·9$, 3·0 and 3·3 Å, and
the same value of $\bar{\epsilon}$ as before (i.e. $z\sqrt{(\bar{\epsilon}/k)} = 283$).   For the parameters character-
istic of the interaction of a pair of krypton atoms we have taken the values
$\epsilon_{A/k} = 171·0°$ and $\sigma_A = 3·60$ [4].   The calculated values of $C_{\text{Kr}}$ are given in table 3
and are compared graphically with experiment in figure 1.   It will be seen that at
temperatures sufficiently high for the classical assumptions of the theory to be a
valid approximation, the agreement between experiment and theory is undoubtedly
much better for $\bar{\sigma} = 2·9$ and 3·0 Å than for $\bar{\sigma} = 3·3$ Å.   A similar comparison between
theory and experiment is shown in figure 2 for the argon clathrates and again

demonstrates the superiority of the lower $\bar{\sigma}$ values.    Inspection of figures 1 and 2 perhaps indicates a preference for $\bar{\sigma} = 3 \cdot 0$ Å, as giving slightly better agreement with experiment than $\bar{\sigma} = 2 \cdot 9$ Å.
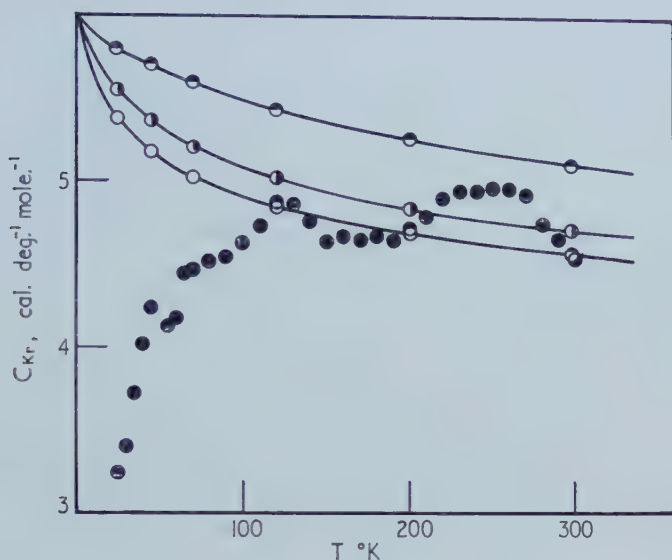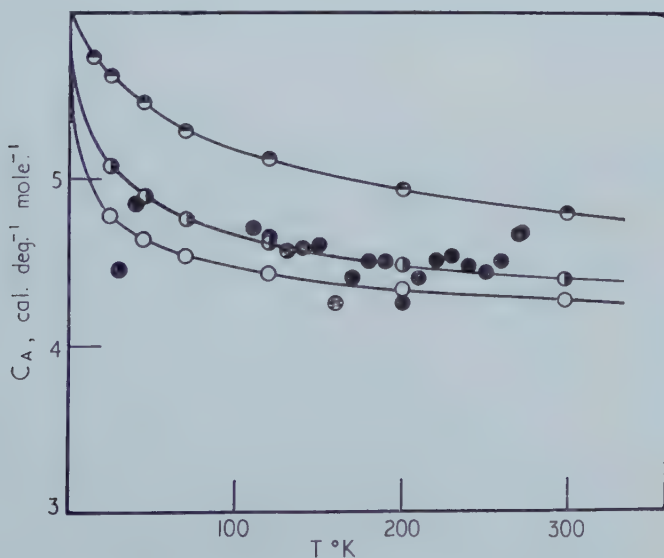


Figure 1.   Comparison of observed and calculated values of $C_{Kr}$ for the krypton clathrate in cal deg$^{-1}$ mole$^{-1}$.  ● experimental points.   Calculated values:  ○ for $\bar{\sigma} = 2 \cdot 9$ Å; ◑ for $\bar{\sigma} = 3 \cdot 0$ Å; ◓ for $\bar{\sigma} = 3 \cdot 3$ Å.



Figure 2.   Comparison of observed and calculated values of $C_A$ for the argon clathrate in cal deg$^{-1}$ mole$^{-1}$.  ● experimental points.   Calculated values:  ○ for $\bar{\sigma} = 2 \cdot 9$ Å; ◑ for $\bar{\sigma} = 3 \cdot 0$ Å; ◓ for $\bar{\sigma} = 3 \cdot 3$ Å.

In the light of this result, it is desirable briefly to reconsider the analysis of $CH_4$, the contribution made by a mole of methane to the heat capacity of the methane clathrate.   The quantity of interest here is $C_{rot} = C_{CH_4} - C_{vib} - C_{int}$, where $C_{vib}$ is the contribution from the movement of the molecules within the cavities (the rattling, as it were) estimated from van der Waals theory and $C_{int}$ that from the intramolecular vibrations.   We have estimated $C_{vib}$ for the methane clathrate using both $\sigma = 2 \cdot 9$ and $3 \cdot 0$ Å and the resulting values of $C_{rot}$ are given in table 4.   It will be seen that use of these lower $\bar{\sigma}$ values gives figures for $C_{rot}$ which, within experimental error, still agree sufficiently well with $2 \cdot 97$ cal deg$^{-1}$ mole$^{-1}$ ($= \frac{3}{2}R$) to leave unaltered the conclusion that from $\sim 150\,^\circ$K upwards the molecules virtually rotate freely.   (The experimental error associated with $C_{rot}$ is $\sim 0 \cdot 2$ cal deg$^{-1}$ mole$^{-1}$ up to $250\,^\circ$K and rather more at room temperature where the relative contribution of $C_{CH_4}$ to the measured heat capacity is least.)

| $T(^\circ K)$ | $C_{rot}$ | $C_{rot}$ |
| --- | --- | --- |
| | $\bar{\sigma} = 2 \cdot 9$ | $\bar{\sigma} = 3 \cdot 0$ Å |
| 150 | 2·45 | 2·60 |
| 200 | 2·75 | 2·88 |
| 230 | 2·73 | 2·87 |
| 250 | 2·69 | 2·80 |
| 300 | 2·26 | 2·39 |

Table 4.   Revised values of $C_{rot}$, the contribution per mole from the rotational movement of the methane molecules in the methane clathrate.   $C_{rot} = C_{CH_4} - C_{vib} - C_{int}$ where $C_{CH_4}$ = measured total heat capacity per mole of methane, $C_{vib}$ = contribution from the vibrational movement of the molecules within the cavity as computed from van der Waals theory using $\bar{\sigma} = 2 \cdot 9$ and $\bar{\sigma} = 3 \cdot 0$ Å, and $C_{int}$ = contribution from intramolecular vibrations.

The calculated value of $S_{Kr}$ at $25\,^\circ$c (the contribution made to the entropy of the clathrate by the non-configurational entropy of a mole of krypton) is $15 \cdot 93$ cal deg$^{-1}$ mole$^{-1}$ for $\bar{\sigma} = 3 \cdot 0$ Å and $16 \cdot 04$ cal deg$^{-1}$ mole$^{-1}$ for $\bar{\sigma} = 2 \cdot 9$ Å.   The experimental figure estimated from our heat capacity results is $13 \cdot 05$ cal deg$^{-1}$ mole$^{-1}$, so that for this system as for the argon and methane clathrates the calculated figure is significantly higher than the experimental value.   This difference probably arises from the interaction between the trapped molecules and the lattice, which must in principle affect the vibrational frequencies of the quinol molecules.   In particular, the vibrations of lower frequency might be sufficiently perturbed for their contribution to the entropy to be significantly reduced while scarcely affecting the heat capacity at higher temperatures where it has almost attained the classical value.   (Thus the entropy contribution from one dimensional vibrations of frequencies 120 and 150 cm$^{-1}$ differ by $0 \cdot 43$ cal deg$^{-1}$ mole$^{-1}$ at $25\,^\circ$c, whereas the heat capacity contributions differ by only $0 \cdot 03$ cal deg$^{-1}$ mole$^{-1}$.)   It is worth noting that the discrepancy between the observed and calculated non-configurational entropies is greater for krypton with its larger molecule and its stronger field of force than for argon.

Four measurements were made of the heat of solution of the krypton clathrate sample with $x = 0.795$ with the differential calorimeter used for similar measurements on the methane clathrates. The heat of solution of the clathrates in dilute hydrochloric acid ($0.002$ N) was compared with that of $\alpha$-quinol. Taking $0.5$ k cal as the heat content difference between three moles of $\alpha$- and $\beta$-quinol, the resulting values of $\Delta U_m$, the heat of formation of the clathrate per mole of krypton at constant volume were $-5.3$, $-6.8$, $-5.0$, $-5.7$ k cal, with a mean of $-5.7$ k cal. The calculated values are $-5.73$, $-5.98$ and $-6.53$ k cal for $\bar{\sigma} = 2.9$, $3.0$ and $3.3$ Å respectively. Thus the observed values of $\Delta U_m$ are consistent with the revised value of $\bar{\sigma}$.

REFERENCES

[1] PARSONAGE, N. G., and STAVELEY, L. A. K., 1959, *Mol. Phys.*, **2**, 212.
[2] PARSONAGE, N. G., and STAVELEY, L. A. K., 1960, *Mol. Phys.*, **3**, 59.
[3] VAN DER WAALS, J. H., 1956, *Trans. Faraday Soc.*, **52**, 184.
[4] HIRSCHFELDER, J. O., CURTISS, C. F., and BIRD, R. B., 1954, *Molecular Theory of Gases and Liquids* (New York: Wiley).

# The polarized charge-transfer spectrum of crystalline anthracene-TNB complex†

by STEPHEN K. LOWER, ROBIN M. HOCHSTRASSER
and C. REID

The University of British Columbia, Vancouver 8,
Canada

The intermolecular charge-transfer spectrum of the crystalline anthracene-TNB complex has been measured, using polarized light. The crystal spectrum differs from that of the solution to a much greater degree than is the case for ordinary aromatic systems. The transition is polarized along the inter-molecular axis and is blue-shifted with respect to the solution. There is pronounced vibrational structure, including a prominent 250 cm⁻¹ interval. A Davydov splitting of approximately 200 cm⁻¹ is observed, and this is shown to be in reasonable agreement with the known crystal structure and with the symmetry assignment of the transition, which is $A' \leftarrow A'$ for the complex in solution and $A \leftarrow A$ in the crystal.

## 1. Introduction

The electron transfer theory of Mulliken [1, 2] provides a description of the bonding and spectra of many well-known complexes between aromatic hydrocarbon donors and various acceptors such as iodine or 1, 3, 5-trinitrobenzene (TNB). The theory was applied to the TNB-polyacene complexes by McGlynn and Boggus [3] and the subject has been reviewed by McGlynn [4]. The emission spectra of TNB complexes were first studied by Reid [5] while the absorption spectra were extensively examined by Czekalla and his group [6 8].

All previous studies on TNB complexes were concerned with the complex in solution; there have been no detailed studies of the crystal spectra of these compounds, although Nakamoto [9] observed the dichroism in crystalline chloranil-hexamethylbenzene and several other molecular complexes, and confirmed the theoretical prediction that the charge-transfer absorption is polarized perpendicular to the planes of the benzene rings, i.e. in the direction of the intermolecular bond.

More knowledge of such crystal spectra would clearly be of interest, and for this study the anthracene-TNB complex was selected, since it forms good crystals between pressed discs, has a known crystal structure [10], the polarized infra-red spectrum is known [11], and this complex has recently been discussed in detail by McGlynn [4, 12].

## 2. EXPERIMENTAL

The complex was prepared from twice-recrystallized portions of Eastman 'white label' anthracene and 1, 3, 5-trinitrobenzene, and then recrystallized from a concentrated alcoholic solution of TNB. The orange crystals were melted between a quartz disc and a microscope cover glass and cooled slowly under pressure, yielding a crystalline film of 5–10 microns thickness†. A polarizing microscope was used to locate a uniform area giving perfect straight extinction, and the crystal (elongated along the $c$-axis) was oriented in front of a pinhole in the metal Dewar cell. Light from a tungsten lamp was focused on the crystal, and the transmitted light was made parallel and passed through a Wollaston prism so mounted that either of the two oppositely polarized beams could be directed onto the slit. The spectrometer was a Hilger E–2 quartz prism instrument equipped with an automatic scanning unit and a 1P28 photomultiplier. All the spectra except one were run at liquid nitrogen temperature, and separate runs were made for the incident light intensity in each polarization. Values of optical density were calculated with respect to an assumed optical density of zero at a point well outside the absorption band. In two cases the observation was extended into the ultra-violet region, and the tungsten source was replaced by an Osram xenon arc lamp. Eight different samples were studied.
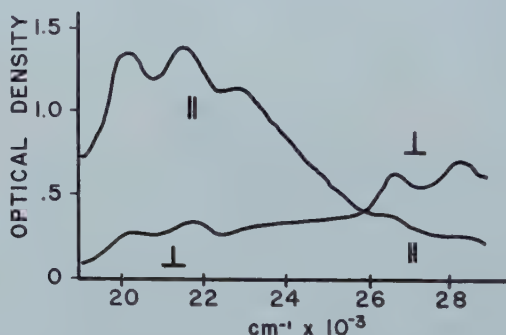


Figure 1.    Absorption spectrum of a thin crystal of the complex.    Only the main peaks are resolved, but the optical density ratio is more accurate.    The signs ‖ and ⊥ refer to the direction of polarization with respect to the needle ($c$-) axis.

Three representative spectra are shown in figures 1 and 2. As expected, the charge-transfer absorption is greatest for light polarized in the direction of the needle ($c$) axis. It extends roughly from 20 000 to 25 000 cm$^{-1}$, and shows three prominent peaks beginning at 20 150 cm$^{-1}$ and spaced 1300–1500 cm$^{-1}$ apart. Superimposed on these is a weak vibration of very low frequency, around 250 cm$^{-1}$. The peak positions and intensities appear to vary somewhat between samples, and their broadness makes exact location of the maxima difficult. Slight errors in the alignment of the crystal and of the optical system affect the shapes of the broad peaks (and hence their apparent positions), and this probably explains most of

† The thickness was measured by splitting the discs apart (the film usually adheres completely to one or the other), measuring the surface of a selected area, and then dissolving this area in ethanol and measuring the absorption at 3800 Å. From this, and the molar volume (286 gm$^3$ mol$^{-1}$) of the complex, the thickness was readily estimated.

the variation. The presence of the low-frequency intervals also contributes to the difficulty of exact measurement.

From the spectrum in figure 1 we can calculate a maximum optical density ratio of 5·2 : 1, assuming a reflection loss of 10 per cent. It was possible to record spectra at optical densities of up to 3·5. Values greater than 2·5 are considered unreliable because of attenuation of the strongly absorbing peaks, resulting in a flattening of the upper curves of figure 2.
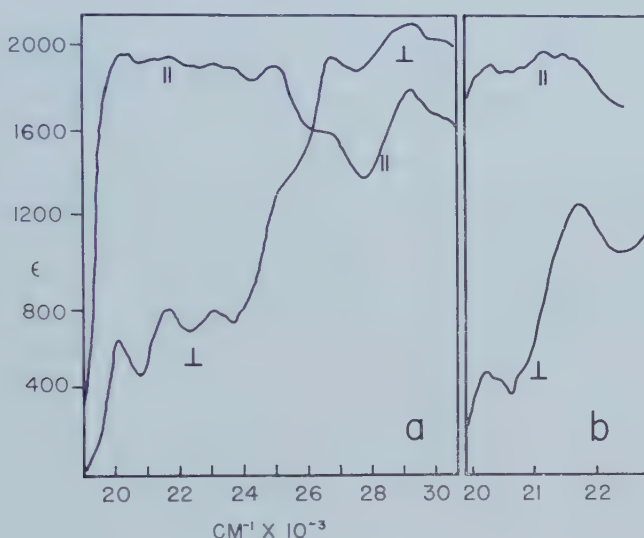


Figure 2. Absorption spectra of two other samples, showing more detail. The ordinate scale refers only to (*a*). In both cases, the maximum optical density is about 2·8.

Beyond 26 200 cm⁻¹, the maximum absorption occurs perpendicular to the needle axis, corresponding to excitation in the planes of the aromatic rings. The broad peaks at 26 000 cm⁻¹ and 26 500 cm⁻¹ are presumably those of anthracene, and that at 29 200 cm⁻¹ may arise from the TNB. The most interesting feature of this portion of the spectrum is the low intensity of the anthracene bands, which in the pure crystal have extinction coefficients of around 20 000. Even if we correct for the smaller number of anthracene molecules in a given thickness of the sample, and allow for an error of 1000 in our measured extinction coefficient, it appears that this transition suffers an attenuation by a factor of 0·2 in the crystalline complex.

## 3. DISCUSSION

### 3.1. *The crystal structure and vibrational intervals*

In solution, the anthracene-TNB charge-transfer absorption occupies a broad band centred at 22 300 cm⁻¹. The extinction coefficient is 1200–1600, and the spectrophotometrically determined heat of formation is −4·4 kcal per mole. In a rigid glass at 77 °K, the charge–transfer absorption shows no vibrational structure [8, 12] and in this way the crystal and solution spectra differ to a greater degree than is the case for ordinary aromatic molecules. The broadness of the solution spectrum is related to the shallowness (4·4 kcal = 1540 cm⁻¹) of the ground-state

potential energy curve.    Additional broadening could arise from contact charge-transfer and from multiple configurational isomerism, which have been discussed by Orgel and Mulliken [13] and more recently by Murrell [14].

According to Wallwork [10], the anthracene-TNB complex belongs to the monoclinic point group C2/c, with $\beta = 133 \cdot 5°$.    There are eight molecules (four complexes) per unit cell and the molecules are stacked alternately in columns parallel to the *c*-axis, but tilted by about 6° from the perpendicular to that axis. The distance between molecules along the *c*-axis is 3·29 Å.    Figure 3 (*a*) shows the locations of the molecules in projection on the 110 plane.    An individual molecule such as TNB is located midway between two anthracene molecules, but is tilted in the direction of only one of them, the other differing in inclination by 12°; only to this extent can the crystal be regarded as consisting of discrete 1 : 1 complex pairs.

The crystal structure places a physical constraint upon the molecules which does not exist in solution, and markedly alters the shape of the upper- and ground-state potential energy curves, both of which should now be sharper and of greater height.    The charge-transfer spectrum should itself be sharper, and the presence of more vibrational structure is expected.
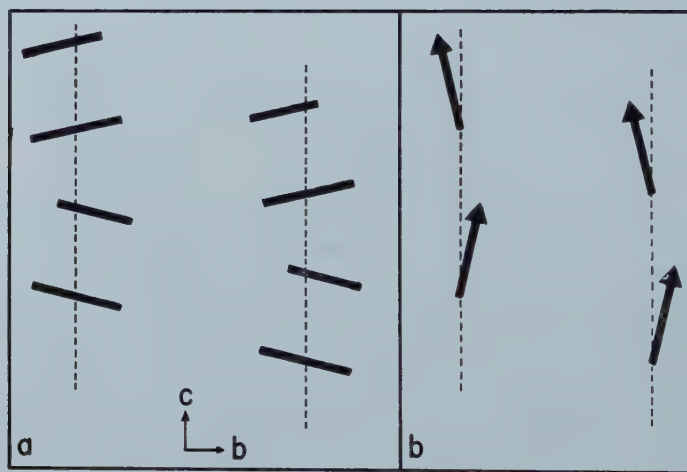


Figure 3.    A projection of the 110 plane of a unit cell on to 100.    In (*a*), the molecules are represented edgewise by the heavy lines, the longer ones, centred on the *c*-axis, denoting anthracenes.    The transition dipole moments alone are shown in (*b*).    In both diagrams, the inclination (5° 20′) is exaggerated for clarity.

In this connection it is interesting to note that although the charge-transfer absorption in solution is structureless, there is considerable vibrational detail in the emission spectrum of the complex, and McGlynn *et al.* [12] have recently studied it in some detail.    They find that the anthracene phosphorescence causes most of the structure, and includes fundamentals of 1139 cm$^{-1}$, 1414 cm$^{-1}$ and 1573 cm$^{-1}$, which correspond to the $a_g$ vibrations of the same frequency which appear in the phosphorescence of pure anthracene.    The 1266 cm$^{-1}$ (C–H bending) fundamental of anthracene does not occur in the phosphorescence of the complex, but a broad 1250 cm$^{-1}$ interval is present in the charge transfer

complex fluorescence, the curve for which was derived by subtracting the phos-
phorescence from the total emission.

The vibrational structure in the present spectra is not well enough resolved
to permit positive identification of the fundamentals. The exact peak positions
can in most cases be determined only to within $30$-$60$ cm$^{-1}$, and an accurate
vibrational analysis is thus precluded. Nevertheless, it seems worth while to
present a rough analysis for five of the better spectra. Two of these are given in
table 1, and correspond to the spectra of figures 1 and 2 (*b*). The 'assignments'
are very approximate and sometimes rather ambiguous (e.g. it is not possible to
distinguish a $1530$ cm$^{-1}$ vibration from $1250+250$ cm$^{-1}$) but they do seem to
correlate satisfactorily the various spectra studied, and certainly suggest the
general form of the vibrational structure, even if their relationship to the actual
fundamentals is somewhat equivocal. The existence of fundamentals of approxi-
mately $250$ cm$^{-1}$ and $1070$ cm$^{-1}$ is fairly certain; those of $1150$ cm$^{-1}$, $1250$
and/or $1500$ cm$^{-1}$ are also likely.

| Peak | Parallel[b] | | Perpendicular | | Assignment | Splitting[c] |
|---|---|---|---|---|---|---|
| Figure 1 | $\nu$ | $\nu-\nu_0$ | $\nu$ | $\nu-\nu_0$ | | |
| 1 ($\nu_0$) | 20100 | 0 | 20280 | 0 | $^1A \leftrightarrow {}^1A$ | −180 |
| 2 | 21430 | 1330 | 21670 | 1390 | $1070+250=1320$ | −240 |
| 3 | 22720 | 2620 | — | — | $2(1070+250)=2640$ | |
| Figure 2 (*b*) | | | | | | |
| 1 (*a*) ($\nu_0$) | 20150 | 0 | 20270 | 0 | $^1A \leftrightarrow {}^1A$ | −120 |
| 1 (*b*) | 20380 | 230 | [20500] | 230 | 250 | −120 |
| 1 (*c*) | 20600 | 450 | [20800] | 530 | $2(250)=500$ | −200 |
| 1 (*d*) | 20840 | 690 | — | — | $3(250)=750$ | |
| 2 (*a*) | 21220 | 1070 | — | — | 1070 | |
| 2 (*b*) | 21500 | 1350 | — | — | $1070+250=1320$ | |
| 2 | — | — | 21750 | 1480 | $1250+250=1500$ | |
| 2 (*c*) | [21780] | [1630] | — | — | $1070+2(250)=1570$ | |
| 3 | — | — | 23150 | 2850 | $2(1070+250)\pm250=2890$ | |

Table 1. Vibrational analysis of the charge-transfer absorption[a].

a All values of $\nu$ are in cm$^{-1}$. Figures in brackets denote extremely poorly defined peaks.
b Directions of polarization are with respect to the needle (*c*-) axis.
c Splittings are given in cm$^{-1}$, as $\nu_{parallel}-\nu_{perpendicular}$.

It is interesting to compare these with the vibrations which appear in the
polarized infra-red spectrum of the complex [11], some of which are listed in
table 2. In general, we should expect vibrations involving those bonds which
are most sensitive to changes in the electron densities in the two rings to be
strongly excited in the charge-transfer process, and these should include C–C
ring stretching as well as motions of the nitro groups. It appears likely that at
least one vibration of the latter type is active in the absorption spectrum, but more
definite assignment must await further work, perhaps at liquid Helium
temperature.

The appearance of *intermolecular vibrations* (crystal modes) in the spectra of crystals is not uncommon, and is to be expected in the present case, where such vibrations may have a marked effect on the charge-transfer 'bond' between two molecules. The low-frequency interval of approximately $250 \text{ cm}^{-1}$ may involve change in the anthracene-TNB intermolecular distance.

| Frequency (cm$^{-1}$) | Assignment[b] |
|---|---|
| 1620 | C–C stretch of both rings |
| 1526 | asymmetric $-NO_2$ stretch |
| 1439 | C–H in-plane bending of both molecules |
| 1341 | symmetric $-NO_2$ stretch |
| 1167 | CN stretch (?) of TNB |
| 1068 | degen. TNB ring stretch |

Table 2. The infra-red absorption of anthracene-TNB[a].

[a] This is a portion of table 2 of Kross *et al.* [11].
[b] The assignments are those of the above authors. All the bands listed here are polarized along the needle axis, perpendicular to the ring planes.

### 3.2. *Selection rules and polarizations*

Observation of a crystal of the complex under a polarizing microscope reveals distinct dichroism, the light polarized parallel to the needle ($c$) axis being more strongly absorbed. There is no dichroism when one views a thin section cut normal to the $c$-axis, indicating that the transition moment must lie along that axis.

In solution, the complex exists as bimolecular species belonging to the point group $C_s$, where the $z$-axis is taken perpendicular to the ring planes. The observed polarization on the crystal and the fact that our present concept of the charge-transfer process predicts a $z$-polarized transition moment, has led to the assignment of $^1A'$ for the upper state.

It is now well known† that the spectra of molecular crystals must be interpreted in terms of crystal interaction effects, for which purpose it is necessary to replace the 'oriented gas' model by the 'weak coupling' model of Davydov [21.] Electrostatic interaction between the transition dipole moments is of two kinds; interaction between translationally equivalent dipoles causes a net shift ('crystal shift') of the transition, usually to lower energy, while that between non-translationally equivalent moments can result in a splitting (Davydov splitting) of the bands into components differing slightly in energy and polarization. Most of these effects have been observed in the present study, and will be discussed in turn.

Ordinarily the space group of the crystal is of decisive importance in determining the nature of the crystal wave functions. In the present case the designation C2/c refers to the separate anthracene and TNB molecules, but since we are considering intermolecular charge-transfer effects, we are interested in the

† Recent reviews of this subject include those of Tanaka [15], McClure [16] and Wolf [17]. The group-theoretical aspects have been discussed in some detail by Winston [18], and Craig [19, 20] has applied the theory to anthracene.

symmetry properties of *pairs* of molecules, or more exactly, of the transition dipoles, since is from the latter than the crystal interaction effects arise.   There are four such dipoles per C2 c unit cell, but (see figure 3 *b*) only two of these are non-translationally equivalent, so the crystal can be represented (for our present purpose) as consisting of smaller 'unit cells' of two differently oriented complexes or dipole moments, which are related to each other by the space group P2$_1$.   The site group isogonal to P2$_1$ is C$_2$.   The wave functions $\phi_1$ and $\phi_2$ of the two individual non-equivalent molecular complexes are combined to belong to the $\alpha$ and $\beta$ site-group representations, giving rise to two crystal wave functions

$$\psi^\alpha = \frac{1}{\sqrt{2}}(\phi_1 + \phi_2), \quad \psi^\beta = \frac{1}{\sqrt{2}}(\phi_1 - \phi_2).$$

The operation C$_2$ changes the sign of $\psi^\beta$, so that the characters of the $\alpha$ and $\beta$ site-group representations are $+1$ and $-1$, corresponding respectively to the A and B representations of the site group.   If the transition is totally symmetric in the molecular point group, then it must belong to the A site group representation, and we note that the transition connecting the ground and excited states is now polarized in the *z*-direction, as is observed experimentally.

The fact that the observed optical density ratio in the two polarizations is as low as 5 : 1 suggests that crystal-induced mixing of the charge-transfer transition with a nearby transition of opposite polarization and greater intensity (such as the $^1L_a$ transition of anthracene) probably occurs.

To find the net shift of the spectrum in the crystal, it is desirable to compare the locations of the O-O bands.   In the crystal this is probably the first peak, which occurs at 20 150 cm$^{-1}$.   In the solution, the shapes of the upper and lower potential energy curves differ so much that the O–O band is not observed (see figure 5 in reference [12]), but extrapolation of the mirror-image emission and absorption curves places that band at about 18 400 cm$^{-1}$, which means that the charge-transfer band undergoes a *blue* shift of 1750 cm$^{-1}$ in the crystal.   A possible explanation of this effect might be that the anthracene and TNB molecules are not acting as isolated pairs, but each anthracene molecule, say, engages in charge-transfer bonding to both adjacent TNB molecules.   The effective ionization potential of the donor molecule is slightly increased, and hence the energy required to excite the charge-transfer state increases.

### 3.3. *The splitting*

Inspection of table 1 reveals a splitting of 120 200 cm$^{-1}$ between oppositely polarized components of what are assumed to be corresponding peaks.   Similar splittings occur in the other spectra, although the broadness of the peaks and the presence of the 250 cm$^{-1}$ interval makes it difficult to see.

According to the theory, the energy of the transition is given by

$$E = W + \sum_p I_{jp} \pm \sum_q I_{jq}$$

where the positive sign refers to the *A* state and the negative sign to the *B* state. The index *p* runs over all translationally equivalent molecules, and *q* runs over all others.   The sums of the two interaction integrals $I_{jp}$ and $I_{jq}$ thus contribute to the crystal shift and splitting, respectively.   Other contributions to the shift are given by *W*.   The Davydov splitting is clearly

$$\Delta E = 2 \sum_q I_{jq}.$$

The equation given by Craig [19] for the calculation of the interaction integrals can be modified to a somewhat more convenient form:

$$I_{jk} = -\frac{e^2}{r^3}|M|^2(3\cos\theta_j\cos\theta_k - \cos\phi_{jk})$$

where $r$ is the intermolecular distance, $M$ the transition moment length (in angstroms), $\theta_j$ is the angle between the dipole $j$ and the axis connecting its centre with that of the dipole $k$, and $\phi_{jk}$ is the angle between the two dipoles. Because of the strong inverse dependence on $r$ it is usually unnecessary to carry the calculation beyond 15 Å, and in the present case, nearly all the splitting is due to interaction with the two adjacent dipoles in the same stack.

There is strong interaction between adjacent 'unpaired' molecules, but these individual interactions cancel within a dipole–dipole approximation and in this sense we are still justified in regarding the crystal as a collection of discrete complex molecules. The system would appear to correspond to the 'weak coupling' situation discussed by Simpson and Peterson [22], in which excitons remain localized at a given lattice position for a relatively long time, making it necessary to consider the interaction as deriving from individual vibronic bands, rather than from the total electronic transition. Considering the interaction between one dipole and its fourteen nearest neighbours, we calculate a value of $-850\text{ cm}^{-1}$ for $\sum_q I_{jq}$, corresponding to a Davydov splitting of $1700\text{ cm}^{-1}$ for the total electronic band intensity. If we assume that the transition is divided up into about six vibronic bands, which are individually split in a 'weak coupling' situation, then the predicted splitting is $280\text{ cm}^{-1}$, a value in reasonable agreement with experiment.

Because the summed interaction integral is negative, the $z$-axis polarized transition to the $A$ state is at lower energy, in accordance with the data in table 1.

#### REFERENCES

[1] MULLIKEN, R. S., 1950, *J. Amer. Chem. Soc.*, **72**, 600.
[2] MULLIKEN, R. S., 1952, *J. Amer. Chem. Soc.*, **74**, 811.
[3] McGLYNN, S. P., and BOGGUS, J. D., 1958, *J. Amer. Chem. Soc.*, **80**, 5096.
[4] McGLYNN, S. P., 1958, *Chem. Rev.*, **58**, 113.
[5] REID, C., 1952, *J. chem. Phys.*, **20**, 1212.
[6] CZEKALLA, J., BRIEGLAB, G., HERRE, W., and GLIER, R., 1957, *Z. Elektrochem.*, **61**, 537.
[7] CZEKALLA, J., SCHMILLEN, A., and MAGER, K. J., 1957, *Z. Elektrochem.*, **61**, 1053.
[8] CZEKALLA, J., 1959, *Z. Elektrochem.*, **63**, 1157.
[9] NAKAMOTO, K., 1952, *J. Amer. Chem. Soc.*, **74**, 390, 392.
[10] WALLWORK, S. C., 1954, *Acta cryst., Camb.*, **7**, 648.
[11] KROSS, R. D., NAKAMOTO, K., and FASSEL, V., 1956, *Spectrochim. Acta.*, **8**, 142.
[12] McGLYNN, S. P., BOGGUS, J. D., and ELDER, E., 1960, *J. chem. Phys.*, **32**, 357.
[13] ORGEL, L., and MULLIKEN, R. S., 1957, *J. Amer. Chem. Soc.*, **79**, 4839.
[14] MURRELL, J. N., 1959, *J. Amer. Chem. Soc.*, **81**, 5037.
[15] TANAKA, J., 1959, *Progr. theor. Phys.*, Japan, Supplement No. **12**, 183.
[16] McCLURE, D. S., 1959, *Solid State Physics*, **8**, 1.
[17] WOLF, H., 1959, *Solid State Physics*, **9**, 1.
[18] WINSTON, H., 1951, *J. chem. Phys.*, **19**, 156.
[19] CRAIG, D. P., 1955, *J. chem. Soc.*, p. 2303.
[20] CRAIG, D. P., and HOBBINS, P. C., 1955, *J. chem. Soc.*, pp. 539, 2309.
[21] DAVYDOV, A. S., 1948, *J. exp. theor. Phys.*, **18**, 210.
[22] SIMPSON, W., and PETERSON, D., 1957, *J. chem. Phys.*, **26**, 588.

# Electron spin resonance of $(CO_2H)CH_2CH_2\dot{C}H(CO_2H)$ in irradiated glutaric acid

by A. HORSFIELD, J. R. MORTON and D. H. WHIFFEN

Basic Physics Division, National Physical Laboratory,
Teddington, Middlesex

It is concluded from electron spin resonance spectra that the radical $(CO_2H)CH_2CH_2\dot{C}H(CO_2H)$ remains trapped in a glutaric acid crystal after $\gamma$-irradiation. This radical is found in two different conformations. Approximate hyperfine coupling constants are given for each, although exact interpretation is hindered by the overlapping of spectra. Reasons for the formation of the two forms of the radical are discussed.

## 1. Introduction

The free radicals $\dot{C}H(CO_2H)_2$ in irradiated malonic acid [1] and $(CO_2H)CH_2\dot{C}H(CO_2H)$ in irradiated succinic acid [2, 3] have been the subject of recent electron resonance studies. Continuing this series, irradiated glutaric acid has been examined in the hope of observing the radical

$$(CO_2H)CH_2CH_2\dot{C}H(CO_2H).$$

This radical was of special interest since it might have been possible to detect hyperfine interactions from the protons on the methylene group furthest from the radical centre. Unfortunately no such coupling was detected and therefore it must be less than the line width of approximately 9 Mc/s.

## 2. Experimental

### 2.1. *Materials and instrumental*

The spectra were observed with a superheterodyne electron resonance spectrometer operating at 9000 Mc/s, with phase-sensitive detection and derivative recorder presentation. Single crystals of glutaric acid could be rotated about an axis from outside the cavity and spectra at 10 intervals were examined. The glutaric acid crystals were grown from water and formed monoclinic plates of the type described by Morrison and Robertson [4]. Care was taken to choose single crystals for irradiation by prior examination under the polarizing microscope. The unit cell data of Morrison and Robertson [4] were confirmed by optical goniometry and x-ray diffraction. Single crystals were irradiated with 1·0 Mev $\gamma$-rays at the Spent Fuel Irradiation Unit, A.E.R.E., Harwell. The total dose was approximately five megarads per crystal. The E.S.R. measurements were made at room temperature, and the same spectra were obtained whether the crystal had been irradiated at room temperature or at liquid nitrogen temperature.

When it was realized that two distinguishable radicals were present (see below) heating experiments were undertaken to see if one of these could be destroyed preferentially.   The spectrum at a certain orientation was unchanged after heating the crystal for three hours at 60°c.   Heating to 70°c for half an hour caused the spectrum to diminish in intensity by 90 per cent, possibly due to a phase change in the crystal, but remain unchanged in shape.

### 2.2. *Spectra obtained for magnetic field perpendicular to crystal b-axis*

If the glutaric acid crystal possesses the space group $C_{2h}^6(I2/a)$, with four molecules per unit cell [4], any one chemical species of radical in any of the four unit cell sites is expected to give identical spectra when the magnetic field $H$ is perpendicular to the unique $b$-axis.   Consequently these orientations were examined first by rotating the crystal about the $b$-axis.   A typical spectrum is shown in figure 1, which relates to the orientation $H$ perpendicular to $a$ and $b$, that is, parallel to $c^*$.   Although this spectrum is approximately symmetrical about its centre, it is not exactly so; neither are the other spectra for the field perpendicular to $b$.   This lack of symmetry means that at least two species of radical are present,
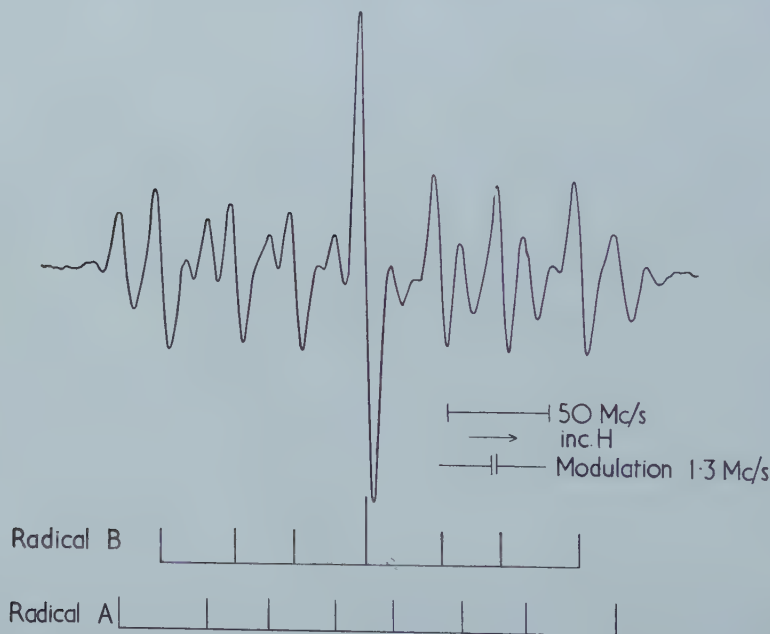


**Figure 1.**   Derivative spectrum of $\gamma$-irradiated glutaric acid ($H\|c^*$).

and they possess different $g$-values.   The strong lines in each spectrum can be grouped into two sets of eight lines of equal intensity.   The lines of each set are symmetrically disposed to the centre of that set.   This indicates the presence of two radicals designated A and B.   In the spectrum presented in figure 1 two of the lines due to radical B coalesce to give the strong central peak which partially obscures the neighbouring peaks due to radical A.   The very weak lines are 13 Mc/s from the stronger lines and are attributed to 'spin-flip' transitions [5] which are apparent in the spectra of most organic materials.   The two species A and B appear to be present in approximately equal amounts.   Quantitative estimates are difficult,

since lines due to radical A, which appear at first sight to be weaker, are also rather broader, so that the integrated absorption of A is probably as great as that of B.

In the set of spectra with the magnetic field perpendicular to $b$ overlapping did not seriously hinder the interpretation. This was in terms of the species $(CO_2H)CH_2CH_2\dot{C}H(CO_2H)$, in two conformations A and B, in both of which the free electron exhibits hyperfine interaction with three protons. If the terms involving the interaction of the nuclei with the magnetic field are omitted from the Hamiltonian the square of the proton hyperfine couplings when the crystal is rotated about $b$ should vary sinusoidally [6]. In figures 2, 3 and 4 this function is plotted against $\theta$, where $\theta$ is the angle of rotation, for the three protons whose couplings have been measured. These figures show that both A and B radicals have one $\alpha$-proton whose hyperfine coupling is strongly anisotropic, and two $\beta$-protons whose anisotropy is much less.

### 2.3. *Spectra obtained for magnetic field not perpendicular to crystal b-axis*

When the magnetic field is not perpendicular to the unique crystal axis there is a further complication of the spectra. Each species of radical can be trapped in two non-equivalent sites related by the two-fold axis. These magnetically non-equivalent radicals give different spectra except when $H$ is perpendicular to or parallel to $b$. It was in fact not possible to analyse the spectra of the general orientations completely, although some lines, especially those in the wings of the spectrum, could be identified. The separation of the extreme lines was obtained for an A and a B species in most orientations. Since two of the protons of each species gave almost isotropic couplings for $b$ perpendicular and parallel to $H$, an average value for these protons was subtracted from the total splitting to give the coupling for the most anisotropic $\alpha$-hydrogen. This enabled the complete
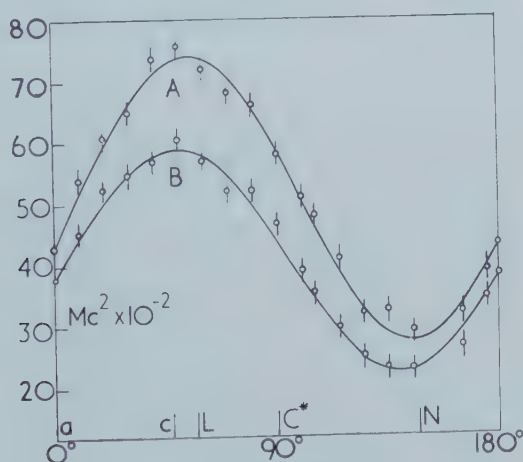


Figure 2. Square of $\alpha$-hydrogen hyperfine coupling ($H \perp b$).

coupling tensor (apart from signs) to be obtained for the third hydrogen. The spectra were obtained for two sets of orthogonal rotation axes, namely the crystal axes $b$, $a$ and $c^*$ and also the molecular axes $b$, $L$ and $N$ [4]. Either set sufficed to yield the coupling tensor for the most anisotropic hydrogen, and the two sets of data were shown to be self-consistent, within the experimental errors. Table 1 shows the principal values of the $\alpha$-hydrogen coupling, and also gives the principal
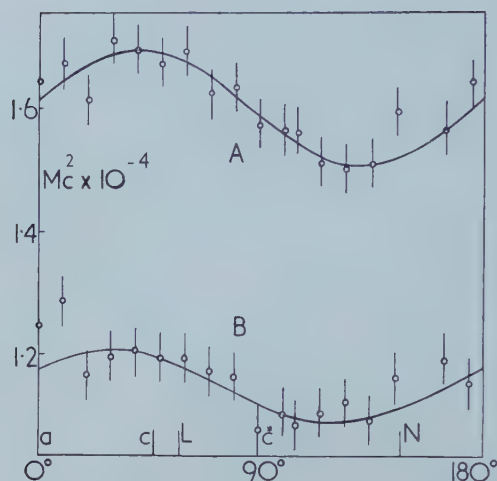
Figure 3.   Square of $\beta_1$ (larger) hydrogen hyperfine coupling ($H \perp b$).
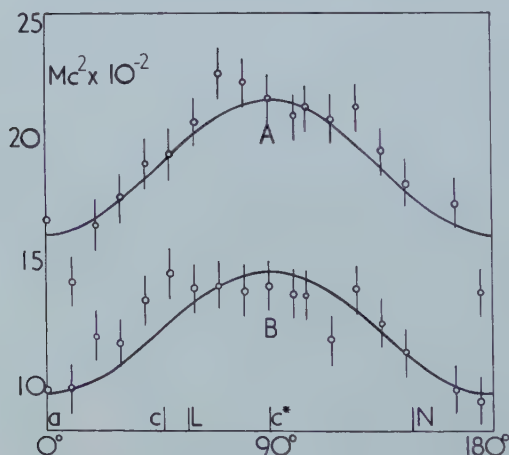


Figure 4.   Square of $\beta_2$ (smaller) hydrogen hyperfine coupling ($H \perp b$).

|              | Coupling (Mc/s) | Direction cosines in $L$, $M$, $N$ axes |
|--------------|-----------------|------------------------------------------|
| Species A    | $-88$           | $(0.96, \pm 0.25, 0.10)$                 |
|              | $-53$           | $(-0.16, \pm 0.21, 0.97)$                |
|              | $-26$           | $(-0.22, \pm 0.95, -0.24)$               |
|              | $-56$           | Isotropic component                      |
| Species B    | $-79$           | $(0.94, \pm 0.29, 0.20)$                 |
|              | $-52$           | $(-0.31, \pm 0.39, 0.87)$                |
|              | $-23$           | $(-0.18, \pm 0.88, -0.45)$               |
|              | $-51$           | Isotropic component                      |

Table 1.   Principal values and directions of the $\alpha$-hydrogen tensors.   The $\pm$ signs refer to radicals related to each other by the two-fold axis.

| Radical species and hydrogen | | Couplings in $LN$ plane | | Parallel to $M$ | Isotropic |
|---|---|---|---|---|---|
| | | Max. | Min. | | |
| A | $\beta_1$ | 131 | 123 | 111 | 122 |
|   | $\beta_2$ | 46 | 40 | 54 | 47 |
| B | $\beta_1$ | 110 | 104 | 107 | 107 |
|   | $\beta_2$ | 38 | 31 | 30 | 33 |

Table 2.   The $\beta$-hydrogen coupling (Mc/s).

directions in terms of the molecular $L$, $M$, $N$ coordinate system.   Table 2 refers to the other hydrogens and gives the maximum and minimum couplings in the $LN$ plane, and also the values for $H$ parallel to $M$ (i.e. $b$).   The almost isotropic nature of the $\beta$-hydrogen couplings means that the true isotropic coupling constant will not differ greatly from the value quoted.

## 3. Discussion

### 3.1. *The $\alpha$-hydrogen coupling tensor*

The most likely radicals to be trapped in irradiated glutaric acid are

$$(CO_2H)CH_2\dot{C}HCH_2(CO_2H)$$

which would show hyperfine interaction with five protons, and

$$(CO_2H)CH_2CH_2\dot{C}H(CO_2H)$$

which would couple to three protons.   The A and B radicals whose spectra have been observed are clearly both of the latter type.   Moreover, the $\alpha$-hydrogen, i.e. that attached to the free radical centre, is expected to have an isotropic coupling of approximately $-55$ Mc/s, and principle values of the anisotropic tensor of approximately $-25$, $-55$ and $-85$ Mc/s [1, 2, 3, 7, 8, 9].   These values are fully consistent with the data of table 1, showing that both A and B radicals have one $\alpha$-hydrogen atom.   The coupling constants have been given negative signs by virtue of this assignment, since their signs are not derivable from the spectra. It may be seen from table 1 that the least negative, intermediate, and most negative principal axes of the coupling tensor lie approximately parallel to the molecular directions $M$, $N$ and $L$ respectively.   These directions were defined by Morrison and Robertson [4].   $L$ is the chain extension direction, $N$ is perpendicular to the plane of the three central carbon atoms, and $M$, which is perpendicular to $L$ and $N$, was also assumed to be a two-fold axis.   It is expected [7, 8] that the least negative, intermediate, and most negative principal axes of the coupling tensor will be parallel to the $\dot{C}$–H bond, perpendicular to the radical plane, and in the radical plane but perpendicular to the $\dot{C}$–H bond respectively.   This indicates that the $\dot{C}$–H direction in the radical is approximately parallel to $M$, the calculated angles between them being $19° \pm 5°$ for A and $29° \pm 5°$ for B.   The crystal structure [4] indicates that the plane of the three terminal carbon atoms is inclined $14°$ to that of the three central carbon atoms, and the radical is more nearly coplanar with the former than the latter.   The calculated angle between the intermediate axis of the tensor and the normal to the plane of the terminal carbon atoms was $3°$ for A and $15°$ for B, with an error of $\pm 5°$.

### 3.2. *The β-hydrogen coupling tensor*

The expected principal values of the β-hydrogen tensor are less well known, the only other example being in the radical $(CO_2H)CH_2\dot{C}H(CO_2H)$ in irradiated succinic acid [3]. In this case the β-hydrogens were distinguishable and had isotropic couplings of 80 and 100 Mc/s. The corresponding figures for the glutaric acid radical (table 2) show an even greater difference between the isotropic coupling constants of the β-hydrogen atoms. This presumably confirms the findings of the α-hydrogen tensor, i.e. that the radical plane does not bisect the HCH angle of the methylene group. In succinic acid [3] a twist of 5° was suggested, and similar calculations for glutaric acid indicate a twist of 25° ± 5° for both A and B species.

### 3.3. *The nature of the free radicals*

It seems certain that both A and B radicals are of the same chemical species, namely $(CO_2H)CH_2CH_2\dot{C}H(CO_2H)$ and that both are trapped in the crystal in the approximate orientations of the undamaged molecule. The only difficulty is to explain why the two species are distinguishable, for this can only be due to differences in their precise geometrical shape or their orientation in the trapping site. It is not certain if A and B are in equilibrium with each other, or if one is unstable with respect to the other but with a very high activation energy for their interconversion. The existence of a dynamic equilibrium would not be apparent providing the half-life of exchange were longer than $10^{-7}$ sec. Faster exchanges would cause broadening and loss of hyperfine structure. It would be difficult to explain why species A and B are energetically equivalent, so that equal amounts of each are present at equilibrium.

One possibility is that the difference between A and B lies in the position of the hydrogen atom in one of the carboxylic acid groups of the radical. There is, however, no other reason to suggest that the configuration of the carboxylic acid group in the radical is reversed with respect to that in the molecule. Alternatively it is possible that the B radical contains the ionized carboxylic acid group $-CO_2^-$.

Although other explanations may be envisaged, for example a pyramidal free radical centre, or isomers obtained by hindered rotation in the $H\dot{C}-CH_2$ bond, considerable objections to them arise.

The final possibility is that in the crystal the molecule does not possess a two-fold axis parallel to $M$. This would explain all the present observations, for the two ends of the molecule would then be non-equivalent, and geometrically distinguishable radicals would result depending on whether hydrogen is removed from one end or the other.

Morrison and Robertson [4] state that the missing reflections permit the space group $C_s^4(Ia)$ in addition to $C_{2h}^6(I2/a)$ assumed in their analysis. Should the lower symmetry be correct, the molecule would not possess a two-fold axis of symmetry in the crystal. However, the structure apparently refined well for projections along two axes, with an overall discrepancy in the structure factors of 18·6 per cent. Speakman [10] has applied statistical tests to the $h0l$ intensities and these support the more symmetrical structure. He has commented, however, that even if the individual molecules do not have a two-fold axis, provided deviations from it are random, they will appear to possess such an axis in the macroscopic crystal.

We wish to thank Dr. J. C. Speakman for discussions on the x-ray structure, and Dr. D. E. Henn for checking the unit cell dimensions of our crystals. This work forms part of the research programme of the Basic Physics Division of the National Physical Laboratory and is published by permission of the Director.

## REFERENCES

[1] McConnell, H. M., Heller, C., Cole, T., and Fessenden, R. W., 1960, *J. Amer. chem. Soc.*, **82**, 766.
[2] Heller, C., and McConnell, H. M., 1960, *J. chem. Phys.*, **32**, 1535.
[3] Pooley, D., and Whiffen, D. H., 1961, *Mol. Phys.*, **4**, 81.
[4] Morrison, J. D., and Robertson, J. M., 1949, *J. chem. Soc.*, p. 1001.
[5] Trammel, G. T., Zeldes, H., and Livingston, R., 1958, *Phys. Rev.*, **110**, 630.
[6] Holmberg, R. W., Livingston, R., and Smith, W. T., 1960, *J. chem. Phys.*, **33**, 541.
[7] McConnell, H. M., and Strathdee, J., 1959, *Mol. Phys.*, **2**, 159.
[8] Ghosh, D. K., and Whiffen, D. H., 1959, *Mol. Phys.*, **2**, 285.
[9] Atherton, N. M., and Whiffen, D. H., 1960, *Mol. Phys.*, **3**, 1 and 103.
[10] Speakman, J. C., 1960, personal communication.

# Molecular two-centre integrals between $2p\pi$ and $3p\pi$ atomic orbitals

## II. Coulomb integrals

by ALF LOFTHUS

Department of Physics, University of Oslo, Blindern, Oslo, Norway

All possible two-centre Coulomb integrals between $2p\pi$ and $3p\pi$ atomic orbitals with equal orbital exponent $\alpha$ have been evaluated analytically and tabulated for $\alpha = 1\cdot00\ (0\cdot25)\ 10\cdot00$.

## 1. INTRODUCTION

In a previous work [1] (hereafter called Part I) all possible two-centre hybrid and exchange integrals between $2p\pi$ and $3p\pi$ atomic orbitals with equal orbital exponent $\alpha$ were reduced to finite expressions involving tabulated auxiliary functions. In the present work the corresponding Coulomb integrals are evaluated analytically and tabulated.

The two-centre Coulomb integrals are defined as

$$C = (\psi_a\psi_a' \mid \psi_b''\psi_b''') = \int\int \psi_a(1)\psi_a'(1)(e^2/r_{12})\psi_b''(2)\psi_b'''(2)\,d\tau_1 d\tau_2 \qquad (1)$$

where $\psi, \psi', \psi''$ and $\psi'''$ denote various Slater atomic orbitals of the form

$$(2p\pi) = (2p) = (k^5/\pi)^{1/2}\exp(-kr)r\sin\vartheta\cos\varphi, \qquad (2\,a)$$

$$(3p\pi) = (3p) = (2k^7/\pi)^{1/2}\exp(-kr)r^2\sin\vartheta\cos\varphi, \qquad (2\,b)$$

and where $k = Z/2a_0$, $Z$ the effective nuclear charge, and $a_0 = 0\cdot5292$ Å is the Bohr radius. $a$ and $b$ denote the two centres (see figure in Part I).

## 2. METHOD OF INTEGRATION

Following the method of Barnett and Coulson [2], we first integrated over the space of electron 1, having

$$G(\psi, \psi'; 2) = \int \psi_a(1)\psi_a'(1)r_{12}^{-1}\,d\tau_1. \qquad (3)$$

As pointed out by Barnett and Coulson, these $G$ functions are effectively identical with one-electron Coulomb integrals, electron 2 in the former corresponding to nucleus $b$ in the latter.

The Coulomb integrals can thus be expressed as

$$C = \int G(\psi, \psi'; 2)\psi_b''(2)\psi_b'''(2)\,d\tau_2. \qquad (4)$$

The final integration, being very involved and laborious, was performed in elliptical coordinates; the general methods used are outlined elsewhere [3].

M

## 3. RESULTS

The three $G$ functions evaluated here are listed in table 1. The first of these was also evaluated by Barnett and Coulson [2], whereas the latter two form an extension of their table 7. To be more general, we have here allowed different $k$ on different orbitals, whereas in the present application $k_1 = k_2 = k$.

The $j_n$ functions involved in the $G$ functions are listed in table 2. $j_7$ and $j_8$ were also listed by Barnett and Coulson, whereas the rest extends their table 11. These functions arise in the integration of $G$ with respect to $r$.

There are altogether six different Coulomb integrals which can be constructed from $2p\pi$ and $3p\pi$ orbitals:

$$
\left.
\begin{aligned}
C_0 &= (2p_a 2p_a \,|\, 2p_b 2p_b), & C_3 &= (2p_a 2p_a \,|\, 2p_b 3p_b), \\
C_1 &= (2p_a 2p_a \,|\, 3p_b 3p_b), & C_4 &= (2p_a 3p_a \,|\, 3p_b 3p_b), \\
C_2 &= (2p_a 3p_a \,|\, 2p_b 3p_b), & C_5 &= (3p_a 3p_a \,|\, 3p_b 3p_b).
\end{aligned}
\right\}
\tag{5}
$$

The analytical expressions for these integrals are given in table 3, as functions of $\alpha = kR = ZR/2a_0$, where $R$ is the internuclear distance. Numerical values of the integrals, for $\alpha = 1 \cdot 00 \, (0 \cdot 25) \, 10 \cdot 00$, are given in table 4. These values were obtained from the analytical expressions by an electronic computer, and are believed to be correct to $\pm 1$ in the last figure.

By letting $R = (2a_0/Z)\alpha \to 0$, we obtain the mononuclear integrals

$$
M(\psi_a \psi_a' \,|\, \psi_a'' \psi_a''') = C(\psi_a \psi_a' \,|\, \psi_b'' \psi_b''')_{\alpha=0}.
\tag{6}
$$

These integrals are added in table 4 under $\alpha = 0$.

## 4. CHECKS OF THE CALCULATIONS

From the definitions of the Coulomb integral (equation (1)) and the atomic orbitals (equation (2)), and recalling that $\alpha = kR = ZR/2a_0$, it is readily seen that the following relations must exist between the integrals:

$$
\left.
\begin{aligned}
C_3 &= (2/15)^{1/2} \, \alpha^{11}/4 \, d/d\alpha \, (-C_0/\alpha^{10}), \\
C_4 &= (2/15)^{1/2} \, \alpha^{13}/4 \, d/d\alpha \, (-C_2/\alpha^{12}), \\
C_1 + C_2 &= (2/15)^{1/2} \, \alpha^{12}/2 \, d/d\alpha \, (-C_3/\alpha^{11}).
\end{aligned}
\right\}
\tag{7}
$$

It is found that these relations are fulfilled by the formulae given in table 3.

A formula and some numerical values for $C_0$ did already exist in the literature [3], but were repeated here as a means of checking the methods. Complete agreement was found.

All integrals were recalculated numerically for $\alpha = 4 \cdot 00$ by means of the Barnett–Coulson method [2], and agreement between the two methods was found.

## REFERENCES

[1] LOFTHUS, A., 1961, *Mol. Phys.*, **4**, 17.
[2] BARNETT, M. P., and COULSON, C. A., 1951, *Phil. Trans.* A, **243**, 221.
[3] PREUSS, H., 1956, *Integraltafeln zur Quantenchemie* (Berlin: Springer-Verlag).

$$G(2p, 2p\,;\,2) = (1/16)(k_1^5 k_2^5)^{1/2} k_a^{-7} r_{a2}^{-3}$$
$$\times \{j_8(2k_a r_{a2}) + (1/2)\sin^2\vartheta\,\cos^2\varphi j_7(2k_a r_{a2})\}$$
$$G(2p, 3p\,;\,2) = (1/32)(2/15)^{1/2}(k_1^5 k_2^7)^{1/2} k_a^{-8} r_{a2}^{-3}$$
$$\times \{j_{10}(2k_a r_{a2}) + (1/2)\sin^2\vartheta\,\cos^2\varphi j_9(2k_a r_{a2})\}$$
$$G(3p, 3p\,;\,2) = (1/480)(k_1^7 k_2^7)^{1/2} k_a^{-9} r_{a2}^{-3}$$
$$\times \{j_{12}(2k_a r_{a2}) + (1/2)\sin^2\vartheta\,\cos^2\varphi j_{11}(2k_a r_{a2})\}$$

Table 1.  $G(\psi, \psi'\,;\,2)$ integrals.  $(k_a = (k_1 + k_2)/2.)$

$j_7(t) = 144 - \exp(-t)(144 + 144t + 72t^2 + 24t^3 + 6t^4 + t^5)$
$j_8(t) = -24 + 4t^2 + \exp(-t)(24 + 24t + 8t^2 + t^3)$
$j_9(t) = 1008 - \exp(-t)(1008 + 1008t + 504t^2 + 168t^3 + 42t^4 + 8t^5 + t^6)$
$j_{10}(t) = -168 + 20t^2 + \exp(-t)(168 + 168t + 64t^2 + 12t^3 + t^4)$
$j_{11}(t) = 8064 - \exp(-t)(8064 + 8064t + 4032t^2 + 1344t^3 + 336t^4 + 66t^5 + 10t^6 + t^7)$
$j_{12}(t) = -1344 + 120t^2 + \exp(-t)(1344 + 1344t + 552t^2 + 124t^3 + 16t^4 + t^5)$

Table 2.  $j_n(t)$ functions.

$$C_0 = (2p_a 2p_a | 2p_b 2p_b) = \{(81/8)\alpha^{-5} - (3/2)\alpha^{-3} + (1/2)\alpha^{-1}$$
$$- \exp(-2\alpha)((81/8)\alpha^{-5} + (81/4)\alpha^{-4} + (75/4)\alpha^{-3} + (21/2)\alpha^{-2}$$
$$+ (17/4)\alpha^{-1} + (3851/2560) + (651/1280)\alpha + (389/2688)\alpha^2$$
$$+ (47/1680)\alpha^3 + (3/1120)\alpha^4)\}Z(e^2/a_0)$$

$$C_1 = (2p_a 2p_a | 3p_b 3p_b) = \{(189/10)\alpha^{-5} - (43/20)\alpha^{-3} + (1/2)\alpha^{-1}$$
$$- \exp(-2\alpha)((189/10)\alpha^{-5} + (189/5)\alpha^{-4} + (713/20)\alpha^{-3} + (209/10)\alpha^{-2}$$
$$+ (44/5)\alpha^{-1} + (231601/76800) + (35761/38400)\alpha$$
$$+ (10133/38400)\alpha^2 + (3677/57600)\alpha^3 + (2399/201600)\alpha^4$$
$$+ (19/12600)\alpha^5 + (1/10080)\alpha^6)\}Z(e^2/a_0)$$

$$C_2 = (2p_a 3p_a | 2p_b 3p_b) = \{(1323/80)\alpha^{-5} - (7/4)\alpha^{-3} + (5/12)\alpha^{-1}$$
$$- \exp(-2\alpha)((1323/80)\alpha^{-5} + (1323/40)\alpha^{-4} + (1253/40)\alpha^{-3}$$
$$+ (371/20)\alpha^{-2} + (953/120)\alpha^{-1} + (35509/12800) + (16607/19200)\alpha$$
$$+ (13981/57600)\alpha^2 + (183/3200)\alpha^3 + (37/3600)\alpha^4 + (1/800)\alpha^5$$
$$+ (1/12600)\alpha^6)\}Z(e^2/a_0)$$

$$C_3 = (2p_a 2p_a | 2p_b 3p_b) = (2/15)^{1/2}\{(567/16)\alpha^{-5} - (9/2)\alpha^{-3} + (5/4)\alpha^{-1}$$
$$- \exp(-2\alpha)(567/16)\alpha^{-5} + (567/8)\alpha^{-4} + (531/8)\alpha^{-3} + (153/4)\alpha^{-2}$$
$$+ (127/8)\alpha^{-1} + (56419/10240) + (9059/5120)\alpha + (1949/3840)\alpha^2$$
$$+ (439/3840)\alpha^3 + (233/13440)\alpha^4 + (3/2240)\alpha^5)\}Z(c^2/a_0)$$

$$C_4 = (2p_a 3p_a | 3p_b 3p_b) = (2/15)^{1/2}\{(1323/20)\alpha^{-5} - (49/8)\alpha^{-3} + (5/4)\alpha^{-1}$$
$$- \exp(-2a)((1323/20)\alpha^{-5} + (1323/10)\alpha^{-4} + (5047/40)\alpha^{-3}$$
$$+ (1519/20)\alpha^{-2} + (331/10)\alpha^{-1} + (1781717/153600)$$
$$+ (272597/76800)\alpha + (75157/76800)\alpha^2 + (27157/115200)\alpha^3$$
$$+ (2683/57600)\alpha^4 + (101/14400)\alpha^5 + (73/100800)\alpha^6$$
$$+ (1/25200)\alpha^7)\}Z(e^2/a_0)$$

$$C_5 = (3p_a 3p_a | 3p_b 3p_b) = (1/100)\{3528\alpha^{-5} - 280\alpha^{-3} + 50\alpha^{-1}$$
$$- \exp(-2\alpha)(3528\alpha^{-5} + 7056\alpha^{-4} + 6776\alpha^{-3} + 4144\alpha^{-2} + 1842\alpha^{-1}$$
$$+ (5018647/7680) + (763927/3840)\alpha + (34567/640)\alpha^2$$
$$+ (1559/120)\alpha^3 + (3839/1440)\alpha^4 + (4/9)\alpha^5 + (7079/124740)\alpha^6$$
$$+ (157/31185)\alpha^7 + (1/4158)\alpha^8)\}Z(e^2/a_0)$$

Table 3.  Formulae for two-centre Coulomb integrals.  $(\alpha = ZR/2a_0\,;\ Z = $ effective nuclear charge, $R = $ internuclear distance (Å), $a_0 = 0{\cdot}5292$ Å, $e^2/a_0 = 27{\cdot}206$ ev.)

M 2

| $\alpha$ | $C_0 =$ $(2p_a2p_a\|2p_b2p_b)$ | $C_1 =$ $(2p_a2p_a\|3p_b3p_b)$ | $C_2 =$ $(2p_a3p_a\|2p_b3p_b)$ | $C_3 =$ $(2p_a2p_a\|2p_b3p_b)$ | $C_4 =$ $(2p_a3p_a\|3p_b3p_b)$ | $C_5 =$ $(3p_a3p_a\|3p_b3p_b)$ |
|---|---|---|---|---|---|---|
| 0·00 | 1·957031 (−1) | 1·576953 (−1) | 1·358594 (−1) | 1·607865 (−1) | 1·364243 (−1) | 1·399701 (−1) |
| 1·00 | 1·843097 (−1) | 1·519924 (−1) | 1·305530 (−1) | 1·533518 (−1) | 1·320213 (−1) | 1·360429 (−1) |
| 1·25 | 1·786115 (−1) | 1·489805 (−1) | 1·277734 (−1) | 1·495198 (−1) | 1·296795 (−1) | 1·339373 (−1) |
| 1·50 | 1·722294 (−1) | 1·454773 (−1) | 1·245581 (−1) | 1·451398 (−1) | 1·269404 (−1) | 1·314588 (−1) |
| 1·75 | 1·653997 (−1) | 1·415725 (−1) | 1·209955 (−1) | 1·403501 (−1) | 1·238671 (−1) | 1·286570 (−1) |
| 2·00 | 1·583347 (−1) | 1·373588 (−1) | 1·171746 (−1) | 1·352848 (−1) | 1·205255 (−1) | 1·255855 (−1) |
| 2·25 | 1·512139 (−1) | 1·329269 (−1) | 1·131805 (−1) | 1·300663 (−1) | 1·169818 (−1) | 1·222987 (−1) |
| 2·50 | 1·441809 (−1) | 1·283620 (−1) | 1·090913 (−1) | 1·248012 (−1) | 1·132995 (−1) | 1·188505 (−1) |
| 2·75 | 1·373442 (−1) | 1·237406 (−1) | 1·049756 (−1) | 1·195782 (−1) | 1·095378 (−1) | 1·152925 (−1) |
| 3·00 | 1·307806 (−1) | 1·191290 (−1) | 1·008916 (−1) | 1·144675 (−1) | 1·057494 (−1) | 1·116726 (−1) |
| 3·25 | 1·245397 (−1) | 1·145823 (−1) | 9·688648 (−2) | 1·095217 (−1) | 1·019802 (−1) | 1·080340 (−1) |
| 3·50 | 1·186492 (−1) | 1·101446 (−1) | 9·299669 (−2) | 1·047782 (−1) | 9·826849 (−2) | 1·044144 (−1) |
| 3·75 | 1·131202 (−1) | 1·058492 (−1) | 8·924910 (−2) | 1·002608 (−1) | 9·464522 (−2) | 1·008459 (−1) |
| 4·00 | 1·079510 (−1) | 1·017201 (−1) | 8·566197 (−2) | 9·598241 (−2) | 9·113413 (−2) | 9·735485 (−2) |
| 4·25 | 1·031311 (−1) | 9·777273 (−2) | 8·224637 (−2) | 9·194736 (−2) | 8·775255 (−2) | 9·396205 (−2) |
| 4·50 | 9·864456 (−2) | 9·401593 (−2) | 7·900742 (−2) | 8·815357 (−2) | 8·451212 (−2) | 9·068318 (−2) |
| 4·75 | 9·447166 (−2) | 9·045279 (−2) | 7·594562 (−2) | 8·459424 (−2) | 8·141968 (−2) | 8·752930 (−2) |
| 5·00 | 9·059115 (−2) | 8·708212 (−2) | 7·305792 (−2) | 8·125941 (−2) | 7·847805 (−2) | 8·450747 (−2) |
| 5·25 | 8·698122 (−2) | 8·389948 (−2) | 7·033874 (−2) | 7·813713 (−2) | 7·568690 (−2) | 8·162134 (−2) |

| R | | | | | | |
|---|---|---|---|---|---|---|
| 5·50 | 8·362048 (−2) | 8·089811 (−2) | 6·778078 (−2) | 7·521438 (−2) | 7·304347 (−2) | 7·887176 (−2) |
| 5·75 | 8·048840 (−2) | 7·806976 (−2) | 6·537555 (−2) | 7·247774 (−2) | 7·054320 (−2) | 7·625737 (−2) |
| 6·00 | 7·756573 (−2) | 7·540521 (−2) | 6·311414 (−2) | 6·991392 (−2) | 6·818027 (−2) | 7·377508 (−2) |
| 6·25 | 7·483461 (−2) | 7·289481 (−2) | 6·098733 (−2) | 6·751000 (−2) | 6·594803 (−2) | 7·142053 (−2) |
| 6·50 | 7·227862 (−2) | 7·052880 (−2) | 5·898603 (−2) | 6·525374 (−2) | 6·383942 (−2) | 6·918850 (−2) |
| 6·75 | 6·988283 (−2) | 6·829760 (−2) | 5·710142 (−2) | 6·313365 (−2) | 6·184715 (−2) | 6·707316 (−2) |
| 7·00 | 6·763365 (−2) | 6·619196 (−2) | 5·532509 (−2) | 6·113905 (−2) | 5·996398 (−2) | 6·506841 (−2) |
| 7·25 | 6·551881 (−2) | 6·420306 (−2) | 5·364912 (−2) | 5·926009 (−2) | 5·818284 (−2) | 6·316802 (−2) |
| 7·50 | 6·352721 (−2) | 6·232261 (−2) | 5·206611 (−2) | 5·748775 (−2) | 5·649694 (−2) | 6·136578 (−2) |
| 7·75 | 6·164885 (−2) | 6·054288 (−2) | 5·056921 (−2) | 5·581377 (−2) | 5·489983 (−2) | 5·965566 (−2) |
| 8·00 | 5·987470 (−2) | 5·885667 (−2) | 4·915207 (−2) | 5·423063 (−2) | 5·338543 (−2) | 5·803182 (−2) |
| 8·25 | 5·819662 (−2) | 5·725733 (−2) | 4·780890 (−2) | 5·273148 (−2) | 5·194806 (−2) | 5·648872 (−2) |
| 8·50 | 5·660723 (−2) | 5·573876 (−2) | 4·653433 (−2) | 5·131007 (−2) | 5·058245 (−2) | 5·502113 (−2) |
| 8·75 | 5·509989 (−2) | 5·429531 (−2) | 4·532349 (−2) | 4·996073 (−2) | 4·928370 (−2) | 5·362413 (−2) |
| 9·00 | 5·366855 (−2) | 5·292181 (−2) | 4·417191 (−2) | 4·867829 (−2) | 4·804730 (−2) | 5·229313 (−2) |
| 9·25 | 5·230776 (−2) | 5·161351 (−2) | 4·307547 (−2) | 4·745805 (−2) | 4·686907 (−2) | 5·102385 (−2) |
| 9·50 | 5·101254 (−2) | 5·036606 (−2) | 4·203046 (−2) | 4·629571 (−2) | 4·574518 (−2) | 4·981234 (−2) |
| 9·75 | 4·977836 (−2) | 4·917546 (−2) | 4·103342 (−2) | 4·518736 (−2) | 4·467209 (−2) | 4·865492 (−2) |
| 10·00 | 4·860109 (−2) | 4·803803 (−2) | 4·008122 (−2) | 4·412940 (−2) | 4·364655 (−2) | 4·754819 (−2) |

Table 4. Two-centre Coulomb integrals, in units of $Z(e^2/a_0)$. ($\alpha = ZR/2a_0$; $Z$ = effective nuclear charge, $R$ = internuclear distance (Å), $a_0 = 0.5292$ Å, $e^2/a_0 = 27.206$ ev, $(-p) = 10^{-p}$.)

# Charge transfer states and optical absorption in octahedrally hydrated paramagnetic salts

## II. Intensities in the manganous ion

by ROBERT ENGLMAN

Department of Physics, Technion-Israel Institute of Technology, Haifa

The theory of optical absorption assisted by states of charge transfer is extended to inter-system (spin–change) transitions. The transition probabilities are calculated. By some very special choice of the overlap integrals agreement is obtained between the theory and the experiments on hydrated manganous ions.

---

## 1. INTRODUCTION

The absorption spectra of the manganese ion $Mn^{2+}$ in octahedral surroundings have of late been observed in the water-coordinated state [1, 2, 3], in the oxide [4], the fluoride [5], the bromide and the chloride [6]. Generally speaking, the theory of an octahedral Stark-field gives convincing assignments of the bands, and satisfactory fits to the band energies.

In table 1, the *intensity* data are collected. On the whole, these show a variation of unexpected complexity from column to column and defy attempts to sense some regularity (e.g. some monotonic variation with the field strength or some other parameter). At the present stage, then, there is little a theoretician can do by way of comparison of his expressions with the empirical data. On the other hand, the independent works of Heidt *et al.* [1], of Holmes and McClure [2] and of Jorgensen [3] point to some pattern in the hydrated complex, and this can form the basis of comparison. (The ' pattern ' is exhibited in figure 2. The reason for the factor 2 needed to bring [2] in line with the other results is not known to this writer. The discrepancy of the uppermost line ($^4T_{1g}^{(2)}$) is commented on in §4).

| | [1] | [2] | [3] | [4] | [5] | [6] | [6] |
|---|---|---|---|---|---|---|---|
| $^4T_{1g}^{(2)}$ 32 800 cm⁻¹ | 3 | 0·7 | 5·5 | | | | |
| $^4E_g^{(2)}$ 29 200 cm⁻¹ | 1·3 | 0·6 | 0·8 | | 3·3 | 22 | 23 |
| $^4T_{2g}^{(2)}$ 28 100 cm⁻¹ | 1·6 | 0·8 | 1·3 | | 2·0 | 21 | 87 |
| $^4A_{1g}, {}^4E_g$ 25 000 cm⁻¹ | 1·5 | 0·5 | 1 | (0·4) | 4·0 | 23 | 29 |
| $^4T_{2g}^{(1)}$ 23 000 cm⁻¹ | 1·8 | 0·7 | 1·2 | (0·25) | 2·7 | 50 | 40 |
| $^4T_{1g}^{(1)}$ 18 800 cm⁻¹ | 2·5 | 0·9 | 1·9 | (1) | 3·3 | 23 | |
| $^6A_{1g}$ (ground state) → | [1] | [2] | [3] | [4] | [5] | [6] | [6] |
| | Mn²⁺ 6 H₂O | | | MnO | MnF₂ | MnCl₂ | MnBr₂ |
| | Room temperature | | | (78°K) | R.T. | (78°K) | |

Table 1. Oscillator strength × 10⁷.

(*a*) The energy values listed are those of the hydrated complex.

(*b*) Oscillator strengths are listed by [2], [5] and [6]. For [1] and [3] the values are calculated from half-widths and molar extinction coefficients. The values given for [4] are obtained graphically and should be regarded as purely relative.

So far the only theoretical treatment of the intensities of the $Mn^{2+}$–$6H_2O$ is that of Koide and Pryce [7] who interpreted the tiny peaks on Pappalardo's [8] absorption curve of the $^6A_{1g} \rightarrow {}^4A_{1g}$, $^4E_g$ transition. The positions of the peaks were associated with discrete vibrational energies of the ligand molecules which were absorbed *en passe* in the electronic jumps to the higher Stark-levels. The authors succeeded in getting agreement with the observed oscillator strengths of many lines. Later Liehr [9] expressed doubts as to the efficacy of an analysis of such sophistication.

As already noted, the authors Koide and Pryce were concerned with details of the transitions $^6A_{1g} \rightarrow {}^4A_{1g}$, $^4E_g$, which is one (the sharpest) of the six observed intersystem transitions of the manganous ion. In this work, where the total band intensities of each of the six bands are calculated and compared to experiment, we shall not consider the details on any line. The main difference is, however, much deeper, since the mechanism which is here assumed for the operation of the transitions differs in essentials from that considered by Koide and Pryce.
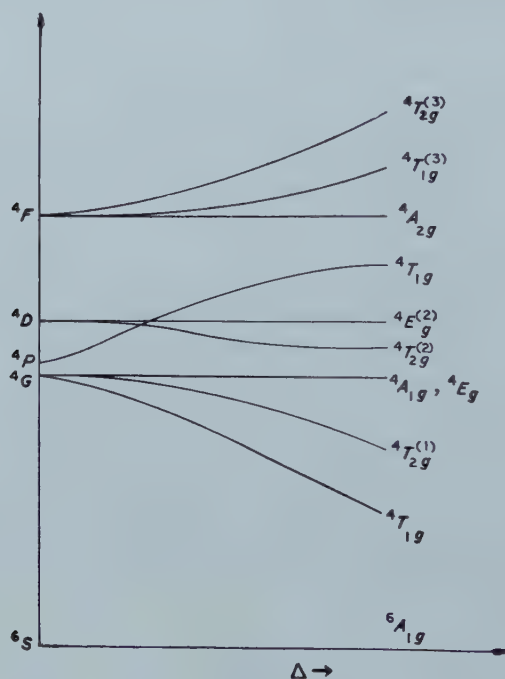


Figure 1.

The situation hinges on what are to be regarded as the intermediate (virtual) odd states in the transition. These are essential in the process in order that the odd electric dipole vector may connect the initial and final states. Koide and Pryce, in common with Liehr and Ballhausen [10], drew on the high-lying odd states of the free manganese ion. In the present work we shall follow, in spirit as well as for notation, the earlier works of the author [11, 12]. In these the odd states in question were supposed to belong to the manganese-water complex as a whole and to be identical with the states associated with the charge transfer spectra observed in the near ultra-violet [13]. The theory was considerably simplified and was found to agree well with experiment for the spin-conserved transitions of

the iron-group ions. ($V^{2+}$ played a special role in 'proving the rule'.) In a forthcoming publication we intend to discuss some further evidence in favour of this theory.

## 2. THE MATRIX ELEMENTS

The following quantities enter the transition probabilities between the ground state sextet and the excited quartet states:

The electric dipole vector $P = e \sum_i \mathbf{r}_i$, the spin-orbit interaction operator $H_{so} = \sum_i \xi(r_i) \mathbf{l}_i . \mathbf{s}_i$ and the odd vibrational Hamiltonian

$$H_v = \sum_i \tfrac{1}{2}(Z_3 + Z_6 - 2Z_0) \frac{\partial}{\partial z_i} (V_3 + V_6) + \text{(same with } x \text{ and } y).$$

Two additional terms (in each direction), corresponding to transverse vibrational modes of the complex, are not written down since, according to the argument given in [12], their matrix elements involving charge transfer states are small.

The strong field representation of the states of the ion is given by Pappalardo ([6], §4). In usual practice, and according to the convention chosen by Koide and Pryce for their spin-orbit matrix elements, the $x$-components of Pappalardo's $T$-states would be taken as *minus* the $y$-component and his $y$-component as the $x$-component. If the charge transfer states are brought into the picture, each ionic state ought to be orthogonalized by augmenting it with linear combinations of the c.t. states. However, with a reasonably low overlap (see §5 of [12]) and the approximate nature of the theory, this mental reservation need not be translated into practice.

The matrix elements are given by perturbation theory:

$$'\langle {}^4T|P|{}^6A\rangle' = \sum_{CX} \frac{\langle {}^4T|H_r|C\rangle\langle C|P|{}^4X\rangle\langle {}^4X|H_{so}|{}^6A\rangle}{(E_T - E_C)(E_A - E_X)}$$

$$+ \sum_{CX} \frac{\langle {}^4T|P|C\rangle\langle C|H_r|{}^4X\rangle\langle {}^4X|H_{so}|{}^6A\rangle}{(E_A - E_X)(E_A - E_C)}$$

$$+ \sum_{CY} \frac{\langle {}^4T|H_{so}|{}^6Y\rangle\langle {}^6Y|H_r|C\rangle\langle C|P|{}^6A\rangle}{(E_T - E_Y)(E_T - E_C)}$$

$$+ \sum_{CY} \frac{\langle {}^4T|H_{so}|{}^6Y\rangle\langle {}^6Y|P|C\rangle\langle C|H_r|{}^6A\rangle}{(E_T - E_Y)(E_A - E_C)}$$

$$+ \sum_{CC'} \frac{\langle {}^4T|H_r|C\rangle\langle C|H_{so}|C''\rangle\langle C'|P|{}^6A\rangle}{(E_T - E_C)(E_T - E_{C'})}$$

$$+ \sum_{CC'} \frac{\langle {}^4T|P|C'\rangle\langle C'|H_{so}|C\rangle\langle C|H_v|{}^6A\rangle}{(E_A - E_C)(E_A - E_{C'})}.$$

The $C$-states are those in which one of the $3d$ electrons is transferred onto the ligand. The last two terms do not occur in Koide and Pryce, since there is only one, ${}^6A_{1g}$ (${}^6S$), sextet state on the ion (though not of course on the *complex*). The vibrational quantum number is here, unlike in [12], suppressed.

Before calculating the matrix elements in the next section, we wish to make some preliminary points. The following integrals enter:

$$R = \langle u|z|\alpha_z\rangle, \qquad 2I = \left\langle u\left|\frac{\partial}{\partial z}(V_3 + V_6)\right|\alpha_z\right\rangle,$$

$$Q = \langle \xi|y|\alpha_z\rangle, \qquad 2J = \left\langle \eta\left|\frac{\partial}{\partial z}(V_3 + V_6)\right|\alpha_x\right\rangle.$$

($Q$ and $I$ have already been defined in [12].)

Latest information [14] on the integrated spin–orbit coupling constant in the free $Mn^{2+}$ is $\zeta_d(Mn^{2+}) = 294$ cm$^{-1}$. For the coordinated ion we shall take $\zeta = 260$ cm$^{-1}$. (In [7] $\simeq 300$ cm$^{-1}$.) Since the last two terms of the matrix elements require the corresponding quantity on the ligand, we first calculated

$$\zeta_p(OI, s^2 p^4 {}^3P) = 151 \pm 7 \text{ cm}^{-1}, \qquad \zeta_p(OII, sp^4 {}^4P) = 185 \pm 7 \text{ cm}^{-1}$$

and then, assuming roughly that the transferred electron $\alpha_z$ moves as on $O^-$, we obtained the value $\zeta_\alpha \simeq 120$ cm$^{-1}$.

This being rather smaller than $\zeta_d$ we would feel justified in neglecting contributions arising from it. What clinches the matter is, however, that $\alpha_z$ is presumably predominantly a mixture of $2p$, $3s$, $3p$ states of oxygen and therefore at most one of the $\alpha_z$, $\alpha_z'$ states which appear in $\langle \alpha_z | \xi \mathbf{l} . \mathbf{s} | \alpha_z' \rangle$ has effective overlap with the paramagnetic ion. (The other will be oriented perpendicularly to the ion-ligand direction.) We shall therefore neglect the effect of the spin–orbit interaction on the ligand.

For facility in calculation, $H_v$ is supposed to have only the component explicitly written out at the beginning of this section (i.e. that involving $z$). In cubic symmetry, this merely means that the total transition probabilities have to be tripled.

## 3. CALCULATED MATRIX ELEMENTS

It would be too lengthy to quote the full result of our calculation. We shall therefore give only results for the transition to $^4A_{1g}$ and to the two components of $^4E_g$. (The other matrix elements may be obtained from the author on application.)

$${}'\langle {}^4A(S_z = \tfrac{3}{2}) | P | {}^6A(S_z = \tfrac{5}{2}) \rangle'$$

$$= \frac{\zeta \hbar^2}{\sqrt{5}} (\hat{x} + i\hat{y}) \left\{ QI \left[ \frac{3}{\sqrt{2}} - \tfrac{1}{2} \sum_n \frac{\epsilon_n}{E_{\cdot A} - E_{\cdot T(n)}} \left( \frac{\lambda_n}{E_{\cdot A} - E_C} + \frac{\nu_n}{E_{\cdot A} - E_C} \right) \right] + \frac{3JR}{\sqrt{2}} \right.$$

$$\times \frac{1}{(E_{\cdot A} - E_C)(E_{\cdot A} - E_{C'})} - \frac{2JQ}{\sqrt{6}} \left[ \frac{1}{(E_{\cdot A} - E_C)(E_{\cdot A} - E_{C'})} + \frac{1}{(E_{\cdot A} - E_C)(E_{\cdot A} - E_{C'})} \right] \right\}.$$

$${}'\langle {}^4E_{(1)}(\tfrac{3}{2}) | P | {}^6A(\tfrac{5}{2}) \rangle'$$

$$= \frac{\zeta \hbar^2}{\sqrt{5}} (\hat{x} + i\hat{y}) \left\{ \frac{QI}{2} \left[ \frac{\beta}{\sqrt{2}} \frac{\sqrt{15}}{(E_A - E_C)(E_A - E_{C'})} + (\sqrt{3}\beta - \alpha) \sum_n \frac{\epsilon_n}{E_A - E_{T(n)}} \right. \right.$$

$$\times \left. \left( \frac{\lambda_n}{E_E - E_C} + \frac{\nu_n}{E_A - E_C} \right) \right]$$

$$+ \frac{\sqrt{15}}{\sqrt{6}} JQ\alpha \left[ \frac{1}{(E_A - E_C)(E_A - E_{C'})} + \frac{2}{(E_E - E_C)(E_E - E_{C'})} \right.$$

$$\left. \left. - 3 \left( \frac{1}{E_E - E_C} + \frac{1}{E_A - E_C} \right) \sum_n \frac{\epsilon_n \mu_n}{E_A - E_{T(n)}} \right] \right\}.$$

$${}''\langle {}^4E_{(2)}(\tfrac{3}{2}) | P | {}^6A(\tfrac{5}{2}) \rangle'$$

$$= -\frac{\zeta \hbar^2}{\sqrt{5}} (\hat{x} - i\hat{y}) \left\{ \frac{QI}{2} \left[ \sqrt{5} (\sqrt{3}\alpha - \beta) \sum_n \frac{\epsilon_n}{E_A - E_{T(n)}} \left( \frac{\lambda_n}{E_E - E_C} \frac{\nu_n}{E_A - E_C} \right) \right. \right.$$

$$\left. - \frac{\beta\sqrt{10}}{(E_A - E_C)(E_A - E_{C'})} \right] + JR \frac{\beta\sqrt{10}}{(E_E - E_C)(E_E - E_{C'})} - \frac{\sqrt{5}}{\sqrt{2}} JQ\alpha$$

$$\times \left[ \frac{1}{(E_A - E_C)(E_A - E_{C'})} + \left( \frac{1}{E_E - E_C} + \frac{1}{E_A - E_C} \right) \sum_n \frac{\epsilon_n \mu_n}{E_A - E_{T(n)}} \right] \right\}.$$

The $n$-summation is over the three $^4T_{1g}^{(n)}$ states, which have spin–orbit matrix elements with the sextet state. Transition matrices between states of other $S_z$ are proportional to those written down, with constants of proportionality given by the coefficients of $\sigma_n$ in table 2 of [7].

$$\epsilon_n = \sqrt{2}(\lambda_n + \nu_n) - \mu_n, \quad \text{and} \quad \lambda_n, \quad \nu_n, \quad \mu_n, \quad \alpha \text{ and } \beta$$

are defined and given numerically by Pappalardo [8].

## 6. THE OSCILLATOR STRENGTH

The oscillator strength is defined as

$$\text{o.s.} = \frac{2m}{3\hbar^2 e^2} \sum \frac{E_f - E_i}{2j+1} |\langle f|P|i\rangle|^2$$

for transitions between the initial states $i$ of multiplicity $2j+1$ ($=6$) and final states $f$. The summation is over all initial and final states in the band.

It is now necessary to consider the integrals $P$, $Q$, $I$ and $J$. These are all of the same sign and it may be assumed that $R \geqslant Q$, $I \geqslant J$. In [12] it has been assumed that $RJ(E_i - E_c)^{-1}$ is negligible compared with $QI(E_f - E_c)^{-1}$. For inter-system transitions the situation is more complex, since some band-intensities depend on $QI$, others on $RI$. Some exact numerical relationships would be required. As these are lacking, we fit the data the best we can. Thus in table 2 we give the figures for the oscillator strengths assuming

$$(a) \quad \frac{R}{Q} = \frac{I}{J} = 1, \quad (b) \quad \frac{R^2}{Q^2} = \frac{I^2}{J^2} = 2.$$

The absolute values of $Q^2$ and $I^2$, as estimated in [12], are $0\cdot 02 R_0^2$ and

$$1\cdot 66 \times 10^{-22} R_0^{-2} \text{ (erg/cm)}^2$$

respectively. $E_C(\simeq E_{C'})$ is taken from [13] as $55\,000\,\text{cm}^{-1}$.

| | 2 | 4 |
|---|---|---|
| $^4T_{1g}^{(2)}$ | 2 | 2·6 |
| $^4E_g^{(2)}$ | 2·2 | 1·8 |
| $^4T_{2g}^{(2)}$ | 4·3 | 2·7 (1, 1·7) |
| $^4A_{1g}, ^4E_g^{(1)}$ | 3·4 (1·2, 2·2) | 1·7 |
| $^4T_{2g}^{(1)}$ | 2·4 | $1 \times 10^{-7}$ |
| $^4T_{1g}^{(1)}$ | $4\cdot 1 \times 10^{-7}$ | $(b)$ |
| $^6A_{1g} \rightarrow$ | $(a)$ | |

Table 2. Calculated oscillator strengths.

The order of magnitude agreement with table 1 is no worse (within a factor 2–5) than can be hoped for. The better relative fits are given by case $(a)$ and this possibility multiplied by a suitable scaling factor, is compared graphically in figure 2. It is seen that the general trend is maintained by the theoretical quantities. (The comparison of columns $(a)$ and $(b)$ show that as regards relative strengths (within each column) it is the uppermost state $^4T_{1g}^{(2)}$ which is most sensitive to the nature of the assumptions. One wonders whether to connect this with the variation, already noted, of the experimental data of this line.)

Nonetheless, as the intensities depend so critically on the assumed ratio of the integrals, we conclude that while by a suitable choice agreement can be secured between this theory and experiment, the great sensitivity of the results does not allow the theory to be conclusively confirmed by these experiments. It would be

interesting to establish whether or not the predictions of the theory with respect to absorption of polarized light are borne out by experiment. (The matrix elements for the transitions to the orbital triplets indicate a mixture of linear and circular polarizations in different proportions.)



Figure 2. Comparison of experimental and theoretical oscillator strengths. The boxes represent case (*a*) of table 2, suitably scaled. Lines are experimental results:
———————— [1]
– – – – – – – – – [2]  multiplied by 2.
– · – · – · – · – · – [3]

It may also be noted that the present interpretation associates the higher, more intense component of the $25\,000\,\text{cm}^{-1}$ band with the $^4E_g$ transition. This is opposed by the conclusion of [5] and [7] who investigated the removal of the accidental degeneracy of the $^4E_g$, $^4A_{1g}$ states by covalency effects. The present result seems to be confirmed, however, by Stout's experiments [5] with polarized light, in which the higher component is more affected, presumably by the tetra-gonal field, indicating that this component should be $E_g$.

I am thankful to Mr. Y. Shadmi for a discussion and to Dr. C. K. Jorgensen for written clarification.

## References

[1] HEIDT, L. J., KOSTER, G. F., and JOHNSON, A. M., 1958, *J. Amer. chem. Soc.*, **80**, 6471.
[2] HOLMES, O. H., and McCLURE, D. S., 1957, *J. chem. Phys.*, **26**, 1686.
[3] JORGENSEN, C. K., 1957, *Acta chem. scand.*, **11**, 53.
[4] PRATT, G. W., and COELHO, R., 1960, *Phys. Rev.*, **116**, 281.
[5] STOUT, J. W., 1959, *J. chem. Phys.*, **31**, 709.
[6] PAPPALARDO, R., 1959, *J. chem. Phys.*, **31**, 1050.
[7] KOIDE, S., and PRYCE, M. H. L., 1958, *Phil. Mag.*, **3**, 607.
[8] PAPPALARDO, R., 1957, *Phil. Mag.*, **2**, 1397.
[9] LIEHR, A. D. (private communication).
[10] LIEHR, A. D., and BALLHAUSEN, C. J., 1957, *Phys. Rev.*, **106**, 1161.
[11] ENGLMAN, R., 1960, *J. chem. Phys.*, **32**, 299.
[12] ENGLMAN, R., 1960, *Mol. Phys.*, **3**, 48.
[13] ORGEL, L. E., 1954, *Quart. Rev.*, **8**, 423.
[14] SHADMI, Y., Ph.D. Thesis, The Hebrew University, Jersusalem.

# The effect of deuterium and chlorine substitution on triplet→singlet transition probabilities in naphthalene

by M. S. DE GROOT and J. H. VAN DER WAALS

Koninklijke/Shell-Laboratorium, Amsterdam

(Shell Internationale Research Maatschappij N.V.)

Recently Hutchison and Mangum [1] studied the phosphorescent state of naphthalene dissolved in a durene single crystal. They discovered that the phosphorescence lifetime, at 77 K, increases from $2\cdot1 \pm 0\cdot1$ sec for ordinary naphthalene to $16\cdot9 \pm 0\cdot9$ sec for the deuterated compound and tentatively attributed the effect to the difference in mass between H and D.

We are now measuring the effect of substitution in aromatic molecules on the radiative transition probability from the triplet phosphorescent state $(T)$ to the ground $(S_0)$ state. This is done by irradiating a glassy solution of the phosphorescent substance, at 77 K, in a microwave cavity as described earlier [2]. The relative concentration of molecules in their triplet state is determined from the (integrated) intensity of the magnetic resonance signal. After the exciting light has been switched off the corresponding phosphorescence intensity and decay time are measured by means of a photomultiplier and a recording instrument. In the table some preliminary results on naphthalene $(C_{10}H_8)$, deuteronaphthalene $(C_{10}D_8)$ and $\beta$-chloronaphthalene $(C_{10}H_7Cl)$ are given. Further experiments with greater accuracy are planned.

When comparing $C_{10}H_8$ and $C_{10}D_8$ it will be noticed that (within the experimental accuracy) the phosphorescence intensity is proportional to the number of triplet-state molecules. This proves that deuterium substitution has no influence on the radiative lifetime $\tau^r$. Hence the spectacular increase in decay time $\tau$ must be due to suppression of the non-radiative return to the ground state, as suggested by recent work of Wright *et al.* on benzene [3]. Apparently 18 sec is a lower limit for the radiative lifetime of both light and heavy naphthalene $(\tau_H^r \simeq \tau_D^r \geqslant 18 \text{ sec})$. The non-radiative lifetime follows from

$$1/\tau^d = 1/\tau - 1/\tau^r; \tag{1}$$

for naphthalene one obtains $2\cdot5 \text{ sec} \geqslant \tau_H^d > 2\cdot2 \text{ sec}$.

The difference between deuterium and chlorine substitution is striking. The phosphorescence intensity of $\beta$-chloronaphthalene per unit of triplet concentration is about five times as high as that of naphthalene. When taking $\tau_{\beta \, Cl}^r \geqslant 18/5 = 3\cdot6 \text{ sec}$ and $\tau_{\beta \, Cl} = 0\cdot42 \text{ sec}$ one obtains from (1):

$$0\cdot48 \text{ sec} \geqslant \tau_{\beta \, Cl}^d > 0\cdot42 \text{ sec}.$$

Apparently the rate constants for the radiative and dark processes $T \to S_0$ are about equally enhanced by chlorine substitution as the rate constant of the excited singlet-to-triplet conversion $S^* \to T$ [4], which is in agreement with previous predictions [5]. The difference between the decay times of $\beta$-chloronaphthalene given in the table may be due to a concentration effect.

The present results give a higher limiting value to the radiative lifetime $\tau_H^r$ of naphthalene (18 sec) than that following from the quantum yield measurements of Gilmore *et al.* (11·0 sec.) [5]. An elucidation of the effect of deuterium substitution on all different rate processes responsible for the fluorescence and phosphorescence of naphthalene is needed. In some simple experiments in which we have compared $C_{10}H_8$ and $C_{10}D_8$ it was found that their fluorescence yields are the same to within 10% and so is their rate of internal conversion $S^* \rightarrow T$.

| Compound | Concentration (mole/1000 g solution) | Steady-state triplet concentration from e.s.r. (relative units) | Corresponding photomultiplier output (relative units) | Phosphoresc. decay time (sec) |
|---|---|---|---|---|
| $C_{10}H_8$ | $3\cdot58 \times 10^{-3}$ | $1\cdot00$ | $1\cdot00$ | $2\cdot2$ |
| $C_{10}D_8$ | $3\cdot57 \times 10^{-3}$ | $0\cdot55$ | $0\cdot55$ | $18\cdot0$ |
| $C_{10}H_8$ | $3\cdot59 \times 10^{-3}$ | $1\cdot00$ | $1\cdot00$ | $2\cdot0$ |
| $C_{10}D_8$ | $3\cdot57 \times 10^{-3}$ | $0\cdot75$ | $0\cdot89$ | $17\cdot7$ |
| $C_{10}H_8$ | $15\cdot6 \times 10^{-3}$ | $1\cdot00$ | $1\cdot00$ | $2\cdot2$ |
| $C_{10}D_8$ | $15\cdot6 \times 10^{-3}$ | $0\cdot62$ | $0\cdot60$ | $18\cdot7$ |
| $C_{10}H_8$ | $3\cdot59 \times 10^{-3}$ | $1\cdot00$ | $1\cdot00$ | $2\cdot3$ |
| $\beta\text{-}C_{10}H_7Cl$ | $3\cdot42 \times 10^{-3}$ | $0\cdot81$ | $3\cdot2$ | $0\cdot48$ |
| $C_{10}H_8$ | $16\cdot0 \times 10^{-3}$ | $1\cdot00$ | $1\cdot00$ | $2\cdot1$ |
| $\beta\text{-}C_{10}H_7Cl$ | $15\cdot1 \times 10^{-3}$ | $0\cdot61$ | $3\cdot8$ | $0\cdot35$ |

Comparison of steady-state triplet concentration with corresponding photomultiplier output.

The deuteronaphthalene contained 99·2 mole per cent D, the purity of $\beta$-chloronaphthalene was better than 99 per cent. The solvent was Alphanol 79, a mixture of primary aliphatic alcohols. All solutions were degassed by repeated freezing and heating, except in the first two experiments of the table.

The simple analysis given here is only feasible if the proportionality constants relating the low-field magnetic resonance signal to the number of triplet molecules are the same for all molecules under consideration. This requires the zero-field splitting patterns to be nearly the same; for the present substances this must be so since their resonance signals all occur at the same field strength [2].

REFERENCES

[1] HUTCHISON, JR., C. A., and MANGUM, B. W., 1960, *J. chem. Phys.*, **32**, 1261.
[2] DE GROOT, M. S., and VAN DER WAALS, J. H., 1960, *Mol. Phys.*, **3**, 190.
[3] WRIGHT, M. R., FROSCH, R. P., and ROBINSON, G. W., 1960, *J. chem. Phys.*, **33**, 934.
[4] ERMOLAEV, V., and TERENIN, A., 1958, *J. chim. Phys.*, **55**, 698.
[5] GILMORE, E. H., GIBSON, G. E., and McCLURE, D. S., 1952, *J. chem. Phys.*, **20**, 829; 1955, *Ibid.*, **23**, 399.

# The diamagnetic susceptibilities of some hydrogen-bonded molecules

by R. MASON

Department of Chemistry, Imperial College of Science and Technology, London, S.W.7

The diamagnetic anisotropy due to the $\pi$ electrons of conjugated molecules arises from the enhancement of the out-of-plane susceptibility (usually $K_3$) following the formation of molecular orbitals, together with a decrease in the in-plane susceptibilities, $K_1$ and $K_2$, due to a positive contribution from the localized atomic orbitals [1]. In heteronuclear molecules, the second effect may often be more important than the ring current contribution and an observed aniso-tropy, in the benzene sense, may not constitute *a priori* evidence for delocalization phenomena.

The table lists the molecular susceptibilities (in units of $10^{-6}$ c.g.s. e.m.u.) of some carboxylic acids and succinimide, as obtained from measurements of the diamagnetic anisotropy of single crystals and a knowledge of the respective molecular orientation.

The effective delocalization term is given more adequately by

$$\Delta K' = K_3 - \sum \chi_{\text{atomic}},$$

with $\chi_H = -2 \cdot 0$, $\chi_C = -7 \cdot 4$, $\chi_N = -9 \cdot 0$ and $\chi_O = -5 \cdot 3$, rather than by

$$\Delta K = K_3 - \tfrac{1}{2}(K_1 + K_2).$$

These atomic susceptibilities are derived from careful magnetic measurements of the average susceptibilities of simple saturated molecules [1]. When applied

| Molecule | $K_1$ | $K_2$ | $K_3$ | $\sum \chi_{\text{atomic}}$ | $\Delta K$ | $\Delta K'$ | $\tfrac{1}{2}(K_1+K_2)$ obs | $\tfrac{1}{2}(K_1+K_2)$ calc |
|---|---|---|---|---|---|---|---|---|
| Succinic acid [2] | $-48 \cdot 6$ | $-53 \cdot 1$ | $-60 \cdot 7$ | $-62 \cdot 8$ | $-9 \cdot 8$ | $2 \cdot 1$ | $-50 \cdot 9$ | $-53 \cdot 6$ |
| Succinimide [3] | $-41 \cdot 6$ | $-45 \cdot 1$ | $-55 \cdot 1$ | $-59 \cdot 0$ | $-11 \cdot 7$ | $4 \cdot 1$ | $-43 \cdot 4$ | $-45 \cdot 0$ |
| Oxalic acid dihydrate [4] | $-52 \cdot 7$ | $-53 \cdot 1$ | $-62 \cdot 4$ | $-58 \cdot 6$ | $-9 \cdot 5$ | $-3 \cdot 8$ | $-52 \cdot 9$ | $-49 \cdot 4$ |
| Maleic acid [5] | $-42 \cdot 0$ | $-44 \cdot 3$ | $-62 \cdot 3$ | $-58 \cdot 8$ | $-19 \cdot 1$ | $-3 \cdot 5$ | $-43 \cdot 2$ | $-42 \cdot 0$ |

Magnetic data of hydrogen-bonded molecules.

to calculations of unsaturated molecules they must be modified to take account of the changes in the symmetry of the electron distribution. Thus Hoarau [1] showed that for a number of aromatic hydrocarbons,

$$\tfrac{1}{2}(K_1 + K_2)_{\text{obs}} = \sum \chi_{\text{atomic}} + n\alpha$$

with $n$ the number of trigonally hybridized carbon atoms and $\alpha$ a constitutive

correction $(\sim +3.8 \times 10^{-6}$ c.g.s. e.m.u.$)$, so that $\chi^{\parallel}{}_{C(sp^2)} = -3.6$ and $\chi^{\perp}{}_{C(sp^2)} = -7.4$ as before. In a similar way, the values $\chi^{\parallel}{}_{=O} = -4.5$ and $\chi^{\parallel}{}_N = -4.0$ have been derived to give the best agreement between the observed and calculated in-plane susceptibilities for the molecules of the table.

The most serious shortcoming in these empirical relations lies in their neglect of the magnetic anisotropy due to $\sigma$ bond formation, which is partly reflected by the fact that $\Delta K'$ is positive for succinic acid and succinimide; judging by this fact alone, the anisotropy due to $\sigma$ bonds is of the same sign as the total anisotropy of conjugated systems. But these difficulties do not detract from the fact that the $\Delta K'$ values for oxalic and maleic acids are quite different from those of succinic acid and succinimide. The implication that delocalization, as a result of hydrogen bond formation, is more important for these former molecules, is entirely in accord with what might be expected on the basis of the known geometry of the hydrogen bonds which are formed by these molecules in their respective crystals. Thus in maleic acid, an intramolecular hydrogen bond of only 2·46 Å links the hydroxyl and carbonyl groups [6]; a short hydrogen bond of 2·50 Å also occurs in oxalic acid dihydrate [7]. In succinimide [3] and succinic acid [8] the N—H . . . O and O—H . . . O distances are 2·869 Å and 2·64 Å respectively. A more sophisticated theory than that originally concerned with the possibility of delocalization in hydrogen-bonded molecules [9] and its associated magnetic effects is being developed.

## REFERENCES

[1] HOARAU, J., 1956, *Ann. Chim.*, **13**, 544.
[2] LONSDALE, K., 1939, *Proc. roy. Soc.* A, **171**, 541.
[3] MASON, R., 1961, *Acta cryst.*, Camb. (in the press).
[4] LONSDALE, K., 1938, *J. chem. Soc.*, p. 364.
[5] GUPTA, M. P., 1954, *Proc. phys. Soc. Lond.*, **67**, 643.
[6] SHAHAT, M., 1952, *Acta cryst.*, Camb., **5**, 763.
[7] DUNITZ, J. D., and ROBERTSON, J. M., 1947, *J. chem. Soc.*, p. 142.
[8] MORRISON, J. D., and ROBERTSON, J. M., 1949. *J. chem. Soc.*, p. 980.
[9] EVANS, M. G., and GERGELY, J., 1949, *Biochim. biophys. Acta*, **3**, 188.

# Atomic orbitals with angularly dependent $Z_{\text{eff}}$ to be used in molecular orbitals calculations

by E. SCROCCO and J. TOMASI

University of Pisa, Italy

A new type of atomic orbital is proposed for use in molecular problems of quantum mechanics. This orbital is formally similar to Slater's orbitals but is characterized by an effective nuclear charge $Z_{\text{eff}}$ which is an explicit function of the angles $\theta$ and $\phi$. The fundamental state of the molecule $H_2^+$ is studied using such an orbital.

The Hartree Fock wave-functions are generally considered to be the most suitable, at present, to describe the electronic configurations of complex atoms. Such many-electron functions consist of antisymmetrized products of mono-electronic orbitals, the last being formed by a radial function $R_{nl}(r)$ multiplied by a spherical harmonic:

$$\psi_{nlm} = R_{nl}(r)\, S_{lm}(\theta\phi). \tag{1}$$

In the self-consistent method of Hartree–Fock the potential energy of a moving electron, in the field caused by the nucleus and by the remaining electrons, has spherical symmetry

$$V(r) = -\frac{Z_{\text{eff}}}{r} \tag{2}$$

where the charge $Z_{\text{eff}}$ is a function of the distance of the electron from the nucleus only.

For an atom in a molecule, this method of approach can be generalized by using a charge $Z_{\text{eff}}$ which is a function of the distance from the nucleus and of the $\theta$ and $\phi$ angles, i.e. the coordinates of the electron with respect to a system having its origin in the nucleus.
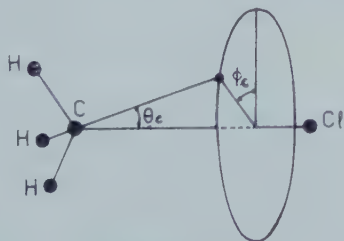


Figure 1.

For instance, in a molecule such as $CH_3Cl$ (see figure 1), if the symmetry axis is taken as polar axis, one could use, in the orbitals of the valence shell of carbon:

$$Z_{\text{eff}\,c} = Z_{\text{eff}}(r_c\theta_c\phi_c) \tag{3}$$

where the dependence on $\phi$ has a threefold symmetry. For a diatomic molecule

A–B, taking the bond axis as polar axis, $Z_{eff}$ is independent of $\phi$ and one could write for atom A:

$$Z_{eff\,A} = Z_{eff}(r_A \theta_A). \tag{4}$$

A function sufficiently general to represent $Z_{eff}$ according to this scheme could be a series expansion of spherical harmonics of the type:

$$Z_{eff} = z(r) \sum_{pq} C_{pq} S_{pq}(\theta\phi) \tag{5}$$

which can be used instead of the usual constant value of $Z_{eff}$ in the expression of any of the atomic orbitals of the type generally used in the study of molecular problems (Slater's orbitals and hydrogenoid orbitals).

In the present note the results of a preliminary study of the $H_2^+$ molecule with such orbitals are reported for the simplest case, i.e. for Slater's functions with a $Z_{eff}$ of the type (5):

$$\chi_{nlm} = N r^{n-1} \exp\left[ -z(r)\left( \sum_{pq} C_{pq} S_{pq}(\theta\phi) \right) r \right] S_{lm}(\theta\phi). \tag{6}$$

For the $H_2^+$ molecule there is no dependence on the angle $\phi$ since the problem has an axial symmetry. With regard to the other two variables, since our aim was to make clear the importance of the angular dependence of $Z_{eff}$, $z$ has been kept constant at all distances and the expansion of (5) has been limited to the second term. With these assumptions $Z_{eff}$ has the form:

$$Z_{eff} = z(1 + \gamma \cos\theta) \tag{7}$$

where $z$ and $\gamma$ are to be computed by minimizing the energy.

The molecular orbital used is:

$$\phi = \frac{\chi_a + \chi_b}{2^{1/2}\left(\int \chi_a^2 \, d\tau + \int \chi_a \chi_b \, d\tau\right)^{1/2}} \tag{8}$$

with

$$\chi' = \exp\left[-z(1 + \gamma\cos\theta)r\right]. \tag{8a}$$

Therefore the total energy of the molecule in atomic units is written as:

$$\mathcal{E} = \frac{\int \chi_a(-\nabla^2)\chi_a \, d\tau + \int \chi_a(-\nabla^2)\chi_b \, d\tau - \int \chi_a^2 (2/r_a) \, d\tau}{\int \chi_a^2 \, d\tau + \int \chi_a \chi_b \, d\tau}$$

$$+ \frac{-\int \chi_a^2(2/r_b)\,d\tau - 2\int \chi_a\chi_b(2/r_a)\,d\tau}{\int \chi_a^2 \, d\tau + \int \chi_a\chi_b \, d\tau} + 2/R_{ab}. \tag{9}$$

It can be easily seen that the integrals involved have the following expressions:

$$\int \chi_a(-\nabla^2)\chi_a \, d\tau = \frac{\pi}{z(1-\gamma^2)},$$

$$\int \chi_a(-\nabla^2)\chi_b \, d\tau = -\frac{\pi \exp\left[-zR(1+\gamma)\right]}{z}\left\{ \left( \frac{z^2 R^2}{3} - zR - 1 \right) + \left( \frac{2z^2 R^2}{3} + \frac{2zR}{3} \right)\gamma \right.$$

$$\left. + \left( \frac{z^2 R^2}{3} + zR + 1 \right)\gamma^2 \right\},$$

$$\int \chi_a^2 \left( \frac{2}{r_a} \right) d\tau = \frac{2\pi}{z^2(1-\gamma^2)},$$

$$\int \chi_a^2 \left(\frac{2}{r_b}\right) d\tau = \frac{2\pi}{z^2} \left\{ \frac{1}{\gamma(1-\gamma^2)} - \frac{\exp[-2zR(1+\gamma)]}{\gamma(1+\gamma)} - \frac{zR}{\gamma^2} \exp\left[-\frac{zR}{\gamma}(1-\gamma^2)\right]\right.$$
$$\left. \times \left(E_i\left[-\frac{zR}{\gamma}(1+\gamma)^2\right] - E_i\left[-\frac{zR}{\gamma}(1-\gamma^2)\right]\right)\right\},$$

$$\int \chi_a \chi_b \left(\frac{2}{r_a}\right) d\tau = \frac{2\pi}{z^2} \exp\left[-zR(1+\gamma)\right] (zR+1),$$

$$\int \chi_a \chi_b \, d\tau = \frac{\pi}{z^3} \exp\left[-zR(1+\gamma)\right] \left(\frac{z^2R^2}{3} + zR + 1\right),$$

$$\int \chi_a^2 \, d\tau = \frac{\pi}{z^3(1-\gamma^2)^2}. \tag{10}$$

The calculation has been carried out by minimizing the energy with respect to $z$ and $\gamma$, the distance $R$ being $2u.a$. The results are reported in the table together with the values obtained by means of other variational functions.

| Molecular orbital used | | Optimum values of parameters | Bond energy (v.e.) | Relative error |
|---|---|---|---|---|
| $\dfrac{\exp(-r_a) + \exp(-r_b)}{\sqrt{N}}$ | | $R = 1\cdot32$ Å | $1\cdot76$ | $37\%$ |
| $\dfrac{\exp(-Zr_a) + \exp(-Zr_b)}{\sqrt{N}}$ | (a) $\begin{cases} \\ \end{cases}$ | $R = 1\cdot06$ Å $Z = 1\cdot228$ Å | $2\cdot25$ | $19\cdot4$ |
| $\dfrac{[\exp(-Zr_a) + Cr_a \cos\theta_a \exp(-\epsilon Zr_a)]}{\sqrt{N}}$ $+ \dfrac{[\exp(-Zr_b) + Cr_b \cos\theta_b \exp(-\epsilon Zr_b)]}{\sqrt{N}}$ | (b) $\begin{cases} \\ \\ \\ \end{cases}$ | $R = 1\cdot06$ Å $\epsilon = 1\cdot15$ Å $Z = 1\cdot247$ Å $C = 0\cdot145$ Å | $2\cdot652$ | $5\cdot0$ |
| $\dfrac{\exp[-z(1+\gamma\cos\theta_a)r_a]}{\sqrt{N}}$ $+ \dfrac{\exp[-z(1+\gamma\cos\theta_b)r_b]}{\sqrt{N}}$ | (c) $\begin{cases} \\ \\ \end{cases}$ | $R = 1\cdot06$ Å $z = 1\cdot275$ Å $\gamma = -0\cdot19$ Å | $2\cdot734$ | $2\cdot08$ |
| Exact solution | (d) | — | $2\cdot792$ | — |

(a) Finkelstein and Horowitz; (b) Dickinson; (c) this paper; (d) exact solution.

The virial theorem has given the following values:
$$\mathscr{E} = -16\cdot34 \text{ v.e.,}$$
$$V/2 = -16\cdot34,$$
$$T = \phantom{-}16\cdot35.$$

These results are really encouraging; in fact, one obtains, with only two variational parameters, a better value for the bond energy than that obtained using Dickinson's three-parameter function.

A further proof of the goodness of the molecular orbital (8 a) is given in figure 2 where a comparison is made between some variational functions and the exact function. Such a comparison has been made in both the plane orthogonal to the

bond axis through its centre and in a plane passing through the two nuclei. For the sake of simplicity only the orbital $(\exp(-r_a)+\exp(-r_b))/N^{1/2}$, Dickinson's orbital and the proposed one are reported. Furthermore, only the central part of the exact orbital has been drawn since, everywhere else, this is practically coincident with the proposed orbital, within the limits of accuracy of the drawing.
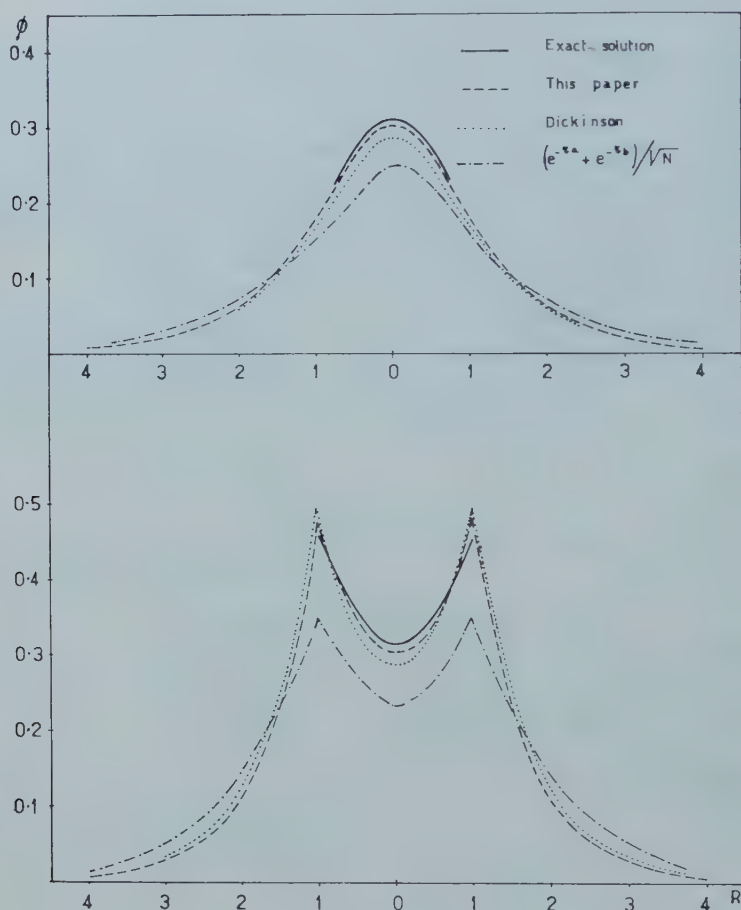


Figure 2.

It may be noted that the computed value of $\gamma = -0.19$ leads to a higher charge density in the bonding region and a lower charge density in the external regions.

A similar effect is obtained with a certain hybridization $2p$, as in the Dickinson function, but it can be shown that a larger hybridization corresponds to the function (8 a). In fact, if such a function is expanded in a series of powers of $\gamma$, one obtains:

$$\chi = N \exp(-zr)\left(1 - z\gamma r \cos\theta + \frac{z^2\gamma^2 r^2}{2}\cos^2\theta - \ldots\right), \tag{11}$$

which can be written as:

$$\chi = N\left\{\left(\frac{\pi}{z^3}\right)^{1/2} 1s - z\gamma\left(\frac{\pi}{z^5}\right)^{1/2} 2p_\sigma + \frac{z^2\gamma^2}{2}\left(\frac{5\pi}{2z^7}\right)^{1/2} 3s + \frac{z^2\gamma^2}{2}\left(\frac{2\pi}{z^7}\right)^{1/2} 3d\sigma + \ldots\right\} \tag{12}$$

and also:

$$\chi = (1 - \gamma^2) \left\{ 1s - \gamma 2p_\sigma + \sqrt{\tfrac{5}{8}} \gamma^2 3s + \frac{\sqrt{2}}{2} \gamma^2 3\,d_\sigma + \dots \right\}. \tag{13}$$

In this last expression the orbitals clearly show the form of generalized hybrids which mix an infinite number of Slater's orbitals of the right symmetry.

A study of the $H_2$ molecule using the orbital proposed in the present paper is being carried out.

<div align="center">REFERENCES</div>

[1] FINKELSTEIN, B. N., and HOROWITZ, G. E., 1928, *Z. Phys.*, **48**, 118.
[2] DICKINSON, B. N., 1933, *J. chem. Phys.*, **1**, 317.
[3] BATES, D. R., LEDSHAM, K., and STEWART, A. L., 1953, *Phil. Trans.* A, **246**, 215.

# Excess free energy of solid solutions of Kr–CH₄ mixtures at 90·67°K

by C. LEFEBVRE and J. GUISSET

University of Brussels, Belgium

The excess free energy of the solid system Kr–CH₄ has been determined from 'frost-point' pressure measurements at 90·67°K, the triple-point temperature of pure CH₄. A new method of calculating $g^E(x)$ from the experimental 'frost curve' $P(y)$ has been used. The results are in good agreement with those deduced from the average potential theory of solutions.

## 1. Introduction

Of all the tentative molecular theories of solutions so far advanced, the 'average potential model' appears to be the most appropriate to solid solutions, since this theory depends very little on the structure model of the condensed phase [1]. Experimental investigation of such solutions is restricted to a fairly narrow range of systems, as the consequence of the fundamental hypothesis underlying the theory, i.e. the Law of Corresponding States. The most suitable substances for such a study are the simple, non-polar, spherical molecules of A, Kr, Xe, CH₄, etc. Numerous papers have been published on investigations of liquid binary systems of these molecules. However, as a result of the difficulty of obtaining thermodynamic equilibrium in a solid mixture, very few accurate results have been published for solid solutions. A new method† of investigating solid solutions from 'frost point' pressure measurements has been suggested recently by Walling and Halsey [2]. The advantage of this method is that it permits the estimation of the gas–solid equilibrium with a vanishing small quantity of solid. Thus all problems due to diffusion and to solid phase thermodynamic equilibrium are avoided. The 'frost curve' $P(y)$ as a function of $y$, the composition of the gaseous phase in equilibrium with the solid phase for the Kr–CH₄ system is established and from this curve, $g^E(x)$, the excess free energy of the solid in terms of $x$, the solid composition is deduced using a new method of calculation [3, 4]. The Kr–CH₄ system has been chosen for study, partly for experimental reasons: knowledge of the phase diagram [5], ease of maintenance at a constant temperature and of pressure measurement, and partly to complete the data already established on the excess thermodynamic properties of the system [6].

## 2. Experimental procedure

The method consists of measuring the pressure $P$ at which the first crystal of solid appears, when increasing amounts of the gaseous mixture of known composition $y$ are introduced into the experimental chamber, maintained at constant temperature. Graphs of $p/n$ as a function of $p$ are constructed for each mixture: where $p$ is the total pressure and $n$ is the number of moles introduced into the

† This method has been used to study liquid solutions from dew point curves [7] and [8].

experimental chamber.    At the 'frost point' pressure $P$, of each mixture, dis-
continuities are evident in the relative curves (see figure 1).    The 'frost curve'
$P(y)$ can be constructed from the condensation pressure values thus obtained for a
series of mixtures of varying composition.    From graphs of $p/n(p)$, $P$ can be
determined to $\pm 0\cdot1$ mm Hg, the error in $y$ is of the order of $1/1000$.    The method
of calculating $g^E(x)$ from the 'frost curve', including a correction for gas imper-
fection, is described in references [3] and [4].
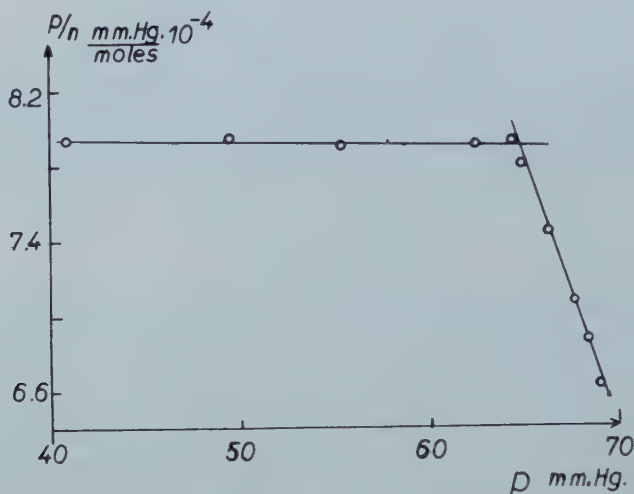


Figure 1.    Graph of $p/n(p)$ for a gas composition $y = 0\cdot8196$.    The subscripts 1 and 2 refer
          to $CH_4$ and Kr respectively.    The change in slope occurs at $P$, the 'frost point'
          pressure of the mixture.

The krypton and methane used in these measurements were purified by low-
temperature fractional distillation.    Their purity after distillation was checked
by a series of vapour-pressure measurements during melting.    In this way it was
shown that the pressure interval during melting was less than $0\cdot1$ mm Hg, which
corresponds to a temperature variation of the order of $0\cdot005°$.    The average
values obtained for the triple-point vapour pressure of Kr and $CH_4$, corrected to
the international mm Hg, are $547\cdot45 \pm 0\cdot04$ mm Hg and $87\cdot77 \pm 0\cdot02$ mm Hg,
respectively.

| $y_1$ | $P$ |
|---|---|
| 0·2027 | 27·1 |
| 0·4467 | 36·3 |
| 0·6266 | 46·7 |
| 0·7384 | 56·0 |
| 0·7548 | 57·8 |
| 0·8186 | 64·9 |
| 0·8837 | 72·3 |
| 0·9660 | 83·1 |

Table 1.    Values of the 'frost point' pressure $P$, in international mm Hg for different gas
          compositions of $y_1$.
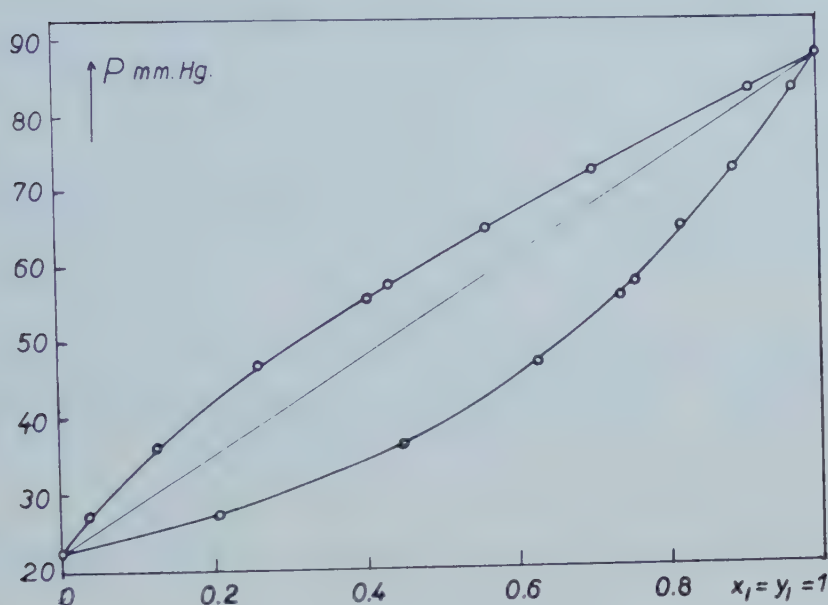
Figure 2. The lower curve represents the 'frost curve' $P(y)$, constructed from the experimental values given in table 1. The upper curve is the total vapour-pressure curve, constructed from values of $x$, calculated by Bellemans *et al.* [4].
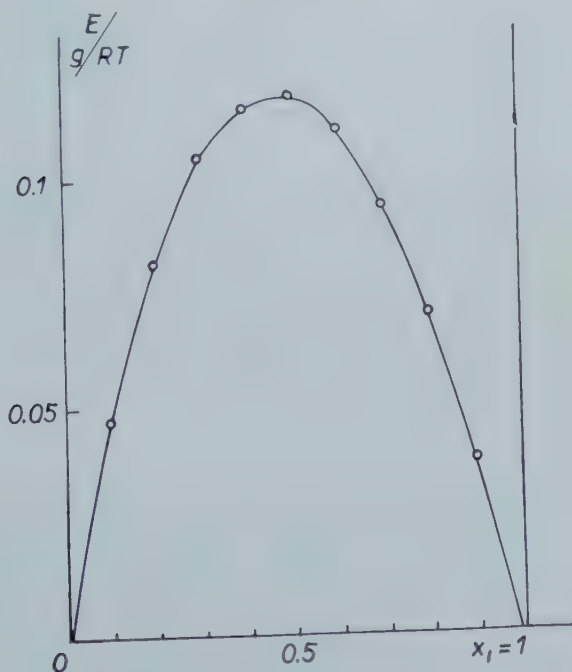


Figure 3. Graph of $g^E(x)/RT$ assumed to be given by $g^E(x)/RT = x_1 x_2 [A + B(x_1 - x_2)]$. The values of $A$ and $B$, calculated from the 'frost curve' $P(y)$ are $A = 0.473$ and $B = 0.063$, see [4]. For $x_1 = x_2 = 0.5$, $g^E = 21 \pm 1$ cals/mole.

The apparatus used in this work is a refined form of that used by V. Mathot et al. [7] and has been constructed largely by V. Mathot and N. Janson. The volume of the experimental chamber A, has been increased to about $70 \ cm^3$, thus permitting a more exact determination of the quantity of substances introduced.

Fine thermostatic control of A was ensured by immersing it in a bath of pure $CH_4$ maintained at its triple-point, i.e. $90 \cdot 67^\circ K$, see [9]. From vapour-pressure determinations it was shown that the temperature of this $CH_4$ bath remained constant to within $0 \cdot 002^\circ$.

## 3. CONCLUSIONS

The theoretical value of $g^E$ has been calculated from equation (9-5-4), as given by I. Prigogine et al. [1], where it is assumed that $\epsilon_{12}^2 = \epsilon_{11}\epsilon_{22}$ (dispersion forces), i.e. for $\theta = \delta^2/8$. The normalized parameters $\rho$ and $\delta$ given by

$$\rho_1 = (r_{22}^* - r_{11}^*)/r_{11}^*, \qquad \rho_2 = (r_{11}^* - r_{22}^*)/r_{22}^*,$$
$$\delta_1 = (\epsilon_{22}^* - \epsilon_{11}^*)/\epsilon_{11}^*, \qquad \delta_2 = (\epsilon_{11}^* - \epsilon_{22}^*)/\epsilon_{22}^*,$$

have been determined as the mean value of these parameters calculated from table 2.

|  | $\rho_1$ | $\delta_1$ | $\rho_2$ | $\delta_2$ |
|---|---|---|---|---|
| (1) Second virial coefficient | $-0 \cdot 066$ | $0 \cdot 152$ | $0 \cdot 071$ | $-0 \cdot 132$ |
| (2) Critical data | $-0 \cdot 027$ | $0 \cdot 099$ | $0 \cdot 027$ | $-0 \cdot 090$ |
| (5) Crystal data | $-0 \cdot 043$ | $0 \cdot 074$ | $0 \cdot 044$ | $-0 \cdot 069$ |
| (4) Viscosity | $-0 \cdot 070$ | $0 \cdot 387$ | $0 \cdot 075$ | $-0 \cdot 279$ |

Table 2.

Data from viscosity measurements have not, however, been considered since these values deviate systematically from values given by all other methods. Thus

$$\bar{\rho}_1 = -0 \cdot 04 \pm 0 \cdot 01, \qquad \bar{\rho}_2 = 0 \cdot 05 \pm 0 \cdot 01,$$
$$\bar{\delta}_1 = 0 \cdot 11 \pm 0 \cdot 02, \qquad \bar{\delta}_2 = -0 \cdot 10 \pm 0 \cdot 02,$$

giving, for $x_1 = x_2 = 0 \cdot 5$, with 1 as reference component: $g^E = 19$ cals/mole, with 2 as reference component: $g^E = 28$ cals/mole.

Let us consider the mean value:

$$\bar{g}^E = 23 \cdot 5 \ \text{cals/mole}.$$

There is good agreement between theoretical predictions and experimental results. For in fact, the Kr–$CH_4$ system is suitable for comparison with the theory, since both $\rho$ and $\delta$ are small and since, in addition, the spherical molecules of Kr and $CH_4$ obey, to a large extent, the Law of Corresponding States. It should be remarked, however, that the scatter in the values of measured $\epsilon^*$ and $r^*$ as obtained from second virial coefficient, critical and crystalline data, introduces a large error in the calculated value of $g^E$, and represents the real limitation in the estimation of the validity of the theoretical model. In fact, if one takes the r.m.s. errors on $\rho$ and $\delta$ indicated above, the error on calculated $g^E$ amounts to $\pm 10$.

References

[1] PRIGOGINE, I., BELLEMANS, A., and MATHOT, V., 1957, *The Molecular Theory of Solutions* (Amsterdam: North-Holland Publishing Co.).
[2] WALLING, J. F., and HALSEY, G. D., 1959, *J. chem. Phys.*, **30**, 1514.
[3] BELLEMANS, A., 1959, *Bull. Soc. chim. Belg.*, **68**, 355.
[4] BELLEMANS, A., LEFEBVRE, C., and GUISSET, J., 1960, *Bull. Soc. chim. Belg.*, **69**, 441.
[5] VEITH, H., and SCHRÖDER, E., 1937, *Z. phys. Chem.* A, **179**, 16.
[6] THORP, N., and SCOTT, R., 1956, *J. phys. Chem.*, **60**, 670.
[7] MATHOT, V., STAVELEY, L., YOUNG, J., and PARSONAGE, N., 1956, *Trans. Faraday Soc.*, **52**, 1488.
[8] HOLST, G., and HAMBURGER, L., 1916, *Z. phys. Chem.*, **91**, 513.
[9] CLUSIUS, K., and WEIGAND, K., 1940, *Z. phys. Chem.* B, **46**, 1.

# The mobility of holes and electrons in organic crystals

by J. N. MURRELL

Department of Chemistry, The University of Sheffield

Overlap integrals between the molecular orbitals of different anthracene molecules in the crystal lattice have been calculated. In the $c'$ direction the highest occupied orbitals overlap to a greater extent than the lowest vacant orbitals (a ratio of 4·7 : 1). This result explains the experimental fact that holes are more mobile than electrons in this direction. It is predicted that in the $ab$ plane the mobilities of the holes and electrons should be approximately equal, and considerably greater than in the $c'$ direction.

Experiments on the photoconduction of organic crystals, mainly of anthracene, have shown that the positive holes are more mobile than electrons [1–6]. At first sight this is a rather surprising result. A negatively charged molecule is expected to have a wave function which spreads out over a larger area than that of the corresponding positively charged molecule, hence the overlap between the wave function of a negatively charged molecule with that of a neutral molecule on a neighbouring lattice site is expected to be larger than the corresponding overlap for a positively charged molecule and its neighbours. The larger the overlap the more mobile should be the charge carrier, whether one considers a localized or a delocalized formulation of the electronic states of the crystal.

In this paper I shall show by examining in detail the overlap integrals between orbitals of neighbouring molecules in the anthracene crystal that the experimental results on the mobilities of the charge carriers are in qualitative agreement with the theoretical expectations.

Anthracene crystals are monoclinic prismatic with a space group $C_{2h}^5-P_{2_1/a}$. The detailed crystal structure of anthracene has been obtained by x-ray analysis by Sinclair *et al.* [7]. The relationship between neighbouring molecules in the crystal is shown in the figure. Molecules are centred at the corners of the prism, and lie in parallel planes whose normal is (1·000, −0·533, 0·500), in orthogonal coordinates. The centres of the $ab$ faces define the positions of a second set of molecules which are also parallel to one another and have the normal (1·000, 0·533, 0·500). The two molecules of the unit cell, 1 and 9 (say), make equal and opposite angles of 64° with the $ac$ plane.

Equivalent positions in the lattice are $(X', Y', Z)$, $(-X', -Y, -Z')$, $(4·280 -X', 3·018 +Y, -Z')$ and $(4·280 +X', 3·018 -Y, Z')$ in orthogonal angstrom coordinates, so that knowing the coordinates of atom $A_1$, one can construct the coordinates of $A_1'$, $A_9$ and $A_9'$, and then by translation along the $ab$ or $c$ axes, obtain the coordinates of any other equivalent position. The coordinates of atoms A . . . G are given in reference [7].
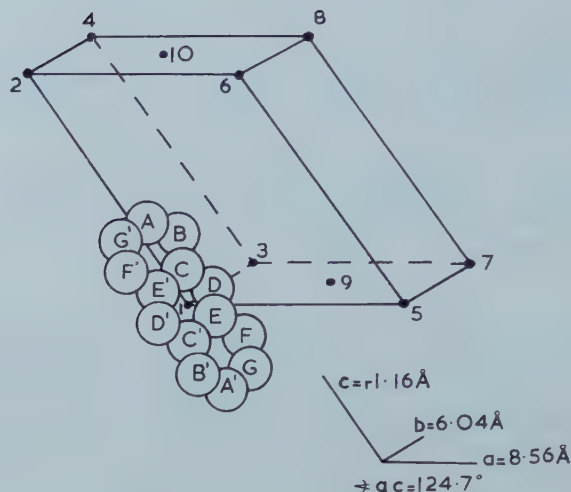
The closest approach of any two atoms in the lattice is between $F_1$ and $C_9'$, or their equivalents, and is 3·60 Å. To evaluate the overlap integral between molecular orbitals on different sites we expand these orbitals as a linear combination of atomic orbitals, and evaluate the individual atomic orbital overlap integrals. For an exact calculation this would involve the computation of 196 terms for each pair of sites. Fortunately the overlap integrals fall off inverse-exponentially with the separation of the two atomic centres, so that for large distances many terms can be neglected. For convenience I have chosen to neglect any overlap integral between two atomic orbitals which are more than 4·50 Å apart. This still entails the calculation of the following numbers of terms: for the overlap of 1 and 9, 31 terms; 1 and 10, 4 terms; 1 and 3, 10 terms; 1 and 2, 3 terms. Molecules 4, 5, 6, 7 and 8 have all their atoms at distances greater than 4·50 Å from any atom of 1.

The positive holes or the excess electrons of the anthracene ions are contained in the $\pi$-molecular orbitals, that is those orbitals which are antisymmetric with respect to reflection in the planes of the molecules. These molecular orbitals are compounded of the carbon $2p\pi$ atomic orbitals. If two of these atomic orbitals are defined by vectors $\mathbf{n}_1$ and $\mathbf{n}_2$, and the separation of the orbitals by $\mathbf{R}$, then their overlap integral can be split up as follows:

$$-S_{12} = \frac{(\mathbf{n}_1 \cdot \mathbf{R})(\mathbf{n}_2 \cdot \mathbf{R})}{n_1 n_2 R^2} S_\sigma - \left[ \frac{\mathbf{n}_1 \cdot \mathbf{n}_2}{n_1 n_2} - \frac{(\mathbf{n}_1 \cdot \mathbf{R})(\mathbf{n}_2 \cdot \mathbf{R})}{n_1 n_2 R^2} \right] S_\pi$$

where $S_\sigma$ is the component of the overlap in the direction $\mathbf{R}$, and $S_\pi$ is the component of the overlap perpendicular to $\mathbf{R}$. The $S_\sigma$ is about $10 \times S_\pi$ for the same interatomic distance, in the region we are studying.

Expressions for $S_\sigma$ and $S_\pi$ are given, and tabulated for some cases, by Mulliken *et al.* [8]. For two equivalent atomic orbitals the integrals are a function of a parameter $p = \zeta R$, where $R$ is the interatomic distance expressed in atomic units, and $\zeta$ is the exponential factor of the radial part of the atomic orbital. For both the positive and negative ions I have chosen the $\zeta$-value by the Slater recipe. For a neutral carbon atom ($\zeta = 1·625$); that is the atomic orbitals have the radial dependence $\exp(-1·625r)$.

The density of the unpaired electrons in the anthracene ions appears to be satisfactorily given by the simple Hückel theory [9]. The Hückel functions for the highest occupied and lowest vacant orbitals of anthracene, which will represent the wave functions for the hole and the electron respectively, are given below:
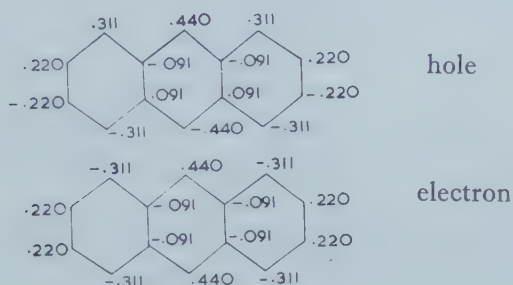


The results of the calculation are given in the table.

| Overlap | Hole | Electron |
|---------|------|----------|
| 1 and 2 | −0·05 | − 0·22 |
| 1 and 3 | 15·5 | −12·7 |
| 1 and 9 | −13·1 | −19·3 |
| 1 and 10 | 3·3 | 0·7 |

Overlap integrals between nearest neighbours, all to be multiplied by $10^{-4}$.

Since the overlap integrals between atomic orbitals vary roughly as $\exp(-p)$ neglect of the overlap between orbitals farther apart than 4·50 Å will mean that those neglected will be smaller by a factor of about 0·05 than the largest overlap integrals calculated. The values given in the table are therefore expected to have an accuracy of about 5 per cent.

Experimentally it has been found by Mette and Pick [10] that conduction in the *ab* plane is larger by a factor of 5 than conduction in the *c'* direction, perpendicular to this plane. This is supported by the calculations. It appears that this *c'* conduction arises from the interaction of molecules 1 and 10 rather than 1 and 2. In all experimental measurements the holes are found to be more mobile than the electrons in the *c'* direction. Kepler [6] finds a hole/electron mobility ratio of 1·3, Le Blanc [5] of 2·0, in the *c'* direction. Mette and Pick found that conduction in the *ab* plane was isotropic, but Kepler reports some anisotropy in this plane. The calculations predict that the holes should be more mobile in the **b** direction but electrons in the **a** + **b** direction.

One must conclude that the conduction properties of organic crystals are likely to be specific for each compound. Thus one finds for anthracene that holes are more mobile than electrons in the *c'* direction, but this is a result of an almost equal overlap between the atom pairs $A_1G_{10}$ and $B_1G_{10}$, which are of the same sign for the hole but of opposite sign for the electron. It cannot be expected that such a cancellation will occur as a general case.

On completion of this work I received a manuscript by Dr. O. H. Le Blanc on the band structure of anthracene. The author calculates resonance integrals between nearest neighbours rather than overlap integrals, but since these are roughly proportional to one another, his findings agree with mine. I wish to thank Dr. Le Blanc and the General Electric Company for allowing me to see this manuscript prior to publication.

REFERENCES

[1] PUTSEIKO, E. K., 1954, *C.R. Acad. Sci. U.R.S.S.*, **67**, 1009.
[2] CHYNOWETH, A. G., and SCHNEIDER, W. G., 1954, *J. chem. Phys.*, **22**, 1021.
[3] COMPTON, D. M. J., SCHNEIDER, W. G., and WADDINGTON, T. C., 1957, *J. chem. Phys.*, **27**, 160.
[4] KOMMANDEUR, J., and SCHNEIDER, W. G., 1958, *J. chem. Phys.*, **28**, 582.
[5] LE BLANC, O. H., 1960, *J. chem. Phys.*, **33**, 626.
[6] KEPLER, R. G., 1960, *Phys. Rev.*, **119**, 1226.
[7] SINCLAIR, V. C., ROBERTSON, J. M., and MATHIESON, A. McL., 1950, *Acta cryst., Camb.*, **3**, 245, 251.
[8] MULLIKEN, R. S., RIEKE, C. A., ORLOFF, D., and ORLOFF, H., 1949, *J. chem. Phys.*, **17**, 1248.
[9] BALK, P., DE BRUIJN, S., and HOIJTINK, G. J., 1957, *Rec. Trav. chim. Pays-Bas*, **76**, 860.
[10] METTE, H., and PICK, H., 1953, *Z. Phys.*, **134**, 560.

# Molecular two-centre integrals between 2 $p\pi$ and 3 $p\pi$ atomic orbitals
## III. Penetration integrals

by ALF LOFTHUS

Department of Physics, University of Oslo, Blindern, Oslo, Norway

The evaluation of two-centre Coulomb-penetration and exchange-penetration integrals is discussed. All possible penetration integrals between $2p\pi$ and $3p\pi$ atomic orbitals exponent α are reduced analytically and tabulated for $\alpha = 1.00$ (0.25) 10.00.

## 1. INTRODUCTION

In quantum-chemical calculations the potential of an electron in the field of a neutral atom must sometimes be considered. This potential is represented by an operator denoted $H_a^*(1)$, where $a$ indicates the atom, and 1 the electron under consideration. The penetration integrals are then defined as follows:

Coulomb-penetration: $Q = (\psi_b | -H_a^* | \psi_b') = -\int H_a^*(1)\psi_b(1)\psi_b'(1)\,d\tau_1,$

Exchange-penetration: $R = (\psi_a | -H_a^* | \psi_b') = -\int H_a^*(1)\psi_a(1)\psi_b'(1)\,d\tau_1,$ \qquad (1)

where $\psi$ and $\psi'$ denote various atomic orbitals. (The minus sign is introduced to make the integrals positive.)

As pointed out by Barnett and Coulson [4], the Coulomb-penetration integral measures the energy of one electron based on one atom $(b)$, due to the field of a different, neutral atom $(a)$. The exchange-penetration integral measures the resonance energy between two orbitals, one of which is based on the neutral atom.

The penetration integrals were first introduced by Goeppert-Mayer and Sklar [1] in their pioneer work on the ASMO method, applied to benzene. They showed that the penetration operator could be written

$$H_a^*(1) = -\int_{r_{a1}}^{\infty} (r/r_{a1} - 1)\sigma(r)r\,dr \qquad (2)$$

where $r_{a1}$ denotes the distance of the electron (1) from the nucleus $(a)$, and where

$$\sigma(r) = 4\pi\{|\psi_{2s}|^2 + |\psi_{2px}|^2 + |\psi_{2py}|^2 + |\psi_{2pz}|^2\}. \qquad (3)$$

(The various atomic orbitals are defined below, equation (8).)

Explicit formulae for $\sigma(r)$ and $H_a^*(1)$ were not given by Goeppert-Mayer and Sklar, but following Parr and Crawford [3] we readily have

$$\sigma(r) = 2k^3 \exp(-2kr)(2 - 4kr + 4(kr)^2), \qquad (4)$$

and (in atomic units $e^2/a_0 = 27.206$ ev),

$$H_a^*(1) = -(2/r_{a1})\exp(-2kr_{a1})(2 + 3kr_{a1} + 2(kr_{a1})^2 + (kr_{a1})^3), \qquad (5)$$

where $k$ is the orbital exponent (equation (8)).

It must here be noted that Parr and Crawford used the hydrogen-like instead of the (node-less) Slater-type $2s$ atomic orbitals. (Hydrogen-like and Slater-type $2p\pi$ orbitals are the same.) This is of course an advantage, but if Slater orbitals are used elsewhere in calculations where penetration integrals are involved, it may be more appropriate to use Slater orbitals throughout.

O

Using Slater-type $2s$ orbitals, we have now instead of (4) and (5),

$$\sigma(r) = (16/3)k^3 \exp(-2kr)(kr)^2 \tag{6}$$

and

$$H_a^*(1) = -(2/r_{a1}) \exp(-2kr_{a1})(2 + 3kr_{a1} + 2(kr_{a1})^2 + (2/3)(kr_{a1})^3). \tag{7}$$

The purpose of the present work is to evaluate analytically all possible penetration integrals between $2p\pi$ and $3p\pi$ orbitals with equal orbital exponent, when hydrogen-like as well as Slater-type $2s$ AO are used.

The orbitals involved here are of the form

$$
\left.
\begin{aligned}
\psi_{2s} &= (k^5/\pi)^{1/2} \exp(-kr)r & \text{Slater-type,} \\
\psi_{2s} &= (k^3/\pi)^{1/2} \exp(-kr)(1-kr) & \text{Hydrogen-like,} \\
(2p\pi) = \psi_{2px} &= (k^5/\pi)^{1/2} \exp(-kr)r \sin\vartheta \cos\varphi, \\
\psi_{2py} &= (k^5/\pi)^{1/2} \exp(-kr)r \sin\vartheta \sin\varphi, \\
\psi_{2pz} &= (k^5/\pi)^{1/2} \exp(-kr)r \cos\vartheta, \\
(3p\pi) = \psi_{3px} &= (2k^7/\pi)^{1/2} \exp(-kr)r^2 \sin\vartheta \cos\varphi,
\end{aligned}
\right\} \tag{8}
$$

where $k = Z/2a_0$, $Z$ the effective nuclear charge, and $a_0 = 0.5292$ Å is the Bohr radius.

## 2. Results

There are altogether three Coulomb-penetration and four exchange-penetration integrals which can be constructed from $2p\pi$ and $3p\pi$ orbitals :

$$
\left.
\begin{aligned}
Q_0 &= (2p_b | -H_a^* | 2p_b), & R_0 &= (2p_a | -H_a^* | 2p_b), \\
Q_1 &= (3p_b | -H_a^* | 3p_b), & R_1 &= (3p_a | -H_a^* | 3p_b), \\
Q_2 &= (3p_b | -H_a^* | 2p_b), & R_2 &= (3p_a | -H_a^* | 2p_b), \\
& & R_3 &= (2p_a | -H_a^* | 3p_b).
\end{aligned}
\right\} \tag{9}
$$

On introducing elliptical coordinates, these integrals were reduced analytically ; general methods of integration are outlined elsewhere [6]. The resulting formulae, given as functions of $\alpha = kR = ZR/2a_0$, where $R$ is the internuclear distance, are listed in table 1. From these formulae numerical values were calculated for $\alpha = 1.00\ (0.25)\ 10.00$; and these are listed in table 2. These values, obtained by an electronic computer, are believed to be correct to $\pm 1$ in the last figure.

To check the calculations, all integrals were recalculated numerically for $\alpha = 4.00$ by means of the Barnett–Coulson method [4], and agreement was found.

A few scattered values for some of the penetration integrals, agreeing with the present, are found elsewhere in the literature [1–5].

## REFERENCES

[1] GOEPPERT-MAYER, M., and SKLAR, A. L., 1938, *J. chem. Phys.*, **6**, 645.
[2] SKLAR, A. L., and LYDDANE, R. H., 1939, *J. chem. Phys.*, **7**, 374.
[3] PARR, R. G., and CRAWFORD, B. L., 1948, *J. chem. Phys.*, **16**, 1049.
[4] BARNETT, M. P., and COULSON, C. A., 1951, *Phil. Trans.* A, **243**, 221.
[5] JACOBS, J., 1949, *Proc. phys. Soc., Lond.*, **62**, 710; 1955, *Ibid.*, **68**, 72.
[6] PREUSS, H., 1956, *Integraltafeln zur Quantenchemie* (Berlin: Springer-Verlag).

| (a) Hydrogen-like $2s$ AO |
|---|

$$Q_0 = (2p_b|-H_a^*|2p_b) = \exp(-2\alpha)\{(75/256) + (75/128)\alpha + (461/960)\alpha^2$$
$$+ (43/240)\alpha^3 + (67/1680)\alpha^4 + (1/210)\alpha^5\}Z(e^2/a_0)$$

$$Q_1 = (3p_b|-H_a^*|3p_b) = \exp(-2\alpha)\{(17/192) + (17/96)\alpha + (1597/9600)\alpha^2$$
$$+ (1391/14400)\alpha^3 + (1871/50400)x^4 + (53/6300)\alpha^5 + (47/37800)\alpha^6$$
$$+ (1/9450)\alpha^7\}Z(e^2/a_0)$$

$$Q_2 = (3p_b|-H_a^*|2p_b) = (2/15)^{1/2}\exp(-2\alpha)\{(409/1024) + (409/512)x + (909/1280)\alpha^2$$
$$+ (2387/6720)\alpha^3 + (349/3360)\alpha^4 + (61/3360)\alpha^5 + (1/560)\alpha^6\}Z(e^2/a_0)$$

$$R_0 = (2p_a|-H_a^*|2p_b) = \{\exp(-\alpha)[(1701/512)\alpha^{-3} + (1701/512)\alpha^{-2}$$
$$- (629/128)\alpha^{-1} + (19/8)] - \exp(-3\alpha)[(1701/512)\alpha^{-3} + (5103/512)\alpha^{-2}$$
$$+ (67/8)\alpha^{-1} + (213/64) + (11/16)\alpha + (1/16)\alpha^2]\}Z(e^2/a_0)$$

$$R_1 = (3p_a|-H_a^*|3p_b) = \{\exp(-\alpha)[-(26931/5120)\alpha^{-3} - (26931/5120)\alpha^{-2}$$
$$+ (37923/5120)\alpha^{-1} - (801/256) + (469/640)\alpha]$$
$$+ \exp(-3\alpha)[(26931/5120)\alpha^{-2} + (80793/5120)\alpha^{-1}$$
$$+ (11399/1920) + (479/320)\alpha + (13/60)\alpha^2 + (7/480)\alpha^3]\}Z(e^2/a_0)$$

$$R_2 = (3p_a|-H_a^*|2p_b) = (2/15)^{1/2}\{\exp(-\alpha)[(27243/2048)\alpha^{-3} + (27243/2048)\alpha^{-2}$$
$$- (4005/256)\alpha^{-1} + (1407/256)] - \exp(-3\alpha)[(27243/2048)\alpha^{-3}$$
$$+ 81729/2048)\alpha^{-2} + (19233/512)\alpha^{-1} + (2323/128) + (327/64)\alpha$$
$$+ (53/64)\alpha^2 + (1/16)\alpha^3]\}Z(e^2/a_0)$$

$$R_3 = (2p_a|-H_a^*|3p_b) = (2/15)^{1/2}\{\exp(-\alpha)[-(17961/2048)\alpha^{-3}$$
$$- (17961/2048)\alpha^{-2} + (7619/512)\alpha^{-1} - (1887/256) + (19/8)\alpha]$$
$$+ \exp(-3\alpha)[(17961/2048)\alpha^{-3} + (53883/2048)\alpha^{-2} + (5171/256)\alpha^{-1}$$
$$+ (927/128) + (43/32)\alpha + (7/64)\alpha^2]\}Z(e^2/a_0)$$

| (b) Slater $2s$ AO |
|---|

$$Q_0 = (2p_b|-H_a^*|2p_b) = \exp(-2\alpha)\{(35/128) + (35/64)\alpha + (71/160)\alpha^2$$
$$+ (19/120)\alpha^3 + (9/280)\alpha^4 + (1/315)\alpha^5\}Z(e^2/a_0)$$

$$Q_1 = (3p_b|-H_a^*|3p_b) = \exp(-2\alpha)\{(61/768) + (61/384)\alpha + (179/1200)\alpha^2$$
$$+ (623/7200)\alpha^3 + (119/3600)\alpha^4 + (91/12600)\alpha^5 + (2/2025)\alpha^6$$
$$+ (1/14175)\alpha^7\}Z(e^2/a_0)$$

$$Q_2 = (3p_b|-H_a^*|2p_b) = (2/15)^{1/2}\exp(-2\alpha)\{(187/512) + (187/256)\alpha + (1241/1920)\alpha^2$$
$$+ (51/160)\alpha^3 + (151/1680)\alpha^4 + (73/5040)\alpha^5 + (1/840)\alpha^6\}Z(e^2/a_0)$$

$$R_0 = (2p_a|-H_a^*|2p_b) = \{\exp(-\alpha)[(693/256)\alpha^{-3} + (693/256)\alpha^{-2}$$
$$- (265/64)\alpha^{-1} + (67/32)] - \exp(-3\alpha)[(693/256)\alpha^{-3} + (2079/256)\alpha^{-2}$$
$$+ (107/16)\alpha^{-1} + (41/16) + (1/2)\alpha + (1/24)\alpha^2]\}Z(e^2/a_0)$$

$$R_1 = (3p_a|-H_a^*|3p_b) = \{\exp(-\alpha)[-(1331/320)\alpha^{-3} - (1331/320)\alpha^{-2}$$
$$+ (15337/2560)\alpha^{-1} - (1653/640) + (201/320)\alpha]$$
$$+ \exp(-3\alpha)[(1331/320)\alpha^{-3} + (3993/320)\alpha^{-2} + (5451/512)\alpha^{-1}$$
$$+ (4363/960) + (89/80)\alpha + (37/240)\alpha^2 + (7/720)\alpha^3]\}Z(e^2/a_0)$$

$$R_2 = (3p_a|-H_a^*|2p_b) = (2/15)^{1/2}\{\exp(-\alpha)[(10929/1024)\alpha^{-3} + (10929/1024)\alpha^{-2}$$
$$- (1653/128)\alpha^{-1} + (603/128)] - \exp(-3\alpha)[(10929/1024)\alpha^{-3}$$
$$+ (32787/1024)\alpha^{-2} + (7623/256)\alpha^{-1} + (451/32) + (123/32)\alpha$$
$$+ (19/32)\alpha^2 + (1/24)\alpha^3]\}Z(e^2/a_0)$$

$$R_3 = (2p_a|-H_a^*|3p_b) = (2/15)^{1/2}\{\exp(-\alpha)[-(7203/1024)\alpha^{-3}$$
$$- (7203/1024)\alpha^{-2} + (3139/256)\alpha^{-1} - (795/128) + (67/32)\alpha]$$
$$+ \exp(-3\alpha)[(7203/1024)\alpha^{-3} + (21609/1024)\alpha^{-2} + (127/8)\alpha^{-1}$$
$$+ (11/2) + (31/32)\alpha + (7/96)\alpha^2]\}Z(e^2/a_0)$$

Table 1. Formulae for two-centre Coulomb-penetration ($Q$) and exchange-penetration ($R$) integrals. ($\alpha = ZR/2a_0$; $Z$ = effective nuclear charge, $R$ = internuclear distance (Å), $a_0 = 0.5292$ Å, $e^2/a_0 = 27.206$ ev.)

A.  Lofthus

(a)  Hydrogen-like 2s AO

| α | $Q_0 =$ $(2p_b\|-H_a^*\|2p_b)$ | $Q_1 =$ $(3p_b\|-H_a^*\|3p_b)$ | $Q_2 =$ $(3p_b\|-H_a^*\|2p_b)$ | $R_0 =$ $(2p_a\|-H_a^*\|2p_b)$ | $R_1 =$ $(3p_a\|-H_a^*\|3p_b)$ | $R_2 =$ $(3p_a\|-H_a^*\|2p_b)$ | $R_3 =$ $(2p_a\|-H_a^*\|3p_b)$ |
|---|---|---|---|---|---|---|---|
| 0·00 | 2·9297 (−1) | 8·8542 (−2) | 1·4585 (−1) | 2·9297 (−1) | 8·8542 (−2) | 1·4585 (−1) | 1·4585 (−1) |
| 1·00 | 2·1423 (−1) | 7·7880 (−2) | 1·1798 (−1) | 2·2869 (−1) | 8·1169 (−2) | 1·2131 (−1) | 1·3470 (−1) |
| 1·25 | 1·8367 (−1) | 7·2238 (−2) | 1·0542 (−1) | 2·0229 (−1) | 7·7201 (−2) | 1·1007 (−1) | 1·2793 (−1) |
| 1·50 | 1·5410 (−1) | 6·5832 (−2) | 9·2323 (−2) | 1·7590 (−1) | 7·2583 (−2) | 9·8214 (−2) | 1·1984 (−1) |
| 1·75 | 1·2687 (−1) | 5·8972 (−2) | 7·9384 (−2) | 1·5076 (−1) | 6·7470 (−2) | 8·6336 (−2) | 1·1077 (−1) |
| 2·00 | 1·0274 (−1) | 5·1965 (−2) | 6·7123 (−2) | 1·2764 (−1) | 6·2035 (−2) | 7·4896 (−2) | 1·0111 (−1) |
| 2·25 | 8·1983 (−2) | 4·5083 (−2) | 5·5892 (−2) | 1·0695 (−1) | 5·6445 (−2) | 6·4218 (−2) | 9·1224 (−2) |
| 2·50 | 6·4559 (−2) | 3·8542 (−2) | 4·5889 (−2) | 8·8830 (−2) | 5·0854 (−2) | 5·4497 (−2) | 8·1434 (−2) |
| 2·75 | 5·0234 (−2) | 3·2500 (−2) | 3·7191 (−2) | 7·3222 (−2) | 4·5396 (−2) | 4·5829 (−2) | 7·1991 (−2) |
| 3·00 | 3·8663 (−2) | 2·7054 (−2) | 2·9782 (−2) | 5·9966 (−2) | 4·0177 (−2) | 3·8233 (−2) | 6·3084 (−2) |
| 3·25 | 2·9461 (−2) | 2·2251 (−2) | 2·3587 (−2) | 4·8836 (−2) | 3·5275 (−2) | 3·1672 (−2) | 5·4839 (−2) |
| 3·50 | 2·2244 (−2) | 1·8095 (−2) | 1·8490 (−2) | 3·9581 (−2) | 3·0745 (−2) | 2·6075 (−2) | 4·7327 (−2) |
| 3·75 | 1·6653 (−2) | 1·4561 (−2) | 1·4356 (−2) | 3·1947 (−2) | 2·6615 (−2) | 2·1351 (−2) | 4·0577 (−2) |
| 4·00 | 1·2369 (−2) | 1·1602 (−2) | 1·1047 (−2) | 2·5692 (−2) | 2·2896 (−2) | 1·7398 (−2) | 3·4584 (−2) |
| 4·25 | 9·1204 (−3) | 9·1592 (−3) | 8·4306 (−3) | 2·0597 (−2) | 1·9584 (−2) | 1·4117 (−2) | 2·9317 (−2) |
| 4·50 | 6·6791 (−3) | 7·1679 (−3) | 6·3838 (−3) | 1·6466 (−2) | 1·6663 (−2) | 1·1412 (−2) | 2·4730 (−2) |
| 4·75 | 4·8601 (−3) | 5·5638 (−3) | 4·7987 (−3) | 1·3133 (−2) | 1·4109 (−2) | 9·1944 (−3) | 2·0768 (−2) |
| 5·00 | 3·5153 (−3) | 4·2855 (−3) | 3·5825 (−3) | 1·0452 (−2) | 1·1893 (−2) | 7·3860 (−3) | 1·7370 (−2) |
| 5·25 | 2·5284 (−3) | 3·2770 (−3) | 2·6572 (−3) | 8·3026 (−3) | 9·9844 (−3) | 5·9177 (−3) | 1·4474 (−2) |
| 5·50 | 1·8090 (−3) | 2·4886 (−3) | 1·9590 (−3) | 6·5844 (−3) | 8·3501 (−3) | 4·7303 (−3) | 1·2020 (−2) |
| 5·75 | 1·2878 (−3) | 1·8777 (−3) | 1·4359 (−3) | 5·2141 (−3) | 6·9589 (−3) | 3·7732 (−3) | 9·9506 (−3) |
| 6·00 | 9·1248 (−4) | 1·4081 (−3) | 1·0468 (−3) | 4·1236 (−3) | 5·7808 (−3) | 3·0042 (−3) | 8·2139 (−3) |
| 6·25 | 6·4367 (−4) | 1·0497 (−3) | 7·5921 (−4) | 3·2574 (−3) | 4·7879 (−3) | 2·3879 (−3) | 6·7623 (−3) |
| 6·50 | 4·5215 (−4) | 7·7829 (−4) | 5·4794 (−4) | 2·5704 (−3) | 3·9545 (−3) | 1·8952 (−3) | 5·5536 (−3) |
| 6·75 | 3·1634 (−4) | 5·7400 (−4) | 3·9363 (−4) | 2·0264 (−3) | 3·2578 (−3) | 1·5022 (−3) | 4·5507 (−3) |
| 7·00 | 2·2049 (−4) | 4·2123 (−4) | 2·8154 (−4) | 1·5962 (−3) | 2·6775 (−3) | 1·1891 (−3) | 3·7210 (−3) |
| 7·25 | 1·5313 (−4) | 3·0764 (−4) | 2·0052 (−4) | 1·2564 (−3) | 2·1957 (−3) | 9·4033 (−4) | 3·0367 (−3) |
| 7·50 | 1·0599 (−4) | 2·2367 (−4) | 1·4225 (−4) | 9·8821 (−4) | 1·7969 (−3) | 7·4283 (−4) | 2·4737 (−3) |
| 7·75 | 7·3117 (−5) | 1·6191 (−4) | 1·0053 (−4) | 7·7679 (−4) | 1·4676 (−3) | 5·8627 (−4) | 2·0117 (−3) |
| 8·00 | 5·0285 (−5) | 1·1672 (−4) | 7·0784 (−5) | 6·1025 (−4) | 1·1966 (−3) | 4·6233 (−4) | 1·6334 (−3) |
| 8·25 | 3·4480 (−5) | 8·3812 (−5) | 4·9668 (−5) | 4·7917 (−4) | 9·7396 (−4) | 3·6432 (−4) | 1·3243 (−3) |
| 8·50 | 2·3576 (−5) | 5·9953 (−5) | 3·4737 (−5) | 3·7606 (−4) | 7·9150 (−4) | 2·8688 (−4) | 1·0722 (−3) |
| 8·75 | 1·6076 (−5) | 4·2731 (−5) | 2·4217 (−5) | 2·9501 (−4) | 6·4227 (−4) | 2·2576 (−4) | 8·6696 (−4) |
| 9·00 | 1·0934 (−5) | 3·0351 (−5) | 1·6831 (−5) | 2·3134 (−4) | 5·2045 (−4) | 1·7756 (−4) | 7·0014 (−4) |
| 9·25 | 7·4180 (−6) | 2·1485 (−5) | 1·1664 (−5) | 1·8134 (−4) | 4·2118 (−4) | 1·3958 (−4) | 5·6478 (−4) |
| 9·50 | 5·0207 (−6) | 1·5161 (−5) | 8·0608 (−6) | 1·4210 (−4) | 3·4043 (−4) | 1·0966 (−4) | 4·5509 (−4) |
| 9·75 | 3·3904 (−6) | 1·0665 (−5) | 5·5557 (−6) | 1·1132 (−4) | 2·7484 (−4) | 8·6120 (−5) | 3·6633 (−4) |
| 10·00 | 2·2845 (−6) | 7·4803 (−6) | 3·8192 (−6) | 8·7174 (−5) | 2·2164 (−4) | 6·7603 (−5) | 2·9459 (−4) |

| $R$ | $(2p_b|-H_a|2p_b)$ | $(3p_b|-H_a\cdot3|p_b)$ | $(3p_b|-H_a^n|2p_b)$ | $(2p_a|-H_a|2p_b)$ | $(3p_a|-H_a|3p_b)$ | $(3p_a|-H_a|2p_b)$ | $(3p_a|-H_a|2p_b)$ |
|---|---|---|---|---|---|---|---|
| 0·00 | 2·7344 (−1) | 7·9427 (−2) | 1·3336 (−1) | 2·7344 (−1) | 7·9427 (−2) | 1·3336 (−1) | 1·3336 (−1) |
| 1·00 | 1·9728 (−1) | 6·9740 (−2) | 1·0706 (−1) | 2·1212 (−1) | 7·2794 (−2) | 1·1034 (−1) | 1·2329 (−1) |
| 1·25 | 1·6809 (−1) | 6·4594 (−2) | 9·5284 (−2) | 1·8711 (−1) | 6·9211 (−2) | 9·9873 (−2) | 1·1709 (−1) |
| 1·50 | 1·4007 (−1) | 5·8749 (−2) | 8·3074 (−2) | 1·6229 (−1) | 6·5035 (−2) | 8·8877 (−2) | 1·0964 (−1) |
| 1·75 | 1·1450 (−1) | 5·2497 (−2) | 7·1079 (−2) | 1·3873 (−1) | 6·0410 (−2) | 7·7912 (−2) | 1·0128 (−1) |
| 2·00 | 9·2031 (−2) | 4·6124 (−2) | 5·9786 (−2) | 1·1715 (−1) | 5·5494 (−2) | 6·7403 (−2) | 9·2375 (−2) |
| 2·25 | 7·2883 (−2) | 3·9881 (−2) | 4·9509 (−2) | 9·7922 (−2) | 5·0442 (−2) | 5·7636 (−2) | 8·3269 (−2) |
| 2·50 | 5·6960 (−2) | 3·3970 (−2) | 4·0418 (−2) | 8·1140 (−2) | 4·5395 (−2) | 4·8783 (−2) | 7·4258 (−2) |
| 2·75 | 4·3988 (−2) | 2·8531 (−2) | 3·2568 (−2) | 6·6737 (−2) | 4·0475 (−2) | 4·0922 (−2) | 6·5578 (−2) |
| 3·00 | 3·3606 (−2) | 2·3651 (−2) | 2·5930 (−2) | 5·4545 (−2) | 3·5777 (−2) | 3·4059 (−2) | 5·7402 (−2) |
| 3·25 | 2·5424 (−2) | 1·9368 (−2) | 2·0417 (−2) | 4·4339 (−2) | 3·1373 (−2) | 2·8152 (−2) | 4·9845 (−2) |
| 3·50 | 1·9061 (−2) | 1·5680 (−2) | 1·5913 (−2) | 3·5875 (−2) | 2·7310 (−2) | 2·3130 (−2) | 4·2971 (−2) |
| 3·75 | 1·4173 (−2) | 1·2561 (−2) | 1·2285 (−2) | 2·8910 (−2) | 2·3612 (−2) | 1·8902 (−2) | 3·6803 (−2) |
| 4·00 | 1·0458 (−2) | 9·9627 (−3) | 9·4009 (−3) | 2·3217 (−2) | 2·0289 (−2) | 1·5376 (−2) | 3·1335 (−2) |
| 4·25 | 7·6618 (−3) | 7·8288 (−3) | 7·1351 (−3) | 1·8588 (−2) | 1·7334 (−2) | 1·2456 (−2) | 2·6536 (−2) |
| 4·50 | 5·5765 (−3) | 6·0988 (−3) | 5·3740 (−3) | 1·4842 (−2) | 1·4732 (−2) | 1·0054 (−2) | 2·2364 (−2) |
| 4·75 | 4·0339 (−3) | 4·7125 (−3) | 4·0187 (−3) | 1·1824 (−2) | 1·2460 (−2) | 8·0889 (−3) | 1·8764 (−2) |
| 5·00 | 2·9012 (−3) | 3·6135 (−3) | 2·9850 (−3) | 9·4008 (−3) | 1·0492 (−2) | 6·4896 (−3) | 1·5680 (−2) |
| 5·25 | 2·0753 (−3) | 2·7508 (−3) | 2·2032 (−3) | 7·4607 (−3) | 8·7993 (−3) | 5·1934 (−3) | 1·3055 (−2) |
| 5·50 | 1·4771 (−3) | 2·0800 (−3) | 1·6165 (−3) | 5·9117 (−3) | 7·3520 (−3) | 4·1467 (−3) | 1·0833 (−2) |
| 5·75 | 1·0462 (−3) | 1·5627 (−3) | 1·1794 (−3) | 4·6776 (−3) | 6·1216 (−3) | 3·3044 (−3) | 8·9616 (−3) |
| 6·00 | 7·3775 (−4) | 1·1669 (−3) | 8·5597 (−4) | 3·6966 (−3) | 5·0809 (−3) | 2·6285 (−3) | 7·3923 (−3) |
| 6·25 | 5·1801 (−4) | 8·6641 (−4) | 6·1812 (−4) | 2·9181 (−3) | 4·2047 (−3) | 2·0875 (−3) | 6·0819 (−3) |
| 6·50 | 3·6226 (−4) | 6·3979 (−4) | 4·4424 (−4) | 2·3012 (−3) | 3·4702 (−3) | 1·6554 (−3) | 4·9917 (−3) |
| 6·75 | 2·5238 (−4) | 4·7002 (−4) | 3·1785 (−4) | 1·8131 (−3) | 2·8567 (−3) | 1·3111 (−3) | 4·0878 (−3) |
| 7·00 | 1·7519 (−4) | 3·4361 (−4) | 2·2644 (−4) | 1·4274 (−3) | 2·3462 (−3) | 1·0372 (−3) | 3·3407 (−3) |
| 7·25 | 1·2119 (−4) | 2·5002 (−4) | 1·6067 (−4) | 1·1229 (−3) | 1·9227 (−3) | 8·1963 (−4) | 2·7249 (−3) |
| 7·50 | 8·3563 (−5) | 1·8112 (−4) | 1·1356 (−4) | 8·8284 (−4) | 1·5725 (−3) | 6·4709 (−4) | 2·2186 (−3) |
| 7·75 | 5·7439 (−5) | 1·3065 (−4) | 7·9969 (−5) | 6·9365 (−4) | 1·2836 (−3) | 5·1042 (−4) | 1·8034 (−3) |
| 8·00 | 3·9365 (−5) | 9·3866 (−5) | 5·6116 (−5) | 5·4471 (−4) | 1·0460 (−3) | 4·0230 (−4) | 1·4636 (−3) |
| 8·25 | 2·6901 (−5) | 6·7177 (−5) | 3·9246 (−5) | 4·2754 (−4) | 8·5089 (−4) | 3·1686 (−4) | 1·1861 (−3) |
| 8·50 | 1·8334 (−5) | 4·7899 (−5) | 2·7360 (−5) | 3·3542 (−4) | 6·9113 (−4) | 2·4939 (−4) | 9·5988 (−4) |
| 8·75 | 1·2463 (−5) | 3·4033 (−5) | 1·9015 (−5) | 2·6304 (−4) | 5·6055 (−4) | 1·9617 (−4) | 7·7583 (−4) |
| 9·00 | 8·4513 (−6) | 2·4099 (−5) | 1·3176 (−5) | 2·0619 (−4) | 4·5402 (−4) | 1·5423 (−4) | 6·2632 (−4) |
| 9·25 | 5·7171 (−6) | 1·7009 (−5) | 9·1048 (−6) | 1·6158 (−4) | 3·6726 (−4) | 1·2118 (−4) | 5·0504 (−4) |
| 9·50 | 3·8587 (−6) | 1·1968 (−5) | 6·2744 (−6) | 1·2658 (−4) | 2·9672 (−4) | 9·5177 (−5) | 4·0682 (−4) |
| 9·75 | 2·5987 (−6) | 8·3952 (−6) | 4·3127 (−6) | 9·9128 (−5) | 2·3945 (−4) | 7·4719 (−5) | 3·2736 (−4) |
| 10·00 | 1·7465 (−6) | 5·8723 (−6) | 2·9569 (−6) | 7·7610 (−5) | 1·9303 (−4) | 5·8634 (−5) | 2·6318 (−4) |

Table 2. Two-centre Coulomb-penetration (Q) and exchange-penetration (R) integrals, in units of $Z(e^2/a_0)$. ($\alpha = ZR/2a_0$; $Z$ = effective nuclear charge, $R$ = internuclear distance (Å), $a_0 = 0.5292$ Å, $e^2/a_0 = 27.206$ ev, $(-p) = 10^{-p}$).

# Energy levels and π bonding in polynuclear complexes

by C. K. JØRGENSEN

Office of the Science Adviser, N.A.T.O.,

Place du Maréchal de Lattre de Tassigny, Paris XVI†

and L. E. ORGEL

University Chemical Laboratory, Lensfield Road, Cambridge

The influence of π bonding of nitrogen and oxygen on the energy of the d orbitals of polynuclear iridium and ruthenium complexes is estimated from absorption spectra in the visible region.

Delépine [1] and one of the authors [2] have recently presented evidence that the green nitrido-iridium sulphates prepared by Delépine in 1909 should be formulated as $K_4[N\{Ir(H_2O)(SO_4)_2\}_3]$. These formulations imply resonance between two Ir (IV) and one Ir (III) ion in each complex unit leading to three equivalent iridium ions of intermediate valency.

The proposed formulae are closely related to those of the well-known trinuclear acetates, for example to that of the chromium compound which may be formulated to contain the $[O\{Cr(C_5H_5N)(CH_3CO_2)_2\}_3]^+$ ion [3]. It seems plausible that there is a single basic structure common to all of the compounds, involving an equilateral triangle of metal ions surrounding and coplanar with a central oxygen or nitrogen atom (figure 1 (*a*) [4]).
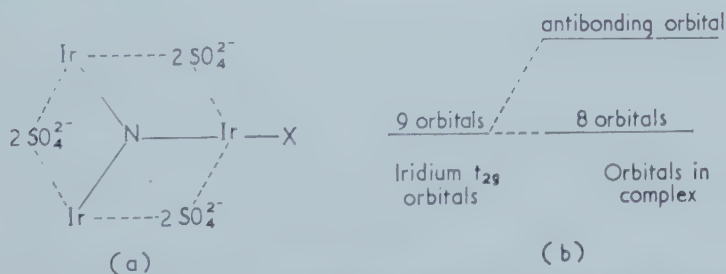


Figure 1. (*a*) Proposed structure of trinuclear iridium complexes; (*b*) proposed orbital energy scheme.

We suppose that these compounds, like all other Ir (III) and Ir (IV) complexes, are of the low-spin type. There is then room in all for eighteen electrons in the $t_{2g}$ orbitals of the three iridium atoms, each being considered to have approximately octahedral local symmetry. However, the central nitrogen atom

carries two electrons in its $p_z$ orbital† which combine with one linear combination of iridium orbitals,

$$\psi = (\phi_1 + \phi_2 + \phi_3)/\sqrt{3}$$

where $\phi_i$ is the 5d orbital on the $i$th iridium atom which is antisymmetric with respect to the iridium plane and symmetric with respect to the perpendicular plane containing the nitrogen atom and the $i$th iridium atom (cf. figure 1 of reference [4]). The bonding combination of these orbitals is stable and will always be filled, while the antibonding combination will separate out above the eight other linear combinations of $t_{2g}$ orbitals (figure 1 (b)). If we suppose that there is a tendency for this unstable antibonding orbital to remain empty we can understand the existence of the nitrido-iridium sulphates with an average metal valency of 11/3. On the reduction of Delépine's complexes the anti-bonding orbital becomes filled giving the yellow trinuclear iridium (III) complexes [2]. It is perhaps worth noting that if Lecoq de Boisbaudran's blue sulphates [2] can be formulated as $K_{10}[O\{Ir(H_2O)(SO_4)_2\}_3]$ then they contain one electron in the antibonding orbital.

From the absorption spectra of the iridium complexes [2] it can be concluded that $\pi$ bonding between the $p_z$ orbital of the nitrogen atom and the $\psi$ orbital is very strong; the transitions between 15 000 and 23 000 $cm^{-1}$ can hardly be caused by anything else but transitions from the eight filled combinations of $t_{2g}$ orbitals to the ninth orbital, that is the antibonding combination of $p_z$ and $\psi$. The identification of the symmetry types of the excited states is not possible without a thorough calculation based on reasonable estimates of the M.O. energy differences, the interelectronic repulsion parameters, and the spin orbit coupling parameter. The last factor is very important since the Landé parameter $\zeta_{5d}$ is roughly 2500 $cm^{-1}$ in the complexes [5]. However, the general picture of $\pi$ antibonding effects on the ninth $t_{2g}$ orbital amounting to some 20 000 $cm^{-1}$ is clearly established.

It is well known that the stabilization energy of a bonding M.O. in general is a good deal smaller than the destabilization of the corresponding antibonding M.O. Hence, the $\pi$ bonding stabilization of the Ir (III, IV, IV) must be of the order of 10 000 $cm^{-1}$ for each of the two electrons involved. This is significant when compared to usual bond energies (in the $H_2$, 18 000 $cm^{-1}$ per electron and in $Li_2$ only 4500 $cm^{-1}$ per electron).

We believe that the influence of $\pi$ bonding in transition-metal complexes can often be estimated most readily from absorption spectra, though in some cases chemical evidence is also convincing. Dunitz and one of the authors [6] discussed the M.O. configuration of $[Cl_5RuORuCl_5]^{4-}$ (figure 2 (a)) in which the set of six $t_{2g}$ orbitals of the two ruthenium atoms is split by a mechanism similar to that mentioned above, the two anti-bonding molecular orbitals of symmetry $\pi_g$ (figure 2 (b)) (in which oxygen p electrons participate) being empty in the ground state, leaving eight 4d electrons in a closed-shell diamagnetic M.O. configuration. The first electron transfer band [7] of the mononuclear $[RuCl_6]^{2-}$ appears at 17 100 $cm^{-1}$. Fletcher [8] has drawn our attention to the fact that the pure oxodecachloro dinuclear complex does not show such bands before 26 000 $cm^{-1}$. The main part of this shift must be attributed to the $\pi$

---

† We take the threefold axis as the $z$ axis.

antibonding effect on the empty $4d(t_{2g})$ orbitals. Actually, a weak band seems to be present at 13 800 cm$^{-1}$ for [Cl$_5$RuORuCl$_5$]$^{4-}$, presumably corresponding to the internal $xy \rightarrow (xz, yz)$ transition. In the mononuclear ion [MoOCl$_5$]$^{2-}$ the transition [9] at 14 050 cm$^{-1}$ must have the same origin.
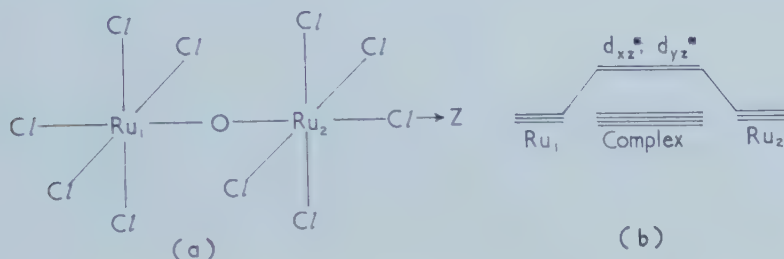


Figure 2. (a) Structure of the binuclear ruthenium complex; (b) proposed orbital energy scheme showing two antibonding orbitals.

By extrapolation from existing data [7] one deduces with great confidence that if RuCl$_6$ exists it must have a first electron-transfer band at about 7000 cm$^{-1}$. Fletcher [8] does not find the first band of the mononuclear [RuO$_2$Cl$_4$]$^{2-}$ ion until 30 500 cm$^{-1}$ (with a possible shoulder at 27 500 cm$^{-1}$). This is a most eminent proof of the stronger $\pi$ antibonding effects of oxygen than of chlorine. Recently, Lott and Symons [10] have suggested the same interaction in [OsO$_2$Cl$_4$]$^{2-}$ and [OsO$_2$(OH)$_4$]$^{2-}$.

Fletcher [8] has also studied ruthenium red and has established the average oxidation number $+ 3 \cdot 33$ and the relative composition 3Ru : 14NH$_3$. He suggests a linear structure

$$[(NH_3)_5RuORu(NH_3)_4ORu(NH_3)_5]^{6+}$$

for the complex ion [8]. Again $\pi$ bonding may explain the particular stability of this structure. Among the nine $t_{2g}$ orbitals, four ($\pi_g$ and $\pi_u$) are $\pi$ antibonding. However, it may be expected that the overlap, and hence the antibonding effects, are roughly twice as large for the $\pi_g$ orbital as for the $\pi_u$, since only the outer Ru ions are involved in the latter orbital while all are involved in the former. Thus, it is quite reasonable that the 14 electrons fill the seven lowest orbitals, leaving only the two $\pi_g$ orbitals empty. It may be noted that the complex can be reversibly oxidized in acid solution to a yellow Ru (III, IV, IV) ion. This reaction presumably involves the loss of one of the less antibonding $\pi_u$ electrons. The absorption maxima of the red (at 18 900 cm$^{-1}$) and of the yellow (at 21 800 cm$^{-1}$) forms may also indicate a large destabilization of the empty $\pi_g$ orbital, though the high intensity of the transitions may indicate that they involve electron transfer from the bonding M.O. rather than d–d transitions.

We believe that these examples indicate the way in which molecular-orbital theory can help to rationalize the stability of certain rather complicated poly-nuclear anions, although we are well aware that stereochemical considerations are also of great importance. Consideration of the d electron orbitals is likely to be specially important for the robust polynuclear complexes, sometimes involving metals in different oxidation states, which were reported long ago by

experimental chemists.  Our arguments may also apply to the more recently investigated labile hydroxy-aquo complexes [11].

REFERENCES

[1] DELÉPINE, M., 1959, *Ann. Chim.*, **4**, 1115.
[2] JØRGENSEN, C. K., 1959, *Acta chem. scand.*, **13**, 196.
[3] WEINLAND, R. F., and GUSSMANN, E., 1910, *Z. anorg. Chem.*, **67**, 167.
[4] ORGEL, L. E., 1960, *Nature, Lond.*, **187**, 504.
[5] JØRGENSEN, C. K., 1960, *Mol. Phys.*, **3**, 201.
[6] DUNITZ, J. D., and ORGEL, L. E., 1953, *J. chem. Soc.*, p. 2594.
[7] JØRGENSEN, C. K., 1959, *Mol. Phys.*, **2**, 309.
[8] FLETCHER, J. M., private communications.
[9] JØRGENSEN, C. K., 1957, *Acta chem. scand.*, **11**, 73.
[10] LOTT, K. A. K., and SYMONS, M. C. R., 1960, *J. chem. Soc.*, p. 973.
[11] SILLÉN, L. G., 1959, *Quart. Rev.*, **13**, 146.

# Electron spin resonance of γ-irradiated adipic acid

by J. R. MORTON and A. HORSFIELD

Basic Physics Division, National Physical Laboratory, Teddington, Middlesex

The radical $(CO_2H)\dot{C}H(CH_2)_3(CO_2H)$ has been detected in a γ-irradiated single crystal of adipic acid. It has been calculated from the anisotropy of the spectra on rotation of the crystal that the radicals have almost the same orientation as the undamaged molecules, although the plane of the free radical carbon is twisted approximately 10° from the original plane of the three terminal carbon atoms.

## 1. Introduction

Recent work on electron spin resonance has included studies of irradiated single crystals of the aliphatic dicarboxylic acids, $(CO_2H)(CH_2)_n(CO_2H)$ [1–5]. At least two chemically distinct species have been observed in irradiated malonic acid, the member with $n=1$, the species being $\dot{C}H(CO_2H)_2$ [1] and $\dot{C}H_2(CO_2H)$ [2]. The anisotropy of the hyperfine coupling of the α-protons (attached to free-radical carbon) was studied in both these radicals. In irradiated succinic acid ($n=2$) [3, 4] the radical $(CO_2H)\dot{C}HCH_2(CO_2H)$ was detected, and the anisotropy of the hyperfine coupling of the β-protons (attached to the carbon atom next to the free radical carbon atom) was also detected and studied. Irradiated glutaric acid ($n=3$) was examined [5] in the hope of detecting γ-proton couplings, and the two chemical species $(CO_2H)\dot{C}H(CH_2)_2$ $(CO_2H)$ and $(CO_2H)CH_2\dot{C}HCH_2(CO_2H)$. These hopes were not fulfilled, however, and only the first of these radicals was detected. This radical was found in two conformations, probably owing to the lack of the previously assumed molecular two-fold axis of symmetry.

The present investigation of adipic acid ($n=4$) was also undertaken in the hope of observing two chemically distinct species on irradiation, and further, to discover if the lack of molecular symmetry in glutaric acid was a particular or a general phenomenon in the higher dibasic acids.

## 2. Experimental

### 2.1. *Materials and Instrumental*

Small single crystals of adipic acid were grown with some difficulty from dilute (10 per cent) aqueous nitric acid solution by slow removal of water in a desiccator. The crystals formed hexagonal plates, the best developed face being the (001) face of the monoclinic crystal. Examination under the polarising microscope indicated that the crystals tended to elongate in the direction of the *b*-axis, and this was confirmed by x-ray diffraction. A single crystal was γ-irradiated at the Spent Fuel Irradiation Unit, A.E.R.E., Harwell, the total dose being five Megarads. The spectra were observed with a super-heterodyne X-band spectrometer which has already been described in the

literature [6]. The electron resonance spectra were obtained every 15° by rotating the crystal about the orthogonal $a$, $b$ and $c^*$ axes in turn. The axis of rotation was in each case held perpendicular to the magnetic field. The adipic acid molecules possess a centre of symmetry in the crystal [7], which means that the two ends of the molecule are indistinguishable. The unit cell contains two molecules related to each other by the two-fold $b$-axis. It was therefore anticipated that two magnetically distinguishable sites would be observed during rotation about the $a$ and $c^*$ axes, but that these would not be distinguishable on rotation about the $b$-axis.
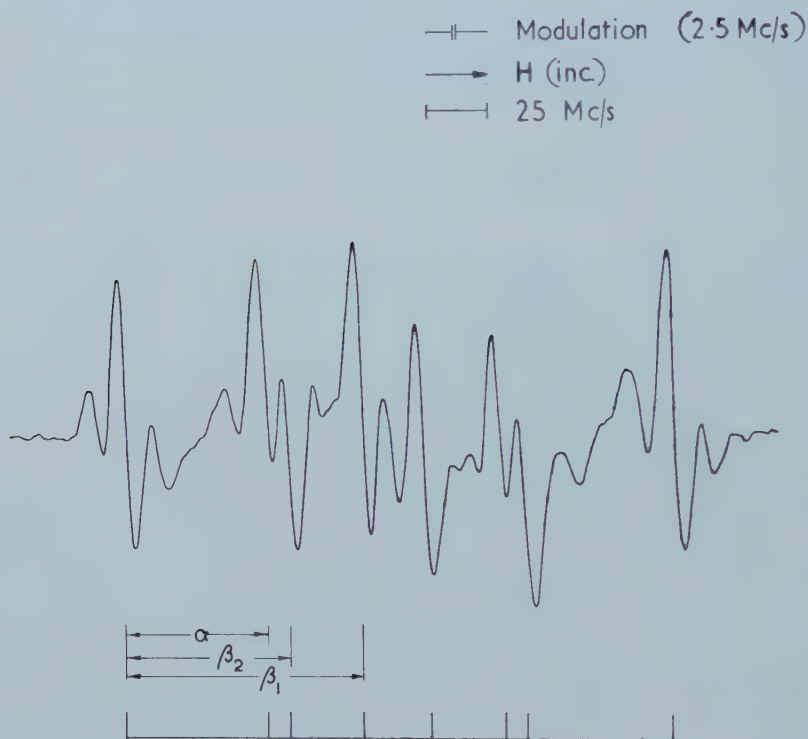


The derivative spectrum of a $\gamma$-irradiated single crystal of adipic acid (H‖$a$) after annealing at 100° c for 30 min. ' Spin-flip ' transitions 13 Mc/s on either side of the main lines are prominent in this spectrum.

## 2.2. *Analysis of the spectra*

The spectra of a freshly irradiated single crystal of adipic acid for orientations H perpendicular to $b$ were not symmetric about their own centre. This indicates the presence of more than one chemical species of radical. However, on heating the crystal to 100° c for 30 min symmetrical spectra for H perpendicular to $b$ were obtained, of which the figure is an example, and for which the orientation of the crystal was $a$ parallel to H. The spectra of annealed adipic acid were interpreted in terms of the radical $(CO_2H)\dot{C}H(CH_2)_3(CO_2H)$, and hyperfine coupling to three protons. The analysis of the spectrum of the figure is indicated, and is seen to be in terms of one $\alpha$- and two $\beta$- protons ($\beta_1$ and $\beta_2$). The analysis is based on the observed large anisotropy of the

α-proton couplings, for those orientations having *b* perpendicular to H. As explained in § 2.1 for other orientations the spectra were complicated by the presence of two magnetically distinguishable radicals. The total splitting for each radical could be determined from the still comparatively well resolved wings of the spectra. The α-proton couplings for these orientations were obtained as the difference between the total splitting and a mean $(\beta_1 + \beta_2)$ splitting of 186 Mc/s. determined for orientations *b* perpendicular to H.

No coupling to γ-protons could be detected, neither could any deductions be drawn as to the nature of the other chemical species, although the most probable radical is $(CO_2H)CH_2\dot{C}H(CH_2)_2(CO_2H)$.

# 3. Discussion

## 3.1. *The α-proton coupling tensor*

Rotation of the crystal about the crystallographic axes *a*, *b* and *c*\* enabled the α-proton coupling tensor to be determined. The tensor is given in table 1, together with its principal values and their direction cosines in the *a*, *b*, *c*\* axis system. The principal values quoted are typical of α-proton tensors [1–5] and as such have been given the negative sign required by theory [8] although this is not determined from the spectra. The least negative, intermediate, and most negative principal directions of the coupling tensor are parallel to the Ċ–H bond, perpendicular to the radical plane, and in the radical plane but perpendicular to the Ċ–H bond respectively. The orientation of the radical could therefore be compared with that of the undamaged molecule, since atomic coordinates of the latter in the *a*, *b*, *c*\* axis system are available [7].

| Tensor in *a*, *b*, *c*\* axis system | | | Principal values | Direction cosines in *a*, *b*, *c*\* axis system |
|---|---|---|---|---|
| 57·8 | ± 16·9 | 16·0 | (−) 27·8 | (0·418, ∓0·894, 0·162) |
| ± 16·9 | 38·6 | ± 16·0 | (−) 49·6 | (0·744, ±0·235, −0·626) |
| 16·0 | ± 16·0 | 74·7 | (−) 93·6 | (0·521, ±0·382, 0·763) |

Table 1. Coupling tensor (Mc/s) of α-proton in radical $(CO_2H)\dot{C}H(CH_2)_3(CO_2H)$.

From the atomic coordinates of the molecule the following vectors have been calculated: perpendicular to the plane of the three terminal carbon atoms $(-0·646, 0·381, 0·661)$; perpendicular to the plane of the carboxylic acid group $(-0·534, 0·551, 0·641)$; the internal bisector of the angle between the terminal C–C bonds $(0·459, 0·886, -0·063)$. These vectors were compared with the principal directions listed in table 1. It was clear that the lower signs were relevant, the upper signs relating to the other molecule in the unit cell. From the above vectors and the data in table 1 (lower signs) it may be calculated that the angle between the perpendicular to the plane of the three terminal carbon atoms in the molecule, and the perpendicular to the radical plane is 10·4° ± 5°. Furthermore, the angle between the perpendicular to the carboxylic acid group and the perpendicular to the radical plane is 21·9° ± 5°. It may be inferred, therefore, that the terminal carbon plane in the radical is twisted approximately

$10°$ from its position in the undamaged molecule, and that this twist is away from the plane of the carboxylic acid group. The calculated angle of $13\cdot1° \pm 5°$ between the $\dot{C}$–H bond in the radical and the internal bisector of the terminal C–C bonds in the molecule is consistent with this conclusion.

### 3.2. The β-proton coupling tensors

Owing to the complexity of the spectrum when $b$ was not perpendicular to H, it was not possible to derive the complete β-proton tensors. The maximum and minimum values of the couplings $\beta_1$ and $\beta_2$ in the (010) plane are, however, given in table 2. It will be seen that $\beta_1$ and $\beta_2$ differ considerably, but that, compared with an α-proton, their anisotropy is very small. It is this very small anisotropy in the β-proton coupling which justifies the method by which the α-proton tensor was obtained.

| Proton | Coupling in (010) plane | | Isotropic |
|---|---|---|---|
| | Maximum | Minimum | |
| $\beta_1$ | 116 | 108 | (+) 112 |
| $\beta_2$ | 76 | 72 | (+)  74 |

Table 2.   The β-proton couplings (Mc/s) in the radical $(CO_2H)\dot{C}H(CH_2)_3(CO_2H)$.

Since the average, or isotropic parts of the β-proton couplings differ, the radical plane presumably is twisted with respect to the adjacent methylene group of which the β-protons are part. This conclusion supports that already arrived at in the previous section. If the β-proton coupling is of the form $B\cos^2\theta$ as previously assumed [3, 4], and the angle of twist is $\psi$, then the observed couplings lead to the equations

$$B\cos^2(30-\psi) = 112\cdot0 \text{ Mc/s}$$
$$\text{and } B\cos^2(30+\psi) = 74\cdot5 \text{ Mc/s}$$

The solution of these equations is $\psi = 10\cdot0°$ and $B = 127$ Mc/s.

The β-proton couplings therefore support the conclusion from the α-proton anisotropy that the angle between the plane of the terminal carbon atoms in the radical and the undamaged molecule, is approximately $10°$.

### 3.3. The g-tensor

The smallest principal value of the g-tensor had direction cosines ($-0\cdot587$, $0\cdot620$, $0\cdot521$) and makes an angle of $25°$ with the intermediate axis of the α-proton tensor. Within the overall limits of the experimental error it would appear therefore that the minimum value of g lies perpendicular to the radical plane, in agreement with previous observations [1, 4, 9]. The average value of g, $2\cdot0031$, is slightly greater than the free spin value of $2\cdot0023$, as has been predicted theoretically [10].

### 3.4. *Conclusion*

The conclusions from the electron spin resonance spectra of irradiated adipic acid are similar in some respects to those from irradiated glutaric acid [5]. The glutaric acid spectra [5] were complicated by lack of a two-fold axis in the molecule, and in both cases there were the unrealized prospects of γ-proton couplings. There was evidence from the spectra of both radicals that the radical plane was twisted with respect to the original terminal carbon plane. In adipic acid it seems that the twist is away from the carboxylic acid group, and is no doubt due to intermolecular crystalline forces.

REFERENCES

[1] McCONNELL, H. M., HELLER, C., COLE, T., and FESSENDEN, R. W., 1960, *J. Amer. chem. Soc.*, **82**, 766.
[2] HORSFIELD, A., MORTON, J. R., and WHIFFEN, D. H., 1961, *Nature, Lond.*, **189**, 481.
[3] HELLER, C., and McCONNELL, H. M., 1960, *J. chem. Phys.*, **32**, 1535.
[4] POOLEY, D., and WHIFFEN, D. H., 1961, *Mol. Phys.*, **4**, 81.
[5] HORSFIELD, A., MORTON, J. R., and WHIFFEN, D. H., 1961, *Mol. Phys.* (in the press).
[6] HORSFIELD, A., MORTON, J. R., and WHIFFEN, D. H., 1961, *Trans. Faraday Soc.* (in the press).
[7] MORRISON, J. D., and ROBERTSON, J. M., 1949, *J. chem. Soc.*, p. 987.
[8] McCONNELL, H. M., and STRATHDEE, J., 1959, *Mol. Phys.*, **2**, 159.
[9] ATHERTON, N. M., and WHIFFEN, D. H., 1960, *Mol. Phys.*, **3**, 1 and 103.
[10] McCONNELL, H. M., and ROBERTSON, R. E., 1957, *J. phys. Chem.*, **61**, 1018.

# The paramagnetic Faraday effect in permanganate and titanium tetrachloride

by A. J. STONE

Department of Theoretical Chemistry, University Chemical Laboratory,
Lensfield Road, Cambridge

The paramagnetic Faraday effect in molecules which have no unpaired electrons is related to the temperature-independent paramagnetism. Comparison of the calculated and observed Verdet constants of $TiCl_4$ indicates that the excited state $t_1^{-1}2e^1$ does not lie below $t_1^{-1}3t_2^1$, as in other tetrahedral complexes, but above it.

The dispersion (i.e. variation with frequency) of the Faraday rotation of most substances is of a type described as diamagnetic. For molecules containing an unpaired electron, there is an additional term whose dispersion is of a different nature; this term is called a paramagnetic rotation. It has been found that for some substances, in particular permanganate ion, which have no unpaired electrons but exhibit temperature-independent paramagnetism, the Faraday rotation includes a paramagnetic term [1]. The purpose of this investigation was to seek a connection between the temperature-independent paramagnetism and the paramagnetic rotation.

Kramers [2] showed that the rotation of the plane of polarization, per unit length, of light travelling parallel to the applied magnetic field is given by

$$\theta = - \frac{8\pi\nu^2 N_1}{hc\bar{n}S} \sum_{0,g} \frac{\mathrm{Im}\{\langle 0|X|g\rangle\langle g|Y|0\rangle\}}{\nu^2 - \nu_{0g}^2} \exp\left(-\frac{h\nu_0}{kT}\right), \tag{1}$$

where the magnetic field is taken to be in the $z$ direction; $N_1$ = number of molecules per unit volume, $\bar{n}$ = mean refractive index, $S$ = partition function, and $\langle 0|X|g\rangle$ is the matrix element of the $x$ component of the dipole moment between states $|0\rangle$ and $|g\rangle$. The summation is over all excited states $|g\rangle$ and all occupied states $|0\rangle$. $h\nu_0$ is the energy of $|0\rangle$ relative to some arbitrary zero and $h\nu_{0g} = h\nu_g - h\nu_0$.

Molecules with an odd number of electrons have a ground state of even degeneracy [2], usually a doublet (the Kramers doublet). The paramagnetic rotation of these molecules is due to the splitting of this doublet by the magnetic field and the consequent difference in population of the two states [2], and is approximately proportional to

$$\sum_g \frac{A(g)\nu^2}{\nu^2 - \nu_{0g}^2} \tanh\frac{\lambda\beta H}{kT}, \tag{2}$$

where $A(g)$ is a constant which will depend on $|g\rangle$, $\pm\lambda\beta H$ are the Zeeman energies of the two components $|0_1\rangle$ and $|0_2\rangle$ of the doublet, and $\nu_{0g}$ is the mean of $\nu_{0_1g}$ and $\nu_{0_2g}$.

For molecules containing no unpaired electrons and having a non-degenerate ground state $|0\rangle$, (1) can be re-written as

$$\theta = - \frac{8\pi\nu^2 N_1}{hc\bar{n}} \sum_g \frac{\mathrm{Im}\{\langle 0|X|g\rangle\langle g|Y|0\rangle\}}{\nu^2 - \nu_{0g}^2}. \tag{3}$$

In this case the application of a magnetic field has two effects.    In the first place, the ground state is altered by the perturbation

$$\frac{eh}{2mc} H_z \hat{L}_z = \beta H_z \hat{L}_z,$$

and becomes, to the first order,

$$|0'\rangle = |0\rangle - \sum_{f \neq 0} |f\rangle \frac{\langle f|\beta H_z \hat{L}_z|0\rangle}{h\nu_{0f}}. \tag{4}$$

This is the effect which gives rise to the temperature-independent paramagnetic term of the magnetic susceptibility, which is [3]

$$\chi_T = \tfrac{2}{3}N_1 \sum_{f \neq 0} \frac{|\langle f|\beta H_z \hat{L}_z|0\rangle|^2}{h\nu_{0f}}. \tag{5}$$

In the second place, degenerate excited states are split by the field (the Zeeman effect).    The increase in energy of a state $|g\rangle$ is $\langle g|\beta H_z \hat{L}_z|g\rangle = \beta H_z \lambda_g$, say, so that $\nu_{0g}$ becomes

$$\nu_{0g}' = \nu_{0g}' + \frac{1}{h}\beta H_z \lambda_g.$$

Then

$$\frac{1}{\nu^2 - (\nu_{0g}')^2} = \frac{1}{\nu^2 - \nu_{0g}^2}\left\{1 + \frac{2\beta H_z \lambda_g \nu_{0g}^0}{h(\nu^2 - \nu_{0g}^2)} + \cdots\right\}. \tag{6}$$

Substituting (4) and (6) in (3), and neglecting terms of the second order and higher in $H_z$, we obtain $\theta = \theta_p + \theta_d$, where

$$\theta_p = \frac{8\pi\nu^2 N_1}{\hbar c\bar{n}} \sum_{g,f} \frac{\text{Im}\{\langle 0|X|g\rangle\langle g|Y|f\rangle\langle f|\beta H_z \hat{L}_z|0\rangle + \langle 0|\beta H_z \hat{L}_z|f\rangle\langle f|X|g\rangle\langle g|Y|0\rangle\}}{h\nu_{0f}(\nu^2 - \nu_{0g}^2)}$$

$$= \frac{32\pi^2\nu^2 N_1 \beta H_z}{h^2 c\bar{n}} \sum_{g,f} \frac{\text{Im}\{\langle 0|X|g\rangle\langle g|Y|f\rangle\langle f|\hat{L}_z|0\rangle\}}{\nu_{0f}(\nu^2 - \nu_{0g}^2)}, \tag{7}$$

$$\theta_d = -\frac{32\pi^2\nu^2 N_1 \beta H_z}{h^2 c\bar{n}} \sum_{g} \frac{\text{Im}\{\langle 0|X|g\rangle\langle g|Y|0\rangle\lambda_g \nu_{0g}\}}{(\nu^2 - \nu_{0g}^2)^2}. \tag{8}$$

$\theta_p$ varies with frequency as $\nu^2/(\nu^2 - \nu_{0g}^2)$, as does (2), and so is a paramagnetic rotation.    The dispersion of the diamagnetic rotation takes the form $\nu^2/(\nu^2 - \nu_{0g}^2)^2$, so we see that $\theta_d$ is a diamagnetic term.    We will consider $\theta_p$ first.

In permanganate ion, the ground state is $A_1$.    Since $X$ is $T_2$ and $L_z$ is $T_1$ in the tetrahedral group $T_d$, $|g\rangle$ must be a $T_2$ state and $|f\rangle$ a $T_1$ state.    The electron configuration of the ground state is $(1a_1)^2(1t_2)^6(1e)^4(2t_2)^6(t_1)^6(2e)^0(3t_2)^0(2a_1)^0$. The first two optical absorptions, at $18\,320\text{ cm}^{-1}$ and $32\,210\text{ cm}^{-1}$, are due to transitions from the ground state to $(1a_1)^2(1t_2)^6(1e)^4(2t_2)^6(t_1)^5(2e)^1(3t_2)^0(2a_1)^0$ (which will be written $t_1^{-1}2e^1$ for brevity) and to $t_1^{-1}3t_2^1$, respectively [4].    In the neighbourhood of these absorptions, the only terms in $\theta_p$ which we need consider are those for which $|g\rangle$ is $t_1^{-1}2e^1$ or $t_1^{-1}3t_2^1$, because of the denominator $(\nu^2 - \nu_{0g}^2)$. It is found that if overlap between oxygen atoms is neglected, and metal $4p$ orbitals are ignored, the only one of these terms which does not disappear is that for which $|g\rangle = t_1^{-1}2e^1(T_2)$ and $|f\rangle = t_1^{-1}3t_2^1(T_1)$.    The temperature-independent paramagnetism, on the other hand, is almost entirely due to the excited state $|f\rangle = 1t_2^{-1}2e^1(T_1)$ [5], which, to the approximations used, does not contribute to $\theta_p$ at any frequency.

In order to compare theory with experiment, it is necessary to calculate $\theta_d$ also. The three components of a $T_2$ set are $\frac{1}{2}(T_{2x}+iT_{2y})$, $T_{2z}$, and $\frac{1}{2}(T_{2x}-iT_{2y})$. The contribution to $\theta_a$ arising from these states is

$$-\frac{32\pi^2\nu^2 N_1\beta\nu_{0g}H_z}{h^2c\bar{n}(\nu^2-\nu_{0g}{}^2)^2}$$

$$\times \operatorname{Im}\{\tfrac{1}{2}\langle 0|X|T_{2x}+iT_{2y}\rangle\langle T_{2x}-iT_{2y}|Y|0\rangle\lambda_+ + \tfrac{1}{2}\langle 0|X|T_{2x}-iT_{2y}\rangle$$

$$\times \langle T_{2x}+iT_{2y}|Y|0\rangle\lambda_-\} = \frac{32\pi^2\nu^2 N_1\beta\nu_{0g}H_z\lambda_+}{h^2c\bar{n}(\nu^2-\nu_{0g}{}^2)^2}|\langle 0|X|T_{2x}\rangle|^2,$$

since $\qquad \lambda_- = -\lambda_+$ and $\langle 0|Y|T_{2y}\rangle = \langle 0|X|T_{2x}\rangle$.

The quantities required for the calculation were determined as follows: the matrix elements were calculated, using molecular orbitals which were linear combinations of Slater atomic orbitals. The orbital coefficients were found by comparing the calculated and observed [4] dipole strengths of the first two transitions. The sign of $\langle 0|X|g\rangle$ was determined by calculation. The $\nu_{0g}$ are the absorption frequencies; $\nu_{0f}$ was given the value $25\,000\text{ cm}^{-1}$, as estimated by Carrington [5]. In the case of $\theta_d$, $|\langle 0|X|T_{2r}\rangle|^2$ is obtained from the observed dipole strength, so that only $\lambda_-$ has to be calculated.

Figure 1 shows the calculated molecular Verdet constant $\Lambda$, in minutes of arc $\text{cm}^{-1}$ gauss $^1$ (mole $\text{cm}^3$)$^{-1}$, and its paramagnetic and diamagnetic parts, together with Gassmann's experimental values [1], which were obtained using dilute solid solutions of $Ba(MnO_4)_2.3H_2O$ in $Ba(ClO_4)_2.3H_2O$. The variation with temperature found by Gassmann is probably a secondary effect due to change in absorption with temperature, as he points out. If this is ignored, the calculated curve fits the experimental one quite well; the agreement is necessarily limited by the assumption that the absorption lines are infinitely sharp. We note that there
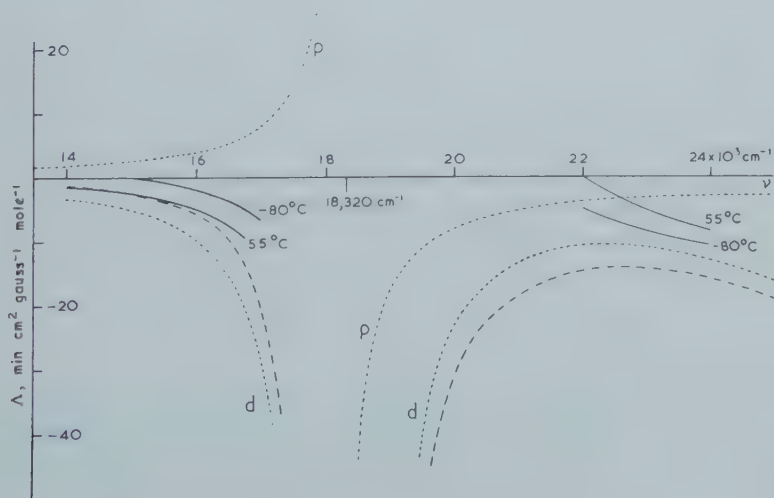


Figure 1. The magnetic rotation of $MnO_4{}^-$.
———————— Observed.
– – – – – – Calculated (total).
·················· Calculated; $p$ paramagnetic, $d$ diamagnetic.

is a connection between the temperature-independent paramagnetism and the anomalous paramagnetic rotation, in that the immediate effect of the magnetic field is the same in both cases, but that the presence in (7) of the frequency factor and the other matrix elements precludes any direct relation.

The case of titanium tetrachloride is interesting. The experimental curve [6, 7] varies very nearly as $\nu^2/(\nu^2 - \nu'^2)^2$ where $\nu' = 35\,700$ cm$^{-1}$, the frequency of the first absorption [8]. This indicates a rotation which is principally due to the diamagnetic contribution of the first absorption, which will be written as $\theta_{d_{35\,700}}$. If the absorption bands are assigned in the usual way with the first one corresponding to the $|0\rangle$ to $t_1^{-1}2e^1$ transition and the second (which is at about 45 000 cm$^{-1}$) to the $|0\rangle$ to $t_1^{-1}3t_2^1$ transition, $\theta_{d_{35\,700}}$ turns out to be small, and the principal contribution to $\theta$ comes from $\theta_{d_{45\,000}}$ with a smaller paramagnetic contribution $\theta_{p_{35\,700}}$. If the $t_1^{-1}2e^1$ state is taken to be *above* the $t_1^{-1}3t_2^1$ state, however, $\theta_{d_{35\,700}}$ is found to be quite close to the experimental value, and $\theta_p$ is small (see figure 2). This may be taken as an indication that the $t_1^{-1}2e^1$ state is above the
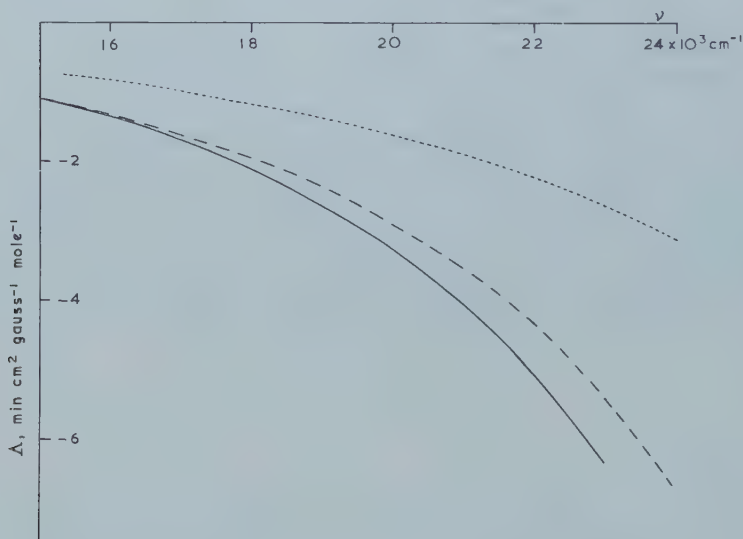


Figure 2. The magnetic rotation of TiCl$_4$.
——————— Observed.
— — — — — Calculated, assuming $t_1^{-1}2e^1$ above $t_1^{-1}3t_2^1$.
·················· Calculated, assuming $t_1^{-1}2e^1$ below $t_1^{-1}3t_2^1$.

$t_1^{-1}3t_2^1$ state, but as the normal order applies in those tetrahedral complexes which have been studied [4], further evidence is necessary to substantiate this suggestion. It should be noted, however, that this does not necessarily imply that the $2e$ orbital lies above the $3t_2$ orbital; the energies of states depend on coulomb and exchange terms, as well as orbital energies.

REFERENCES

[1] GASSMANN, G., 1939, *Ann. Phys., Lpz.*, **35**, 638.
[2] KRAMERS, H. A., 1930, *Proc. K. Neder. Akad. Weten. Amst.*, **33**, 959.
[3] VAN VLECK, 1931, *Electric and Magnetic Susceptibilities* (Oxford: University Press).
[4] CARRINGTON, A., and SCHONLAND, D. S., 1960, *Mol. Phys.*, **3**, 331.
[5] CARRINGTON, A., 1960, *Mol. Phys.*, **3**, 271.
[6] DE MALLEMANN, R., and SUHNER, F., *C.R. Acad. Sci., Paris*, **227**, 546.
[7] SIERTSEMA, L. H., 1916, *Proc. K. Neder. Akad. Weten. Amst.*, **18**, 925.
[8] MASON and VANGO, 1956, *J. phys. Chem.*, **60**, 622.

# Electron transfer spectrum of caesium rhodium (IV) hexachloride at relatively low wave-number

by CHR. KLIXBÜLL JØRGENSEN

Cyanamid European Research Institute, Cologny (Geneva), Switzerland

(*Received* 1 *May* 1961)

The dark green crystals of $Cs_2RhCl_6$ have electron transfer bands at lower wave-number than any other hexahalide complex yet studied. The transitions are compared to those occurring in analogous compounds, and the influence of covalent bonding on the orbital energies is discussed.

## 1. Introduction

Dwyer and Nyholm [1, 2] prepared $Cs_2RhCl_6$ and found by x-ray crystallography that the dark green crystals are isomorphous with $(NH_4)_2PtCl_6$. The compound is exceedingly oxidizing and owes probably its existence to a very low solubility. By contact with water, chlorine is evolved (having a rather particular smell, possibly of admixed $O_3$ or $ClO_2$) and pink Rh (III) is regenerated.

## 2. Experimental

The precipitate, resembling the dye malachite green, decomposes partly at room temperature during a few hours to a dark bluish colour, which remains for several weeks. Mixed crystals of the composition $Cs_2Rh_{0.2}Pt_{0.8}Cl_6$ were also prepared: $0.15$ g $Na_3RhCl_6$, $12H_2O$ (H. Drijfhout and Zoon, Amsterdam) and $0.56$ g $Na_2PtCl_6$, $6H_2O$ were dissolved in $10$ ml ice water, and saturated with chlorine (no colour change). $0.5$ g $(NH_4)_2 Ce(NO_3)_6$ was dissolved in $2$ ml $0.2$ M $HNO_3$, and $0.45$ g $CsCl$ in $2$ ml $H_2O$, both solutions containing small pieces of ice. After subsequent mixing, the bright green precipitate was filtered on a small piece of paper in a Büchner funnel, and not washed, but only sucked dry. The dry crystals are remarkably stable in air.

It has not yet been possible to prepare, e.g. $[N(C_4H_9)_4]_2 RhCl_6$, which presumably would be soluble in dichloroethane [3] and furnish one of the few chances of studying the ion $RhCl_6^{--}$ in solution.

The reflection spectra of $Cs_2RhCl_6$ and of the mixed crystals with $Cs_2PtCl_6$ are given in the figure, and the wave-numbers of the absorption maxima (in $kK = 1000$ cm$^{-1}$) in the table. By comparison with the spectra of analogous ions, such as $IrCl_6^{--}$ and $RuCl_6^{---}$ [4], it becomes quite evident that $RhCl_6^{--}$ has the central ion configuration low-spin $4d^5$.

As will be discussed in another paper [5], solid salts of $IrCl_6^{--}$ of alkali metal ions have their band maxima slightly shifted, compared to the aqueous solution, while much more profound changes occur in the silver (I) and thallium (I) salts. Hence, the bands of $Cs_2IrCl_6$ are also given in the table.

## 3. Theoretical Discussion

The wave-numbers of the electron transfer transitions, which previously have been theoretically interpreted [4] extrapolate in a very smooth way, going

| | Laporte-forbidden | Laporte-allowed | Laporte-allowed $\pi\gamma_{8u} \to d\gamma_{5g}$ | | |
|---|---|---|---|---|---|
| | $\pi\gamma_{4g} \to d\gamma_{5g}$ | $\pi\gamma_{5u} \to d\gamma_{5g}$ | 1 and 2 components | | Centre |
| $Cs_2RhCl_6$ | (10·0) | 12·0 | (15·6) | (16·7) | 16·3 |
| $Cs_2Rh_{0·2}Pt_{0·8}Cl_6$ | — | 12·0 | (15·8) | (16·4) | 16·0 |
| $Cs_2IrCl_6$ | 16·8 | 19·4 | — | — | 23·2 |
| $IrCl_6^{--}$ | 16·95 | 20·5 | 23·05 | 24·4 | 23·7 |
| $RuCl_6^{---}$ | 25·6 | 28·65 | Small splitting | | 32·4 |
| $OsCl_6^{---}$ | 32·6 | 35·45 | 38·2 | 39·4 | 38·8 |

Wave-numbers (in kK = 1000 cm$^{-1}$) of electron transfer bands of $4d^5$- and $5d^5$-hexachloro complexes.

from $Cs_2IrCl_6$ to $Cs_2RhCl_6$. In particular, the wave-numbers are all $\sim 7$ kK lower in $4d^n$ than in $5d^n$, as found in many other hexahalide complexes.

From one point of view, it is nearly unexpected that the extrapolation should be so linear, when we are so close to the wave-number zero. Approaching the situation of equal electronegativities of the central ion and of the halide ligand, the M.O. energies are not expected simply to cross, but to have a minimum distance roughly equal to twice the non-diagonal element of one-electron operators between the original metal orbital (belonging to the partly filled shell) and the original halide $\pi$ orbital. This argument is only strictly valid for the symmetry types also occurring in the partly filled shell, here $\gamma_{5g}$.

It would therefore be specially interesting to identify the transition $\pi\gamma_{5g} \rightarrow 4d\gamma_{5g}$ which unfortunately is the weakest of all the $\pi \rightarrow 4d$ transitions. The shoulder at 13·5 kK, perceptible in the figure, may represent this transition, in which case the splitting of $\pi\gamma_{4u} \rightarrow d\gamma_{5g}$ observable in most hexahalides (see table) should be ascribed to effects of intermediate coupling. The weak band at 21·8 kK in pure $Cs_2RhCl_6$ ($PtCl_6^{--}$ has also a weak transition there, while $RhCl_6^{---}$ has maxima at other wave-numbers) is presumably a 'ligand field' transition $\gamma_{5g} \rightarrow \gamma_{3g}$ between the two anti-bonding subshells.

Anyhow, these energy differences 13–16 kK give an absolute upper limit, some 8 kK, to the non-diagonal element between $\pi\gamma_{5g}$ and $4d\gamma_{5g}$. It is a well-known fact, as also expressed in the Helmholz Wolfsberg model [6] that, in the linear combination of orbitals from two atoms, the bonding M.O. will be stabilized slightly less and the anti-bonding M.O. de-stabilized somewhat more than the non-diagonal element $H_{ij}$, due to the occurrence of the overlap integral $S_{ij}$ in $H_{ij}-S_{ij}E$. Hence, the typical single bonds such as H–H and C–C are characterized by non-diagonal elements of the order of magnitude 20 kK, two electrons being thus stabilized.

It is a common belief that a bi-unique relation exists between the ionicity of a heteropolar, chemical bond and the difference between the electronegativities of the two atoms, i.e. the diagonal elements $H_{ii}$ and $H_{jj}$. This belief is equivalent to a roughly invariant value of all $H_{ij}$. The hypothesis seems more than dubious, since the bond-energies in homonuclear molecules vary considerably. Thus, $Cl_2$ or $Na_2$ have much smaller stabilizations than $H_2$ and C—C. There is no serious reason to believe that $H_{ij}$ in heteropolar bonds should show less variation, and it is only possible to predict that the order of magnitude will be the same.

With a second-order perturbation theory argument, the stabilization of a given M.O. is expected to be roughly $(H_{ij})/4$, if $H_{ii}-H_{jj} = 4 H_{ij}$ and so on. Energy differences between $\pi$-orbitals in hexahalides amounting to 4 kK (table) or some 8 kK in tetroxo complexes [7] suggest hence values of $H_{ij}$ 15–25 kK, when $\psi_j$ is the first, empty $p$-orbital of the central ion, while the $\pi$-bonding effect on the $d$-shell is much smaller in $RhCl_6^{--}$, as discussed above.

On the other hand, the value of $\Delta$ (the energy difference between $\gamma_{3g}$ and $\gamma_{5g}$ in octahedral complexes) in $4d^n$ and $5d^n$ hexahalides, some 20–30 kK, is now known to be mainly caused by $\sigma$-antibonding effects on $\gamma_{3g}$. The energy of the set of $\sigma$-orbitals $\gamma_{4u}$ is estimated from absorption spectra of $OsI_6^{--}$ and $PtBr_6^{--}$ [4] to be 45 kK below $\gamma_{3g}$ of the partly filled shell. Consequently, in these cases, nearly equal $H_{ii}$ occur, with $H_{ij}$ slightly smaller or slightly larger than $\Delta$.

References

[1] DWYER, F. P. J., and NYHOLM, R. S., 1947, *Nature, Lond.*, **160**, 502.
[2] DWYER, F. P., NYHOLM, R. S., and ROGERS, L. E., 1947, *Proc. roy. Soc. N.S. Wales*, **81**, 267.
[3] JØRGENSEN, C. K., to be published.
[4] JØRGENSEN, C. K., 1959, *Mol. Phys.*, **2**, 309.
[5] JØRGENSEN, C. K., *Mol. Phys.*, **4**, 235.
[6] WOLFSBERG, M., and HELMHOLZ, L., 1952, *J. chem. Phys.*, **20**, 837.
[7] CARRINGTON, A., and JØRGENSEN, C. K., *Mol. Phys.* (to be published).

# Reflection spectra of (alkali metal, thallium (I), silver (I)) iridium (IV) hexachlorides

by CHR. KLIXBÜLL JØRGENSEN

Cyanamid European Research Institute, Cologny (Geneva), Switzerland

While the effect of rubidium and caesium ions in solid salts of $IrCl_6^{--}$ is a shift to lower wave-numbers, comparable to that occurring in organic solvents relative to water, the dark blue silver (I) and thallium (I) salts have a new, broad band in the red. Mixed crystals of $Cs_2IrCl_6$ and $Tl_2IrCl_6$ are prepared, and the absorption spectra are discussed in terms of a tendency to 'ferroelectric rattling' and strong covalent bonding of Ag and Tl. Analogous cases are pointed out in solid salts of other $5d$-hexahalides.

Delépine [1] prepared dark red alkali metal salts from the aqueous, orange–brown solution of $IrCl_6^{--}$. He obtained also a dark blue-green $Tl_2IrCl_6$ and a dark blue silver (I) salt. The present author accepts Delépine's argument that the latter material really is $Ag_2IrCl_6$ and not some hydroxo compound like the blue, colloidal iridium (IV) compounds, though it is known that, e.g. $Ag_2PtCl_6$ may decompose to $Ag_2PtCl_4(OH)_2$ with an excess of $Ag^+$ removing the chloride. The chemical behaviour of Delépine's silver salt is rather remarkable; if more than two $Ag^+$ is added per mole of $IrCl_6^-$, a rather spontaneous reduction to the yellow iridium (III) hexachloride takes place [1]:

$$2Ag_2IrCl_6 + 2Ag^+ + H_2O \longrightarrow 2Ag_3IrCl_6 + 2H^+ + O \qquad (1)$$
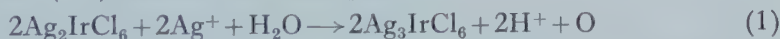
and in general, the blue $Ag_2IrCl_6$ is rather difficult to keep for more than a few hours.

The deviation from the principle of additivity of ionic colours is rather conspicuous, and the present author therefore measured the reflection spectra of a series of iridium (IV) hexachlorides. Figure 1 shows the spectra of $Cs_2IrCl_6$ and $Tl_2IrCl_6$ and of the mixed crystals containing 20 per cent and 50 per cent thallium.

Further, the spectrum of $Ag_2IrCl_6$ is indicated. While $Cs_2IrCl_6$ has roughly the same spectrum as the aqueous solution, but shifted some 4 per cent to lower wave-number, all the salts containing the two heavy metals develop a broad band between 750 and 550 m$\mu$. This band seems to be somewhat stronger than the narrow electron transfer bands (caused by transfer of $\pi$ electrons from the chloride ligands to the single hole in the nearly filled $\gamma_{5g}$ subshell in the central ion [2]) since the last of these bands at $\sim 440$ m$\mu$ is only visible as a weak shoulder in the silver salt.

Before attempting a theoretical interpretation of the corresponding energy levels, it is worth contemplating the crystal structure $A_2MX_6$ of cubic symmetry, which is remarkably common among solid hexahalide complexes. Figure 2 shows a unit cell (containing 4 $MX_6$ groups arranged in a regular tetrahedron) and the atoms in the three first layers I, II, and III. The layers I and III only contain A atoms, while two of the four M atoms in the unit cell are situated in
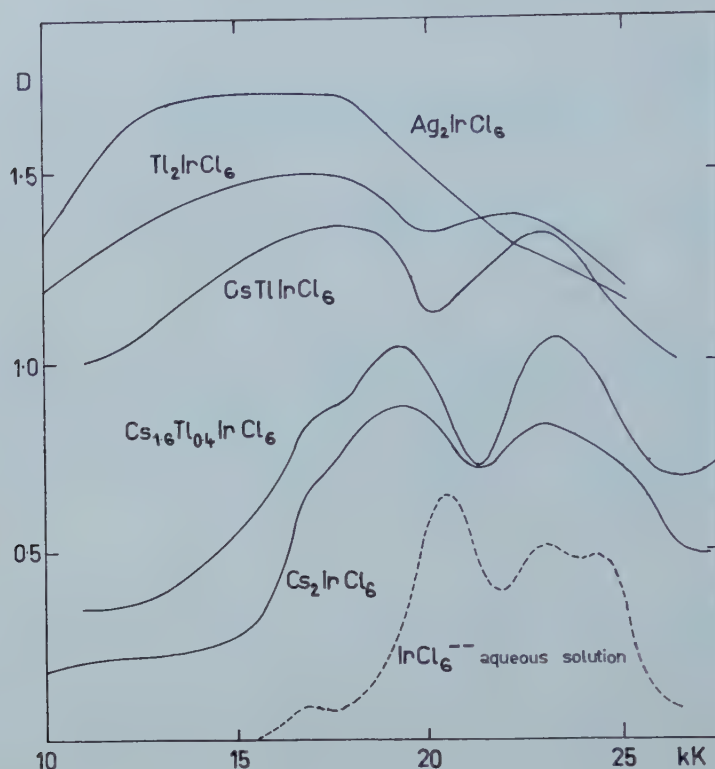
Figure 1.   Optical density D as function of wave-number (1 kK = 1000 cm$^{-1}$).

layer B, circumscribed by a regular octahedron consisting of six X. Each A is surrounded by twelve X, disposed in four equilateral triangles with the four three-fold axes of the cubic symmetry in the centres.   Each group $MX_6$ is surrounded by eight A in a regular cube, and have twelve other $MX_6$ groups as nearest neighbours.   Owen [3] pointed out that the superexchange phenomenae between adjacent iridium atoms are conducted via the two bridges of double chlorine atoms, two such bridges being exemplified in layer II on figure 2.
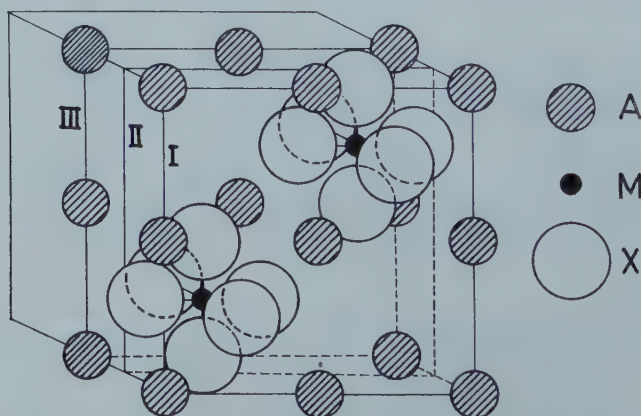


Figure 2.

The lattice parameter **a** (here the length of a side of the unit cell) does not depend in a very clear-cut way on the ionic radii $r_A$, $r_M$, and $r_X$. The lattice, considered as a fluorite structure of A and $MX_6$ would give

$$\mathbf{a}\sqrt{3} = 4r_A + 4r(MX_6) \tag{2}$$

which distinctly does not hold, if $MX_6$ is considered as a spherical entity with the radius $r_M + 2r_X$. The octahedrons are adapted to the presence of the eight A considerably closer to M. Group theory does not demand any special position of the X atoms. If however their centres are on the adjacent layers in figure 2,

$$\mathbf{a} = 4r_M + 4r_X. \tag{3}$$

This relation seems rather accurate for $K_2PtCl_6$, having $\mathbf{a} = 9.725$ Å, while the $MX_6$ groups must be more distant in $Cs_2PtCl_6$ with $\mathbf{a} = 10.192$ Å. If the rich material of **a** parameters [4] is studied as function of A, M and X, it transpires that for smaller $r_A$, there is only a quite small variation of **a** with A, suggesting relation (3), while with larger $r_A$ (Rb, Cs, $N(CH_3)_4$), **a** seems to contain linear contributions somewhere between 1.5 and 2 times the change of $r_A$ and roughly $4r_X$ (Cl compared with Br) still somewhat less than expected from (2).

This indicates the possibility of 'rattling' of A in the holes between the $MX_6$ groups, when $r_A$ is smaller than a certain threshold value, possibly close to the ionic radius of $Rb^+$, 1.49 Å, in our case. Orgel [5] gave a general explanation of ferroelectricity in terms of these rattling opportunities, but the present author is not aware of studies of the individual or collective vibration modes in $A_2MX_6$ crystals. Anyhow, it is well known that $K^+$ is the lower limit of $r_A$, before the $A_2MX_6$ structure breaks down, and $K_2SnBr_6$ and $K_2TeCl_6$ are actually somewhat distorted.

The Goldschmidt radii of $Ag^+$ and $Tl^+$ being 1.13 and 1.44 Å respectively, it would not be unexpected if a certain local distortion would bring the ions close to a few of the surrounding $MX_6$ groups. Said in another way, the coordination number 12 of A in figure 2 seems much too high for silver and thallium. These metric and electrostatic arguments, which would be valid already for anhydrous $Li^+$, are reinforced by the peculiar stereochemistry of covalent bonds of these two elements [6].

Returning to our optical transitions, the filled 4d-shell of $Ag^+$ and the filled 6s-shell of $Tl^+$ might be suspected to transfer electrons to the $\gamma_{5g}(5d)$ sub-shell of $IrCl_6^{--}$. Silver (I) complexes with a centre of inversion have their first empty odd orbital (behaving as 5p close to the silver nucleus) at a very high energy; and consequently, the electron transfer must go to the empty even orbital, approximately being 5s. Fromherz and Menschick [7] found in silver (I) halogen complexes that transitions $4d \longrightarrow 5s$ occur at only a few kK ($1\,kK = 1000\,cm^{-1}$) higher wave-number than $\pi$ chloride $\rightarrow 5s$. Consequently the M.O. energy of the highest filled sub-shell of Ag (I) should be only 5 kK higher than the filled ligand orbitals. Good arguments can be found [8] that 6s has much higher energy than the halide orbitals in thallium (I) complexes.

Hence, it might seem very natural that electron transfer occurs in $Tl\,IrCl_6$ and $Ag_2IrCl_6$ at some 5 to 8 kK lower wave-number than in the isolated $IrCl_6^{--}$. However, this would be neglecting the large influence of interelectronic repulsion parameters on electron transfer transitions between fairly distant atoms. For instance, it is clear that the position of the band $\sim 30\,kK$ of iridium (III) pyridine complexes [9] representing a transition from the $\gamma_{5g}$ sub-shell of Ir (III) to the

empty $\pi^*$ orbitals of pyridine by no means correspond to the relative electro-negativities of the two sets of orbitals, but are increased by at least 20 kK by the separation effects [8]. In the same way, a binuclear complex with weakly inter-acting metal atoms, such as $ox_2Cr(OH)_2Cr\ ox_2^{-4}(ox^{--} = C_2O_4^{--})$ is not expected to have very low wave-numbers for transitions Cr (III), Cr (III) $\rightarrow$ Cr (II), Cr (IV), though by definition the electronegativities of the two $3d$ subshells are the same.

As discussed above, it would probably not be permitted to use arguments from the full cubic symmetry for Ag (I) and Tl (I) in the dark-coloured iridium (IV) hexachlorides. It is not easy to give a convincing proof that the separation effect might be sufficiently small to place the proposed electron transfer bands at the observed position. A not too close analogy may be found in the ion-pair $Co(NH_3)_6I^{++}$ as compared with $Co(NH_3)_5I^{++}$. The former ion-pair has a broad absorption maximum at 37 kK [10–12] as compared with the first strong band at 26·1 kK of the iodo-complex. However, the possible interaction between several monovalent ions and several $IrCl_6^{--}$ groups may be much more compli-cated in our solids.

On the other hand, it cannot be argued that many other metal ions are much more reducing than $Ag^+$ and $Tl^+$ and consequently should give electron transfer bands at even lower wavenumbers. While chemical reactions would occur with $Fe(H_2O)_6^{++}$, ions such as $Mn(H_2O)_6^{++}$ would still be more reducing than $Ag^+$. However, all such ions would be hydrated and hence have a radius about 3 Å, much larger than $Cs^+$, and having much greater separation effects on the electron transfer spectrum. Actually, $Na^+$, $Li^+$ and $H^+$ introduce also 3 $H_2O$ per positive ion in their very soluble iridium (IV) hexachlorides [1]; it is not known whether these salts retain a crystal structure resembling $A_2MX_6$.

Similar deviations from the additivity of ionic colours occur in many other $5d$-hexahalides. The effect of small ionic size of $K^+$ [2] is evident in the dark-red $K_2OsCl_6$, compared with yellow $[N(C_2H_5)_4]_2\ OsCl_6$ or solutions of $OsCl_6^{--}$; or dark-red $K_2ReBr_6$ versus yellow $[N(CH_3)_4]_2\ ReBr_6$; and cannot be explained as an effect of grain size. This phenomenon is probably caused by two different tendencies: analogous to the effect of organic solvents, $K^+$ and $Rb^+$ shift the bands $\pi\gamma_{5u} \rightarrow 5d\gamma_{5g}$ and $\pi\gamma_{4u} \rightarrow 5d\gamma_{5g}$ to lower wave-numbers, which seem to be related to decreased interatomic distances [13]; and the first, Laporte-forbidden transition $\pi\gamma_{4g} \rightarrow 5d\gamma_{5g}$ becomes intensified and broadened by inter-action between adjacent $MX_6$ groups, which may be rather strong (cf. equation (3)) in potassium salts. The halogen–halogen anti-bonding effects, which are already rather strong on $\pi\gamma_{4g}$ in the isolated $MX_6$, would be accentuated in the anti-bonding combinations with the 24 closely adjacent halides on the 12 closest $MX_6$ neighbours.

Rosenheim and Sasserath [14] prepared the indigo–blue cheesy precipitate $Ag_2OsBr_6$ from the red–orange solution of $OsBr_6^{--}$. Violet solutions of $IrBr_6^{--}$ (even in methanol) immediately decompose with $Ag^+$, forming the greenish-yellow $Ag_3IrBr_6(?)$. Thallium (I) perchlorate produces a similar precipitate with $IrBr_6^{--}$, which however becomes grey with bromine water. Here it is difficult to exclude formation of Tl (III). No doubt, the possibility of forming anhydrous, and fairly covalent salts of Ag (I) and Tl (I) changes the chemical behaviour of the $5d$-hexahalides much from that of the isolated ions $MX_6^{--}$.

## EXPERIMENTAL

Solutions were prepared of $0.1$ M $Na_2IrCl_6$, $6H_2O$ in $1$ M $HClO_4$ ($5.60$ g from H. Drijfhout and Zoon, Amsterdam, to $100$ ml), $0.1$ M $TlClO_4$ in $0.1$ M $HClO_4$ (from B.D.H. thallium (I) carbonate), $0.04$ M $CsClO_4$ (from $3.4$ g CsCl in $20$ ml water, added $4$ ml $10$ M AnalaR perchloric acid, the white $CsClO_4$ washed with ice water, and dissolved in $500$ ml hot water) and $0.1$ M $AgClO_4$ (from $Ag_2O$ and $HClO_4$) and stoichiometric amounts mixed.

The precipitates were either filtered on paper and measured on the reflection attachment to the Beckman DU spectrophotometer every $20$ or $10$ m$\mu$, or (since the crystals are very small and difficult to filter) the slurry of the precipitate put on a porous porcelain assiette, which was cut after drying in the air. The measurements of the dark-grey $CsTlIrCl_6$ were not very reproducible, and the relative optical density in figure 1 cannot be considered reliable.

## REFERENCES

[1] DELÉPINE, M., 1917, *Ann. Chim.*, **7**, 277.
[2] JØRGENSEN, C. K., 1959, *Mol. Phys.*, **2**, 309.
[3] OWEN, J., 1958, *Disc. Faraday Soc.*, **26**, 53.
[4] LANDOLT-BÖRNSTEIN, 1955, *Zahlenwerte . . .* , 6. Auflage, I.Band, 4. Teil, Kristalle, (Berlin: Springer Verlag).
[5] ORGEL, L. E., 1958, *Disc. Faraday Soc.*, **26**, 138.
[6] ORGEL, L. E., 1958, *J. chem. Soc.*, p. 4186, 1959, p. 3815.
[7] FROMHERZ, H., and MENSCHICK, W., 1929, *Z. Phys. Chem. B*, **3**, 1.
[8] JØRGENSEN, C. K., 1961, *Absorption Spectra and Chemical Bonding in Complexes* (London: Pergamon).
[9] JØRGENSEN, C. K., 1957, *Acta chem. scand.*, **11**, 166.
[10] LINHARD, M., 1944, *Z. Elektrochem.*, **50**, 224.
[11] EVANS, M. G., and NANCOLLAS, G. H., 1953, *Trans. Faraday Soc.*, **49**, 363.
[12] KING, E. L., ESPENSON, J. H., and VISCO, R. E., 1959, *J. phys. Chem.*, **63**, 755.
[13] JØRGENSEN, C. K. (to be published).
[14] ROSENHEIM, A., and SASSERATH, E. A., 1899, *Z. anorg. Chem.*, **21**, 122.

# Excess charges in carbonium ions and their influence on the magnetic shielding of hydrogen

by C. MACLEAN and E. L. MACKOR

Koninklijke/Shell-Laboratorium, Amsterdam

(Shell Internationale Research Maatschappij N.V.)

*(Received* 15 *January* 1961)

The N.M.R. spectra at 40 Mc/s of a number of aromatic carbonium
ions are presented. The chemical shifts of the various types of hydrogen
are discussed in terms of localized charges and $\pi$-electron ring currents. It is
concluded that the excess charges are more uniformly distributed than pre-
dicted on the basis of simple molecular orbital calculations.

## 1. Introduction

When an aromatic molecule is transformed into its conjugate acid by protona-
tion the magnetic shielding of the hydrogens is modified in two different ways.
In the first place protonation causes large excess charges on various carbon atoms
which are reflected in the chemical shift of the adjacent hydrogen atoms. Secondly
the introduction of a $CH_2$ group in a conjugated system necessitates the interruption
of a $\pi$-electron path, thereby decreasing the number of ring currents [1]. In the
discussion of the N.M.R. spectra of aromatic carbonium ions given in the present
paper the observed chemical shifts are first corrected for the effect of ring currents
and the remaining shifts are then compared with localized charge densities pre-
dicted on the basis of M.O. theories.

For the experimental details we refer to a previous paper [2] in which high-
resolution spectra of a number of aromatic carbonium ions, measured at 40 Mc/s,
were given. The conjugate acid ions were obtained by dissolving basic aromatic
hydrocarbons in strong acids. If N.M.R. spectra are to be recorded, the basicity
should be sufficiently high because proton exchange can lead to blurring [2].
Methyl substitution enhances the basicity considerably and stable aromatic
carbonium ions could in general more easily be obtained from methyl-substituted
aromatic molecules [3]. The temperature is 22 c unless stated otherwise.

Before analysing the magnetic shielding of the substituent methyl groups in
these ions we shall discuss the effect of $\pi$-electron ring currents on their chemical
shift as derived from the spectra of neutral molecules.

### 1.1. *Effect of ring currents on chemical shifts of substituted methyl groups*

The chemical shifts of hydrogens in methyl groups substituted in a number of
aromatic molecules ($\nu_{methyl}$) have been measured together with those of the ring
hydrogens in the corresponding position in the unsubstituted molecule ($\nu_{ar}$).
The results are collected in tables 1 and 2.

On the basis of the ring-current model [1] one may calculate the contributions
of the ring current for the different types of hydrogen in these molecules. The
constants used in the calculation were: radius aromatic ring: 1·4 Å, average
distance ring carbon atom methyl hydrogen: 1·8 Å. The data in the tables

M.P.

Q

confirm the assumptions of Pople *et al.* [1] for the shifts of the ring hydrogens and show their calculations to be also valid for methyl groups in aromatic molecules. More in particular, one would expect a linear relationship between $\nu_{methyl}$ and $\nu_{ar}$ and this is indeed found (figure 1). Hydrogen atoms in positions adjacent to the more olefinic double bond between carbon atoms 9 and 10 in phenanthrene and 3 and 4 in 1, 2-benzanthracene seem to be exceptions.
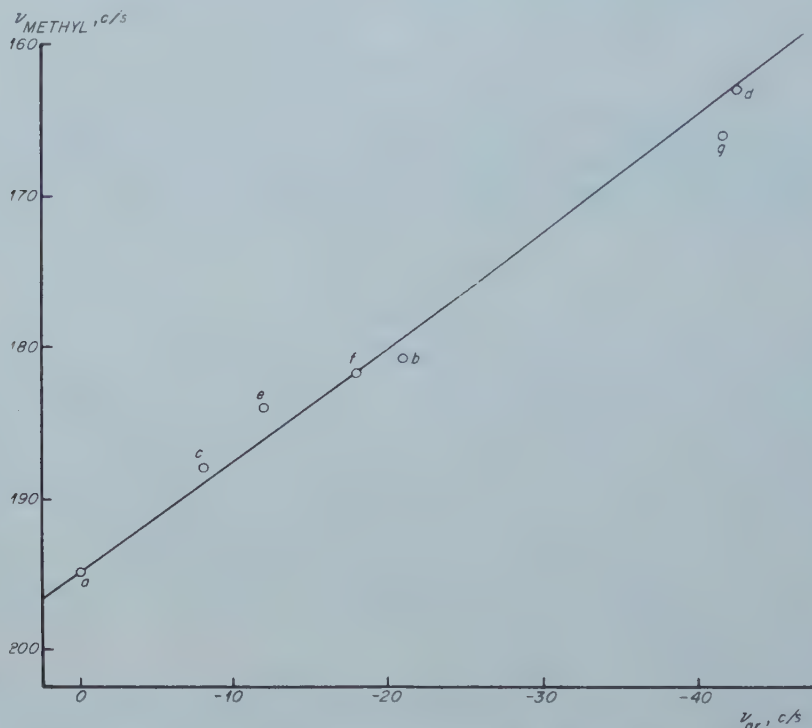


Figure 1.   Chemical shifts in c/s of hydrogens in substituted methyl groups plotted against shifts of aromatic hydrogens in the corresponding positions in the unsubstituted molecule (table 1).

In the interpretation of the spectra we shall correct the chemical shifts for the contributions of ring currents and compare these corrected shifts with the following reference points, derived from the data in tables 1 and 2:

Reference point for methyl hydrogen         +228 c/s from benzene.

Reference point for aromatic hydrogen   + 75 c/s from benzene.

It may be pointed out that the value of 228 c/s is nearly equal to the chemical shift for methyl hydrogens near olefinic carbon atoms (cf. table 11-4 of ref. [1]). The chemical shift of hydrogen atoms near olefinic carbon atoms is near the value of + 75 c/s from benzene, but the shifts in different molecules scatter over a range of about 44 c/s (cf. table 11-3 of ref. [1]).

The influence of localized excess charges induced by the substituent methyl groups might be expected to manifest itself in the form of a correlation between the variation in magnetic shielding of the methyl-group hydrogen and the self-polarizability of the carbon atom to which the substituent is bonded (column 5 of table 2). Such a linear correlation is indeed found. However, the

self-polarizabilities themselves prove to be approximately proportional to the resultant dipolar field of the induced ring currents. Apparently it is not possible to separate the contributions of these two effects.

## 2. Aromatic carbonium ions

### 2.1. *Pentamethylbenzene*

The N.M.R. spectrum of the proton complex of pentamethylbenzene is reproduced in figure 2. It is clearly different from that of the molecule which consists of a single line due to the ring hydrogen ( + 26 c s, with respect to benzene) and a barely split doublet (1 c s) of the hydrogens in the methyl groups ( + 208 c/s).

Protonation occurs in the unsubstituted position. If $HF + BF_3$ is used as the solvent the proton complex has a sufficiently long lifetime and the signal of the $CH_2$ group is observed at + 112 c/s with respect to benzene.

| | Methyl hydrogen | | | Ring hydrogen | | |
|---|---|---|---|---|---|---|
| | $\nu_{exp}$ | Ring-current contribution | Net shift, $\Delta\nu$ | $\nu_{exp}$ | Ring-current contribution | Net shift, $\Delta\nu$ |
| *a.* toluene | 195 | − 32 | 227 | 0 | − 72 | 72 |
| *b.* 1-me-naphthalene | 181 | − 48 | 229 | − 21 | − 97 | 76 |
| *c.* 2-me-naphthalene | 188 | − 39 | 227 | − 8 | − 82 | 74 |
| *d.* 9, 10-dime-anthracene | 164 | − 64 | 228 | − 43 | − 123 | 80 |
| *e.* 9-me-phenanthrene | 184 | − 55 | 239 | − 12 | − 106 | 94 |
| *f.* 1-me-phenanthrene | 182 | − 52 | 234 | − 18 | − 101 | 83 |
| *g.* 4-me-phenanthrene† | 167 | − 65 | 232 | − 42 | − 124 | 82 |
| *h.* 2-me-phenanthrene | — | — | — | − 8 | − 83 | 75 |
| *j.* 3-me-phenanthrene | — | — | — | − 8 | − 86 | 78 |

† Sterically hindered.

Table 1. Chemical shifts in c s at 40 Mc s relative to benzene of hydrogen in substituent methyl groups and of ring hydrogens in corresponding position in the unsubstituted aromatic molecule.

Solvent: $CS_2$. Concentrations are of the order of a few per cent m. The shifts in the table $\nu_{exp}$, with respect to benzene, have been recalculated fom the experimental shifts (internal reference $C_6H_{12}$) using the value 230 c s for the difference in chemical shift between benzene and cyclohexane. The chemical shifts of the hydrogens of phenanthrene have been obtained from the spectrum by trial and error using the coupling constants of naphthalene.

The three resonance peaks at 180, 187 and 198 c/s, with intensity ratio 1 : 2 : 2 are attributed to the methyl hydrogens at the para, ortho and meta positions, respectively. This assignment is in agreement with the spectra of the proton complexes of metaxylene, mesitylene, 1, 3, 4-trimethylbenzene, 1, 2, 4, 5- and 1, 3, 4, 5-tetramethylbenzene, and hexamethylbenzene at − 85 c in $HF + BF_3$†. In these molecules, apart from hexamethylbenzene, the position of protonation

† The spectra of mesitylene and of hexamethylbenzene at room temperature display a single narrow methyl peak. The collapse of the multiplet in the proton complex of mesitylene is caused by proton exchange with free molecules and with the acid. In the case of hexamethylbenzene, 1, 2, 3, 5- and possibly 1, 2, 4, 5-tetramethylbenzene, however, the collapse is caused by proton exchange *within* the ion. Another point is that the low temperature spectra display a splitting of the signal of the methyl group in para position to the $CH_2$ group. These phenomena will be discussed in a later paper.

is invariably an unsubstituted position. For mesitylene the signal of the methyl groups consists of a doublet with intensity ratio of $1:2$ situated at 180 c/s (para) and 187 c/s (ortho), respectively. The resonance peak of the two-ring hydrogens in meta position with respect to the $CH_2$ group is found at $-16$ c/s.

In the proton complex of 1, 3, 4, 5-tetramethylbenzene only a single methyl group is present in meta position with respect to the $CH_2$ group and the signal of the methyl groups is a triplet with intensity ratio of $1:2:1$ at 180, 187 and 198 respectively. The resonance of the ring hydrogen in meta position is again found at $-16$ c/s. The spectrum of the proton complex of 1, 2, 4, 5-tetramethylbenzene (durene) at $-85°c$ displays a doublet methyl group with intensity ratio $1:1$ (189 c/s and 197 c/s). The resonance of the para ring hydrogen is located at $-53$ c/s with respect to benzene; it practically coincides with the solvent peak.

Both metaxylene and 1, 3, 4-trimethylbenzene possess different carbon atoms of comparable proton affinity. It appears from the spectrum that protonation takes place on carbon atom 4 (or 6) in metaxylene and on carbon atom 6 in 1, 3, 4-trimethylbenzene. The signals of the ring hydrogens in ortho and meta position with respect to the $CH_2$ group are located at $-40$ c/s and $-16$ c/s from benzene, respectively.

| Position | $\nu_{exp}$ | Ring-current contribution | Net shift, $\Delta\nu$ | Self-polarizability $\beta^{-1}$ |
|---|---|---|---|---|
| 3 | 183 | $-57$ | 240 | 0·448 |
| 4 | 186 | $-60$ | 246 | 0·447 |
| 5 | 177 | $-56$ | 233 | 0·452 |
| 6 | 187 | $-42$ | 229 | 0·410 |
| 7 | 185 | $-42$ | 227 | 0·410 |
| 8 | 173 | $-58$ | 231 | 0·449 |
| 9† | 156 | — | — | 0·496 |
| 10 | 168 | $-69$ | 237 | 0·514 |
| 2′ | 184 | $-44$ | 228 | 0·410 |
| 3′ | 188 | $-42$ | 230 | 0·404 |
| 4′ | — | $-53$ | — | 0·439 |

† Sterically hindered.

Table 2.    Chemical shifts in c/s of methyl hydrogens in monomethyl-substituted 1, 2-benzanthracenes (see table 1).

## 2.2. Hexamethylbenzene

The N.M.R. spectrum of the hexamethylbenzenium ion in $HF + BF_3$ as measured at $-85°c†$ is reproduced in figure 3. The resonance of the single hydrogen in the
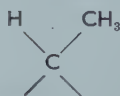


group is found at $+131$ c/s from benzene. This peak has been found to display a quadruplet structure due to spin–spin interaction with the nearby methyl group. The resonance of the latter is a doublet (6·7 c/s), as expected, situated at 227 c/s. The triplet is assigned, as in the preceding case, to the methyl hydrogens in the para, ortho and meta positions. The spacings and the chemical shifts correspond

† See footnote on page 243.

well with those obtained for the pentamethylbenzenium ion. It should be noted that the 'out of plane' methyl peak (227 c/s) nearly coincides with the reference point.

A recent publication [4] considers the N.M.R. spectrum of the 1, 1, 2, 3, 4, 5, 6-heptamethylbenzenium ion. The spacings of the methyl groups in the spectrum correspond excellently with those measured by us. On an absolute scale the correspondence between the values is bad, partly because the values of ref. [4] have to be corrected for bulk susceptibility effects and possibly for solvent effects, as the solutions contained metal ions.
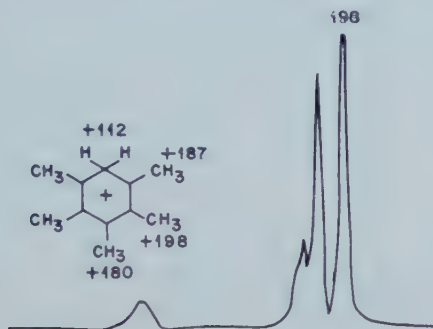


Figure 2. Proton resonance spectrum of pentamethylbenzenium ion in HF + BF$_3$ at 40 Mc/s. Internal reference: benzene.

### 2.3. 9, 10-*dimethylanthracene*

The spectrum of the molecule (figure 4 *a*) is similar to that of naphthalene [1] (case A$_2$B$_2$). The coupling constants obtained from the spectrum are $J_{\beta\beta} = 5\cdot9$ c/s, $J_{\alpha\beta} = 8\cdot1$ c/s (ortho) and $1\cdot4$ c/s (meta).

In the spectrum of the proton complex (figure 4 *b*) the low-field part, which is due to the aromatic hydrogens, is similar to that of the proton complex of anthrone (see §3). The doublet resonance peak of the out-of-plane methyl group in position 10 (223 and 231 c/s), near which protonation has taken place, has the same chemical shift as the out-of-plane methyl group in the hexamethylbenzenium ion. Evidently the influence of the ring currents in the two outer rings—the central ring current is interrupted—is negligible. The contribution to the shielding of these ring currents is decreased to a small value by the factor $(1-3\cos^2\delta)$ in which $\delta$ is the angle between the induced diamagnetic dipole vector, which is
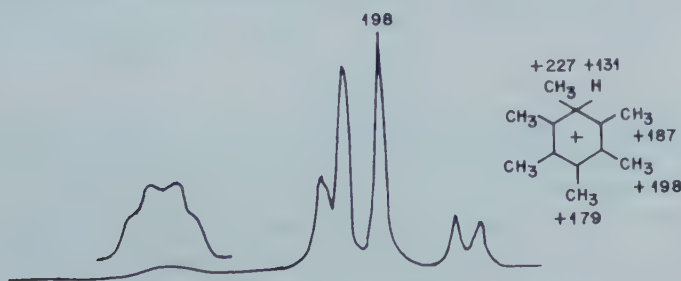


Figure 3. Proton resonance spectrum of hexamethylbenzenium ion in HF + BF$_3$ at $-85°$c at 40 Mc/s; the resonance of the single hydrogen at $+131$ c/s has been enlarged for clarity. Internal reference: benzene.

perpendicular to the aromatic nucleus, and the vector joining the dipole and the out-of-plane methyl group considered.

The hydrogens of the 'in-plane' methyl group in the 9 position at 148 c/s are −80 c/s from the reference point. This shift to lower field is only partly caused by the positive charge on the adjacent carbon atom because the ring currents in the outer rings produce a shift to lower field of −32 c/s. Thus the shift caused by the positive charge on the carbon atom in the 9 position amounts to −48 c/s.

The case of 9, 10-dimethyl-1, 2-benzanthracene is similar. Here protonation takes place exclusively in the 9 position [2]. The resonance of the hydrogens of the methyl group in the 10 position is shifted to lower field over −49 c/s by the positive charge on the adjacent carbon atom.
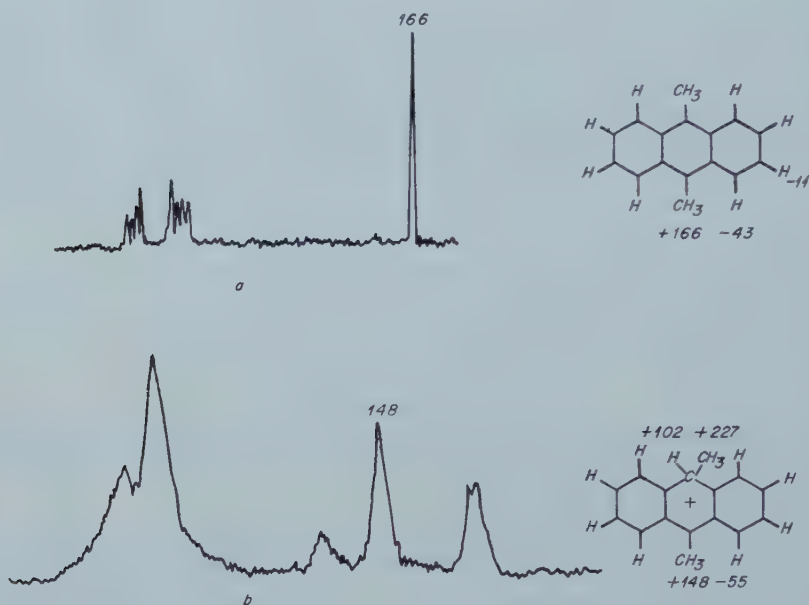


Figure 4.   Proton resonance spectra of (a) 9, 10-dimethylanthracene in $CCl_4$ and (b) its conjugate acid in $CF_3COOH + H_2O . BF_3$ at 40 Mc/s.   Internal reference: benzene.

### 3. OXYGEN-SUBSTITUTED AROMATIC CARBONIUM IONS

Oxygen-substituted aromatic molecules are much more basic than the corresponding parent compounds and stable aromatic carbonium ions can readily be obtained from them. Three examples will be discussed: anthrone, 4, 4-dimethyl-1-ketonaphthalene, and 2, 2-dimethyl-1-ketonaphthalene.

### 3.1. *Anthrone*

The N.M.R. spectrum of the carbonium ion of this highly basic molecule (figure 5) displays, apart from the $CH_2$ resonance, a well-resolved quadruplet and a strong broad peak of relative intensities 1 : 3. The splittings in the quadruplet, 7·9 and 1·8 c/s, can only be explained if the peaks are caused by protons either in the 1 and 8 or the 4 and 5 positions. Molecular-orbital calculations predict a positive charge on the carbon atoms in the 1, 3, 6 and 8 positions and therefore one would be inclined to assign the quadruplet signal to the hydrogens in the 1 and 8 positions. Their chemical shift is −59 c/s as compared with −36 c/s

in the molecule. The best correspondence between the calculated† and the measured spectrum is obtained if the constants given in the diagram (figure 5) are used in the calculations.

Anthrone is known to exist in two tautomeric forms of which the keto modification is the more stable. This fact is confirmed by its N.M.R. spectrum in $CS_2$, in which the $CH_2$ peak is found at $+119$ c s with respect to benzene. The spectrum is similar to that of its conjugate acid and does not resemble an $A_2B_2$ spectrum. This indicates that in anthrone in its keto modification the α-protons 1 and 8 carry an excess positive charge.

### 3.2. 4, 4-dimethyl-1-ketonaphthalene

The low-field part of the spectra of this molecule and its conjugate acid are reproduced in figure 6 (*a* and *b*).

In the molecule the olefinic hydrogens in the 2 and 3 positions give rise to a quadruplet which is clearly visible in figure 6 (*a*). These hydrogens are only to a
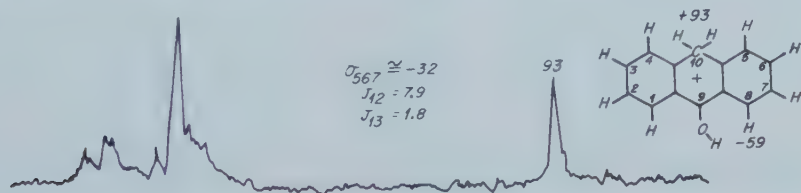
Figure 5.   Proton resonance spectrum of anthrone in $CF_3COOH + H_2O . BF_3$ at 40 Mc/s. Internal reference: benzene.
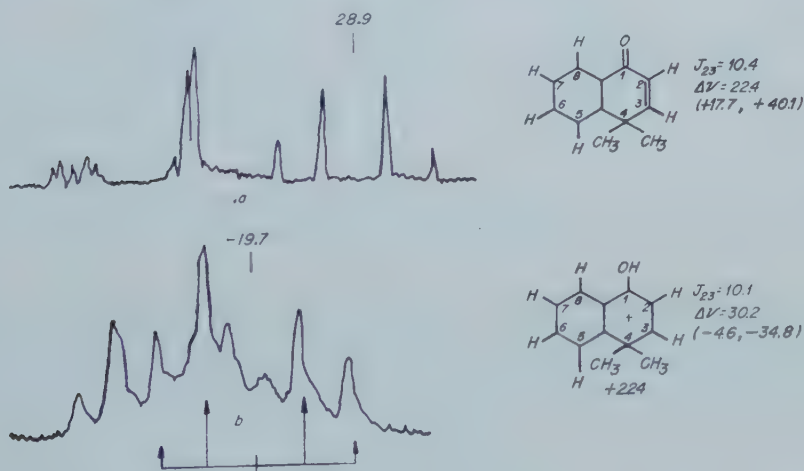
Figure 6.   Spectra of the ring protons of 4, 4-dimethyl-1-keto naphthalene in $CS_2$ and in $CF_3COOH + H_2O . BF_3$ at 40 Mc/s.   Internal reference: benzene.

minor extent subject to the ring current in the aromatic ring and they appear on the high-field side. Their chemical shifts with respect to benzene are indicated in the diagram together with their coupling constant. The aromatic hydrogens give a spectrum resembling the one of the ring hydrogens in anthrone.

† A computer programme has been made with which the N.M.R. spectra of systems of four coupled spins can be calculated.

On the formation of the ion the centre of the quadruplet—as indicated in figure 6 (a)—is strongly shifted to lower field over $-48.6$ c/s. The shift of hydrogen 2 is different from that of hydrogen 3 but it is difficult to assign the variations in chemical shift; one would expect the assignment in the ion to be: $\nu_3 = -34.8$ c/s and $\nu_2 = -4.6$ c/s.

### 3.3. 2, 2-dimethyl-1-ketonaphthalene

The low-field part of the spectra of the molecule and the carbonium ion are reproduced in figure 7 (a and b). The resonance of the hydrogens in the 3 and 4 positions is readily recognizable. Chemical shifts are indicated in the diagram. The centre of the quadruplet in the molecule is situated at $+38.8$ c/s and in the ion at $+20.3$ c/s. Again it is difficult to assign the chemical shifts of the pair of hydrogens in the ion but one would expect hydrogen 3 to have the smaller magnetic shielding ($\nu_3 = +12.9$ c/s and $\nu_2 = +27.7$ c/s).
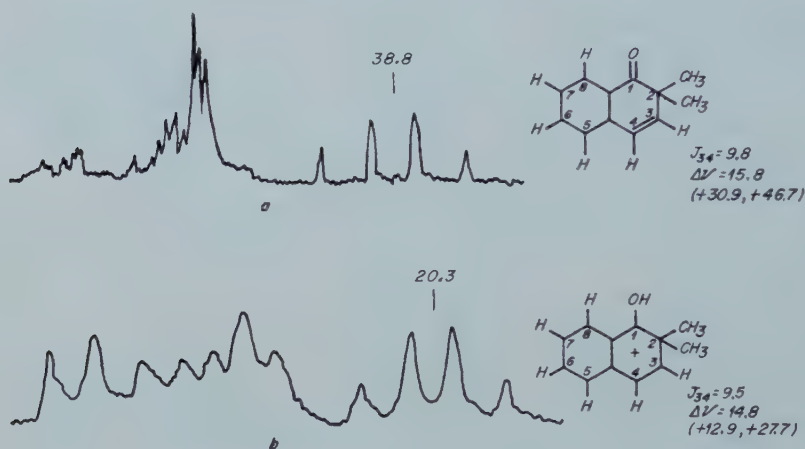


Figure 7. Spectra of the ring protons of 2, 2-dimethyl-1-keto naphthalene in $CS_2$ and in $CF_3COOH + H_2O . BF_3$ at 40 Mc/s. Internal reference: benzene.

## 4. Discussion

The N.M.R. spectrum of a proton complex of an aromatic hydrocarbon consists in general of three groups of lines, which, in order of increasing magnetic field, can be assigned to the aromatic hydrogens, the hydrogens in the methylenic
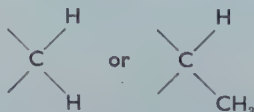


groups and finally the hydrogens in the methyl groups (figures 2–7).

A detailed discussion of the spectra displayed by the aromatic hydrogens will not be attempted because the multiplet structure is often blurred by proton exchange. This exchange may be due to interaction with other molecules in which case it can be slowed down by lowering the temperature or by making the solution more acidic [2]. It can also be caused by an exchange of the same proton over carbon atoms of equal proton affinity in the ion. This type of exchange can

only be slowed down by lowering the temperature. For instance, the multiplet structure of the methyl-group resonance in the hexamethylbenzenium ion in $HF + BF_3$ became apparent at $-85\,°c$.

This discussion will be concerned with the question whether a relation exists between the chemical shifts of aromatic and methyl-group hydrogens and the positive charges on the adjacent carbon atoms in the complex.

### 4.1. *Hydrogens in methyl groups*

As was pointed out above, the reference point for the chemical shift of hydrogens in methyl groups substituted in aromatic rings, after correcting for the effect of ring currents, is $+228\,c$'s with respect to benzene. Table 3 gives the values of the shifts from this reference point for the carbonium ions investigated.

| Proton complex of | $\nu_{me}$ relative to benzene, c/s | $\nu_{me}$ corrected for ring-current, c/s | $\Delta\nu_{me}$ relative to reference point, c/s | Total shift per electronic charge, c/s | Charge density calculated from shift |
|---|---|---|---|---|---|
| Pentamethyl-benzene | 180 (para) | 180 | $-48$ | 190 | 0·25 |
| | 187 (ortho) | 187 | $-41$ | | 0·21⁵ |
| | 198 (meta) | 198 | $-30$ | | 0·16 |
| Hexamethyl-benzene | 179 (para) | 179 | $-49$ | 189 | 0·25 |
| | 187 (ortho) | 187 | $-41$ | | 0·21⁵ |
| | 198 (meta) | 198 | $-30$ | | 0·16 |
| | 227 (out of plane) | 227 | $-1$ | | small |
| 9, 10-dimethyl-anthracene | 148 (meso) | 180 | $-48$ | — | 0·25 |
| | 227 (out of plane) | 227 | $-1$ | | small |
| 9, 10-dimethyl-1, 2-benzanthracene | 142 (meso) | 179 | $-49$ | — | 0·26 |
| | 220 (out of plane) | 220 | $-8$ | | small |

Table 3. Chemical shifts in c/s of methyl hydrogen in proton complexes of methyl-substituted aromatic molecules

It is tempting to interpret the results for the benzene derivatives as shifts caused by positive charges alone, since the ring current is interrupted in the proton complex. The methyl groups in these carbonium ions in the para, ortho and meta positions are found at $+180$, $+187$ and $+198\,c/s$ with respect to benzene or at $-48$, $-41$ and $-30\,c/s$ from the reference point. If one may assume that the influence of charge on shift is linear, the shift of the hydrogens in a methyl group adjacent to a positively charged carbon atom amounts to $-190\,c/s$ per electronic charge. The charge distribution calculated on this basis from the chemical shifts for the proton complex of benzene is given in figure 8 (*a*).

This charge distribution (*a*) is very different from either the distributions (*b*) and (*c*) as predicted by molecular orbital calculations without or including electron interaction [5]. The experimental charge distribution is much more uniform than predicted by these calculations.

It has been suggested previously [3, 6] that in order to calculate the charge distribution in systems carrying a net positive charge the method of Wheland and
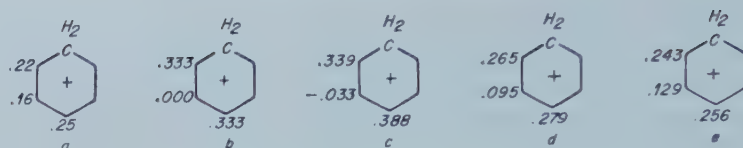
Figure 8.  Charge distribution in the benzenium ion.  (a) Derived from N.M.R. shifts of methyl-group protons;  (b) molecular-orbital calculation without electron interaction;  (c) molecular-orbital calculation with electron interaction;  (d) calculated by perturbation method of Wheland and Mann ($f = 1\cdot4$);  (e) calculated by perturbation method of Wheland and Mann with $f = 2\cdot8$.

Mann should be used [7].   These authors assume that the Coulomb integral $\alpha_r$ of carbon atom $r$ is changed by a net positive charge $\delta q_r$ according to:

$$\delta \alpha_r = f \beta \delta q_r,$$

where $f$ is a constant related to the electron interaction integral $\gamma_{11}$ ($= 10\cdot53$ ev) and the resonance integral $\beta$ ($\sim -4$ ev) by $-2f \approx \gamma_{11}/\beta$ [8].   $f = 1\cdot4$ seems to be a reasonable value [6], and has been used.   Wheland-and-Mann-type calculations were made for the benzenium ion (figure 8 (d)), the anthracenium ion (figure 9 (b)) and the two naphthalenium ions (figure 10 (a) and (b)).

The calculated distribution of the positive charge in the benzenium ion (figure 8 (d)) corresponds much better with the 'measured' distribution of diagram (a) than do (b) and (c).   The agreement can be made more quantitative if one arbitrarily increases the value of the parameter $f$.   For $f = 2\cdot8$ one obtains the distribution of charge as in diagram (e).

The shifts of the hydrogens in the methyl group in 9 position in the proton complexes of 9, 10-dimethylanthracene and 9, 10-dimethylbenzanthracene is $-48$ c/s, with respect to the reference point (cf. table 3).   This shift can be interpreted as caused by a charge density of $0\cdot25$ electrons in agreement with the calculated values in figure 9 (b).
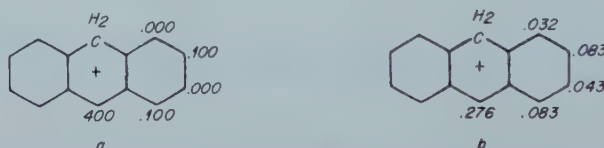


Figure 9.  Charge distribution in the anthracenium ion.  (a) Molecular-orbital calculation without electron interaction;  (b) calculated by perturbation method of Wheland and Mann ($f = 1\cdot4$).

## 4.2. Hydrogen in aromatic CH bonds

An estimate of the chemical shift, $\Delta\nu$, of ring hydrogens caused by excess charges on ring carbon atoms can be obtained with the aid of the spectrum of the carbonium ions of metaxylene, mesitylene, 1, 3, 4-trimethylbenzene, 1, 2, 4, 5- and 1, 3, 4, 5-tetramethylbenzene, where the ring hydrogens in meta, ortho or para position to the $CH_2$ group are found at $-16$ c/s, $-40$ c/s and $-52$ c/s from benzene or at $-91$ c/s, $-115$ c/s and $-127$ c/s from the reference point.   This leads to a shift of $-539$ c/s per unit positive charge and again to the charge distribution of figure 8 (a).

One might attempt to apply this value to the case of the proton complex of anthrone in order to estimate the positive charge on carbon atoms 1 and 8. The adjacent hydrogens have a chemical shift of $-59$ c/s with respect to benzene† or $-53$ c/s when one corrects for the ring current in the other aromatic ring. This would mean a positive charge of $0\cdot1$ of an electron which compares well with the calculated value $0\cdot083$ (see figure 9 (b)).

The theoretically predicted charge distributions in the carbonium ions of 4, 4-dimethyl-1-ketonaphthalene and 2, 2-dimethyl-1-ketonaphthalene are given in figure 10 (a) and (b).

In the carbonium ion of the first compound the hydrogens in the 2 and 3 positions are shifted from the reference point over $-80$ c/s and $-110$ c/s. The influence of the ring current in the unsubstituted ring is approximately 10 c/s giving $-70$ c s and $-100$ c s. The total shift of $-170$ c/s is expected to be caused by $0\cdot31$ electrons in good agreement with the calculated value $0\cdot33$. Analogously, the total charge shift of the hydrogen pair in positions 3 and 4 in the second compound is $-74$ c s and this value leads to a positive charge of $0\cdot13$ electrons. The calculated value is $0\cdot17$.
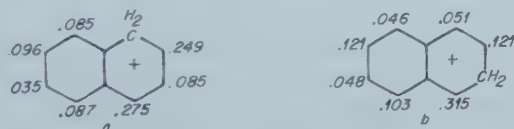


Figure 10.    Charge distribution in carbonium ions of 4, 4-dimethyl-1-keto naphthalene (a) and 2, 2-dimethyl-1-keto naphthalene (b) calculated by the perturbation method of Wheland and Mann ($f=1\cdot4$).

### 4.3. *Hydrogens at the protonated carbon atoms*

The fate of the added proton has not yet been considered in detail apart from the statement that it is present as a hydrogen atom in an aliphatic
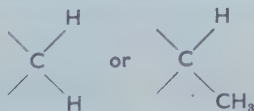


group.    The chemical shift of this hydrogen is between that of an aliphatic and an aromatic hydrogen.    Less information is available for the chemical shift of this atom since it is more subject to exchange broadening.    Therefore only the chemical shifts will be considered of the quadruplet of the single hydrogen in the
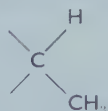


groups in the following sequence of proton complexes: hexamethylbenzene ($+131$ c/s), 9, 10-dimethylanthracene ($+102$ c/s) and 9, 10-dimethyl-1, 2-benzanthracene ($+69$ c/s). If one corrects for the ring currents by 0 c/s, 60 c/s and 85 c/s, respectively, one obtains the values $+131$ c/s, $+162$ c/s and $+154$ c/s. It is not certain that one may assign a meaningful reference point to the single hydrogen in such a configuration but we expect it to be at about $+200$ c/s. The low value of the corrected shift in hexamethylbenzenium ion ($+131$ c s) probably

† These hydrogens are bonded to a ring which carries a ring current.

is caused by the high value of the charge of $+0.2$ units on the ortho carbon atoms. The excess charge on the nearby carbon atoms in the proton complexes of 9, 10-dimethylanthracene and 9, 10-dimethyl-1, 2-benzanthracene is about half as high, leading to a smaller downfield shift.

## 5. CONCLUDING REMARKS

In the calculation of the excess charge densities we have considered only the linear term in the expansion of the chemical shift due to charge, $\Delta \nu$, in powers of the excess charge, $q$:

$$\Delta \nu = a_1 q + a_2 q^2 + \ldots .$$

The first term $a_1$ has been discussed by Fraenkel *et al.* [9] in a paper which came to our attention after the completion of our manuscript. These authors have made a new determination of the chemical shifts of ring hydrogens due to excess charges on adjacent carbon atoms in the systems $C_5H_5^-$, $C_6H_6$ and $C_7H_7^+$ [10] and it is gratifying to find that their value of 10 p.p.m. per unit charge corresponds satisfactorily with our value of 13.4 p.p.m. per unit charge for ring protons in aromatic carbonium ions.

The second term has been treated by several authors [11]. Part of this term can be accounted for by the distortion of the hydrogen 1s orbital by the electrostatic field of the excess charge, whereas the linear term originates from bond polarization [9]. The sign of the experimental shifts is determined by the sign of the excess charge [9, 12] and this indicates that the linear term dominates.

As far as the quadratic term is concerned, a simple electrostatic model [11] predicts a charge shift $\Delta \nu = -20 \, (q^2/b^4)$ p.p.m. in which $q$ is the excess charge and $b$ the distance. For a CH-fragment one calculates a value of $a_2$ of about $-15$ p.p.m./(charge)$^2$.

It might well be that the lack of strict proportionality between charge shift and excess charge in the data of Fraenkel *et al.* [9] is due to the second term. The inclusion of this second term in the calculation of the charge shifts in the present paper would affect the charge-distribution in the carbonium ions to a small extent; in fact an even more uniform charge distribution would be obtained.

Our inferred charge densities for the aromatic carbonium ions are very different from densities calculated in the simple Hückel approximation. It is remarkable that the correspondence is even worse if the electron interaction is explicitly taken into account. Wheland-and-Mann-type calculations predict a more uniform charge distribution in agreement with the chemical shift data.

Alternatively one can include† in a configuration interaction method not only singly, but also doubly excited states. This has a very small effect on the energy levels but causes a more uniform distribution of charge.

It may be stressed that in calculating the charge distributions only two aspects of the magnetic shielding have been taken into account, i.e. the interruption of the ring currents and the localization of excess charges, which both produce large shifts. The concentrations of the solutes invariable were of the order of a few mole per cent so that dilution shifts can be ignored. Possible solvent effects have been neglected, but these are probably small compared with the charge shifts.

† J. P. Colpa (to be published).

We gratefully acknowledge the experimental assistance of Mr. J. Gaaf. We are indebted to Dr. J. P. Colpa and Mr. G. ter Maten for their help in the calculation of charge densities, and to Mr. J. Knotnerus who prepared the two ketonaphthalenes.

## REFERENCES

[1] POPLE, J. A., SCHNEIDER, W. G., and BERNSTEIN, H. J., 1959, *High Resolution Nuclear Magnetic Resonance* (McGraw-Hill).
[2] MacLEAN, C., VAN DER WAALS, J. H., and MACKOR, E. L., 1958, *Mol. Phys.*, **1**, 247.
[3] MACKOR, E. L., HOFSTRA, A., and VAN DER WAALS, J. H., 1958, *Trans. Faraday Soc.*, **54**, 186.
[4] VON E. DOERING, W., *et al.*, 1958, *Tetrahedron*, **4**, 178.
[5] POPLE, J. A., and BRICKSTOCK, A., 1954, *Trans. Faraday Soc.*, **50**, 901.
[6] MULLER, N., PICKET, L. W., and MULLIKEN, R. S., 1954, *J. Amer. chem. Soc.*, **76**, 4770.
[7] WHELAND, G. W., and MANN, D. E., 1949, *J. chem. Phys.*, **17**, 264.
[8] AALBERSBERG, W. J., and MACKOR, E. L., 1960, *Trans. Faraday Soc.*, **56**, 1351.
[9] FRAENKEL, G., CARTER, R. E., McLACHLAN, A., and RICHARDS, J. H., 1960, *J. Amer. chem. Soc.*, **82**, 5846.
[10] LETO, J. R., COTTON, F. A., and WAUGH, J. S., 1957, *Nature, Lond.*, **180**, 978.
[11] FRANK, P. J., and GUTOWSKY, H. S., 1958, *Arch. Sci., Genève*, **11**, 215.
MARSHALL, T. W., and POPLE, J. A., 1958, *Mol. Phys.*, **1**, 199.
[12] MacLEAN, C., and MACKOR, E. L., 1960, *Mol. Phys.*, **3**, 223.

# A hydrodynamic model for diamagnetic induced currents in molecules

by ANDREW D. McLACHLAN† and MILTON R. BAKER

Conant Chemical Laboratory, and Lyman Laboratory of Physics,
Harvard University, Cambridge, Massachusetts, U.S.A.

The current set up when a single bound electron moves in a magnetic field obeys simple hydrodynamic equations, which arise from a variational principle. When the ground state is not degenerate they have a unique solution, determined by the unperturbed electron density. The theory is closely related to Wick's irrotational flow model for the currents in a rotating molecule, to Tillieu and Guy's variational method, and London and Rebane's ideas of gauge invariance. Difficulties arise when there is more than one electron, when the wave function has nodes, or when it is degenerate; but the method may be useful for calculating magnetic properties of some small molecules.

## 1. Introduction

In 1948 Wick [1] put forward a hydrodynamic theory of the electronic currents which are set up when a molecule rotates. In this model, which is only strictly true for a single electron, the electron cloud of the molecule is carried round rigidly with the nuclei, but electrons within the clouds can slip past the nuclei instead of rotating like a rigid body. The current density and velocity field of the rotating electrons obey equations of continuity and irrotational flow which can be solved if the charge distribution is known.

The diamagnetic currents induced in a molecule by a magnetic field‡ pose a very similar theoretical problem, because of Larmor's theorem [2]. However, the ideas which are used to discuss the chemical shifts in nuclear magnetic resonance, for example [3, 4, 5], are developed from Van Vleck's theory of magnetic susceptibilities [6], and use a perturbation theory. The current is arbitrarily divided into 'diamagnetic' and 'paramagnetic' parts, depending on the vector-potential chosen to represent the field. On the other hand, London's macroscopic theory of super-conductivity [7] uses hydrodynamic equations for the electronic current, and is closely connected with the theory of the diamagnetic ring currents [8–11] which flow in conjugated molecules like benzene.

In this paper we show that the currents induced in a molecule by a magnetic field also obey hydrodynamic equations, which only involve the unperturbed ground state wave function of the electrons, and have a simple physical interpretation.

‡ We use the term ' diamagnetic current ' for the entire current induced in a molecule by the magnetic field.

However, we also find exceptional difficulties in the method when there are nodes in the wave function, or it is almost degenerate. As a result the theory is only useful in special cases. Wick's theory, and some other treatments of diamagnetism, have the same drawbacks.

## 2. Diamagnetism of a single electron: the velocity field and current density

We consider a single electron moving round a fixed set of nuclei in a constant magnetic field **H**. Spin–orbit coupling is neglected.

Although the values of any physical quantity, such as the probability density $\rho$, or current density **j**

$$\rho = \psi^* \psi, \tag{2.1}$$

$$\mathbf{j} = \frac{e\hbar i}{2mc} [\psi^* \nabla \psi - \psi \nabla \psi^*] - \frac{e^2}{mc^2} \mathbf{A} \psi^* \psi, \tag{2.2}$$

associated with an electron are uniquely fixed by the form of the magnetic field $\mathbf{H}(\mathbf{H} = \text{curl}\,\mathbf{A})$, the electronic wave function $\psi$ and the Schrödinger equation

$$\left[ \frac{1}{2m} (-i\hbar\nabla + e\mathbf{A}/c)^2 + V \right] \psi = W\psi \tag{2.3}$$

depend on the choice of vector potential **A**. In fact if $\mathbf{A}_0$ is our first choice of **A**, and $\lambda(\mathbf{r})$ an arbitrary scalar function, the substitution

$$\frac{e}{c}\mathbf{A} = \frac{e}{c}\mathbf{A}_0 + \nabla\lambda \tag{2.4}$$

leaves the magnetic field unchanged, but the solution of the new Schrödinger equation differs from the original solution by a phase factor:

$$\psi = \psi_0 \exp\left[\lambda(\mathbf{r})/i\hbar\right]. \tag{2.5}$$

Our first object will be to make a change of variables, and derive a transformed Schrödinger equation which does not depend directly on the choice of **A**. Suppose that we write the complex wave function $\psi$ of a single electron in the form

$$\psi(\mathbf{r}) = \theta(\mathbf{r}) \exp\left[S(\mathbf{r})/i\hbar\right] \tag{2.6}$$

with $\theta$ and $S$ both real functions $(\theta \geq 0)$. Then in the gauge transformation (2.5) $\theta$ is invariant, but $S_0$ becomes $(S_0 + \lambda)$, and the quantities

$$\rho = \theta^2, \tag{2.7}$$

$$\mathbf{j} = -\frac{e}{mc}\left(\frac{e}{c}\mathbf{A} - \nabla S\right)\theta^2, \tag{2.8}$$

are obviously also invariant. Substitution of (2.6) into the Schrödinger equation, and separation of the real and imaginary parts, gives the coupled equations

$$-\frac{\hbar^2}{2m}\nabla^2\theta + \frac{1}{2m}\left(\frac{e}{c}\mathbf{A} - \nabla S\right)^2\theta + V\theta = W\theta, \tag{2.9}$$

$$2\nabla\theta \cdot \left(\nabla S - \frac{e}{c}\mathbf{A}\right) + \theta\nabla^2 S = 0, \tag{2.10}$$

which now only involve gauge invariant quantities. Next we may avoid all reference to $S$ and **A** by substituting a vector

$$\mathbf{v} = \frac{1}{m}\left(\frac{e}{c}\mathbf{A} - \nabla S\right) \tag{2.11}$$

into (2.9) and (2.10). The form of **v** is subject to only one subsidiary condition:

$$\text{curl } \mathbf{v} = \frac{e\mathbf{H}}{mc,} \qquad (2.12)$$

which follows because $\mathbf{H} = \text{curl } \mathbf{A}$. Apart from this restriction we may treat **v** as an independent variable. Equations (2.8) and (2.10) then take the form

$$\mathbf{j} = -\frac{e}{c}(\rho\mathbf{v}), \qquad (2.13)$$

$$\text{div }(\rho\mathbf{v}) = 0; \qquad (2.14)$$

while $\theta$ is found from the modified Schrödinger equation

$$-\frac{\hbar^2}{2m}\nabla^2\theta + (\tfrac{1}{2}m\mathbf{v}^2 + V)\theta = W\theta. \qquad (2.15)$$

The vector **v** should clearly be interpreted as the velocity field of a single electron precessing in the magnetic field. (2.14) is the hydrodynamic equation of continuity, and the additional term $\tfrac{1}{2}m\mathbf{v}^2$ in (2.15) represents the kinetic energy which arises from the precession. Indeed, very similar equations govern the flow of classical charged particles in a magnetic field, or the flow of superconducting electrons in London's macroscopic theory [7]. As we shall see in §4, the velocity field described above is completely analogous to Wick's and Espe's [1, 12] irrotational flow field for the currents in a rotating molecule.

Before discussing the solution of the equations by perturbation theory we shall note two useful general theorems. The first follows at once from (2.12) by Stokes' theorem, and states that

$$\oint \mathbf{v} \cdot d\mathbf{l} = \frac{e}{mc}\int \mathbf{H} \cdot d\mathbf{S}. \qquad (2.16)$$

The line integral of **v** round any closed circuit in the molecule is equal to the magnetic flux through the circuit (provided that $S$ is a single-valued function). The second is a variational principle; $\theta$ and **v** are the functions which make

$$W = \int\left[\frac{\hbar^2}{2m}(\nabla\theta)^2 + V\theta^2\right]d\tau + \int \frac{1}{2}m\mathbf{v}^2\theta^2\, d\tau \qquad (2.17)$$

a minimum, subject to the conditions that

$$\int \theta^2\, d\tau = 1; \quad \text{curl } \mathbf{v} = \frac{e\mathbf{H}}{mc}. \qquad (2.18)$$

## 3. PERTURBATION THEORY

Suppose that in the absence of a magnetic field $\psi_0$ is the real wave function of an electron in a non-degenerate state. In a small magnetic field the usual first order perturbation theory shows that $\psi_0$ changes to $\psi_0 + i\psi_1$ where $\psi_1$ is a real function, proportional to the strength of $H$. Hence, if $\psi_0$ *has no nodes*, the phase $S$ of the perturbed wave function is small everywhere. An expansion of equations (2.12)–(2.15) in powers of $H$ then shows that **v** and **j** are proportional to $H$, while the change in $\theta$ is proportional to $H^2$. Under these conditions **v** is determined, to first order in $H$, by the equations

$$\text{div }(\rho_0\mathbf{v}) = 0, \qquad (3.1)$$

$$\text{curl } \mathbf{v} = \frac{e\mathbf{H}}{mc}, \qquad (3.2)$$

**R**

where $\rho_0$ is the unperturbed probability density. Furthermore, the second-order change of energy, according to (2.17), is just

$$w = \int \frac{1}{2} m \rho_0 \mathbf{v}^2 \, d\tau. \tag{3.3}$$

Alternatively $\mathbf{v}$ may be calculated from the variational principle that $w$ is a minimum, with (3.2) as a restrictive condition. (3.1) is then the condition for $w$ to be stationary.

It is important to establish that the velocity field found in this way is unique. so that one can use the hydrodynamic equations instead of ordinary perturbation theory. In fact there is only one solution which is finite everywhere and satisfies the flux theorem (2.16). For let $\mathbf{u}$ and $\mathbf{v}$ be two solutions of (3.1) and (3.2). Then curl $(\mathbf{u} - \mathbf{v}) = 0$, or

$$\mathbf{u} - \mathbf{v} = \nabla \phi \tag{3.4}$$

where $\phi$ is some scalar function, single valued because

$$\oint \nabla \phi \cdot d\mathbf{l} = 0 \tag{3.5}$$

for all closed circuits. We now show that $\nabla \phi \equiv 0$. Consider the integral

$$\int \rho (\nabla \phi)^2 \, d\tau = \int (\phi \rho \nabla \phi) \cdot d\mathbf{S} - \int \phi [\nabla \cdot (\rho \nabla \phi)] \, d\tau. \tag{3.6}$$

The first term on the right vanishes when the surface $S$ encloses the whole of space, and the second vanishes because $\mathbf{u}$ and $\mathbf{v}$ satisfy (3.1). Thus $\nabla \phi = 0$ everywhere, and $\mathbf{u} = \mathbf{v}$.

We therefore conclude, that for a non-degenerate nodeless electronic state, the velocity distribution in a magnetic field can be found uniquely by this variational method, and only requires a knowledge of the unperturbed electron density.

One simple example is the hydrogen atom in a uniform field $\mathbf{H}$. In this case

$$\mathbf{v} = \left(\frac{e}{2mc}\right) \mathbf{H} \times \mathbf{r}, \tag{3.7}$$

so that the lines of flow are along 'circles of latitude', and the charge distribution precesses like a rigid body. Another case occurs when there is a nuclear spin, of magnetic moment $\boldsymbol{\mu}$, at the centre. Then

$$\mathbf{v} = \left(\frac{e}{mc}\right) \frac{\boldsymbol{\mu} \times \mathbf{r}}{r^3} \tag{3.8}$$

so that the lines of flow are the same but the velocity is proportional to the local magnetic field.

## 4. Analogy between rotation and a magnetic field

In his treatment of the electrons in a rotating molecule Wick [1] uses a set of axes rotating with the nuclei at an angular velocity $\boldsymbol{\omega}$. Relative to these axes the stationary states of the electrons are found from the Hamiltonian

$$\mathscr{H}' = \mathscr{H} - \boldsymbol{\omega} \cdot \mathbf{L}\hbar, \tag{4.1}$$

in which $\mathbf{L}\hbar$ is the orbital angular momentum of the electrons, and $\mathscr{H}$ is their Hamiltonian when the nuclei are at rest. Comparison of (4.1) with the Schrödinger equation (2.3) for an electron in a uniform magnetic field $\mathbf{H}$,

for which $\mathbf{A} = \frac{1}{2}\mathbf{H} \times \mathbf{r}$, shows that they are the same to the first order in $\mathbf{H}$ (or $\boldsymbol{\omega}$) provided that

$$\boldsymbol{\omega} = \frac{-e\mathbf{H}}{2mc}. \tag{4.2}$$

This result, which is Larmor's theorem, means that the theory of the previous sections can also be used to calculate the wave function for electrons in a rotating molecule. However, there are some important differences in the physical interpretation of the equations. The analogue of (2.2), for example:

$$\mathbf{j} = \frac{e\hbar i}{2mc}\left[\psi^*\nabla\psi - \psi\nabla\psi^*\right] + \frac{e}{c}(\boldsymbol{\omega} \times \mathbf{r})\psi^*\psi \tag{4.3}$$

gives the apparent 'slippage current' *relative to an observer rotating with the molecule.* Similarly

$$\mathbf{w} = \frac{1}{m}\left[m(\boldsymbol{\omega} \times \mathbf{r}) - \nabla S\right] \tag{4.4}$$

is the velocity relative to this observer. The currents and velocities relative to a fixed observer are therefore

$$\mathbf{J} = \mathbf{j} - \frac{e}{c}\rho(\boldsymbol{\omega} \times \mathbf{r}) = \left(\frac{e}{mc}\right)\rho\nabla S, \tag{4.5}$$

$$\mathbf{v} = \mathbf{w} + (\boldsymbol{\omega} \times \mathbf{r}) = -\nabla S/m \tag{4.6}$$

and the velocity field of a single electron is irrotational.

Another analogy is between the energy changes. The second order change of energy may be written in the form

$$w = \frac{1}{2}I\omega^2 \tag{4.7}$$

where $I$ is called the rotational moment of inertia [13–16], and

$$w = \int \frac{1}{2}m\rho v^2 d\tau = \frac{1}{2m}\int \rho(\nabla S)^2 \, d\tau: \tag{4.8}$$

$\mathbf{v}$ is now the velocity of the electron relative to fixed axes. Also derived from the second order energy change is the rotational magnetic moment [13] of the electrons, which is measured in molecular beam experiments:

$$\mathbf{M} = \left(\frac{-e\hbar}{2mc}\right)[I\omega/\hbar]. \tag{4.9}$$

Finally the magnetic field at the nucleus, which causes spin-rotational coupling effects [17], is the result of the total current $\mathbf{J}$, instead of the slippage current $\mathbf{j}$. The difference between them is simply the magnetic field produced by a rigid rotation of the entire electron distribution about the nucleus with an angular velocity $\boldsymbol{\omega}$—the diamagnetic term in Ramsey's formula [3, 18].

### 5. NODES AND DEGENERATE STATES

It is disappointing that although the equations (2.12)–(2.15) for the current density and velocity field hold quite generally, their solutions cannot usually be found by perturbation theory. This is because $\mathbf{v}$ cannot be treated as a small quantity when the unperturbed wave function has a node, since $S$ changes very rapidly from approximately 0 to approximately $\hbar\pi$ on passing across the node.

In particular $\mathbf{v} \propto 1/H$, $\mathbf{j} \propto H$, and $\frac{1}{2}\rho\mathbf{v}^2 \propto 1$ at the node itself. Although the energy integral (3.3) associated with the exact wave function in a magnetic field still exists it no longer represents the second energy order change.

Consider the energy integral (3.3) belonging to the exact wave function in the magnetic field. Then we split it in two:

$$w = \left(\frac{e}{2mc}\right)\int \theta^2\left(\frac{e}{c}\mathbf{A} - \nabla S\right).\,\mathbf{A}\,d\tau - \frac{1}{2}m\int \theta^2\left(\frac{e}{c}A - \nabla S\right).\,\nabla S\,d\tau \qquad (5.1)$$

$$= -\frac{1}{2}\int \mathbf{j}.\,\mathbf{A}\,d\tau + (c/2e)\int \mathbf{j}.\,\nabla S\,d\tau. \qquad (5.2)$$

The first term on the right of (5.2) is always proportional to $H^2$ and represents the second-order energy change, even if there is a node. On the other hand, the second term need not always vanish:

$$\int \mathbf{j}.\,\nabla S\,d\tau = \int \operatorname{div}(\mathbf{j}S)\,d\tau - \int S\operatorname{div}\mathbf{j}\,d\tau \qquad (5.3)$$

$$= \int_\Sigma S\mathbf{j}.\,d\mathbf{S}, \qquad (5.4)$$

where the surface $\Sigma$ encloses the region of integration. If $S$ is a single-valued function on $\Sigma$, the integral in (5.4) vanishes; but $S$ need not be when the surface is divided by a node. Consider, for example, an electron in the $2p_y$ orbital of an atom. (We suppose that some external perturbation removes the degeneracy of
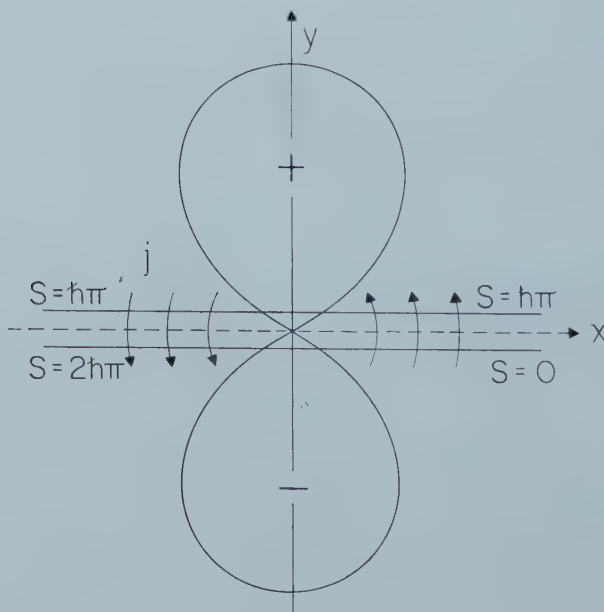


Currents crossing the node of a $2p$ orbital.

$2p_x$, $2p_y$, and $2p_z$.) In a magnetic field along the $z$-axis the wave function becomes $p_y + i\epsilon p_x$, where $\epsilon$ is a small real number, and a current flows across the nodes. Now let us start from a point on the negative $y$-axis (figure) and move in the $xy$ plane round a circle. $S$ changes from $0$ to $+\hbar\pi$ as we cross the positive $x$-axis,

and then, not back to 0 but on to $+2h\pi$, as we cross $Ox$ the second time. In fact $S$ changes by $\pm h$ round any circuit that encircles the $z$-axis just once. The integral in (5.4) is then $h$ times the total current which flows across the half of the $xz$ plane where $x > 0$, and (5.1) will only represent the second-order energy change in special cases, when no current flows across the nodes.

Another kind of difficulty arises when the electronic state is degenerate. In this case the wave function need not be real in the absence of a magnetic field, and carries a current whose velocity field is irrotational, according to (2.12). An external magnetic field may mix the original state strongly with some other component of the degenerate level, so that the initial current distribution is completely altered in the zeroth order. The first-order changes of current and charge density also obey rather complicated equations.

A related effect occurs when two states are almost degenerate. In a magnetic field a large current can arise, owing to the mixing of the sestates, and the size of the current is very sensitive to the precise energy difference between them. Although the results of §2 are still valid if one knows the *exact* unperturbed electron densities of the two states, the velocity distribution **v** may have large errors if it is claculated from slightly inaccurate electron densities.

## 6. The many-electron wave function

The antisymmetric wave function $\Psi(1, 2, \ldots N)$ for $N$ electrons may be written in the form

$$\Psi(1, 2, \ldots N) = \theta(1, 2, \ldots N) \exp\left[S(1, 2, \ldots N)/i\hbar\right] \tag{6.1}$$

where $\theta$ is an antisymmetric real function, and $S$ is a symmetric function of the coordinates of all the electrons, in order that $\Psi$ itself may be antisymmetric. The many-electron Hamiltonian

$$\mathcal{H} = \sum_{i=1}^{N} \left\{ \frac{1}{2m}\left[ -i\hbar\nabla_i + \frac{e}{c}\mathbf{A}(\mathbf{r}_i) \right]^2 + V(\mathbf{r}_i) \right\} + \sum_{i<j} \frac{e^2}{r_{ij}} \tag{6.2}$$

then leads to a transformation very similar to the one in §2. For example, equation (2.10) becomes

$$\sum_{i=1}^{N} \nabla_i \cdot \theta^2 \left[ \nabla_i S - \frac{e}{c}\mathbf{A}(\mathbf{r}_i) \right] = 0, \tag{6.3}$$

and **v** is now a vector in $3N$ dimensions, whose components in the sub-space of electron $i$ are

$$\mathbf{v}_i(1, 2, \ldots N) = \frac{1}{m}\left[ \frac{e}{c}\mathbf{A}(\mathbf{r}_i) - \nabla_i S(1, 2, \ldots N) \right]. \tag{6.4}$$

The electric current is obtained by integrating over the coordinates of all the electrons but the first:

$$\mathbf{j}(\mathbf{r}) = \frac{-Ne}{mc} \int \theta^2(\mathbf{r}, \mathbf{r}_2, \ldots \mathbf{r}_N)\left[ \frac{e}{c}\mathbf{A}(\mathbf{r}) - \nabla S(\mathbf{r}, \mathbf{r}_2, \ldots \mathbf{r}_N) \right] d\tau_2 \ldots d\tau_N, \tag{6.5}$$

and still obeys the equation of continuity (2.14). The functions $\theta$ and $S$ for many electrons obey a variational principle, just as in §2, but the equations no longer have a direct physical interpretation, nor are they easy to solve. However, there is one particularly simple approximation that is useful. We take $S$ to be a sum of one-electron terms:

$$S(1, 2, \ldots N) = s(\mathbf{r}_1) + s(\mathbf{r}_2) + \ldots s(\mathbf{r}_N) \tag{6.6}$$

and vary the function $s(\mathbf{r})$ to give the minimum energy. The change of energy, however, is just

$$w' = N \int \frac{1}{2m} \theta^2 \left[ \nabla s(\mathbf{r}_1) - \frac{e}{c} \mathbf{A}(\mathbf{r}_1) \right]^2 d\tau_1 \dots d\tau_N = \frac{1}{2} \int m\rho_0 \mathbf{v}^2 ; \qquad (6.7)$$

where $\rho_0$ is now the *total* unperturbed electron density at $r$, and $\mathbf{v}$ is the average electron velocity

$$\mathbf{v}(\mathbf{r}) = \frac{1}{m} \left[ \frac{e}{c} \mathbf{A}(\mathbf{r}) - \nabla s(\mathbf{r}) \right]. \qquad (6.8)$$

The condition that $w'$ is a minimum now gives exactly the same equations as those for one electron in § 3, and since the total electron density in a molecule has no nodes, the velocity $\mathbf{v}$ found by this approximation is unique, and will always be finite. Since $w'$ is found by the approximate solution of a variational problem, the true second-order energy change in a magnetic field is always smaller, and a molecule is always more paramagnetic than this calculation would suggest. (Of course the exact electron density must be used to calculate $w'$.) We also notice that since $w' \geqslant 0$, a molecule is always diamagnetic in our simple approximation ! *A posteriori* one concludes that the approximation is very bad if the molecule is not diamagnetic.

## 7. Discussion

The theory we have outlined in this paper is almost equivalent to Wick's theory of rotational currents; but it also resembles a variational method of Tillieu and Guy [19–22], [26] who write the wave function in a magnetic field as a multiple of the unperturbed one

$$\psi = \psi_0(1 + gH). \qquad (7.1)$$

The small correction function $g(\mathbf{r})$ is chosen to give the least energy. Their wave function is of precisely the same form as (2.6) when $S$ is small, if we replace $gH$ by $S/i\hbar$. Thus Tillieu and Guy's method is subject to the same difficulties as ours when the wave function has a node, and leads them to the mistaken conclusion that all non-degenerate molecules are diamagnetic [23]. On the other hand their method gives good results for the magnetic properties of some simple saturated molecules [21–22] in which the localized wave functions have no nodes.

One may also follow an idea put forward recently by Rebane [24] and interpret the velocity field in terms of a transformation to a new vector potential $\mathbf{A}^+$;

$$\frac{e}{c} \mathbf{A}^+ = \left( \frac{e}{c} \mathbf{A} - \nabla S \right), \quad \frac{e}{mc} \mathbf{A}^+ = \mathbf{v}. \qquad (7.2)$$

With this new vector potential, which does not generally satisfy the condition that

$$\mathrm{div}\ \mathbf{A}^+ = 0, \qquad (7.3)$$

the phase function $S$ is transformed away, and the wave function in the magnetic field is real, equal to $\theta(\mathbf{r})$. From his point of view $S$ is also the transformation function $\lambda$ in (2.4) which converts $\mathbf{A}_0$ into $\mathbf{A}^+$, and corresponds closely to the 'superpotential' ([7], p. 70) in London's macroscopic theory of superconductivity. When there is more than one electron Rebane's proposed gauge transformation would involve a vector potential in many dimensions which has singularities at the nodes. However, one can also derive $\mathbf{A}^+$ in another way, taking $S$ from (6.8) instead. In this case $\mathbf{A}^+$ is the vector potential which makes the

paramagnetic part of the magnetic susceptibility in Van Vleck's formula [25] as small as possible, as one may see from (6.7). In the theory of rotational currents the choice of $S$ in (6.6) is precisely analogous to Espe's irrotational flow approximation [12] for a molecule with many electrons.

It is unfortunate that the hydrodynamic equations and Tillieu and Guy's variational method are useful in such restricted conditions, as it is convenient to calculate the magnetic properties of a molecule from its ground state wave function. The methods are likely to be most useful in molecules where the paramagnetic terms in Van Vleck's formula are small: small saturated molecules like $H_2$ and methane. The worst molecules are ones with almost degenerate orbitals and with low-lying excited states, such as transition metal complexes.

## References

[1] WICK, G. C., 1948, *Phys. Rev.*, **73**, 51; 1933, *Z. Phys.*, **85**, 25; 1933, *Nuovo Cim.*, **10**, 118.

[2] Reference [6], page 22.

[3] RAMSEY, N. F., 1950, *Phys. Rev.*, **78**, 699.

[4] POPLE, J. A., BERNSTEIN, H. J., and SCHNEIDER, W. G., 1958, *High Resolution Nuclear Magnetic Resonance* (New York: McGraw-Hill).

[5] POPLE, J. A., 1959, *Ann. rev. phys. Chem.*, **10**, 331.

[6] VAN VLECK, J. H., 1932, *Electric and Magnetic Susceptibilities* (Oxford: Clarendon Press).

[7] LONDON, F., 1950, *Superfluids*, Volume I (New York: John Wiley and Sons).

[8] LONDON, F., 1937, *J. Phys. Radium*, **8**, 397; *J. chem. Phys.*, **5**, 837.

[9] POPLE, J. A., 1956, *J. chem. Phys.*, **24**, 1111.

[10] POPLE, J. A., 1958, *Mol. Phys.*, **1**, 175.

[11] McWEENY, R., 1958, *Mol. Phys.*, **1**, 311.

[12] ESPE, I., 1956, *Phys. Rev.*, **103**, 1254.

[13] RAMSEY, N. F., 1956, *Molecular Beams* (Oxford: Clarendon Press).

[14] RAMSEY, N. F., 1940, *Phys. Rev.*, **58**, 226.

[15] ESHBACH, J. R., and STRANDBERG, M. W. P., 1952, *Phys. Rev.*, **85**, 24.

[16] RAMSEY, N. F., 1952, *Phys. Rev.*, **87**, 1075.

[17] RAMSEY, reference [13], page 166.

[18] RAMSEY, N. F., 1952, *Phys. Rev.*, **86**, 243.

[19] TILLIEU, J., and GUY, G., 1956, *J. chem. Phys.*, **24**, 1117.

[20] TILLIEU, J., and GUY, G., 1954, *Comptes Rendus*, **239**, 1203, 1283; 1955, *Ibid.*, **240**, 1402; 1955, *Ibid.*, **241**, 382; 1956, *Ibid.*, **242**, 1279.

[21] DAS, T. P., and BERSOHN, R., 1956, *Phys. Rev.*, **104**, 849; 1959, *Ibid.*, **115**, 897.

[22] STEPHEN, M. J., 1957, *Proc. roy. Soc.* A, **243**, 264.

[23] GUY, G., TILLIEU, J., and BARDET, J., 1958, *Comptes Rendus*, **246**, 574.

[24] REBANE, T. K., 1960, *Soviet Physics, J.E.T.P.* (English translation), **11**, 694; Russian original, 1960, *J.E.T.P.*, **38**, 963.

[25] VAN VLECK, J. H., reference [6], page 275.

[26] TILLIEU, J., 1957, *Ann. Phys.*, **2**, 471, 631.

# The nuclear magnetic resonance spectrum
## of 1: 2 : 4-trichlorobenzene

by C. N. BANWELL

University Chemical Laboratories, Lensfield Road, Cambridge†

Although the magnitudes of nuclear spin–spin coupling constants between the hydrogen nuclei of aromatic systems have long been well established [1], interest has recently arisen in their relative signs [2, 3]. The purpose of this note is to show that in 1:2:4-trichlorobenzene the three coupling constants are all of the same sign. The 40 Mc/s spectrum of this compound was previously published by Pople *et al.* [4] but these authors made no specific statements regarding the relative signs of the coupling constants.

The spectrum of the pure liquid was obtained using a Varian 4300B Spectrometer equipped with sample spinner and operating at 40 and 16·2 Mc/s. Resonance positions were measured by the side-band technique of Arnold and Packard [5]. The analysis of the spectrum of this ABC-type molecule [6] was carried out by the methods previously described [7], the assignment of resonances to specific nuclei being made on the basis of the magnitudes of coupling constants.

The 40 Mc/s spectrum is shown in figure 1 together with a calculated spectrum. It was found possible to fit the observed frequency and intensity data to within
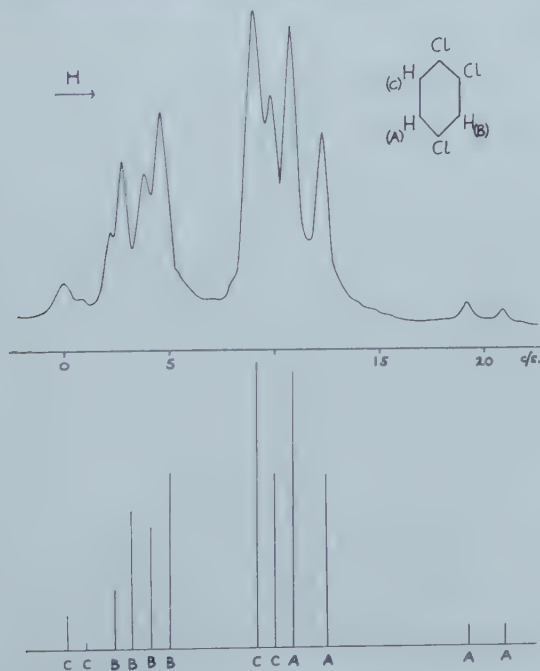


Figure 1. Observed and calculated 40 Mc/s spectra of 1 : 2 : 4-trichlorobenzene.

† Present address: Laboratorium für phys. Chemie, Eidgenössische Technische Hochschule, Zürich.

experimental errors by spectra calculated from either of the following sets of parameters:

| | $\sigma_B - \sigma_A$ | $\sigma_C - \sigma_A$ | $J^{AC}_{ortho}$ | $J^{AB}_{meta}$ | $J^{BC}_{para}$ |
|---|---|---|---|---|---|
| (a) | 9·7 | 6·3 | +8·7 | +2·4 | +0·2 c/sec |
| (b) | 9·6 | 6·3 | +8·8 | −2·0 | −0·5 c/sec |

Since the calculated spectra are virtually identical only one is shown in the figure. Spectra calculated with other possible sign combinations of coupling constants were in wide disagreement with the experimental data.

Figure 2 illustrates the 16·2 Mc/s spectrum and includes spectra (a) and (b) calculated from the parameters of (a) and (b) above after reduction of the chemical shifts by a factor of 16·2/40. In order to aid visual summation of overlapped lines in the calculated spectra Lorentzian curves have been drawn about each line and summed (dotted curve). The half-width was chosen to give an apparent resolving power comparable to that of the observed spectrum.
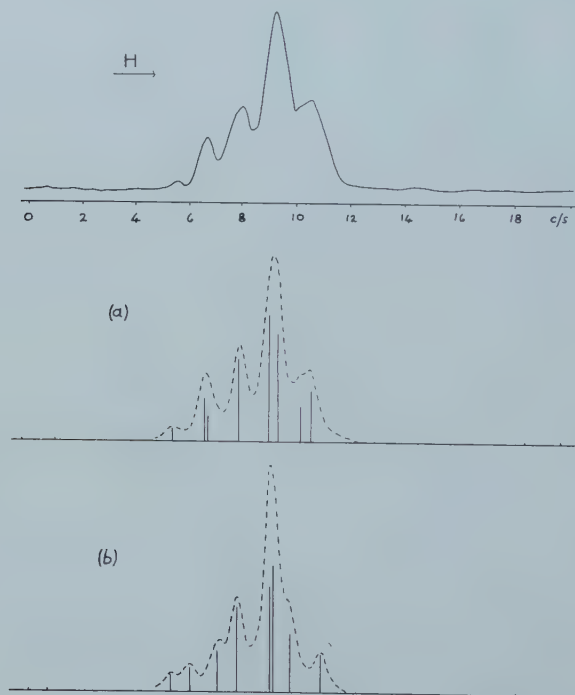


Figure 2. The observed 16·2 Mc/s spectrum of 1:2:4-trichlorobenzene together with spectra calculated from the parameters (a) and (b) given in the text.

It is evident that figure 2 (a) is in better agreement with the observed data than 2 (b) and, accordingly, we are able to choose the nuclear magnetic resonance parameters of 1:2:4-trichlorobenzene as follows:

$$\sigma_B - \sigma_A = +0·24 \pm 0·02 \text{ p.p.m.} \qquad J^{AC}_{ortho} = \ 8·7\dagger \pm 0·2 \text{ c/sec.}$$
$$\sigma_C - \sigma_A = +0·16 \pm 0·02 \text{ p.p.m.} \qquad J^{AB}_{meta} = +2·4 \ \pm 0·2 \text{ c/sec.}$$
$$J^{BC}_{para} = +0·2 \ \pm 0·2 \text{ c/sec.}$$

† Assumed positive; the signs of the other coupling constants are relative to this.

The magnitudes of the three coupling constants are comparable with those reported earlier for other substituted aromatic compounds [1] and their relative signs agree with those established by Bak *et al.* for fluorobenzene [2] and by Fessenden and Waugh for 2 : 4-dichloroaniline and 2 : 5-dichloroaniline [3]. Furthermore the sign and magnitude of $J_{para}$ reported above and by Fessenden and Waugh is in good agreement with the value calculated by McConnell [8] for benzene and naphthalene, assuming that the $\pi$-electron contribution is the only factor of importance in this constant.

McConnell further showed that the $\pi$-electron contribution gives a small negative coupling (about $-0.2$ c sec) to $J_{meta}$; however, the observed magnitudes of this constant (1 to 3 c sec) are sufficiently large to show that the $\sigma$-electron contribution, and not the $\pi$-contribution, is the dominating factor. The careful reasoning of Bak *et al.* [2], leading to the conclusion that if $J_{ortho}$ and $J_{meta}$ are the same sign then their sign is positive, indicates that the $\sigma$-electron contribution is about $+2$ c sec at the *meta* position. Thus the behaviour of aromatic systems is in sharp contrast to that of unsaturated aliphatic compounds where the $\sigma$-contribution to the coupling is more strongly attenuated, and the 'alternating sign' rule predicted by the Dirac vector model appears to be obeyed by the coupling constants [7, 9].

References

[1] SCHNEIDER, W. G., BERNSTEIN, H. J., and POPLE, J. A., 1957, *Canad. J. Chem.*, **35**, 1060.
GUTOWSKY, H. S., HOLM, C. H., SAIKA, A., and WILLIAMS, G. A., 1957, *J. Amer. chem. Soc.*, **79**, 4596.
RICHARDS, R. E., and SCHAEFER, T. P., 1958, *Trans. Faraday Soc.*, **54**, 1280.
LEANE, J. B., and RICHARDS, R. E., 1959, *Trans. Faraday Soc.*, **55**, 707.
CLOUGH, S., 1959, *Mol. Phys.*, **2**, 349.
[2] BAK, B., SHOOLERY, J. N., and WILLIAMS, G. A., 1958, *J. mol. Spec.*, **2**, 525.
[3] FESSENDEN, R. W., and WAUGH, J. S., 1959, *J. chem. Phys.*, **31**, 996.
[4] POPLE, J. A., SCHNEIDER, W. G., and BERNSTEIN, H. J., 1959, *High-Resolution Nuclear Magnetic Resonance* (McGraw-Hill Book Co. Inc.), p. 264.
[5] ARNOLD, J. T., and PACKARD, M. E., 1951, *J. chem. Phys.*, **19**, 1608.
[6] BERNSTEIN, H. J., POPLE, J. A., and SCHNEIDER, W. G., 1957, *Canad. J. Chem.*, **35**, 65.
[7] BANWELL, C. N., and SHEPPARD, N., 1960, *Mol. Phys.*, **3**, 351.
[8] MCCONNELL, H. M., 1959, *J. chem. Phys.*, **30**, 126.
[9] ALEXANDER, S., 1958, *J. chem. Phys.*, **28**, 358.
ELVIDGE, J. A., and JACKMAN, L. M., 1959, *Proc. chem. Soc.*, p. 89.

# On the electronic structures of $NO_2$ and its plane dimer $N_2O_4$

by JOSIANE SERRE

Laboratoire de Chimie, Ecole Normale Supérieure, Paris

The present work was undertaken to study the electronic structures of $NO_2$ and its dimer $N_2O_4$, in connection with the interpretation by Coulson and Duchesne [1] of the nature of the $N$—$N$ bond between the two $NO_2$ groups of the plane dimer $N_2O_4$. The method used is the self-consistent field method simplified by the approximations of Parr and Pariser.

The value chosen for the resonance integral $\beta_{N-O}$ is equal to the half-sum of the values of $\beta_{N\ N}$ and $\beta_{O-O}$ empirically determined for the bond lengths of $NO_2, r = 1\cdot19$ A [2]. The integral $\beta_{O-O}$ in the oxygen molecule has been determined by Parr and Fumi [3]. In the present work the integral $\beta_{N-N}$ is evaluated in the same way, fitting it to the excitation energy $^1\Sigma_u \leftarrow {}^1\Sigma_g^+$ obtained from Morse curves for these two states of $N_2$. The configuration interaction was included in this part of the calculation. For $r = 1\cdot19$ Å, we found $\beta_{N\ O} = -4\cdot30$ ev.

We computed $NO_2$ with eight electrons, each of the oxygens in the valence-state $(O, V_2, s^2 p_x^2 p_y p_z)$ contributing one $2p_y$ electron and one $2p_x$ lone-pair and the nitrogen in the valence state $(N, V_3, s p_z p_x p_y^2)$ contributing two $2p_y$ electrons.

The unpaired electron of $NO_2$ was considered as a core electron, localized on the nitrogen [4]. Watanabe [5] and his co-workers found at least two electronic transitions in the $NO_2$ absorption system between 2000 A and 2700 Å. We computed four transitions and found them at 1388 Å, 1844 Å, 1967 Å and 2398 Å. Our agreement with the experiment is rather good although our computation is much less extensive than McEwen's [6] work.

If $N_2O_4$ is built up as Coulson and Duchesne claimed, the orbital of the lone-pair electrons of $N$ must be very close to a pure $s$ orbital. The nitrogen atoms then are in the valence state $(N, V_3, s^2 p_x p_y p_z)$. A new calculation of $NO_2$ and $N_2O_4$ was undertaken with the nitrogens in this valence state; $NO_2$ with seven electrons and $N_2O_4$ with fourteen: one $2p_y$ electron and one $2p_x$ lone-pair from each oxygen and one $2p_y$ electron from each nitrogen. There are eight orbitals $\phi_1, \ldots, \phi_8$ in which the fourteen electrons may be disposed. The orbitals $\phi_2$, $\phi_3$, $\phi_4$ and $\phi_5$ are those of the four lone-pairs. The orbitals $\phi_1$, $\phi_6$, $\phi_7$ and $\phi_8$ respectively belong to the $B_{1u}$, $B_{3g}$, $B_{2g}$ and $A_{1u}$ species of the $N_2O_4$ symmetry group. The coefficients of $\phi_7$ and $\phi_8$ are entirely determined by symmetry; those of $\phi_1$ and $\phi_6$ are given by the S.C.F. method.

The S.C.F. computation has been done for four configurations: the two closed-shell singlets of $^1A_{1g}$ symmetry $\phi_1^2 \phi_2^2 \phi_3^2 \phi_4^2 \phi_5^2 \phi_6^2 \phi_7^2$ and $\phi_1^2 \phi_2^2 \phi_3^2 \phi_4^2 \phi_5^2 \phi_6^2 \phi_8^2$ and the two $\phi_1^2 \phi_2^2 \phi_3^2 \phi_4^2 \phi_5^2 \phi_6^2 \phi_7^1 \phi_8^1$ corresponding to the singlet and triplet of $B_{2u}$ symmetry. For these four configurations we found the following energy values:

$$E_I(A_{1g}) = -32\cdot50 \text{ A.U.}, \quad E_{II}(A_{1g}) = -32\cdot51 \text{ A.U. and } E(^1B_{2u}) = -32\cdot40 \text{ A.U.},$$
$$E(^3B_{2u}) = -32\cdot62 \text{ A.U.}$$

The singlets I and II were calculated independently without orthogonality restrictions. But, even in the S.C.F. method we have a non-zero configuration interaction element between these nearly degenerate $^1A_{1g}$ configurations. By a configuration interaction method† two better mutually orthogonal $^1A_{1g}$ wave functions were obtained. With this procedure the energy value of the lower $A_{1g}$ singlet becomes $E' = -32\cdot62$ a.u. which is identical with that of the $^3B_{2u}$ triplet. For the triplet as well as for the singlet state a more refined configuration interaction calculation could possibly change the energies. This calculation is in progress but it is not yet possible to predict any result. In conclusion we can say that in our computation based on Coulson's and Duchesne's model the lowest triplet and the lowest singlet seem to be nearly degenerate, which is not in agreement with experimental data.

By a calculation founded on another method Green and Linnett [7] in a paper published after this work had been finished† also arrived at a conclusion contrary to the model of Coulson and Duchesne.

## REFERENCES

[1] COULSON, C. A., and DUCHESNE, J., 1957, *Bull. Acad. Belg. Cl. Sci.*, **43**, 522.
[2] MOORE, C. E., 1953, *J. opt. Soc. Amer.*, **43**, 1045.
[3] FUMI, F. G., and PARR, R. G., 1953, *J. chem. Phys.*, **21**, 1864.
[4] WALSH, A. D., 1953, *J. chem. Soc.*, p. 2266.
[5] NAKAYAMA, T., KITAMURA, M. Y., and WATANABE, K., 1959, *J. chem. Phys.*, **30**, 1180.
[6] McEWEN, K. L., 1960, *J. chem. Phys.*, **32**, 1801.
[7] GREEN, M., and LINNETT, J. W., 1961, *Trans. Faraday Soc.*, **57**, 1 and 10.

† The author wants to thank the Referee of this note for having drawn her attention to this point.

# The effects of orbital degeneracy in the E.S.R. spectrum of the coronene positive ion

by J. R. BOLTON and A. CARRINGTON

Department of Theoretical Chemistry,
University of Cambridge

Recent theoretical interest in the electron spin resonance spectra of aromatic negative ions having orbitally degenerate ground states has been stimulated by the experimental results of Townsend and Weissman [1]. They found that hyperfine lines in the spectra of the benzene and coronene negative ions are unusually broad and furthermore, that these ions have enhanced spin–lattice relaxation times, so that their spectra are not easily saturated at high microwave power levels. The suggestion by Townsend and Weissman that the broadening of the hyperfine lines is due to Jahn-Teller distortions which modulate the spin density has been examined in detail by McConnell and McLachlan [2, 3] and found to be essentially correct. McConnell [4] has suggested that spin–orbit coupling effects, especially large in the case of a degenerate or near degenerate state, might be responsible for the shorter relaxation time.

Experimental study of such systems is limited to these observations and further information is obviously desirable. We have found that the coronene positive ion, which should also have a degenerate ground state, gives a good e.s.r. spectrum exhibiting the features described above. One expects to observe a maximum of thirteen equally spaced hyperfine lines arising from interaction of the twelve equivalent protons. We have definitely observed eleven of these lines with a spacing of 1·53 gauss and a width between the points of maximum slope of 450 milligauss, compared with a normal width of 50–100 milligauss. The spectrum, obtained by dissolving coronene in concentrated sulphuric acid, is shown in figure 1. This system is free of certain complications present in the
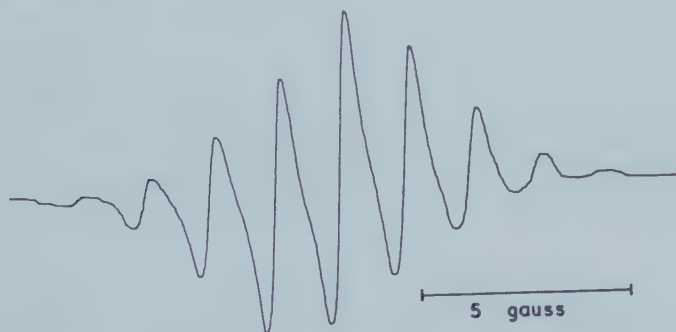


Figure 1. E.S.R. spectrum of the coronene positive ion showing the nine central components. The remaining four components can be observed on increasing amplification.

benzene and coronene negative ion systems. Factors which can contribute to the line width in these cases include rapid electron exchange between the mono-negative ion and the hydrocarbon or its di-negative ion, and unresolved alkali-metal hyperfine structure.

Figure 2 summarizes the results of a comparative study of the coronene and perylene positive ions. The three spectra of each ion were recorded at different microwave power levels, other instrumental controls remaining constant to
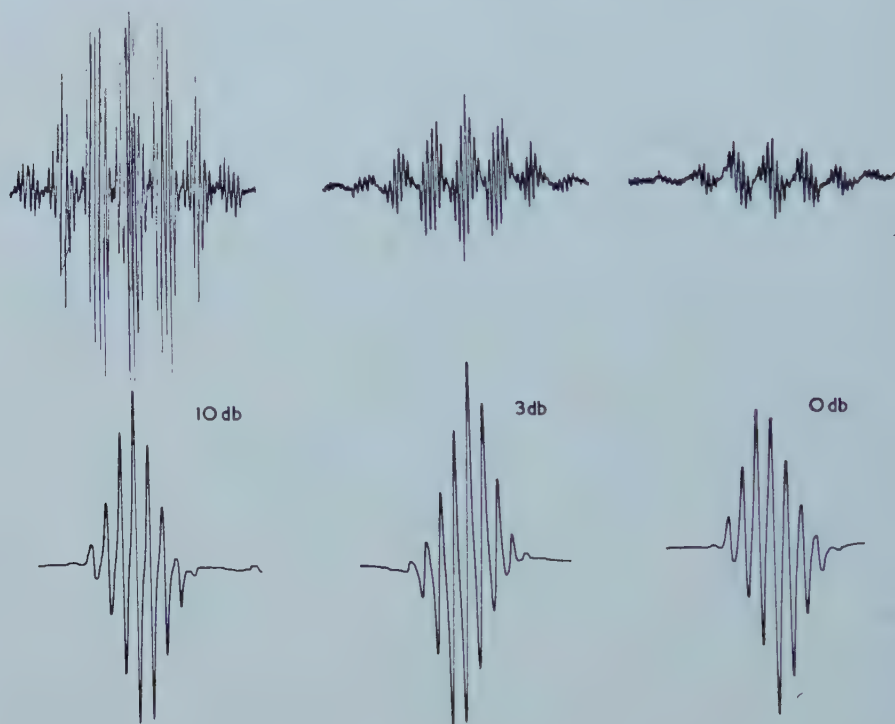


Figure 2. A comparative study of the perylene (top) and coronene (bottom) positive ions with the microwave power increasing from left to right.

within ±5 per cent. The perylene positive ion, which has a non-degenerate ground state, gives a spectrum [5] which is easily saturated, whilst we are unable to saturate the coronene spectrum under comparable conditions.

An accurate measurement of the $g$-value would also be desirable but we are at present unable to determine this with sufficient precision.

The apparatus used was a Varian 100 kc E.S.R. spectrometer employing a Varian VA6315/V–153 klystron with a maximum power output of approximately 100 milliwatts.

REFERENCES

[1] TOWNSEND, M. C., and WEISSMAN, S. I., 1960, *J. chem. Phys.*, **32**, 309.
[2] McCONNELL, H. M., and McLACHLAN, A. D., 1961, *J. chem. Phys.*, **34**, 1.
[3] HOBEY, W. D., and McLACHLAN, A. D., 1960, *J. chem. Phys.*, **33**, 1695.
[4] McCONNELL, H. M., 1961, *J. chem. Phys.*, **34**, 13.
[5] CARRINGTON, A., DRAVNICKS, F., and SYMONS, M. C. R., 1959, *J. chem. Soc.*, p. 947.

# Intramolecular excitation transfer. The lowest $n \rightarrow \pi^*$ transitions in pyrazine†

by M. A. EL SAYED and G. W. ROBINSON

Gates and Crellin Laboratories of Chemistry‡, California Institute of
Technology, Pasadena, California

In the pyrazine molecule, which has filled non-bonding orbitals *para* to
each other, two orbitally degenerate $n \rightarrow \pi^*$ transitions are expected, one
symmetry forbidden and one symmetry allowed. Interelectronic inter-
actions remove this degeneracy. The lowest pair of $(n, \pi^*)$ triplet states
and the corresponding pair of singlet states are studied with a view towards
determining the magnitude of such interactions and the ordering of the
forbidden and allowed components. Absorption spectra are obtained of
pyrazine in crystalline hydrogen and rare gases at $4 \cdot 2°$K, of pure crystalline
pyrazine at $4 \cdot 2°$K, and of 42 metres of pyrazine vapour at various pressures.
The phosphorescence spectrum of pyrazine in crystalline rare gases at $4 \cdot 2°$K
also is studied. The splitting between the two singlet components is found
to be approximately 435 cm$^{-1}$ with the forbidden component lying lowest.
The forbidden singlet–singlet transition gains some of its intensity through
vibronic mixing with a $(\pi, \pi^*)$ state, but vibronic coupling between the two
$(n, \pi^*)$ states also may be present. The strongest part of the singlet–triplet
absorption spectrum is found to involve the same upper state as the phos-
phorescence spectrum, and the transition is shown to be symmetry allowed.
It is strongly suggested that the ordering of the allowed and forbidden com-
ponents of the triplet state is inverted from that of the singlet, or the two
states may lie very close together. Using an ' independent systems ' model,
a calculation of the splitting, with the inclusion of exchange is made. The
theory indicates that the singlet states are indeed split by a coulomb term
having roughly the expected magnitude with the forbidden component lying
lowest; in addition, there is a very small exchange term with the opposite
sign. The splitting between the triplets is shown to involve only the small
exchange term, and the order of the allowed and forbidden components
becomes reversed. There is no indication of pyrazine fluorescence at $4 \cdot 2°$K
in any of the solids used. This fact illustrates the high efficiency of the
singlet–triplet radiationless process even under these conditions where the
rate might be expected to be a minimum for condensed phases. An interest-
ing alternation of spacing has been discovered in the first few quantum levels
of the 600 cm$^{-1}$$a_{1g}$ ring-bending vibration of the ground electronic state of
the molecule.

---

## 1. INTRODUCTION

In pyrazine (*p*-diazabenzene) orbitally degenerate $(n, \pi^*)$ transitions can
occur from each end of the molecule. Pyrazine is of point-group symmetry $D_{2h}$.
The representations $B_{1u}$, $B_{2u}$ and $B_{3u}$ are those of the vectors **z**, **y**, **x**, while

M.P.

S

the representations $B_{1g}$, $B_{2g}$ and $B_{3g}$ correspond to the rotations $R_z$, $R_y$ and $R_x$ respectively. There is an ambiguity in assigning molecule-fixed axes to $x$, $y$ and $z$. As illustrated in figure 1, we have chosen the $N \dots N$ axis to be the $z$ axis and the $yz$ plane to be the molecular plane. This notation conforms to the recommendations published by Mulliken [1] but unfortunately introduces a third notation for pyrazine. The correlation between the representation subscripts used by various authors is given in the following table:

| Molecular plane<br>$N \dots N$ axis | $yz$<br>$z$ | $xz$<br>$z$ | $xy$<br>$y$ |
|---|---|---|---|
| Correlation | 1<br>2<br>3 | 1<br>3<br>2 | 2<br>3<br>1 |
| References in text | This<br>paper | [11], [15]<br>[17] | [6], [7],<br>[8], [9]<br>[10] |

Thus the allowed component of the first $(n, \pi^*)$ singlet state has symmetry $^1B_{3u}$ in our notation, $^1B_{2u}$ in the Goodman-Kasha [11] notation and $^1B_{1u}$ in the notation of Ito *et al.* [8]. Electronic repulsion interactions are expected to remove the two-fold degeneracy of the excited $(n, \pi^*)$ states. This molecule therefore presents a prototype example of the same kind of interactions which occur between molecules in crystals [2] and between chromophores in 'double molecules' [3] and in long-chain molecules [4]. For this reason it is important to know the magnitude of the splitting and to try to understand its origin for both the multiplicity allowed and the multiplicity forbidden transitions.
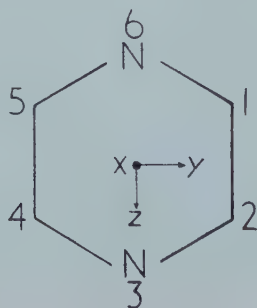


Figure 1.   Pyrazine coordinates used in this paper.

Nitrogen heterocyclics usually are characterized by rather sharp, linelike absorptions to the long wavelength side of the stronger and broader $\pi \to \pi^*$ absorption spectra. These are known [5] to be due to an electronic transition from the approximately $sp^2$-nitrogen atomic orbital to the lowest vacant anti-bonding $\pi^*$-molecular orbital of the ring and are designated $n \to \pi^*$ transitions. The $s$-character of the hybrid $n$-orbital is responsible for the dipole allowedness of

these transitions; consequently, the polarization is perpendicular to the molecular plane. This has been shown to be indeed the case by the recent high resolution studies of Innes *et al.* [6] for the three diazabenzenes.

The absorption spectrum of pyrazine near 3200 Å was first identified as $n \to \pi^*$ by Halverson and Hirt [7]. Ito and co-workers [8] analysed the vapour spectrum in this region, and because of the apparent presence of two kinds of band shapes and the existence of two different ring vibrations near 600 cm$^{-1}$, they concluded that the absorption is caused by two transitions, one weak and one strong, with nearly coinciding (0, 0) bands. These were identified as the two expected singlet singlet (S'–S) components of the first orbitally degenerate $n \to \pi^*$ transition, but no explanation was given as to why the electronic splitting was so small. Hirt [9] reanalysed the spectrum in terms of a single transition but paid little attention to vibronic selection rules. Very recently, Innes and his co-workers [6, 10] have reported on the analysis of the rotational structure in the vapour-phase spectrum under extremely high resolution. In this way the band origins, and the vibrational frequencies, could be determined to within better than 0·1 cm$^{-1}$; and, of greatest importance, the polarization of the bands could be ascertained unequivocally. In the more recent paper [6] the authors felt that there was no need to make the two-transition hypothesis if it is assumed that the molecule becomes non-planar in the excited state.

The corresponding singlet–triplet (T S) system has been identified by Goodman and Kasha [11] through the solution absorption spectrum and phosphorescence studies of pyrazine and a dimethyl derivative. This system occurs near 3850 Å.

Spectra of many molecules in simple non-polar crystalline solids [12] at low temperatures (4·2 K) are known to be relatively sharp. Because of the absence of hot bands such spectra of complex molecules are simpler than vapour-phase spectra. In addition, external perturbations may be altered rather smoothly by employing 'solvents' with a wide range of polarizabilities; e.g. H$_2$, Ne, A, Kr, Xe and the pure molecular crystal. In this way spectral shifts and intensity perturbations can be studied rather precisely as a function of environment, and the results of such studies are very often useful in the interpretation of a complex spectrum. For these reasons it was thought that the spectrum of pyrazine obtained under these conditions might be quite helpful in the study of the transition. This paper reports the results of this work. The singlet–triplet absorption spectrum of gaseous pyrazine, excitation transfer splitting in the singlet and triplet $n \to \pi^*$ states, and the analysis of the singlet–singlet $n \to \pi^*$ transition are discussed in light of the low temperature results.

## 2. EXPERIMENTAL

### 2.1. *Low-temperature spectra*

Pyrazine was obtained commercially† and was purified by several vacuum sublimations. The crystalline material was further purified by a number of zone refining passes. The pyrazine and the solvent gas were co-crystallized in the usual way [12] by passing the solvent gas (pressure ∼3 mm Hg) through a

† Aldrich Chemical Co., 3747 N. Booth Street, Milwaukee, Wisconsin, U.S.A.

$-53\,°c$ cold trap containing the pyrazine.    Since the vapour pressure of pyrazine at this temperature is roughly $10\,\mu$ Hg, the mole ratio of solvent gas to pyrazine is about $300:1$.    Ratios very much lower than $50:1$ were found to result in considerable dimer formation†.    The gaseous mixture was condensed at $4\cdot2\,°\text{k}$ on a quartz window through which the spectra were observed.

A crude 'crystal' spectrum was obtained by similarly condensing pure pyrazine vapour at liquid nitrogen temperature; liquid nitrogen was then replaced by liquid helium.    The bands in the condensed crystal spectrum are intrinsically rather diffuse, and little sharpening was apparent at the lower temperature.    A thin crystal prepared from the melt between quartz plates showed a similar broadening.    In spite of the poor quality of the crystal spectrum, it nevertheless served its intended purpose of showing the pyrazine spectrum under conditions of a moderately strong *asymmetric* perturbation, unlike that present when the environment is a rare gas.

The light source used for the low-temperature absorption spectra and for excitation of the phosphorescence spectra was a Hanovia high-pressure Xe lamp. Since the phosphorescence yield of pyrazine in the low-temperature crystals is very high and the spectrum is very sharp, the phosphorescence was easily detectable, even without filtering, above the background continuum used to excite it. A Corning ultra-violet filter No. 9863 improved the contrast in the longer wavelength region.    More recent phosphorescence spectra devoid of background were obtained through excitation with radiation from an $f/10$ monochromator. Exposure times in this case were of the order of five minutes.    The low temperature spectra were photographed on a medium Bausch and Lomb quartz prism instrument giving better than 1 Å unit resolution in the region of interest. An iron comparison spectrum was used.

### 2.2. *Long path length spectra*

The hot band structure of the (S′–S) absorption, as well as the (T–S) absorption of the pure vapour, was obtained by use of the multiple-pass technique described by Bernstein and Herzberg [13].    Spherical mirrors having 150 cm radii of curvature were adjusted until a path length of 42 metres was obtained. Several pictures were taken, using a Pyrex filter to prevent any possible photolysis, while the vapour pressure was gradually increased from a few microns up to 8 mm. A large Bausch and Lomb spectrograph employing quartz optics was used for photographing the spectra, and the iron spectrum served as wavelength standard.

### 3. SINGLET–SINGLET SYSTEM

### 3.1. *Results*

Figure 2 shows the S′$(n, \pi^*)$–S absorption spectrum of pyrazine in the vapour phase at room temperature compared with the spectrum in solid A, Kr and Xe at $4\cdot2\,°\text{k}$, and the crystal spectrum at $4\cdot2\,°\text{k}$.    The spectrum of pryazine in solid $H_2$ is very similar to that in solid A except that it is shifted $20\,\text{cm}^{-1}$ to the *high* frequency side of the gas-phase spectrum.    With the exception of the hot band structure and the frequency shift, the striking similarity between the argon spectrum and the vapour spectrum should be noted.    The spectrum becomes

---

† This interesting aspect will be discussed in a future paper.
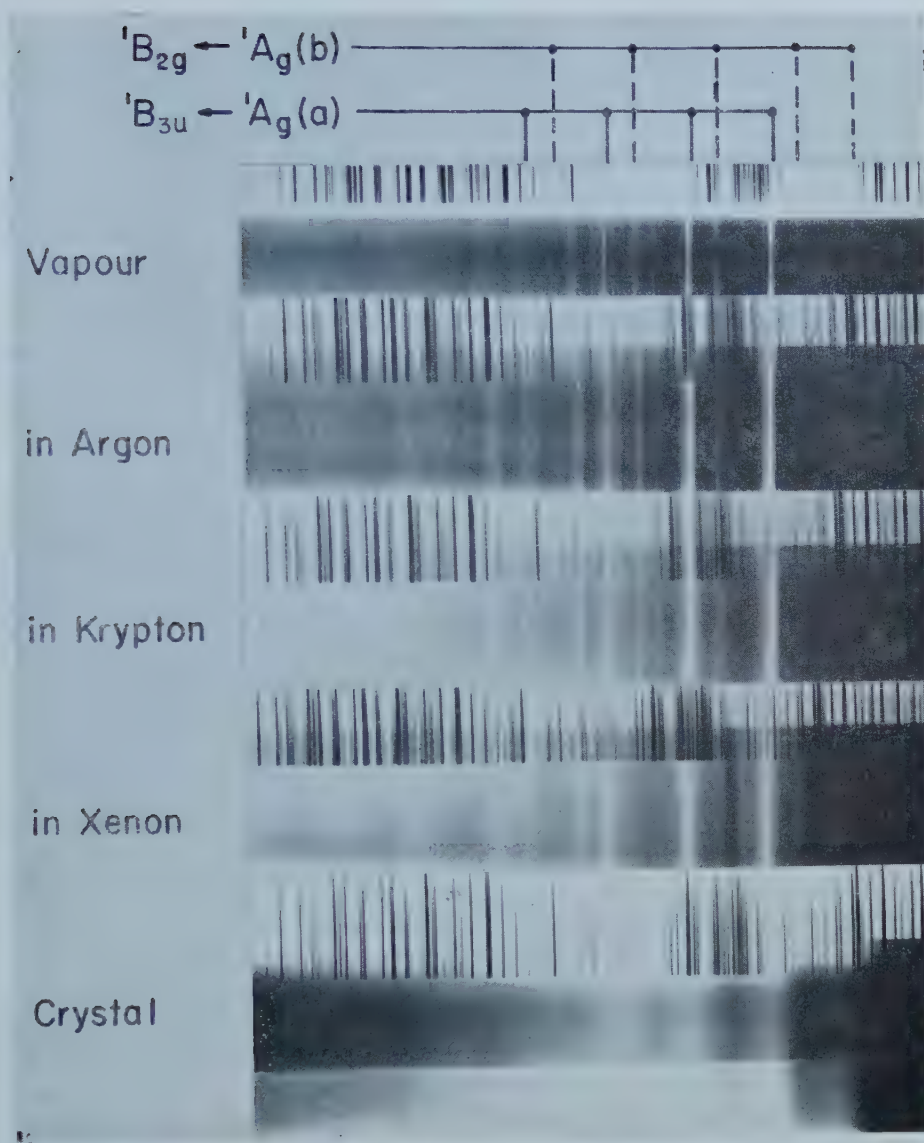
Figure 2. The first $n \rightarrow \pi^*$ singlet–singlet absorption spectrum of pyrazine in various environments. The (0, 0) band of the $^1B_{2g} \leftarrow {}^1A_g$ system can be seen clearly in the lower crystal spectrum. Bands in the vapour spectrum below the first two dotted lines on the right are hot bands of the $^1B_{3u} \leftarrow {}^1A_g$ system. Only in the cases of xenon and the pure crystal does the photograph clearly show either of the first two weak bands of the forbidden system.

somewhat broader in solid krypton and quite a bit broader in solid xenon and in the pure crystal. The characteristic features of the spectrum can be described in terms of a few leading bands which form progressions with totally symmetric vibrations, in particular the 560–580 cm$^{-1}$ ring-bending mode. Table 1 gives the position of the (0, 0) band of the allowed transition in each of the environments used. The spectra are shifted progressively to lower frequency (red-shift)

| Pyrazine environment | $^1B_{3u}-^1A_g$ | | $^3B_{3u}-^1A_g$ | |
|---|---|---|---|---|
| | $\nu$ (cm$^{-1}$) | $\Delta\nu$ (cm$^{-1}$) | $\nu$ (cm$^{-1}$) | $\Delta\nu$ (cm$^{-1}$) |
| Vapour | 30875 | — | 26818[b] | — |
| Hydrogen | 30895 | + 20 | 26802 | − 16 |
| Argon | 30684 | −191 | 26693 | −125 |
| Krypton | 30590 | −285 | 26612 | −206 |
| Xenon | 30470 | −405 | 26580 | −238 |

Table 1.   The positions and shifts[a] of the (0, 0) band of the $^{1,\,3}B_{3u}(n,\,\pi^*)-^1A_g$ transitions of pyrazine in crystalline rare gases and hydrogen at 4·2°K.

    a. The shift, $\Delta\nu=\nu$ (solid)$-\nu$ (vapour).
    b. From absorption spectrum of 42 metre path of vapour.

as the polarizability of the solvent increases.   This effect has been discussed in reference [12] and is normal.   The crystal shift, which is about the same size as the shift in solid krypton, may at first sight appear small.   However, for the $^1B_{2u}(\pi,\,\pi^*)-^1A_{1g}$ transition in benzene, the krypton, xenon and crystal red-shifts relative to the vapour are 251 cm$^{-1}$, 396 cm$^{-1}$ and 280 cm$^{-1}$ respectively [12]. These should be compared with 285 cm$^{-1}$, 405 cm$^{-1}$ and 270 cm$^{-1}$ in the present case.   An alternate way by which the crystal spectrum can be correlated with the other spectra would cause the crystal red-shift to be 850 cm$^{-1}$, which seems far too large.

    There are two important new features brought out by the low temperature spectra:

    I. There is a new band 195 cm$^{-1}$ to the *low* frequency side of the (0, 0) band of the allowed transition ($^1B_{3u}\leftarrow^1A_g$).   This band has not been observed in the spectrum of the vapour.   Its intensity is perturbed by a polarizable environment, being relatively strong in solid xenon, weaker in krypton and essentially missing in argon, in hydrogen and probably in the pure crystal as well.   It would be expected to have very low intensity in the vapour spectrum, and furthermore it would be overlapped by the strong hot band at − 182 cm$^{-1}$.

    II. Because of site-group symmetry lower than the point-group symmetry of the molecule, and non-zero intermolecular interactions, a symmetry forbidden (0, 0) band may gain intensity in the crystal spectrum [2].   The new band which appears in the crystal spectrum of pyrazine about 500 cm$^{-1}$ to lower frequency than the $^1B_{3u}\leftarrow^1A_g$ (0, 0) band therefore is identified as the (0, 0) band of the forbidden transition ($^1B_{2g}\leftarrow^1A_{1g}$).   The presence of this band was confirmed by increasing the absorbing path of pyrazine in solid krypton.   Eventually a very weak band appeared about 450 cm$^{-1}$ to the red of the $^1B_{3u}\leftarrow^1A_g$ (0, 0) band. Previous work on the 2600 Å singlet–singlet transition in benzene [12] showed that it was also possible to perturb by Kr and Xe the symmetry forbidden (0,0) band in that molecule.

    In addition to these two features, another new band appears in the solid solution spectra 260 cm$^{-1}$ to the high frequency side of the $^1B_{3u}\leftarrow^1A_g$ (0, 0) band. Its intensity is also enhanced as the rare gas environment becomes more polarizable.

## 3.2. *The arguments for two transitions*

The arguments which lead to the assignment of the bands in terms of two electronic transitions will now be discussed. The most important point is that weak bands, which cannot be ascribed to hot bands, have been found on the *low* frequency side of the strong (0, 0) band of Ito *et al.* [8]. Ito's (0, 0) band was the one also taken by Innes and his group [6] as their (0, 0) band, in terms of which the spectrum was interpreted as only a single electronic transition. The occurrence of weak bands to the red of this strong band definitely suggests the presence of some sort of forbiddenness in the transition.

A second important point deals with the polarization of the individual bands. The paper by Ito *et al.* [8] pointed out that some of the bands, including the strong (0, 0) band, appear sharp and some diffuse at the dispersion and resolution available in the second order of a 3 metre grating instrument. This point was more definitely established in the Innes experiments, where an examination of the rotational structure showed that the sharp bands were polarized, as expected for an allowed $n \rightarrow \pi^*$ transition, perpendicular to the molecular plane. The polarization of the diffuse bands has not yet been established [14].

To summarize, the presence of the weak band at $(0, 0) - 195$ cm$^{-1}$, the enhancement of the forbidden component at $\sim (0, 0) - 500$ cm$^{-1}$ by the crystal perturbations, and the polarization of the strong (0, 0) band all point strongly to the presence of two transitions, one allowed and one forbidden, with the forbidden component roughly 500 cm$^{-1}$ to the low frequency side of the allowed component. In addition, the presence and relative positions of the components are exactly what is expected theoretically for the molecule (§ 5). The relative simplicity of the phosphorescence spectrum (§ 4) compared with the absorption spectrum gives further experimental evidence for essentially a single transition in the one case and two transitions in the other.

## 3.3. *The vibrational analysis*

Table 2 gives an analysis of the important parts of the spectrum. A more precise value of the $^1B_{3u} - {}^1B_{2g}$ splitting can be obtained from this analysis. The value obtained† is 435 cm$^{-1}$, which is in good agreement with the values 450 cm$^{-1}$ from the solid Kr spectrum and the rough value 500 cm$^{-1}$ from the crystal spectrum. Some weak bands in the absorption spectrum have not been included in table 2 because it is not certain to which transition they belong. All of these weak bands were reported in [8], and two of them were reported by the Innes group [6, 10]. They occur at 1034 cm$^{-1}$, 1106 cm$^{-1}$, 1244 cm$^{-1}$ and 1371 cm$^{-1}$ to the short wavelength side of the (0, 0) band of the allowed transition. They are not associated with hot band structure since they occur at 4·2°K. There is indication in the low temperature spectrum that the 1106 cm$^{-1}$ band is actually 526 cm$^{-1}$ in combination with $\nu_{6a}'$. The 1371 cm$^{-1}$ band is probably the totally symmetric ring vibration $\nu_{8a}'$; and 1106 cm$^{-1}$ (if real) or 1244 cm$^{-1}$ could be $\nu_{9a}'$.

An alternation of energy level spacing of the $\nu_{6a}''(a_g)$ 600 cm$^{-1}$ ring-bending vibration is apparent in the hot-band structure of the $(S' \leftarrow S)$ absorption spectrum (table 2) and in the $(T \rightarrow S)$ phosphorescence spectrum (table 3). It

† The value 435 cm$^{-1}$ was obtained from the analysis before the pure crystal spectrum and the Kr spectrum were obtained.

| $\nu-\nu_{0,\,0}$ cm$^{-1}$ | $^1B_{3u} \leftarrow {}^1A_g$ Assignments[a] | $\nu-\nu_{0,\,0}$ cm$^{-1}$ | $^1B_{2g} \leftarrow {}^1A_g$ Assignments[a] |
|---|---|---|---|
| $-1827$[b] | $-3\nu_{6a}''$ | $-419$ [g] | $-\nu_{16b}''\,(b_{3u})$ |
| $-1229$[c] | $-2\nu_{6a}''$ | 0[h] | (0, 0) near 30440 cm$^{-1}$ |
| $-\,596$[c, d] | $-\nu_{6a}''$ | 105[i] | $-\nu_{6a}''+\nu_{11}'$ |
| $-\,182$[c] | (1, 1) of $\nu_{16b}$ | 240[h] | $\nu_{16b}'\,(b_{3u})$ |
| 0 | (0, 0) at 30876 cm$^{-1c}$ | 695[h] | $\nu_{11}'\,(b_{3u})$ |
| 58[c, e] | (1, 1) of $\nu_{16a}$ | 820[j] | |
| 583[c] | $\nu_{6a}'\,(a_g)$ | 1258[k] | $\nu_{11}'+\nu_{6a}'$ |
| 823[c, f] | $\nu_1'\,(a_g)$ | | |
| 1168[c] | $2\nu_{6a}'$ | | |

a. The notation is that of [15] except $b_{3u}=b_{2u}$; prime and double prime refer to excited and ground states respectively.
b. From absorption spectrum of 42 metre path of vapour.
c. Taken from [10].
d. Note the alternation of spacing in this hot band progression.
e. Assignment tentative; it means $\nu_{16a}'-\nu_{16a}''=58$ cm$^{-1}$.
f. Assignment tentative; this band is overlapped by $\nu_{11}'+\nu_{6a}'$ of $^1B_{2g} \leftarrow {}^1A_g$; see § 3.4.
g. B′ series of [8].
h. Observed at 4·2°K under environmental perturbation.
i. A′ series of [8].
j. C′ series of [8]. See § 3.4.
k. Overlapped by 823 cm$^{-1}$ band of $^1B_{3u} \leftarrow {}^1A_g$.

Table 2.   Analysis of prominent bands of the lowest $n-\pi^*$ absorption spectrum of pyrazine.

therefore is definitely a ground state phenomenon and, since it occurs in the vapour, it cannot be caused by environmental perturbations.   One tentatively can attribute the alternation to the fact that this vibration is derived from a doubly degenerate vibration in a regular hexagonal molecule $(D_{6h})$.   The pyrazine potential function has approximately this symmetry.   The coupling between the two 'doubly degenerate' components, 609 cm$^{-1}$ $(a_g)$ and 516 cm$^{-1}$ $(b_{2g})$ can occur only in even quantum levels because of symmetry considerations. Such a coupling is the most obvious explanation of the vibrational anomaly, but this hypothesis requires a more quantitative study.

### 3.4. $n, \pi^*$ vibronic coupling

One might expect a certain amount of vibronic coupling between the $(n, \pi^*)$ states themselves and, if so, the coupling vibrations should be of species $b_{1u}$.   In the forbidden system the vibronic polarization of such bands would be identical with that of the allowed system.   Ring vibrations of $b_{1u}$ symmetry have frequencies 1490 cm$^{-1}$ and 1022 cm$^{-1}$ in the ground state [15].   The bands 1034 cm$^{-1}$ and 526 cm$^{-1}$ become 1470 cm$^{-1}$ and 961 cm$^{-1}$ respectively in the forbidden system and could therefore be accounted for in the manner suggested above.   If these two bands comprise all the $(n, \pi^*)$ mixing in this molecule, then only about 10 per cent of the total intensity of the forbidden component is derived from this source.   The polarization of the important series labelled C′ in [8] is in doubt

| $\nu_0$, $_{0-\nu}$ cm$^{-1}$ | Int. | Assignment |
|---|---|---|
| 0 | vs | 0, 0 at 26818 cm$^{-1}$ (vapour) |
| 598[a] | s | $0, 0-\nu_{6a}''$ |
| 1023 | m | $0, 0-\nu_1''$ |
| 1232 | s | $0, 0-2\nu_{6a}''$ |
| 1509[b] | m | $0, 0-\nu_{8a}''$ |
| 1624 | m | $0, 0-\nu_1''-\nu_{6a}''$ |
| 1843 | s | $0, 0-3\nu_{6a}''$ |
| 2122 | m | $0, 0-\nu_{8a}''-\nu_{6a}''$ |
| 2246 | mw | $0, 0-\nu_1''-2\nu_{6a}''$ |
| 2461 | m | $0, 0-4\nu_{6a}''$ |
| 2754 | w | $0, 0-\nu_{8a}''-2\nu_{6a}''$ |
| 2855 | w | $0, 0-\nu_1''-3\nu_{6a}''$ |
| 3077 | mw | $0, 0-5\nu_{6a}''$ |
| 3673 | w | $0, 0-6\nu_{6a}''$ |

a. Note the alternation of spacing in the first few members of the $0, 0-n\nu_{6a}''$ progression. Because of lower instrumental dispersion, these differences are not as reliable as those in table 2.

b. The assignment of the progression is tentative since it is not in agreement with the Raman polarization work [15].

Table 3.   Analysis of the phosphorescence spectrum of pyrazine $[^3B_{3u}(n, \pi^*) \rightarrow {}^1A_g]$.

[14]. The series very likely belongs to the forbidden system because the separation of its first member from the allowed (0, 0) band is too small to be explained by a totally symmetric vibration. If the series is polarized in-plane, it can be assigned $\nu'_{16b} + n\nu'_{6a}$, with $n = 1, 2 \ldots$. The low relative intensity of the $n = 0$ member would then be puzzling. If it is polarized out-of-plane, over 90 per cent of the forbidden intensity is derived from $(n, \pi^*)$ vibronic coupling. One might also wonder about the assignment of the out-of-plane polarized band in table 2 with separation 823 cm$^{-1}$ from the (0, 0) band of the allowed system or 1258 cm$^{-1}$ from the (0, 0) band of the forbidden system. The rotational $\bar{B}$ constant for the upper state of this band is very low [10], a fact which may signal that some peculiarity is associated with it.

## 3.5. *The geometry of the excited state*

In-plane vibronic polarization in an $n \rightarrow \pi^*$ transition does not necessarily mean, as suggested by Innes *et al.* [6], that the molecule is non-planar in the excited state. Such an observation in this case would simply establish the fact that there is a forbidden component whose intensity is gained through mixing with a state having $B_{1u}$ or $B_{2u}$ symmetry. The most probable $(\pi, \pi^*)$ state is the one near 1600 Å [16], which is analogous to one component of the $^1E_{1u}$ state of benzene. If a molecule is non-planar in one of its combining states and planar in the other, the vibronic selection rules are governed by the $\pm$ symmetry property of the inversion doublets. An alternate progression (0, 2, 4 ... or 1, 3, 5 ...) of non-planar vibrations is expected to occur. Such a progression either does not exist or is very weak in the pyrazine spectrum showing that the molecule in its excited state cannot deviate greatly, if at all, from the planar equilibrium configuration.

## 4. SINGLET–TRIPLET SYSTEM

Sidman [17] calculated the spin–orbit coupling in pyrazine and found that the $^3B_{3u}$ $(n, \pi^*)$ state would mix primarily through the $y$-component of the spin–orbit operator; i.e. with a $^1B_{1u}$ $(\pi, \pi^*)$ state rather than with $^1B_{3u}$ $(n, \pi^*)$ or $^1B_{2u}$ $(\pi, \pi^*)$ states. The $^3B_{2g}$ state requires vibronic mixing by a $u$-vibration in addition to the spin–orbit coupling for it to combine through electric dipole transitions with the ground state.

The phosphorescence spectrum of pyrazine in EPA at $77°$K has been previously studied by Goodman and Kasha [11], who assigned the transition to $^3B_{3u}$ $(n, \pi^*) \rightarrow {}^1A_{1g}$. The (T–S) absorption spectrum of a concentrated solution of pyrazine in isopentane also was recorded by these authors; but it was not certain that the absorption and emission transitions involved the same upper state,
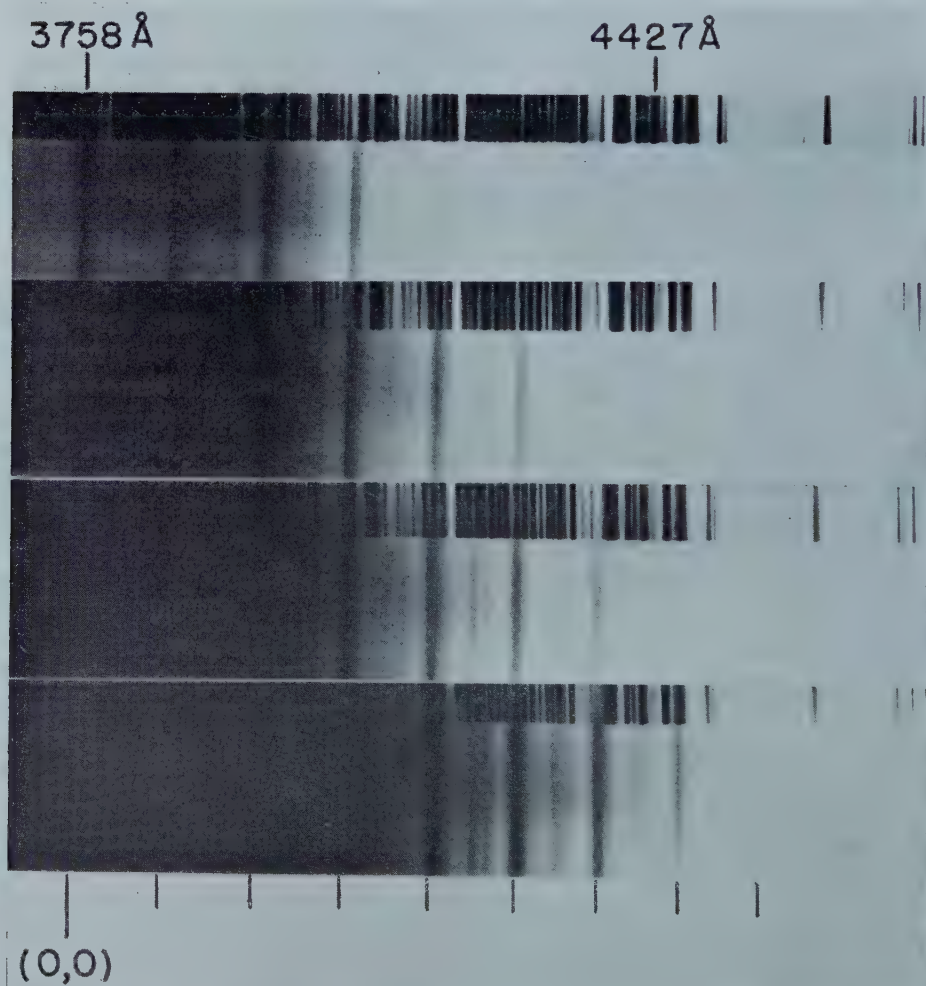


Figure 3. The phosphorescence spectrum $(^3B_{3u}(n,\ \pi^*) \rightarrow {}^1A_g)$ of pyrazine in crystalline krypton at $4·2°$K. The (0, 0) band is at 3756 Å. The exposure time increases from top to bottom. A Corning 9863 ultra-violet filter has been used to decrease the background radiation to the long wavelength side of 4000 Å.

nor was it clear that the transition was symmetry allowed, i.e. showed a (0, 0) band. While the intensity of the absorption indicated a symmetry allowed but multiplicity forbidden transition, the frequency measurements did not throw much light on the relationship between absorption and emission. The reported absorption–emission shift of 560 cm$^{-1}$ was considered [18] to be a rather large environmental shift of some kind, but it could indeed be taken to mean that the transitions in emission and absorption did not involve the same upper state. This is an important point. A more detailed examination of the (T–S) spectrum was required to settle it.

The phosphorescence spectrum of pyrazine in crystalline $H_2$ and the rare gases at 4·2°K is very sharp, and the bands are well resolved (figure 3). The bands are listed along with their probable assignment in table 3.

The absorption spectrum of 42 metres of pyrazine vapour at 8 mm Hg pressure reveals the singlet–triplet system; the first (longest wavelength) strong band of this system was found to lie at $26818 \pm 4$ cm$^{-1}$. This could be compared with the positions given in table 1 of the shortest wavelength solid solution phosphorescence bands. If this vapour absorption band and these phosphorescence bands in the different environments are taken to be the (0, 0) band of the same electronic system, it is seen that the resulting shifts relative to the vapour and relative to each other are highly consistent with those found for the (S′–S) transition. It is almost certain therefore that: (1) The (T–S) absorption spectrum has the same upper state as the phosphorescing state; and (2) the (0, 0) band occurs, showing that this upper state is $^3B_{3u}$, not $^3B_{2g}$. The Goodman–Kasha absorption–emission shift of 560 cm$^{-1}$ is therefore very likely an environmental effect. Because of the long lifetime of triplet states, it is virtually certain that energy relaxation to the lowest triplet state has occurred before emission. Since the phosphorescing state is $^3B_{3u}$, the $^3B_{2g}$ state must either be essentially degenerate† with $^3B_{3u}$ or lie above it. It appears therefore that while the singlet $(n, \pi^*)$ components are in the order $^1B_{3u}$ above $^1B_{2g}$, the order of the triplet $(n, \pi^*)$ components is reversed. Unfortunately, the magnitude of the splitting cannot be determined from the available data. In the next section it will be shown that the experimental results are in exact accord with what is expected theoretically. An estimate of the splitting of the two triplet components shows it to be very small and of sign opposite that of the singlet splitting.

## 5. The theoretical splitting

In $n \rightarrow \pi^*$ transitions in conjugated molecules the excited electron in the $\pi^*$-orbital is very probably highly localized‡ in the vicinity of the non-bonding positive hole because of the strong coulomb attraction of the electron with the hole. *Only in the case where the initial and final orbitals are both delocalized can the electron in the final state orbital realize considerable delocalization.* Thus, in the azabenzenes, the nature of the final $\psi_{-2}$ $\pi^*$-orbital is expected to depend heavily upon the type of transition under consideration, whether it be $n \rightarrow \pi^*$ or $\pi \rightarrow \pi^*$. Experimentally, the localization of $n \rightarrow \pi^*$ transitions in conjugated

---

† To within the order of $kT$, which in our experiments is 3 cm$^{-1}$.
‡ We acknowledge Professor W. T. Simpson for pointing out to us the importance of this effect in other molecules.

systems is evidenced by the fact that such transitions in many different molecules retain their identity with respect to the approximate magnitude of their transition energy. Variations in singlet–singlet transition probabilities do occur because of variations in the molecular $sp$-hybridization†.

Because of the probable localization of $n \rightarrow \pi^*$ excitation in the azabenzenes, we adopt an 'independent systems' approach for the calculation of the energy splittings. We consider here the case of two heterocyclic nitrogens labelled A and B. The extension to more complicated molecules is straightforward. Let the zero-order eigenfunctions $\Psi$ for the excited $(n, \pi^*)$ states be the symmetric and antisymmetric combinations of simple product functions,

$$\Psi_\pm = 2^{-1/2}(\Psi_A'\Psi_B \pm \Psi_A\Psi_B'), \tag{5.1}$$

where the $(')$ denotes, as the case may be, singlet or triplet $n \rightarrow \pi^*$ (localized) excitation. The energy splitting $(E_+ - E_-)$ between the $+$ and $-$ components is simply

$$\Delta E_\pm \equiv (E_+ - E_-) = 2 \langle \Psi_A'\Psi_B | H_{AB} | \Psi_A\Psi_B' \rangle, \tag{5.2}$$

where the non-vanishing elements of $H_{AB}$ involve only the sum over electron repulsion interactions of the A electrons with the B electrons. Labelling $n_A$, $\pi_A^*$, $n_B$, $\pi_B^*$ as $\psi_1$, $\psi_2$, $\psi_3$, $\psi_4$ respectively, neglecting all but four electrons, and allowing for exchange, one may write in a common notation,

$$\Psi_A'\Psi_B = 2^{-1/2}\{|\psi_1'(1)\bar{\psi}_2(2)\psi_3(3)\bar{\psi}_3(4)| - |\bar{\psi}_1'(1)\psi_2(2)\psi_3(3)\bar{\psi}_3(4)|\} \tag{5.3}$$

for the singlet state; and

$$\Psi_A'\Psi_B = 2^{-1/2}\{|\psi_1'(1)\bar{\psi}_2(2)\psi_3(3)\bar{\psi}_3(4)| + |\bar{\psi}_1'(1)\psi_2(2)\psi_3(3)\bar{\psi}_3(4)|\} \tag{5.4}$$

$$\begin{array}{c}|\psi_1'(1)\psi_2(2)\psi_3(3)\bar{\psi}_3(4)| \\ |\bar{\psi}_1'(1)\bar{\psi}_2(2)\psi_3(3)\bar{\psi}_3(4)|\end{array}$$

for the $M = +1$, $0$, $-1$ components respectively of the triplet state. A prime labels the excited state non-bonding orbital, and the factor $24^{-1/2}$ has been absorbed in all the determinants. Similar expressions may be written for $\Psi_A\Psi_B'$. If two-centre overlap effects are neglected, the splitting $\Delta E_-$ involves only the integrals,

$$\left. \begin{array}{l} J = e^2 \langle \psi_1(1)\psi_2(1) | r_{12}^{-1} | \psi_3(2)\psi_4(2) \rangle \\ \\ K = e^2 \langle \psi_1(1)\psi_2(2) | r_{12}^{-1} | \psi_3(1)\psi_4(2) \rangle. \end{array} \right\} \tag{5.5}$$

and

$$S_{n'n} = \langle \psi_1'(1) | \psi_1(1) \rangle$$

In the case of the singlet and the $M = 0$ triplet component, expansion of $\Delta E_\pm$ yields a sum of four major terms, each of which involves a product of two determinants. The two terms containing spin factors of the type $\alpha(1)\alpha(1)$ $\alpha(2)\alpha(2)$ contribute for both the singlet and the triplet a total of $2 S^2_{n'n}(J-K)$ to $\Delta E_\pm$, while the two cross terms, because of spin orthogonality, contain factors of the form $\alpha(1)\alpha(1)$ $\beta(2)\beta(2)$ and contribute only a term $+2 S^2_{n'n}J$ to the singlet splitting and $-2 S^2_{n'n}J$ to the triplet splitting. The splitting in the $M = \pm 1$

† In formaldehyde, because of symmetry, the highest filled lone pair orbital must be, except for configuration interaction, essentially pure p; the transition probability is accordingly very small. In the azabenzenes the hybridization is approximately $sp^2$ and relatively strong $n \rightarrow \pi^*$ transitions occur. Platt [19] has called these two types of transitions U–A and W–A, respectively.

triplet components is, of course, the same as that for $M=0$. Thus, the ' excitation transfer splitting ' becomes

$$\Delta E_{\pm} \text{(singlet)} = 2 \, S^2_{n'n}(2J - K),$$

$$\Delta E_{\pm} \text{(triplet)} = -2 \, S^2_{n'n}K.$$

$$(5.6)$$

This is a special case of the exciton problem, where exchange has been included [20].

Taking the ground state non-bounding orbital to be a hybrid of the form

$$n = [(1/3)^{1/2}(2s) + (2/3)^{1/2}(2p_z)],$$

the effective nuclear charge on nitrogen to be 3·82 [21], and using an $N \ldots N$ distance of 2·74 Å [22]†, one can obtain numerical values of the integrals $J$ and $K$ directly from the literature. The values of these integrals have been derived from Slater-type AO's; they are listed in terms of the parameter $\rho$ (or $\alpha$) = $\zeta$ (or $\delta$) $R$ where $\zeta$ is half the effective nuclear charge on each centre and $R$ is the distance in atomic units between the two centres. The required value of $\rho$ for the nitrogens in pyrazine is 9·9. The coulomb integrals are given by Roothaan [23] or by Kotani *et al.* [24], both compilations giving identical values for the integrals required in the present problem. The exchange integrals are obtained from [24] by a (straight line) logarithmic extrapolation from $\rho = 8·5$, the limit of the table, to the required value of 9·9. The results are :

$$J = 221 \text{ cm}^{-1}, \quad K \sim 12 \text{ cm}^{-1}.$$

The theoretical values for the splitting are therefore $\Delta E_{\pm}$ (singlet) = $+860$ $S^2_{n'n}$ cm$^{-1}$ and $\Delta E_{\pm}$ (triplet) $\approx -24 \, S^2_{n'n}$ cm$^{-1}$. The value of $S^2_{n'n}$ probably lies between 0·67 and 1·00 [25, 26]. Using this same method, the splittings in the other diazabenzenes are found to be, except for the factor $S^2_{n'n}$, $\Delta E_{\pm}$ (singlet) = $+1590$ cm$^{-1}$, $\Delta E_{\pm}$ (triplet) = $-275$ cm$^{-1}$ for pyrimidine (meta); and $\Delta E_{\pm}$ (singlet) = $+12,400$ cm$^{-1}$, $\Delta E_{\pm}$ (triplet) = $-5500$ cm$^{-1}$ for pyridazine (ortho). The neglect of overlap is more serious and the ' independent systems ' approximation may be less good in these cases. Work is now being carried out on these other two molecules in order to determine the experimental splittings [26]‡.

An alternative method by which $J$ can be found is through the dipole–dipole approximation. It is well known [27] that the repulsion term $e^2/r_{ij}$ can be expressed as a two-centre expansion. The first non-vanishing term in the expansion of the coulomb integral corresponds to the interaction between transition dipoles $M$ on centres A and B a distance $R$ apart. The singlet splitting is then given by

$$\Delta E_{\pm} \text{(singlet)} = 4J = 2M^2R^{-3}. \qquad (5.7)$$

† Since it is the excited state distance which should be used, an error is introduced at this point.

‡ The experimental singlet splittings have been found to be $840 \pm 100$ cm$^{-1}$ and $9030 \pm 100$ cm$^{-1}$ for pyrimidine and pyridazine, respectively, where the uncertainty is in the determination of the frequency of the vibration causing the forbidden components to become allowed. For s-triazine pyrimidine-type splittings should occur while for s-tetrazine both pyrimidine- and pyridazine-type splittings are expected.

Using 0·01 for the oscillator strength of pyrazine [28], dividing by two to obtain the value for the individual $n \to \pi^*$ transitions at each end of the molecule, and again taking $R = 2\cdot74$ Å, the value of $\Delta E_{\pm}$ (singlet) by this method is $+165$ cm$^{-1}$. It is noteworthy that both calculations give a direction and magnitude of the singlet splitting which are in accord with the experimental findings.

### REFERENCES

[1] MULLIKEN, R. S., 1955, *J. chem. Phys.*, **23**, 1997; see figure 1.
[2] McCLURE, D. S., 1959, *Solid State Physics* (New York: Academic Press), Vol. 8, pp. 1–48.
[3] McCLURE, D. S., 1958, *Canad. J. Chem.*, **36**, 59.
[4] TINOCO, I., 1960, *J. Amer. chem. Soc.*, **82**, 4785.
[5] SIDMAN, J. W., 1958, *Chem. Rev.*, **58**, 689. KASHA, M., 1950, *Disc. Faraday Soc.*, **9**, 14.
[6] INNES, K., MERRITT, J., TINCHER, W., and TILFORD, S., 1960, *Nature, Lond.*, **187**, 500.
[7] HALVERSON, F., and HIRT, R., 1949, *J. chem. Phys.*, **17**, 1165.
[8] ITO, M., SHIMADA, R., KURAISHI, T., and MIZUSHIMA, M., 1957, *J. chem. Phys.*, **26**, 1508.
[9] HIRT, R. C., 1958, *Spectrochim. Acta*, **12**, 114.
[10] MERRITT, J. A., and INNES, K. K., 1960, *Spectrochim. Acta*, **16**, 945.
[11] GOODMAN, L., and KASHA, M., 1958, *J. mol. Spectroscop.*, **2**, 58.
[12] ROBINSON, G. W., 1961, *J. mol. Spectroscop.*, **6**, 58.
[13] BERNSTEIN, H., and HERZBERG, G., 1948, *J. chem. Phys.*, **16**, 30.
[14] INNES, K., private communication.
[15] LORD, R. C., MARSTON, A. L., and MILLER, F. A., 1957, *Spectrochim. Acta*, **9**, 113.
[16] EL SAYED, M., and KASHA, M. (unpublished work).
[17] SIDMAN, J. W., 1958, *J. mol. Spectroscop.*, **2**, 333.
[18] KRISHNA, V. G., and GOODMAN, L., 1960, *J. chem. Phys.*, **33**, 381.
[19] PLATT, J. R., 1951, *J. chem. Phys.*, **19**, 101; 1953, *J. opt. Sci. Amer.*, **43**, 252.
[20] MERRIFIELD, R. E., 1955, *J. chem. Phys.*, **23**, 402.
[21] GOODMAN, L., and HARRELL, R. W., 1959, *J. chem. Phys.*, **30**, 1131.
[22] SCHOMAKER, V., and PAULING, L., 1936, *J. Amer. chem. Soc.*, **61**, 1769.
[23] ROOTHAAN, C. C. J., 1955, *Special Technical Report of the Laboratory of Molecular Structure and Spectra*, University of Chicago.
[24] KOTANI, M., ISHIGURO, E., and HIJIKATA, K., 1954, *J. phys. Soc. Japan*, **9**, 553.
[25] GOODMAN, L., 1961, *J. mol. Spectroscop.*, **6**, 109; see especially pp. 125–126.
[26] EL SAYED, M. A., and ROBINSON, G. W., 1961, *J. chem. Phys.*, **34**, 1840; and important correction to this communication, *ibid.*, in press.
[27] HIRSCHFELDER, J. O., CURTISS, C. F., and BIRD, R. B., 1954, *Molecular Theory of Gases and Liquids* (New York: John Wiley and Sons), p. 843 *et seq.*
[28] MASON, S. F., 1959, *J. chem. Soc.*, p. 1240.

# Spin–orbit coupling constant and $\langle r^{-3} \rangle$ in transuranic ions

by M. E. FOGLIO† and M. H. L. PRYCE

H. H. Wills Physics Laboratory, University of Bristol, Royal Fort, Bristol 8

The spin–orbit coupling parameter $\zeta$, the quantum average $\langle r^{-3} \rangle$, and binding energy $-E$ for atomic number $Z = 92$, 94, 96 and net ionic charge approximately 1 and 5, have been calculated for the $5f$ electrons. The potential assumed in the one-electron wave function calculation is that given by the Thomas–Fermi model of a positive ion.

It is shown that the ratio $\zeta / \langle r^{-3} \rangle$ is fairly insensitive to changes in the surroundings of the ion, and can be used for estimating one of the parameters with the experimental value of the other.

The $5g$ electrons are shown to be effectively free in the considered range of $Z$ and $n$.

The behaviour of the wave function as a function of $n$ and $Z$ is discussed.

---

It is generally assumed [1] that the $5f$ electron shell begins to be filled in the neighbourhood of uranium ($Z = 92$). It is therefore interesting to study some properties of these electrons as a function of the atomic number and of the net ionic charge $n$. We have calculated the values of the spin–orbit coupling constant $\zeta$ and of $\langle r^{-3} \rangle$—the quantum average of $r^{-3}$, where $r$ is the radial coordinate of the $5f$ electron, taking the nucleus as centre of spherical polar coordinates—which are important in the study of the spectroscopy, paramagnetic resonance and magnetic susceptibility of compounds of these ions.

We can relate the values of $\zeta$ and $\langle r^{-3} \rangle$ in compounds of transuranic ions to the values of the same quantities in the free ions, as the most important contributions to $\zeta$ and $\langle r^{-3} \rangle$ come from small values of $r$. In that region, the relative values of the wave function for different $r$ are hardly affected by external conditions and even by the value of $n$. Thus, these conditions will change the value of $\zeta$ and $\langle r^{-3} \rangle$ in an approximate proportionality to the probability of finding the electron inside a small range of $r$, less than 0·5 Å for the $5f$ electrons in the transuranic ions. The ratio $\zeta / \langle r^{-3} \rangle$ will accordingly be fairly constant on changing the surroundings of the ion, and it will be of value in predicting the value of $\langle r^{-3} \rangle$ when $\zeta$ is known experimentally, or vice versa. The variations of $\zeta / \langle r^{-3} \rangle$ with $Z$ is small, because $Z \gg 1$, but in the present case it proves to be considerably more than its variation with $n$.

In order to obtain $\zeta$ and $\langle r^{-3} \rangle$, it is necessary to calculate the wave functions for the $5f$ electrons in a one-electron approximation. The potential assumed

in our calculations is the one obtained from the Thomas–Fermi model for a positive ion [2] and we have calculated it numerically for values of $(n+1)/Z$ equal to 0·06488 and 0·02207, and $Z=92$, 94, 96. These values correspond roughly to $n=1$ and $n=5$ respectively.

The table shows the results of the computation, together with rough inter-polations for $Z=93$, 95, and an even rougher extrapolation for $Z=91$.

The change in the calculated parameters due to the differences of $n$ from the nearest integer can easily be interpolated. We have not obtained the Thomas–Fermi function for integer values of $n$, as the change in the calculated parameters will be small, and our approximation for the potential does not justify the increase of computational work necessary to obtain the parameter for integer values of $n$.

| $Z$ | $n$ | $\zeta$ (cm$^{-1}$) | $\langle r^{-3}\rangle$ (A.U.) | $\zeta/\langle r^{-3}\rangle$ (cm$^{-1}$/A.U.) | $-E$ (ev) | $W(0\cdot4$ Å$)$ | $W(1\cdot6$ Å$)$ |
|---|---|---|---|---|---|---|---|
| 91 | 1·008 | 16 | 0·047 | 341 | 3·2 | 0·9987 | (0·99) |
| 92 | 1·031 | 89·3 | 0·259 | 346 | 3·44 | 0·995 | 0·89 |
| 93 | 1·053 | 430 | 1·24 | 352 | 3·9 | 0·985 | 0·71 |
| 94 | 1·075 | 901 | 2·46 | 360 | 4·47 | 0·965 | 0·328 |
| 95 | 1·097 | 1480 | 4·0 | 370 | 5·6 | 0·924 | 0·12 |
| 96 | 1·119 | 2210 | 5·78 | 381·8 | 8·16 | 0·865 | 0·07 |
| 91 | 4·904 | 1300 | 3·74 | 348 | 40 | 0·925 | 0·095 |
| 92 | 4·969 | 1460 | 4·11 | 355·7 | 43 | 0·91 | 0·044 |
| 93 | 5·034 | 1800 | 4·96 | 363 | 45·5 | 0·895 | 0·025 |
| 94 | 5·099 | 2080 | 5·62 | 370·4 | 48·4 | 0·88 | 0·015 |
| 95 | 5·164 | 2210 | 5·87 | 377 | 51·5 | 0·865 | 0·010 |
| 96 | 5·228 | 2540 | 6·63 | 383·5 | 54·6 | 0·85 | 0·008 |

Values of the computed 5f electron parameters. The symbols in the table have the following meaning:

$Z$: atomic number of the ion.

$n$: net ionic charge.

$\zeta$: one-electron spin–orbit coupling parameter, in cm$^{-1}$.

$\langle r^{-3}\rangle$: quantum average of $r^{-3}$ in atomic units $(me^2/\hbar^2)^3$.

$-E$: 5f electron binding energy, in electron volts.

$W(r)$: probability of finding a given 5f electron outside the radius $r$.

The effective potential energy—the electric potential energy plus the centri-fugal term $\hbar^2 l(l+1)/2mr^2$—was plotted for $f$ and $g$ electrons. For $f$ electrons the graph shows a deep minimum about 0·1 Å; for $g$ electrons it only shows the flat minimum of the function $-(e^2(n+1)/r)+\hbar^2 l(l+1)/2mr^2$ which appears at large distance from the nucleus. This shows that according to the Thomas–Fermi model, the 5g electrons are still effectively free in the transuranic ions.

It is most interesting to compare our values for the effective potential, the wave function and the energy, with those of Mayer [3].

In her calculation, the potential corresponds to the Thomas–Fermi potential of a $Z-1$ neutral atom, plus a unit positive charge at $r=0$. This assumption corresponds approximately to our potential with $n=0$. For a given value of $n$, and up to a critical value of $Z$ the wave functions have two relative minima (maxima in absolute value) after the first node. The outer minimum strongly

decreases the probability of finding the electron near the nucleus. Above the critical value of $Z$ (for each $n$) the outer minimum disappears, and the energy decreases abruptly.

For the potential used by Mayer [3], this value of $Z$ is less than 86 while for our calculations with $n=1$ it is about 94. With $n=5$ the value is much less than 92 for our calculations, but we have not obtained a definite value. Correspondingly, the binding energy $-E$, $\zeta$ and $\langle r^{-3} \rangle$ have a minimum around $n=1$.

Mayer computes 8·5 and 14 ev for the binding energies of neutral $Z=91$ and 93 respectively, which can be compared with the values in the table, column 6.

This strange behaviour of the wave function for constant $Z$ is a consequence of the slight changes with $n$ of the values of the effective potential, and in particular, of the position of its outer minimum. This minimum depends very little on $Z$, and is located around $12h^2/me^2$ for $n=0$ and approaches the nucleus with increasing $n$. For larger values of $n$, it disappears into the inner minimum of the effective potential. It is then apparent that the critical value of $Z$ will have a maximum at an intermediate value of $n$. As the Thomas–Fermi approximation is not expected to hold accurately, these results are only qualitative.

The probability $W(r)$ of finding the $5f$ electron outside a radius $r$ can be obtained from the wave function. We see from the table that at a distance from the nucleus approximately twice the crystallographic radius [4] these probabilities are too big for $U^{--}$ and $Pu^{++}$. This is a failing of the Thomas–Fermi model for low $n$.

This fact makes the values of $\zeta$ and $\langle r^{-3} \rangle$ very low, as can be seen from the fact that $Th^{+-}$ has $\zeta=1035 \text{ cm}^{-1}$ (deduced spectroscopically [5]), and that the value of $\zeta$ must increase with $Z$.

The values of $\zeta_{5f}$ for certain compounds as deduced, with perhaps dubious theoretical assumption, from experimental values, can be found in the literature: $2400 \text{ cm}^{-1}$ in $NpF_6$ [6], [7]; $1900 \text{ cm}^{-1}$ in $NpO_2^-$ [8]; $2200 \text{ cm}^{-1}$ in $PuO_2^{++}$ [8] and 2250 or $2200 \text{ cm}^{-1}$ in $NpO_2^{--}$ [7, 9]. From the change of $\zeta$ between $NpF_6$ and $NpO_2^-$ and between $NpF_6$ and $NpO_2^{++}$ we see that $\zeta$ is very sensitive in the ligand field. This fact agrees with the large probabilities of finding the $5f$ electrons outside the crystallographic radius in these ions. From this comparison we see that the model assumed gives values of $\zeta$ lower than the experimental ones. These experimental values of $\zeta$ are another confirmation of the fact that the Thomas–Fermi approximation is the cause of the calculated low values of $\zeta$, as the effect of the ligand field is to lower the value of $\zeta$ in comparison with the free ion value, and we see that the values calculated for the free ion are lower than the experimental values for the ion in the ligand field in the said compounds.

From the table, we see that the ratio $\zeta/\langle r^{-3} \rangle$ is fairly constant, and we can expect a similar behaviour in compounds of the transuranic ions. The value of the ratio is rather low for $U^{++}$, as the value of $\langle r^{-3} \rangle$ is more affected than that of $\zeta$ by the incorrectness of the wave functions already mentioned, and we can expect a slightly higher value.

We can conclude that the calculated ratio $\zeta/\langle r^{-3} \rangle$ will be fairly accurate, and that can be used for calculating $\langle r^{-3} \rangle$ from the experimental value of $\zeta$ or vice versa [7].

REFERENCES

[1] JORGENSEN, C. KLIXBULL, 1958, Paper presented 14 April to the Symposium of the Chemistry of the Less Familiar Elements in connection with the 33rd National Meeting of the American Chemical Society in San Francisco.
[2] FERMI, 1930, *Mem. R. Accad. Ital.*, **1,** 1.
[3] MAYER, M. G., 1941, *Phys. Rev.*, **60,** 184.
[4] KATZ, J. J., and SEABORG, G. T., 1957, *The Chemistry of Actinide Elements* (London: Methuen).
[5] RACAH, G., 1950, *Physica*, **16,** 651.
[6] WEINSTOCK, B., and MALM, J. G., 1956, *J. Inorg. Nucl. Chem.*, **2,** 380.
[7] EISENSTEIN, J. C., and PRYCE, M. H. L., *The Electronic Structure and Magnetic Properties of Uranyl-like Ions.* III. Neptunyl (to be published).
[8] GRUEN, D. M., 1952, *J. chem. Phys.*, **20,** 1818.
[9] McGLYNN, S. P., and SMITH, J. K., 1961, *J. mol. Spectrosc.*, **6,** 188.

# On the magnetically dilute Heisenberg and Ising ferromagnetics

## II. High-temperature expansions

by D. J. MORGAN† and G. S. RUSHBROOKE

Physics Department, King's College, Newcastle upon Tyne,
University of Durham

The problem of a randomly dilute Heisenberg or Ising ferromagnetic is discussed on the basis of expansions of susceptibility in inverse powers of temperature. The first six significant coefficients in such expansions have been found, for any lattice and any spin value. The series are used to estimate the dependence of Curie temperature, $\theta_c$, on concentration of magnetic elements, $p$, for simple cubic, body-centred cubic and face-centred cubic lattices and spins $\frac{1}{2}$ and 1. Near $p=1$, it is found that for the Ising models $\theta_c(p)=p\theta_c(1)$ whereas for the Heisenberg models $\theta_c(p)<p\theta_c(1)$.

---

## 1. INTRODUCTION

In an earlier paper with the same main title [1] we discussed the general theory of randomly dilute Heisenberg and Ising ferromagnetics and proved, in particular, that the limiting concentration of magnetic elements, $p_c$, is the same for all such models, whether Heisenberg or Ising and regardless of the spin value concerned. We gave preliminary estimates of $p_c$ for various lattices. And in two cases, namely $H(\frac{1}{2})$ b.c.c. and $I(\frac{1}{2})$ s.c.‡, we attempted to indicate the dependence of the Curie temperature on the concentration, $p$, of magnetic elements over the full range $p_c \leqslant p \leqslant 1$. These Curie temperature curves were derived, basically, from expansions of the susceptibility, $\chi$, in powers of $p$: but reference was made also to conclusions drawn from expansions of $\chi$ in powers of inverse temperature. It is this latter work, hitherto unpublished (although in fact completed before the investigation reported in [1]), which forms the content of the present paper. Physically, we are now primarily concerned not with estimating $p_c$ but with determining the effect on the Curie temperature of a small random admixture of non-magnetic material.

The only previous high-temperature expansion work on this problem is due to Behringer who has recently [2] treated the $H(\frac{1}{2})$ model, for the face-centred cubic lattice, in this way. We have ourselves dealt with the models $H(s)$ and $I(s)$ in terms of general lattice parameters: which enables subsequent particularization to any lattice and any spin value.

---

† Now at Department of Applied Mathematics, University College, Cathays Park, Cardiff.

‡ We use the same notation as in [1]: thus $H(s)$ denotes the Heisenberg problem for spin $s$, and b.c.c. stands for ' body-centred cubic lattice '.

## 2. General theory: Heisenberg model

Being concerned with the extension to random mixtures of the high-temperature formulae derived for pure Heisenberg ferromagnetics by Rushbrooke and Wood [3], we shall use the notation of [3] without full recapitulation. We start with the Hamiltonian

$$\mathscr{H} = -2J \sum_{\langle i,j \rangle} S^{(i)} \cdot S^{(j)} - g\beta H \sum_i S_3^{(i)} \tag{1}$$

where the spin variables, $S$, now relate only to the randomly distributed magnetic elements, occupying a fraction $p$ of the lattice sites. And from (1) we derive expressions for the susceptibility, and inverse susceptibility, of the form

$$\bar{\chi}\theta = \tfrac{1}{3}s(s+1)p \sum_{n=0}^{\infty} \frac{a_n(p)}{\theta^n}, \tag{2}$$

and

$$\frac{1}{\bar{\chi}\theta} = \frac{3}{s(s+1)p} \sum_{n=0}^{\infty} \frac{b_n(p)}{\theta^n} \tag{3}$$

where $a_0$ and $b_0$ are each unity. As in [3], $s$ denotes the maximum value of $S_3$, $\theta$ denotes $kT/J$, and $\bar{\chi}$ stands for $J\chi/Ng^2\beta^2$, where $N$ is the total number of lattice sites (whether occupied by magnetic elements or not).

Just as for the pure ferromagnetic, $a_n$, though now dependent on $p$, is given by

$$a_n(p) = \frac{3}{s(s+1)p} \cdot \frac{2^n}{n!} \{\text{coefficient of } N \text{ in } \langle \mathscr{P}^n \mathscr{Q}^2 \rangle\} \tag{4}$$

where

$$\mathscr{P} \equiv \sum_{\langle ij \rangle} S^{(i)} \cdot S^{(j)}, \quad \mathscr{Q} \equiv \sum_i S_3^{(i)},$$

and, for any operator A, $\langle A \rangle$ denotes (trace A)$/(2s+1)^N$, for any matrix representation.

Equation (4), limited to the case $p = 1$, is the basic formula from which Rushbrooke and Wood derived $a_0, a_1, \ldots a_6$, and thence $b_0, b_1, \ldots b_6$, in terms of $s$ and appropriate lattice parameters. That work fell naturally into two parts: the calculation of the traces of products of spin operators and the enumeration of the occurrences of diagrams (localized graphs) on the lattice. The diagrams pertaining to $a_n$ comprised $n$ lines and two crosses, each line representing a factor of the type $S^{(i)} \cdot S^{(j)}$ and each cross a factor of the type $S_3^{(k)}$. The only difference in the present case, for general $p$, is that these occurrence factors now involve $p$, the probability that any particular lattice site is occupied by a magnetic element. The traces themselves, when they occur, are unchanged and may be taken over from the earlier calculations†.

At first sight we might expect that if a diagram involves $m$ points then, for the case of general $p$, the occurrence factor appropriate to $p = 1$ should be multiplied by $p^m$. But while this is fairly self-evident for a diagram of one part only, it is by no means obvious (and indeed not true) for a diagram of two

---

† We are indebted to Dr. P. J. Wood for placing at our disposal his thesis 'A Contribution to the Theory of the Magnetic Properties of Solids', Durham (1958), in which these trace values are tabulated.

or more separate pieces. The problem involved is best illustrated by a specific example: consider the two-part diagram
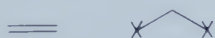


for which the occurrence when $p=1$ is given by

$$\tfrac{1}{4}N^2z^2(z-1) - Nz[(z-1)^2 - r_3] - \tfrac{1}{2}Nz(z-1)(z-2) - Nz(z-1) - \tfrac{1}{2}Nzr_3. \quad (5)$$

Here $z$, as always, is the lattice coordination-number and $\tfrac{1}{6}Nzr_3$ is the number of nearest-neighbour triangles among the sites of an $N$-point lattice. The first term in (5) is, of course, the product of the occurrences of the two separate parts of the above diagram: the later terms enumerate the unwanted, over-lapping, configurations corresponding respectively to the four possibilities



We have thus to decide between

    ($a$) multiplying (5) by $p^5$

or

    ($b$) replacing (5) by

$$\tfrac{1}{4}N^2z^2(z-1)p^5 - Nz[(z-1)^2 - r_3]p^4 - \tfrac{1}{2}Nz(z-1)(z-2)p^4 - Nz(z-1)p^3$$
$$- \tfrac{1}{2}Nzr_3p^3. \quad (6)$$

Even further possibilities, which we need not elaborate, suggest themselves: and we have failed to see an entirely convincing direct argument pointing to the correct procedure. Nevertheless the method exemplified in (6) above is in fact correct (for this problem of random mixing), and has been used throughout. We establish that this method is correct by the following, indirect, argument.

    Consider an $N$-site pseudo-lattice, of the type described by Rushbrooke and Wood in §6 of [3], in which there are isolated sets of points, those within any set being all nearest neighbours: we illustrate for the case of four points in each set, when we have $N/4$ units each equivalent to

     (7)

The general theory applies unchanged to such a pseudo-lattice. If we now randomly decimate this pseudo-lattice by introducing a probability $p$ for the existence of each point, we are left with a mixed pseudo-lattice comprising

$$\frac{N}{4}p^4 \quad \text{units}$$



$$4\frac{N}{4}p^3(1-p) \quad \text{units}$$



$$6\frac{N}{4}p^2(1-p)^2 \quad \text{units}$$



$$4\frac{N}{4}p(1-p)^3 \quad \text{isolated points}$$

It follows, from the additivity of free-energies and from (2) above, that $p a_n(p)$ for the $N$-site pseudo-lattice (7) equals

$p^4 a_n(1)$ for the $N$-site pseudo-lattice with units

$+3p^3(1-p)a_n(1)$ for the $N$-site pseudo-lattice with units

$+3p^2(1-p)^2 a_n(1)$ for the $N$-site pseudo-lattice with units

$+p(1-p)^3 a_n(1)$ for a pseudo-lattice of $N$ isolated points

Now for any $N$-site lattice, including pseudo-lattices, the general expressions of [3] provide values for $a_n(1)$, $n=0$, 1, ... 6. Consequently for any such pseudo-lattice $a_n(p)$, $n=0$, 1, ... 6 can be unambiguously determined. We have therefore only to compute $a_n(p)$ for an arbitrary lattice by the methods (a), (b), etc., above, and then particularize to a pseudo-lattice to see which method is correct. We are led to adopt method (b), as already stated.

Having thus settled the correct procedure, which some may indeed feel to be self-evident, we have thereby calculated the coefficients $a_0(p) \ldots a_6(p)$ for an arbitrary lattice and general spin $s$. The calculations are lengthy, and a checking procedure is necessary. This can, however, be obtained by particularizing the results to a *variety* of pseudo-lattices of the type already described: for which purpose we have considered the following units

$(z=1)$     $(z=2)$     $(z=3)$     $(z=4)$     and     $(z=5)$
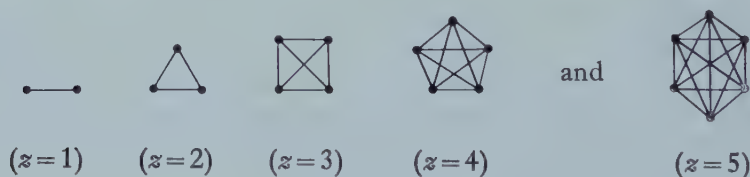
For all such pseudo-lattices, $a_n(p)$ has been calculated both from first principles, using method (b), and also by the method of linear combinations of $a_n(1)$'s described above. Agreement in all cases gives us confidence in our results.

From the values of $a_n(p)$, $n=0$, 1, ... 6, expressed in terms of general lattice parameters, it is easy to convert to the corresponding values of the coefficients $b_n(p)$, $n=0$, 1, ... 6. All these coefficients are polynomials in $p$, and also in $X$, where $X=s(s+1)$. The general expressions, in terms of lattice parameters, are very lengthy (especially for $n=6$), for which reason it seems better to present here, in Appendix I, simply the expressions for the $a_n(p)$ coefficients appropriate to the three cubic lattices, s.c., b.c.c., and f.c.c.[†]. By particularizing to $s=\frac{1}{2}$, i.e. $X=\frac{3}{4}$, in the f.c.c. expressions we can compare our

---

[†] The authors will be pleased to supply the general expressions to anyone particularly concerned with their application to other lattices.

results with the values of $b_1$, $b_2$, $b_3$ and $b_4$ reported by Behringer [2] for this H($\frac{1}{2}$) f.c.c. problem. Our expressions for $b_1$, $b_2$ and $b_3$ reproduce Behringer's values, but with $b_4$ this is not so. We are grateful to Dr. Behringer for acknowledging, in correspondence, a counting error in his calculation of $b_4$.

Finally, it is worth observing that in these Heisenberg calculations diagrams involving two crosses on the same site can be disregarded. This is essentially due to the isotropy of the interactions, and follows from theorem II of [3].

## 3. General theory: Ising model

For the Ising model, in place of (1) we start with the Hamiltonian

$$\mathscr{H} = -2J \sum_{\langle i,j \rangle} S_3^{(i)} S_3^{(j)} - g\beta H \sum_i S_3^{(i)}. \tag{8}$$

The calculation of the $a_n(p)$ and $b_n(p)$ coefficients, still defined by (2) and (3), follows precisely the same lines as in the Heisenberg case: we have to find traces of products of $S_3$ operators and the occurrences, involving $p$, of localized lattice graphs. The occurrence factors can, of course, be taken over unchanged from the Heisenberg problem: but since the Ising interaction is non-isotropic (except in the special case $s = \frac{1}{2}$), we have now to include diagrams involving double crosses. This point is perhaps worth illustrating, specifically, for the two graphs



$$(a) \qquad\qquad (b)$$

In the Heisenberg case, the trace pertaining to both ($a$) and ($b$) is effectively $\frac{1}{9}X^3$: 'effectively' because for ($a$) we omit a factor $(2s+1)^3$ and for ($b$) a factor $(2s+1)^2$, since these ultimately cancel with factors $2s+1$ in the definition of $\langle A \rangle$. Therefore, for the Heisenberg problem, the contribution to $\langle \mathscr{P}^2 \mathscr{Q}^2 \rangle$ from ($a$) is $\frac{1}{9}X^3[\frac{1}{2}N^2zp^3 - Nzp^2]$, while that from ($b$) is $\frac{1}{9}X^3[Nzp^2]$: and the resulting coefficient of $N$ vanishes. In the Ising case, however, again omitting irrelevant $2s+1$ factors, the trace pertaining to ($a$) is $\frac{1}{27}X^3$ while that for ($b$) is $\frac{1}{45}X^2(3X-1)$: the contribution from these two diagrams to the coefficient of $N$ in $\langle \mathscr{P}^2 \mathscr{Q}^2 \rangle$ is thus $zp^2X^2(4X-3)/135$, and vanishes only when $s = \frac{1}{2}$. But even with this small complication, the Ising problem is appreciably simpler than the Heisenberg problem: for the trace calculations, which had to be performed *ab initio*, are relatively elementary. Using a representation in which the $S_3^{(i)}$ matrices are all diagonal, the computation of traces amounts to evaluating the sums of powers of integers.

For the Ising problem, as for the Heisenberg problem, we have found $a_n(p)$, $n = 0, 1, \ldots 6$, and thence $b_n(p)$, $n = 0, 1, \ldots 6$, in terms of general lattice parameters. But rather than present these lengthy expressions it seems better to give here, in Appendix II, simply the $a_n(p)$ coefficients appropriate to the three cubic lattices: each coefficient is, of course, a polynomial in $p$ and also in $X$.

For the normal Ising ferromagnetic model, namely for $s = \frac{1}{2}$ and $p = 1$, $a_1, \ldots a_9$ (and likewise $b_1, \ldots b_9$) are known for the simple and body-centred cubic lattices both from the work of Domb and Sykes [4] and from unpublished,

concordant, calculations of Rushbrooke and Scoins. Domb and Sykes also give $a_1, \ldots a_8$ for the face-centred cubic lattice: and we have confirmed that in all these cases our general expressions reduce, with $p=1$ and $X=\frac{3}{4}$, to these known values on substituting the appropriate lattice parameters. Rather little work has been done on the Ising model for general spin, but Domb and Sykes (equations (15) in [4]) give expressions in terms of $s$ for $a_1, \ldots a_4$ for the face-centred cubic lattice only. Our general results again agree with these expressions.

## 4. ESTIMATION OF CURIE POINTS FROM HIGH-TEMPERATURE EXPANSIONS

As is well known, there are two possible ways of determining the Curie temperature from expansions of $\chi$, or $\chi^{-1}$, in inverse powers of $\theta$. If working with the $\chi^{-1}$ expansion, (3) above, we curtail the expansion at $n=m$, and then find the greatest value of $\theta$ for which $\chi^{-1}=0$: this gives $\theta_c^{(m)}$, the $m$th approxima-tion to $\theta_c$; and in the present case, when the coefficients depend on $p$, we should write this $\theta_c^{(m)}(p)$. We ought then to seek to extrapolate the sequence of successive approximations, $\theta_c^{(1)}(p) \ldots \theta_c^{(6)}(p)$ to find $\theta_c(p)$ as $m \to \infty$; and can perhaps best do this by plotting successive approximations against $1/m$. Behringer [2] adopted this method, but without the final extrapolation: for the $H(\frac{1}{2})$ f.c.c. problem he presents plots of $\theta_c^{(1)}(p) \ldots \theta_c^{(4)}(p)$—the last of these being subject to error. Alternatively, working with the $\chi$ expansion, we can attempt to estimate the radius of convergence of the series (2). In this case various procedures are possible, but for definiteness we might, for any fixed $p$, consider $\theta_c(p)=\lim a_n(p)/a_{n-1}(p)$, attempting to find this limit by plotting $a_n(p)/a_{n-1}(p)$ against $1/n$ and extrapolating, $n \to \infty$. For reasons already discussed by Rushbrooke and Wood [3] and [5], we prefer this second approach, and shall use it here.

First for the Heisenberg and then for the Ising problem, for the three lattices s.c., b.c.c., and f.c.c., and for the two spin values $s=\frac{1}{2}$ and 1, we have deter-mined $\theta_c(p)$ for values of $p$ decreasing from unity by intervals of $0.02$ down to $p=0.9$ and then by intervals of $0.05$ down to such a $p$-value that $\theta_c(p)$ is too uncertain to be worth recording. In fact for the Heisenberg problem we stop at $p=0.5$ and for the Ising problem at $p=0.3$. In every case we have con-sidered four plots, namely $a_n(p)/a_{n-1}(p)$, $a^{\frac{1}{2}}_n(p)/a^{\frac{1}{2}}_{n-2}(p)$, $a_n(p)a_{n-1}(1)/a_{n-1}(p)a_n(1)$ and $a^{\frac{1}{2}}_n(p)a^{\frac{1}{2}}_{n-2}(1)/a^{\frac{1}{2}}_{n-2}(p)a^{\frac{1}{2}}_n(1)$, against $1/n$, and have attempted extrapolation to $1/n=0$. It is impossible to present all this data here, and perhaps only the final conclusions need concern us. But by way of illustration, figure 1 shows $a^{\frac{1}{2}}_n(p)/a^{\frac{1}{2}}_{n-2}(p)$ for $H(\frac{1}{2})$, f.c.c., and $p=0.9$, $0.85$, $\ldots$ $0.45$. These $p$-values label the curves at their right-hand ends, and against the left-hand vertical axis are marked the extrapolated values of $\theta_c(p)$, with some indication of their un-certainties when based on this plot alone. We shall refer to this figure again below: it shows fairly well how the sequence of coefficients $a_n(p)$ changes as $p$ decreases, and how eventually the series (2) comes to have an infinite radius of convergence, corresponding to $\theta_c(p)=0$, for finite $p$.

The whole corpus of conclusions about $\theta_c(p)$ obtained in this way is con-veniently summarized in figures 2 and 3, which present the results for the Heisenberg and Ising problems, respectively.

For the Heisenberg models, we feel justified in assigning something like a 1 per cent accuracy to $\theta_c(p)$ for $p \geqslant 0\cdot8$: for smaller $p$-values confidence diminishes to perhaps a 3 per cent accuracy when $p \sim 0\cdot6$, and thereafter the results are less reliable. These are fairly conservative judgments, based on agreement between the alternative extrapolation procedures we have used: but of course any prediction drawn from the initial terms of an infinite series, however many of
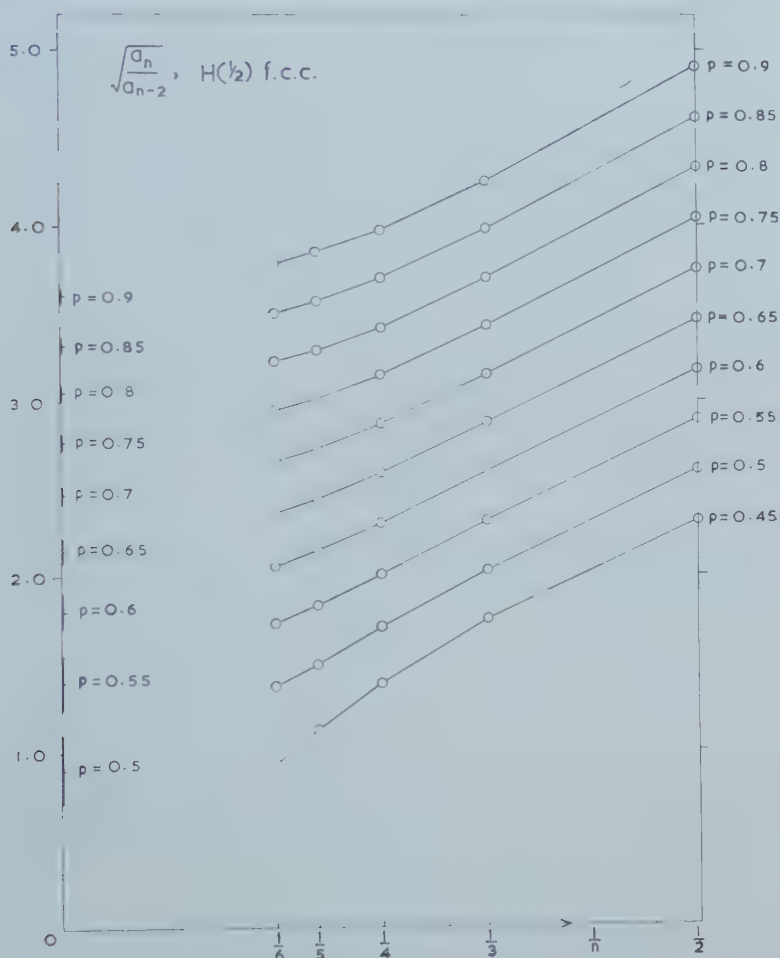


Figure 1.   Plots of $a^{\frac12}_n / a^{\frac12}_{n-2}$ against $1/n$, $n = 2, 3, \ldots 6$, for the face-centred cubic lattice, Heisenberg spin $\frac12$ problem.   Each sequence, joined by straight lines, corresponds to a specific value of $p$ as indicated.

them, implies an unjustified, if not unjustifiable, optimism.   Moreover, an exception to these judgements must be made for the problem $H(\frac12)$ s.c. (curve 6): here the coefficients behave very irregularly, and it is difficult to draw conclusions from them with much certainty.   Indeed, for both Heisenberg and Ising models, the larger $s$ is, and the greater $z$ (the lattice coordination number), the smoother is the behaviour of the coefficients and the easier it is to make

confident extrapolations: though for the Ising model even the $I(\frac{1}{2})$ s.c. co-efficients behave regularly. In fact for the Ising model we would assign something like a 1 per cent accuracy to $\theta_c(p)$ for $p \geqslant 0.75$, falling to perhaps 2·5 per cent when $p \sim 0.5$, with, of course, greater uncertainty for smaller values of $p$.
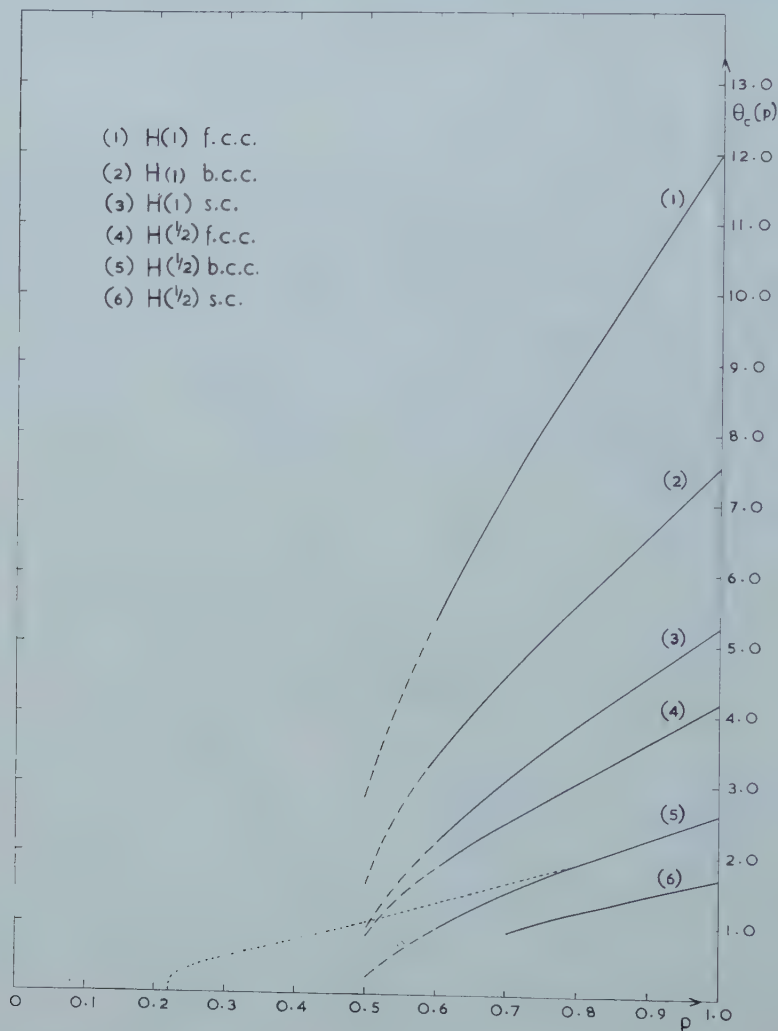


Figure 2. Summary of inferred Curie temperatures for Heisenberg problems. Dotted curve is taken from figure 3 of [1].

## 5. DISCUSSION AND CONCLUSIONS

Despite a superficial similarity, there is a striking difference between the curves of figure 2, for Heisenberg models, and those of figure 3, for Ising models. In the latter, Ising, case

$$\frac{d\theta_c(p)}{dp} = 1 \text{ at } p = 1$$

while in the former, Heisenberg, case

$$\frac{d\theta_c(p)}{dp} > 1 \text{ at } p = 1.$$

In other words, with the Ising model the lowering of the Curie temperature due to random non-magnetic 'impurities' starts by following the predictions of a simple Curie–Weiss treatment, whereas with the Heisenberg model it
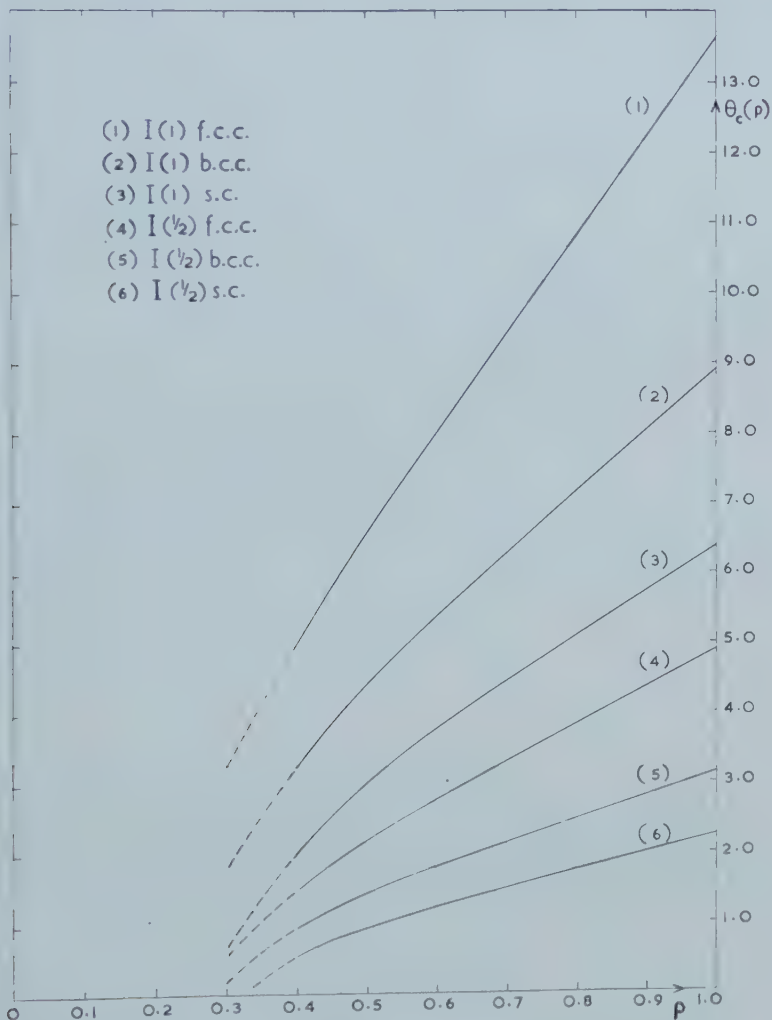


Figure 3. Summary of inferred Curie temperatures for Ising problems.

does not. This is at the same time the most unexpected and, perhaps, also the most reliable result of this high-temperature investigation. Crudely, but by no means inaccurately, we may say that

for the Ising problems $\theta_c(p) = p\theta_c(1)$

while

(9)

for the Heisenberg problems $\theta_c(p) = (p - 0.25)\,\theta_c(1)$,

these linear relations holding, in both cases, till $\theta_c(p)$ has been reduced to

approximately $\theta_c(1)/2$. This implies that if instead of plotting $\theta_c(p)$ versus $p$ we had plotted $\theta_c(p)/\theta_c(1)$ versus $p$, then the six curves of figure 2, and likewise the six curves of figure 3, would have been virtually coincident: i.e. the reduced $\theta_c(p)/\theta_c(1)$ plots are very insensitive, at least in their upper portions, to either spin value or detailed lattice structure (we are, of course, only considering three-dimensional lattices).

As we have said already, the lower parts of the curves shown in figures 2 and 3 should not be regarded as particularly reliable. This is for two reasons. First, because in general the behaviour of the $a_n(p)$ coefficients becomes increasingly irregular as $p$ decreases and, secondly, because there would in any case seem to be greater flexibility, for smaller $p$, in conclusions produced by different extrapolatory assumptions. This is well illustrated by figure 1. For were we to assume that the plots of figure 1 have eventually to cut the left-hand vertical axis at right angles, this would make very little difference to the upper part of the appropriate curve in figure 2, but an appreciable difference to the lower part. The curves given in figures 2 and 3 are those we obtained without making any such assumption (for which there is no real evidence).

Since these extrapolations were made, and the above curves drawn, the work reported in [1] has shown that, for a given lattice, $p_c$ is the same for both Heisenberg and Ising models, and independent of the spin value. And we have been led [1] to estimate $p_c$ from a simple random-cluster-size problem. For the three lattices here under discussion our estimates were, s.c. $p_c = 0.28$, b.c.c. $p_c = 0.22$, f.c.c. $p_c = 0.18$, all values to within some 10 per cent. Since then Domb and Sykes [6] have added two more terms to the series (see (11) of [1]) determining $p_c$ for the simple cubic lattice, and still support the value $0.28$. Work on two-dimensional lattices (Fisher [7]) certainly strongly suggests that conclusions drawn from too few terms of this cluster-size series may lead to serious underestimates of $p_c$: but there is as yet no evidence that our preliminary estimates of $p_c$ for the cubic lattices are unreasonable. We have also seen, in [1], that $\theta_c(p)$ versus $p$ curves ultimately drop very steeply and have a vertical tangent at $p_c$.

For the Ising problem there is no difficulty in reconciling the present curves with the conclusions of [1]. For the Heisenberg problem, unless the true $p_c$ values are appreciably greater than the above estimates, we must suppose that as $p$ decreases the $\theta_c(p)$ curves, which start by falling steadily, bend to the left before finally descending vertically at $p = p_c$. We indicated such behaviour in figure 3 of [1], and reproduce this, shown dotted, in figure 2 above. We now incline, however, to believe that the high-temperature curves can be trusted to rather lower $p$-values than this dotted curve allows, and consequently that the leftward swing may be more pronounced than that indicated. Yet a further possibility (to which the next approximation in the scheme outlined in § 5 of [1] appears to lend some rather uncertain support) is that for the Heisenberg problem $\theta_c(p) = 0$ for $p_c \leqslant p \leqslant p_c^*$, where $p_c^*$ lies in the range $0.4$ to $0.5$, and that then $\theta_c(p)$ follows the predictions of the 'high-temperature' curves. We are examining this matter further.

## Appendix I

$a_n(p)$ coefficients for the Heisenberg model, general spin. $X = s(s+1)$.

### (i) *Face-centred cubic lattice*

$a_0 = 1$, $a_1(p) = 8pX$, $a_2(p) = \frac{4}{3}pX[44pX - 3]$,

$a_3(p) = \frac{16}{45}pX[1170p^2X^2 - 185pX + 6(1 - X - X^2)]$,

$a_4(p) = \frac{4}{135}pX[98000p^3X^3 - 24860p^2X^2 + 6pX(377 - 272X - 272X^2)$
$$+ 15(-3 + 6X + 4X^2)],$$

$a_5(p) = \frac{8}{14175}pX[35590800p^4X^4 - 12471200p^3X^3$
$$+ 105p^2X^2(18203 - 11088X - 11088X^2)$$
$$+ 42pX(-2751 + 4644X + 2888X^2 - 608X^3)$$
$$+ 9(192 - 522X - 67X^2 + 240X^3 + 160X^4)],$$

$a_6(p) = \frac{4}{6075}pX[209828800p^5X^5 - 93833200p^4X^4$
$$+ 60p^3X^3(333517 - 180736X - 180736X^2)$$
$$+ 15p^2X^2(-147911 + 215824X + 136272X^2 - 36480X^3)$$
$$+ 6pX(16824 - 43845X - 4428X^2 + 24096X^3 + 9120X^4)$$
$$+ 9(-138 + 444X - 163X^2 - 296X^3 - 160X^4)].$$

### (ii) *Body-centred cubic lattice*

$a_0 = 1$, $a_1(p) = \frac{16}{3}pX$, $a_2(p) = \frac{8}{9}pX[28pX - 3]$,

$a_3(p) = \frac{32}{135}pX[490p^2X^2 - 105pX + 6(1 - X - X^2)]$,

$a_4(p) = \frac{8}{405}pX[26480p^3X^3 - 9020p^2X^2 + 42pX(31 - 16X - 16X^2)$
$$+ 15(-3 + 6X + 4X^2)],$$

$a_5(p) = \frac{16}{42525}pX[6286000p^4X^4 - 2878400p^3X^3$
$$+ 105p^2X^2(6083 - 2928X - 2928X^2)$$
$$+ 7350pX(-9 + 12X + 8X^2)$$
$$+ 9(192 - 522X - 67X^2 + 240X^3 + 160X^4)],$$

$a_6(p) = \frac{8}{18225}pX[24011200p^5X^5 - 13976400p^4X^4$
$$+ 60p^3X^3(69665 - 28384X - 28384X^2)$$
$$+ 3p^2X^2(-242439 + 264336X + 176432X^2 - 14592X^3)$$
$$+ 6pX(9528 - 20901X - 5172X^2 + 5120X^3 + 2592X^4)$$
$$+ 9(-138 + 444X - 163X^2 - 296X^3 - 160X^4)].$$

### (iii) *Simple cubic lattice*

$a_0 = 1$, $a_1(p) = 4pX$, $a_2(p) = \frac{2}{3}pX[20pX - 3]$,

$a_3(p) = \frac{8}{45}pX[250p^2X^2 - 75pX + 6(1 - X - X^2)]$,

$a_4(p) = \frac{2}{27}pX[1936p^3X^3 - 892p^2X^2 + 6pX(31 - 16X - 16X^2)$
$$+ 3(-3 + 6X + 4X^2)],$$

$a_5(p) = \frac{4}{14175}pX[1649200p^4X^4 - 1002400p^3X^3$
$$+ 105p^2X^2(2987 - 1392X - 1392X^2)$$
$$+ 5250pX(-9 + 12X + 8X^2)$$
$$+ 9(192 - 522X - 67X^2 + 240X^3 + 160X^4)],$$

$$a_6(p) = \frac{2}{42525}pX[31595200p^5X^5 - 24206000p^4X^4$$
$$+ 420p^3X^3(23445 - 9280X - 9280X^2)$$
$$+ 21p^2X^2(-118343 + 125632X + 85104X^2 - 4864X^3)$$
$$+ 30pX(9528 - 20901X - 5172X^2 + 5120X^3 + 2592X^4)$$
$$+ 63(-138 + 444X - 163X^2 - 296X^3 - 160X^4)].$$

## APPENDIX II

$a_n(p)$ coefficients for the Ising model, general spin.    $X = s(s+1)$.

### (i) *Face-centred cubic lattice*

$a_0 = 1$,   $a_1(p) = 8pX$,   $a_2(p) = \frac{8}{15}pX[110pX - 3 + 4X]$,

$a_3(p) = \frac{16}{225}pX[5850p^2X^2 + 130pX(-3 + 4X) + 3 - 18X + 2X^2]$,

$a_4(p) = \frac{8}{4725}pX[1715000p^3X^3 + 62440p^2X^2(-3 + 4X)$
$$+ pX(6717 - 24792X + 5248X^2)$$
$$- 45 + 249X - 204X^2 - 64X^3],$$

$a_5(p) = \frac{16}{496125}pX[622839000p^4X^4 + 31644200p^3X^3(-3 + 4X)$
$$+ 70p^2X^2(92529 - 307764X + 84156X^2)$$
$$+ 42pX(-3411 + 19899X - 19372X^2 - 6128X^3)$$
$$+ 5(135 - 810X + 1584X^2 + 216X^3 - 304X^4)],$$

$a_6(p) = \frac{16}{1488375}pX[12852014000p^5X^5 + 838037200p^4X^4(-3 + 4X)$
$$+ 70p^3X^3(3562824 - 11405664X + 3602176X^2)$$
$$+ 28p^2X^2(-440001 + 2263719X - 2249412X^2 - 507208X^3)$$
$$+ pX(232425 - 1490436X + 2832414X^2 - 303312X^3 - 902768X^4)$$
$$- 945 + 5445X - 11124X^2 + 4206X^3 + 4512X^4 - 352X^5].$$

### (ii) *Body-centred cubic lattice*

$a_0 = 1$,   $a_1(p) = \frac{16}{3}pX$,   $a_2(p) = \frac{16}{45}pX[70pX - 3 + 4X]$,

$a_3(p) = \frac{32}{675}pX[2450p^2X^2 + 70pX(-3 + 4X) + 3 - 18X + 2X^2]$,

$a_4(p) = \frac{16}{14175}pX[463400p^3X^3 + 21280p^2X^2(-3 + 4X)$
$$+ pX(3633 - 11928X + 2912X^2)$$
$$- 45 + 249X - 204X^2 - 64X^3],$$

$a_5(p) = \frac{32}{1488375}pX[110005000p^4X^4 + 6830600p^3X^3(-3 + 4X)$
$$+ 70p^2X^2(26397 - 85932X + 24948X^2)$$
$$+ 42pX(-1575 + 8715X - 7140X^2 - 2240X^3)$$
$$+ 5(135 - 810X + 1584X^2 + 216X^3 - 304X^4)],$$

$a_6(p) = \frac{32}{4465125}pX[1470686000p^5X^5 + 116208400p^4X^4(-3 + 4X)$
$$+ 70p^3X^3(633504 - 1959984X + 659216X^2)$$
$$+ 28p^2X^2(-116847 + 538773X - 484044X^2 - 77456X^3)$$
$$+ pX(104265 - 610596X + 969654X^2 - 69552X^3 - 254128X^4)$$
$$- 945 + 5445X - 11124X^2 + 4206X^3 + 4512X^4 - 352X^5].$$

### (iii) *Simple cubic lattice*

$$a_0 = 1, \quad a_1(p) = 4pX, \quad a_2(p) = \tfrac{4}{15}pX[50pX - 3 + 4X],$$

$$a_3(p) = \tfrac{8}{225}pX[1250p^2X^2 + 50pX(-3+4X) + 3 - 18X + 2X^2],$$

$$a_4(p) = \tfrac{4}{4725}pX[169400p^3X^3 + 10360p^2X^2(-3+4X)$$
$$+ pX(2595 - 8520X + 2080X^2)$$
$$- 45 + 249X - 204X^2 - 64X^3],$$

$$a_5(p) = \tfrac{8}{496125}pX[28861000p^4X^4 + 2322600p^3X^3(-3+4X)$$
$$+ 70p^2X^2(12879 - 41724X + 12436X^2)$$
$$+ 42pX(-1125 + 6225X - 5100X^2 - 1600X^3)$$
$$+ 5(135 - 810X + 1584X^2 + 216X^3 - 304X^4)],$$

$$a_6(p) = \tfrac{8}{1488375}pX[276458000p^5X^5 + 27930000p^4X^4(-3+4X)$$
$$+ 70p^3X^3(206022 - 641712X + 218688X^2)$$
$$+ 28p^2X^2(-56385 + 257835X - 228240X^2 - 34400X^3)$$
$$+ pX(74475 - 436140X + 692610X^2 - 49680X^3 - 181520X^4)$$
$$- 945 + 5445X - 11124X^2 + 4206X^3 + 4512X^4 - 352X^5].$$

## REFERENCES

[1] RUSHBROOKE, G. S., and MORGAN, D. J., 1961, *Mol. Phys.*, **4**, 1.
[2] BEHRINGER, R. E., 1957, *J. chem. Phys.*, **26**, 1504.
[3] RUSHBROOKE, G. S., and WOOD, P. J., 1958, *Mol. Phys.*, **1**, 257.
[4] DOMB, C., and SYKES, M. F., 1957, *Proc. roy. Soc.* A, **240**, 214.
[5] RUSHBROOKE, G. S., and WOOD, P. J., 1955, *Proc. phys. Soc., Lond.* A, **68**, 1161.
[6] DOMB, C., and SYKES, M. F., 1961, *Phys. Rev.*, **122**, 77.
[7] FISHER, M. E., 1961, *J. math. Phys.*, **2**, 609.

# An acoustic continuum model of molecular friction in simple dense fluids

by STUART A. RICE†

Department of Theoretical Chemistry, University of Cambridge‡

An acoustic model is presented with the aim of calculating an upper bound for the molecular friction constant. Problems arising from the use of macroscopic boundary conditions at molecular surfaces are circumvented by treating the molecule in a continuum as a distributed force centre modifying the propagation of acoustic waves. The computed friction constant is a factor of two larger than experiment. Physical arguments are given for the validity of the relation.

$$\zeta_0 < \zeta \text{ (real system)} < \zeta \text{ (acoustic)}$$

with $\zeta_0$ and $\zeta$ defined by equations (1) and (14). Other acoustic models are briefly discussed.

## 1. INTRODUCTION

In 1946 Kirkwood [1] demonstrated that dissipative processes in a dense medium could be described in terms of frictional forces generated by the fluctuating intermolecular force field of the medium surrounding a given molecule or set of molecules. Provided that the mean momentum, exchange per ' encounter ' [2] was small, it was shown that the singlet distribution function satisfied a Fokker–Planck equation. Higher-order distribution functions also satisfy Fokker–Planck type equations, suitably generalized to account for the multidimensional nature of the phase space. In this representation the forces leading to dissipation of energy can be described by a friction tensor which is defined in terms of the autocorrelation function of the intermolecular forces. In the application of the theory to specific transport phenomena, the transport coefficients are ultimately expressed in terms of the friction tensor (constant).

There have been a number of attempts to calculate the friction constant. We wish to mention the following studies:

(1) Kirkwood *et al.* [3], on the basis of dimensional arguments in which the relaxation time for the force autocorrelation function is identified as the interval of time smoothing, $\tau$, suggested the formula

$$\zeta_0{}^2 = \frac{Nm}{3v} \int \nabla^2 V(R_{12}) g_2(R_{12}) d^3 R_{12} \tag{1}$$

with $V(R_{12})$ the potential of intermolecular force, $g_2(R_{12})$ the pair correlation function, $N$ the number of molecules, $m$ the mass of a molecule and $v$ the volume of the system.

(2) Rice and Kirkwood [4] derived equation (1) from three hypotheses:

(*a*) The average displacement of a pair of molecules in time $\tau$ is small compared to the intermolecular spacing.

---

(*b*) The distribution function in pair space can be approximated as the product of the local equilibrium distribution function in configuration space and a momentum distribution function Maxwellian about the mean velocity.

(*c*) The pair diffusion tensor can be approximated *at all distances* as the direct sum of singlet diffusion tensors.

(3) Rice [5] showed that, aside from a factor of $(2/\pi)^{1\cdot2}$, equation (1) could be derived on the assumption that the autocorrelation function of momentum is gaussian in the time.

(4) Collins and Raffel [6] derived equation (1) by assuming that the momentum of a molecule as a function of time can be represented as having equal but opposite curvatures in the steady state and in the initial decay of the fluctuation.

(5) Gray [7] has shown that if the non-equilibrium singlet number density returns to equilibrium with relaxation time $\tau$, and the velocity relaxation time has the same value $\tau$, then equation (1) follows for the friction constant.

(6) Naghizadeh and Rice [8] have derived equation (1) from the equipartition theorem using assumption (*c*) of Rice and Kirkwood as well as the condition that a time $\tau$ may be so chosen that both the increment of momentum of a molecule in time $\tau$ is independent of the momentum and the displacement of a pair of molecules in time $\tau$ is small compared to the intermolecular spacing.

The six studies cited all have as a common feature the underestimation of the correlations between forces, momenta or coordinates. In the first study, the argument identifying $\tau$ as the relaxation time for force correlation, and in the third study the assumption of a gaussian form for the autocorrelation function of momentum, both imply that within a time $\tau$ an increment in force or momentum is rendered independent of the initial state†. With the restrictions imposed on the magnitude of $\tau$ by the general theory and in a dense medium where a positive displacement has large probability of being followed by a negative displacement due to the effective ' cage ' of near neighbours, such an assumption can only be approximately correct. In the studies cited as (2) and (6) the underestimate of correlation effects enters through the spatial decoupling effected when the pair diffusion tensor is set equal, at all distances, to the direct sum of singlet diffusion tensors. It is clear that this assumption is valid as $R_{12} \to \infty$, but at small distances it cannot be correct. Unfortunately, the derivations also require consideration of the pair diffusion tensor for small pair displacements. The derivation of Collins and Raffel (4) requires that the time derivative of the force acting on a molecule be of equal magnitude but opposite sign in the two limits, $t \to \infty$ and $t \to 0$. This severely restricts the rate at which the velocity can decay since in the initial transient state the coupling of the regressing fluctuation to the medium is not as complete as in the steady state. Finally, the fifth study restricts the coordinate and velocity relaxation times to be the same, a condition by no means in agreement with what is known of relaxation phenomena in dilute gases. Indeed, even though in the dense rigid sphere fluid the relaxation time for a perturbation in momentum space returning to thermal equilibrium corresponds to but one collision [9], it is not at all clear that configuration space relaxation can be as rapid because of the ' cage ' of neighbours tending to restrict the motion of a particle.

In this paper we seek a different representation of the interactions between molecules which will enable an upper bound to be placed on the effectiveness

† The use of a gaussian autocorrelation function leads to a lower bound for $\zeta$.

of the intermolecular correlations. If the interaction between a given molecule and the rest of the system is represented by a model in which the molecule is in contact with a continuum, then the correlation between particles will be over-estimated. The reason for this is easy to see, since the use of boundary conditions of a mechanical nature at the surface between the selected molecule and the continuum requires complete coherence between medium and molecule. That is, such conditions preclude all possible fluctuations which are characteristic of the real, molecularly coarse, fluid. It is, of course, just the existence of these fluctuations in the real system which limit the extent, both spatial and temporal, of possible intermolecular correlations.

The model used in this paper attempts to incorporate into a continuum the essential features of a real molecular sustem. Thus, the density of matter as a function of distance from the molecule will be taken to agree with the pair correlation function, and the molecule and the accompanying density variations about it will be taken to constitute a distributed force field affecting the amplitude and propagation of acoustic waves. A discussion of the relationship between this model and the elegant calculations of Fixman [10] and Kotin [11] will be found in § 3.

## 2. THE CONTINUUM MODEL

The starting point for our considerations is the same as that of Rice and Kirkwood [4], namely, the time averaged force acting on a given molecule. We write this force in the form

$$\langle \mathbf{F}_1 \rangle = -\frac{N}{\upsilon\tau} \int_0^\tau \int \nabla V(R_{12}(t+s)) g_2(R_{12}(t+s)) d^3R_{12} \, ds. \tag{2}$$

As in earlier work, the force acting at time $t+s$ is expanded about the force acting at time $t$,

$$\nabla V(R_{12}(t+s)) = \nabla V(R_{12}) + \Delta \mathbf{R}_{12}(s) \cdot \nabla\nabla V(R_{12}) + \cdots. \tag{3}$$

We shall also implicitly use the expansion

$$g_2(R_{12}) = g_2^0(R_{12}) + \Delta g_2(R_{12}) \tag{4}$$

with $g_2^0(R_{12})$ the local equilibrium pair correlation function and $\Delta g_2(R_{12})$ the perturbation to the local equilibrium function. In all of the following analysis we shall make the assumption that contributions to the mean force from $\Delta g_2(R_{12})$ can be neglected relative to the terms we shall retain [12]. We remind the reader that $g_2^0(R_{12})$ is defined by the local thermodynamic variables, and may vary from point to point in the fluid. With the use of the Liouville theorem to transform the integrand of equation (2) [13], and noting that the mean force acting on a molecule vanishes in an equilibrium ensemble, one finds

$$\langle \mathbf{F}_1 \rangle = -\frac{N}{\upsilon\tau} \int_0^\tau \int \Delta \mathbf{R}_{12}(s) \cdot \nabla\nabla V(R_{12}) g_2^0(R_{12}) d^3R_{12} \, ds$$

$$= -\frac{\rho_m}{m\tau} \int_0^\tau \int \Delta \mathbf{R}_{12}(s) \cdot \nabla\nabla V(R_{12}) g_2^0(R_{12}) d^3R_{12} \, ds \tag{5}$$

with $\rho_m$ the mass density of the fluid.

We now consider the transformation to the continuum model. We interpret $V(R_{12})/m$ as the potential of the force acting between a molecule and a unit mass

of the surrounding medium. Further, the density variation of the medium surrounding the molecule is described by $g_2(R_{12})$, now interpreted in terms of the mass density of the continuum.

In the continuum model, the relative displacement $\Delta \mathbf{R}_{12}(s)$ can be thought of as arising from a variation in density accompanying an acoustic wave. However, the presence of a molecule at the origin modifies the acoustic field by generating a force per unit mass, $-\nabla V(R_{12})/m$, and we may therefore regard the molecule as a distributed force centre. Under these circumstances, the displacement of an element of the continuum satisfies the inhomogeneous wave equation

$$\frac{1}{c^2} \frac{\partial^2 \Delta \mathbf{R}_{12}}{\partial s^2} - \nabla^2 \Delta \mathbf{R}_{12} = -\frac{g_2(R_{12}(t+s))}{mc^2} \nabla V(R_{12}(t+s)) \tag{6}$$

with $c$ the velocity of sound in the medium. We take as our boundary conditions that the displacement and its first derivative with respect to time both vanish at the surface of the containing volume, i.e. in the limit as $R_{12} \to \infty$. Under these circumstances, the solution to equation (6) can be shown to be [14]

$$\Delta \mathbf{R}_{12}(s) = -\frac{1}{4\pi mc^2} \int \frac{g_2(R_{12}{}^*)}{R_{12}} \nabla V(R_{12}{}^*) \, d^3 R_{12} \tag{7}$$

where the asterisk refers to the retarded value of $R_{12}$, i.e.

$$R_{12}{}^* = R_{12}\left(t + s - \frac{R_{12}}{c}\right). \tag{8}$$

The expansion of equation (7) using equations (3) and (4) gives

$$\Delta \mathbf{R}_{12}(s) = -\frac{1}{4\pi mc^2} \int \frac{g_2{}^0(R_{12})}{R_{12}} \Delta \mathbf{R}_{12}{}^*(s) \cdot \nabla \nabla V(R_{12}) \, d^3 R_{12} \tag{9}$$

to terms of the same order as retained in equation (5). With the expansion

$$\Delta \mathbf{R}_{12}{}^*(s) = \Delta \mathbf{R}_{12}(s) - \frac{R_{12}}{c} \frac{\partial \Delta \mathbf{R}_{12}}{\partial s} + \cdots \tag{10}$$

and substitution of equations (9) and (10) into equation (5), we obtain for the mean force the relation

$$\langle \mathbf{F}_1 \rangle = -\frac{\rho_m}{4\pi m^2 c^3 \tau}\left[ \int_0^\tau \int g_2{}^0(R_{12}) \frac{\partial \Delta \mathbf{R}_{12}}{\partial s} \cdot \nabla \nabla V(R_{12}) \, d^3 R_{12} \right.$$
$$\left. \cdot \int g_2{}^0(R_{12}) \nabla \nabla V(R_{12}) \, d^3 R_{12} \, ds \right]. \tag{11}$$

In equation (11) the only term dependent on $s$ is the time derivative. With the identification

$$\frac{1}{\tau} \int_0^\tau \frac{\partial \Delta \mathbf{R}_{12}}{\partial s} \, ds = \mathbf{u}, \tag{12}$$

with $\mathbf{u}$ the mean velocity of the molecule relative to the medium and the fundamental definition of the friction constant

$$\langle \mathbf{F}_1 \rangle = -\zeta \mathbf{u}, \tag{13}$$

we find, after integration over angles,

$$\zeta = \frac{\rho_m}{36\pi m^2 c^3}\left[ \int \nabla^2 V(R_{12}) g_2{}^0(R_{12}) \, d^3 R_{12} \right]^2. \tag{14}$$

In terms of $\zeta_0$, defined by equation (1),

$$\zeta = \frac{\zeta_0{}^4}{4\pi m^2 c^3 \rho m}. \tag{15}$$

For the case of liquid argon at 90°K, $\zeta_0$ has been calculated and has the value $4.84 \times 10^{-10}$ g/sec [3]. The measured velocity of sound, $8.196 \times 10^4$ cm/sec [15], and density, $1.374$ g/cm³ [15], give for the acoustic frictional constant, $\zeta = 1.21 \times 10^{-9}$ g/sec. In terms of the observable diffusion coefficient, this value corresponds to $D = 1.03 \times 10^{-5}$ cm²/sec. As anticipated, this is smaller than the observed value, $D = 2.07 \times 10^{-5}$ cm²/sec [16].

## 3. Discussion

The model discussed in this paper is very simple and its physical interpretation is clear. The real molecularly coarse fluid is replaced by an acoustic continuum with a distributed force field. The distributed force field, representing the interaction between a molecule and the medium is chosen to duplicate the local mean density variations of a real fluid. The uncertainties involved in the definition of a proper molecular size and in the use of macroscopic boundary conditions at a surface of molecular dimensions have been avoided by using conditions on the wave amplitude and its derivative in the limit as $R_{12} \to \infty$.

In the model discussed a strong correlation is always maintained between the origin of the distributed force and fluid displacements, independent of the separation of the displacement from the origin. This correlation arises from the coherence of the acoustic wave, which we have taken to be non-dissipatively propagated. The natural damping of correlations by intervening fluctuations is thereby destroyed, and the molecular friction overestimated.

Fixman [10] and Kotin [11] have also used an acoustic model to calculate the friction constant. In the first calculation, Fixman showed that the propagation of acoustic waves can serve as a correlating mechanism whereby the initial momentum of a selected molecule can be conveyed to a distant point in the fluid. In this calculation the random force of classical Brownian motion theory is assumed to be the acoustic force acting on a molecule as a result of fluid compression in the neighbourhood of the molecule. In the limit that the time of smoothing becomes very large, Fixman finds for the dilute gas the result

$$v\eta = NmD, \tag{15}$$

which is 20 per cent higher than the result of Chapman–Enskog theory [17]. Kotin treated the same problem (i.e. diffusion in the dilute gas) by two continuum models in which, as above, the molecule is assumed to be subject to fluid pressure waves arising from density fluctuations in the surrounding medium. The motion of the molecule is associated with acoustic radiation into the medium, resulting in an acoustic impedance which gives rise to a frictional force on the molecule. Whether the model is that of a hard sphere molecule in a continuum, or the inhomogeneity of the surrounding fluid is included via multiple scattering, the friction constant obtained has the same functional form as that of the Chapman–Enskog theory, but is somewhat smaller (15–40 per cent).

The calculations of Fixman and Kotin provide a very incisive analysis of one particular physical interpretation of the friction constant and in our opinion are of great interest. The calculations differ considerably from that presented

herein where the acoustic model is used only in the sense of predicting in an approximate way the displacement of a molecule collectively interacting with a large number of neighbours. Our method is not suited to the dilute gas [18], but for the dense fluid has the advantages of keeping, through the distributed force centre, a representation of the average behaviour of the fluid in the neighbourhood of a molecule. Since the approximations made by Fixman and Kotin to render the calculations tractable are useful only in the dilute gas case, the models are complementary to one another.

In closing, we wish to remark that although we have no analytic verification of limits, the physical picture discussed makes it very likely that the friction constant calculated herein is an upper bound to possible values. We thus anticipate that

$$\zeta_0 < \zeta \text{ (real system)} < \zeta \text{ (acoustic)} \tag{16}$$

## REFERENCES

[1] KIRKWOOD, J. G., 1946, *J. chem. Phys.*, **14**, 180.
[2] For a brief summary of the theory and a physical analysis of the meaning of ' encounter' in this usage as well as a description of the various time scales involved in transport processes, see S. A. Rice and H. L. Frisch, 1960, *Ann. Rev. phys. Chem.*, **11**, 187.
[3] KIRKWOOD, J. G., BUFF, F. P., and GREEN, M., 1949, *J. chem. Phys.*, **17**, 988.
[4] RICE, S. A., and KIRKWOOD, J. G., 1959, *J. chem. Phys.*, **31**, 901.
[5] RICE, S. A., 1960, *J. chem. Phys.*, **33**, 1376.
[6] COLLINS, F. C., and RAFFEL, H., 1958, *J. chem. Phys.*, **29**, 699.
[7] GRAY, P., private communication.
[8] NAGHIZADEH, J., and RICE, S. A., to be submitted to *J. chem. Phys.*
[9] HARRIS, R. A., and RICE, S. A., 1960, *J. chem. Phys.*, **33**, 1055.
[10] FIXMAN, M., 1957, *J. chem. Phys.*, **26**, 1421; 1958, *Ibid.*, **28**, 397; **29**, 540.
[11] KOTIN, L., 1960, Thesis, Harvard University, January.
[12] This assumption is implicit in all previous calculations of the friction constant.
[13] We use the Liouville Theorem to transform volume elements and distribution functions as in the arguments of reference [4].
[14] SNEDDON, I., 1957, *Elements of Partial Differential Equations* (New York: McGraw-Hill Book Company), p. 249.
[15] VAN ITTERBECK, A., and VERBEKE, O., 1960, *Physica*, **26**, 931.
[16] CORBETT, J. W., and WANG, J. H., 1956, *J. chem. Phys.*, **25**, 422.
[17] See, for example, J. O. Hirschfelder, C. F. Curtiss and R. B. Byrd, 1954, *Molecular Theory of Gases and Liquids* (New York: John Wiley & Sons).
[18] Amongst other factors, the series expansions of the force cannot be truncated after so few terms if the medium is gaseous.

# The NMR spectra of some epoxides

by J. I. MUSHER

Lyman Laboratory, Harvard University

The high resolution NMR spectra of a series of eight epoxides has been studied. Five of these, with the epoxide group axially affixed to a saturated ring, show ABX spectra and the analysis provides accurate values for the NMR parameters of the three-spin system. These are then compared with the data in the literature. Three of the epoxides, with the epoxide group equatorial to the ring, show, however, AA′B or AA′K spectra and cannot be interpreted explicitly without extensive fitting with machine calculations.

Recently there has been considerable interest [1, 2, 3] in obtaining experimental values for proton–proton coupling constants to serve as aids in the development of a proper theoretical treatment [2, 4, 5] of electron-coupled I.I interactions. With this in mind, Reilly and Swalen [6] have examined in detail four epoxides and Gutowsky *et al.* [2] have studied one of these, styrene oxide†. We have studied a series of eight epoxides of the form:

$$\begin{array}{ccc} [B]H & & R \\ \backslash\,^{\beta} & & ^{\alpha}/ \\ & C-C & \\ /\,\backslash & & /\,\backslash \\ [A]H & O & H[X] \end{array}$$
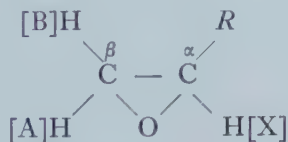
where $R$ is a saturated cyclic alcohol containing no protons on the carbon bonded to the epoxy group. The eight compounds were the four isomeric (2-methyl-1-hydroxy-cyclohexyl)-ethylene oxides (I–IV) and four of the eight possible 1-hydroxy-decalyl-ethylene oxides (V–VIII) [7–11]‡.

The high resolution 60 Mc/s NMR spectra were taken in degassed $CCl_4$, with the exception of VI which was taken in degassed $CDCl_3$, and referred to internal hexamethyldisiloxane. Frequency shifts were measured by audio sideband interpolation sweeping upfield and downfield on alternate calibrations. Four calibrations were made for each spectrum. The small quantities of the compounds available caused some difficulties but the standard deviations of the peak separations within a single multiplet were less than 0·15 c/s and between peaks in separate multiplets (affecting the screening parameters only) less than 0·30 c/s. Spectra were also taken at 40 Mc/s, providing properly corresponding data.

† These authors have also examined propylene oxide but with an incomplete analysis due to the complexity of the spectrum and for this reason it will not be included in our discussion here. However, they do show the A proton to be to low field from the B proton for an hydrocarbon $R$ group contrary to our data presented below.

‡ The structural formulae and several spectra of the compounds are given in ref. [11] according to the same system of numbering (I–VIII) as we employ here.

Since the epoxide structure is linked to a tertiary ring carbon and since we can neglect long-range couplings, the epoxy group protons can be considered as a closed system of three interacting spins. By analogy with data from vinyl compounds [12] we expect a spectrum of the form ABX [13] with the protons assigned as above; the X proton should lie to lowest field and the A proton to highest field. The first expectation has been verified by the four epoxides of ref. [6] but the second has only held for glycidonitrile and has been contradicted by the other three epoxides. We shall make our assignments based upon the experimental observation [6] that $J_{cis} = J_{AX} > J_{trans} = J_{BX}$ and upon the assumption that the X proton (observed to be to low field) is the one on the $\alpha$ carbon atom from the analogy with vinyl compounds.

In five of these epoxides† the spectrum is of the expected ABX type with either 11 or 12 non-overlapping peaks in each spectrum spread over a minimum of 32 c/s. From the data and ABX calculations‡ the NMR parameters as listed in the table are obtained. The coupling constants are probably valid to $\pm 0.25$ c/s and the chemical shifts to $\pm 0.5$ c/s.

From these data and the two assumptions above we observe that proton B does lie to low field from proton A in agreement with the vinyl compounds and contrary to three of the four epoxides previously studied. Thus an alkyl substituent can have the same effect on the chemical shift for epoxy protons as it has for vinyl protons. We further note that the screening parameter for the X proton is changed the most by the different substituents and that the sum of the screening parameters for the A and X protons is not relatively constant over the series, both contrary to the conclusions of Reilly and Swalen.

In three of these epoxides instead of the 12-peak ABX spectrum we find a six- or seven-peak AA′B or AA′K spectrum with all the peaks contained within 19 c/s. The six-peak spectra of (trans-2-methyl-1-hydroxy-cyclohexyl)-ethylene oxide, m.p. 75–75·5° (III), and (1α-hydroxy-9β-H)-trans-decalyl-ethylene oxide, m.p. 116·5–117·5° (VI) are almost of A₂B form (with B to low field) centred on 156·2 and 162·6 c/s respectively. (The latter is taken in $CDCl_3$ which should be corrected to $\sim 155$ c/s for comparison with data taken in $CCl_4$ [14].)

(Trans-2-methyl-1-hydroxy-cyclohexyl)-ethylene oxide, m.p. 40·5–41° (IV), has an AA′K spectrum containing seven peaks† with the peak for the K proton lying to low field. An explicit analysis of this spectrum is not feasible without

† The sample of II given us was found to contain a mixture of 55 per cent (probably of) I and 45 per cent II. (This mixture was originally considered to be a mixture of II [11].) We were unable to separate these but could, with difficulty, distinguish parts of the two sets of multiplets. Only the approximate values as indicated in the table could be determined. In this compound (or rather mixture of compounds) the hydroxyl peak is rather independent of concentration and only slightly dependent on temperature. It is rather broad and over-laps the epoxy proton peaks—it is (at room temperature) 0·4 p.p.m. to lower field than any of the other hydroxyl proton peaks. Probably there is rather strong intra-molecular bonding involved, perhaps between the hydroxyl proton and the epoxy oxygen.

‡ It will be observed from the work of Reilly and Swalen that the error introduced into $J_{AX}$ and $J_{BX}$ by using an ABX calculation instead of the exact ABC calculation is small unless $\sigma_A - \sigma_B$ or $\sigma_B - \sigma_X$ is very small. VII and VIII have these values in the range of those for styrene oxide in which the agreement between the two calculations is within 0·1 c/s, and I and V should admit an error of $< 0.2$ c/s. The error in $J_{AX}$ and $J_{BX}$ in IV (below) should be larger and certainly accounts for the apparent equality of these two coupling constants. In all cases the error introduced into $J_{AB}$ and the screening parameters should be $< 0.05$ c/s.

| Compound | $J_{AB}$ | $J_{AX}$ | $J_{BX}$ | $\eta H_0(1-\sigma_A)$ | $\eta H_0(1-\sigma_B)$ | $\eta H_0(1-\sigma_X)$ |
|---|---|---|---|---|---|---|
| I (cis-2-methyl-1-hydroxy-cyclohexyl)-ethylene oxide, m.p.42·5–43° | 5·69 | 3·51 | 2·81 | 153·0 | 165·0 | 177·3 |
| II (cis-2-methyl-1-hydroxy-cyclohexyl)-ethylene oxide, b.p. 88–9°/10 mm | ~5·7 | $\lvert J_{AX}\dagger + J_{BX}\rvert\dagger \approx 6\cdot4$ | | $\sim 15 - \frac{\delta}{2}\dagger$ | $\sim 151 + \frac{\delta}{2}\dagger$ | ~180 |
| V (1α-hydroxy-9α-H)-1·1 trans-decalyl-ethylene oxide, m.p. 112–112·5° | 5·58 | 3·61 | 2·79 | 155·3 | 166·7 | 181·9 |
| VII (1α-hydroxy-9 β-H)-cis-decalyl-ethylene oxide, m.p. 100–101° | 5·55 | 3·72 | 2·78 | 152·8 | 161·7 | 194·0 |
| VIII (1α-hydroxy-9 β-H)-cis-decalyl-ethylene oxide, m.p. 88–90° | 5·50 | 3·75 | 2·89 | 156·7 | 166·9 | 193·3 |
| IV (trans-2-methyl-1-hydroxy-cyclohexyl)-ethylene oxide, m.p. 40·5–4·1° | $\dfrac{\delta^2 - 0\cdot7}{1\cdot7}$ | ~3·45 | ~3·45 | $147\cdot1 - \frac{\delta}{2}\dagger$ | $147\cdot1 + \frac{\delta}{2}\dagger$ | 160·9 |
| Range of parameters (excluding II and IV) | 0·19 | 0·24 | 0·10 | 3·9 | 5·2 | 16·0 |

Epoxide NMR parameters. The data are given in c/s referred to internal hexamethyldisiloxane.
† These values could not be determined from the spectra.

machine calculations because of the inability to observe the several peaks of low intensity. However, it is possible, based on an ABX calculation to determine $J_{AX}$, $J_{BX}$, $\eta H_0(1-\sigma_X)$, $\frac{1}{2}\eta H_0(2-\sigma_A-\sigma_B)$ and a linear equation relating $J_{AB}$ to $\delta = \eta H_0(\sigma_A - \sigma_B)$. These values are also given in the table except that the assignment of resonances to particular protons on the epoxide structure is chosen only to be consistent with the other assignments. It is interesting to note that $J_{AX} + J_{BX}$ (which is independent of the error in either of the coupling constants considered separately†) is 0·3 c/s greater than the same sum for any of the other molecules in the series. The range of $J_{AX} + J_{BX}$ for the six molecules is 6·3–6·9 c/s.

The original assignments of cis- and trans- configurations (for the non-hydroxyl substituents) of I–IV were verified by chemical conversion to the known cis- and trans-1, 2-dimethylcyclohexanols. By conformational analysis I and II are expected to have their epoxy groups axial and III and IV are expected to have their epoxy groups equatorial. From our evidence, therefore, when the epoxy group is equatorial to the ring the α proton is $> 0.25$ p.p.m. to high field from its position when the epoxy group is axial‡ thus overlapping the peaks from the β protons and causing an ABX spectrum to collapse into an AA′B or AA′K spectrum. The pair of β protons also coalesce and contribute in a major way to the reduction in the number of peaks of the spectra. The explicit expression of this shift has not been determined, but it is the cause of the AB part of the ABX spectrum's going into the AA′ part of the AA′K spectrum. From the instances examined here this effect is very definite and specific and can serve as a method for identifying conformations of expoxy groups. On the basis of this, with Dr. Akhrem [11] we have reversed the configurational assignments of V–VIII which were previously identified only by qualitative chemical information. The corrected assignments have been used here.

*Note added in proof.*—It is unfortunate that we have used here the nomenclature AA′K, etc. as consistent with ref. [6] for which A′ signifies a nucleus with chemical shift slightly different from that of A. In more recent work, the author and others have found it more meaningful to use a prime to indicate a nucleus which has the same chemical shift as the unprimed nucleus but which is not magnetically equivalent to it: e.g. 1, 1-difluoroethylene and butadiene-1, 3 are

---

† The peaks relative to internal hexamethyldisiloxane were at: 145·05, 145·9, 148·5, 149·35, 157·5, 160·87, 164·87 c/s with appropriate intensities, and are assigned to transitions 3(A), 5(B), 4(A), 6(B), 9(X), 10–11(X), 12(X) respectively according to ref. [13]. The equation relating $J_{AB}$ and $\delta$ is: $1·7J_{AB} + 0·7 = \delta^2$ with $\delta > 0$. For example: $J_{AB} = 5·7$ c/s means that $\delta = 3·2$ c/s.

‡ This is analogous to the observation [14] that in 1, cis-3, trans-5-trimethylcyclohexane the protons on the axial methyl group are 0·14 p.p.m. deshielded from the protons on the equatorial methyl groups. With the epoxides, of course, the α-proton does not have the same time-average positions as the proton in the methyl groups.

·called AA′XX′ and AA′BB′XX′ systems respectively and not $A_2B_2$ and $A_2B_2X_2$. This is to alleviate confusion between 'chemical equivalence' and 'magnetic ·equivalence'.

## REFERENCES

[1] KARPLUS, M., ANDERSON, D. H., FARRAR, T. C., and GUTOWSKY, H. S., 1957, *J. chem. Phys.*, **27**, 597.
[2] GUTOWSKY, H. S., KARPLUS, M., and GRANT, D. M., 1959, *J. chem. Phys.*, **31**, 1278.
[3] MUSHER, J. I., 1961, *J. chem. Phys.*, **34**, 594.
[4] KARPLUS, M., and ANDERSON, D. H., 1959, *J. chem. Phys.*, **30**, 6.
[5] KARPLUS, M., 1959, *J. chem. Phys.*, **30**, 11.
[6] REILLY, C. A., and SWALEN, J. D., 1960, *J. chem. Phys.*, **32**, 1378.
[7] AKHREM, A. A., 1959, *Bull. Acad. Sci. U.R.S.S.*, 750.
[8] NAZAROV, I. N., and AKHREM, A. A., 1958, *J. gen. Chem.*, Moscow, **28**, 1791.
[9] NAZAROV, I. N., KAMERNITZKII, A. V., and AKHREM, A. A., 1958, *J. gen. Chem.*, Moscow, **28**, 1458.
[10] NAZAROV, I. N., ALEKZANDROVA, G. V., and AKHREM, A. A., 1948, *J. gen. Chem.*, Moscow, **28**, 2187, 2199.
[11] MUSHER, J. I., and AKHREM, A. A., 1960, *C.R. Acad. Sci. U.R.S.S.*, **134**, 354.
[12] ALEXANDER, S., 1958, *J. chem. Phys.*, **28**, 358.
[13] POPLE, J. A., SCHNEIDER, W. G., and BERNSTEIN, H. J., 1959, *High-Resolution Nuclear Magnetic Resonance* (New York: McGraw-Hill Book Company Inc.).
[14] MUSHER, J. I., unpublished results.

# The rate of molecular collisions in gases composed of 'soft' molecules

by J. S. ROWLINSON

Department of Chemical Engineering and Chemical Technology,
Imperial College of Science and Technology, London, S.W.7

Equations are derived for the number of collisions per unit time in which the centres of the molecules approach to some arbitrary distance, $d$, or less, for molecules with spherical intermolecular potentials. The collision rates based upon this criterion of closeness-of-approach have a different dependence on temperature from those based upon cross sections determined from the viscosity. It is suggested that the rates calculated in this paper are the more appropriate for the discussion of experiments on the exchange of molecular energy and on the kinetics of chemical reactions.

---

A knowledge of $Z$, the number of collisions made by one molecule in unit time, is required for the interpretation of many experiments on the rates of chemical reactions and on the rates of equilibration of different kinds of molecular energy. The calculation of this collision rate is straightforward if the molecules are supposed to be rigid elastic spheres, a supposition that has often been made in practice since calculations of $Z$ have not needed to be very accurate.

However, there is now a substantial body of accurate information on the rates of equilibration of vibrational and translational energy over very wide ranges of temperature [1, 2] from which it would be useful to calculate with precision $Z_{10}$, the mean number of collisions required for a molecule with one vibrational quantum of energy to revert to the ground state. The quantal theory of this process can be put into the form where it yields directly the mean life of the excited molecule [3], and not $Z_{10}$. This mean life is more closely related than $Z_{10}$ to the experimental observations. Nevertheless the expression of the life of an excited molecule as a number of collisions has several advantages and is very widely used. The value of $Z_{10}$ shows at once the rate of deactivation on a natural scale on which the ultimate limit is $Z_{10} \approx 1$. Moreover the use of $Z_{10}$ rather than a lifetime in seconds is the most meaningful way of comparing one molecule with another in its efficiency in removing vibrational energy.

$Z_{10}$ can be found only if $Z$ is known as a function of density and temperature. A common procedure, both in studies of energy transfer and of chemical kinetics [4], has been to calculate $Z$ for an assembly of rigid spheres†

$$Z^* = 4n(\sigma^*)^2 (\pi kT/m)^{1/2}, \tag{1}$$

where the asterisk denotes the rigid-sphere approximation. $Z^*$ is the number of collisions made by one molecule in one second in a pure gas of $n$ molecules per cubic centimetre, whose mass is each $m$. The diameter, $\sigma^*$, is that of the rigid

† Equations quoted without derivation can be found in standard works on the kinetic theory of gases [5].

spherical molecule (in centimetres). This is usually obtained from the observed viscosity at room temperature by assuming again that the gas is composed of rigid spheres:

$$\eta^* = \frac{5}{16} \frac{1}{(\sigma^*)^2} \left(\frac{mkT}{\pi}\right)^{1/2}. \tag{2}$$

The collision rate so calculated, $Z^*$, is proportional to $T^{1/2}$ at constant density and to $T^{-1/2}$ at constant pressure. But at no temperature does it represent any definable estimate of the collision number for the real molecules. If the interaction between molecules is a central force which is a continuous function of their separation then the viscosity is a measure of the mean angle of deflection of molecules on neighbouring trajectories. At low temperatures many of these will be attractive deflections of molecules whose centres are never close at any point of their trajectories. $Z^*$ of (1) and (2) is therefore more a measure of trajectories that result in a deflection, rather than in a collision, as this term is usually understood.

The criterion for a collision that would appear to be most relevant for exchange of energy, or for chemical reaction, is the number of times the molecular centres approach to within some chosen distance. It is the object of this note to calculate such rates for molecules with continuous force-fields.

Let the potential energy of two molecules at separation $r$ be $u(r)$. The detailed form of this function is immaterial but its general behaviour is, as follows: at small $r$, $u(r)$ is positive and decreases with increasing $r$; it becomes zero at a separation $\sigma$ (commonly called the collision diameter); it has a minimum value of $-\epsilon$ at a separation $r_m$; and it approaches zero as $r$ approaches infinity.

Consider two molecules of mass $m$ on trajectories between which the perpendicular distance is initially $b$. (The word 'initially' describes the situation before the mutual force has distorted the trajectories from straight lines.) The distance $b$ is called the impact parameter. The closest distance of approach, $d$, of two such molecules is given by

$$b^2 = d^2 \left(1 - \frac{4u(d)}{mv^2}\right) \tag{3}$$

where $v$ is the initial relative velocity.

The collision rate required is the number of collisions in which the centres of molecules approach to $d$ or less, where the choice of $d$ can be made later in the calculation to suit the phenomenon under discussion. Thus the number of collisions is that number in which (3) specifies the maximum allowable value of $b$ for each velocity $v$. If $u(d)$ is negative $(d > \sigma)$ then for each velocity between 0 and $\infty$ there is a corresponding maximum value of $b$. If $u(d)$ is positive $(d < \sigma)$ then there is no real value of $b$ which will lead to a satisfactory collision, unless $v$ exceeds a critical value that is found by putting $b$ equal to zero in (3).

Consider first, therefore, the case where $u(d)$ is negative. The number of collisions made by one molecule in which the initial relative velocity is between $v$ and $v + dv$ and of impact parameter $b$ or less is just that fraction of the collision rate for hypothetical rigid spheres of diameter $b$ that lie in this velocity range, namely

$$Z = n \frac{\pi^{1/2}}{2} \left(\frac{m}{kT}\right)^{3/2} b^2 v^3 \exp\left(-\frac{mv^2}{4kT}\right) dv. \tag{4}$$

Substitute for $b$ from (3) and integrate over all velocities:

$$Z[d] = 4nd^2 \left(\frac{\pi kT}{m}\right)^{1/2} \left(1 - \frac{u(d)}{kT}\right)$$

$$= Z_d^* \left(1 - \frac{u(d)}{kT}\right) \qquad (d \geqslant \sigma), \tag{5}$$

where $Z_d^*$ is the collision rate for hypothetical rigid spheres of diameter $d$.

Two particular cases of (5) are:

$$Z[\sigma] = Z_\sigma^*, \tag{6}$$

$$Z[r_m] = Z_{r_m}^* \left(1 + \frac{\epsilon}{kT}\right). \tag{7}$$

The first of these equations shows that the number of collisions in which the molecules approach to $\sigma$ or less is just the collision rate for hypothetical spheres of this diameter. Thus $Z[\sigma]$ is proportional to $T^{1.2}$ at constant density. The second equation shows that the number of collisions in which the centres approach to $r_m$ or less exceeds the number which approach to $\sigma$ not only by the factor of $(r_m \sigma)^2$ but also by the factor $(1 - \epsilon kT)$. The second factor is a measure of the number of trajectories that are brought within $r_m$ by the attractive forces of the molecules. A special case of this equation was derived by Sutherland for rigid spheres surrounded by an attractive potential, and a collision rate of this kind was used by Eucken [6].

If $u(d)$ is positive $(d < \sigma)$ then the integration of (4) is taken only over those velocities for which (3) has a real solution for $b$. Substitution from (3) and integration, gives

$$Z[d] = Z_d^* \exp\left[-u(d)/kT\right] \qquad (d \leqslant \sigma). \tag{8}$$

Here $Z$ increases with temperature more rapidly than $T^{1/2}$ (at constant density) because of the failure of molecules with low velocities to make effective collisions.

The choice of $d$, and so the choice of (5) or (8) for the calculation of $Z$, depends upon one's assessment of the type of collision to be counted in each kind of experiment.

The figure shows, for oxygen, the ratios of $Z[r_m]$, $Z[\sigma]$ and $Z[0.95\sigma]$ to the conventional $Z^*$ of (1) and (2). A Lennard-Jones 12:6 potential is used with $\sigma = 3.61$ Å and $\epsilon/k = 113$ K. The conventional $Z^*$ of (1) and (2) is calculated from the viscosity of oxygen at 0 C [5]. It is seen that $Z[\sigma]$ has the same dependence upon temperature as $Z^*$ (cf. (6)), but that $Z[0.95\sigma]$, falls rapidly at low temperature.

Oxygen is a gas for which there are experimental measurements [1, 2] of the relaxation time for vibrational energy from room temperature to 3100 K, and it is seen that the choice of $d$ can affect the derived collision number $Z_{10}$ by a factor of two or more.

Herzfeld and Litovitz [1] (p. 195, equation 36-4; p. 203, equation 38-1; p. 243, table 50-2) use (1) with $(\sigma^*)^2$ replaced by $(\sigma^2\Omega)$, where $\sigma$ and $\Omega$ are the collision diameter and the reduced cross section appropriate to the viscosity for a Lennard-Jones potential. Cottrell and McCoubrey [2] make the same choice. Their curve for $Z$ naturally crosses the usual curve, $Z^*$, at 0 C in this case since this was the temperature chosen for the calculation of $Z^*$ from the viscosity. It crosses $Z[\sigma]$ at the temperature at which $\Omega$ is unity, which is 396 K for oxygen. The figure shows that, in its dependence upon temperature, this curve resembles
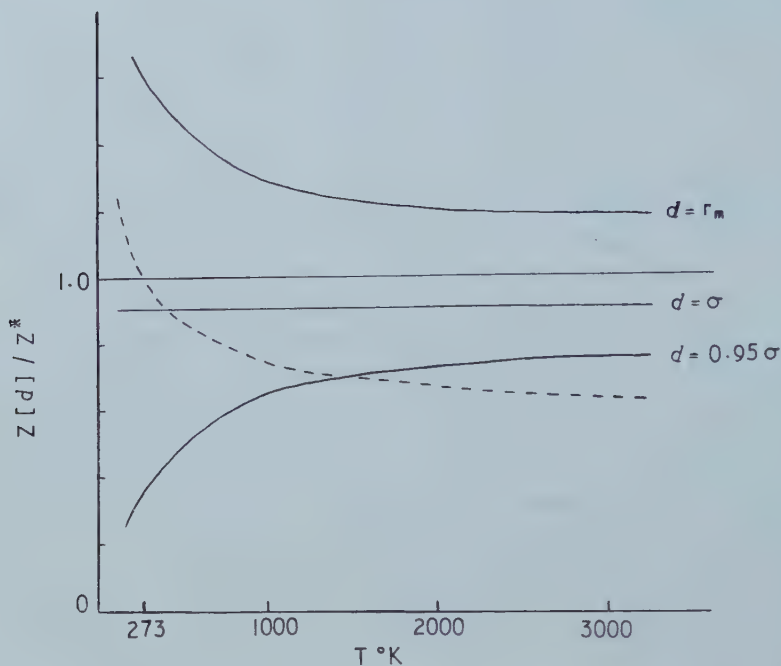
The ratios for oxygen of $Z[d]$ to the conventional collision rate for rigid spheres defined by
(1) and (2). The three values of $d$ are $r_m$, $\sigma$ and $0.95\sigma$. The dashed line is the
collision rate chosen by Herzfeld and Litovitz and by Cottrell and McCoubrey.

$Z[r_m]$, although it is only half the absolute size. This resemblance arises since
both are collision rates that are heavily weighted at low temperatures by the
attractive deflections. It is probable that the collision number of Herzfeld and
Litovitz and of Cottrell and McCoubrey, which is an average based upon
deflections, not upon separations of molecules, is less appropriate to this
phenomenon than is $Z[\sigma]$ or even $Z[0.95\sigma]$.

I wish to thank Dr. J. C. McCoubrey for a discussion of this problem.

REFERENCES

[1] HERZFELD, K. F., and LITOVITZ, T. A., 1959, *Absorption and Dispersion of Ultrasonic Waves* (New York: Academic Press), Part B.
[2] COTTRELL, T. L., and McCOUBREY, J. C., *Molecular Energy Transfer in Gases* (London: Butterworths), Chap. 5 (in the press).
[3] COTTRELL, T. L., and REAM, N., 1955, *Trans. Faraday Soc.*, **51**, 159, 1453.
[4] HINSHELWOOD, C. N., 1940, *Kinetics of Chemical Change* (Oxford: University Press), p. 14.
[5] KENNARD, E. H., 1938, *Kinetic Theory of Gases* (New York: McGraw-Hill), Chap. 3; CHAPMAN, S., and COWLING, T. G., 1939, *Mathematical Theory of Non-Uniform Gases* (Cambridge: University Press), Chap. 5; HIRSCHFELDER, J. O., CURTISS, C. F., and BIRD, R. B., 1954, *Molecular Theory of Gases and Liquids* (New York: Wiley), Chap. 8.
[6] EUCKEN, A., and BECKER, R., 1934, *Z. phys. Chem.* B, **27**, 235.

# Determination of the relative signs of proton spin coupling constants by double irradiation

by R. FREEMAN and D. H. WHIFFEN

Basic Physics Division, National Physical Laboratory, Teddington, Middlesex

The method of Evans [1] for determining relative signs of nuclear spin coupling constants by double irradiation experiments has been extended to the case where the three coupled nuclei are all protons. It is thus possible to demonstrate from the high resolution proton magnetic resonance spectrum of the ring protons of 2-Furoic acid that the three spin coupling constants are all of like sign.

## 1. Introduction

The exact analysis of certain types of high resolution nuclear magnetic resonance spectra can be made to yield the relative signs of some of the coupling constants in the molecule. Examples are relatively few and are limited entirely to strongly coupled spin systems [2]. Recently Evans [1] has suggested an elegant method of obtaining such relative signs by an adaptation of the technique of spin decoupling to systems of three coupled nuclei, and has demonstrated in this way the opposite signs of the two thallium–hydrogen spin coupling constants in the thallium diethyl cation. The method has the advantage of being applicable to molecules which have 'first order' spectra, that is, the coupling constants ($J$) may be small compared with the chemical shifts, and this clearly widens the possible field of investigation. There is some theoretical interest in the possibility of negative coupling constants, and indeed in order to determine relative signs, spectra have been deliberately recorded at low magnetic field so that the field independent coupling constants become comparable with the chemical shifts.

This paper extends the work of Evans to a system of three coupled protons. This is a test of the generality of the method, for the spin decoupling technique is all the more difficult when the values of the three coupling constants are close together, as they will be when all three nuclei are protons.

## 2. Principle of the method

### 2.1. *The spectrum of 2-Furoic acid*

The method is best described by means of an example, and since the molecule investigated experimentally represents a particularly simple case, it will be used as the model. The substance is 2-Furoic acid and it has been studied as a saturated solution in acetone on a Varian Associates 60 Mc/s high resolution spectrometer at about 24°c. This substance has been investigated previously at 30 Mc/s [3], 40 Mc/s [4] and 60 Mc/s [5] as an ABX type molecule (the acid proton does not couple into the ring). At 60 Mc/s the spectrum is very nearly of the first order type (figure 1) but the ABX nomenclature has been retained and a normal ABX
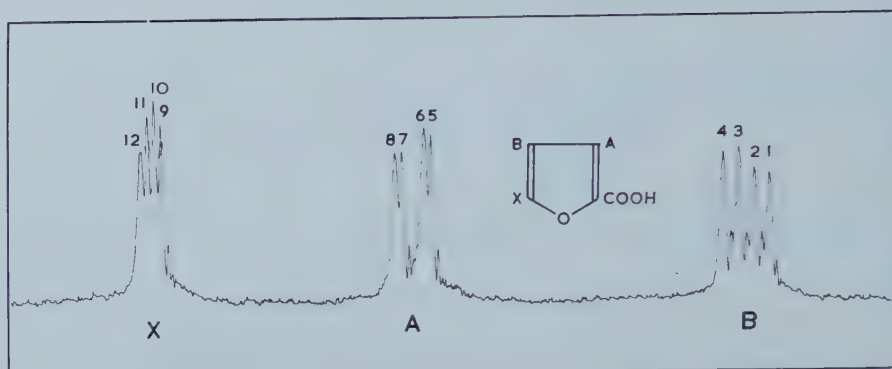
Figure 1.   The high resolution nuclear resonance spectrum of the ring protons of 2-Furoic acid at 60 Mc/s.   The magnetic field increases from left to right.

analysis [6] gives $|J_{AB}| = 3 \cdot 5$ c/s, $|J_{BX}| = 1 \cdot 8$ c/s, $|J_{AX}| = 0 \cdot 8$ c/s, $\nu_A - \nu_B = 39 \cdot 2$ c/s, $\nu_X - \nu_A = 31 \cdot 6$ c/s.

## 2.2.  Double irradiation, $J_{AB}$ and $J_{BX}$ of like sign

If one assumes first of all that all three coupling constants are positive, then it is possible to tabulate the spin states of the proton neighbours for each of the twelve observed transitions† numbered in figure 1.   Here $\alpha$ represents $M_I = +\frac{1}{2}$ and $\beta$ represents $M_I = -\frac{1}{2}$.

|  |  | X | | | | A | | | | B | | | |
|---|---|---|---|---|---|---|---|---|---|---|---|---|---|
|  |  | 12 | 11 | 10 | 9 | 8 | 7 | 6 | 5 | 4 | 3 | 2 | 1 |
| Spin states | A | α | β | α | β |  |  |  |  | α | α | β | β |
| of neighbours | B | α | α | β | β | α | α | β | β |  |  |  |  |
|  | X |  |  |  |  | α | β | α | β | α | β | α | β |

Table 1.

As a result of the difference between $|J_{AB}|$ and $|J_{AX}|$ it is feasible to irradiate near the frequency of transitions 5 and 6 without appreciably perturbing transitions 7 and 8, and yet still apply sufficient power to meet the condition $\gamma H_1 > \pi |J_{AX}|$.   Under these conditions transitions 9 and 10 should collapse to a single line, but 11 and 12 should *remain unchanged* since these transitions are confined to those molecules where the proton B has spin state $\alpha$, and these are not affected by the strong radio-frequency field.

If the coupling constants are all negative $\alpha$ and $\beta$ are interchanged throughout table 1.   The argument is unaffected, and the absolute signs of the coupling constants are not determined in this experiment.

## 2.3.  Double irradiation, $J_{AB}$ and $J_{BX}$ of opposite sign

One may deduce from §2.2 that the behaviour of the X spectrum when part of the A spectrum is strongly irradiated is quite independent of the sign of $J_{AX}$, the coupling which is being 'washed out'.   For this reason the only cases which

† The nuclear resonance absorptions are transitions $\alpha \leftarrow \beta$, where $\beta$ states are of lower energy, because the magnetic field is assumed to be in the $-z$ direction in accordance with the normal convention in nuclear resonance [7].

now remain to be considered are the two where $J_{AB}$ and $J_{BX}$ are of opposite sign. If $J_{AB}$ is positive and $J_{BX}$ negative then in table 1, row B of column X (and row X of column B) should have $\alpha$ and $\beta$ interchanged. Then irradiation of lines 5 and 6 would collapse 11 and 12 but leave 9 and 10 unchanged because molecules with proton B in spin state $\alpha$ are not affected. Exactly the same behaviour would be observed if $J_{AB}$ were negative and $J_{BX}$ positive; in this case $\alpha$ and $\beta$ are interchanged in row B of column A (and row A of column B) and it is now molecules with B in spin state $\beta$ which are unaffected.

Hence the relative signs of the coupling constants $J_{AB}$ and $J_{BX}$ may be determined by observing what happens to the X group of lines when part of the A group is irradiated.

## 3. Experimental

The method of spin decoupling used is an adaptation of the sideband modulation method described in detail elsewhere [8], with one important difference. When the chemical shift involved is less than about 50 c/s it is preferable to use two sets of modulation sidebands rather than one. The high field sideband of the first set is used to record the spectrum with the aid of a lock-in detector fed with a reference signal at the modulation frequency. It is preferable that this be field modulation rather than modulation of the 60 Mc/s oscillator [9]. A second modulation is then imposed at such a frequency that the new high field sideband falls on the part of the spectrum that is to be strongly irradiated. In the present experiment it was found convenient to make this a modulation of the oscillator, for now a somewhat higher modulation index is required in order that the effective radio-frequency field in the sideband be high enough for spin decoupling.

One advantage of the 'double modulation' method is that the two modulation frequencies can be made high enough to ensure that the two unused sidebands do not overlap any part of the spectrum. Furthermore, since one frequency may be chosen arbitrarily, it is convenient to make the modulation frequency of the sideband used to record spectra a fixed frequency (in the present experiment 506·0 c/s) so that a tuned amplifier stage can be used in the lock-in detector.

The spectra are recorded by sweeping the magnetic field. This may be considered as equivalent to holding the field constant and sweeping both the measuring and decoupling frequencies through the spectrum keeping a constant separation between them. Spin decoupling then occurs only during the relatively short period when the measuring sideband frequency is in the vicinity of the collapsed line.

## 4. Results

### 4.1. *Relative signs of $J_{AB}$ and $J_{BX}$*

With the simple apparatus described above it is not possible to observe simultaneously both the part of the spectrum that has to be strongly irradiated and the region containing the collapsing multiplet. However, once the spectrum has been measured up carefully in the conventional way, it is sufficient to know the difference between the two modulation frequencies on two occasions,

(a) when the transitions 9 and 10 are seen to collapse, and
(b) when transitions 11 and 12 collapse.

These two critical frequencies may be calculated from a knowledge of $\nu_X - \nu_A$, $|J_{AB}|$ and $|J_{BX}|$, for the case that $J_{AB}$ and $J_{BX}$ have the same or opposite sign (table 2).

|                                    | (a)          | (b)          |
|------------------------------------|--------------|--------------|
| $J_{AB}$ and $J_{BX}$ same sign    | 32·5         | 30·8         |
| $J_{AB}$ and $J_{BX}$ opposite sign| 29·0         | 34·3         |
| Experimental                       | 32·4 ± 0·2   | 30·6 ± 0·2   |

Table 2.   Critical frequencies (c/s).

In order that the frequencies be critical, the effective radio-frequency power in the sideband used for decoupling has to be reduced until it is only just sufficient to 'wash out' the $J_{AX}$ spin coupling. In this way the experimental determinations of the critical frequencies have been made (table 2) and it is clear that $J_{AB}$ and $J_{BX}$
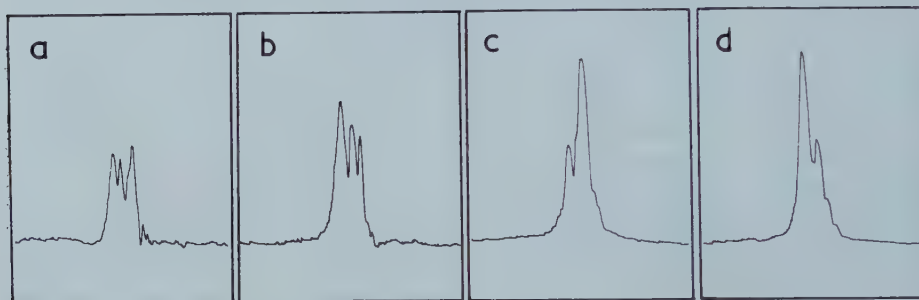


Figure 2.   The X spectrum of figure 1 recorded with simultaneous strong irradiation of (a) transitions 5 and 6, (b) 7 and 8, (c) 1 and 2, (d) 3 and 4.

must have the same sign. Figures 2 (a) and 2 (b) show actual records of the X spectrum obtained at the two critical frequencies. As in figure 1, these spectra are presented with magnetic field increasing from left to right. The collapsed lines are rather broad and are not necessarily twice as tall as the unperturbed lines.

### 4.2.   Relative signs of $J_{AX}$ and $J_{AB}$

The determination of the relative signs of $J_{AX}$ and $J_{AB}$ is the same in principle but rather more difficult in practice. Consideration of table 1 shows that, if $J_{AX}$ and $J_{AB}$ are of like sign, irradiation of transitions 1 and 2 should collapse lines 9 and 11 leaving 10 and 12 unchanged. The X spectrum would then appear to consist only of lines 12 and 10, the latter having three times its original intensity. The sideband used for decoupling must now be made stronger so as to meet the new condition $\gamma H_1 > \pi |J_{BX}|$ without perturbing transitions 3 and 4, a nicer compromise than in the first experiment. The difference between the two modulation frequencies when

(c) transitions 9 and 11 collapse, and
(d) transitions 10 and 12 collapse,

may be calculated for like and opposite signs of $J_{AX}$ and $J_{AB}$ from a knowledge of $\nu_X - \nu_B$, $|J_{AX}|$ and $|J_{AB}|$, and these four critical frequencies are set out in table 3 and compared with the experimentally determined values.

|                                    | (c)          | (d)          |
|------------------------------------|--------------|--------------|
| $J_{AX}$ and $J_{AB}$ same sign    | 72·2         | 69·5         |
| $J_{AX}$ and $J_{AB}$ opposite sign| 68·7         | 73·0         |
| Experimental                       | 72·0 ± 0·2   | 69·3 ± 0·2   |

Table 3.   Critical frequencies (c/s).

As before the choice is between frequencies separated by $J_{AB}$ (3·5 c/s) so that there is no difficulty in deciding that $J_{AX}$ and $J_{AB}$ have like signs. Figures 2(c) and 2 (d) are actual recordings of the X group of lines under the critical conditions. Once again the decoupled lines are rather broad.

The agreement between calculated and experimental values in tables 2 and 3 is surprisingly good. The chemical shift data and coupling constants are probably reliable to ±0·1 c/s since four separate spectra were calibrated and measured up. Leane and Richards [3] reported concentration shifts of a few cycles per second for this compound so that it is important to determine the chemical shifts in the actual sample used in the decoupling experiments. The modulation frequencies were measured by an electronic frequency meter reading to ±0·1 c/s. This does not of course mean that the best setting may be chosen with this accuracy by observation of the partically decoupled X pattern of lines. Out of 130 recordings made during the second experiment it was possible to pick out 55 that could reasonably be considered to have the shape of figures 2 (c) or 2 (d). Of these only two fell outside the range ±0·2 c/s from the quoted experimental values, and all spectra recorded when the frequency fell inside this range had the required shape.

One may conclude that the spin decoupling method can be a powerful tool for determining relative signs of spin coupling constants in high resolution proton magnetic resonance spectra. The additional equipment required is rather simple.

## REFERENCES

[1] EVANS, D. F., and MAHER, J. P., 1961, *Proc. chem. Soc.*, p. 208.
[2] ALEXANDER, S., 1958, *J. chem. Phys.*, **28**, 358.
[3] LEANE, J. B., and RICHARDS, R. E., 1959, *Trans. Faraday Soc.*, **55**, 518.
[4] COREY, E. J., SLOMP, G., DEV, S., TOLINAGA, S., and GLAZIER, E. R., 1958, *J. Amer. chem. Soc.*, **80**, 1204.
[5] ABRAHAM, R. J., and BERNSTEIN, H. J., 1961, *Canad. J. Chem.*, **39**, 905.
[6] BERNSTEIN, H. J., POPLE, J. A., and SCHNEIDER, W. G., 1957, *Canad. J. Chem.*, **35**, 65,
[7] POPLE, J. A., SCHNEIDER, W. G., and BERNSTEIN, H. J., 1959, *High Resolution Nuclear Magnetic Resonance* (New York: McGraw-Hill Book Company).
[8] FREEMAN, R., 1960, *Mol. Phys.*, **3**, 435.
[9] FREEMAN, R., and POUND, R. V., 1960, *Rev. sci. Instrum.*, **31**, 103.

# Electron spin resonance of γ-irradiated malonic acid

A. HORSFIELD, J. R. MORTON and D. H. WHIFFEN

Basic Physics Division, National Physical Laboratory, Teddington, Middlesex

The electron spin resonance spectrum of a γ-irradiated single crystal of malonic acid indicates the presence of at least two chemically distinct radicals. The most stable radical is $\dot{C}H(CO_2H)_2$, but the present paper primarily concerns the structure and orientation of the radical $\dot{C}H_2(CO_2H)$. The anisotropy of the spectra of this radical with respect to the direction of the main magnetic field $H$ shows that the free radical carbon atom has gone over to planar $sp^2$ hybridization, the HĊH angle being $116° \pm 5°$. Since the two ends of the undamaged malonic acid molecule are distinguishable in the crystal, two sites were expected for the radical $\dot{C}H_2(CO_2H)$. It appears, however, that approximately 80 per cent of the radicals occupy one site, and only about 20 per cent the other. Comparison of the orientation of the main $\dot{C}H_2(CO_2H)$ radical with that of the undamaged molecule indicates that in the radical the plane of the $\dot{C}H_2$ group is approximately perpendicular to the plane of the $(CO_2H)$ group.

The spectra of the less predominant $\dot{C}H_2(CO_2H)$ radicals were too weak and too overlapped for detailed analysis.

## 1. Introduction

The electron spin resonance spectrum of the radical $\dot{C}H(CO_2H)_2$ in irradiated malonic acid was first detected by H. M. McConnell and his co-workers [1, 2], who discussed the anisotropy of the coupling due to the α-proton (attached to the free radical carbon). The anisotropy of the $^{13}C$ coupling in the radical $^{13}\dot{C}H(CO_2H)_2$ has also been investigated [3, 4]. More recently the radical $\dot{C}H_2(CO_2H)$ was identified in irradiated malonic acid [5] by the present authors. This paper presents the detailed results of that investigation.

## 2. Experimental

### 2.1. *Materials and instrumental*

Single crystals of malonic acid were grown from aqueous solution by slow evaporation. Most of the crystals had the form indicated in figure 1, in which the crystal faces are identified. The unit cell is triclinic [6], and contains two molecules related to each other by a centre of symmetry. Single crystals of malonic acid were irradiated at the Spent Fuel Irradiation Unit, A.E.R.E., Harwell, with γ-rays of mean energy 1·0 MeV, the dose being five megarads per crystal. The electron spin resonance spectra were observed a few days later at room temperature with a superheterodyne spectrometer operating at 9000 Mc/s. Magnetic field calibration was carried out with the aid of an automatic proton magnetometer [7] which provided field markers every 18 gauss. The spectra were obtained every 15° by rotating the crystal about each of the right-handed orthogonal axes $x$, $y$ and $z$ in turn. The orientation of these axes with respect

to the crystal is indicated in figure 1, the $xy$ plane coinciding with the crystallo-graphic (010) face. The axis of rotation of the crystal was in each case held perpendicular to the main magnetic field of the spectrometer.
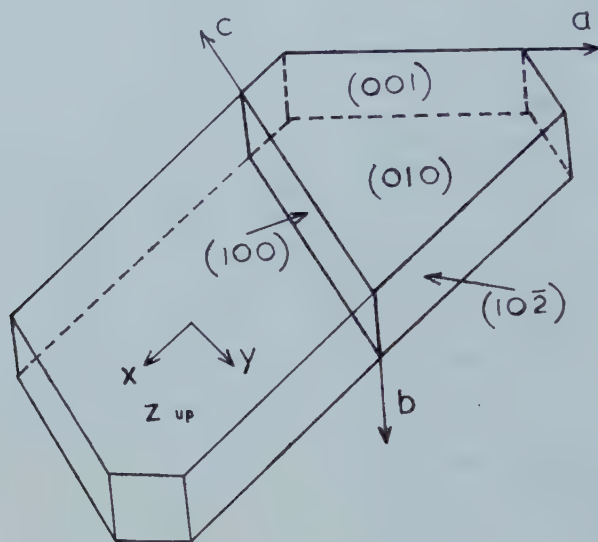


Figure 1.    Single crystal of malonic acid showing reference axes.

## 2.2. Analysis of the spectra

The derivative spectrum of a freshly irradiated single crystal of malonic acid for the orientation $H||z$ is shown in figure 2. Here may be seen the two strong lines due [1, 2] to $\dot{C}H(CO_2H)_2$. In addition, for this, and all other orientations, four lines were observed which have been ascribed [5] to the radical $\dot{C}H_2(CO_2H)$. In order to confirm this analysis the crystal was heated to 50°c and its spectrum for the orientation $H||z$ examined after various time intervals. It was found that the four lines due to $\dot{C}H_2(CO_2H)$ decreased to approximately half-strength after every 30 min at 50°c, whereas the spectrum of $\dot{C}H(CO_2H)_2$ was unaffected. The two molecules per unit cell of malonic acid are related by a centre of symmetry, and therefore could not be distinguished spectroscopically. However, the two $(CO_2H)$ groups in the molecule are distinguishable [6], one being twisted 15° from the plane of the three carbon atoms, the other being twisted approximately 90°. Two radical sites for $\dot{C}H_2(CO_2H)$ were therefore envisaged, depending on which $(CO_2H)$ group was detached as a result of the $\gamma$-ray damage. A doubling in the spectra could only be observed clearly for a limited number of orientations of the crystal, since it appeared that over 80 per cent of the $\dot{C}H_2(CO_2H)$ radicals were in one orientation and only 20 per cent in the other. The authors are now of the opinion that the third radical mentioned in [3] is, in fact, the 'weaker' orientation of the radical $\dot{C}H_2(CO_2H)$, the spectra of which were, however, so badly overlapped by the much stronger lines of the other orientation and of $\dot{C}H(CO_2H)_2$ that it was im-possible to obtain complete coupling tensors for it. For the remainder of this

paper reference to ' the radical $\dot{C}H_2(CO_2H)$ ' implies the main orientation of that radical unless otherwise stated.

Rotation of the crystal about the $x$, $y$ and $z$ axes enabled the two $\alpha$-proton coupling tensors of the radical $\dot{C}H_2(CO_2H)$ to be determined from the hyperfine splittings. The $\alpha$-proton splitting in $\dot{C}H(CO_2H)_2$ was also remeasured in order to compare the principal values of the coupling tensor with those of McConnell *et al.* [2]. The $g$-tensor of the radical $\dot{C}H_2(CO_2H)$ was also determined.



Figure 2.   Derivative spectrum of a freshly irradiated single crystal of malonic acid $(H\|z)$.

## 3. Discussion

### 3.1. *The α-proton coupling tensors.*

The $\alpha$-proton coupling tensors of the radicals $\dot{C}H(CO_2H)_2$ and $\dot{C}H_2(CO_2H)$ are given in table 1, together with their principal values and the principal direction cosines in the $x$, $y$, $z$ axis system. The principal values quoted are typical of $\alpha$-proton coupling tensors, and as such have been given the negative sign required by theory [8] although this is not determined from the spectra. The principal values obtained for the radical $\dot{C}H(CO_2H)_2$ agree reasonably well with those of McConnell *et al.* [2], who found 29, 61 and 91 Mc/s (experimental error $\pm 2$ Mc/s).

It is expected [8, 9] that the least negative, intermediate, and most negative principal directions of the $\alpha$-proton coupling tensor will be parallel to the $\dot{C}$–H bond, perpendicular to the radical plane, and in the radical plane but perpendicular to the $\dot{C}$–H bond, respectively. The intermediate axes of the $\alpha$-proton tensors of $\dot{C}H_2(CO_2H)$ should therefore be parallel to each other. The angle between

them may be calculated from table 1 to be $\cos^{-1} 0.997$, or $4.4°$. The estimated experimental error is approximately $5°$. The major and minor axes of each tensor should intersect at an angle equal to the HĊH angle. This was calculated from the tensors to be $116° \pm 5°$. This angle would be $120°$ for strict $sp^2$ hybridization of the free radical carbon atom, so that, within the experimental error, the plane trigonal hybridization of the free radical carbon atom is established.

| Radical | | Tensor in x, y, z axis system | | | Principal values | Direction cosines in x, y, z axis system |
|---|---|---|---|---|---|---|
| ĊH(CO₂H)₂ | (−) | 53 | 7 | 17 | (−) 28 | (0·52, 0·16, −0·84) |
| | | 7 | 82 | 15 | (−) 58 | (0·79, −0·47, 0·39) |
| | | 17 | 15 | 41 | (−) 91 | (0·33, 0·87, 0·37) |
| | | Isotropic component | | | (−) 59 | |
| ĊH₂(CO₂H) (α₁) | (−) | 47 | −10 | −24 | (−) 30 | (0·80, 0·00, 0·60) |
| | | −10 | 68 | 14 | (−) 55 | (0·35, 0·81, −0·47) |
| | | −24 | 14 | 61 | (−) 91 | (0·48, −0·59, −0·65) |
| | | Isotropic component | | | (−) 62 | |
| ĊH₂(CO₂H) (α₂) | (−) | 54 | 14 | 18 | (−) 37 | (0·76, −0·59, −0·28) |
| | | 14 | 54 | 3 | (−) 59 | (0·41, 0·77, −0·49) |
| | | 18 | 3 | 80 | (−) 92 | (0·50, 0·26, 0·82) |
| | | Isotropic component | | | (−) 63 | |
| ĊH₂(CO₂H) (g) | | 2·0033 −0·0005 0·0000 | | | 2·0020 | (0·27, 0·77, −0·58) |
| | | −0·0005 2·0028 0·0010 | | | 2·0034 | (0·90, 0·02, 0·44) |
| | | 0·0000 0·0010 2·0033 | | | 2·0042 | (0·35, −0·64, −0·68) |

Table 1. Coupling tensors (Mc/s) of radicals ĊH(CO₂H)₂ and ĊH₂(CO₂H), and g-tensor of ĊH₂(CO₂H).

### 3.2. The orientation of the free radicals in the crystal

The atomic coordinates of one molecule of malonic acid are tabulated by Goedkoop and MacGillavry [6] using the triclinic unit cell axes $a$, $b$, $c$ as reference axes. It was necessary to relate these atomic coordinates to the crystal axes $x$, $y$, $z$ before the orientation of the radicals could be compared with that of the undamaged molecules. It was calculated that

$$\begin{vmatrix} x \\ y \\ z \end{vmatrix} = \begin{vmatrix} -0.3203 & 0.1881 & -0.4407 \\ 0.9473 & 0.1526 & -0.8976 \\ 0.0000 & -0.9702 & 0.0000 \end{vmatrix} \begin{vmatrix} a \\ b \\ c \end{vmatrix}$$

This equation relates the atomic coordinates in the orthogonal $x$, $y$, $z$ axis system, to the atomic coordinates expressed in Å in the triclinic $a$, $b$, $c$ axis system. The relative orientation of the two sets of axes is indicated in figure 1. Using the above equation, the atomic coordinates in the $x$, $y$, $z$ axis system were calculated and are tabulated in table 2. In this table the central carbon atom is designated $C_0$, and the two carboxylic acid groups are $(C_1O_{11}O_{12}H)$ and $(C_2O_{21}O_{22}H)$. The plane of $(C_1O_{11}O_{12}H)$ is approximately parallel (angle $14.7°$) to the plane of the central carbon atoms $C_0C_1C_2$, whereas the group $(C_2O_{21}O_{22}H)$ is approximately perpendicular (angle $85.8°$) to the plane $C_0C_1C_2$.

From the data of table 1 it may be calculated that the internal bisector of the angle between $\dot{\text{C}}$–H bonds in the radical $CH_2(CO_2H)$ is, in $x$, $y$, $z$ coordinates, (0·039, 0·556, 0·830). This vector is approximately parallel (angle 24°) to the $C_0$–$C_1$ bond, but is nearly perpendicular to the $C_0$–$C_2$ bond, From this it was inferred that the main radical $\dot{\text{C}}H_2(CO_2H)$ is in fact $\dot{\text{C}}_0H_2(C_1O_{11}O_{12}H)$. However, it may also be calculated that the plane of the group $(C_1O_{11}O_{12}H)$ is approximately perpendicular to the plane of the free radical carbon atom. The perpendicular to $(C_1O_{11}O_{12}H)$ is (0·885, −0·455, 0·102) and makes angles of 84° and 88° with the intermediate principal tensor directions. These considerations imply that

( i) The main orientation of $\dot{\text{C}}H_2(CO_2H)$ is formed by the loss of that carboxylic acid group which was, in the crystal, nearly perpendicular to the plane of the central carbon atoms, i.e. the group $(C_2O_{21}O_{22}H)$.

( ii) The plane of the $\dot{\text{C}}H_2$ group in the main conformation of $\dot{\text{C}}H_2(CO_2H)$ is nearly perpendicular to the plane of the carboxylic acid group. This is a surprising conclusion, for one would expect the radical to be completely planar, enabling the $p$-orbital on the central carbon to mix with the $\pi$-system of the carboxylate group. It appears, however, that crystal forces prevent the rotation about the $\dot{\text{C}}$–C bond which would be necessary for the radical to adopt the planar configuration.

| Atom | $x$ | $y$ | $z$ |
|------|-----|-----|-----|
| $C_0$ | −2·173 | +0·707 | −0·643 |
| $C_1$ | −2·467 | −0·560 | −1·481 |
| $O_{11}$ | −2·280 | −0·469 | −2·703 |
| $O_{12}$ | −3·035 | −1·523 | −0·848 |
| $C_2$ | −1·335 | +1·687 | −1·446 |
| $O_{21}$ | −1·908 | +2·572 | −2·070 |
| $O_{22}$ | −0·046 | +1·457 | −1·366 |

Table 2.  Atomic coordinates of one malonic acid molecule in the $x$, $y$, $z$ axis system.

### 3.3. *The g-tensor of the radical $\dot{\text{C}}H_2(CO_2H)$*

The $g$-tensor of the main orientation of $\dot{\text{C}}H_2(CO_2H)$ was determined by remeasuring the spectra using an irradiated malonic acid crystal which had been smeared with a speck of DPPH. The $g$-value of the DPPH radical was assumed to be 2·0036 ± 0·0002. The $g$-tensor of $\dot{\text{C}}H_2(CO_2H)$ in the $x$, $y$, $z$ axis system is given in table 1, together with its principal values and their direction cosines. The absolute accuracy of the principal $g$-values was estimated to be ± 0·0005, and the relative accuracy ± 0·0003. It may be calculated that the smallest principal $g$-value makes angles of 10° and 8° with the intermediate axes of the $\alpha$-proton tensors. Within the experimental error (± 10°) the minimum $g$-value therefore lies perpendicular to the plane of the free radical carbon atom, in accord with previous observations [2, 10, 12]. The principal in-plane $g$-values, 2·0042 and 2·0034, are nearly equal and so the directions for which they occur are not accurately determined. The higher value lies closer to the $\dot{\text{C}}$–C bond direction. The average value of $g$, 2·0032, is slightly greater than the free spin value of 2·0023, as has been predicted theoretically [12].

This work forms part of the research programme of the Basic Physics Division of the National Physical Laboratory and is published by permission of the Director.

REFERENCES

[1] COLE, T., HELLER, C., and MCCONNELL, H. M., 1959, *Proc. nat. Acad. Sci., Wash.*, **45,** 525.
[2] MCCONNELL, H. M., HELLER, C., COLE, T., and FESSENDEN, R. W., 1960, *J. Amer. chem. Soc.*, **82,** 766.
[3] MCCONNELL, H. M., and FESSENDEN, R. W., 1959, *J. chem. Phys.*, **31,** 1688.
[4] COLE, T., and HELLER, C., 1961, *J. chem. Phys.*, **34,** 1085.
[5] HORSFIELD, A., MORTON, J. R., and WHIFFEN, D. H., 1961, *Nature, Lond.*, **189,** 481.
[6] GOEDKOOP, J. A., and MACGILLAVRY, C. H., 1957, *Acta cryst., Camb.*, **10,** 125.
[7] HORSFIELD, A., MORTON, J. R., and MOSS, D. G., 1961, *J. sci. Instrum.*, **38,** 322.
[8] MCCONNELL, H. M., and STRATHDEE, J., 1959, *Mol. Phys.*, **2,** 129.
[9] GHOSH, D. K., and WHIFFEN, D. H., 1959, *Mol. Phys.*, **2,** 285.
[10] POOLEY, D., and WHIFFEN, D. H., 1961, *Mol. Phys.*, **4,** 81.
[11] ATHERTON, N. M., and WHIFFEN, D. H., 1960, *Mol. Phys.*, **3,** 1 and 103.
[12] MCCONNELL, H. M., and ROBERTSON, R. E., 1957, *J. phys. Chem.*, **61,** 1018.

# Electron spin resonance of an X-ray irradiated single crystal of α-glycylglycine

by W. C. LIN and C. A. McDOWELL

Department of Chemistry, University of British Columbia,
Vancouver 8, B.C., Canada

The electron spin resonance of an x-ray irradiated single crystal of α-glycylglycine has been measured at 9 GC/sec for various orientations of the crystal in the static magnetic field. The resonance pattern was found to be a doublet for all orientations and from the measurement of the anisotropy of the doublet splitting it has been possible to calculate the coupling tensor for the σ-hydrogen attached to a carbon atom in the radical. Further it has been established that the main radical produced by x-ray irradiation is $H_3N^+CH_2CONH\,\dot{C}H\,CO_2^-$. It has also been shown that the σ–CH bond in the radical must lie within 2° of the $b$ axis of the monoclinic host crystal and that the 'molecular' plane of the radical is inclined at an angle of about 7° to the $b–c$ plane of the host crystal.

## 1. INTRODUCTION

It is well known that the irradiation of certain organic crystals by x-rays or γ-rays leads to the production of free radicals with a fairly long lifetime. The study of the electron spin resonance spectra of such radicals formed in irradiated single crystals of compounds in which the molecules are strongly hydrogen-bonded, has led to the identification of the paramagnetic species. In the case of the radicals produced in single crystals of malonic acid [1], succinic acid [2], glycollic acid [3], glycine [4, 5], *d-l*-alanine [6], and glutamic acid [7], it has been possible to analyse the e.s.r. spectra of the oriented radicals fairly completely and to understand the origins of the hyperfine structure observed in these. Recently Gordy and his co-workers have studied the e.s.r. spectra of γ-irradiated single crystals of the more complex compounds N-acetylglycine [8] and *l*-cystine-HCl [9], and identified the radicals formed. We wish here to report other results on the e.s.r. spectra of x-ray irradiated single crystals of α-glycylglycine, $H_3N^+CH_2CONH\,CH_2CO_2^-$. This compound would be expected to form two types of radicals by the loss of a hydrogen atom from one of the two methylene groups (a common result of x-ray irradiation, see refs. [1 9]). The two possible radicals would be $H_3N^+\dot{C}H\,CONH\,CH_2\,CO_2^-$(I) or $H_3N^+CH_2CONH\,\dot{C}H\,CO_2^-$(II).

In the case of γ-irradiated N-acetylglycine, Miyagawa *et al.* [8] showed that the radical formed was $CH_3CONH\,\dot{C}H\,COOH$ (III). The hyperfine structure of the e.s.r. spectrum of the radical III consists of two broad lines due to the interaction of the unpaired electron with the σ-proton attached to the carbon atom. The broadening of the lines is probably caused by the interaction with the neighbouring NH groups. The hyperfine structure of the glycine type of radical, formula I, is essentially a 24-line structure [4, 5] attributed to electron spin and nuclear spin interaction from one σ-proton attached to the carbon atom

and the nuclei in the $NH_3^+$ group. It should therefore, be easy to determine the nature of the radicals formed by x-ray irradiation of $\alpha$-glycylglycine from the nature of the hyperfine structure observed in the e.s.r. spectra. The results which are presented below indicate that the main radical formed is of type II. Our observations and their interpretation have been confirmed by a report of results of Box *et al.* [12], which appeared after this work was concluded.

## 2. THEORETICAL

The energy levels of an oriented radical in a single crystal involving the unpaired electron and a nuclear magnetic moment in an externally applied magnetic field can be calculated from the following Hamiltonian:

$$\mathcal{H} = g\beta\mathbf{H}.\mathbf{S} + \mathbf{S}.\mathbf{A}.\mathbf{I} - g_n\beta_n\mathbf{H}.\mathbf{I}. \tag{1}$$

The first term in equation (1) represents the interaction between the electron spin and the external magnetic field $\mathbf{H}$. The second term represents the interaction between the electron spin and the nuclear spin with the interaction constant being expressed as a tensor $\mathbf{A}$. The last term represents the interaction between the nuclear spin and the external magnetic field.

Under normal conditions in an e.s.r. experiment, the external field is sufficiently strong for the electron spin to be quantized in the direction of the field. One may therefore write

$$\mathcal{H} = g\beta H M_s + \left(M_s\frac{\mathbf{H}}{H}.\mathbf{A} - g_n\beta_n\mathbf{H}\right).\mathbf{I} \tag{2}$$

where $M_s = \pm\frac{1}{2}$ is the spin quantum number of the unpaired electron. If the hyperfine interaction tensor $\mathbf{A}$ is expressed in its principal axes coordinates

$$\mathbf{A} = A_{xx}\mathbf{ii} + \mathbf{A}_{yy}\mathbf{jj} + A_{zz}\mathbf{kk} \tag{3}$$

and if the magnetic field $H$ has direction cosines $\lambda$, $\mu$, $\nu$ with respect to the principal axes, then equation (2) becomes

$$\mathcal{H} = g\beta H M_s + \{(M_s A_{xx} - g_n\beta_n H)\lambda\mathbf{i} + (M_s A_{yy} - g_n\beta_n H)\mu\mathbf{j}$$
$$+ (M_s A_{zz} - g_n\beta_n H)\nu\mathbf{k}\}.\mathbf{I}. \tag{4}$$

The expression within the braces can be regarded as a resultant field vector which acts upon the nuclear moment. The nuclear spin is quantized in the direction of this resultant field so that the energy levels can be written as:

$$W = g\beta H M_s + \{(M_s A_{xx} - g_n\beta_n H)^2\lambda^2 + (M_s A_{yy} - g_n\beta_n H)^2\mu^2$$
$$+ (M_s A_{zz} - g_n\beta_n H)^2\nu^2\}^{1/2} M_I \tag{5}$$

where $M_I$ is the quantum number of the nuclear spin state. For the hyperfine interaction due to a single proton, this expression gives rise to four levels and hence four hyperfine lines. However, usually only two are strong corresponding to the $\Delta M_I = 0$ transition where the axis of quantization is fixed in space [13].

Equation (5) is useful for the calculation of energy levels when the principal components of the interaction tensor $A_{xx}$, $A_{yy}$, $A_{zz}$ are known. It is not, however, a convenient formula for the reverse process of determining the interaction tensor components from the observed hyperfine splittings. For this latter purpose, use may be made of an approximate formula which derives from the

assumption that the nuclear spin is also quantized in the external magnetic field direction; thus writing both $\mathbf{S}$ and $\mathbf{I}$ as

$$\mathbf{S} = S(\lambda\mathbf{i} + \mu\mathbf{j} + \nu\mathbf{k}), \tag{6a}$$

$$\mathbf{I} = I(\lambda\mathbf{i} + \mu\mathbf{j} + \nu\mathbf{k}). \tag{6b}$$

Equation (2) becomes

$$\mathcal{H} = g\beta HS + (\lambda^2 A_{xx} + \mu^2 A_{yy} + \nu^2 A_{zz})SI - g_n\beta_n HI \tag{7}$$

and the energy levels are given by:

$$W = g\beta H M_s + A M_s M_I - g_n\beta_n H M_I \tag{8}$$

with

$$A = \lambda^2 A_{xx} + \mu^2 A_{yy} + \nu^2 A_{zz}. \tag{9}$$

If an arbitrary reference system of coordinates is used instead of the principal axes which are usually unknown prior to an experiment, then the expression for the hyperfine interaction tensor component becomes

$$A = l^2 A_{aa} + m^2 A_{bb} + n^2 A_{xx} + 2(mn A_{bc} + nl A_{ca} + lm A_{ab}) \tag{10}$$

where $l$, $m$, $n$ are the direction cosines of the external magnetic field, and $A_{ij}$ the tensor components are both expressed in the arbitrary coordinate axes $a$, $b$, $c$.

## 3. EXPERIMENTAL

The α-glycylglycine crystals were grown from a mixture of $n$-propyl alcohol and water from which they were obtained as plates with dimensions about $5 \times 5 \times 1$ mm. In the literature α-glycylglycine has been reported as belonging to the monoclinic system; there are, however, discrepancies between the crystal parameters reported by the various workers. For these reasons the unit cell dimensions were redetermined for us by Dr. J. Trotter of this department from x-ray diffraction photographs taken with a Weissenberg camera. Table 1 lists the various crystal parameters in the literature with those recently found by Dr. Trotter. In our calculations we used the latter set of data.

| Unit cell parameter | Bernal (a) | B.H. + W. (b) | Wyckoff (c) | Trotter (d) |
|---|---|---|---|---|
| $a$ | 7·7 | 7·70 | 7·76 | 7·85 |
| $b$ | 9·56 | 9·57 | 9·46 | 9·57 |
| $c$ | 9·5 | 9·48 | 7·67 | 9·46 |
| $\beta$ | 125° 20′ | 124° 35′ | 99° 30′ | 125 |
| $Z$ | 4 | 4 | 4 | 4 |
| Space group | $P2_1/a$ | $P2_1/a$ | $P2_1/a$ | $P2_1/a$ |

Table 1.   Crystal parameters for α-glycylglycine.

(a) BERNAL, J. D., 1931, *Z. Kristallogr.*, **78**, 363.

(b) BESWAS, A. B., HUGHES, E. W., and WILSON, J. N., 1950, *Struct. Rep. Utrecht*, **13**, 488.

(c) WYCKOFF, R. G. W., 1959, *Crystal Structures*, IV, Table XIII, C 2(6).

(d) TROTTER, J. (private communication).

The prominent face of the crystals we had was the (001) plane (see figure 1). The crystals were easy to cleave along the edges. For our purpose it is most convenient to use an orthogonal system of reference axes. A right-handed orthogonal system $a'$, $b'$, $c'$ was used; the relation of this to the crystal is shown
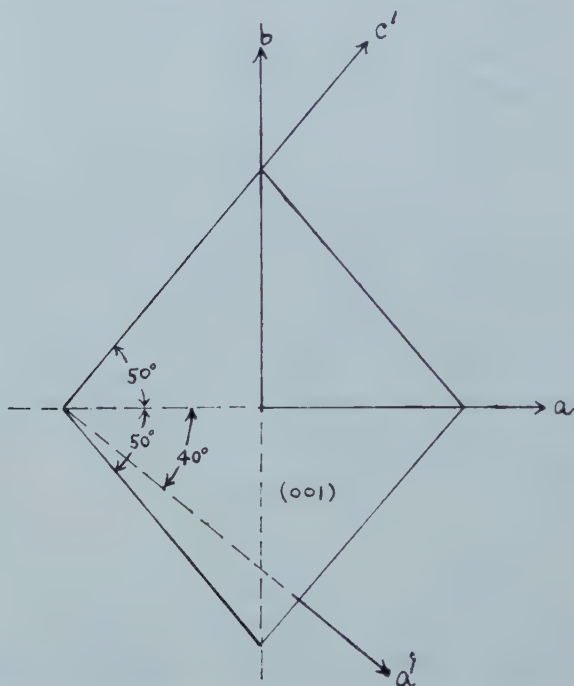


Figure 1.    Crystal axes $a$, $b$ and $c$, and reference axes $a'$, $b'$, and $c'$, for α-glycylglycine.

in figure 1; $b'$ was taken to be perpendicular to the 001 face of the plate-like crystal and $c'$ to be along one edge. With this choice, the alignment of the crystal can be made quite accurately.

The crystal to be irradiated was mounted at the appropriate orientation on a Perspex rod which itself was covered with a lead shield during the irradiation. The irradiations of several hours duration were carried out at room temperature with 50 kv x-rays. After irradiation the crystals were studied at room temperature in our 9 Gc/sec e.s.r. spectrometer which has 10 kc/s modulation and uses a Varian 6' magnet with pole shims to provide a homogeneous magnetic field. The angular rotation of the crystal could be measured with an accuracy of about 2°. A rectangular cavity operating in the $TE_{012}$ mode was used.

The description used for the various orientations is as follows: orientation $c'b'a'$ 30 means that the crystal has been studied with the $c'$ axis vertical, that $b'$ was initially parallel to the external magnetic field, and that $a'$ has been rotated through an angle of 30° towards $b'$.

## 4. Results and discussion

All the spectra observed were very simple and consisted of two rather broad lines ($\sim$ 12 gauss wide) except for a few orientations for which there was a slight splitting into two unresolved doublets. These two types of spectra are shown
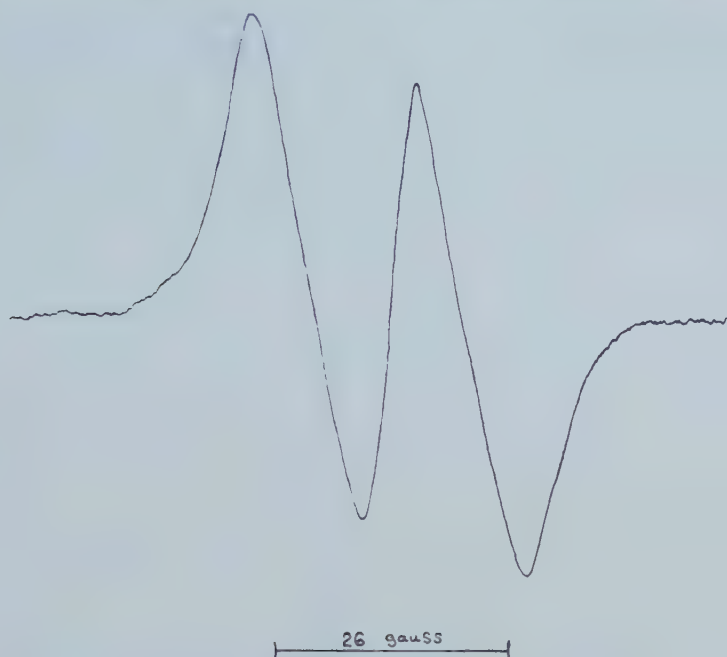
Figure 2. E.s.r. spectrum of x-ray irradiated single crystal of α-glycylglycine. Orientation *c′, b′, a′*, 90° ($\mathbf{H}_0\|a$). Direction cosines of $\mathbf{H}_0$, 1, 0, 0.
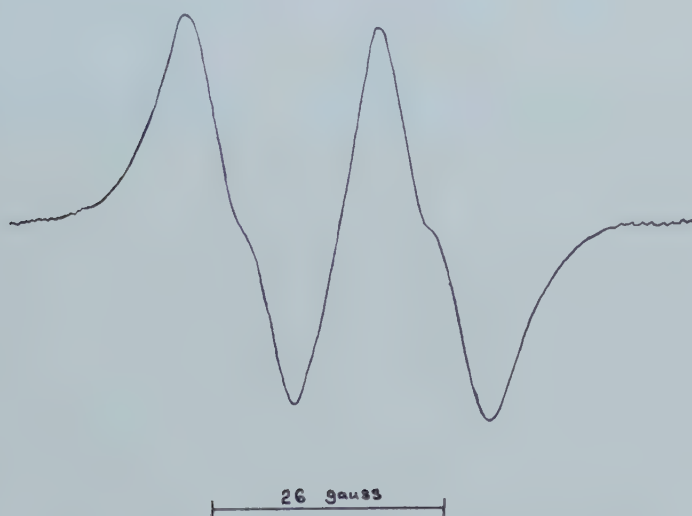


Figure 3. E.s.r. spectrum of x-ray irradiated single crystal of α-glycylglycine. Orientation *b′, a′, c′*, 35°. Direction cosines of $\mathbf{H}_0$, 0·82, 0, 0·57.

in figures 2 and 3. The spectra observed resemble those for γ-irradiated N-acetylglycine. This strongly suggests that the radicals formed have the structure II. We shall show later that there is also quantitative agreement between the principal values of the interaction tensors for the two radicals.

Y

The most surprising result of the present work is that only two-line spectra were observed at all orientations. In general, for a monoclinic crystal one would expect a two-line spectrum only when the external magnetic field was either perpendicular or parallel to the $b$ axis of the crystal. For any other orientation, a four-line structure should result owing to the two magnetically non-equivalent molecules in the crystal. In the very special case when one of the principal axes
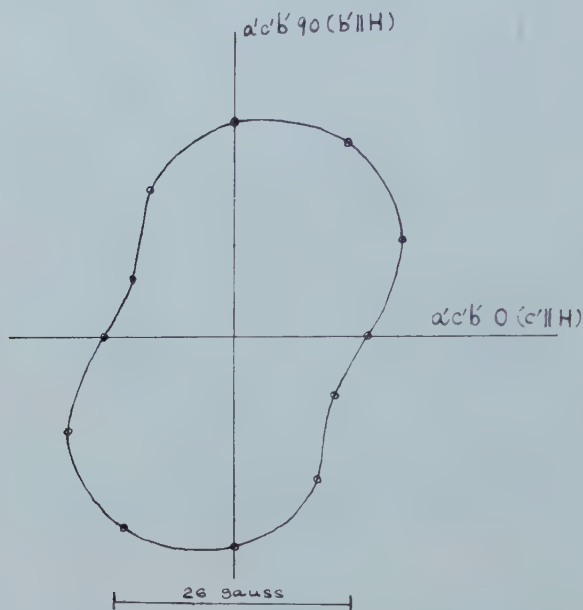


Figure 4. Angular variation of the doublet splitting of the e.s.r. spectrum of x-ray irradiated single crystal of α-glycylglycine. (*a'* axis vertical.)
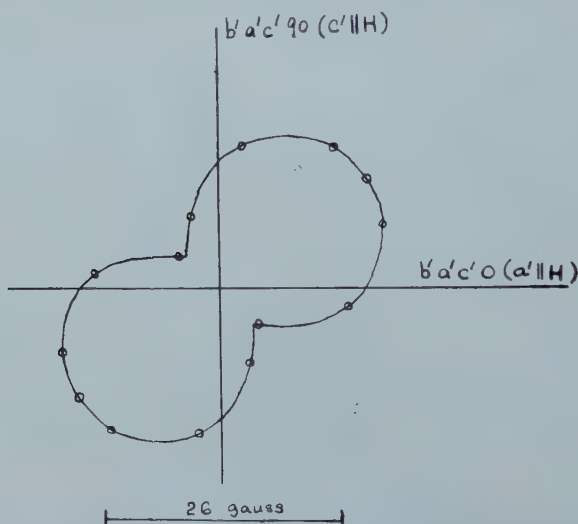


Figure 5. Angular variation of the doublet splitting of the e.s.r. spectrum of x-ray irradiated single crystal of α-glycylglycine. (*b'* axis vertical.)

Figure 6. Angular variation of the doublet splitting of the e.s.r. spectrum of x-ray irradiated single crystal of α-glycylglycine. (*c'* axis vertical.)
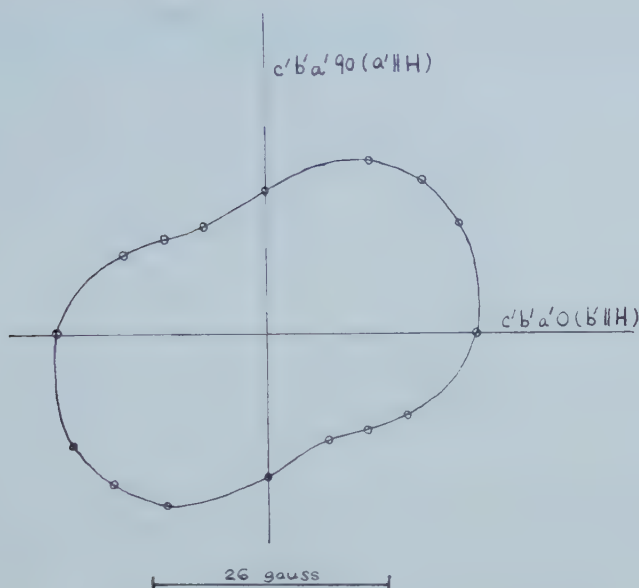
of the hyperfine interaction tensor is parallel to the *b* axis, the two tensors corresponding to the two non-equivalent molecules should be the same for all orientations. This is shown later to be the case for irradiated α-glycylglycine.

The experimentally determined splittings of the doublets for the three sets of spectra with the reference axes *a'*, *b'*, and *c'* vertical are presented in the form of polar diagrams in figures 4, 5 and 6 respectively. Experimental values taken from these diagrams were used to calculate the hyperfine interaction tensor with respect to the *a'*, *b'*, *c'* system of axes using equation (10) the tensor resulting was

$$\mathbf{A} = \begin{pmatrix} 16\cdot1 & 4\cdot6 & 6\cdot9 \\ 4\cdot6 & 23\cdot8 & 4\cdot4 \\ 6\cdot9 & 4\cdot4 & 15\cdot0 \end{pmatrix}. \tag{11}$$

The principal values of the interaction tensor (11) together with the respective direction cosines of the principal axes w.r.t. *a'*, *b'* and *c'* were calculated to be:

| Principal values | *l* | *m* | *n* |
|---|---|---|---|
| $A_{xx} = -16\cdot8$ gauss | 0·56 | −0·67 | 0·49 |
| $A_{yy} = -29\cdot5$ | 0·49 | 0·74 | 0·46 |
| $A_{zz} = -8\cdot6$ | −0·67 | −0·01 | 0·74 |

Table 2. Principal values and direction cosines of the interaction tensor w.r.t. *a'*, *b'* and *c'*.

For comparison we list in table 3 these three principal values of the hyperfine interaction tensor for the glycylglycine radical and three for the radical from

N-acetylglycine as determined by Miyagawa et al. [8], together with theoretical values for a C–H fragment calculated by McConnell and Strathdee [10].

| | Glycylglycine | N-acetylglycine | CH fragment | 80 per cent of CH value |
|---|---|---|---|---|
| $A_{xx}$ | −16·8 | −17 | −24·7 | −19·8 |
| $A_{yy}$ | −29·5 | −27 | −36·7 | −29·3 |
| $A_{zz}$ | − 8·6 | −10 | − 7·6 | − 6·1 |
| Isotropic component $1/3\,(A_{xx}+A_{yy}+A_{zz})$ | −18·3 | −18 | −23·0 | −18·4 |

Table 3.   Comparison of the principal values of the interaction tensors of the glycylglycine and N-acetylglycine radicals with the theoretical values for a C–H fragment.

The data in table 3 indicate that the electron density at the carbon atom attached to the σ-proton is apprxoimately 80 per cent its full value (i.e. pure $2p_z$). This may be compared with the corresponding value found for the radical formed by x-ray irradiation of malonic acid, i.e. 93 per cent.

From the direction cosines of the principal axis $A_{zz}$, it can be deduced that the C–H bond of the radical lies in the $a'–c'$ plane and that it makes an angle of 42° with the $c'$ axis and 132° with the $a'$ axis. By reference to figure 1 it can be seen that this means the CH bond is within 2° of the $b$ axis of the crystal. As mentioned earlier, this is the reason for the two-line spectra observed for all orientations of the crystal. It is at present not certain that the small splitting ($\sim 2$ gauss) shown in figure 3 is due to a difference in the two non-equivalent radicals in the unit cell or to hyperfine-interaction with the proton attached to the nitrogen atom.
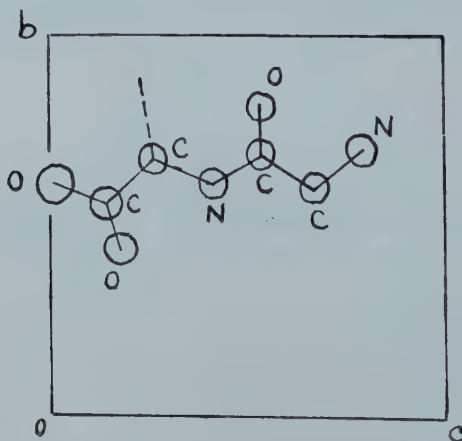


Figure 7.   Projection of one molecule in the crystal of α-glycylglycine along the $a$ axis onto the (100) face showing the position of the C–H bond (dotted line). (From ref. [11].)

Although full details of the crystal structure determinations made by Beswas et al. (ref. (b), table 1) are not available some of their results have been given by Pauling and Corey [11]. Figure 7 which is based on this latter information

shows the structure of crystals of α-glycylglycine projected along the *a* axis on to the (100) face of the crystal. It can be seen that the CH bond of the radical would be parallel to the *b* axis and that the molecular plane coincides with the *b*–*c* planes.

From the interaction tensor w.r.t. the *abc″* system with *a* and *b* being the crystal axes and *c″* the normal to the *a*–*b* plane, the direction cosines of the principal axes can be calculated as:

$$
\begin{array}{cccc}
 & a & b & c'' \\
A_{xx} & 0\cdot74 & 0 & 0\cdot67 \\
A_{yy} & 0\cdot67 & 0 & -0\cdot74 \\
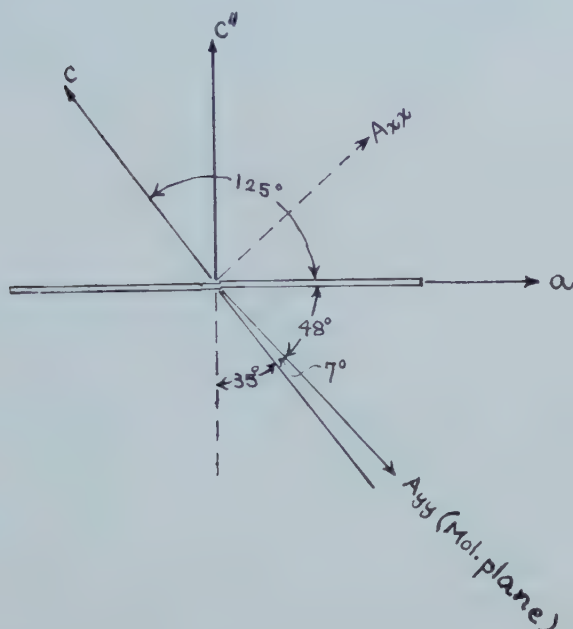A_{zz} & 0 & 1 & 0
\end{array}
\qquad (12)
$$



Figure 8. The relation between the 'molecular' plane of the radical and the crystal axes in α-glycylglycine.

These values again show that the C–H bond ($A_{zz}$ axis) is parallel to the *b* axis of the crystal while the 'molecular' plane which contains the $A_{yy}$ and $A_{zz}$ axes makes an angle with the *a*–*b* plane equal to the angle between $A_{yy}$ and the *a* axis, i.e. $\cos^{-1} 0\cdot67 = 48°$. This means that the 'molecular' plane of the radical is inclined at an angle of 7° to the *b*–*c* plane of the crystal. These descriptions of the geometry of the radical are depicted in figure 7.

References

[1] McConnell, H. M., Heller, C., Cole, T., and Fessenden, R. W., 1960, *J. Amer. chem. Soc.*, **82,** 76.

[2] Heller, C., and McConnell, H. M., 1960, *J. chem. Phys.*, **32,** 1535.

[3] Atherton, N. M., and Whiffen, D. H., 1960, *Mol. Phys.*, **3,** 1.

[4] Ghosh, D. K., and Whiffen, D. H., 1959, *Mol. Phys.*, **2,** 285.

[5] Horsfield, A. J., Lin, W. C., and McDowell, C. A. (unpublished work).

[6] Miyagawa, I., and Gordy, W., 1959, *J. chem. Phys.*, **30,** 1590.

[7] Lin, W. C., McDowell, C. A., and Rowlands, J. R., 1961, *J. chem. Phys.*, **35,** 757.

[8] Miyagawa, I., Kurita, Y., and Gordy, W., 1960, *J. chem. Phys.*, **33,** 1599.

[9] Kurita, Y., and Gordy, W., 1961, *J. chem. Phys.*, **34,** 282.

[10] McConnell, H. M., and Strathdee, J., 1959, *J. chem. Phys.*, **2,** 129.

[11] Pauling, L., and Corey, R. B., 1945, *Fortschr. Chem. org. Naturst.*, **11,** 188.

[12] Box, H. C., Freund, H. G., and Lilga, K., 1961, *Free Radicals in Biological Systems* (New York: Academic Press), p. 239.

[13] Trammell, G. T., Zeldes, H., and Livingston, R., 1958, *Phys. Rev.*, **110,** 630.

# Electron spin resonance of X-ray irradiated single crystals of potassium hydrogen malonate

by W. C. LIN and C. A. McDOWELL

Department of Chemistry, University of British Columbia,
Vancouver, 8, B.C., Canada

The electron spin resonance of x-rayed single crystals of potassium hydrogen malonate has been examined in detail. The results enable experimental tests to be made of the theory of second order, or forbidden lines arising from the simultaneous transitions between nuclear spin states (i.e. $\Delta M_I \neq 0$) during an electron spin transition.

## 1. INTRODUCTION

In the study of hyperfine splittings in e.s.r. of irradiated single crystals of organic compounds, there exist two factors which very often cause difficulties in the analysis of the result. The first factor is what may be called the crystal symmetry effect. This arises because of the existence of symmetry elements in crystals and so all molecules in a single crystal are not similarly orientated.

The second complicating factor is the presence of the so-called 'forbidden lines' in the e.s.r. spectrum arising from the simultaneous transition of the nuclear spin state (i.e. $\Delta M_I \neq 0$) during the electron spin transition. As a result, electron interaction with a single proton gives rise to four hyperfine lines instead of two. These four lines form two pairs of unequal intensities and the intensity ratio between the two pairs varies with the orientation of the radical in the external field. Further complication is due to the fact that the splitting between the two lines of a pair is, in general, not a direct measure of the interaction tensor component.

At present, these two complicating factors can be studied in detail only in extremely simple cases. The malonic acid radical $OOC\,\dot{C}H\,COO^-$ offers such an opportunity, for the hyperfine interaction involved is that due to a single proton. McConnell et al. [1] made a detailed study of this radical in irradiated malonic acid. The crystals of malonic acid belong to the triclinic system, and for this reason, the first complicating factor does not exist. We have chosen potassium acid malonate which belongs to the monoclinic class. The presence of two magnetically non-equivalent positions in the crystal offers a chance for the study of the first factor. Fortunately, irradiation of $HOOC\,CH_2COO\,K$ seems to produce only one radical, namely $OOC\,\dot{C}H\,COO^-$. McConnell et al. [1] found that irradiation of malonic acid produced, besides the radical mentioned, others which had to be removed by a process of ageing. The absence of other radical species in the case of the potassium acid malonate made it particularly easy to study the intensities of the so-called 'forbidden lines'.

The crystal structure of the acid salt has not been studied. However, because of the simplicity of the molecule, the knowledge of the anisotropic hyperfine interaction tensor of the radical completely determines the orientations of the molecules in the crystal.

## 2. THEORETICAL

The theory applicable to the present case has been treated in detail by several workers [1, 2, 3, 4]. Here we shall only present the equations necessary for the subsequent calculations.

The spin Hamiltonian for a system consisting of an unpaired electron (with quenched orbital angular momentum) and a single nuclear spin in an externally applied magnetic field can be written as:

$$\mathcal{H} = g_e \beta_e \mathbf{S} . \mathbf{H} - g_n \beta_n \mathbf{I} . \mathbf{H} + \mathbf{S} . \mathbf{A} . \mathbf{I}. \tag{1}$$

To use this equation for calculation, it can be cast into the following form:

$$\mathcal{H} = H_e S_H - \{(H_n - S_H A_x)^2 \lambda^2 + (H_n - S_H A_y)^2 \mu^2 + (H_n - S_H A_y)^2 \nu^2\}^{1/2} I_\mu, \tag{2}$$

where $I_\mu$ is now the scalar operator of the nuclear spin in the resultant field direction, and $\lambda$, $\mu$ and $\nu$ are the direction cosines of $H$ in the $x$, $y$, $z$ system (the principal axes of tensor $A$ chosen as the coordinate axes). $A_x$, $A_y$, and $A_z$ being the principal values of the tensor $A$. In this equation (2) $H_e = g_e \beta_e H$ and $H_n = g_n \beta_n H$.

## 3. EXPERIMENTAL

The monoclinic crystals of $CH_2(COO)_2KH$ were grown from an aqueous solution containing malonic acid and a small excess of KOH. The crystals were all of the form shown by Groth [6] except for the fact that the 011 face was more prominent at the expense of the 001 face, while the 010 face was absent. The crystals were elongated along the $c$ axis which was therefore the easiest to identify. The $c$ axis was used as one of the axes of our reference system together with the $b$ axis. An $a'$ axis was then chosen to be orthogonal to both $b$ and $c$ and the three form a right-hand system. Thus $a'$ was in the $a–c$ plane. Our subsequent calculation and discussion are all based on this arbitrary $a'bc$ system of axes.

The crystals were irradiated at room temperature with 50 kv x-rays for several hours, and the e.s.r. spectra taken as previously described [7].

The orientation of the crystal is described in the figures by a scheme which can be explained best as follows: orientation $cba'$ 30 means the $c$ axis is vertical and points upwards in the horizontal magnetic field, the $b$ axis was originally in the field direction while the $a'$ axis has been rotated through an angle of 30 degrees towards the $b$ axis. Thus $cba'$ 30 corresponds to a magnetic field having direction cosines $l = \frac{1}{2}$, $m = \sqrt{3}/2$, $n = 0$ with respect to the $a'bc$ system.

## 4. RESULTS

The spectra are all very simple and generally consist of two lines except in certain orientations. The spectrum shown in figure 1 corresponds to an orientation in which none of the axes $a'$, $b$ and $c$ is vertical in the magnetic field. Spectra corresponding to such skew orientations were required to determine the sign of one of the non-diagonal components of the interaction tensor. The forbidden lines are however all comparatively weak, but can easily be distinguished

from the main lines.   In the cases where there are three lines, such as in figure 2, one line is always twice as strong as the other two and is, in fact, the superposition of two lines.   Two line-spectra occur only in orientations in which the external field is either parallel to the *b* axis (*b*‖**H**) or perpendicular to it (*b*⊥**H**).   In all
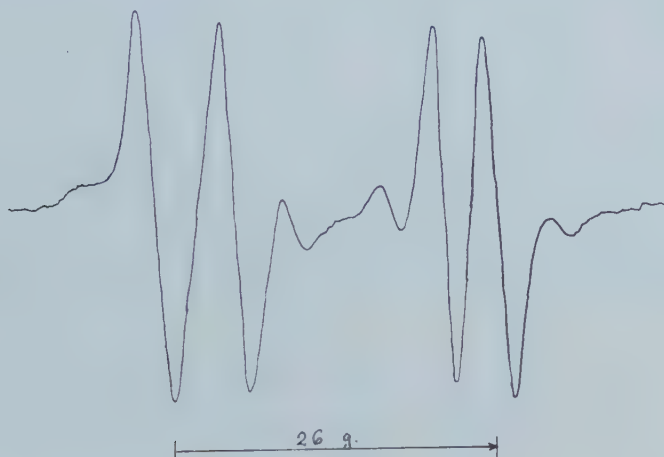


Figure 1.   E.s.r. spectrum of x-ray irradiated potassium hydrogen malonate at a skew angle. Direction cosines of external magnetic field, 0·50, 0·75, 0·43.
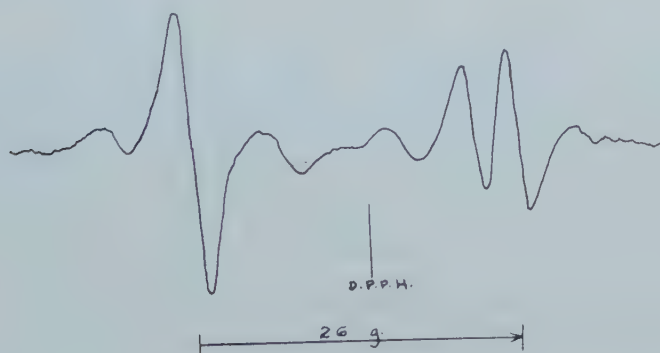


Figure 2.   E.s.r. spectrum of x-ray irradiated potassium hydrogen malonate for the orientation *cba'*, 30°.   Direction cosines of external magnetic field; $\frac{1}{2}$, $\sqrt{3}/2$, 0.

other orientations, the spectra consist of either three or four lines.   These observations are therefore entirely in accordance with what is expected from the crystal symmetry.

## 5. Discussion

The strong line splitting is not a direct measure of the hyperfine interaction unless the external field is parallel to one of the principal axes of the interaction tensor.   However, to facilitate calculation, the splittings may first be assumed equal to the interaction tensor components and the cross terms

of the tensor calculated. This procedure is justified by the fact that the principal values and principal axes thus determined give correct values for both the strong line and the weak line splittings when used in the exact equation (2).

### 5.1. *The principal values and principal axes of the hyperfine interaction tensor*

The interaction tensor in the $a'bc$ system is evaluated from our results as

$$\mathbf{A} = \left\{ \begin{array}{ccc} 10\cdot0 & \pm1\cdot8 & 0\cdot3 \\ \pm1\cdot8 & 26\cdot5 & \pm4\cdot3 \\ 0\cdot3 & \pm4\cdot3 & 23\cdot2 \end{array} \right\}, \tag{3}$$

where the upper signs refer to molecular position which we shall call A and the lower signs to molecular position B. The signs of the cross terms in the interaction tensor (3) were assigned by measuring the angular variation of the spectra with the crystal mounted in a skew orientation.

The diagonalization of the A matrix above gave the following principal values and principal axes, the direction cosines of the latter being referred to the $a'bc$ system:

$$\begin{array}{cccc} & a & b & c \\ A_x = 19\cdot1 \text{ gauss} & 0\cdot06 & \pm0\cdot49 & -0\cdot87 \\ A_y = 30\cdot7 \text{ gauss} & 0\cdot08 & \pm0\cdot86 & 0\cdot50 \\ A_z = 10\cdot0 \text{ gauss} & 0\cdot99 & \pm0\cdot11 & 0\cdot01 \end{array} \right\} . \tag{4}$$

The signs of the direction cosines have been chosen so that, when they form a matrix in this order, the determinant equals $+1$ for the A position.

The three principal values should be compared with those of the malonic acid radical [1]:

$$A_x = 21\cdot6, \qquad A_y = 32\cdot2, \qquad A_z = 10\cdot3 \text{ gauss.}$$

We shall assume that in the planar radical $^-O_2C-\dot{C}H-CO_2^-$, the CH bond bisects the C–C–C angle and lies in the molecular plane. The direction of the bond is the principal axis $A_z$, and the direction of the symmetry axis of the unpaired $\pi$-electron is the principal axis $A_x$. Thus the molecular plane containing the $O_2$–C–C–$CO_2$ skeleton should contain both $A_y$ and $A_z$ with the latter bisecting C–C–C and with $A_x$ perpendicular to the plane. The two planes corresponding to the two molecular positions A and B are then oriented as shown in figure 3.

### 5.2. *The calculation of the theoretical hyperfine splitting*

The method for the calculation of the energy levels and hence the splittings from the exact Hamiltonian (2) can be found in the paper of McConnell *et al.* [1].

The calculated hyperfine splittings for both the strong and the weak lines are shown in figure 4 corresponding to orientations $cba'$. Experimental points are shown as small circles in this figure.

### 5.3. *The relative intensities of the weak and the strong lines*

The theoretical intensity ratios, being equal to $[\cos(\beta/2)/\sin(\beta/2)]^2$ in our case can be calculated when $\beta$ is known. $\beta$ is the angle of rotation of the proton quantization axis during electronic transition and can be calculated (see refs. [1, 5]).

As a first approximation, the experimental intensity ratios can be taken as the ratio of the height of the derivative curves. Both the theoretical and the experimental intensity ratios are plotted in figure 5. It should be noted that
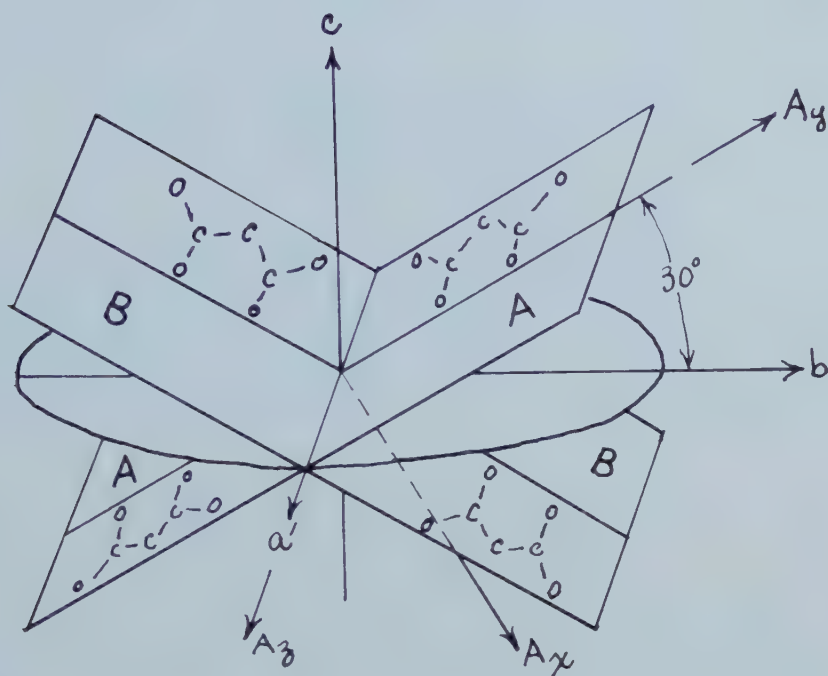
Figure 3.    Orientations of the two $O_2$–C–C–C–$O_2$ planes of the malonate radical in x-ray irradiated potassium hydrogen malonate. These correspond to the two molecular positions A and B in the crystal. The $a'$ axis bisects the C–C–C– angle. The principal axes, $A_x$, $A_y$, $A_z$ shown are those for position A.
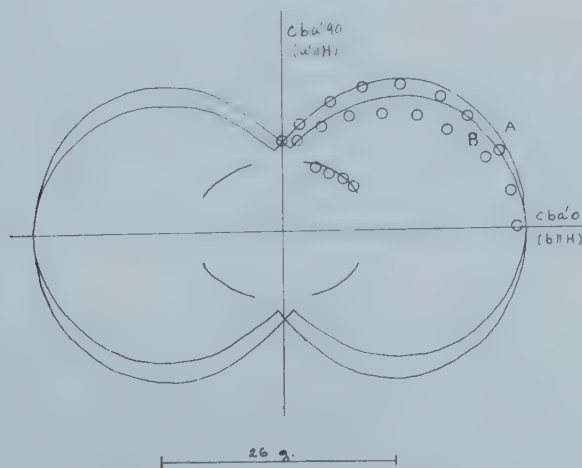


Figure 4.    Calculated angular variation of the hyperfine splitting constants for x-ray irradiated single crystals of potassium hydrogen malonate for orientations $cba'$. The circles represent experimental observations.
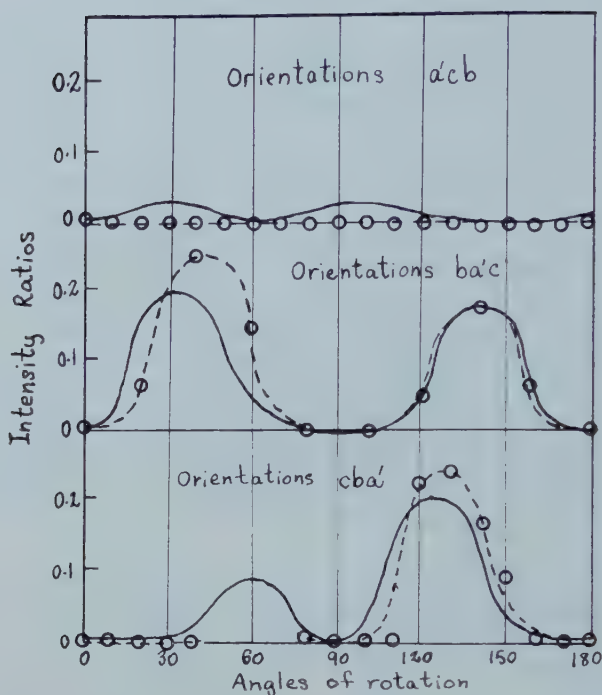
Figure 5. Ratios of the intensities of the weak and strong lines in the e.s.r. spectrum of x-ray irradiated single crystals of potassium hydrogen malonate as a function of the angle of rotation of the crystal with respect to the static magnetic field. The full line represents the calculated values and the circles are experimental observations.

owing to many factors, both the calculated and the experimental intensities are only semi-quantitative; the agreement between the two can therefore be considered as quite good.

### 5.4. The spectroscopic splitting factor g

The $g$ value of the radical can be calculated by means of the following equation

$$g = (1 - \Delta H/H) g_0,$$

where $H$ is the external field magnitude taken as 3370 gauss (for X band); $\Delta H$ = the difference in gauss between the centre of the spectrum and that of the D.P.P.H. line; $g_0$ the $g$ factor for D.P.P.H. taken as 2·0036. The $g$ values for the radical in the three principal axes directions were found to be $g_x = 2\cdot0031$; $g_y = 2\cdot0054$; $g_z = 2\cdot0041$. These values are somewhat larger than the values found for the malonic acid radical by McConnell et al. [1], namely, $g_x = 2\cdot0026$; $g_y = 2\cdot0035$; $g_z = 2\cdot0033$.

### References

[1] McConnell, H. M., Heller, C., Cole, T., and Fessenden, R. W., 1960, J. Amer. chem. Soc., 82, 766.
[2] Trammell, G. T., Zeldes, H., and Livingston, R., 1958, Phys. Rev., 110, 630.
[3] Miyagawa, I., and Gordy, W., 1959, J. chem. Phys., 30, 1590.
[4] Atherton, N. M., and Whiffen, D. H., 1960, Mol. Phys., 3, 1.
[5] Rose, M. E., 1957, Elementary Theory of Angular Momentum (New York: Wiley & Sons, Inc.), pp. 62, 73.
[6] Groth, P., 1910, Chemische Kristallographie, III (Leipzig: Engelmann).
[7] Lin, W. C., and McDowell, C. A., 1961, Mol. Phys., 4, 333.

# Electron spin resonance of $CH_3CH_2\dot{C}(COOH)_2$ in ethyl malonic acid

by J. R. ROWLANDS and D. H. WHIFFEN

Basic Physics Division, National Physical
Laboratory, Teddington

The study of the electron spin resonance spectra of aliphatic free radicals trapped in single crystals leads to information about the hyperfine couplings, especially of hydrogen nuclei. Typical values are now well established for hydrogens attached to the free radical carbon [1–7], but the range for hydrogens on an adjacent carbon is less fully established. The present work is part of a programme to investigate such $\beta$ hydrogens and in particular to confirm the
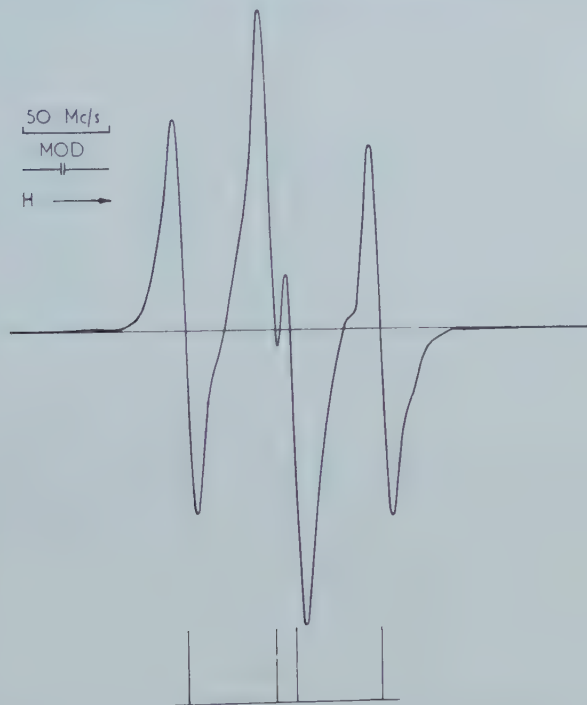


Figure 1. Derivative of absorption spectrum, for a crystal orientation in which the central line is just resolved into a doublet.

expression $B \cos^2 \theta$ proposed for such atoms [4, 5, 8] where $\theta$ is the angle between the projection of the C–H bond and the projection of the normal to the radical plane onto a plane perpendicular to the C–C bond.

A single crystal of ethyl malonic acid was grown from a saturated solution in water and subjected to 5 megarads of $\gamma$-radiation of 1 Mev at the Spent Fuel Irradiation Unit, Harwell. Measurements were made at 9000 Mc/s with a

superheterodyne spectrometer [9] under conditions normal for such work
[3, 6, 9]. Nothing appears to be known about the crystal structure of the
ethyl malonic acid. The present results suggested a triclinic cell with only one
magnetically distinct radical.

Figure 1 shows a typical spectrum, and similar figures were obtained for all
orientations except that the individual lines were sometimes broader and the
central doublet less well resolved. Clearly this is a four line spectrum derived
from the couplings to two nearly equivalent hydrogen atoms. The detailed
measurements showed that the central line was always broader than the wings
and apparently, there was no special orientation for which the hydrogens had
exactly equal couplings. The anisotropy is small and it is clear that the electron
couples with no $\alpha$ hydrogen and only two $\beta$ hydrogens, so the radical must be
$CH_3CH_2\dot{C}(COOH)_2$.

Two tensors were deduced and the principal values of the coupling for one
hydrogen ($\beta_1$) were 75, 71 and 64 Mc/s and for the other 62, 56 and 53 Mc/s.
The average couplings are 70 Mc/s for $\beta_1$, and 57 Mc/s for $\beta_2$; these correspond
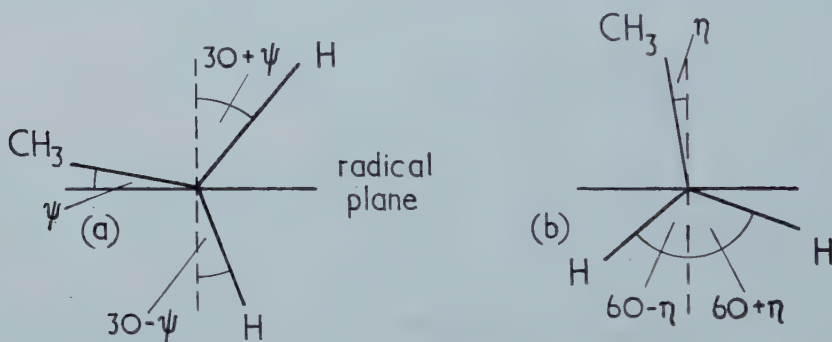


Figure 2. Possible geometrical arrangements.

to the contact term and theory [8] requires these to have a positive sign. If the
radical is viewed along the $C_2H_5-\dot{C}$ bond, the appearance might be essentially
as in figure 2 (a) or 2 (b). If 2 (a) is correct and the coupling is strictly of the
form $B \cos^2 \theta$. Then

$$B \cos^2 (30 - \psi) = 70,$$
$$B \cos^2 (30 + \psi) = 57,$$

whose solution is $B = 84$ Mc/s and $\psi = 5°$.

If 2 (b) is correct

$$B \cos^2 (60 - \eta) = 70,$$
$$B \cos^2 (60 + \eta) = 57,$$

whose solution is $B = 254$ Mc/s and $\eta = 2°$.

Both of these values for $B$ are outside the range of values currently being
suggested for $B$; this range is from 112 Mc/s from the methyl group in
$(CH_3)_2\dot{C}OH$ [4] to 152 Mc/s which would be obtained from the methyl coupling
in $CH_3\dot{C}H_2$ [10]. It is apparent that the form $B \cos^2 \theta$, with $B$ independent
of the nature of the radical is not wholly correct, but it is not yet clear whether
the trouble lies in the neglect of the angle independent term, in the variation of

$B$ with other substituents in the radical, in the variation of $B$ with substituents at the $\beta$ carbon atom, or in a more complicated angular dependence of the isotropic coupling.

This work forms part of the research programme of the Basic Physics Division of the National Physical Laboratory and is published by permission of the Director.

REFERENCES

[1]  McConnell, H. M., Heller, C., Cole, T., and Fessenden, R. W., 1960, *J. Amer. chem. Soc.*, **82**, 766.
[2]  Ghosh, D. K., and Whiffen, D. H., 1959, *Mol. Phys.*, **2**, 285.
[3]  Atherton, N. M., and Whiffen, D. H., 1960, *Mol. Phys.*, **3**, 1 and 103.
[4]  Heller, C., and McConnell, H. M., 1960, *J. chem. Phys.*, **32**, 1535.
[5]  Pooley, D., and Whiffen, D. H., 1961, *Mol. Phys.*, **4**, 81.
[6]  Horsfield, A., Morton, J. R., and Whiffen, D. H., 1961, *Nature, Lond.*, **189**, 481.
[7]  McConnell, H. M., and Strathdee, J., 1959, *Mol. Phys.*, **2**, 129.
[8]  McLachlan, A. D., 1958, *Mol. Phys.*, **1**, 233.
[9]  Horsfield, A., Morton, J. R., and Whiffen, D. H., 1961, *Mol. Phys.* (in the press).
[10]  Fessenden, R. W., and Schuler, R. H., 1960, *J. chem. Phys.*, **33**, 935.

# A one-centre S.C.F. wave function for the methane molecule

by E. L. ALBASINY and J. R. A. COOPER

National Physical Laboratory, Teddington, Middlesex

A Hartree–Fock single-determinant wave function is calculated for the ground state of the methane molecule. The one-electron molecular orbitals in this determinant are expanded up to third-order terms as a series of spherical harmonics about the central carbon nucleus. The potential field due to the nuclei is correspondingly expanded up to sixth-order terms and the complete Hartree–Fock S.C.F. equations are set up and solved numerically for the six radial functions occurring in the molecular orbitals. The numerical techniques employed differ in certain respects from those used in previous atomic calculations. The total molecular energy obtained from this approximation is $-39.90$ A.U.

The spherically symmetric model, in which only the first term in each expansion is retained, is re-examined to settle an uncertainty in the associated energy value; this energy value is here found to be $-39.53$ A.U.

## 1. Introduction and historical survey

This paper describes the numerical calculation of the self-consistent field (S.C.F.) for the ground state of the methane molecule $CH_4$ using the one-centre method. Each one-electron molecular orbital (M.O.) wave function, together with the nuclear potential, is expanded as a series of products of a spherical harmonic and a radial function with the central carbon nucleus as origin. The total electronic wave function is then taken to be the Hartree–Fock determinant composed of these molecular orbitals.

Early one-centre calculations of the electronic structure of methane assumed spherical symmetry for the averaged nuclear potential and the electron charge distribution. The problem is then mathematically equivalent to that of a 10-electron atom and permits the usual methods developed by Hartree [1] for central-field atomic problems to be applied. These assumptions make pointless, however, the investigation of molecular properties dependent upon the directional variation of the electron distribution.

Buckingham *et al.* [2] made the first calculation for methane using this spherical model and solved the Hartree S.C.F. equations neglecting exchange. In this approximation each molecular orbital contains just a single harmonic term corresponding to the electron configuration $(1s)^2(2s)^2(2p)^3$. Exchange terms were later included by both Bernal [3] and Mills [4]. Whereas, however, Bernal used analytic radial functions containing parameters to be determined by minimizing the electronic energy, Mills solved the Hartree Fock equations to obtain numerical radial functions. Mills also estimated the effects of the second non-zero harmonic term in the expansion of the nuclear potential by means of a modified form of perturbation theory. This latter calculation has been queried, however, in a recent paper by Saturno and Parr [5] since it appears to yield too good a resulting energy value for the method employed.

Carter [6] was the first to show the effect of higher harmonic terms in the one-centre M.O. expansions. He carried out calculations for both methane and silane, and noted that the inclusion merely of a second harmonic term in the $2t_2$ M.O. expansion for methane led to a considerable improvement in the calculated values of certain physical quantities.

Koide *et al.* [7] extended this work by including higher harmonic terms in the expansions of the molecular orbitals as well as in the expansion of the nuclear potential about the carbon nucleus. Their work included exchange terms but, due to the difficulty of solving numerically the now more complicated Hartree–Fock S.C.F. equations, they assumed analytic radial functions in the molecular orbitals, with associated parameters which were determined by minimizing the energy. Unfortunately, their expression for the electronic energy, upon which the calculation is based, contains several terms which the present work has revealed to be in error. This is discussed further in Appendix 1.

The present work follows on from that of [7]. The same higher harmonic terms are included in the M.O. and nuclear potential expansions and a single determinant total wave function assumed. But whereas Koide and his co-workers minimize the energy with respect to five parameters occurring in the molecular orbitals they assume, we derive the full Hartree–Fock S.C.F. equations and solve them numerically to obtain the 'best' radial functions in the M.O. expansions. The spherical model considered by Mills [4] is also re-examined and a deficiency in the energy value conjectured in [5] is confirmed.

Whilst the present work was in progress Saturno and Parr [5] published an account of a further one-centre treatment of methane. Their work differs from that described previously in that they represent the ground state wave function by a linear combination of determinants rather than a single determinant. Analytic radial functions are used with variable non-integral principal quantum numbers as well as variable orbital exponents. As in the present paper, higher harmonic terms are incorporated to take into account the departure from spherical symmetry of the electron distribution and nuclear potential under the tetrahedral symmetry of the molecule.

## 2. Nuclear potential and molecular orbitals

A Cartesian coordinate system is chosen for $CH_4$ in which the four protons have fixed coordinates $(t, t, t)$, $(t, -t, -t)$, $(-t, t, -t)$, $(-t, -t, t)$ and the carbon nucleus is at the origin. A C–H bond length of $R = t\sqrt{3} = 2\cdot0$ atomic units† is assumed for convenience; the experimental value is $2\cdot0665$ A.U. $(1\cdot0936$ Å$)$.

The Hamiltonian $H$ for the 10-electron system may be written in atomic units as

$$H = \sum_{i=1}^{10} \left[ -\frac{1}{2}\nabla_i^2 + V(\mathbf{r}_i) \right] + \sum_{i<j} \frac{1}{r_{ij}} \tag{1}$$

with

$$V(\mathbf{r}_i) = -\frac{Z}{r_i} - \sum_{k=1}^{4} \frac{1}{r_{ik}}. \tag{2}$$

Here $Z$ is the charge on the central carbon nucleus (equal to 6 A.U.), $\mathbf{r}_i$ is the vector coordinate of the $i$th electron, $\mathbf{r}_k$ that of the $k$th proton and $r_{ij} = |\mathbf{r}_i - \mathbf{r}_j|$.

† The atomic units of length and energy are $0\cdot52917 \times 10^{-8}$ cm and $27\cdot210$ ev respectively (see [1], p. 5).

$V(\mathbf{r})$ is the potential energy of an electron at $\mathbf{r}$ due to the five nuclei. This potential may be expanded in a series of harmonics about the carbon nucleus in the form

$$V(\mathbf{r}) = V_0(r) + V_3(r)A_3(\theta, \phi) + V_4(r)A_4(\theta, \phi) + V_6(r)A_6(\theta, \phi) + \ldots, \quad (3)$$

where

$$
\left.
\begin{aligned}
&V_0(r) = -\frac{6}{r} - \frac{4}{r_>}, \\[4pt]
&V_3(r) = -\frac{8}{21}(35\pi)^{1/2}\frac{r_<^3}{r_>^4}, \quad A_3(\theta, \phi) = \frac{1}{2}\left(\frac{105}{\pi}\right)^{1/2} xyz, \\[4pt]
&V_4(r) = -\frac{8}{27}(21\pi)^{1/2}\frac{r_<^4}{r_>^5}, \quad A_4(\theta, \phi) = \frac{1}{8}\left(\frac{21}{\pi}\right)^{1/2}[3 - 5(x^4 + y^4 + z^4)], \\[4pt]
&V_6(r) = -\frac{32}{117}(26\pi)^{1/2}\frac{r_<^6}{r_>^7}, \\[4pt]
&A_6(\theta, \phi) = \frac{21}{32}\left(\frac{26}{\pi}\right)^{1/2}\left[22x^2y^2z^2 + x^4 + y^4 + z^4 - \frac{17}{21}\right].
\end{aligned}
\right\} \quad (4)
$$

In the above $x = \sin\theta\cos\phi$, $y = \sin\theta\sin\phi$, $z = \cos\theta$, and $r_<$ and $r_>$ denote the lesser and greater of $r$ and $R$. The angular functions $A_i$ have been normalized so that

$$\int_0^\pi \int_0^{2\pi} A_i^2(\theta, \phi)\sin\theta\, d\theta\, d\phi = 1, \quad (i = 3, 4, 6).$$

The absence of the first-, second- and fifth-order harmonics in the expansion (3) is due to the tetrahedral symmetry of the methane molecule and illustrates an advantage of the one-centre method in this instance. The retention of the first term $V_0(r)$ only in the expansion corresponds to the spherical approximation in which the proton charges are averaged out over a sphere of radius $R$.

The type of molecular orbitals possible for $CH_4$ has been discussed by Mulliken [8]. The appropriate spherical harmonics occurring in each molecular orbital depend upon the symmetry group of the molecule and have been tabulated up to the fourth order for $CH_4$ (tetrahedral group $T_d$) by Carter [6]. The equilibrium configuration for $CH_4$ may be written as

$$(1a_1)^2(2a_1)^2(2t_{2x})^2(2t_{2y})^2(2t_{2z})^2,$$

where $a_1$ and $t_2$ denote the two types of molecular orbitals corresponding to the irreducible representations $A_1$ and $T_2$ of the tetrahedral symmetry group.

The following forms, in which harmonic terms up to the third order are taken into account, are assumed for the molecular orbitals:

$$
\left.
\begin{aligned}
&r\psi(1a_1) = \left(\frac{1}{4\pi}\right)^{1/2} P_1(r), \\[4pt]
&r\psi(2a_1) = \left(\frac{1}{4\pi}\right)^{1/2} P_2(r) + \left(\frac{105}{4\pi}\right)^{1/2} P_3(r)xyz, \\[4pt]
&r\psi(2t_{2x}) = \left(\frac{3}{4\pi}\right)^{1/2} P_4(r)x + \left(\frac{15}{4\pi}\right)^{1/2} P_5(r)yz + \left(\frac{7}{16\pi}\right)^{1/2} P_6(r)x(5x^2 - 3), \\[4pt]
&r\psi(2t_{2y}) = \left(\frac{3}{4\pi}\right)^{1/2} P_4(r)y + \left(\frac{15}{4\pi}\right)^{1/2} P_5(r)zx + \left(\frac{7}{16\pi}\right)^{1/2} P_6(r)y(5y^2 - 3), \\[4pt]
&r\psi(2t_{2z}) = \left(\frac{3}{4\pi}\right)^{1/2} P_4(r)z + \left(\frac{15}{4\pi}\right)^{1/2} P_5(r)xy + \left(\frac{7}{16\pi}\right)^{1/2} P_6(r)z(5z^2 - 3).
\end{aligned}
\right\} \quad (5)
$$

As in the work of Koide *et al.* [7], the third-order harmonic has been omitted from the $\psi(1a_1)$ orbital since the inner electrons are assumed to be insufficiently affected by the surrounding protons for the departure from spherical symmetry to be significant. The first- and second-order harmonics in $\psi(1a_1)$ and $\psi(2a_1)$ are excluded by the symmetry conditions. The six radial functions $P_1(r)$ to $P_6(r)$ are to be determined numerically from a variation principle as explained in the next section. The angular functions are normalized to unity when integrated over the unit sphere.

If only the first term is retained in each molecular orbital expansion the electron configuration corresponds to that for the neon atom, viz. $(1s)^2(2s)^2(2p)^6$. This is the closed-shell configuration with a spherically symmetric charge distribution used originally by Buckingham *et al.* [2].

## 3. ENERGY AND VARIATIONAL EQUATIONS

The total energy of the molecule is taken as the sum of the normal electronic energy $E$ and the classical repulsion energy $N$ of the nuclei given by

$$N = \left[ 4Z + 3\sqrt{\frac{3}{2}} \right] \Big/ R. \tag{6}$$

According to the variation principle, $E$ may be approximated by

$$E' = \int \Psi^* H \Psi \, d\tau \tag{7}$$

where $\Psi$ is an approximation to the ground state wave function, normalized so that $\int \Psi^* \Psi \, d\tau = 1$, and the integrations extend over the coordinates of all the electrons. $E'$ has the property that it is an absolute minimum for the normal state of the system.

The ground state wave function $\Psi$ assumed for the methane molecule is the normalized $10 \times 10$ Hartree–Fock determinant made up from the five one-electron molecular orbitals given by (5), each orbital being associated with both spin functions. The radial functions $P_1(r)$ to $P_6(r)$ occurring in the molecular orbitals in $\Psi$ are to be determined by minimizing $E'$. If the orthonormality conditions

$$\int_0^\infty P_1^2(r) \, dr = \int_0^\infty \{P_2^2(r) + P_3^2(r)\} \, dr = \int_0^\infty \{P_4^2(r) + P_5^2(r) + P_6^2(r)\} \, dr = 1, \tag{8}$$

$$\int_0^\infty P_1(r) P_2(r) \, dr = 0 \tag{9}$$

are imposed, the analysis given by Hartree ([1], Ch. 3) for atomic structure calculations is applicable. This shows that $E'$ may be expressed as a sum of integrals in the form

$$E' = \sum_\alpha I_\alpha + \sideset{}{'}\sum_{\alpha, \beta} J_{\alpha\beta} - \sideset{}{''}\sum_{\alpha, \beta} K_{\alpha\beta}, \tag{10}$$

where the second sum includes all pairs of electrons $\alpha \neq \beta$ taken once only and the third sum includes all pairs $\alpha \neq \beta$ with the same spin. $I_\alpha$, $J_{\alpha\beta}$ and $K_{\alpha\beta}$ are defined by

$$I_\alpha = \int \psi_\alpha^*(\mathbf{r}_i)[-\tfrac{1}{2}\nabla_i^2 + V(\mathbf{r}_i)]\psi_\alpha(\mathbf{r}_i) \, d\tau_i,$$

$$J_{\alpha\beta} = \int\int |\psi_\alpha(\mathbf{r}_i)|^2 \frac{1}{r_{ij}} |\psi_\beta(\mathbf{r}_j)|^2 \, d\tau_i \, d\tau_j, \qquad (11)$$

$$K_{\alpha\beta} = \int\int \psi_\alpha^*(\mathbf{r}_i)\psi_\beta(\mathbf{r}_i) \frac{1}{r_{ij}} \psi_\alpha(\mathbf{r}_j)\psi_\beta^*(\mathbf{r}_j) \, d\tau_i \, d\tau_j.$$

$I_\alpha$ is a one-electron integral whilst $J_{\alpha\beta}$ and $K_{\alpha\beta}$ are the two-electron Coulomb and exchange integrals respectively.

The integrations over the angular coordinates can be carried out analytically when use is made of the expansions in spherical harmonics of $V(r_i)$ and the $\psi_\alpha$'s given by equations (3) and (5). The resulting integrals which occur involve integrations over radial coordinates only. A similar procedure is adopted in atomic calculations, but the higher harmonic terms in the potential $V(r_i)$ and the orbitals $\psi_\alpha$ lead, in the molecular case, to more complicated expressions than those appearing for atoms. Thus, in addition to the usual atomic-type terms, cross-products of the radial functions occur in the one-electron integrals. Indeed,

$$\sum_\alpha I_\alpha = 2I(1a_1) + 2I(2a_1) + 6I(2t_{2x}),\tag{12}$$

where

$$I(1a_1) = \int_0^\infty P_1(r)\left[-\frac{1}{2}\frac{d^2}{dr^2} + V_0(r)\right]P_1(r)\,dr,\tag{13}$$

$$
\left.\begin{aligned}
I(2a_1) &= \int_0^\infty P_2(r)\left[-\frac{1}{2}\frac{d^2}{dr^2} + V_0(r)\right]P_2(r)\,dr\\
&\quad -\int_0^\infty P_3(r)\left[-\frac{1}{2}\frac{d^2}{dr^2} + V_0(r) + \frac{1}{11}\left(\frac{21}{\pi}\right)^{1/2}V_4(r)\right.\\
&\qquad\qquad \left.\pm\frac{10}{143}\left(\frac{26}{\pi}\right)^{1/2}V_6(r) + \frac{6}{r^2}\right]P_3(r)\,dr\\
&\quad +\left(\frac{1}{\pi}\right)^{1/2}\int_0^\infty P_2(r)P_3(r)V_3(r)\,dr,
\end{aligned}\right\}\tag{14}
$$

$$
\left.\begin{aligned}
I(2t_x) &= I(2t_y) = I(2t_z)\\
&= \int_0^\infty P_4(r)\left[-\frac{1}{2}\frac{d^2}{dr^2} + V_0(r) + \frac{1}{r^2}\right]P_4(r)\,dr\\
&\quad +\int_0^\infty P_5(r)\left[-\frac{1}{2}\frac{d^2}{dr^2} + V_0(r) + \frac{1}{21}\left(\frac{21}{\pi}\right)^{1/2}V_4(r) + \frac{3}{r^2}\right]P_5(r)\,dr\\
&\quad +\int_0^\infty P_6(r)\left[-\frac{1}{2}\frac{d^2}{dr^2} + V_0(r) - \frac{1}{22}\left(\frac{21}{\pi}\right)^{1/2}V_4(r)\right.\\
&\qquad\qquad \left.+\frac{25}{858}\left(\frac{26}{\pi}\right)^{1/2}V_6(r) + \frac{6}{r^2}\right]P_6(r)\,dr\\
&\quad +\frac{1}{7}\left(\frac{21}{\pi}\right)^{1/2}\int_0^\infty P_4(r)P_6(r)V_4(r)\,dr\\
&\quad -\frac{2}{3}\left(\frac{1}{\pi}\right)^{1/2}\int_0^\infty \{P_4(r)V_4(r) + P_5(r)V_3(r)\}P_6(r)\,dr.
\end{aligned}\right\}\tag{15}
$$

A similar complexity occurs with the two-electron integrals $J_{\alpha\beta}$ and $K_{\alpha\beta}$. The angular integrations may be performed with the help of prepared tables (see [9], p. 178) after using a Legendre function expansion for the reciprocal interelectronic distance $1/r_{ij}$. The resulting radial integrals which remain are of the form

$$I_n(ij:kl) = \int_0^\infty\int_0^\infty \frac{r_<^n}{r_>^{n+1}}P_i(r)P_j(r)P_k(r')P_l(r')\,dr\,dr',\tag{16}$$

where $r_<$ and $r_>$ denote now the lesser and greater of $r$ and $r'$ respectively. In atomic calculations only integrals having either $j=i$, $l=k$ or $k=i$, $l=j$ appear; these are usually denoted by $F_n$ and $G_n$ respectively.

Thus $E'$ may be expressed as a linear combination of 3 single and 74 double radial integrals,

$$E' = 2I(1a_1) + 2I(2a_1) + 6I(2t_{2x}) + \sum a_n(ij:kl)I_n(ij:kl). \tag{17}$$

The numerical coefficients $a_n(ij:kl)$ have been given in [7], but certain of the values are in error. Amended values are given in Appendix 1 with numerical values of the $I_n$.

The six differential equations for the 'best' S.C.F. radial functions $P_1(r)$ to $P_6(r)$ are obtained from the energy expression (17) by using the variation principle. This requires that $E'$ be stationary with respect to all small variations $\Delta P_i(r)$ in the radial functions which are consistent with the orthonormality conditions (8) and (9). As with atomic calculations, it is convenient for the subsequent analysis to introduce the following functions

$$Z_n(kl;r) = \int_0^r \left(\frac{r'}{r}\right)^n P_k(r')P_l(r')\,dr' \tag{18}$$

and

$$Y_n(kl;r) = Z_n(kl;r) + \int_r^\infty \left(\frac{r}{r'}\right)^{n+1} P_k(r')P_l(r')\,dr'. \tag{19}$$

The double integrals in $E'$ may then be written as

$$I_n(ij:kl) = \int_0^\infty P_i(r)P_j(r)\frac{1}{r}Y_n(kl;r)\,dr = \int_0^\infty P_k(r)P_l(r)\frac{1}{r}Y_n(ij;r)\,dr. \tag{20}$$

The variation $\Delta E_i'$ due to the variation of a particular radial function $P_i(r)$ can be written in the form

$$\Delta E_i' = \int_0^\infty \Delta P_i(r)\left[Q_i(r) + \sum_j \epsilon_{ij} P_j(r)\right]dr, \tag{21}$$

where $Q_i(r)$ consists of contributions from all the single and double integrals involving the particular radial function $P_i(r)$ and the $\epsilon_{ij}$ are Lagrange multipliers introduced to incorporate the orthonormality conditions (8) and (9). Four such multipliers are required corresponding to the four conditions imposed on the radial functions. The condition for stationary energy $\Delta E_i' = 0$ therefore gives the Hartree–Fock equation for the 'best' radial function $P_i(r)$ as

$$Q_i(r) + \sum_j \epsilon_{ij}P_j(r) = 0. \tag{22}$$

The contribution from the single integrals (13), (14) and (15) to $Q_i(r)$ is of the general form

$$\left[-\frac{d^2}{dr^2} + \sum_s a_s V_s(r) + \frac{l(l+1)}{r^2}\right]P_i(r) + \sum_{s,j} b_s V_s(r)P_j(r), \tag{23}$$

where $l$ is the order of the harmonic term containing $P_i(r)$. (For atomic calculations, the nuclear potential coefficients are such that $a_s = 0$ for $s \neq 0$ and $b_s = 0$ for all $s$.) The double integrals $I_n(ij:kl)$ yield the following type of contribution, differing according to the other three radial functions in the

integrand but all expressible in terms of functions of the type $Y_n(kl;r)$,

$$i=j=k=l, \qquad \frac{4}{r} Y(ii;r)P_i(r),$$

$$i=j=k,l, \qquad \frac{2}{r} Y(il;r)P_i(r) + \frac{1}{r} Y(ii;r)P_l(r),$$

$$i=j,k,l, \qquad \frac{2}{r} Y(kl;r)P_i(r),$$

$$i=k,j,l, \qquad \frac{1}{r} Y(il;r)P_j(r) + \frac{1}{r} Y(ij;r)P_l(r),$$

$$i,j,k,l, \qquad \frac{1}{r} Y(kl;r)P_j(r).$$

In atomic calculations only the combinations $i=j=k=l$, $i=j$, $k=l$ and $i=k$, $j=l$ occur.

## 4. COMPUTATIONAL PROCEDURE

The full differential equations for $P_1(r)$ to $P_6(r)$ are complicated and will not be set down explicitly apart from the simplest—that for $P_1(r)$—which is

$$\left[\frac{d^2}{dr^2} + \frac{2}{r}\{Y(r) + Y_0(11)\} - \epsilon_{11}\right]P_1 + \frac{2}{r}\left\{Y_0(12)P_2 + \frac{1}{7}Y_3(13)P_3\right.$$

$$\left. + Y_1(14)P_4 + \frac{3}{5}Y_2(15)P_5 + \frac{3}{7}Y_3(16)P_6\right\} - \epsilon_{12}P_2 = 0, \quad (24)$$

where

$$Y(r) = -rV_0(r) - 2Y_0(11) - 2Y_0(22) - 2Y_0(33) - 6Y_1(44) - 6Y_0(55) - 6Y_0(66) \quad (25)$$

and $Y_n(ij)$ has been written for $Y_n(ij;r)$. The $\epsilon_{12}$ parameter may be given the value zero without appreciably affecting the associated orthogonality condition (9). Indeed, the resulting functions $P_1(r)$ and $P_2(r)$ so obtained are such that

$$\int_0^\infty P_1 P_2\, dr = -0.0001.$$

See Appendix 2 for a further discussion.

With $\epsilon_{12}=0$, the equations for $P_1(r)$ to $P_6(r)$ may be written as

$$\frac{d^2 P_i(r)}{dr^2} + \left\{\frac{1}{r}f_i(r) - \epsilon_{ii} - \frac{k_i}{r^2}\right\}P_i(r) + \frac{1}{r}g_i(r) = 0, \qquad i=1, 2, \ldots, 6, \quad (26)$$

where, in general, $f_i(r)$ and $g_i(r)$ are functions of $P_1(r)$ to $P_6(r)$ and $k_i = l_i(l_i+1)$ is a constant. As $i$ goes from 1 to 6, the $l_i$ assume the values 0, 0, 3, 1, 2, 3 respectively. The normalization conditions (8) imposed on the $P_i(r)$ require that $\epsilon_{22} = \epsilon_{33}$ and $\epsilon_{44} = \epsilon_{55} = \epsilon_{66}$.

Equations (26) must be solved numerically subject to the normalization conditions (8) and the conditions

$$P_i(0) = 0, \qquad P_i(r) \to 0 \quad \text{as} \quad r \to \infty, \qquad i=1, 2, \ldots, 6. \quad (27)$$

Frequent changes of the interval $\delta r$ may be avoided by adopting the transformations employed for similar atomic-type calculations by Worsley [10] and Mayers [11], namely

$$x = \log_e cr \qquad (28)$$

and

$$y_i(x) = r^{-1/2}P_i(r), \qquad i=1, 2, \ldots, 6, \qquad (29)$$

where $c$ is a suitably chosen parameter. In terms of the transformed variables, the equations to be solved are of the form

$$\frac{d^2y_i(x)}{dx^2} + \{rf_i(x) - r^2\epsilon_{ii} - k_i - \tfrac{1}{4}\}y_i(x) + r^{1/2}g_i(x) = 0, \quad i = 1, 2, \ldots, 6 \quad (30)$$

with normalization conditions

$$\int_0^\infty r^2 y_1^2(x)\, dx = \int_0^\infty r^2\{y_2^2(x) + y_3^2(x)\}\, dx$$

$$= \int_0^\infty r^2\{y_4^2(x) + y_5^2(x) + y_6^2(x)\}\, dx = 1. \quad (31)$$

It should be noted that equations (31) correspond strictly to conditions such as $\int_{1/c}^\infty P_1^2\, dr = 1$ rather than $\int_0^\infty P_1^2\, dr = 1$. The difference is negligibly small, however, for the values $c = 500$ and $c = 2000$ used in the calculations.

The overall method of solution of the set of six equations is essentially the iterative scheme used by Hartree [1] and his co-workers, for which the various steps are

(1) guess values for $y_1(x)$ to $y_6(x)$;
(2) evaluate $f_i(x)$ and $g_i(x)$ for a particular value of $i$ from the estimates for $y_1(x)$ to $y_6(x)$;
(3) solve the $i$th equation of (30) with these values of $f_i(x)$ and $g_i(x)$ to obtain a new estimate for $y_i(x)$;
(4) repeat steps (2) and (3) with the same or a new value of $i$ until a consistent set of results is achieved.

The work of Koide et al. [7] affords a good initial guess for use in step (1). Step (2) requires the evaluation in terms of the variable $x$ of the functions $Z_n(kl)$ and $Y_n(kl)$ defined by (18) and (19). These satisfy the differential equations

$$\frac{dZ_n(kl)}{dx} = r^2 y_k y_l - nZ_n(kl) \quad (32)$$

and

$$\frac{dY_n(kl)}{dx} = (n+1)Y_n(kl) - (2n+1)Z_n(kl) \quad (33)$$

with boundary conditions†

$$Z_n(kl) = 0 \quad \text{at} \quad x = 0 \quad (34)$$

and

$$Y_n(kl) - Z_n(kl) \to 0 \quad \text{as} \quad x \to \infty. \quad (35)$$

Equations (32) and (33) are both of the form

$$\frac{du}{dx} + ku = v(x) \quad (36)$$

with $k$ a constant. This type of equation may readily be integrated by means of the formula recommended by Mayers [11], namely

$$u_{j+1} = \frac{1}{A} u_j + \frac{\delta x}{24}\left[ -\frac{1}{A^2} v_{j-1} + \frac{13}{A} v_j + 13 v_{j+1} - A v_{j+2} \right], \quad (37)$$

where $A = \exp(k\delta x)$ and $u_j = u(j\delta x)$. $Z_n(kl)$ is obtained from this formula by forward recursion and $Y_n(kl)$ by backward recursion. The conditions $Z_n(kl) = 0$

† As with equations (31), equation (34) is not strictly true but differs negligibly for the values of $c$ used from the true condition $Z_n(kl) = 0$ at $r = 0$.

at $x=0$ and $x=\delta x$ are sufficiently accurate for starting the $Z$ integration whilst condition (35) applied at a suitably large value of $x$ enables the $Y$ integration to be performed.

The overall iterative procedure is such that step (3) requires the solution of a linear second-order differential equation with first derivative term absent. For such an equation the well-known method of Numerov [12] may be used. When applied to the equation

$$\frac{d^2u}{dx^2} + F(x)u + G(x) = 0, \tag{38}$$

this leads to the finite-difference representation

$$\left\{1 + \frac{1}{12}(\delta x)^2 F_{j+1}\right\} u_{j+1} - \left\{2 - \frac{5}{6}(\delta x)^2 F_j\right\} u_j$$
$$+ \left\{1 + \frac{1}{12}(\delta x)^2 F_{j-1}\right\} u_{j-1} + \frac{1}{12}(\delta x)^2 \{G_{j+1} + 10G_j + G_{j-1}\} = 0 \tag{39}$$

with $u_j = u(j\delta x)$. When $u_0$ and $u_m$ are prescribed, the set of $m-1$ equations obtained from (39) by setting $j=1(1)m-1$ may be solved for the unknowns $u_1, u_2, \ldots, u_{m-1}$ by a direct method. This avoids the technique favoured by earlier workers (see Hartree [1], Ch. 5 for example) of performing trial outward and inward integrations until solutions are obtained which match in the middle of the range. The direct method for the set of equations

$$p_{j+1}u_{j+1} - q_j u_j + r_{j-1}u_{j-1} + b_j = 0, \qquad j = 1(1)m-1, \tag{40}$$

with $u_0$ specified and $u_m = 0$, is as follows. Set

$$\alpha_1 = q_1, \qquad \beta_1 = b_1 - r_0 u_0 \tag{41}$$

and compute

$$\alpha_j = q_j - \frac{r_{j-1}p_j}{\alpha_{j-1}}, \qquad \beta_j = b_j + \frac{r_{j-1}\beta_{j-1}}{\alpha_{j-1}}, \qquad j = 1(1)m-1. \tag{42}$$

Then

$$u_j = \frac{1}{\alpha_j}(p_{j+1}u_{j+1} + \beta_j), \qquad j = m-1(1)1. \tag{43}$$

This procedure is equivalent to the process of Gaussian elimination adapted to take advantage of the special form of the equations (40).

When the Numerov process is applied to equation (30) for a particular value of $i$, the resulting finite-difference equation is similar to equation (40). For an appropriate choice of $m$ and $\delta x$ the boundary condition $y_i(x) \to 0$ as $x \to \infty$ may be approximated by $y_i(m\delta x) = 0$, which corresponds to $u_m = 0$ in the preceding analysis, but the assumption that $u_0$ is specified requires a knowledge of $y_i(x)$ at $x=0$ which is not immediately provided from the condition (27) that $P_i(r) = 0$ at $r=0$. However, the analytic forms used in reference [7] for the $P_3(r)$, $P_5(r)$ and $P_6(r)$ functions tend to zero at the origin as $r^1$, $r^3$ and $r^1$ respectively. This indicates that, without appreciable loss of accuracy, $y_3(x)$, $y_5(x)$ and $y_6(x)$ may be set equal to zero at $x=0$ for a value of $c$ in (28) equal to 500 or 2000.

A different starting procedure is adopted for the $y_1(x)$, $y_2(x)$ and $y_4(x)$ functions. Let $P_i(r)$ denote a solution of (26) for $i=1$, 2 or 4 and suppose that, in the neighbourhood of the origin, $P_i(r)$ is approximated by the expression

$$P_i(r) = a_0 + a_1 r + a_2 r^2 + a_3 r^3. \tag{44}$$

A knowledge of $P_i(r)$ at four distinct values of $r$ for which equation (44) is valid enables the coefficients $a_0$ to $a_3$ to be determined. In particular, if values of $r$

corresponding to equal increments in the $x$ variable are taken, with

$$r_j = (1/c)\exp(j\delta x),$$

then $a_0$ may be expressed as

$$a_0 = b_0 P_i(r_0) + b_1 P_i(r_1) + b_2 P_i(r_2) + b_3 P_i(r_3), \qquad i=1, 2, 4, \qquad (45)$$

where the coefficients $b_0$ to $b_3$ depend only upon $\delta x$ and $c$ and not upon the function $P_i(r)$. The required solution $P_i(r)$ must have $a_0 = 0$ to satisfy the first condition of (27). In terms of the $y_i(x)$ variables defined by (29), this means that the approximate relationship

$$c_0 y_i(0) + c_1 y_i(\delta x) + c_2 y_i(2\delta x) + c_3 y_i(3\delta x) = 0, \qquad i=1, 2, 4 \qquad (46)$$

must hold, in which the $c_j$ $(j=0, 1, 2, 3)$ are given by $c_j = b_j c^{-1/2} \exp(\tfrac{1}{2}j\delta x)$ and are constants which may be readily determined for a particular choice of $\delta x$ and $c$. It is clear that the coefficient of $y_i(3\delta x)$ in (46) may be made unity by multiplying throughout by a suitable constant. If this is done only three constants effectively enter into the resulting equation and these depend now only upon $\delta x$ and not upon $c$. Thus the final form of the boundary condition to be imposed at $x=0$ on the $y_1(x)$, $y_2(x)$ and $y_4(x)$ functions is

$$d_0 y_i(0) + d_1 y_i(\delta x) + d_2 y_i(2\delta x) + y_i(3\delta x) = 0, \qquad i=1, 2, 4 \qquad (47)$$

with $d_j$ a function of $\delta x$ $(j=0, 1, 2)$.

The procedure for solving the equation for $y_1(x)$ is as follows. The required solution must satisfy the finite-difference form of equation (30) with $i=1$ and must be normalized so that $\displaystyle\int_0^\infty r^2 y_1^2(x)\,dx = 1$. The boundary conditions are given by equation (47) with $i=1$ and by $y_1(m\delta x)=0$. To obtain the required solution two parameters need to be determined, namely $y_1(0)$ and $\epsilon_{11}$. The direct method of solution ensures that the condition $y_1(m\delta x)=0$ is satisfied, leaving the two parameters to be determined from the two remaining conditions, namely the normalization condition and the boundary condition at $x=0$.

Three trial solutions, which in general are not correctly normalized and do not satisfy condition (47), are computed using slightly different (guessed) values of the two parameters for each integration. The method of inverse interpolation described by Warner [13] is then applied to improve the parameters and a new solution is calculated. The process is continued until a solution satisfying all the required conditions is obtained.

The procedure may be defined mathematically as follows. Let $y_s$ and $\epsilon_s$ denote the values of the parameters $y_1(0)$ and $\epsilon_{11}$ at the $s$th stage and let

$$N_s = 1 - \left[\int_0^\infty r^2 y_1^2(x)\,dx\right]^{1/2}, \qquad (48)$$

$$a_s = d_0 y_1(0) + d_1 y_1(\delta x) + d_2 y_1(2\delta x) + y_1(3\delta x), \qquad (49)$$

where $y_1(x)$ in the above equations refers to the solution obtained with parameters $y_s$ and $\epsilon_s$. Then $y_{s+1}$ and $\epsilon_{s+1}$ are computed from the formulae

$$\gamma y_{s+1} = y_{s-2}(a_{s-1}N_s - a_s N_{s-1}) + y_{s-1}(a_s N_{s-2} - a_{s-2}N_s)$$
$$+ y_s(a_{s-2}N_{s-1} - a_{s-1}N_{s-2}), \qquad (50)$$

$$\gamma\epsilon_{s+1} = \epsilon_{s-2}(a_{s-1}N_s - a_s N_{s-1}) + \epsilon_{s-1}(a_s N_{s-2} - a_{s-2}N_s)$$
$$+ \epsilon_s(a_{s-2}N_{s-1} - a_{s-1}N_{s-2}), \qquad (51)$$

with

$$\gamma = a_{s-2}(N_{s-1} - N_s) + a_{s-1}(N_s - N_{s-2}) + a_s(N_{s-2} - N_{s-1}). \qquad (52)$$

The process is terminated when $|N_s|$ and $|a_s|$ differ from zero by less than a prescribed tolerance. Essentially the same procedure is applied in the case of the $y_2(x)$ and $y_4(x)$ functions, except that $N_s$ is now defined as

$$\left[1 - \int_0^\infty r^2 y_3^2(x)\, dx\right]^{1/2} - \left[\int_0^\infty r^2 y_2^2(x)\, dx\right]^{1/2} \tag{53}$$

or

$$\left[1 - \int_0^\infty r^2\{y_5^2(x) + y_6^2(x)\}\, dx\right]^{1/2} - \left[\int_0^\infty r^2 y_4^2(x)\, dx\right]^{1/2} \tag{54}$$

respectively and the associated eigenvalues are $\epsilon_{22}$ or $\epsilon_{44}$.

$y_3(x)$ is computed with a single application of the direct method—specified by equations (40) to (43)—on using the conditions $y_3(0) = y_3(m\delta x) = 0$ and $\epsilon_{33} = \epsilon_{22}$, the last value obtained for $\epsilon_{22}$ in the overall iterative procedure being used. $y_5(x)$ and $y_6(x)$ are obtained similarly but now $\epsilon_{55} = \epsilon_{44}$ or $\epsilon_{66} = \epsilon_{44}$ gives the appropriate value for the $\epsilon$ parameter.

By means of the techniques described, step (3) of the overall iterative procedure may be accomplished. As with atomic calculations, the convergence can in some instances be improved by taking as the new estimate for $y_i(x)$ not the newly computed function itself but a linear combination of this and the old estimate. In particular, the combination $(y_4)_{new} = \frac{1}{2}(y_4)_{old} + \frac{1}{2}(y_4)_{computed}$ proves beneficial. The work of Koide *et al.* [7] and Mills [4] enables good estimates of the $y_i(0)$ and $\epsilon_{ii}$ parameters to be made which ensure the success of the inverse interpolation scheme outlined.

The computations were carried out on the ACE computer at the National Physical Laboratory. The order in which the improved functions were to be computed was controlled by an external set of switches and was left to the discretion of the operator. It was found that the convergence was better if the $y_1$, $y_5$ and $y_6$ functions were allowed to settle before the others. A similar situation occurs in atomic calculations where experience shows that the outer electron functions are the most sensitive. A record was kept in the machine of the order in which iterations were performed so that unnecessary recomputations of the functions $Z_n(kl)$ and $Y_n(kl)$ could be avoided.

## 5. Results and Discussion

The results of the numerical calculations are given in table 1. The values of $P_1(r)$ to $P_6(r)$ were computed with $x = \log_e 500r$ at an interval of $\delta x = \frac{1}{12}$ and are listed at twice this interval. Calculations carried out at intervals of $\delta x = \frac{1}{4}$ and $\delta x = \frac{1}{8}$ indicate that the $P_1(r)$ function is correct to the number of figures given but that errors of a few units in the fourth significant figure exist in the $P_2(r)$ and $P_4(r)$ functions, both being somewhat too large in absolute value. The $P_3(r)$, $P_5(r)$ and $P_6(r)$ functions are too small in absolute value and are liable to errors of as much as a unit in the third decimal place in the region $r = 2$ where the absolute values are maximal. The $\epsilon_{11}$, $\epsilon_{22}$ and $\epsilon_{44}$ parameters were obtained by extrapolation from the results computed with $\delta x = \frac{1}{4}$, $\frac{1}{8}$ and $\frac{1}{12}$ and should be correct to the number of figures given.

The electronic energy $E'$ was also computed for each of these three approximations. The resulting values obtained were $-53.66$, $-53.73$ and

| | | | | | $r = A \times 10^p$ | | | | |
|---|---|---|---|---|---|---|---|---|---|
| $x$ | $A$ | $p$ | $P_1(r)$ | $P_2(r)$ | $P_3(r)$ | $P_4(r)$ | $P_5(r)$ | $P_6(r)$ |
| 0 | 2·0000 | −3 | 0·0546 | −0·0100 | — | — | — | — |
| | 2·3627 | −3 | 0·0644 | −0·0118 | — | — | — | — |
| | 2·7912 | −3 | 0·0759 | −0·0139 | — | — | — | — |
| 0·5 | 3·2974 | −3 | 0·0894 | −0·0164 | — | — | — | — |
| | 3·8955 | −3 | 0·1052 | −0·0193 | — | 0·0001 | — | — |
| | 4·6020 | −3 | 0·1238 | −0·0227 | — | 0·0001 | — | — |
| 1·0 | 5·4366 | −3 | 0·1455 | −0·0267 | — | 0·0001 | — | — |
| | 6·4225 | −3 | 0·1709 | −0·0313 | — | 0·0002 | — | — |
| | 7·5873 | −3 | 0·2004 | −0·0367 | — | 0·0002 | — | — |
| 1·5 | 8·9634 | −3 | 0·2348 | −0·0430 | — | 0·0003 | — | --- |
| | 1·0589 | −2 | 0·2748 | −0·0503 | — | 0·0005 | — | — |
| | 1·2509 | −2 | 0·3209 | −0·0588 | — | 0·0007 | — | — |
| 2·0 | 1·4778 | −2 | 0·3740 | −0·0685 | — | 0·0009 | — | — |
| | 1·7458 | −2 | 0·4348 | −0·0796 | — | 0·0013 | — | — |
| | 2·0625 | −2 | 0·5040 | −0·0922 | — | 0·0017 | — | — |
| 2·5 | 2·4365 | −2 | 0·5823 | −0·1065 | — | 0·0024 | — | — |
| | 2·8784 | −2 | 0·6700 | −0·1224 | — | 0·0033 | — | — |
| | 3·4004 | −2 | 0·7673 | −0·1401 | — | 0·0045 | — | — |
| 3·0 | 4·0171 | −2 | 0·8738 | −0·1593 | — | 0·0062 | — | — |
| | 4·7457 | −2 | 0·9886 | −0·1798 | — | 0·0085 | — | — |
| | 5·6063 | −2 | 1·1099 | −0·2013 | — | 0·0116 | — | — |
| 3·5 | 6·6231 | −2 | 1·2349 | −0·2229 | — | 0·0157 | 0·0001 | — |
| | 7·8243 | −2 | 1·3593 | −0·2438 | — | 0·0212 | 0·0001 | — |
| | 9·2433 | −2 | 1·4776 | −0·2625 | — | 0·0284 | 0·0002 | — |
| 4·0 | 1·0920 | −1 | 1·5829 | −0·2773 | — | 0·0379 | 0·0002 | — |
| | 1·2900 | −1 | 1·6667 | −0·2858 | — | 0·0501 | 0·0004 | — |
| | 1·5240 | −1 | 1·7200 | −0·2854 | — | 0·0658 | 0·0006 | — |
| 4·5 | 1·8003 | −1 | 1·7337 | −0·2732 | 0·0001 | 0·0857 | 0·0010 | — |
| | 2·1269 | −1 | 1·7000 | −0·2460 | 0·0001 | 0·1103 | 0·0016 | — |
| | 2·5126 | −1 | 1·6141 | −0·2009 | 0·0002 | 0·1405 | 0·0024 | −0·0001 |
| 5·0 | 2·9683 | −1 | 1·4758 | −0·1359 | 0·0004 | 0·1767 | 0·0037 | −0·0002 |
| | 3·5066 | −1 | 1·2911 | −0·0500 | 0·0007 | 0·2192 | 0·0058 | −0·0003 |
| | 4·1425 | −1 | 1·0726 | +0·0556 | 0·0012 | 0·2678 | 0·0087 | −0·0006 |
| 5·5 | 4·8938 | −1 | 0·8388 | 0·1772 | 0·0022 | 0·3217 | 0·0132 | −0·0010 |
| | 5·7814 | −1 | 0·6113 | 0·3085 | 0·0040 | 0·3796 | 0·0196 | −0·0018 |
| | 6·8299 | −1 | 0·4105 | 0·4402 | 0·0070 | 0·4394 | 0·0289 | −0·0033 |
| 6·0 | 8·0686 | −1 | 0·2507 | 0·5613 | 0·0123 | 0·4983 | 0·0421 | −0·0058 |
| | 9·5319 | −1 | 0·1376 | 0·6608 | 0·0213 | 0·5532 | 0·0604 | −0·0101 |
| | 1·1261 | 0 | 0·0671 | 0·7295 | 0·0358 | 0·6011 | 0·0854 | −0·0174 |
| 6·5 | 1·3303 | 0 | 0·0291 | 0·7615 | 0·0580 | 0·6386 | 0·1182 | −0·0291 |
| | 1·5715 | 0 | 0·0115 | 0·7538 | 0·0885 | 0·6610 | 0·1577 | −0·0462 |
| | 1·8566 | 0 | 0·0044 | 0·7024 | 0·1199 | 0·6580 | 0·1955 | −0·0658 |
| 7·0 | 2·1933 | 0 | 0·0019 | 0·5965 | 0·1230 | 0·6062 | 0·2043 | −0·0715 |
| | 2·5910 | 0 | 0·0009 | 0·4492 | 0·0935 | 0·5031 | 0·1756 | −0·0586 |
| | 3·0609 | 0 | 0·0004 | 0·2997 | 0·0592 | 0·3777 | 0·1315 | −0·0407 |
| 7·5 | 3·6161 | 0 | 0·0002 | 0·1758 | 0·0325 | 0·2558 | 0·0875 | −0·0250 |
| | 4·2719 | 0 | 0·0001 | 0·0895 | 0·0155 | 0·1550 | 0·0519 | −0·0137 |
| | 5·0467 | 0 | — | 0·0388 | 0·0063 | 0·0829 | 0·0271 | −0·0067 |
| 8·0 | 5·9619 | 0 | — | 0·0140 | 0·0022 | 0·0383 | 0·0123 | −0·0028 |
| | 7·0432 | 0 | — | 0·0040 | 0·0006 | 0·0150 | 0·0047 | −0·0010 |
| | 8·3205 | 0 | — | 0·0009 | 0·0001 | 0·0048 | 0·0015 | −0·0003 |
| 8·5 | 9·8295 | 0 | — | 0·0002 | — | 0·0012 | 0·0004 | −0·0001 |
| | 1·1612 | 1 | — | — | — | 0·0002 | 0·0001 | — |

Table 1. Normalized radial wave functions computed with independent variable
$x = \log_e 500r$

$$\int_0^\infty P_1{}^2 \, dr = \int_0^\infty (P_2{}^2 + P_3{}^2) \, dr = \int_0^\infty (P_4{}^2 + P_5{}^2 + P_6{}^2) \, dr = 1.$$

$E' = -53\cdot74; \qquad\qquad \epsilon_{11} = 22\cdot31; \quad \epsilon_{22} = \epsilon_{33} = 1\cdot870; \quad \epsilon_{44} = \epsilon_{55} = \epsilon_{66} = 1\cdot028.$

$-53.74$ respectively, which indicates the convergence of the approximations as $\delta x \to 0$. On adding the nuclear repulsion energy of $13.84$ A.U. to the value of $E'$ computed with $\delta x = \frac{1}{12}$, a calculated total energy of $-39.90$ A.U. is obtained for the methane molecule. This is slightly lower than the value of $-39.85$ A.U. obtained by Saturno and Parr [5]† who assumed a linear combination of determinants for the total wave function rather than a single determinant as in the present work. The improvement is presumably due to the use of numerical as opposed to analytic radial functions. The observed experimental energy is given in [5] as $-40.52$ A.U.

A comparison of their own work with that of Mills [4] led Saturno and Parr [5] to conjecture that the energy value obtained by Mills for the spherical model was too high by about $0.2$ A.U. This approximation has been re-examined and an energy value of $-39.53$ A.U. obtained, which is $0.15$ A.U. lower than the value of $-39.38$ A.U. given by Mills. A direct comparison between the present calculation and that of Mills is not possible as Mills did not transform the variables in the manner discussed in §4. It seems likely, however, that the intervals he used in the numerical procedures were not small enough to determine a sufficiently accurate solution. In this connection it is interesting to note that, in the present calculation of the spherical model, the eigenvalues obtained with $\delta x = \frac{1}{4}$ are $22.165$, $1.787$ and $0.894$ whilst with $\delta x = \frac{1}{12}$ they become $22.170$, $1.796$ and $0.903$. Extrapolated values from results obtained with $\delta x = \frac{1}{4}$, $\frac{1}{8}$ and $\frac{1}{12}$ are $22.171$, $1.797$ and $0.904$ whereas the values quoted by Mills are $22.09$, $1.787$ and $0.902$. The discrepancy between the first two eigenvalues is quite large.

## Appendix 1

The normal electronic energy $E'$ is given by

$$E' = 2I(1a_1) + 2I(2a_1) + 6I(2t_{2x}) + \sum a_n(ij:kl)I_n(ij:kl). \tag{55}$$

The numerical coefficients $a_n(ij:kl)$, together with the values (computed for $\delta x = \frac{1}{12}$) of the various integrals occurring in the above expression, are given in table 2. Koide *et al.* [7] derive a similar energy expression to (55). Apart from a few sign changes, which are accounted for by a printing error in the definition of the $\psi(2a_1)$ orbital, nine of the coefficients given in [7] differ from those listed in table 2. The differences occur in the coefficients of the integrals $I_2(44:55)$, $I_2(55:66)$, $I_2(55:46)$, $I_6(66:66)$, $I_2(46:66)$, $I_2(46:46)$, $I_6(36:36)$, $I_1(45:45)$ and $I_2(44:46)\ddagger$. Because of these differences, the energy value computed in [7] is too high. An estimate of the correction necessary may be obtained by using the final analytic radial functions given by Koide and his colleagues to evaluate the terms which

† The value $-39.80$ given in [5] has been subsequently amended by Saturno and Parr to $-39.85$.

‡ The integral $I_2(44:46)$ does not appear in table 2 as its coefficient is zero.

| $n : ij : kl$ | $a_n(ij : kl)$ | $I_n(ij : kl)$ | $n : ij : kl$ | $a_n(ij : kl)$ | $I_n(ij : kl)$ | $n : ij : kl$ | $a_n(ij : kl)$ | $I_n(ij : kl)$ |
|---|---|---|---|---|---|---|---|---|
| $0 : 11 : 11$ | $1$ | $3{\cdot}502$ | $0 : 44 : 44$ | $15$ | $0{\cdot}402$ | $0 : 12 : 12$ | $-2$ | $0{\cdot}039$ |
| $0 : 11 : 22$ | $4$ | $0{\cdot}724$ | $2 : 44 : 44$ | $-\dfrac{6}{5}$ | $0{\cdot}189$ | $3 : 13 : 13$ | $-\dfrac{2}{7}$ | $0{\cdot}000_0$ |
| $0 : 11 : 33$ | $4$ | $0{\cdot}009$ | $0 : 44 : 55$ | $30$ | $0{\cdot}026$ | $1 : 14 : 14$ | $-2$ | $0{\cdot}035$ |
| $0 : 11 : 44$ | $12$ | $0{\cdot}612$ | $2 : 44 : 55$ | $-\dfrac{12}{35}$ | $0{\cdot}013$ | $2 : 15 : 15$ | $-\dfrac{6}{5}$ | $0{\cdot}000_1$ |
| $0 : 11 : 55$ | $12$ | $0{\cdot}032$ | $0 : 44 : 66$ | $30$ | $0{\cdot}003$ | $3 : 16 : 16$ | $-\dfrac{6}{7}$ | $0{\cdot}000_0$ |
| $0 : 11 : 66$ | $12$ | $0{\cdot}003$ | $2 : 44 : 66$ | $-\dfrac{2}{5}$ | $0{\cdot}001$ | $1 : 24 : 24$ | $-2$ | $0{\cdot}287$ |
| $0 : 22 : 22$ | $1$ | $0{\cdot}508$ | $0 : 55 : 55$ | $15$ | $0{\cdot}002$ | $1 : 35 : 35$ | $-\dfrac{6}{7}$ | $0{\cdot}000_4$ |
| $0 : 22 : 33$ | $2$ | $0{\cdot}008$ | $2 : 55 : 55$ | $-\dfrac{30}{49}$ | $0{\cdot}001$ | $1 : 24 : 35$ | $-4\sqrt{\dfrac{3}{7}}$ | $0{\cdot}010$ |
| $0 : 33 : 33$ | $1$ | $0{\cdot}000_2$ | $4 : 55 : 55$ | $-\dfrac{20}{147}$ | $0{\cdot}000_7$ | $2 : 25 : 25$ | $-\dfrac{6}{5}$ | $0{\cdot}012$ |
| $3 : 23 : 23$ | $\dfrac{4}{7}$ | $0{\cdot}003$ | $0 : 55 : 66$ | $30$ | $0{\cdot}000_2$ | $2 : 34 : 34$ | $-\dfrac{18}{35}$ | $0{\cdot}004$ |
| $4 : 33 : 33$ | $\dfrac{28}{363}$ | $0{\cdot}000_1$ | $2 : 55 : 66$ | $\dfrac{22}{35}$ | $0{\cdot}000_1$ | $2 : 36 : 36$ | $-\dfrac{8}{15}$ | $0{\cdot}000_0$ |
| $6 : 33 : 33$ | $\dfrac{800}{20449}$ | $0{\cdot}000_1$ | $4 : 55 : 66$ | $-\dfrac{100}{77}$ | $0{\cdot}000_1$ | $2 : 25 : 34$ | $-\dfrac{12}{5}\sqrt{\dfrac{3}{7}}$ | $0{\cdot}007$ |
| $0 : 22 : 44$ | $12$ | $0{\cdot}450$ | $2 : 55 : 46$ | $\dfrac{144}{35}\sqrt{\dfrac{3}{7}}$ | $-0{\cdot}001$ | $2 : 25 : 36$ | $\dfrac{8}{5}$ | $-0{\cdot}000_6$ |
| $3 : 23 : 45$ | $\dfrac{48}{7}\sqrt{\dfrac{3}{7}}$ | $0{\cdot}005$ | $4 : 55 : 46$ | $-\dfrac{200}{63}\sqrt{\dfrac{3}{7}}$ | $-0{\cdot}000_8$ | $2 : 34 : 36$ | $\dfrac{8}{5}\sqrt{\dfrac{3}{7}}$ | $-0{\cdot}000_3$ |
| $0 : 22 : 55$ | $12$ | $0{\cdot}029$ | $0 : 66 : 66$ | $15$ | $0{\cdot}000_0$ | $3 : 26 : 26$ | $-\dfrac{6}{7}$ | $0{\cdot}001$ |
| $3 : 23 : 56$ | $-\dfrac{32}{7}$ | $-0{\cdot}000_5$ | $2 : 66 : 66$ | $-\dfrac{7}{30}$ | $0{\cdot}000_0$ | $3 : 35 : 35$ | $-\dfrac{8}{21}$ | $0{\cdot}000_3$ |
| $0 : 22 : 66$ | $12$ | $0{\cdot}003$ | $6 : 66 : 66$ | $-\dfrac{2125}{11154}$ | $0{\cdot}000_0$ | $3 : 26 : 35$ | $\dfrac{8}{7}$ | $-0{\cdot}000_5$ |
| $0 : 33 : 44$ | $12$ | $0{\cdot}008$ | $2 : 46 : 66$ | $-\dfrac{12}{5}\sqrt{\dfrac{3}{7}}$ | $-0{\cdot}000_1$ | $4 : 34 : 34$ | $-\dfrac{8}{21}$ | $0{\cdot}002$ |
| $4 : 33 : 46$ | $-\dfrac{224}{99}\sqrt{\dfrac{3}{7}}$ | $-0{\cdot}000_2$ | $4 : 46 : 66$ | $\dfrac{100}{33}\sqrt{\dfrac{3}{7}}$ | $-0{\cdot}000_1$ | $4 : 36 : 36$ | $-\dfrac{2}{121}$ | $0{\cdot}000_0$ |
| $0 : 33 : 55$ | $12$ | $0{\cdot}000_5$ | $3 : 45 : 45$ | $\dfrac{684}{245}$ | $0{\cdot}010$ | $4 : 34 : 36$ | $\dfrac{8}{33}\sqrt{\dfrac{3}{7}}$ | $-0{\cdot}000_2$ |
| $4 : 33 : 55$ | $\dfrac{16}{33}$ | $0{\cdot}000_2$ | $3 : 45 : 56$ | $-\dfrac{424}{35}\sqrt{\dfrac{3}{7}}$ | $-0{\cdot}000_9$ | $5 : 35 : 35$ | $-\dfrac{680}{2541}$ | $0{\cdot}000_2$ |
| $0 : 33 : 66$ | $12$ | $0{\cdot}000_1$ | $2 : 46 : 46$ | $-\dfrac{108}{35}$ | $0{\cdot}001$ | $6 : 36 : 36$ | $-\dfrac{11200}{61347}$ | $0{\cdot}000_0$ |
| $4 : 33 : 66$ | $-\dfrac{56}{121}$ | $0{\cdot}000_0$ | $4 : 46 : 46$ | $\dfrac{50}{21}$ | $0{\cdot}000_8$ | $1 : 45 : 45$ | $-\dfrac{24}{5}$ | $0{\cdot}016$ |
| $6 : 33 : 66$ | $\dfrac{4000}{20449}$ | $0{\cdot}000_0$ | $3 : 56 : 56$ | $\dfrac{394}{105}$ | $0{\cdot}000_1$ | $1 : 56 : 56$ | $-\dfrac{72}{35}$ | $0{\cdot}000_1$ |
| | | | $5 : 56 : 56$ | $-\dfrac{2500}{2541}$ | $0{\cdot}000_1$ | $1 : 45 : 56$ | $\dfrac{48}{5}\sqrt{\dfrac{3}{7}}$ | $-0{\cdot}001$ |

Table 2.

$I(1a_1) = -19{\cdot}931;\quad I(2a_1) = -5{\cdot}529;\quad I(2t\ ) = \ {\cdot}4{\cdot}885;\quad F' \ \ 52{\cdot}737$

differ in the two energy expressions. The integrals involved may be evaluated analytically and a simple calculation then made to compute the change in the energy value. This indicates that the energy value of $-39\cdot64$ A.U. quoted in [7] should be lowered by $0\cdot16$ A.U.

Of course, the parameters occurring in the radial functions for this calculation were obtained by minimizing an energy expression which contained errors rather than the amended version. This merely means that the energy value for the approximation used in [7] should be at least as low as $-39\cdot80$ A.U.

## APPENDIX 2

In atomic structure calculations with closed-shell configurations it is shown by Hartree ([1], §3.8) that the 'non-diagonal' parameters $\epsilon_{ij}$ $(i \neq j)$ may be taken as zero without loss of generality. The analysis which leads to this conclusion in the atomic case is not applicable, however, in the present instance. It can be shown for the variational equations under consideration that

$$
\begin{aligned}
(\epsilon_{11} - \epsilon_{22}) \int_0^\infty P_1 P_2 \, dr = \epsilon_{12} &\int_0^\infty P_3^2 \, dr + \left(\frac{1}{\pi}\right)^{1/2} \int_0^\infty V_3(r) P_1 P_3 \, dr - 2I_0(12:33) \\
&+ \frac{6}{7} I_3(13:23) + \frac{24}{7}\sqrt{\frac{3}{7}} I_3(13:45) - \frac{16}{7} I_3(13:56) \\
&- 2\sqrt{\frac{3}{7}} I_1(14:35) - \frac{6}{5}\sqrt{\frac{3}{7}} I_2(15:34) + \frac{4}{5} I_2(15:36) \\
&+ \frac{4}{7} I_3(16:35). \quad (56)
\end{aligned}
$$

In an atomic-type calculation there would be no term corresponding to $P_3(r)$ and consequently $\int_0^\infty P_1 P_2 \, dr$ would be zero irrespective of the value given to $\epsilon_{12}$. In the molecular case this is not so and, indeed, calculations for various values of $\epsilon_{12}$ indicate that a value close to $0\cdot078$ is required to satisfy the orthogonality condition exactly.

The radial functions obtained with $\epsilon_{12} = 0\cdot0784$, however, are such that no substantial change is made in the resulting determinantal wave function. The functions $P_3(r)$ to $P_4(r)$ obtained with this value of $\epsilon_{12}$ remain as listed in table 1 whilst the new $P_1(r)$ and $P_2(r)$ functions are essentially linear combinations of the values obtained for these functions with $\epsilon_{12} = 0$. Thus, to four decimal places,

$$
P_1(r)|_{\epsilon=0\cdot0784} = P_1(r)|_{\epsilon=0} - 0\cdot0038 P_2(r)|_{\epsilon=0}, \quad (57)
$$

and

$$
P_2(r)|_{\epsilon=0\cdot0784} = P_2(r)|_{\epsilon=0} + 0\cdot0038 P_1(r)|_{\epsilon=0}. \quad (58)
$$

The change in the $P_2(r)$ function leaves the value of the determinantal wave function unaltered since it is equivalent to replacing $\psi(2a_1)$ as given in equation (5) by $\psi(2a_1) + 0\cdot0038\psi(1a_1)$. The change in the $P_1(r)$ function is equivalent to replacing $\psi(1a_1)$ by $\psi(1a_1) - 0\cdot0038\psi(2a_1)$ apart from the term

$$
-0\cdot0038 \left(\frac{105}{4\pi}\right)^{1/2} P_3(r) xyz/r,
$$

the maximum modulus of which does not exceed $0\cdot00014$ and may be neglected.

The resulting energy value differs from that obtained with $\epsilon_{12} - 0$ by only four units in the fifth decimal place. The values of $\epsilon_{11}$, $\epsilon_{22}$ and $\epsilon_{44}$ remain as given in table 1.

Equation (56) takes on a simpler form if the third-order harmonic term which has been omitted from the $\psi(1a_1)$ expansion is incorporated. Thus if $\psi(1a_1)$ is redefined by

$$r\psi(1a_1) = \left(\frac{1}{4\pi}\right)^{1/2} P_1(r) + \left(\frac{105}{4\pi}\right)^{1/2} P_7(r)xyz, \qquad (59)$$

so that it is analogous to the $r\psi(2a_1)$ expansion, an additional orthogonality condition, $\int_0^\infty P_3 P_7 \, dr = 0$, must be satisfied together with the normalization condition $\int_0^\infty (P_1^2 + P_7^2) \, dr = 1$ rather than $\int_0^\infty P_1^2 \, dr = 1$. There will now be a parameter $\epsilon_{37}$ in the seven variational equations for $P_1(r)$ to $P_7(r)$ and from these can be derived the simpler result that

$$(\epsilon_{11} - \epsilon_{22}) \int_0^\infty (P_1 P_2 + P_3 P_7) \, dr = (\epsilon_{12} - \epsilon_{37}) \int_0^\infty (P_3^2 - P_7^2) \, dr. \qquad (60)$$

It follows from (60) that to make $\int_0^\infty P_1 P_2 \, dr$ and $\int_0^\infty P_3 P_7 \, dr$ simultaneously zero, $\epsilon_{12}$ and $\epsilon_{37}$ must be equal. Since $P_3(r)$ and $P_7(r)$ will both be small $\epsilon_{12} = \epsilon_{37} = 0$ will be a good approximation to the required value.

## REFERENCES

[1] HARTREE, D. R., 1957, *The Calculation of Atomic Structures* (New York: John Wiley & Sons).
[2] BUCKINGHAM, R. A., MASSEY, H. S. W., and TIBBS, S. R., 1941, *Proc. roy. Soc. A*, **178**, 119.
[3] BERNAL, M. J. M., 1953, *Proc. phys. Soc., Lond. A*, **66**, 514.
[4] MILLS, I. M., 1958, *Mol. Phys.*, **1**, 99.
[5] SATURNO, A. F., and PARR, R. G., 1960, *J. chem. Phys.*, **33**, 22.
[6] CARTER, C., 1956, *Proc. roy. Soc. A*, **235**, 321.
[7] KOIDE, S., SEKIYAMA, H., and NAGASHIMA, T., 1957, *J. phys. Soc. Japan*, **12**, 1016.
[8] MULLIKEN, R. S., 1933, *J. chem. Phys.*, **1**, 492.
[9] CONDON, E. U., and SHORTLEY, G. H., 1935, *The Theory of Atomic Spectra* (Cambridge: University Press).
[10] WORSLEY, B. H., 1958, *Canad. J. Phys.*, **36**, 289.
[11] MAYERS, D. F., 1960 (private communication).
[12] NUMEROV, B., 1933, *Publs. observatoire central astrophys. Russ.*, **2**, 188.
[13] WARNER, F. J., 1957, *Math. Tab., Wash.*, **11**, 268.

# A proton magnetic resonance investigation of some weak interactions in solution

by R. J. ABRAHAM

Basic Physics Division, National Physical Laboratory, Teddington, Middlesex†

*(Received 6 May 1961)*

The proton chemical shifts of cyclohexane, methyl iodide and iodoform are measured in a number of solvents. A complete calculation of the contribution to the solute proton chemical shift arising from the magnetic anisotropy of cylindrically symmetric solvents is given. Although the formula predicts the direction of the observed shifts, the observed values for non-polar solutes are always much larger than the calculated values. Some possible reasons for this are given and discussed.

The variation of the proton chemical shifts of the polar solutes methyl iodide and iodoform in aliphatic solvents are shown to agree with present theories of these effects. However, in aromatic solvents considerable deviations from the theoretical line are found and these are postulated to arise from solute solvent complexes in which the dipole axis of the solute lies along the hexagonal axis of symmetry of the benzene ring with the protons towards the ring. From the variation of the proton chemical shifts of methyl iodide and iodoform in toluene solution with temperature the following parameters were obtained. For the methyl iodide toluene complex the energy and entropy of formation are $1 \cdot 3 \pm 0 \cdot 5$ kcals/mole and $4 \cdot 9 \pm 0 \cdot 4$ e.u. respectively. For the iodoform toluene complex the corresponding values are $1 \cdot 6 \pm 0 \cdot 2$ kcals/mole and $6 \cdot 4 \pm 0 \cdot 2$ e.u.

---

## 1. INTRODUCTION

High resolution proton magnetic resonance spectroscopy has been used for some time to study interactions in liquids [1]. Strong interactions can be investigated by many other techniques; however, weak interactions, which are very difficult to investigate by other methods, can be studied quite easily by P.M.R. An example of this is the complex formed between chloroform and mesitylene which was investigated using P.M.R. and other techniques by Reeves and Schneider [2]. Similar complexes have been postulated to occur between aromatic solvents and solutes such as N.N. dimethylformamide [3] and substituted acetylenes [4] on the basis of the dilution shifts of the protons in these solutes.

However, these investigations did not take into account all the factors which may affect the solute proton shifts. Four possible mechanisms have recently been discussed [5].

These are (*a*) the solvent bulk susceptibility, (*b*) the solvent magnetic anisotropy, (*c*) Van der Waals interactions and (*d*) for polar solutes the reaction field [6] of the solvent. Of these four effects (*a*) and (*d*) were evaluated, (*c*) is not a large factor for many solvents, but (*b*) which is appreciable in many cases was only discussed qualitatively. However, for those solvents in which effects (*b*) and (*c*) could be ignored, (*a*) and (*d*) did explain the observed results. The

† Present address: Organic Chemistry Department, University of Liverpool, Liverpool.

2 A

M.P.

reaction field theory was extended to include anisotropic solvents by comparing directly the shifts of a non-polar solute and a polar solute in a given solvent. This procedure removes effect (*b*) (assuming that this is constant for the two solutes considered) and gave good agreement with the observed results for all but one solvent, benzene, in which it was postulated solvent solute complexing occurred [7].

In the present paper these procedures are used to investigate the dilution shifts of some polar and non-polar solutes in a variety of solvents, and in addition effect (*b*) is calculated explicitly for cylindrical solvent molecules.

## 2. EXPERIMENTAL

The proton chemical shifts of cyclohexane, methyl iodide and iodoform were measured in dilute solution in a number of solvents on a Varian 60 Mc/s spectrometer. The solutes were measured in the same solution of each solvent. The concentration of each of the solutes was estimated to vary between 3 and 5 per cent by weight, sufficiently low to be considered as infinite dilution. The chemical shifts were measured from a dioxane external reference by the sideband technique, the reproducibility of the measurements being always better than $\pm 0.2$ c.p.s. The results of these measurements are shown in the first three columns of table 1, and in the fourth column the observed chemical shifts of the cyclohexane protons have been corrected for the difference in the bulk susceptibility between the solvent and the dioxane reference. The values of the solvent volume susceptibilities have been taken from ref. [5] except those for dioxane $(-\chi_v = 0.589 \times 10^{-6})$ [8] and $o$-dichlorobenzene $(-\chi_v = 0.782 \times 10^{-6}$ from Pascal's constants).

## 3. RESULTS AND DISCUSSION

Buckingham *et al.* [5] have discussed the dilution shifts of non-polar solutes in normal (i.e. non-anisotropic) solvents in terms of the Van der Waals interactions between the solvent and solute. The procedure they used to remove the bulk susceptibility corrections was identical to that used here. However, this procedure can introduce considerable errors.

Apart from the error due to the inaccuracies in the solvent bulk susceptibilities there is also a significant error in correcting for the solvent, not solution, susceptibility; e.g. the error involved in this procedure in a 5 per cent (v/v) solution of methyl iodide in $n$-hexane is 2 c.p.s. When this is taken into account, the observed shifts of a non-polar solute in normal solvents are almost constant, within the experimental error; e.g. the cyclohexane chemical shifts for all the normal solvents in table 1 are grouped around the value of 128 c.p.s. with a mean deviation of 2 c.p.s. Similarly all the normal solvents in [5] give a methane chemical shift of $-10$ c.p.s. relative to the methane gas value, with a mean deviation of 3 c.p.s.

This suggests that the effect of the Van der Waals interactions on the chemical shifts of non-polar solutes in normal liquids is either very small or essentially constant. The term normal used here includes all solvents except aromatic solvents, linear molecules, acetylenic compounds and nitro compounds. In contrast to the results of [5], halogenated compounds behave normally in this investigation.

| Solvent | $C_6H_{12}$ | $CH_3I$ | $CHI_3$ | $C_6H_{12}$ (corrected) | $CH_3I–C_6H_{12}$ | | $CHI_3–C_6H_{12}$ | |
|---|---|---|---|---|---|---|---|---|
| | | | | | Direct | Adjusted | Direct | Adjusted |
| 1. *n*-Hexane | 129·8 | 94·3 | − 76·9 | 129·4 | − 35·5 | 0 | − 206·7 | 0 |
| 2. Cyclohexane | 127·9 | 93·9 | − 75·2 | 133·2 | − 34·0 | 1·5 | − 203·1 | 3·6 |
| 3. C Cl₄ | 113·5 | 70·4 | − 94·7 | 125·4 | − 43·1 | − 7·6 | − 208·2 | − 1·5 |
| 4. CS₂ | 105·6 | 61·6 | −102·2 | 117·2 | − 44·0 | − 8·5 | − 207·8 | − 1·1 |
| 5. CH Cl₃ | 109·4 | 64·7 | − 99·9 | 127·2 | − 44·7 | − 9·2 | − 209·3 | − 2·6 |
| 6. CH₂Cl₂ | 109·0 | 64·4 | −101·3 | 127·1 | − 44·6 | − 9·1 | − 210·3 | − 3·6 |
| 7. Acetone | 146·6 | 100·9 | − 87·2 | 130·4 | − 45·5 | − 10·0 | − 233·8 | − 27·1 |
| 8. Acetonitrile | 132·6 | 88·4 | − 82·9 | 119·7 | − 44·2 | − 8·7 | − 215·5 | − 7·8 |
| 9. Benzene | 151·5 | 148·2 | − 4·3 | 157·4 | − 3·3 | 32·2 | − 155·8 | 50·9 |
| 10. Toluene | 147·3 | 140·7 | 5·9 | 152·6 | − 6·6 | 28·9 | − 153·2 | 53·5 |
| 11. Chlorobenzene | 138·1 | 117·0 | − 45·6 | 152·9 | − 21·1 | 14·4 | − 183·7 | 23·0 |
| 12. *o*-Dichlorobenzene | 127·2 | 94·8 | − 71·2 | 151·4 | − 32·4 | 3·1 | − 198·4 | 8·3 |
| 13. Benzaldehyde | 166·5 | 129·5 | − 60·1 | 168·1 | − 37·0 | 1·5 | − 226·6 | − 19·9 |
| 14. Benzonitrile | 150·5 | 109·3 | − 71·0 | 158·7 | − 41·2 | − 5·7 | − 221·5 | − 14·8 |
| 15. Nitrobenzene | 163·2 | 120·0 | − 57·0 | 164·3 | − 43·2 | − 7·7 | − 220·2 | − 13·5 |

Table 1.  Proton chemical shifts of cyclohexane, methyl iodide and iodoform in various solvents (in c.p.s. at 60 Mc/s from a dioxane external reference).

R. J. Abraham

| Solute | Cyclohexane | CH₃X | | | CH₂X₂ | | | CHX₃ | | |
|---|---|---|---|---|---|---|---|---|---|---|
| | | Chloride | Bromide | Iodide | Chloride | Bromide | Iodide | Chloride | Bromide | Iodide |
| Benzene | 155·3 | 103·5 | 125·3 | 154·1 | −18·6 | 0·3 | 62·5 | −130·4 | −107·8 | 3·7 |
| Cyclohexane | 129·7 | 45·4 | 67·8 | 95·5 | −91·8 | −71·0 | −10·0 | −210·0 | −187·4 | −73·8 |
| Difference | 25·6 | 58·1 | 57·5 | 58·6 | 73·2 | 71·3 | 72·5 | 79·6 | 79·6 | 77·5 |

Table 2.   Proton chemical shifts of various solutes in benzene and cyclohexane (in c.p.s. at 60 Mc/s from an external dioxane reference).

We will now consider the solute shift due to the magnetic anisotropy of certain solvents. Although this effect has been recognized for some time, various estimates of this shift have been given; e.g. the high field shift due to this effect in benzene has been quoted as $0.6 \pm 0.05$ p.p.m. [8] and $0.33$ p.p.m. [5]. This is due to the difficulty of isolating this particular contribution from the total shift. The procedure which will be adopted here is to compare directly the shift of a non-polar solute in the anisotropic solvent to be studied with that of the same solute in a similarly constituted normal solvent of identical bulk susceptibility. This procedure removes the contributions due to the bulk susceptibility corrections and the Van der Waals interactions and thus the errors introduced in correcting for them separately in the two solvents.

To estimate this effect in benzene, the normal solvent used as a standard was cyclohexane. This gives for (a) cyclohexane itself as solute a high field shift of $25.6$ c.p.s., i.e. $0.43$ p.p.m. (table 2) and (b) methane as solute $25.3$ c.p.s., i.e. $0.42$ p.p.m. [5]. Similarly for carbon disulphide we take carbon tetrachloride as the standard and obtain for (a) cyclohexane a low field shift of $7.9$ c.p.s., i.e. $0.13$ p.p.m. (table 1) and (b) methane $8.4$ c.p.s., i.e. $0.14$ p.p.m. [5]. Thus, although this procedure does not eliminate the errors due to the uncertainties in the solvent bulk susceptibilities it does provide a consistent set of values which are obtained directly from accurate chemical shift measurements. The benzene shift compares very well with the two previous determinations, but the carbon disulphide shift is considerably lower than the only other quoted value $(-0.5$ p.p.m.) [5].

Two calculations of this effect have been given, both for the simple case, which will be considered here, of a cylindrically symmetric solvent molecule. That by Bothner-By and Glick [8] calculates the average field over the faces of the solvent cylinder but does not include the effect of the sides. Thus this calculation predicts a high field shift for all anisotropic solvents, in contrast with observation. That of Buckingham *et al.* [5] averages separately the radial and angular dependence of the magnetic field and thus can only be regarded as a qualitative picture.

We consider a molecule with different magnetic susceptibilities $\chi_{\parallel}$ and $\chi_{\perp}$ along and perpendicular to the cylinder axis. These can be considered as arising from an equivalent dipole pointing along the cylinder axis. Effect (b) is the average field over the surface of the molecule due to this equivalent dipole. For a molecule of radius $r$ (Å) and height $2h$ (Å), this equivalent dipole procedure gives

$$\delta = 10^{30} \times \tfrac{2}{3}(\chi_{\perp} - \chi_{\parallel}) \frac{r-h}{(r+2h)(r^2+h^2)^{3/2}}, \tag{1}$$

where $\delta$ is the shift in p.p.m. For benzene the dipole procedure also gives

$$\tfrac{2}{3}(\chi_{\perp} - \chi_{\parallel}) = \frac{e^2 a^2}{mc^2},$$

where $a$ is the radius of the benzene ring. For $a = 1.4$ Å equation (1) becomes

$$\delta = 54.4 \frac{r-h}{(r+2h)(r^2+h^2)^{3/2}}. \tag{2}$$

The benzene molecule may be considered as a cylinder of radius $3.4$ Å and half-height $1.5$ Å [9]. Including the Van der Waals radius of the solute proton $(0.9$ Å), the dimensions of the cylinder over which the solute proton moves

become 4·3 and 2·6 Å respectively. These values give a calculated shift from (2) of 0·08 p.p.m. The shift obtained by Bothner-By and Glick [8] was 1·51 p.p.m., using the dimensions of the benzene molecule. (The value in [8] has been multiplied by $4\pi$ to get this figure. There is now agreement that this is the correct figure†.) This may be compared with the corresponding value of 0·34 p.p.m. given by equation (2), thus showing the pronounced effect of including the cylinder sides.

For carbon disulphide $\chi_\perp - \chi_\parallel$ equals $5 \times 10^{-29}$ [5] and the molecular dimensions are 1·60 Å radius and 3·16 Å half-height. Thus the cylinder dimensions are 2·5 Å and 4·06 Å respectively. These values give a calculated shift of $-0·046$ p.p.m. Thus although equation (1) gives the correct qualitative picture, the calculated shifts for the most reasonable value of the inter-molecular distances are much too small.

There are several possible reasons for this.

First there is the possibility that the procedure used to obtain equation (1) may not be valid. It has been shown that the equivalent dipole procedure is a good model for the distances considered here. Thus it is very unlikely that the approximations in the model could account for any but a small fraction of the discrepancy between the observed and calculated shifts.

Secondly there is the approximation involved in using the above values of the Van der Waals distances.

These values are the mean value of a distribution of interatomic distances in the liquid. As the chemical shift of the solute protons is proportional to $1/r^3$, the effect of the smaller distances will be much more noticeable in calculating these shifts than in estimating bulk properties of the liquid. This will tend to make the calculated shift based on the average value of $r$ lower than the correct figure. This is to some extent compensated for by the fact that the mean distances are all taken from measurements of the solid state which in the examples considered here is more dense than the liquid. Thus the mean values of the interatomic distances in the liquid are larger than the values given. It is difficult to estimate these effects but again it is hard to see these influencing the calculated values by the required amount.

A more serious approximation is that the above procedure calculates the shift due to only one solvent molecule, the one immediately adjacent to the solute proton considered. The other solvent molecules surrounding the solute molecule will also produce shifts at the solute proton considered, which will all have the same sign as that of the nearest solvent molecule. This will increase the calculated shift by a considerable factor, which again would be very difficult to estimate, depending on the number of solvent molecules around the solute, etc., but may well be the reason for a large part of the difference between the observed and calculated shifts.

There is also the possibility that the solvent molecules are not packed in a completely random fashion around the solute molecule in these solutions. This will depend on both the types of interaction present in the medium (e.g. solute solvent and solvent solvent) and also on the size and shape of the molecules considered, and would affect very markedly the solute chemical shifts. However it is difficult to see on this mechanism why the solutes, methane and cyclohexane,

† A. A. Bothner-By (private communication).

which are of very different size and shape, should give the same high field shift in benzene as compared with cyclohexane as solvent.

### 3.1. *Polar solutes*

We are now in a position to discuss the results for the polar solutes methyl iodide and iodoform. These results depend on the following breakdown of the chemical shifts of polar solutes in anisotropic as compared to isotropic solvents. It is assumed that the total shift is made up of two parts. Firstly, a non-specific effect due to the averaging of the solvent magnetic anisotropy over its surface, i.e. the effect which gives rise to the shifts of the non-polar solutes discussed in the preceding section; and in addition an effect which is due to the polar nature of the solute and also any specific interactions. The further approximation is made that the non-specific effect is not very dependent on the particular solute considered. This approximation is supported by the fact that this non-specific effect is constant for the two very different solutes methane and cyclohexane.

Thus by referring the chemical shifts of the polar solutes considered to that of cyclohexane in the same solution (i.e. by using cyclohexane as an internal reference), not only are the bulk susceptibility corrections eliminated but also the non-specific part of the solute chemical shifts. The assumptions made above can be considered as providing a reasonable working basis for discussing the chemical shifts of polar solutes in anisotropic liquids. The extent to which they are justified will be demonstrated by the results in this section. The chemical shifts of the solutes iodoform and methyl iodide from the internal reference cyclohexane are given in columns five and seven of table 1, and in columns six and eight, the solute shift in $n$-hexane is taken as zero. This merely removes a constant factor in each of the two cases. The variation of the solute shifts in the different solvents is seen to be quite large. For these polar solutes, some of this variation will be due to the variation of the reaction field of the solvent as the dielectric constant of the solvent is increased. This effect can be calculated by the equation derived by Diehl and Freeman [10], which modifies the Buckingham theory [6] by taking account of the shape of the solute molecule. This can be written as

$$\sigma E = -5 \cdot 76 \times 10^{-4} \frac{\mu \cos \theta}{abc} \xi_a [1 + (n^2 - 1) \xi_a] \frac{\epsilon - 1}{\epsilon + (n^2 \xi_a / 1 - \xi_a)}$$

where $\sigma E$ is in c.p.s. at 60 Mc s, $a$, $b$ and $c$ are the semi-axes of the solute ellipsoid, $\mu$ and $n$ are the dipole moment and the refractive index of the solute respectively, $\theta$ is the angle between the X–H bond of the solute proton considered and the dipole axis, $\epsilon$ is the dielectric constant of the solvent, and $\xi_a$ a solute shape factor.

For iodoform, the molecular distances are $a$ (2·24 Å), $b$, $c$ (3·78 Å). $\xi_a$ was estimated from the data of Ross and Sack [11] as 0·47. Also $n^2 = 3 \cdot 24$, $\mu = 0 \cdot 80^D$, $\cos \theta = 1$. Thus equation (3) becomes

$$\sigma E = -13 \cdot 9 \times \frac{\epsilon - 1}{\epsilon + 2 \cdot 88}.$$

For methyl iodide, $a = 2 \cdot 58$ Å, $b = c = 1 \cdot 93$ A, $\xi_a = 0 \cdot 26$, $n^2 = 2 \cdot 34$, $\mu = 1 \cdot 62^D$ and $\cos \theta = \frac{1}{3}$. Now

$$\sigma E = -11 \cdot 4 \times \frac{\epsilon - 1}{\epsilon + 0 \cdot 82}.$$

The calculated lines are shown together with the observed solvent shifts plotted against $(\epsilon - 1)/(\epsilon + \beta)$ in figures 1 and 2.

We will consider first the results for methyl iodide as solute (figure 1). The aliphatic solvents (Nos. 1 to 8) all agree reasonably well with the calculated line. Thus the chemical shifts of the polar solute methyl iodide in
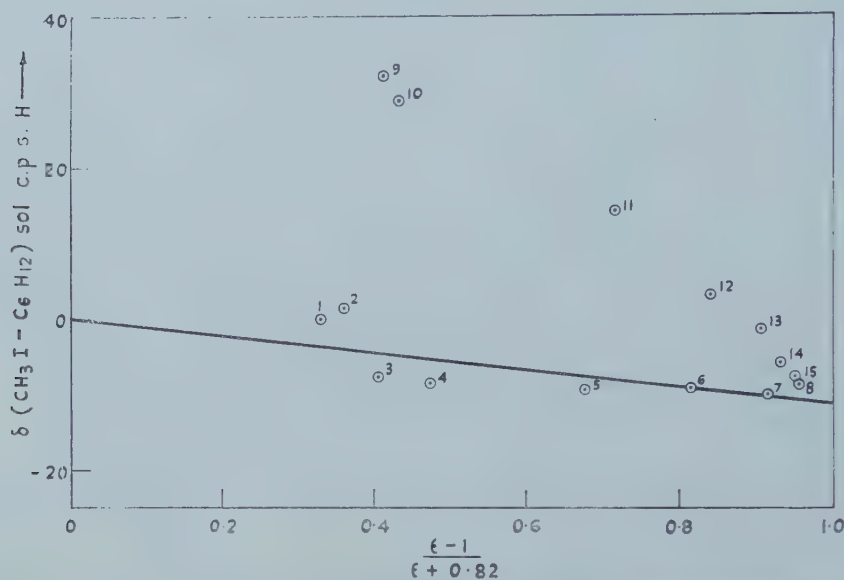


Figure 1. Plot of the proton resonance shift of methyl iodide in various solvents (in c.p.s. at 60 Mc/s) against $(\epsilon-1)/(\epsilon+0.82)$.
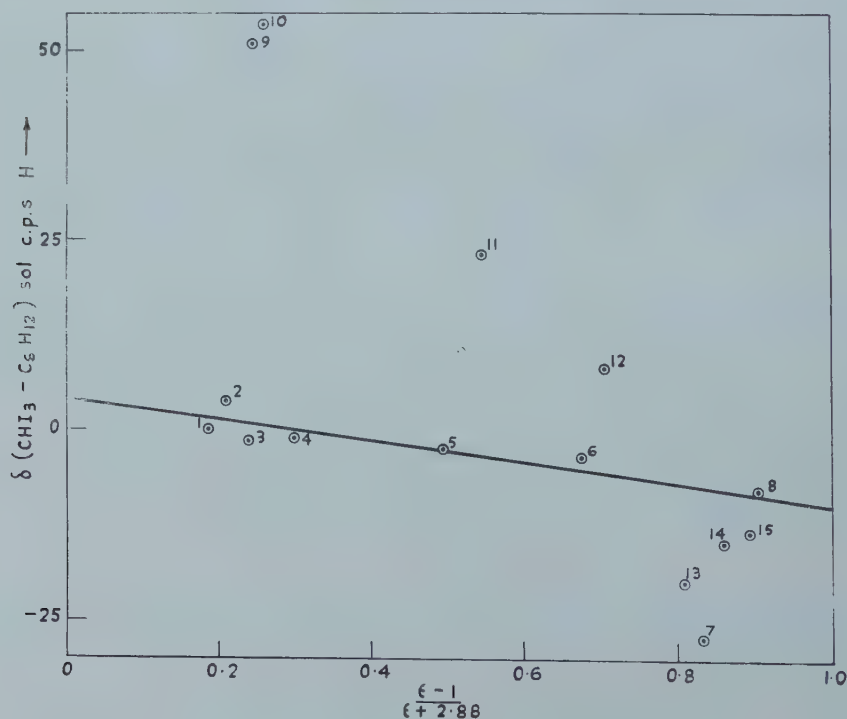


Figure 2. Plot of the proton resonance shift of iodoform in various solvents (in c.p.s. at 60 Mc/s) against $(\epsilon-1)/(\epsilon+2.88)$.

these solvents have now been given a satisfactory quantitative explanation in terms of the three interactions mentioned earlier, i.e. bulk susceptibility corrections and variations in the magnetic anisotropy of the solvent (which are included in the cyclohexane chemical shift values in these solvents) and the variations in the solvent reaction field (which explains the variation of the difference between the methyl iodide and cyclohexane chemical shifts). Also this is support for the validity of the procedure we have used to eliminate the effects of the solvent magnetic anisotropy on the chemical shifts of this solute.

However, the chemical shifts of methyl iodide in aromatic solvents do not follow this simple picture, as can be seen from figure 1. In benzene, for example, there is an excess high field shift of about 0·5 p.p.m. This excess high field shift decreases in substituted aromatics until with the very polar substituent groups such as the cyano and nitro groups there is again reasonable agreement with the calculated line.

The variation of the iodoform chemical shift with solvent (figure 2) agrees almost exactly with this picture. Here again most of the aliphatic solvents agree very well with the calculated line, though now there is one notable exception, acetone (No. 7). Again the aromatic solvents follow much the same pattern as in the methyl iodide case, the largest discrepancy occurring with benzene as solute.

The most obvious explanation of the deviations of the solute shifts from the calculated line is that complex formation is occurring between the solute and solvent.

The postulate of solute solvent complex formation agrees very well with previous work in this field. For example, the behaviour of iodoform in acetone is very similar to that of chloroform in this solvent. The formation of a weak hydrogen bond in this latter case is well established, both by N.M.R. and other methods [12]. The iodoform acetone complex would be expected to be of the same type, though perhaps differing in energy. This is borne out by the experimental data, e.g. the chloroform dilution shift in acetone is 0·75 p.p.m. [13] whilst that of iodoform is somewhat smaller (0·50 p.p.m.), suggesting a weaker hydrogen bond.

In the case of benzene as solvent the high field shifts of the chloroform and iodoform protons are practically equal. This is shown in table 2 which gives in addition the dilution shift in benzene of all the chloro, bromo and iodo substituted methanes. The dilution shifts change with the number of halogen atoms present but are practically independent for the same type of compound, of the halogen atom. Also they are all much larger than the dilution shift of cyclohexane, also given in table 2, which represents the effect of the magnetic anisotropy of the benzene molecule. It is suggested that the dilution shifts of the halogenated methanes in benzene are all due to complex formation with the solvent of the same type as that previously described for the chloroform benzene system. In this model, the solute is attached to the solvent in such a manner that the axis of symmetry of the solute (the dipole axis) is along the sixfold axis of symmetry of the benzene ring, with the protons (i.e. the positive end of the solute dipole) nearest the benzene. In this position the protons experience a high field shift due to the aromatic ring current and this explains the observed shift.

The support for this postulate rests mainly on the similarity of the behaviour of those compounds in aromatic solvents. Figures 1 and 2 demonstrate this very clearly for the two solutes methyl iodide and iodoform. The behaviour of these solutes in the various aromatic solvents studied is very similar. In both cases the high field shift decreases almost linearly with the increasing reaction field of the medium, although the size of this shift is always rather smaller for methyl iodide than for iodoform. It would be very difficult to describe this behaviour in terms of two different types of complex for the two solutes.

There are slight differences in the behaviour of the two solutes in strongly polar aromatic solvents. In these solvents the iodoform proton is to low field of the theoretical line suggesting that weak hydrogen bonding is occurring between the iodoform and the substituent group. This is most noticeable for benzaldehyde as solvent (No. 12) in which hydrogen bonding of exactly the same type as in the iodoform acetone system could occur. However, it should be noted that the disappearance of the solute solvent complex with increasing reaction field of the solvent is not due solely to this latter type of hydrogen bonding as in the case of methyl iodide, there is no evidence of any such hydrogen bonding occurring, yet the high field shift due to the solvent solute complex decreases to almost zero for these strongly polar solutes.

There is the possibility that charge transfer complexes may be formed between the iodine containing solutes and the aromatic solvents. This type of complex is formed by iodine in benzene [14] and such a complex could alter the proton chemical shifts of the solute appreciably. The general similarity between the behaviour of chloroform in aromatic solvents [2] and that of iodoform (figure 2) tends to disprove this idea, as there is no evidence to suggest that chloro compounds form these charge transfer complexes with aromatic solvents. This is further supported by the results of table 2 which show that the shift is unaffected by the type of halogen atom. However, this possibility was tested by measuring the ultra-violet spectra of methyl iodide and iodoform in benzene and carbon tetrachloride. There was no change whatsoever in the spectrum of iodoform in the two solutes. The methyl iodide band at 2620 Å in carbon tetrachloride was displaced to 2870 Å in benzene, but no new band characteristic of a charge transfer complex occurred. Thus this alternative may be eliminated.

### 3.2. *The temperature variation of the solute proton chemical shifts*

In the preceding section it has been postulated that complex formation occurs when a halogenated methane is dissolved in an aromatic non-polar solvent. If this is so the solute proton chemical shift, which depends on the amount of complex present at any temperature, should vary with temperature. In order to test this, the proton chemical shifts of the three solutes cyclohexane, methyl iodide and iodoform in the same toluene solution were measured as a function of temperature. Toluene was used as solvent as it has the same effect as benzene on the solute chemical shifts (shown in table 1) and also has the advantage of a much wider liquid region.

The Varian variable temperature insert was used and the solute chemical shifts measured from the toluene phenyl peak over the range $-60°$c (the lower limit of the apparatus) to $100°$c. The results are shown in table 3. The cyclohexane chemical shift is completely independent of temperature over the entire temperature range. (For the two lowest temperatures, the value shown bracketed

| Temp. (°c) | $C_6H_{12}$ | $CH_3I$ | $CHI_3$ | $CHI_3$ $-C_6H_{12}$ | $CH_3I$ $-C_6H_{12}$ |
|---|---|---|---|---|---|
| − 53 | (337·8) | 344·7 | 219·6 | − 118·2 | 6·9 |
| − 45·5 | (337·8) | 343·6 | 216·3 | − 121·5 | 5·8 |
| − 35·5 | 337·6 | 341·5 | 209·9 | − 127·7 | 3·9 |
| − 18 | 337·9 | 338·8 | 203·6 | − 134·3 | 0·9 |
| − 5·5 | (337·8) | 337·2 | 198·1 | − 139·7 | ~0 |
| 10 | 337·8 | 334·3 | 192·6 | − 145·2 | − 3·5 |
| 26·5 | 337·8 | 331·1 | 184·9 | − 152·9 | − 6·7 |
| 26·5 | 338·1 | 331·8 | 185·9 | − 152·2 | − 6·3 |
| 37 | 337·9 | 330·3 | 182·8 | − 155·1 | − 7·6 |
| 51·5 | 338·1 | 328·9 | 178·6 | − 159·5 | − 9·2 |
| 65·5 | 337·9 | 327·3 | 175·1 | − 162·8 | − 10·6 |
| 82 | 337·5 | 325·9 | 172·4 | − 165·1 | − 11·6 |
| 98·5 | 337·6 | 324·4 | 168·9 | − 168·7 | − 13·2 |
| 103 | 337·7 | 324·0 | 167·6 | − 170·1 | − 13·7 |

Table 3.   The temperature dependence of the proton chemical shifts of cyclohexane, methyl iodide and iodoform in toluene (measured in c.p.s. at 60 Mc/s from the phenyl proton peak).
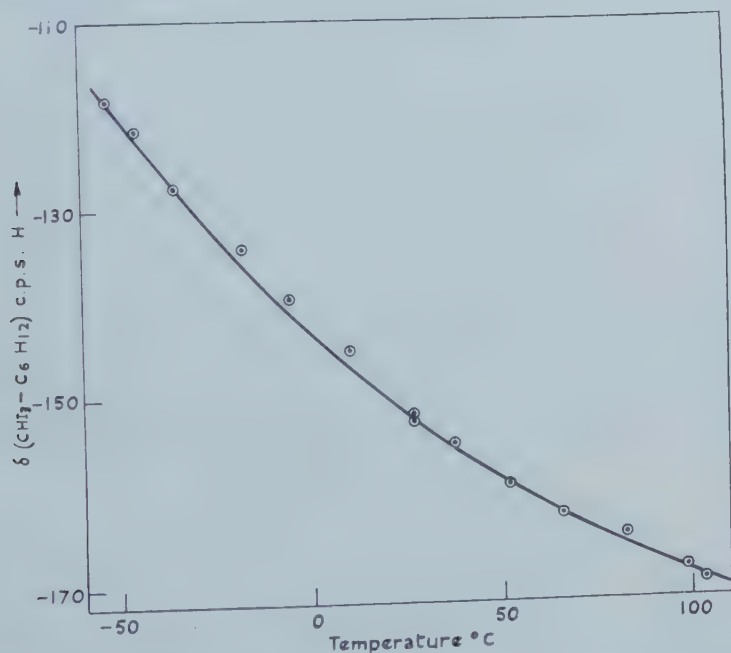


Figure 3.   Plot of the proton resonance shift of iodoform in toluene (in c.p.s. at 60 Mc/s from a cyclohexane internal reference) against temperature.

is the average of the other values, as the cyclohexane peak broadened and could not be measured accurately.  The value at − 5·5 c is also this average value as at this temperature the cyclohexane and methyl iodide peaks could not be separately resolved.)  This temperature independence is to be expected on the theory that the dilution shift of cyclohexane in aromatic solvents is solely due to an averaging of the magnetic field of the aromatic ring current.  Note that the

variation of the density of the medium with temperature, which could affect all the chemical shifts, is removed by using an internal standard.
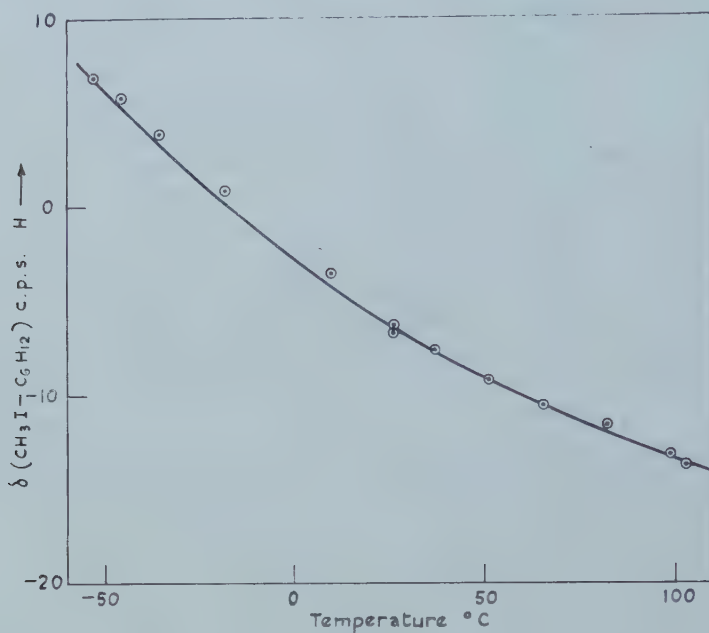


Figure 4.    Plot of the proton resonance shift of methyl iodide in toluene (in c.p.s. at 60 Mc/s from a cyclohexane internal reference) against temperature.

However, the proton chemical shifts of methyl iodide and iodoform change appreciably over the temperature range studied, that of iodoform changing by about 1 p.p.m.   Columns four and five of table 3 give the iodoform and methyl iodide shifts from the cyclohexane internal reference, and these are plotted as functions of temperature in figures 3 and 4.   From the shape of these curves it is possible to obtain values of the parameters which govern the formation of the complex, as follows.

Writing $AH$ for the solute and $B$ for the solvent, the formation of the solute solvent complex can be represented as an equilibrium of the form
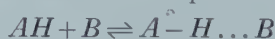
$$AH + B \rightleftharpoons A \overset{\frown}{-} H \ldots B$$

with an equilibrium constant

$$K = \frac{[A-H\ldots B]}{[AH][B]} = \exp\left(\frac{\Delta S}{R}\right)\exp\left(-\frac{\Delta H}{RT}\right).$$

$\Delta S$ is the entropy of formation and $\Delta H$ the heat of formation of the complex. With $K$ in units mf$^{-1}$, the solvent concentration becomes unity (assuming an infinitely dilute solution), thus if a fraction $p$ of the solute is in the complex

$$\frac{p}{1-p} = \frac{[A-H\ldots B]}{[A-H]} = \exp\left(\frac{\Delta S}{R}\right)\exp\left(-\frac{\Delta H}{RT}\right). \qquad (3)$$

The measured chemical shift of the solute protons ($\delta$) will be the weighted mean of the chemical shift of the unassociated solute ($\delta a$) and that in the complex ($\delta c$), i.e.

$$\delta = p\delta c + (1-p)\delta a. \qquad (4)$$

From equations (3) and (4), the required equation giving $\delta$ as a function of the four unknowns $\Delta S$, $\Delta H$, $\delta c$ and $\delta a$ and the temperature is obtained by eliminating $p$.

It is convenient at this point to discuss the significance of equations (3) and (4). When the temperature is very high, so that $\Delta H$ is much less than $kT$, all the solute molecules will be in the unassociated form.   In this state the solute proton chemical shifts (measured from the internal cyclohexane reference) will be due to only the different chemical nature of the solute compared to the cyclohexane and also to the reaction field of the toluene.   Thus this chemical shift will be identical to that of the same solute proton in any non-complexing solvent of the same polarizability (ignoring the effect of other forces such as Van der Waals interactions, etc.).

On lowering the temperature, the random distribution of the solvent molecules around the solute breaks down, as one position is more favoured than the rest, namely that in the complex.   At very low temperatures where $\Delta H$ is much larger than $kT$ all the solute molecules will be associated in this way and the solute chemical shift will now be the shift at high temperatures plus that due to the formation of the complex.

This discussion provides a means of simplifying equations (3) and (4) as follows.   The two solvents $n$-hexane and toluene have similar small polarizabilities, so that the contributions of the reaction fields of these two solvents to the solute chemical shifts are practically identical.   Thus, using the above arguments we can estimate the high temperature shift $\delta a$ as the value of the chemical shift of the particular solute proton considered in $n$-hexane.   Also as the shapes of the curves in figures 3 and 4 remain unchanged whatever the origin of the chemical shifts, we will take this value of $\delta a$ to be the origin and measure all the chemical shifts from this.   Equation (4) now becomes

$$\delta = p\delta c$$

and combining this with equation (3) gives

$$\delta = \frac{\delta c}{1 + \exp\left(-\Delta S/R\right)\exp\left(\Delta H/RT\right)}. \tag{5}$$

$\Delta H$, the heat of formation of the complex, is negative (i.e. the complex is favoured as the temperature is lowered).   It is convenient to include this directly in equation (5) which will be used in the form

$$l\exp\left(-\frac{\Delta H}{RT}\right) = \frac{\delta c}{\delta} - 1, \tag{6}$$

where $l$ is $\exp(-\Delta S/R)$ and $\Delta H$ is now positive.

For iodoform in toluene (figure 3), $\delta a$ was given the value $-206\cdot7$ c.p.s., the iodoform shift in $n$-hexane (table 1).

The results of table 3 are best fitted by the following values: $\Delta H = 1\cdot6 \pm 0\cdot2$ kcals/mole, $\delta c = 140 \pm 20$ c.p.s.  $(2\cdot33 \pm 0\cdot33$ p.p.m.) and $l = 25 \pm 2$.   The calculated curve is shown in figure 3 with the experimental results.   Similarly for methyl iodide in toluene $\delta a$ was taken as $-35\cdot5$ c.p.s. (table 1) and this gave $\Delta H = 1\cdot3 \pm 0\cdot5$ kcals/mole, $\delta c = 70 \pm 20$ c.p.s.  $(1\cdot17 \pm 0\cdot33$ p.p.m.) and $l = 12 \pm 2$.   The percentage errors are larger in this latter case as the variation of the chemical shifts with temperature is much smaller.   Again the calculated curve is shown in figure 4.   From the definition of $l$ (equation (6)) the entropy of formation of the complex in the two cases is found to be $-6\cdot4 \pm 0\cdot2$ e.u. and $-4\cdot9 \pm 0\cdot4$ e.u. respectively.

It would be possible to obtain all four unknowns (i.e. including $\delta a$) directly from the experimental curve using equations (3) and (4), but the range of values of the four parameters which could fit the observed curve would be so wide that very little useful information would be obtained. By eliminating one unknown in the manner above, it is possible to obtain a much narrower range of values of the remaining parameters, although this may introduce a systematic error into these values. The values of $\delta c$ obtained represent the additional fields experienced by the solute protons in the complexes, compared with those in the unassociated molecule, both measured in toluene with respect to the cyclohexane internal reference. To obtain the additional field in the complex as compared to the 'free molecule', i.e. in a normal solvent, the high field shift of cyclohexane itself in aromatic as compared to isotropic solvents must be added. This is 0·40 p.p.m. Thus the high field shift in the complexes is 2·73 and 1·57 p.p.m. for iodoform and methyl iodide respectively. If it is assumed that this additional field is due solely to the magnetic effect of the ring current [17], and that the geometry of the complexes is as postulated above, i.e. the iodoform proton lies on the hexagonal axis of symmetry of the benzene ring whilst the methyl iodide protons are placed symmetrically around this axis, the distance of the iodoform proton from the plane of the ring is found to be $2·5 \pm 0·1$ Å, whilst that of the methyl iodide protons is $2·8 \pm 0·3$ Å. The magnetic field due to the ring current was calculated using the table provided by Johnson and Bovey [18]. This calculation assumes that the observed high field shift of the protons in the complexes is solely due to the benzene ring current. Any other mechanism which contributes to this high field shift would affect these figures. In particular if there is any paramagnetic term similar to that which produces the pronounced low field shifts of protons involved in other hydrogen bonds, the above values would be larger than the real distances.

## 4. Conclusion

The values of $\Delta H$ and $\Delta S$ obtained above are somewhat less than the values of 2·5 kcal/mole [15] and 7·1 e.u. [12] estimated for the chloroform acetone complex. This is in agreement with the heat of solution data for this type of compound [16]. The intermolecular distances obtained above are also much less than the value given for the chloroform mesitylene complex [2]. This is due to the fact that this latter value was calculated from the high field shift of the chloroform proton in mesitylene at room temperature, which is probably only about half of the true value of $\delta c$ (table 2). The values obtained here are only slightly larger than the sum of the Van der Waals radii of the $\pi$ electrons of the benzene ring (1·4 Å) and the solute proton (1·0 Å). This tends to suggest that the complexes studied here may be regarded as arising from hydrogen bonding in which the $\pi$ electrons of the benzene ring act in a similar manner to the unpaired electrons of the more common donor atoms. On this picture, the complexes are essentially similar to other hydrogen bonds, i.e. essentially electrostatic in character, but due to the weak ionic character of the C–H bond, are considerably less stable than the more common hydrogen bonds.

It is not possible at this stage to eliminate entirely other types of association involving the halogen atoms and the aromatic ring, but it is very difficult in particular to explain two observations on the basis of any such interaction, effects which have a reasonable explanation on the basis of the hydrogen bond model.

First the disappearance of the complex when polar substituent groups are introduced into the aromatic ring. This has a reasonable explanation on the above picture as follows. These groups would be expected to disturb the electrostatic equilibrium and thus reduce the energy of formation of the complex and the high field shift of the solute proton. Secondly the high field shift of the solute protons in the complex is not affected by varying the halogen atom in the solute (table 2), i.e. by any change in the solute dipole moment. This behaviour is consistent with the behaviour of other hydrogen bonded systems, in which the energy of formation of the hydrogen bond is not simply related to the dipole moment of the acceptor molecule [12].

However, the formation of such a complex between methyl halides and aromatic compounds is very surprising. It may be due to the fact that these complexes are formed in non-polar media, in which other solvent solute interactions such as dipolar interactions which would normally be of comparable energy and therefore obscure this $\pi$ orbit complex, are absent. A similar type of hydrogen bonding between an acceptor molecule, not normally thought of as capable of forming hydrogen bonds, and benzene has been postulated to explain the P.M.R. shifts of some substituted benzenes in benzene itself as solvent [19].

Whatever the actual nature of the complexes, this investigation does show that the problem of interpreting P.M.R. solute shifts in aromatic solvents is not an easy one, as there may be many possibilities of such weak complex formation with the solvent in the case of larger solute molecules with many active groups.

REFERENCES

[1] POPLE, J. A., SCHNEIDER, W. G., and BERNSTEIN, H. J., 1959, *High Resolution Nuclear Magnetic Resonance* (McGraw-Hill).
[2] REEVES, L. W., and SCHNEIDER, W. G., 1957, *Canad. J. Chem.*, **35**, 251.
[3] HATTON, J. V., and RICHARDS, R. E., 1960, *Mol. Phys.*, **3**, 253.
[4] HATTON, J. V., and RICHARDS, R. E., 1961, *Trans. Faraday Soc.*, **57**, 28.
[5] BUCKINGHAM, A. D., SCHAEFFER, T., and SCHNEIDER, W. G., 1960, *J. chem. Phys.*, **32**, 1227.
[6] BUCKINGHAM, A. D., 1960, *Canad. J. Chem.*, **38**, 1960.
[7] ABRAHAM, R. J., 1961, *J. chem. Phys.*, **34**, 1062.
[8] BOTHNER-BY, A. A., and GLICK, R. E., 1957, *J. chem. Phys.*, **26**, 1651.
[9] WELLS, A. F., 1952, *Structural Inorganic Chemistry* (Oxford: Clarendon Press).
[10] DIEHL, P., and FREEMAN, R., 1961, *Mol. Phys.*, **4**, 39.
[11] ROSS, I. G., and SACK, R. A., 1950, *Proc. phys. Soc., Lond.* B, **63**, 893.
[12] PIMENTEL, G. C., and MCCLELLAN, A. L., 1960, *The Hydrogen Bond* (London: W. H. Freeman & Co.).
[13] KORINEK, G., and SCHNEIDER, W. G., 1957, *Canad. J. Chem.*, **35**, 1157.
[14] BHATTACHARYA, R., and BASU, S., 1958, *Trans. Faraday Soc.*, **54**, 1286.
[15] HUGGINS, C. M., and PIMENTEL, G. C., 1955, *J. chem. Phys.*, **23**, 1244.
[16] HUGGINS, C. M., and PIMENTEL, G. C., 1955, *J. chem. Phys.*, **23**, 896.
[17] Reference [1], chapter 7.
[18] JOHNSON, C. E., and BOVEY, F. A., 1958, *J. chem. Phys.*, **29**, 1012.
[19] SCHAEFFER, T., and SCHNEIDER, W. G., 1960, *J. chem. Phys.*, **32**, 1218.

# The relative signs of N.M.R. spin coupling constants from double irradiation experiments

by R. FREEMAN

Basic Physics Division, National Physical Laboratory, Teddington, Middlesex

The method of double irradiation in high resolution proton magnetic resonance has been used to confirm that the spin coupling constant between the methyl group and the proton in the *cis* position in both *trans*-crotonaldehyde and *trans*-crotonic acid differs in sign from the other coupling constants. Since this is a particularly searching test of the double irradiation method, it is suggested that relative signs of coupling constants could be determined in this way for most molecules containing three coupled hydrogen nuclei provided that the chemical shifts are large compared with the coupling constants.

---

## 1. INTRODUCTION

The use of the technique known as 'spin decoupling' or 'double irradiation' in high resolution proton magnetic resonance requires only quite simple modifications to the conventional spectrometer [1, 2, 3]. It is therefore to be expected that this method, which was originally proposed by Bloch [4], will be developed and used more extensively in the future. It has three principal applications. Complicated spectra can often be simplified if one of the proton spin couplings is destroyed by strong irradiation, so that the remaining spectrum becomes more amenable to analysis [2, 3]. Another application that has been proposed is the determination of the position of a resonance line which itself is completely obscured by other resonances, but which is spin-coupled to a second proton with an observable resonance pattern. For a given power level in the strong irradiation field $H_2$, the extent of collapse of the multiplet structure, which may be thought of as the efficiency of the decoupling process, will be optimum when $H_2$ is separated from the measuring radio-frequency ($H_1$) by the chemical shift. The method is analogous to the determination of the gyromagnetic ratio of $^{13}C$ in methyl iodide by observation of the collapse of the $^{13}C$ satellite lines in the proton spectrum when a strong field is imposed at the resonant frequency of $^{13}C$ [5]. Recently a third application has been suggested. By double irradiation of the thallium diethyl cation, Evans [6] has demonstrated that the two thallium hydrogen coupling constants are of opposite sign. The method may be extended to systems where all the nuclei are protons [7] and should in fact be more generally applicable than the usual analytical method of obtaining the relative signs of proton spin coupling constants [8] where there is the additional requirement that the coupling constants be comparable with the chemical shifts.

The present investigation is an attempt to establish just how far the double irradiation method can be exploited to determine the relative signs of coupling constants before experimental limitations become apparent. A practical example

2 B

has been chosen which provides a particularly searching test and several **points** emerge which could be of importance in the other applications of the spin decoupling method.

## 2. THE DOUBLE IRRADIATION METHOD

For the theoretical treatment of the spin decoupling experiment the reader is referred to the work of Bloch [9] and of Bloom and Shoolery [10]. As Anderson [11] points out, the treatment of Bloom and Shoolery is valid only in the limit of large separation of the resonance frequency of the groups concerned, and should not therefore be applied directly to the double irradiation of protons.

### 2.1. *Relative signs of proton spin coupling constants*

As in the analytical method of determining relative signs of proton spin coupling constants, the molecule to be investigated must contain at least three non-equivalent nuclei, A, R and X, but in the double irradiation method the chemical shifts may be large compared with the spin coupling constants $J_{AR}$,



Figure 1.   A schematic representation of the spectrum of three nuclei when the chemical shifts are very much larger than the spin coupling constants.

$J_{AX}$ and $J_{RX}$. Figure 1 shows schematically how the high resolution spectrum of such a system is built up if $|J_{AR}| > |J_{AX}| > |J_{RX}|$. The operation of the method may be understood pictorially by supposing that the two nuclear neighbours generate small magnetic fields at the nucleus under consideration. The strengths of these fields are proportional to the respective spin coupling constants, and whether they add or subtract from the main field $H_0$ depends both on the spin state of the nuclear neighbour *and* on the sign of the coupling constant. It follows that in a system of only two coupled nuclei the sign of the coupling constant must remain ambiguous, but the introduction of a third nucleus permits the determination of the relative signs of two of the coupling constants. Reference to figure 1 shows how this comes about. At any particular instant the sample can be thought of as divided into two sets of molecules, those in which nucleus A has one of its two possible spin states and those where it has the other. One of these sets of molecules gives rise to transitions 5 and 6 in the R spectrum whereas

transitions 7 and 8 belong to the other set. The first set also produces lines 9 and 10 in the X spectrum if $J_{AR}$ and $J_{AX}$ are of like sign, but lines 11 and 12 if $J_{AR}$ and $J_{AX}$ are of opposite sign. Now it is possible to irradiate at a frequency intermediate between lines 5 and 6 with a power high enough to destroy $J_{RX}$ and yet low enough to avoid perturbing transitions 7 and 8. If at the same time the X spectrum is examined to determine which of the pairs 9, 10 and 11, 12 collapse to a single line, then the relative signs of $J_{AR}$ and $J_{AX}$ are found. An analogous experiment determines the relative signs of $J_{AR}$ and $J_{RX}$.

A complication can arise if the chemical shifts between the resonances of the three nuclei are not large compared with the coupling constants. A simple example would be a molecule of the ABX type in the nomenclature of Pople *et al.* [12]. In such spectra, the transitions of nucleus X can be clearly identified, but the remaining lines may not be divided into exclusively A or exclusively B transitions. They are mixed transitions involving changes in the spin states of both nucleus A and nucleus B. It is conventional however to describe the spectrum in terms of lines that are predominantly A transitions and others that are predominantly B. Strong irradiation of the ' A ' lines with the intention of decoupling the A and X spins then leads to some decoupling of the B and X spins, and this is particularly important if $|J_{AX}| > |J_{BX}|$. Crotonaldehyde, the molecule studied in the present work, provides an example of this kind of situation, and the straightforward double irradiation method for determining the relative signs of the coupling constants gives ambiguous results.

## 3. EXPERIMENTAL
### 3.1. Trans-*crotonaldehyde*

The high resolution proton magnetic resonance spectrum of *trans*-crotonal-dehyde has been studied recently by Pople and Schaefer [13] as an illustration of their general analysis scheme for $ABR_pX_q$ type molecules. It represents an $ABR_3X$ system:

$$H(X)$$
$$H(A) \quad C=O$$
$$C = C$$
$$CH_3(R) \quad H(B)$$
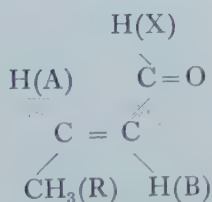
The spectrum of the neat liquid recorded at 24 c on a Varian 60 Mc/s spectro-meter is shown in figure 2. Kowalewski and de Kowalewski [14] have studied and analysed the spectra of the closely related molecules *trans*-crotonic acid and its methyl ester, working with a spectrometer frequency of 40 Mc s. The experiments of both groups lead to the conclusion that the spin coupling constant of the methyl group to the proton in the *cis* configuration ($J_{BR}$) is of opposite sign to the *gem* coupling constant ($J_{AR}$) and thus presumably negative. The two different experimental approaches to the problem of determining these relative signs make an interesting comparison. In both papers the authors point out that close inspection of certain relative intensities suggests that $J_{AR}$ and $J_{BR}$ have opposite signs, but this evidence was not considered conclusive. The Kowalewskis went on to confirm their supposition by re-investigating the spectrum at 25 Mc/s, whereas Pople and Schaefer recorded all spectra at 60 Mc/s but made use of the preferential solvent effect of benzene to reduce the AB chemical
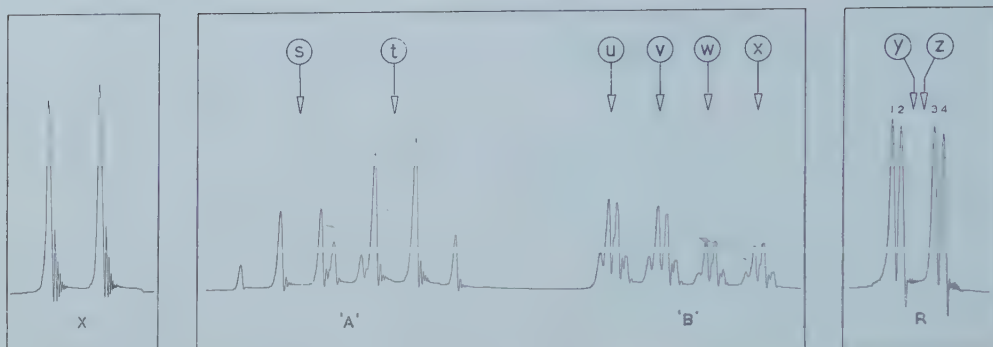
Figure 2.   The spectrum of neat *trans*-crotonaldehyde at 60 Mc/s.   Magnetic field sweep
is from from left to right.   The arrows indicate the location of the strong field $H_2$ in
the double irradiation experiments.

shift.   Both groups were able to establish that the two coupling constants are
indeed of opposite sign.   It is possible to confirm this result by the double
irradiation method even though it is a very unfavourable case experimentally,
which suggests that this technique could in fact be applied rather generally.

The spin coupling constants derived by Pople and Schaefer [13] for *trans*-
crotonaldehyde have been used in the present work to determine suitable
decoupling fields $H_2$.   The complete set is given below.

$$|J_{AB}| = 15 \cdot 6 \pm 0 \cdot 2 \text{ c/s},$$
$$|J_{AR}| = \phantom{0}6 \cdot 8 \pm 0 \cdot 2 \text{ c/s},$$
$$|J_{BR}| = \phantom{0}1 \cdot 6 \pm 0 \cdot 2 \text{ c/s},$$
$$|J_{BX}| = \phantom{0}7 \cdot 8 \pm 0 \cdot 2 \text{ c/s},$$
$$J_{AX} = \phantom{0}0.$$

The required frequency separations were carefully re-measured by the sideband
modulation method and are probably reliable to $\pm 0 \cdot 2$ c/s.   Measured from the
centre of the X doublet (figure 2) the frequencies were

$$(s) = 144 \cdot 0 \pm 0 \cdot 2 \text{ c/s},$$
$$(t) = 159 \cdot 6 \pm 0 \cdot 2 \text{ c/s},$$
$$(u) = 193 \cdot 7 \pm 0 \cdot 2 \text{ c/s},$$
$$(v) = 201 \cdot 4 \pm 0 \cdot 2 \text{ c/s},$$
$$(w) = 209 \cdot 1 \pm 0 \cdot 2 \text{ c/s},$$
$$(x) = 216 \cdot 9 \pm 0 \cdot 2 \text{ c/s},$$
$$(y) = 450 \cdot 3 \pm 0 \cdot 2 \text{ c/s},$$
$$(z) = 451 \cdot 7 \pm 0 \cdot 2 \text{ c/s}.$$

### 3.2.   *The problem of strongly coupled nuclei*

The simplest double irradiation experiment would be to observe the methyl
group spectrum (R) while irradiating at $(s)$ or $(t)$ in the 'A' spectrum (figure 2)
with a radio-frequency field strong enough to 'wash out' the spin coupling $J_{AR}$.
Experimentally one might then observe the collapse of lines 1 and 3 to a single
line.   If such a pattern were produced when the radiation field $H_2$ is at the
frequency $(s)$, then $J_{AB}$ and $J_{BR}$ would have like signs, if at frequency $(t)$ they
would have opposite signs.   Since $(s)$ and $(t)$ are separated by 15·6 c/s there

should be no difficulty in distinguishing these two possibilities, and moreover, the transitions near $(t)$ are unlikely to be perturbed by a radio-frequency at $(s)$ of amplitude $(\gamma/2\pi)H_2 \sim |J_{\mathrm{AR}}|$.

In practice the patterns which are observed are ambiguous, and the reason for this seems to be that not only the AR coupling but also the BR coupling is affected by irradiation of the 'A' spectrum, in the manner discussed in §2.1. Since $|J_{\mathrm{AR}}|$ is more than four times larger than $|J_{\mathrm{BR}}|$, the mixed transitions which have been labelled 'A' in figure 2 are being subjected to quite a strong field compared with $J_{\mathrm{BX}}$.

### 3.3. *The relative signs of* $J_{\mathrm{AB}}$ *and* $J_{\mathrm{BR}}$ *in* trans-*crotonaldehyde*

The problem discussed above can be avoided by reversing the rôles of the two groups to be irradiated, $H_1$ now being used to display the 'A' spectrum and $H_2$ to 'stir' certain R transitions. In figure 2, the collapse of the high field 'A' quadruplet should occur when $H_2$ is at a frequency $(y)$ equidistant between lines 1 and 3 if $J_{\mathrm{AB}}$ and $J_{\mathrm{BR}}$ are of opposite sign; if they are of like sign the optimum frequency for collapse would be $(z)$, equidistant between lines 2 and 4. Now the frequencies $(y)$ and $(z)$ differ by as little as 1·4 c/s, so that if too high a power is used for $H_2$ the two cases become indistinguishable. It is therefore essential that $H_2$ be kept as low as possible compatible with efficient decoupling of A and R. This was ensured in practice by calibration of the radio-frequency field strength of the spectrometer by the method of Anderson [11, 15]. $H_2$ was then set to 2·6 milligauss or about $\frac{3}{2}J_{\mathrm{AR}}$. The importance of this calibration for spin decoupling experiments in general can hardly be over-emphasized.

As described in detail elsewhere [2] spectra were recorded by sweeping the main magnetic field $(H_0)$, with a fixed separation between $H_1$ and $H_2$, that is, at a fixed modulation frequency, for $H_1$ was simply a modulation sideband of $H_2$ at low modulation index. An electronic counter monitored the modulation frequency with an accuracy of $\pm 0.1$ c/s.

An alternative method would have been to maintain $H_0$ constant, fix the frequency of $H_2$ and sweep the frequency of $H_1$ to display the spectrum. The inherent instability of most magnets precludes this method for precise measurements of high resolution proton spectra, so that the field sweep method was adopted. Under these conditions $H_2$ is near its optimum location only during that part of the magnetic field sweep where the collapsed line is being recorded. In the field sweep method, if $H_2$ is kept rather low, the decoupled spectrum has somewhat less total intensity than the unperturbed spectrum, and a theoretical treatment along the lines of the calculation of Bloom and Shoolery [10] predicts generally simpler patterns than for the constant field experiment, in that certain satellite lines are weaker and further removed in frequency, or even absent altogether.

In order to determine the optimum frequency separation of $H_1$ and $H_2$, it was necessary to make recordings of the partially decoupled patterns over a range of modulation frequencies that included the two critical frequencies calculated for like and opposite signs of $J_{\mathrm{AB}}$ and $J_{\mathrm{BR}}$, the separations $(t)-(z)$ and $(t)-(y)$ of figure 2. As the decoupling becomes more efficient, the two central lines of the high field quadruplet come together and eventually coalesce, while the low field quadruplet remains to a large extent unaffected. A reasonable criterion for determining the optimum decoupling would seem to be the peak

height of the coalesced lines, or, when they can be resolved, the height of the minimum between them. This quantity does in fact follow a smooth curve as the modulation frequency is varied (figure 3). Some scatter is to be expected
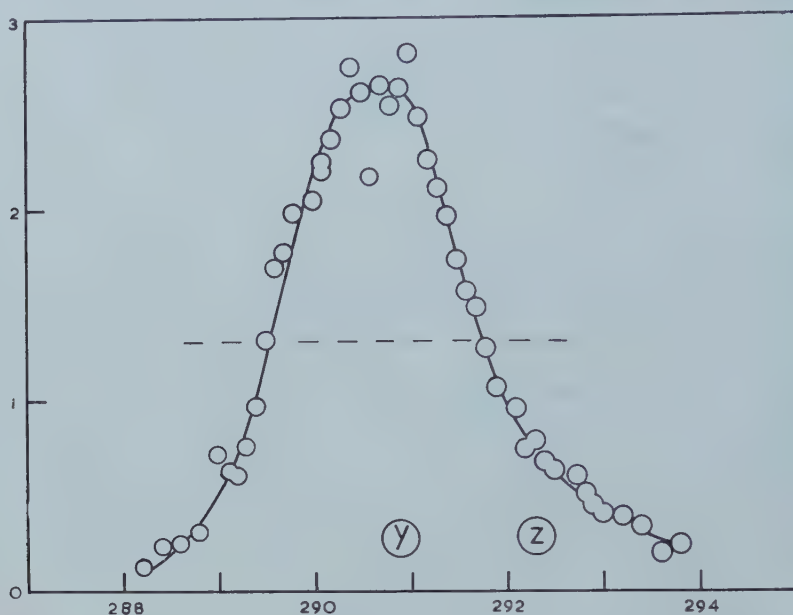


Figure 3. The peak height of the line from the collapsed high field 'A' quadruplet of figure 2 plotted against the modulation frequency in c/s. The point $(y)$ represents the frequency calculated for opposite signs of $J_{AB}$ and $J_{BR}$ while $(z)$ is calculated for like signs. Below the dotted line, the resonance may be resolved into two peaks.
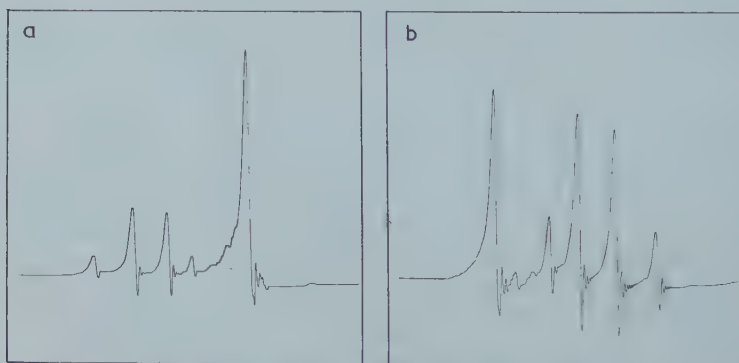


Figure 4. $(a)$ The 'A' spectrum of figure 2 recorded with simultaneous irradiation of the R group at $(y)$ with a radio-frequency field of 2·6 milligauss. The high field quadruplet has collapsed, while a small perturbation of the low field quadruplet can also be discerned. $(b)$ The same except that the strong field is now at $(z)$ of figure 2.

because of occasional degradations of the magnetic field inhomogeneity, but these are apparently not serious. Peak heights were actually measured with respect to the height of one of the lines in the unperturbed quadruplet to allow for the slight frequency dependence of signal intensity. It may be seen that optimum decoupling of the high field quadruplet does in fact occur when $H_2$ is

very close to the frequency $(y)$ corresponding to a modulation frequency 290·9 c/s rather than at $(z)$ which corresponds to 292·3 c/s. This confirms the conclusion that $J_{AB}$ and $J_{BR}$ have opposite signs. Figure 4 $(a)$ shows a typical decoupled spectrum.

Sideband responses are not separated from the centreband by exactly the modulation frequency as Anderson has clearly established [11]. If $\omega_M$ is the modulation frequency in radians sec, $\gamma$ the magnetogyric ratio of the proton, $H_2$ the centreband radio-frequency field in gauss, then $\omega$, the separation of sideband and centreband responses is given by

$$\omega^2 = \omega_M{}^2 - \gamma^2 H_2{}^2.$$

Under the conditions used above this discrepancy is just significant (0·2 c/s) and the critical modulation frequencies shown in figure 3 have been increased by this amount.

The experiment may be repeated in such a way that the low field 'A' quadruplet collapses, and then the optimum modulation frequency is such that $H_2$ falls at the frequency $(z)$, again confirming that $J_{AB}$ and $J_{BR}$ have opposite signs. Figure 4 $(b)$ shows the decoupled spectrum.

### 3.4. *The relative signs of* $J_{AB}$ *and* $J_{AR}$ *in* trans-crotonaldehyde

The 'B' spectrum consists of four quadruplets since it has been 'doubled' by the coupling with proton X. Irradiation at $(u)$ or $(v)$ with a field of
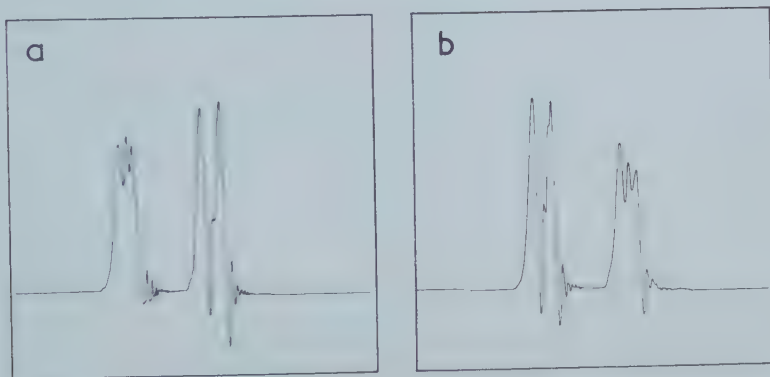


Figure 4. $(a)$ The R spectrum of figure 2 recorded with simultaneous irradiation of the 'B', spectrum at $(u)$ with a radio-frequency field of 0·4 milligauss. In half the molecules of the sample, lines 1 and 2 have coalesced. $(b)$ The same, except that the strong field is at $(x)$ of figure 2.

0·4 milligauss causes lines 1 and 2 of the methyl group spectrum to coalesce for just half the molecules present. Figure 5 $(a)$ shows the spectrum obtained. Irradiation at $(w)$ or $(x)$ produces an analogous pattern involving lines 3 and 4 (figure 5 $(b)$). It follows that $J_{AB}$ and $J_{AR}$ have like signs.

### 3.5. Trans-*crotonic acid*

The high resolution spectrum of this substance at 60 Mc/s very much resembles that of *trans*-crotonaldehyde except that the X proton (carboxylic acid) does not couple to the others, presumably because it is undergoing chemical exchange. Indeed in acetone solution the X line is considerably

broader than the others which suggests a chemical exchange rate comparable with the line width expressed in frequency units. The 'B' spectrum therefore consists of only two quadruplets.

Double irradiation experiments analogous to those performed on *trans*-crotonaldehyde indicate that here again $J_{AB}$ and $J_{BR}$ have opposite signs but $J_{AB}$ and $J_{AR}$ have like signs. At first some experimental difficulties were experienced with spinning sidebands from the strong solvent line but these can be avoided once they have been identified. They appeared to be less serious when the solvent was changed from acetone to dioxan, but this necessitated recalibration of the spectrum, for the chemical shift between A and R increased by 1·3 c/s, enough to invalidate the determination of the relative signs of $J_{AB}$ and $J_{BR}$.

## 4. CONCLUSION

The double irradiation method confirms the conclusions of previous workers [13, 14] that the coupling constant between the methyl group and the *cis* proton in *trans*-crotonaldehyde and *trans*-crotonic acid differs in sign from the other coupling constants. The experiment indicates that even when the 'stirring' field $H_2$ is quite high it must be located quite precisely if the decoupling process is to be efficient. This property is valuable in determining relative signs of proton spin coupling constants, where a decision has to be made between two possible locations of $H_2$. It has been demonstrated experimentally that a decision can be made between two frequencies of the order of 1 c/s apart even when the strength of $H_2$ expressed in frequency units is ten times as great. Such an extreme situation would not normally be encountered in first-order spectra, for the usual conditions are that the two critical frequencies are separated by $J_1$, while $(\gamma/2\pi)H_2$ is of the order of $J_2$, and $|J_1| > |J_2|$ since there is a choice as to which coupling is to be perturbed by $H_2$ and in which part of the spectrum. For example, in figure 1 all the information about the relative signs of $J_{AR}$, $J_{AX}$ and $J_{RX}$ could be obtained in two experiments, irradiation of transitions 1 and 2, and irradiation of transitions 5 and 6, with simultaneous investigation of the X spectrum.

One may conclude that the spin decoupling method should be applicable fairly generally to systems of three coupled hydrogen nuclei provided that the chemical shifts are large compared with the coupling constants. The experiment illustrates what may happen when this last condition is not fulfilled.

One of the experiments provides an example of a situation in which the discrepancy between the modulation frequency and the separation between sideband and centreband responses [11] becomes greater than the normally accepted calibration error. This arises because the centreband power used in spin decoupling experiments is considerably higher than in conventional recording methods where this correction is commonly neglected.

## REFERENCES

[1] ITOH, J., and SATO, S., 1959, *J. phys. Soc., Japan*, **14**, 851.
[2] FREEMAN, R., 1960, *Mol. Phys.*, **3**, 435.
[3] KAISER, R., 1960, *Rev. sci. Instrum.*, **31**, 963.
[4] BLOCH, F., 1954, *Phys. Rev.*, **93**, 944.
[5] ROYDEN, V., 1954, *Phys. Rev.*, **96**, 543.
[6] EVANS, D. F., and MAHER, J. P., 1961, *Proc. chem. Soc.*, p. 208.
[7] FREEMAN, R., and WHIFFEN, D. H., 1961, *Mol. Phys.*, **4**, 321.
[8] ALEXANDER, S., 1958, *J. chem. Phys.*, **28**, 358.
[9] BLOCH, F., 1956, *Phys. Rev.*, **102**, 104.
[10] BLOOM, A. L., and SHOOLERY, J. N., 1955, *Phys. Rev.*, **97**, 1261.
[11] ANDERSON, W. A., 1956, *Phys. Rev.*, **102**, 151.
[12] POPLE, J. A., SCHNEIDER, W. G., and BERNSTEIN, H. J., 1959, *High Resolution Nuclear Magnetic Resonance* (New York: McGraw-Hill Book Company).
[13] POPLE, J. A., and SCHAEFER, T., 1960, *Mol. Phys.*, **3**, 547.
[14] KOWALEWSKI, V. J., and DE KOWALEWSKI, D. G., 1959, *J. chem. Phys.*, **33**, 1794.
[15] ANDERSON, W. A., 1960, *N.M.R. and E.P.R. Spectroscopy* (New York: Pergamon Press).

# Relative molecular orbital energies in tetrahedral complexes

by ALAN CARRINGTON

University Chemical Laboratory, Lensfield Road, Cambridge, England

and CHR. KLIXBULL JØRGENSEN

Cyanamid European Research Institute, Cologny (Geneva), Switzerland

M.O. theory is used for classifying the energy levels of tetroxo complexes, and linear relations are shown to exist between the M.O. energies (and hence the electro-negativities) and the oxidation number and electron configuration of the central ion. The extent of $\pi$-bonding effects is quantitatively studied and compared with the analogous situation in the hexahalides.

## 1. INTRODUCTION

Quite recently, the absorption spectra of tetroxo ions of the first transition group have been interpreted by molecular orbital theory [1, 2], the assignments being supported mainly by arguments concerning the intensity and dichroism [2, 3]. The absorption band of lowest energy has been fairly well identified with a transition from the highest non-bonding molecular orbital, consisting of ligand $\pi$ electrons, to the lowest set of two degenerate molecular orbitals of symmetry $e$ constituting the partly filled shell of the central atom. However, the identification of the higher energy absorption bands seems much more uncertain at present. One of the authors [4] has investigated the order of molecular orbital energies in octahedral hexahalide complexes and suggested an extension to the identification of energy levels of tetrahedral complexes of all three transition groups. We might hope to interpret the orbital energies in terms of the number of electrons in the partly filled shell of the central atom, the principal quantum number (3d, 4d, 5d) and oxidation number of the central atom, and the nature of the ligands. The unexpected success with octahedral complexes encourages us to hope for similar results with tetrahedral complexes, about which there is now considerable experimental information [5, 6].

## 2. $\pi$-ORBITAL ENERGIES

We have first to decide on the energy differences between the three sets of $\pi$ orbitals of the ligands, $t_1$, $t_2$ and $e$, of which we are certain that the non-bonding [7] $t_1$ set has the highest energy. For the hexachlorides of central atoms with oxidation number $+3$ or $+4$, the total spread of the $\pi$ energies seems to be 7 kK ($1 \text{ kK} = 1000$ kayser $= 1000 \text{ cm}^{-1}$). Of this, a fair proportion must be caused by halogen–halogen anti-bonding effects, particularly strong in the $t_{1u}$ orbital, which has four nodal planes between the halogens [6]. The bonding of the empty p orbitals of the central atom lowers the energy of $t_{1u}$ with respect to $t_{2u}$ (which can only be depressed by interaction with central atom $f$ orbitals) by only 3 kK although in neutral platinum group hexafluorides, these energy

differences are greater [8]: about 5 kK between $t_{1g}$ and $t_{2u}$, and about 6 kK between $t_{2u}$ and $t_{1u}$. This shows the increased $\pi$-bonding effect at higher oxidation numbers.

The best evidence for the energy difference between the non-bonding $t_1$ and the bonding $t_2$ orbitals can be obtained from tetroxo ions of the second transition group. We can hardly imagine any explanation of the two first absorption bands (the second having three times the intensity of the first) other than

$$
\begin{array}{ccc}
 & \pi t_1 \rightarrow 4de & \pi t_2 \rightarrow 4de \\
\text{TcO}_4^- \text{ [7]} & 34\cdot6\,\text{kK} & 40\cdot5\,\text{kK} \\
\text{RuO}_4 \text{ [7]} & 26\cdot0 & 32\cdot3
\end{array} \tag{1}
$$

demonstrating an energy difference of 6–8 kK between $\pi t_1$ and $\pi t_2$. The third transition $\pi e \rightarrow 4de$ has no electric dipole moment and would be difficult to detect in the rather high background absorption. Similar arguments apply to the 5d-group, where the two bands of $\text{ReO}_4^-$ at 43 and 50 kK [5] presumably have the same origin. However, the possibly greater effects of intermediate coupling may disturb the simple M.O. configuration picture, and actually, three electronic levels may be distinguished in gaseous $\text{OsO}_4$ [9]. It is not easy to predict whether the spread of the $\pi$ orbital energies will be greater or smaller in the 3d group, and we cannot estimate this spread from the observed spectra before we have determined the value of $-\Delta$, the energy difference between the three $\sigma$- (and $\pi$-) antibonding molecular orbitals of symmetry $t_2$ and the lower $\pi$-antibonding $e$ orbitals.

$\Delta$ (being positive in all octahedral complexes) is $-3\cdot7$ kK in $\text{CoCl}_4^{--}$, $-2\cdot8$ kK in $\text{CoI}_4^{--}$, $-3\cdot8$ kK in Co(II), ZnO [6] and approximately $-5$ kK in $\text{FeCl}_4^-$. We would expect values of $\Delta$ between $-10$ and $-15$ kK in tetroxo complexes of higher oxidation numbers of the 3d-group. It now seems likely that the band at 16·0 kK in $\text{CrO}_4^{---}$ is a 'ligand field' transition $3de \rightarrow 3dt_2$ and the band at 14·8 kK in $\text{MnO}_4^{---}$ is $(3de)^2 \rightarrow (3de)(3dt_2)$. As discussed below, it is less clear whether the transition $3de \rightarrow 3dt_2$ of $\text{MnO}_4^-$ corresponds to the first strong band at 16·6 kK, or whether it has a similar wave-number, but is covered by the electron transfer band $\pi t_1 \rightarrow 3de$ at the latter position. It is plausible to expect a more negative value of $\Delta$ in the 4d- or 5d-groups and since $\text{RuO}_4^{--}$ does not show any bands below one of rather irregular shape [10] at 21·6 kK, it is reasonable to identify this with the transition $(4de)^2 \rightarrow (4de)(4dt_2)$.

Hence the transitions $\pi t_2 \rightarrow 3de$ and $\pi t_1 \rightarrow 3dt_2$ are expected to occur at nearly the same position, some 10 kK higher in energy than $\pi t_1 \rightarrow 3de$ in $\text{MnO}_4^-$ and $\text{CrO}_4^{---}$. It seems probable that the ultra-violet band in $\text{MnO}_4^-$ is in fact a superposition of two bands, one at 28·6 kK and another at 32·3 kK, the latter having pronounced vibrational structure [11]. These bands might very well correspond to the two transitions $\pi t_2 \rightarrow 3de$, and $\pi t_1 \rightarrow 3dt_2$ which are more nearly coincident in $\text{CrO}_4^{--}$ (at 36·6 kK) with a less negative $\Delta$.

It is remarkable that $\text{MnO}_4^-$ does not show any very strong band (with molar extinction above 5000) in the range studied (below 48 kK), but only one further shoulder ($\epsilon \sim 1500$) at 43 kK. The transitions $\sigma t_2 \rightarrow 3dt_2$ would have a very large dipole moment, analogous to $\sigma t_{1u} \rightarrow de_g$ in octahedral complexes, and already the $\sigma + \pi$ mixing in $t_2$ (analogous to $t_{1u}$ in hexahalides [4]) would presumably produce a considerable intensity of $\pi t_2 \rightarrow 3dt_2$ transitions in tetrahedral complexes. This

is the reason why we do not consider transitions from the $\sigma$ orbitals more thoroughly in this paper; they must have rather high wave-numbers.

## 3. ELECTRONEGATIVITY CONSIDERATIONS

The energy difference between electron transfer bands of hexahalides [4] is a well-defined function of the halogen and independent of the central atom. The energy differences observed,

$$\text{F } 44\text{ kK}, \quad \text{Cl } 16\text{ kK}, \quad \text{Br } 10\text{ kK} \text{ relative to I at } 0\text{ kK}, \qquad (2)$$

are fairly close to the differences between the ionization energies of the gaseous halogen *atoms*, while the ionization energies of the gaseous anions are nearly constant, 26 to 30 kK, with fluoride at an intermediate position. We do not argue that the covalent bonding in hexahalide complexes is so pronounced that the ionization energies correspond to neutral halogen atoms; the influence of the Madelung energy in the more electrovalent compounds approximately cancels the decreased ionization energy expected for the more negatively charged halogen.

It is interesting to note that the Pauling electronegativity scale follows the above order of energy differences, each unit corresponding to 30 kK. If we take the rather radical step of assuming that the wave-number of an electron transfer band itself is proportional to the difference in electronegativity of the central atom and the halogen, we obtain very reasonable values for the electronegativities of the $t_{2g}$ orbitals of the partly filled shell, using a value 3·0 for the chlorine:

$$\begin{array}{lll}
\text{4d}^5 \text{ Ru(III) } 2\cdot0 & \text{5d}^5 \text{ Os(III) } 1\cdot8 & \text{5d}^0 \text{ W(VI) } 2\cdot0 \\
\text{4d}^4 \text{ Ru(IV) } 2\cdot3 & \text{5d}^4 \text{ Os(IV) } 2\cdot1 & \text{5d}^2 \text{ Os(VI) } 2\cdot6 \\
& \text{5d}^5 \text{ Ir(IV) } 2\cdot3 & \text{5d}^4 \text{ Pt(VI) } 3\cdot2
\end{array} \qquad (3)$$

It might now be asked whether oxygen is as reducing as fluoride or as chloride. Comparison of the first electron transfer bands of $WO_4^-$ (50·3 kK) and $WF_6$ (57·0 kK) or, *a fortiori*, $OsO_4$ (33·8 kK) and, with lower oxidation number, $OsF_6$ (35·7 kK), might suggest a value of $\sim 40$ kK for oxygen in equation (2). However, it becomes clear that more complicated situations must exist, since the monochloro derivatives such as $CrO_3Cl^-$, $MnO_3Cl$ and $ReO_3Cl$ have nearly the same spectra as the monohydroxo derivatives $CrO_3(OH)^-$, $MnO_3(OH)$, and $ReO_3(OH)$, all shifted some 4 kK to lower wave-number with respect to the corresponding tetroxo ions [3].

The way out of this paradox may be found along two lines: it is evident that oxygen has the lower electronegativity with metals of low oxidation number; and that $\pi$-bonding has a considerable influence on the partly filled shell orbitals, viz. $t_{2g}$ in octahedral and $e$ in tetrahedral complexes. In the gaseous state, $O^{--}$ is unstable with respect to ionization of an electron; and large ions with rather small positive charges do not stabilize $O^{--}$ much, by mere Madelung considerations, explaining the ultra-violet transparency of $Al_2O_3$ as compared to orange $Cs_2O$ and yellow $K_2O$.

The second part of the explanation has been studied quite recently, e.g. Orgel and one of the authors [12] have demonstrated that the $\pi$-bonding effects of oxygen and nitrogen atoms in polynuclear ruthenium and iridium complexes of

mixed oxidation numbers shift the energy of the appropriate, anti-bonding linear combinations of metal $t_{2g}$ orbitals to the extent of 10 to 20 kK. Lott and Symons [13] have explained the diamagnetism of the monomeric $5d^2$ systems $OsO_2(OH)_4^{--}$ and $OsO_2Cl_4^{-}$ by the strong $\pi$-antibonding effects on the d orbitals $(xz, yz)$ from two oxygen atoms on the $z$ axis of a tetragonal complex. When compared with the extrapolated wave-number of the first electron transfer band of the hypothetical $OsCl_6$ at 10 kK, the band of $OsO_2Cl_4^{--}$ at 28 kK suggests a similar strong effect.

Hence we cannot conclude that two ligands have the same electronegativity if their complexes with a given central ion have the electron transfer bands at the same wave-number, since the $\pi$-bonding effects may be different on the excited orbital in the partly filled shell, e.g. the low-spin $RuBr_6^{-}$ and $Ru(CN)_6^{---}$ both having their first strong bands close to 21 kK [8]. While the empty $\pi$-orbitals in cyanide, phosphines and arsines presumably depress the appropriate orbital in the partly filled shell of the transition group elements, the opposite effect evidently occurs in oxygen complexes, as mentioned above. It can be estimated from the monohydroxo complexes $MO_3(OH)$, which have the transition from the highest non-bonding combination of ligand orbitals [3, 13] at 3 to 4 kK below the similar transition in $MO_4$. In other words, the electro-negativities should be perhaps half a unit smaller for oxide than for halide complexes of a given central atom with high oxidation number. This phenomenon occurs also outside the transition groups; thus the weak bands with vibrational structure of $UO_2^{++}$ at 23 kK and $UF_6$ at 27 kK are probably shifted by a comparatively lower energy of the 5f shell in the more electrovalent hexafluoride, though $\pi$-bonding effects are probably of lower importance in this particular case.

The spin-pairing energy, i.e. that part of the interelectronic repulsion energy which is dependent on $S$, is rather important in determining the position of the electron transfer bands. In the hexahalides [4] it has been shown that a very good approximation is to put the spin-pairing energy equal to $-DS(S+1)$. In the tetroxo ions it is conspicuous that the band positions are not always a monotonic function of the number of electrons in the partly filled shell at constant oxidation number. Thus, the bands at 36·8 kK of $VO_4^{---}$, 28·2 kK of $CrO_4^{---}$ and 30·5 kK of $MnO_4^{---}$ suggest a hump at the $3d^2$ system of some 9 kK. This can be readily explained as the hump for half-filled shells, being $(e+1)D$ where $e$ is the orbital degeneracy. It is difficult to be sure of the numerical value of the hump $3D$, going from the excited state $e^2$ in $d^1$ systems to $e^3$ in $d^2$ systems. In the gaseous $Mn^{+5}$ ion, the Racah parameter $B$ is $1·16$ kK, and since $D$ is roughly equal to $6·5B$ the suggested value of $D=3$ kK is equivalent to a nephelauxetic ratio $\beta=0·40$, which compares favourably with the values in the neutral hexafluorides [14]. Since the first electron transfer band occurs at 26·8 kK in $CrO_4^{--}$, it seems reasonable to identify the bands at 16·0 kK in $MnO_4^{--}$ and at 19·6 kK (or 12·7 kK ?) in $FeO_4^{--}$ as the analogous features. The decrease per unit of atomic number in a series with constant oxidation number is, when corrected for the influence of spin-pairing energy, some 7 to 9 kK in the hexahalides, and roughly 10 kK for the tetroxo ions according to the information given above. The variation of the wave-number of the electron transfer band in an isoelectronic series as function of the atomic number (or oxidation number) is 15 kK in the hexahalides and 10 kK in the tetroxo complexes. It is now recognized [8] that the latter quantity is the greater the more electrostatic

is the bonding, and may approach the difference in ionization energy of the gaseous ions, where the order of magnitude is 100 kK per unit of ionic charge. Thus, the electronegativities of tetravalent lanthanides (such as Nd(IV) and Dy(IV)) must be more than 2·5 units higher (cf. equation (3)) than the isoelectronic trivalent lanthanides (Pr(III), Tb(III), etc.).

Finally we must consider the electronegativity differences between the 3d and the two other transition groups. The difference 7 kK (=0·23 Pauling unit) between 4d and 5d, known from the hexahalides, is found again in the tetroxo ions. The latter complexes suggest the difference 17 kK between 3d and 4d. When tetrahalides such as $VBr_4$ with a double band at 21·2 and 24·5 kK [15], $FeCl_4^-$ with a band at 27·3 kK or $CoCl_4^{--}$ at 42·5 kK, are compared with the 4d and 5d hexahalides, it becomes clear that the difference between Fe(III) and Ru(III) is 15 kK after correction for spin-pairing contribution; it may however be difficult to compare high-spin and low-spin complexes. The difference between the oxidation numbers +2 and +3 in the 3d tetrahalides is very great, some 34 kK or more than one Pauling unit of electronegativity, suggesting relatively larger variation of the effective charge of the central atom, i.e. more electrovalent bonding, at least in $CoCl_4^{--}$.

Our conclusions can be summarized as follows:

1. The bonding linear combination of ligand $\pi$-orbitals of symmetry $t_2$ has 6–8 kK lower energy than the non-bonding set $t_1$ in $TcO_4^-$ and $RuO_4$ and hence, the tetroxo ions seem to have a slightly larger splitting of the $\pi$ M.O. energies than have the hexahalides.

2. $\Delta$ is close to $-15$ kK in 3d-group tetroxo ions and $-22$ kK in $RuO_4^{--}$.

3. The energy of the $\sigma$-orbitals is so low that the $\sigma t_2 \rightarrow dt_2$ transitions have not been observed.

4. The effects of $\pi$-bonding on the partly filled shell, increasing the energy of $e$ in tetrahedral and $t_{2g}$ in octahedral complexes, are pronounced in oxygen complexes with central atoms in high oxidation states, and may cause band shifts amounting to 20 kK.

5. The electronegativity of the ligands and central atoms can be correlated with the wave-numbers of the electron transfer bands.

6. The spin-pairing energy is considerable in tetrahedral 3d complexes, $D$ often being above 3 kK.

7. The electronegativity of 4d elements with oxidation number at least +3 is some 0·23 Pauling units (=7 kK) higher than the corresponding 5d elements with the same oxidation number.

8. While the hexahalides and tetroxo ions suggest electronegativity differences of 0·5 Pauling units per unit of oxidation number in isoelectronic series, the electronegativity of tetrahalides of the 3d group with the oxidation number +2 is 1·1 units lower than that of the isoelectronic central atom with the oxidation number +3.

## REFERENCES

[1] CARRINGTON, A., SCHONLAND, D., and SYMONS, M. C. R., 1960, *J. chem. Soc.*, p. 889.
[2] CARRINGTON, A., and SCHONLAND, D. S., 1960, *Mol. Phys.*, **3**, 331.
[3] CARRINGTON, A., unpublished work.
[4] JØRGENSEN, C. K., 1959, *Mol. Phys.*, **2**, 309.
[5] CARRINGTON, A., SCHONLAND, D., and SYMONS, M. C. R., 1957, *J. chem. Soc.*, p. 659.
[6] MCCLURE, D. S., 1959, *Solid State Phys.*, **9**, 399.

[7] WOLFSBERG, M., and HELMHOLZ, L., 1952, *J. chem. Phys.*, **20**, 837.
[8] JØRGENSEN, C. K., 1961, *Advanc. chem. Phys.*, **4** (to be published).
[9] LANGSETH, A., and QVILLER, B., 1934, *Z. phys. Chem.* B, **27**, 79.
[10] CONNICK, R. E., and HURLEY, C. R., 1952, *J. Amer. chem. Soc.*, **74**, 5012.
[11] BOEF, G. DEN, BEEK, H. J. VAN DER, and BRAAF, T., 1958, *Rec. Trav. chim. Pays-Bas*, **77**, 1064.
[12] JØRGENSEN, C. K., and ORGEL, L. E., 1961 (to be published).
[13] LOTT, K. A. K., and SYMONS, M. C. R., 1960, *J. chem. Soc.*, p. 973.
[14] JØRGENSEN, C. K., 1960, *Mol. Phys.*, **3**, 201.
[15] SCAIFE, D. E. (private communication).

# An acoustic model of diffusion in gases† [1]

## by LEONARD KOTIN‡

Institute for the Study of Metals, University of Chicago, Chicago 37, Illinois

Principles of macroscopic acoustical theory are applied to the calculation of the friction constant of a dilute gas of rigid spheres. In the model molecular motions are perturbed by acoustic disturbances arising from the occurrence of density fluctuations in the equilibrium fluid. The friction constant calculated is found to have the same parametric form but a substantially lower numerical coefficient when compared with the result of Chapman and Enskog.

## 1. Introduction

Our present concept of gaseous diffusion is firmly rooted in the kinetic theory of gases. The work of Chapman and Enskog [2] has demonstrated a rigorous statistical approach to the calculation of transport coefficients in gases; and these results have been eminently successful in their agreement with experiment in the case of moderately dilute gases. However, the transport properties of dense gases is currently a matter of great theoretical interest, standing, as it were, at the threshold of the almost prohibitively difficult problem of liquids.

The kinetic theory approach takes as its starting point the Boltzmann equation for the evolution of molecular distribution functions in time. The model of the gas is that of a collection of molecules undergoing chaotic thermal motions in which molecular collisions are solely responsible for the translation of matter, energy, and momentum. At the core of the Chapman–Enskog theory is a detailed dynamical description of a collision between a pair of molecules in the gas.

In a liquid one recognizes the existence of a great deal of order, so that the concept of random molecular collisions as the principal causative influence on the transport properties loses its value. Instead, one is led to a picture of a molecule moving in the field of force provided by the other molecules in the fluid or at least by its nearest neighbours. The translation of a liquid molecule is accomplished by its 'jumping' from one position of equilibrium to another. This process gives rise to the existence of a fluid retardation characterizing the restraining forces on a molecule due to the remainder of the fluid. Indeed, Kirkwood [3] has demonstrated that the equation of motion of a molecule in a fluid contains a dissipative term proportional to the velocity which is in all respects analogous to the corresponding term introduced in an *ad hoc* manner in Einsteins' theory of the Brownian motion [4] of a macroscopic particle in a

homogeneous fluid. Thus, the retarding force on a molecule in a liquid may be characterized by a friction constant.

Although one does not ordinarily think of a friction constant in connection with a gas, it is of theoretical interest to seek a gaseous model which displays a frictional character in order that a more unified viewpoint toward the liquid and gaseous states might be achieved. An approach of this kind has recently been made by Longuet-Higgins and Pople [5] who calculated the self-diffusion coefficient of a gas starting from a quite general molecular definition of the latter and the assumption that the Langevin equation of Brownian motion theory adequately describes the molecular motion.

In the following sections, we shall discuss a model for gaseous diffusion based upon the macroscopic theory of acoustic radiation [6]. In the model a molecule is assumed to be subject to fluid pressure waves arising from density fluctuations in the surrounding fluid. The motion of the molecule is associated with acoustic radiation into the fluid resulting in an acoustic impedance which gives rise to a frictional force on the molecule. Although a continuum theory is employed, the inherent inhomogeneity of the fluid is taken into account through consideration of multiple scattering from molecular centres. A friction constant for a dilute gas of rigid spheres is obtained and compared with the result of the Chapman–Enskog first approximation.

## 2. Fluid force

It is easily shown that the frictional force on a molecule may be related to the occurrence of spontaneous fluctuations in density in the fluid. The latter manifest themselves, in our present acoustical context, as pressure waves perturbing the molecular motion.

A general formula for the instantaneous force acting on a molecule located at $\mathbf{R}_1$ arising from the resultant of the other molecules in the fluid is

$$\mathbf{F}_1 = -\int \nabla_1 V(R_{12}) \rho'(\mathbf{R}_2) \, d\mathbf{R}_2 \tag{1}$$

where $V(R_{12})$ is the intermolecular potential and $\rho'(\mathbf{R}_2)$ is the instantaneous number density at $\mathbf{R}_2$ conditional on the presence of a molecule at $\mathbf{R}_1$. The average value of $\rho'(\mathbf{R}_2)$ at the distance $(R_{12})$ from a molecule at $\mathbf{R}_1$ is given in terms of the potential of average force $W(R_{12})$ and the average number density $\nu$ by the relation

$$\rho'(\mathbf{R}_2) = \nu \exp\left[-W(R_{12})/KT\right]. \tag{2}$$

We assume that the instantaneous density $\rho'(R_2)$ may be expressed by

$$\rho'(\mathbf{R}_2) = \exp\left[-W(R_{12})/KT\right](\nu + n(\mathbf{R}_2)) \tag{3}$$

where $n(\mathbf{R}_2)$ is the fluctuation in density at $\mathbf{R}_2$.

Now, employing a well-known identity, we express the gradient of the potential energy by

$$-\nabla_1 V(R_{12}) = -KT\mathbf{e}_R\left\{\frac{\partial}{\partial R}\exp\left[-V(R)/KT\right]\right\}\exp\left(V/KT\right) \tag{4}$$

where $\mathbf{e}_R$ is a unit vector in the $R_{12}$ direction. At this point one explicitly introduces the rigid sphere molecular model which immediately allows us to

reduce (4) to

$$-\nabla_1 V(R_{12}) = -KT\mathbf{e}_R \, \delta(R-a) \exp(V/KT) \tag{5}$$

where $\delta(R-a)$ is a Dirac delta function and $a$ is the molecular diameter. Introducing (3) and (5) into (1), we obtain the result

$$\mathbf{F} = -KT \int \mathbf{e}_R \, \delta(R-a) \exp[V(R)-W(R)]/KT \, n(\mathbf{R}_2) \, d\mathbf{R}_2$$

$$= -KTa^2 \exp\{[V(a)-W(a)]/KT\} \int \mathbf{e}_R n(\mathbf{e}_R a) \, d\mathbf{e}_R. \tag{6}$$

We immediately proceed to a consideration of a dilute gas by assuming the absence of triplet correlations which may be formally expressed by equating $V(a)$ and $W(a)$; i.e. we omit all extra contributions to $W(a)$ [7]. This operation finally furnishes us with an expression for the force acting on a molecule as a function of the fluctuation in density, namely,

$$\mathbf{F} = KTa^2 \int \mathbf{e}_R n(\mathbf{e}_R a) \, d\mathbf{e}_R. \tag{7}$$

The force expressed in (7) is quite similar in form to the macroscopic equation for the excess force on a large sphere due to a fluctuation in pressure, i.e. formally identical to the ideal gas law.

Having obtained a clearly defined fluid force, we turn to the calculation of the density fluctuation $n(\mathbf{e}_R a)$ from the fluid model. Once $n(\mathbf{e}_R a)$ has been obtained, the complete equation of motion of molecule in the fluid is determined and the diffusion coefficient may be calculated.

## 3. FLUCTUATIONS IN DENSITY

We are now interested in correlating the instantaneous fluctuations with some bulk property of the fluid. To proceed, we seek an equation for the density fluctuations of the form [8]

$$\frac{\partial^2}{\partial t^2} n(\mathbf{R}_1) = \int K(R_{12}) n(\mathbf{R}_2) \, d\mathbf{R}_2; \tag{8}$$

i.e. an equation for the time rate of change of the fluctuation at $\mathbf{R}_1$ due to a fluctuation at $\mathbf{R}_2$. The form chosen for (8) is suggested by the observation that the density fluctuations, being acoustic waves, are assumed to obey the wave equation. Since it may also be shown that all correlations between the first derivative at $\mathbf{R}_1$ and the fluctuation at $\mathbf{R}_2$ vanish identically in an equilibrium ensemble, the choice of the second derivative has the additional virtue of simplicity.

The development from this point follows the linear prediction theory of Fixman [9]. Accordingly, one minimizes the mean square difference of the two sides of (8) to provide the result

$$\left\langle \frac{\partial^2}{\partial t^2} n(\mathbf{R}_1) \, n(\mathbf{R}_2) \right\rangle = \int K(R_{13}) \langle n(\mathbf{R}_2) n(\mathbf{R}_3) \rangle \, d\mathbf{R}_3. \tag{9}$$

Equation (9) affords us a relation between the cross correlation in the left-hand side with the autocorrelation of the density fluctuations.

It will be shown presently that the function $K(R_{12})$ is intimately related to the instantaneous flow potential $\psi(\mathbf{R}, t)$ in the fluid. Before proceeding to this

demonstration, however, we consider the explicit form which must be taken by $K(R_{12})$. Assuming that the correlation functions in (9) are functions only of the relative coordinates indicated, one applies the operator

$$\int d\mathbf{R}_1 \exp\left[i\mathbf{k} \cdot (\mathbf{R}_1 - \mathbf{R}_2)\right]$$

to both sides of (9) to accomplish a Fourier space transformation. This operation leads to

$$\int \left\langle \frac{\partial^2}{\partial t^2} n(\mathbf{R}_1) \cdot n(\mathbf{R}_2) \right\rangle \exp\left[i\mathbf{k} \cdot (\mathbf{R}_1 - \mathbf{R}_2)\right] d\mathbf{R}_1 = \int K(R_{13}) \exp\left[i\mathbf{k} \cdot (\mathbf{R}_1 - \mathbf{R}_3)\right] d\mathbf{R}_1$$

$$\int \langle n(\mathbf{R}_2) \cdot n(\mathbf{R}_3) \rangle \exp\left[i\mathbf{k} \cdot (\mathbf{R}_3 - \mathbf{R}_2)\right] d\mathbf{R}_3.$$

Now defining the Fourier transforms,

$$\left.\begin{aligned}
A(\mathbf{k}) &= \int \left\langle \frac{\partial^2}{\partial t^2} n(\mathbf{R}_1) n(\mathbf{R}_2) \right\rangle \exp\left[i\mathbf{k} \cdot (\mathbf{R}_1 - \mathbf{R}_2)\right] d\mathbf{R}_1, \\[2mm]
B(\mathbf{k}) &= \int -K(R_{13}) \exp\left[i\mathbf{k} \cdot (\mathbf{R}_1 - \mathbf{R}_3)\right] d\mathbf{R}_3, \\[2mm]
C(\mathbf{k}) &= \int \langle n(\mathbf{R}_2) \cdot n(\mathbf{R}_3) \rangle \exp\left[i\mathbf{k} \cdot (\mathbf{R}_3 - \mathbf{R}_2)\right] d\mathbf{R}_3,
\end{aligned}\right\} \tag{10}$$

one obtains an elementary result for $B(\mathbf{k})$, namely,

$$B(\mathbf{k}) = -\frac{A(\mathbf{k})}{C(\mathbf{k})}. \tag{11}$$

Thus, the Fourier transform of $-K(R_{12})$, $B(\mathbf{k})$, is now immediately calculable from an explicit representation of the correlations appearing in the equations for $A(\mathbf{k})$ and $C(\mathbf{k})$. It is shown in Appendix A that the correlations take the form

$$\left.\begin{aligned}
\left\langle \frac{\partial^2}{\partial t^2} n(\mathbf{R}_1) \cdot n(\mathbf{R}_2) \right\rangle &= -KT/m \, \nu \nabla_1^2 \delta(\mathbf{R}_1 - \mathbf{R}_2), \\[2mm]
\langle n(\mathbf{R}_2) \cdot n(\mathbf{R}_3) \rangle &= \nu^2 g(R_{23}) + \nu \delta(\mathbf{R}_2 - \mathbf{R}_3) - \nu^2
\end{aligned}\right\} \tag{12}$$

where $g(R_{23})$ is the radial distribution function.

Now introducing (12) into (10) and (11), we finally obtain

$$B(\mathbf{k}) = \frac{KT/m \, k^2}{1 + \nu \displaystyle\int_{-\infty}^{\infty} [g(R_{23}) - 1] \exp\left[i\mathbf{k} \cdot (\mathbf{R}_3 - \mathbf{R}_2)\right] d\mathbf{R}_3}. \tag{13}$$

The denominator is simplified by the introduction of spherical polar coordinates and carrying out the angular integrations using the direction of $k$ as the polar axis. Thus, (13) becomes

$$B(\mathbf{k}) = \frac{KT}{m} \frac{k^2}{1 + 4\pi\nu/k \displaystyle\int_0^{\infty} R \, dR \sin kR [g(R) - 1]}; \tag{14}$$

$B(\mathbf{k})$ is thus completely determined by a knowledge of the radial distribution function.

We now inquire into the relation of $K(R_{12})$ to a scalar flow potential in the fluid. One defines the latter by the relation

$$\mathbf{J}(\mathbf{R},\, t) = \nabla_R \psi(\mathbf{R},\, t) \tag{15}$$

where $\mathbf{J}$ is the number flux of molecules expressed in terms of molecular quantities by

$$\mathbf{J}(\mathbf{R}) = \sum \delta(\mathbf{R} - \mathbf{R}_i)\mathbf{u}_i \tag{16}$$

where $\mathbf{u}_i$ is the instantaneous velocity of molecule $i$. Also, using the molecular formula for the instantaneous fluctuation $n(\mathbf{R})$,

$$n(\mathbf{R}) = \sum_i \delta(\mathbf{R} - \mathbf{R}_i) - \nu \tag{17}$$

one easily establishes the identity

$$\frac{\partial n(\mathbf{R})}{\partial t} = - \nabla^2 \psi(\mathbf{R},\, t). \tag{18}$$

We may now place an interpretation on the flow potential by asserting that it arises from the presence of instantaneous fluctuations. The latter manifest themselves in fluid disturbances which may be formally described by a scalar potential. It is emphasized that the potential defined above is present in an equilibrium fluid and although it bears a formal similarity to a macroscopic potential it is to be associated with fluctuations rather than macroscopic density gradients.

An equation for $\psi(\mathbf{R},\, t)$ may be derived from equations (8) and (18) (see Appendix B). The result is simply

$$\frac{\partial^2 \psi(\mathbf{R}_1,\, t)}{\partial t^2} = \int K(R_{12})\psi(\mathbf{R}_2,\, t)\, d\mathbf{R}_2. \tag{19}$$

One notes that $\psi(\mathbf{R},\, t)$ satisfies the same integral equation as $n(\mathbf{R})$ (cf. (8) ), and further, that the coefficient $K(R_{12})$ is precisely the one we were occupied with earlier.

Taking the Fourier time transforms of (19) we obtain

$$w^2 \psi_w(\mathbf{R}_1) = \int - K(R_{12})\psi_w(\mathbf{R}_2)\, d\mathbf{R}_2. \tag{20}$$

We may now seek solutions of (20). It may be demonstrated that the solutions of (20) must obey the necessary condition [10]

$$w^2 = B(\mathbf{k}) \tag{21}$$

where $B(\mathbf{k})$ has been defined as the Fourier space transform of $-K(R_{12})$. In addition, any solution of (20) must include one wave component possessing an imaginary propagation number $(k)$ corresponding physically to a damped radiative wave in the fluid; the latter might well be expected in view of the physical requirement that the density fluctuations must be dissipated in an equilibrium fluid.

Now, having established the connection between the fluctuations and the flow potential we proceed with an investigation of the latter.

### 4. ACOUSTIC SCATTERING FROM SPHERICALLY SYMMETRIC CENTRES

In a homogeneous fluid the wave function $\psi_w(\mathbf{R})$ satisfies the scalar Helmholtz equation

$$\nabla^2 \psi_w(\mathbf{R}) + k^2 \psi_w(\mathbf{R}) = 0. \tag{22}$$

However, this result applies only to a fluid which contains no scattering centres. In a fluid with $N$ scatterers (molecules), under the assumption of isotropic scattering, it may be seen that the wave function at any point is determined by the relation

$$\psi(\mathbf{R}) = \psi_0(\mathbf{R}) + \sum_j g_j(k)\psi^j(\mathbf{R}_j) \frac{\exp(i\mathbf{k} \cdot |\mathbf{R} - \mathbf{R}_j|)}{|\mathbf{R} - \mathbf{R}_j|} \tag{23}$$

where $\psi_0(\mathbf{R})$ is an arbitrary incident wave and the second term corresponds to a superposition of the contributions of the scattering centres. $\psi^j(\mathbf{R}_j)$ is the potential at the position of molecule $j$ excluding the contribution of molecule $j$. The subscript $w$ has been suppressed in (23). The scattering coefficient $g_j(k)$ may be determined by an application of boundary conditions at the surface of a molecule.

If the molecules in the fluid are identical (i.e. they have identical scattering coefficients and radii) one may compute the average field at $\mathbf{R}$ by averaging (23) over the position of molecule $j$ assuming it to be uncorrelated with any other molecule to provide

$$\psi(\mathbf{R}) = \psi_0(\mathbf{R}) + g(k)\nu \int d\mathbf{R}_j \psi(\mathbf{R}_j) \frac{\exp(i\mathbf{k} \cdot |\mathbf{R} - \mathbf{R}_j|)}{|\mathbf{R} - \mathbf{R}_j|}. \tag{24}$$

In (24) we have replaced $\psi^j(\mathbf{R}_j)$ by $\psi(\mathbf{R}_j)$ corresponding to the inclusion of the field of the $j$th molecule at $\mathbf{R}_j$. This change renders a great simplification of the following analysis; moreover, it is an excellent approximation for large $N$ [12].

The differential equation satisfied by $\psi(\mathbf{R})$ is derived by application of the operator $(\nabla_R^2 + k^2)$ to both sides of (24). This operation provides

$$(\nabla^2 + k^2)\psi(\mathbf{R}) = -4\pi\nu g(k) \int d\mathbf{R}_j \delta(\mathbf{R} - \mathbf{R}_j)\psi(\mathbf{R}_j)$$

$$= -4\pi\nu g(k)\psi(\mathbf{R}).$$

Hence, $\psi(\mathbf{R})$ satisfies the equation

$$\nabla^2\psi(\mathbf{R}) + [k^2 + 4\pi\nu g(k)]\psi(\mathbf{R}) = 0. \tag{25}$$

Comparison of (23) and (25) shows the alteration which obtains due to the presence of scatterers in the fluid. For a detailed discussion of the multiple scattering problem treated above, the reader is referred to an elaborate development by Foldy [12].

Now, it is assumed that the wave function corresponding to the density fluctuations (see (20)) satisfies the scalar Helmholtz equation

$$\nabla^2\psi_w(\mathbf{R}) + k_0^2\psi_w(\mathbf{R}) = \exp(i\mathbf{k} \cdot \mathbf{R}) \tag{26}$$

where $k_0$ corresponds to the allowed values of the propagation constant arising from (21) and the right-hand side corresponds to the presence of a plane wave source. If one identifies this wave function with $\psi(\mathbf{R})$ in (25), one has in (25) and (26) a pair of differential equations which must be satisfied simultaneously. Subtracting (25) from (26) one obtains

$$[k_0^2 - k^2 - 4\pi\nu g(k)]\psi(\mathbf{R}) = \exp(i\mathbf{k} \cdot \mathbf{R}). \tag{27}$$

In order to derive the solution which obtains due to the superposition of waves

with all possible values of $k$ (i.e. $\psi(\mathbf{R})$ is a function of $k$), namely, $\psi^T(\mathbf{R})$, one integrates $\psi(\mathbf{R})$ over all $k$; hence,

$$\psi^T(\mathbf{R}) = \int \frac{d\mathbf{k} \exp (i\mathbf{k} \cdot \mathbf{R})}{[k_0^2 - k^2 - 4\pi vg(k)]}. \tag{28}$$

In (26) one ought to take a source function which has a function of $k$ for a coefficient corresponding to the amplitude of the wave with propagation constant $k$. However, one has no knowledge of the relative amplitudes and accordingly one can make no progress. Hence, $\psi^T(\mathbf{R})$ must be regarded as solution obtained under the assumption that waves of different values of $k$ have equal amplitudes. The constant factor will be determined later from an application of appropriate boundary conditions.

Dropping the superscript on $\psi^T(\mathbf{R})$, one simplifies (28) by performing the angular integrations taking $R$ as the polar axis to yield

$$\psi(\mathbf{R}) = \frac{2\pi}{iR} \int_0^\infty \frac{dk \, k^2}{[k_0^2 - k^2 - 4\pi vg(k)]} \frac{[\exp (ikR) - \exp (-ikR)]}{k}. \tag{29}$$

Under the assumption that the first factor of the integral in (29) is a symmetric function of $k$, the limits of integration may be altered with the simultaneous absorption of the second term to provide

$$\psi(\mathbf{R}) = \frac{2\pi}{iR} \int_{-\infty}^\infty \frac{dk \, k \exp (ikR)}{[k_0^2 - k^2 - 4\pi vg(k)]}. \tag{30}$$

The scattering factor $g(k)$ is determined by asserting that on the surface of a molecule the fluid velocity of the incident wave must be equal and opposite to the fluid velocity of the scattered wave. The result is found to be (Appendix C)

$$g(k) = \frac{ij_1(ka)}{kh_1(ka)} \tag{31}$$

where $j_1(ka)$ and $h_1(ka)$ are spherical Bessel and Hankel functions of order unity. It is noted that the complex quantity $g(k)$ is itself not invariant to the transformation $k \rightarrow -k$, but its real part is. Hence, from (30) on, the formulae containing $g(k)$ refer only to the real part of (31) in accord with the assumption used in deriving (30). It is interesting to remark that

$$\mathrm{Re}\, g(k) = \tfrac{1}{2}[g(k) + g^*(k)]$$

and it is easily demonstrated that the use of $\mathrm{Re}\, g(k)$ implies that the contributions of both incoming and outgoing waves to the scattering coefficient have been given equal weight.

Equation (30) may now be integrated in the complex $k$ plane by choosing a contour enclosing two of the four poles of the integral (i.e. one on the positive real axis and one on the positive imaginary axis) with an infinite semi-circle in the upper half plane. The poles are located at

$$k_1 = \pm \sqrt{\left(\frac{k_0^2}{1 + 8\pi va^3}\right)}; \quad k_2 = \pm \frac{i}{a}\left(1 - \frac{2\pi va^3 \exp (-2)}{1 + k_0^2a^2}\right). \tag{32}$$

The evaluation of (30) proceeds readily to provide the solution

$$\psi(\mathbf{R}) = -2\pi^2 \left[\frac{\exp (ik_1 R)}{R} + c\frac{\exp (ik_2 R)}{R}\right] \tag{33}$$

where

$$c = \frac{4\pi v a^3 \exp(-2)}{(1 + k_0^2 a^2)^2}. \tag{33'}$$

It is recalled (cf. discussion following (28)) that we must still construct a proper solution for the wave function. In a sense, we may regard (33) as a Green function [6]. One might attempt to develop a solution containing angular character by assuming the function

$$\Psi = (\mathbf{A} \cdot \mathbf{e}_R)\psi(\mathbf{R})$$

as a basis. However, it is easily verified that this function does not satisfy the Helmholtz equation—a major requirement for the proper function. If one chooses the next most obvious construct,

$$\Psi = \mathbf{A} \cdot \mathbf{e}_R \frac{\partial \psi(\mathbf{R})}{\partial R} \tag{34}$$

one finds that $\Psi$ does indeed meet the requirement. Therefore we may complete the remainder of the problem employing (34).

The constant vector $A$ is determined by introducing the definition of the wave function in terms of the instantaneous number flux $\mathbf{J}(\mathbf{R}, t)$ (i.e. (15)). One finds that

$$\mathbf{J} = \nabla_R \Psi = (\mathbf{A} \cdot \mathbf{e}_R)\mathbf{e}_R \frac{\partial^2 \psi}{\partial R^2} + \mathbf{e}_\theta (\mathbf{A} \cdot \mathbf{e}_\theta) \frac{1}{R} \frac{\partial \psi}{\partial R}.$$

Setting $\mathbf{J}$ equal to $\rho \mathbf{v}_f$, the product of the instantaneous number density and the fluid velocity, we determine $A$ by requiring that the radial fluid velocity on the surface of a molecule equal the radial velocity of the molecule, $\mathbf{v}$.

Thus

$$\mathbf{A} = \frac{\rho \mathbf{v}}{(\partial^2 \psi / \partial R^2)_{R=a}}$$

and

$$\Psi = \frac{\rho(\mathbf{v} \cdot \mathbf{e}_R)}{(\partial^2 \psi / \partial R^2)_{R=a}} \frac{\partial}{\partial R} \psi(\mathbf{R}). \tag{35}$$

The fluid force on a molecule may be calculated by employing (7) and (18). Computing the time derivative of the instantaneous density, one finds

$$\frac{\partial \rho(\mathbf{R}, t)}{\partial t} = -\rho \frac{(\mathbf{v} \cdot \mathbf{e}_R)}{(\partial^2 \psi / \partial R^2)_{R=a}} \left\{ \exp(ik_1 R) \frac{k_1^2}{R^2}(1 - ik_1 R) \right.$$

$$\left. + \frac{c}{R^2} \exp(ik_2 R)(1 - ik_2 R) \right\}. \tag{36}$$

Finally, one assumes the time variation of $\rho$ is small; accordingly $\rho$ may be replaced by its average value $v$ on the right-hand side of (36). Since it is convenient to work with the Fourier time transform of the molecular velocity we apply the operator $\int \exp(iwt)\, dt$ to (36). Defining the Fourier time transform of the molecular velocity by $\mathbf{U}(w)$, we obtain the fluctuation at the surface of the molecule by evaluating the transformed equation at $R = a$; hence,

$$-iwn(\mathbf{e}_R a) = \frac{-v[\mathbf{U}(w) \cdot \mathbf{e}_R]c}{ea}. \tag{37}$$

In deriving (37) we have neglected terms of order $(ka)$ compared with unity due to the fact that one seeks a diffusion constant which involves only the low frequency components of the velocity spectrum. Also, terms of $0(va^3)$ have

been neglected compared with unity owing to our limitation of consideration to dilute gases.

Substitution of (37) and (33′) into (7) enables us to compute the Fourier transform of the fluid force acting on a molecule, namely,

$$\mathbf{F}(w) = -\frac{16\pi^2}{3}\frac{v^2 a^4}{e^3}KT\frac{\mathbf{U}(w)}{iw} = -\alpha^2\frac{\mathbf{U}(w)}{iw}, \tag{38}$$

and the equation of motion becomes

$$-iwm\mathbf{U}(w) = -\frac{\alpha^2\mathbf{U}(w)}{iw} + \mathbf{R} \tag{39}$$

where $\mathbf{R}$ is an appropriately chosen constant vector (independent of $w$) which specifies the velocity of the molecule at $t=0$. The molecular velocity $\mathbf{v}(t)$ is obtained by Fourier transformation of $\mathbf{U}(w)$, so that

$$\mathbf{v}(t) = \frac{\mathbf{R}i}{2\pi m}\int_{-\infty}^{\infty}\frac{dw\, w\, \exp(-iwt)}{(w+i\beta)(w-i\beta)} \tag{40}$$

and $\beta = (\alpha^2/m)^{1/2}$.

Equation (40) is integrated in the complex $a$ plane taking a contour along the real axis and an infinite semi-circle enclosing the pole at $w = -i\beta$. Thus,

$$\mathbf{v}(t) = \mathbf{v}(0)\exp(-\beta t). \tag{41}$$

Equation (41) which was derived from our fluid model has a form which is identical to solutions of the Langevin equation. If it is substituted into the general autocorrelation expression for the diffusion constant,

$$D = \tfrac{1}{3}\int_0^{\infty}\langle\mathbf{v}(0)\cdot\mathbf{v}(t)\rangle\,dt$$

and one averages the square of the velocity at $t=0$ over a Maxwellian ensemble, one obtains the familiar result, $D = KT/m\beta$.

Hence, we formally identify $\beta$ as the friction constant:

$$\beta = \left(\frac{16\pi^2}{3e^3}\right)^{1/2}va^2\left(\frac{KT}{m}\right)^{1/2}. \tag{42}$$

## 5. DISCUSSION

The value of the friction constant obtained from our model is approximately 34 per cent of the Chapman–Enskog first approximation. However, both results have precisely the same dependence on the density, molecular diameter and mass, and the temperature.

That the numerical value of the friction constant is found to be smaller than the kinetic theory result may be quite reasonable for the sole source of friction in the model was assumed to arise from radiation impedance associated with the acoustic radiation of a molecule in the fluid. One should like to state that the result shows that 34 per cent of the frictional force arises from the presence of spontaneous density fluctuations (the remainder from other sources); however, it would be unfair to do so in view of the techniques of approximation employed above.

The work outlined must be regarded as a rough preliminary investigation of the model for it would appear extremely doubtful that the methods and boundary conditions of macroscopic acoustics from which we have drawn

extensively are proper. Indeed, Rice [13] has managed to completely avoid the problem of boundary conditions in his application of an acoustic continuum model to a liquid with the resulting friction constant twice as large as experiment.

The author owes a deep debt of gratitude to Dr. Marshall Fixman for his consistently excellent advice and counsel during the course of this research. In addition, we wish to thank Professor Stuart A. Rice for having stimulated new interest in the present work.

## APPENDIX A [11]

Introducing the molecular formula for the instantaneous fluctuation (17) into (9), one finds

$$
\left\langle \frac{\partial^2 n(\mathbf{R}_1)}{\partial t^2} \cdot n(\mathbf{R}_2) \right\rangle = - \left\langle \sum_{ij} \mathbf{u}_i \mathbf{u}_i : \nabla_{R_1} \nabla_{R_1} \delta(\mathbf{R}_1 - \mathbf{R}_i) \delta(\mathbf{R}_2 - \mathbf{R}_j) \right\rangle
$$
$$
+ \left\langle \sum_{ij} \dot{\mathbf{u}}_i \cdot \nabla_{R_1} \delta(\mathbf{R}_1 - \mathbf{R}_i) \delta(\mathbf{R}_2 - \mathbf{R}_j) \right\rangle + \nu \left\langle \sum_i \mathbf{u}_i \mathbf{u}_i : \nabla_{R_1} \nabla_{R_1} \delta(\mathbf{R}_1 - \mathbf{R}_i) \right\rangle
$$
$$
- \nu \left\langle \sum_i \dot{\mathbf{u}}_i \cdot \nabla_{R_1} \delta(\mathbf{R}_1 - \mathbf{R}_i) \right\rangle \tag{A 1}
$$

and

$$
\langle n(\mathbf{R}_2) n(\mathbf{R}_3) \rangle = \left\langle \sum_{ij} \delta(\mathbf{R}_2 - \mathbf{R}_i) \delta(\mathbf{R}_3 - \mathbf{R}_j) \right\rangle - \nu^2. \tag{A 2}
$$

It is easily seen that the last two terms of (A 1) vanish identically in an equilibrium fluid because the average density is independent of position in the fluid. Also, because the velocities and positions of molecules are independent, the ensemble averages in the first two terms of (A 1) decompose into a product of averages.

Now,

$$
\left\langle \sum_{ij} \delta(\mathbf{R}_1 - \mathbf{R}_i) \delta(\mathbf{R}_2 - \mathbf{R}_j) \right\rangle = \sum_{ij} \int \int \frac{d\mathbf{R}_i \cdot d\mathbf{R}_j}{v^2} \delta(\mathbf{R}_1 - \mathbf{R}_i) \delta(\mathbf{R}_2 - \mathbf{R}_j) g(R_{ij})
$$
$$
+ \sum_i \int \frac{d\mathbf{R}_i}{V} \delta(\mathbf{R}_1 - \mathbf{R}_i) \delta(\mathbf{R}_1 - \mathbf{R}_2)
$$
$$
= \nu^2 g(R_{12}) + \nu \delta(\mathbf{R}_1 - \mathbf{R}_2) \tag{A 3}
$$

where $g(R_{ij})$ is the radial distribution function and $V$ is the volume of the system.

Also, the average force on molecule $i$, $m\langle \dot{\mathbf{u}}_i \rangle$, when molecule $j$ is held at $\mathbf{R}_j$ is related to the radial distribution function by

$$
\langle \dot{\mathbf{u}}_i \rangle = \frac{KT}{m} \nabla_i \ln g(R_{ij}). \tag{A 4}
$$

Finally, the average of the dyadic product of the molecular velocities is

$$
\langle \mathbf{u}_i \mathbf{u}_i \rangle = \frac{KT}{m} \mathbf{I} \tag{A 5}
$$

where $\mathbf{I}$ is the idemfactor.

Inserting (A3), (A 4) and (A 5) into (A 1) and (A 2), one finds that

$$
\left\langle \frac{\partial^2 n(\mathbf{R}_1)}{\partial t^2} \cdot n(\mathbf{R}_2) \right\rangle = \frac{KT}{m} \mathbf{I} : \nabla_{R_1} \nabla_{R_1} [\nu^2 g(R_{12}) + \nu \delta(R_{12})]
$$
$$
+ \frac{KT}{m} \nabla_{R_1} \cdot \sum_{ij} \int \int \frac{d\mathbf{R}_i d\mathbf{R}_j}{V^2} \nabla_1 \ln g(R_{ij}) g(R_{ij}) \delta(\mathbf{R}_1 - \mathbf{R}_i) \delta(\mathbf{R}_2 - \mathbf{R}_j)
$$
$$
= -\nu \frac{KT}{m} \nabla_1^2 \delta(R_{12}). \tag{A 6}
$$

## Appendix B

Differentiating (8) with respect to the time, one obtains

$$\frac{\partial^3 n(\mathbf{R}_1)}{\partial t^3} = \int K(R_{12}) \frac{\partial n(\mathbf{R}_2)}{\partial t} \, d\mathbf{R}_2,$$

which is readily transformed by the identity (18) into

$$-\nabla_1^2 \frac{\partial^2}{\partial t^2} \psi(\mathbf{R}_1, t) = \int -K(R_{12}) \nabla_2^2 \psi(\mathbf{R}_2, t) \, d\mathbf{R}_2. \tag{B 1}$$

Now, one employs the vector identity

$$\nabla_2 \cdot [K(R_{12}) \nabla_2 \psi(\mathbf{R}_2, t) - \psi(\mathbf{R}_2, t) \nabla_2 K(R_{12})]$$
$$= K(R_{12}) \nabla_2^2 \psi(\mathbf{R}_2, t) - \psi(\mathbf{R}_2, t) \nabla_2^2 K(R_{12}). \tag{B 2}$$

If (B 2) is integrated over $\mathbf{R}_2$, and one assumes that the surface integral on the left-hand side vanishes, it is found that

$$\int K(R_{12}) \nabla_2^2 \psi(\mathbf{R}_2, t) \, d\mathbf{R}_2 = \int \psi(\mathbf{R}_2, t) \nabla_2^2 K(R_{12}) \, d\mathbf{R}_2. \tag{B 3}$$

Substituting (B 3) in (B 1) with the relationship

$$\nabla_1^2 K(R_{12}) = \nabla_2^2 K(R_{12}),$$

we recover (19).

## Appendix C

In (23) the incident wave at the point $R$ is represented as a plane wave
$$\psi_0(\mathbf{R}) = \text{const.} \times \exp(i\mathbf{k} \cdot \mathbf{R}),$$

which may be written

$$\psi_0(\mathbf{R}) = \text{const.} \times \exp[i\mathbf{k} \cdot (\mathbf{R} - \mathbf{R}_j)] \exp(i\mathbf{k} \cdot \mathbf{R}_j) \tag{C 1}$$

where $\mathbf{R}_j$ is the position of the $j$th scatterer.

If one makes an expansion of the first exponential term in spherical Bessel functions (i.e. these functions are finite at the origin), one has

$$\psi_0(\mathbf{R}) = \sum A_n P_n(\cos\theta) j_n(kr) \exp(i\mathbf{k} \cdot \mathbf{R}_j); \quad r = |\mathbf{R} - \mathbf{R}_j|. \tag{C 2}$$

The scattered wave in (23) may be generally expanded in the series [6]

$$\sum B_n P_n(\cos\theta) h_n(kr). \tag{C 3}$$

If one applies the boundary condition that the radial fluid velocity at the surface of molecule $j$ (i.e. $r = a$) in the incident wave be equal and opposite to the radial velocity of the scattered wave, one finds

$$B_n = -A_n \frac{j_n'(ka)}{h_n'(ka)} \exp(i\mathbf{k} \cdot \mathbf{R}_j). \tag{C 4}$$

Since one is interested only in spherically symmetric scattering, we select the component $n = 0$, and we may write the total potential at $\mathbf{R}$ as

$$A_0 \exp(i\mathbf{k} \cdot \mathbf{R}_j) j_0(kr) - A_0 \frac{j_0'(ka)}{h_0'(ka)} \exp(i\mathbf{k} \cdot \mathbf{R}_j) h_0(kr). \tag{C 5}$$

Finally, if one defines the incident wave at $\mathbf{R}_j$ by

$$\psi_0(\mathbf{R}_j) = A_0 \exp{(i\mathbf{k} . \mathbf{R}_j)}, \qquad (C\,6)$$

and one introduces the functional form of $h_0(kr)$, namely,

$$h_0(kr) = \exp{(ikr)}/kr$$

the total disturbance at $(\mathbf{R})$ becomes

$$\psi(\mathbf{R}) = \psi_0(\mathbf{R}) - \frac{j_0{}'(ka)}{kh_0{}'(ka)} \sum_j \psi(\mathbf{R}_j) \exp{\frac{(i\mathbf{k} . \mid \mathbf{R} - \mathbf{R}_j \mid)}{\mid \mathbf{R} - \mathbf{R}_j \mid}}. \qquad (C\,7)$$

By comparison of (C 7) with (23), the identification between

$$g(k) \quad \text{and} \quad -\frac{j_0{}'(ka)}{kh_0{}'(ka)}$$

may be made. It is readily shown that

$$g(k) = -\frac{j_0{}'(ka)}{kh_0{}'(ka)} = \frac{ij_1(ka)}{kh_1(ka)}.$$

### REFERENCES

[1] For examples of acoustic models in Statistical Mechanics, see FIXMAN, M., 1958, *J. chem. Phys.*, **28**, 397 ; **29**, 540.

[2] CHAPMAN, S., and COWLING, T. G., 1939, *Mathematical Theory of Non-uniform Gases* (Cambridge: University Press).

[3] KIRKWOOD, J. G., 1946, *J. chem. Phys.*, **14**, 180.

[4] CHANDRASEKHAR, S., 1943, *Rev. mod. Phys.*, **15**, 1.

[5] LONGUET-HIGGINS, H. C., and POPLE, J. A., 1956, *J. chem. Phys.*, **25**, 884.

[6] General references to macroscopic acoustical theory: MORSE, P. M., and FESHBACH, H., 1953, *Methods of Theoretical Physics* (New York: McGraw-Hill); RAYLEIGH, J. W. S., 1945, *The Theory of Sound* (New York: Dover Publications).

[7] For example, see GREEN, H. S., 1952, *The Molecular Theory of Fluids* (New York: Interscience Publishers), p. 75.

[8] FIXMAN, M., 1958, *J. chem. Phys.*, **29**, 540.

[9] FIXMAN, M., 1958, *J. chem. Phys.*, **26**, 1421.

[10] This result is stated by M. Fixman, Reference [8].

[11] For an excellent account of the use of the Dirac delta function in Statistical Mechanics, see MASSIGNON, D., 1957, *Mécanique Statistique des Fluides* (Paris: Dunod).

[12] FOLDY, L. L., 1945, *Phys. Rev.*, **67**, 107.

[13] RICE, S. A., *Mol. Phys.*, **4**, 305.

# The crystal structure of phenanthrene

by R. MASON

Department of Chemistry, Imperial College, London, S.W.7

A least squares refinement of Basak's two-dimensional x-ray data is reported. The average e.s.d.'s of the carbon–carbon bond lengths is 0·05 Å and the molecular arrangement in the crystal is compared in some detail with that of anthracene.

## 1. INTRODUCTION

A two-dimensional Fourier analysis of the crystal structure of phenanthrene has been described [1], although no refinement of the data appears to be available. The present analysis was largely prompted by our investigations of the problem of molecular arrangements in crystals of the aromatic hydrocarbons, an account of which will be reported elsewhere. More precise information relating to the molecular orientation in the crystal is also of interest in connection with the diamagnetic anisotropy and ultraviolet absorption of single crystals of phenanthrene.

The unit cell given by Basak has been transformed to the more conventional monoclinic setting,

$$a = 8·57 \text{ Å}, b = 6·11 \text{ Å}, c = 9·47 \text{ Å}, \beta = 97·5°.$$

Space group $P2_1$; F (000) = 188.

## 2. THE REFINEMENT ANALYSIS

In order that the relationship between the crystal structures of phenanthrene and anthracene should be clear, the atomic coordinates have been referred to a new origin, namely the screw axis at $(\frac{1}{2}, 0, \frac{1}{2})$ in the above unit cell. The very limited two-dimensional data preclude the possibility of a complete refinement so that a least-squares adjustment has only been made of the coordinates and isotropic temperature factors of the carbon atoms. Hydrogen atom contributions have, however, been included in the structure factor calculations, their coordinates being defined by C–H bond lengths of 1·1 Å; an isotropic temperature factor $B = 8\pi^2 u^2 = 5·0$ Å$^2$ was applied to their scattering factors.

Unit weights in the least squares minimization of $\sum w\Delta^2$ were used. Corresponding to the reduction of $\sum w\Delta^2$ from $1·19 \times 10^7$ to $0·27 \times 10^7$, the usual discrepancy factor for this kind of analysis was reduced from 0·27 to the present value of 0·12 in six cycles of refinement for the 103 observed $hk0$, $h0l$ and $0kl$ reflections. The final atomic parameters are given in table 1.

## 3. DISCUSSION

The large e.s.d.'s of the bond lengths prevent any realistic comparison of these values with those predicted by the various quantum mechanical models; a three-dimensional analysis of the structure at 95°K is being undertaken with this particular problem in mind. But the present analysis is capable of demonstrating quite clearly the remarkable similarity between the crystallography of

| Atom | $x/a$ | $\sigma(x)$ | $y/b$ | $\sigma(y)$ | $z/c$ | $\sigma(z)$ | $B$ (Å$^2$) |
|------|-------|-------------|-------|-------------|-------|-------------|-------------|
| C1   | 0·1210 | 0·0054 | 0·2853 | 0·0146 | −0·3750 | 0·0050 | 5·2 |
| C2   | 0·2094 | 0·0049 | 0·1195 | 0·0133 | −0·3323 | 0·0048 | 4·5 |
| C3   | 0·0834 | 0·0052 | 0·4586 | 0·0142 | −0·2904 | 0·0047 | 4·3 |
| C4   | 0·2743 | 0·0055 | 0·0600 | 0·0158 | −0·1884 | 0·0054 | 5·8 |
| C5   | 0·1501 | 0·0053 | 0·4478 | 0·0141 | −0·1491 | 0·0050 | 4·8 |
| C6   | 0·2420 | 0·0047 | 0·2440 | 0·0147 | −0·0932 | 0·0042 | 3·7 |
| C7   | 0·1157 | 0·0049 | 0·6260 | 0·0142 | −0·0579 | 0·0045 | 3·5 |
| C8   | 0·2976 | 0·0049 | 0·2381 | 0·0137 | 0·0606 | 0·0043 | 3·5 |
| C9   | 0·1763 | 0·0053 | 0·6051 | 0·0168 | 0·1015 | 0·0048 | 4·5 |
| C10  | 0·4013 | 0·0044 | 0·0642 | 0·0158 | 0·1048 | 0·0041 | 3·0 |
| C11  | 0·2744 | 0·0045 | 0·4366 | 0·0134 | 0·1516 | 0·0042 | 3·0 |
| C12  | 0·4674 | 0·0057 | 0·0290 | 0·0157 | 0·2554 | 0·0056 | 5·8 |
| C13  | 0·3330 | 0·0051 | 0·3772 | 0·0137 | 0·3102 | 0·0047 | 4·0 |
| C14  | 0·4303 | 0·0052 | 0·2010 | 0·0140 | 0·3420 | 0·0048 | 4·5 |

Table 1. Phenanthrene:
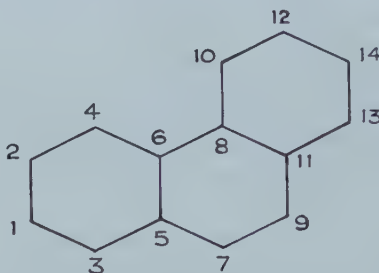


atomic coordinates and temperature factors.

phenanthrene and its isomer, anthracene, a feature which is not evident, for example, from an inspection of the unit cells and space group symmetries.

The orientation of the reference molecule in the unit cell is defined by the direction cosines of the principal axes of inertia. These are respectively:

$$0·2546, \quad -0·0856, \quad 0·9633$$
$$0·4411, \quad -0·8761, \quad -0·1945$$
$$-0·8606, \quad -0·4744, \quad 0·1853$$

referred to the orthogonal axes $a$, $b$ and $c'$ of the crystal. Each molecule at $(x, y, z)$ is surrounded by twelve close neighbours at

$$(x, y, z \pm 1); \qquad (x, y \pm 1, z);$$
$$(\bar{x}, y \pm \tfrac{1}{2}, -z); \qquad (\bar{x}, y \pm \tfrac{1}{2}, -(z+1));$$
$$(\bar{x}+1, y \pm \tfrac{1}{2}, z+1); \qquad (\bar{x}+1, y \pm \tfrac{1}{2}, -z).$$

The anthrancene molecule is similarly approximately close-packed in the crystal with neighbours whose centres are at

$$\pm (0, 1, 0); \qquad \pm (0, 0, 1);$$
$$\pm (\tfrac{1}{2}, \tfrac{1}{2}, 0); \qquad \pm (\tfrac{1}{2}, \tfrac{1}{2}, 1);$$
$$\pm (\tfrac{1}{2}, \bar{\tfrac{1}{2}}, 0); \qquad \pm (\tfrac{1}{2}, \bar{\tfrac{1}{2}}, 1) \quad [2].$$

In both structures, therefore, the molecules are surrounded by four translationally equivalent and eight translationally non-equivalent neighbours. The angles between the planes of the translationally equivalent and non-equivalent molecules are 56 and 52° for phenanthrene and anthracene, respectively.

Table 2 lists a summary of the intermolecular contacts in anthracene and phenanthrene within a distance of 4 Å of each individual carbon and hydrogen atom in the parent molecule.

| $n$ | C–C | | C–H | | H–H | |
|---|---|---|---|---|---|---|
| | Anthracene | Phenanthrene | Anthracene | Phenanthrene | Anthracene | Phenanthrene |
| | 31 | 33 | 98 | 94 | 41 | 42 |
| 1 | $8 \cdot 18 \times 10^0$ | $8 \cdot 78 \times 10^0$ | $28 \cdot 93 \times 10^0$ | $27 \cdot 54 \times 10^0$ | $12 \cdot 42 \times 10^0$ | $12 \cdot 60 \times 10^0$ |
| 2 | $2 \cdot 16 \times 10^0$ | $2 \cdot 34 \times 10^0$ | $8 \cdot 62 \times 10^0$ | $8 \cdot 17 \times 10^0$ | $3 \cdot 85 \times 10^0$ | $3 \cdot 85 \times 10^0$ |
| 3 | $5 \cdot 7 \times 10^{-1}$ | $6 \cdot 3 \times 10^{-1}$ | $2 \cdot 59 \times 10^0$ | $2 \cdot 45 \times 10^0$ | $1 \cdot 22 \times 10^0$ | $1 \cdot 20 \times 10^0$ |
| 4 | $1 \cdot 5 \times 10^{-1}$ | $1 \cdot 7 \times 10^{-1}$ | $7 \cdot 8 \times 10^{-1}$ | $7 \cdot 4 \times 10^{-1}$ | $4 \cdot 0 \times 10^{-1}$ | $3 \cdot 9 \times 10^{-1}$ |
| 5 | $4 \cdot 0 \times 10^{-2}$ | $4 \cdot 5 \times 10^{-2}$ | $2 \cdot 4 \times 10^{-1}$ | $2 \cdot 3 \times 10^{-1}$ | $1 \cdot 3 \times 10^{-1}$ | $1 \cdot 3 \times 10^{-1}$ |
| 6 | $1 \cdot 1 \times 10^{-2}$ | $1 \cdot 2 \times 10^{-2}$ | $7 \cdot 4 \times 10^{-2}$ | $7 \cdot 2 \times 10^{-2}$ | $4 \cdot 5 \times 10^{-2}$ | $4 \cdot 3 \times 10^{-2}$ |
| 7 | $2 \cdot 8 \times 10^{-3}$ | $3 \cdot 3 \times 10^{-3}$ | $2 \cdot 3 \times 10^{-2}$ | $2 \cdot 3 \times 10^{-2}$ | $1 \cdot 6 \times 10^{-2}$ | $1 \cdot 5 \times 10^{-2}$ |
| 8 | $7 \cdot 5 \times 10^{-4}$ | $8 \cdot 8 \times 10^{-4}$ | $7 \cdot 3 \times 10^{-3}$ | $7 \cdot 3 \times 10^{-3}$ | $5 \cdot 5 \times 10^{-3}$ | $5 \cdot 6 \times 10^{-3}$ |
| 9 | $2 \cdot 0 \times 10^{-4}$ | $2 \cdot 4 \times 10^{-4}$ | $2 \cdot 3 \times 10^{-3}$ | $2 \cdot 4 \times 10^{-3}$ | $2 \cdot 0 \times 10^{-3}$ | $2 \cdot 1 \times 10^{-3}$ |
| 10 | $5 \cdot 3 \times 10^{-5}$ | $6 \cdot 5 \times 10^{-5}$ | $7 \cdot 4 \times 10^{-4}$ | $7 \cdot 9 \times 10^{-4}$ | $7 \cdot 1 \times 10^{-4}$ | $8 \cdot 4 \times 10^{-4}$ |
| 11 | $1 \cdot 4 \times 10^{-5}$ | $1 \cdot 8 \times 10^{-5}$ | $2 \cdot 4 \times 10^{-4}$ | $2 \cdot 6 \times 10^{-4}$ | $2 \cdot 6 \times 10^{-4}$ | $3 \cdot 4 \times 10^{-4}$ |
| 12 | $3 \cdot 8 \times 10^{-6}$ | $4 \cdot 9 \times 10^{-6}$ | $7 \cdot 8 \times 10^{-5}$ | $8 \cdot 9 \times 10^{-5}$ | $9 \cdot 8 \times 10^{-5}$ | $1 \cdot 4 \times 10^{-4}$ |
| 13 | $1 \cdot 0 \times 10^{-6}$ | $1 \cdot 3 \times 10^{-6}$ | $2 \cdot 9 \times 10^{-5}$ | $3 \cdot 1 \times 10^{-5}$ | $3 \cdot 7 \times 10^{-5}$ | $6 \cdot 1 \times 10^{-5}$ |
| 14 | $2 \cdot 7 \times 10^{-7}$ | $3 \cdot 7 \times 10^{-7}$ | $8 \cdot 6 \times 10^{-6}$ | $1 \cdot 1 \times 10^{-5}$ | $1 \cdot 4 \times 10^{-5}$ | $2 \cdot 7 \times 10^{-5}$ |

Table 2. Intermolecular contacts in phenanthrene and anthracene, expressed as:

$$\sum_N \frac{1}{r_{ij}^n}$$

with $N$ the number of unique crystallographic vectors and $n$ the force law exponent.

It is difficult to be certain that the small differences between the respective values for anthracene and phenanthrene are significant; a more detailed refinement of phenanthrene can be expected to indicate whether it is possible to correlate the values of

$$\sum_N \frac{1}{r_{ij}^n}$$

with such data as density, heat of sublimation and so on for the two isomers.

I am grateful to Drs. P. Pauling, J. Rollett and R. Sparks for providing copies of their programmes for the University of London 'Mercury' computer.

### REFERENCES

[1] BASAK, B. S., 1950, *Indian J. Phys.*, **24**, 309.
[2] CRUICKSHANK, D. W. J., 1956, *Acta cryst.*, Camb., **9**, 915.

# The wave functions of electronically degenerate states

by A. D. McLACHLAN

Department of Theoretical Chemistry, University Chemical Laboratory, Lensfield Road, Cambridge

The dynamical coupling of nuclear and electronic motions in a degenerate electronic state is described by a complicated vibronic wave equation, because the adiabatic electronic functions vary rapidly during the vibrations. Hobey and McLachlan tried to show how special linear combinations of the electronic wave functions could be found, which vary slowly, and lead to a simpler wave equation. This paper points out a mistake in their argument, but corrects it, and shows that the simple wave equation is still justified. The new method is similar to Van Vleck's transformation in degenerate perturbation theory, and also applies to molecules which are almost degenerate.

---

1

In most molecules one can assume that the electrons adjust themselves instantaneously to the nuclear positions, and the nuclei then move in the average field of the rapidly moving electrons. If $q$ and $Q$ are the coordinates of the electrons and nuclei the Hamiltonian is of the type

$$H = -\partial^2/\partial q^2 + V(q, Q) - \partial^2/\partial Q^2, \tag{1}$$

where $V(q, Q)$ is the potential energy, $-\partial^2/\partial q^2$ represents the kinetic energy of the electrons, and $-\partial^2/\partial Q^2$ is the kinetic energy of the nuclei. In the usual 'adiabatic' [1, 2] or Born and Oppenheimer approximation [3] one first solves the electronic Schrödinger equation at each nuclear configuration

$$\mathscr{H}\psi(q, Q) = E(Q)\psi(q, Q), \tag{2}$$

with

$$\mathscr{H} = -\partial^2/\partial q^2 + V(q, Q). \tag{3}$$

Then the vibrational function $X(Q)$ is fixed by the condition that the total energy of the complete wave function

$$\Psi(q, Q) = \psi(q, Q)X(Q) \tag{4}$$

is stationary for small variations of $X$.

Recent work has made it clear that the electrons cannot follow the nuclei instantaneously if the electronic levels are degenerate [4–9], and then the coupling of nuclear and electronic motion produces special effects [4, 5, 7, 9–15]. The wave function now has to be represented by a series of terms like (4):

$$\Psi(q, Q) = \sum_r \xi_r(q, Q)X_r(Q), \tag{5}$$

in which $\xi_r(q, Q)$ are members of a complete set of electronic wave functions, and $X_r(Q)$ are vibrational amplitudes associated with them [1, 2, 9]. The Schrödinger equation $H\Psi = W\Psi$ leads to a series of coupled equations for the $X$'s

$$[-\partial^2/\partial Q^2 + H_{rr}(Q) - W]X_r(Q)$$
$$+\sum_s{}'[H_{rs}(Q) - 2\langle r \mid \partial/\partial Q \mid s \rangle]X_s(Q) = 0, \qquad (6)$$

where $H_{rr}$ and $\langle r \mid \partial/\partial Q \mid s \rangle$ are the electronic matrix elements of these operators between $\xi_r$ and $\xi_s$; i.e.

$$H_{rr} = \int \xi_r{}^*H\xi_s\, dq \text{ and } \langle r \mid \partial/\partial Q \mid s \rangle = \int \xi_r{}^*(\partial/\partial Q)\xi_s\, dq.$$

So far the functions $\xi_r$ have not been specified, but they must be chosen to make the coupling terms as small as possible and to represent $\Psi'(q, Q)$ in (5) by the smallest number of terms. These requirements are hard to satisfy simultaneously. To fix our ideas consider an electronic state which becomes doubly degenerate at the configuration $Q = 0$. Let $\psi_a(q, Q)$ and $\psi_b(q, Q)$ be the adiabatic wave functions of the degenerate level and $\psi_n(q, Q)$ be the other levels. Since $\mathcal{H}\psi = E\psi$ we find that equation (6) simplifies to

$$[-\partial^2/\partial Q^2 + \langle r \mid -\partial^2/\partial Q^2 \mid r \rangle + E_r(Q) - W]X_r$$
$$+\sum{}'\langle r \mid -\partial^2/\partial Q^2 - 2\partial/\partial Q \mid s \rangle X_s = 0. \qquad (7)$$

If $r$ and $s$ are two different levels the coupling terms in (7) are as small as they are in a non-degenerate electronic state, and can be neglected (for a fuller discussion see [1, 2, 3, 9]). On the other hand, the functions $\psi_a$ and $\psi_b$ vary rapidly with $Q$, so that the terms involving $\partial/\partial Q$ in (7) are very large, and actually diverge as $Q \to 0$. To avoid this difficulty most authors have used a fixed set of electronic functions, independent of $Q$. For instance we might choose the electronic states at $Q = 0$; $\xi_r = \psi_r(q, 0)$, which gives

$$[-\partial^2/\partial Q^2 + \mathcal{H}_{rr}(Q) - W]X_r + \sum_s{}'\mathcal{H}_{rs}(Q)X_s = 0 \qquad (8)$$

instead of (6).

<div align="center">2</div>

To illustrate the difference between (7) and (8), consider the coupling of a doubly degenerate electronic state with a doubly degenerate vibration as it is treated by Longuet–Higgins *et al.* [5]. We use their notation, with $\theta$ for the angular coordinate of the electron, and $(r, \phi)$ for the polar coordinates of the vibrational normal mode. The electron has two states $\exp(i\theta)$ and $\exp(-i\theta)$, while the Hamiltonian is

$$H = \left[ -\frac{1}{2}\left( \frac{\partial^2}{\partial r^2} + \frac{1}{r}\frac{\partial}{\partial r} + \frac{1}{r^2}\frac{\partial^2}{\partial \phi^2} \right) + \tfrac{1}{2}r^2 \right] + 2kr\cos(2\theta - \phi) \qquad (9)$$

$$= H_0 + H'. \qquad (10)$$

The adiabatic wave functions (2) are now

$$\psi_a = \cos(\theta - \tfrac{1}{2}\phi), \quad E_a = \tfrac{1}{2}r^2 + kr, \\ \left.\psi_b = i\sin(\theta - \tfrac{1}{2}\phi), \quad E_b = \tfrac{1}{2}r^2 - kr, \right\} \qquad (11)$$

and we first seek a vibronic wave function of the form

$$\Psi = \psi_a(\theta, \phi)X_a(r, \phi) + \psi_b(\theta, \phi)X_b(r, \phi). \qquad (12)$$

The counterpart of equation (7) is the matrix equation

$$
\begin{vmatrix}
H_0 + \dfrac{1}{8r^2} + kr - E & \dfrac{i}{2r^2}\dfrac{\partial}{\partial\phi} \\[2ex]
\dfrac{i}{2r^2}\dfrac{\partial}{\partial\phi} & H_0 + \dfrac{1}{8r^2} - kr - E
\end{vmatrix}
\begin{vmatrix}
\chi_a \\[2ex]
\chi_b
\end{vmatrix} = 0,
\tag{13}
$$

and contains terms proportional to $1/r^2$ which arise from the variation of $\psi_a$ and $\psi_b$ with the angle $\phi$. On the other hand, if we follow the second method, and take

$$
\Psi = \exp(i\theta)\chi^+(r, \phi) + \exp(-i\theta)\chi^-(r, \phi)
\tag{14}
$$

with fixed electronic wave functions, the vibrational equation is much simpler:

$$
\begin{bmatrix}
H_0 - E & kr\exp(-i\phi) \\[1ex]
kr\exp(+i\phi) & H_0 - E
\end{bmatrix}
\begin{bmatrix}
\chi^+ \\[1ex]
\chi^-
\end{bmatrix} = 0.
\tag{15}
$$

The chief disadvantage of the fixed functions is that they do not allow the electrons to follow the nuclei enough. As $Q$ deviates from 0 the values of $\mathscr{H}_{rs}$ in (8) become quite large, and an accurate wave function of the form (5) needs a large number of terms.

### 3

One would like to choose the electronic wave functions in equation (5) by a third method which allows them to follow the nuclear motion but to avoid the rapid fluctuations of the adiabatic functions. Moffitt and Liehr [4] made the first attempt to achieve this. They expressed their wave functions as fixed linear combinations of atomic orbitals. The orbitals moved with the nuclei so that the electrons did partially follow the molecular vibrations.

More recently Hobey and McLachlan [9] attempted a general solution to the problem. They argued that the main effects of vibrational-electronic coupling in a (doubly) degenerate state could be represented well by a wave function of the form

$$
\Psi = \psi_a(q, Q)\chi_a(Q) + \psi_b(q, Q)\chi_b(Q)
\tag{16}
$$

which only contains the adiabatic electronic wave functions of the degenerate level. (The wave function of a $g$-fold degenerate electronic level would be a similar sum of $g$ products). This is because the coupling terms in equation (7) are all small except for those between components of the degenerate level. They then said that one could reduce the vibronic wave equation (7) to the simpler one (8) by writing the wave function in a new but precisely equivalent form

$$
\Psi = \psi_1(q, Q)\chi_1(Q) + \psi_2(q, Q)\chi_2(Q).
\tag{17}
$$

Here $\psi_1$ and $\psi_2$ are special linear combinations of $\psi_a$ and $\psi_b$, chosen to vary as slowly as possible with nuclear displacements, so that

$$
\langle 1 \mid \partial/\partial Q \mid 2 \rangle = 0
\tag{18}
$$

for each vibrational coordinate $Q$. Suppose $\psi_1$ and $\psi_2$ are given by the transformation

$$
\psi_i(q, Q) = \sum_\mu a_{i\,\mu}(Q)\psi_\mu(q, Q),
\tag{19}
$$

where the suffixes $i$ and $\mu$ respectively take the values $i = 1, 2$ and $\mu = a, b$, and the coefficients $a_{i\mu}(Q)$ are chosen to fulfil (18). Then Hobey and McLachlan showed that $a_{i\mu}(Q)$ must satisfy the sets of simultaneous differential equations

$$\partial a_{i\mu}/\partial Q_x + \sum_\nu a_{i\,\nu}\langle \mu \mid \partial/\partial Q_x \mid \nu \rangle = 0 \qquad (20)$$

for each vibrational coordinate $Q_x$. Unfortunately there is a mistake in their argument, because these equations are generally inconsistent, and it is impossible to satisfy (18) and (19) simultaneously. For let $Q_x$ and $Q_y$ be two coordinates and suppose (20) holds. Then we may use (20) to evaluate $\partial^2 a_{i\,\mu}/\partial Q_x \partial Q_y$ in two different ways as

$$\frac{\partial}{\partial Q_x}\left(\frac{\partial a_{i\,\mu}}{\partial Q_y}\right) \quad \text{or} \quad \frac{\partial}{\partial Q_y}\left(\frac{\partial a_{i\,\mu}}{\partial Q_x}\right). \qquad (21)$$

The expressions will not be equal unless

$$\partial/\partial Q_x\langle \mu \mid \partial/\partial Q_y \mid \nu \rangle = \partial/\partial Q_y\langle \mu \mid \partial/\partial Q_x \mid \nu \rangle \qquad (22)$$

which is generally false (see equation (12) of reference [9]). The only case for which Hobey and McLachlan's condition can be met is that where only one vibrational coordinate $Q_x$ removes the electronic degeneracy. Then equation (20) is clearly integrable.

Nevertheless we shall see that their main argument is still correct. One can replace the rapidly fluctuating functions $\psi_a$ and $\psi_b$ by a new pair $\psi_1$ and $\psi_2$ which vary so slowly during the vibrations that the matrix elements $\langle 1 \mid \partial/\partial Q \mid 2 \rangle$ and $\langle 1 \mid \partial^2/\partial Q^2 \mid 2 \rangle$ are negligible in the wave equation for $\psi_1$ and $\psi_2$. Instead of (18) they satisfy the less stringent condition

$$\langle 1 \mid \partial/\partial Q \mid 2 \rangle \simeq 0. \qquad (23)$$

4

First consider the nuclei fixed at $Q = 0$, where the electronic level is doubly degenerate. Let $\phi_1(q)$ and $\phi_2(q)$ be the two fixed wave functions with energy $E = 0$, while $\phi_n(q)$ are the excited states with energies $E_n(0)$. $\phi_1$ and $\phi_2$ are solutions of

$$\mathscr{H}_0\phi = 0. \qquad (24)$$

When $Q \neq 0$ the potential produced by the nuclei changes from $V(q, 0)$ to $V(q, Q)$, so if we write

$$V(q, Q) - V(q, 0) = U(q, Q) \qquad (25)$$

the electronic Hamiltonian which determines the adiabatic wave functions $\psi_a(q, Q)$ and $\psi_b(q, Q)$ is

$$\mathscr{H} = \mathscr{H}_0 + U(q, Q). \qquad (26)$$

$\psi_a$ and $\psi_b$ will change into solutions of (24) as we approach $Q = 0$, but the precise linear combinations $\phi_a$ and $\phi_b$ depend on the path by which $Q$ tends to 0. Instead let us consider the Hamiltonian

$$\mathscr{H}(\lambda) = \mathscr{H}_0 + \lambda U(q, Q) \qquad (27)$$

with $Q$ fixed, and study its eigenfunctions $\bar\psi_a(\lambda)$ and $\bar\psi_b(\lambda)$ as $\lambda$ varies. When $\lambda = 1$ they are the same as $\psi_a$ and $\psi_b$, but as $\lambda \to 0$ they tend to a certain pair of

degenerate functions $\phi_a$ and $\phi_b$, which depend on $Q$ but not on $\lambda$, with energies $\lambda w_a$ and $\lambda w_b$. These are linear combinations of $\phi_1$ and $\phi_2$:

$$\left.\begin{array}{l} \phi_a = C_{a1}\phi_1 + C_{a2}\phi_2, \\ \phi_b = C_{b1}\phi_1 + C_{b2}\phi_2, \end{array}\right\} \tag{28}$$

and their energies are the roots of the secular equation

$$\left|\begin{array}{cc} U_{11}(Q) - w & U_{12}(Q) \\ U_{21}(Q) & U_{22}(Q) - w \end{array}\right| = 0. \tag{29}$$

Clearly one can recover the fixed functions $\phi_1$ and $\phi_2$ from $\phi_a$ and $\phi_b$ by the inverse transformation

$$\left.\begin{array}{l} \phi_1 = C^*{}_{a1}\phi_a + C^*{}_{b1}\phi_b, \\ \phi_2 = C^*{}_{a2}\phi_a + C^*{}_{b2}\phi_b. \end{array}\right\} \tag{30}$$

Similarly, for each nuclear configuration $Q$ we will define the functions $\psi_1(q, Q)$ and $\psi_2(q, Q)$ to be the *same* linear combinations of $\psi_a(q, Q)$ and $\psi_b(q, Q)$:

$$\left.\begin{array}{l} \psi_1 = C^*{}_{a1}\psi_a + C^*{}_{b1}\psi_b, \\ \psi_2 = C^*{}_{a2}\psi_a + C^*{}_{b2}\psi_b. \end{array}\right\} \tag{31}$$

Let us now examine how $\psi_1$ and $\psi_2$ vary with $Q$. Use the suffix notation $i = 1, 2$ and $\mu = a, b$, Then (31) and (28) become

$$\psi_i = \sum_\mu C^*{}_{\mu i}\psi_\mu \quad : \quad \phi_\mu = \sum_i C_{\mu i}\phi_i. \tag{32}$$

Remembering that $C_{\mu i}$ depends on $Q$ we have

$$\partial\psi_i/\partial Q = \sum_\mu C^*{}_{\mu i}\partial\psi_\mu/\partial Q + \sum_\mu \psi_\mu \partial C^*{}_{\mu i}/\partial Q. \tag{33}$$

But (26) and (29) imply that

$$\frac{\partial\psi_\mu}{\partial Q} = \sum_\nu \psi_\nu \frac{\int \psi^*{}_\nu U'(q, Q)\psi_\mu\, dq}{E_\mu(Q) - E_\nu(Q)}, \tag{34}$$

$$\frac{\partial C^*{}_{\mu i}}{\partial Q} = \sum_\nu C^*{}_{\nu i} \frac{\int \phi^*{}_\mu U'(q, Q)\phi_\nu\, dq}{w_\nu(Q) - w_\mu(Q)}, \tag{35}$$

where $U' = \partial U/\partial Q$. (In equation (34) we have neglected the contributions of the excited levels $\psi_n$ to the sum because $E_\mu - E_n$ is large then.) Substitution of these formulae into (33) gives

$$\frac{\partial\psi_i}{\partial Q} = \sum_{\mu,\,\nu} C^*{}_{\nu i}\psi_\nu \left\{ \frac{\int \psi^*{}_\nu U'\psi_\mu\, dq}{E_\mu - E_\nu} - \frac{\int \phi^*{}_\nu U'\phi_\mu\, dq}{w_\mu - w_\nu} \right\}. \tag{36}$$

Both terms in the bracket of (36) become very large near $Q = 0$, but since $\psi_\mu \to \phi_\mu$ and $E_\mu \to w_\mu$ as $Q \to 0$, the two terms will almost cancel and $\partial\psi_i/\partial Q \to 0$ as $Q \to 0$. On the other hand, when $Q$ is large $(E_\mu - E_\nu)$ and $(w_\mu - w_\nu)$ increase rapidly, and both fractions are small even if they are quite different. When $Q$ is small enough for $U'(q, Q)$ to be treated as a perturbation $\psi_1$ and $\psi_2$ are approximated by

$$\psi_i = \phi_i - \sum_n{}'\phi_n \cdot \frac{\langle n|U|i\rangle}{E_n(0) - E_0(0)}, \tag{37}$$

and our method of choosing them becomes equivalent to Van Vleck's transformation [16, 17] in first order degenerate perturbation theory. Since $\psi_1$ and $\psi_2$

have the required slow variation with $Q$ we can replace the vibronic equation (6) by the simpler one

$$
\begin{bmatrix}
-\dfrac{\partial^2}{\partial Q^2} + \mathcal{H}_{11} - W & \mathcal{H}_{12} \\[2ex]
\mathcal{H}_{21} & -\dfrac{\partial^2}{\partial Q^2} + \mathcal{H}_{22} - W
\end{bmatrix}
\begin{bmatrix}
\chi_1 \\[1ex]
\chi_2
\end{bmatrix} = 0. \tag{38}
$$

However, since the matrix elements of $\mathcal{H}$ in (38) are generally smaller than a typical electronic excitation energy $E_n - E_0$, the terms which are neglected in going from (6) to (38) are comparatively more important than in the adiabatic approximation for a non-degenerate state.

## 5

Our arguments justify the results of previous calculations which used a basis of fixed electronic functions, and also show that the usual adiabatic electronic wave functions $\psi_n(q, Q)$ and their energy curves $E_n(Q)$ play a fundamental part in the coupled motions of a degenerate level.

Besides the exact degeneracy found in symmetrical molecules, which leads to the Jahn–Teller [13, 5] and Renner effects [14, 15] there are also molecules such as dimers [11, 12] where the electronic levels are almost degenerate. In this situation there are also vibronic coupling effects if the minimum separation $\Delta E$ of the electronic states (at $Q=0$) is smaller than the vibrational quanta, and the adiabatic wave functions again vary rapidly when $U \simeq \Delta E$. Let $\phi_1$ and $\phi_2$ be the upper and lower of these levels at $Q=0$. Then we can choose the functions $\psi_1$ and $\psi_2$ in exactly the same way as before, except that the combination coefficients $C_{\mu i}$ are now found from the matrix

$$
\begin{bmatrix}
\Delta E + U_{11} - w & U_{12} \\[1ex]
U_{21} & U_{22} - w
\end{bmatrix}. \tag{39}
$$

## REFERENCES

[1] BORN, M., 1951, *Festchrift Gött. Nachr. Math. Phys. Kl.*, **1**.
[2] BORN, M., and HUANG, KUN, 1954, *Dynamical Theory of Crystal Lattices* (Oxford: University Press), pp. 170, 406–407.
[3] BORN, M., and OPPENHEIMER, J. R., 1927, *Ann. Phys., Lpz.*, **84**, 475.
[4] MOFFITT, W., and LIEHR, A. D., 1957, *Phys. Rev.*, **106**, 1195.
[5] LONGUET-HIGGINS, H. C., ÖPIK, U., PRYCE, M. H. L., and SACK, R. A., 1958, *Proc. roy. Soc. A*, **244**, 1.
[6] LONGUET-HIGGINS, H. C., 1961, *Advances in Spectroscopy*, Vol. II (New York: Interscience Publishers) (in the press).
[7] CHILD, M. S., and LONGUET-HIGGINS, H. C., 1961, *Phil. Trans. A* (to be published).
[8] MOFFITT, W., and THORSON, W. R., 1957, *Phys. Rev.*, **108**, 1251.
[9] HOBEY, W. D., and McLACHLAN, A. D., 1960, *J. chem. Phys.*, **33**, 1695.
[10] McCONNELL, H. M., and McLACHLAN, A. D., 1961, *J. chem. Phys.*, **34**, 1.
[11] SIMPSON, W. T., and PETERSON, D. L., 1957, *J. chem. Phys.*, **26**, 588.

[12] WITKOWSKI, A., and MOFFITT, W., 1960, *J. chem. Phys.*, **33**, 872.

[13] JAHN, H. A., and TELLER, E., 1937, *Proc. roy. Soc.* A, **161**, 220.

[14] POPLE, J. A., and LONGUET-HIGGINS, H. C., 1958, *Mol. Phys.*, **1**, 372; POPLE, J. A., 1960, *Mol. Phys.*, **3**, 16.

[15] DRESSLER, K., and RAMSAY, D. A., 1959, *Phil. Trans.* A, **251**, 553.

[16] VAN VLECK, J. H., 1929, *Phys. Rev.*, **33**, 467, 484.

[17] KEMBLE, E. C., 1937, *Fundamental Principles of Quantum Mechanics* (New York: McGraw-Hill Book Company), p. 394.

# The electron spin resonance spectrum of CH₃ĊHCOOH at 77°K in l-α-alanine

by A. HORSFIELD, J. R. MORTON and D. H. WHIFFEN

Basic Physics Division, National Physical Laboratory, Teddington, Middlesex

The change in the electron resonance spectrum of a $\gamma$-irradiated single crystal of $l$-$\alpha$-alanine on cooling to 77°K has been interpreted in terms of the cessation of rotation of the methyl group of the trapped radical, CH₃ĊHCOOH. The isotropic hyperfine couplings of the three hydrogens of the methyl group are found to be 120, 76 and 14 Mc/s respectively compared to the value of 70 Mc/s each at 300°K. The geometry of the free radical at 77°K is such that, in projection on a plane perpendicular to the Ċ–CH₃ bond, one of the C–H bonds makes an angle of about 12° to the plane of the free radical centre and this hydrogen is probably adjacent to the carboxyl group.

## 1. INTRODUCTION

Miyagawa and Gordy [1] quote unpublished work by H. Shields which indicated that the electron resonance spectrum of x-irradiated $l$-$\alpha$-alanine changed on cooling to liquid air temperature. Since it is known [1, 2] that the trapped free radical is CH₃ĊHCOOH (or possibly CH₃ĊH CO₂⁻), the change might be associated with the loss of rotational motion of the –CH₃ group. At room temperature the three hydrogens of this group are fully equivalent and have an isotropic hyperfine coupling constant of 70 Mc/s [2]. The coupling constants of a non-rotating methyl group would be of interest in relation to the hyperfine couplings in other free radicals with $\beta$-hydrogen atoms, and so the electron resonance spectrum of $\gamma$-irradiated $l$-$\alpha$-alanine was reinvestigated at 77°K.

## 2. EXPERIMENTAL

The electron spin resonance spectra were observed with a superheterodyne spectrometer working at 9000 Mc/s [3]. The second derivative spectra were obtained by use of a phase sensitive detector at 174 c/s with field modulation at 87 c/s. The low temperature cavity was a H₁₀₄ rectangular cavity based on a design of Ingram [4].

The $l$-$\alpha$-alanine crystal was grown from aqueous solution and irradiated to the extent of 5 Mrad with $\gamma$-rays of mean energy 1·0 MeV at the Spent Fuel Irradiation Unit, AERE, Harwell. The spectra at room temperature were in full agreement with earlier work [1, 2] but on cooling to 77°K a change of spectra occurred as indicated in figure 1. This change was reversible and the normal spectra were re-obtained at 300°K. Measurements at 200°K gave the same spectra as at 300°K.

The spectra when the magnetic field was parallel to the *a*, *b* and *c* axes of the orthorhombic crystal were carefully measured, since for these orientations the spectra of all crystallographically related radicals are superimposed.    For other orientations the overlapping of spectra from radicals in differently oriented
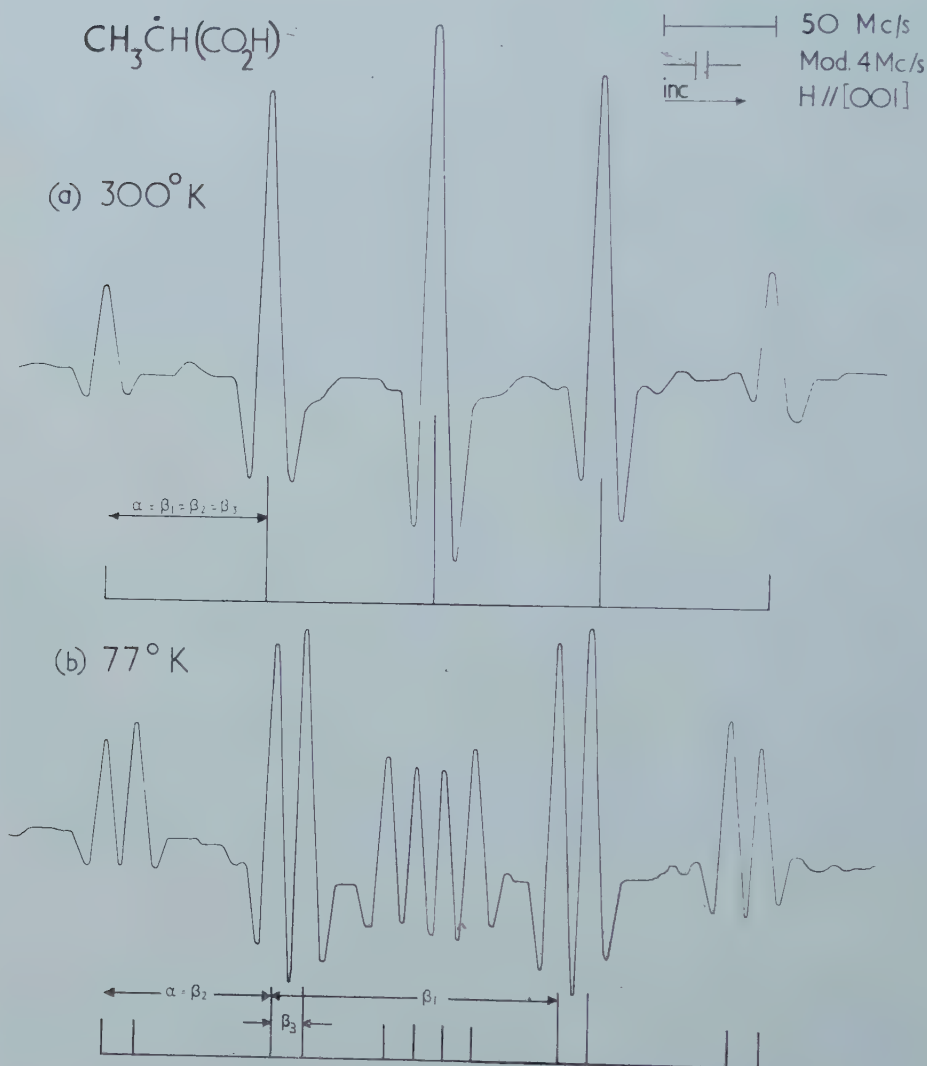


Figure 1.    Second derivative spectra of a $\gamma$-irradiated single crystal of *l*-$\alpha$-alanine, H parallel to *c* axis, (*a*) 300°K, (*b*) 77°K.

sites seriously confuses the central parts of the spectra.    The wings are rather clearer and it was possible to identify enough lines in some orientations in which the magnetic field was not parallel to a crystal axis to enable a coupling tensor to be derived for the hydrogen atom with the smallest coupling.

## 3. THE SPECTRA

Figure 1 shows the spectra obtained with the magnetic field parallel to $c$. It also indicates the interpretation in terms of twelve lines of relative intensity $1 : 1 : 2 : 2 : 1 : 1 : 1 : 1 : 2 : 2 : 1 : 1$ which would be expected for hyperfine coupling to four hydrogen nuclei, with two coupling constants equal. Spectra with the field parallel to $a$ and $b$ were equally straightforward to interpret and required four hydrogens with the effective hyperfine coupling constants of table 1. It seems certain that the methyl group of the $CH_3\dot{C}HCOOH$ radical is rotating slower than $10^7$ times sec at $77°$ K so that each hydrogen atom of this group may have an individual coupling, as opposed to the average value of 70 Mc s attributed to each methyl hydrogen at room temperature. There is no reason to expect the coupling to the λ-hydrogen to vary markedly with temperature. As can be seen in table 1, one of the low-temperature splittings

| Field ∥ | 77°K | | | | | 300°K | |
|---|---|---|---|---|---|---|---|
| | $\beta_1$ | $\beta_2$ | $\beta_3$ | $\alpha$ | $(\beta_1+\beta_2+\beta_3)/3$ | $\alpha$ | $\beta$ |
| $a$ | 116 | 77 | 11 | −51 | 68 | −51 | 67 |
| $b$ | 118 | 76 | 16 | −59 | 70 | −57 | 71 |
| $c$ | 128 | 77 | 14 | −77 | 73 | −73 | 73 |
| Mean | 120 | 76 | 14 | — | 70 | — | 70 |

Table 1. Effective coupling constants (Mc/s).

for each direction is sufficiently close to the λ-hydrogen value at 300°K that it can be assigned unambiguously. The difference between the values 77 and 73 Mc's for the field parallel to $c$ is not necessarily significant as one or all of the methyl hydrogens have the same coupling as $H_{(z)}$ at 77°K and 300°K respectively. This increases the experimental errors somewhat; for instance hydrogen couplings of 75 and 79 Mc s are almost indistinguishable from two hydrogens with 77 Mc/s each.

It is known [5, 6] that hydrogen atoms in a $\beta$ position with respect to the free radical centre, such as those of the $-CH_3$ group here, have only small anisotropies. Therefore the three hydrogens could be confidently assigned to the different couplings, designated $\beta_1$, $\beta_2$ and $\beta_3$, in the manner indicated in table 1 even though it was not possible to confirm this experimentally from measurements with other directions of the field. It was also necessary to assign the same sign to all principal couplings of the $\beta$ hydrogens since only then is there agreement between $(\beta_1+\beta_2+\beta_3)/3$ and the average value at 300°K. Furthermore, although the observed values of $\beta_1$ and $\beta_2$ are each essentially [7, 8] the square root of the diagonal elements of $A^2$, where $A$ is the corresponding coupling tensor, the smallness of off diagonal elements means that the $\beta$ are only slightly greater than the diagonal element of $A$ itself. Consequently the mean value from measurements with the magnetic field parallel to $a$, $b$ and $c$ is essentially the isotropic coupling. The mean values have been rounded off to the nearest lower whole number as a crude correction for the errors arising

from the above difficulty. For $\beta_3$ the hydrogen couples more strongly to the magnetic field than to the electrons and the measurements should represent the diagonal terms in $A$ expressed in $a\ b\ c$ axes.

## 4. Discussion

### 4.1. *Radical geometry and hyperfine coupling*

The simplest expression for the isotropic hyperfine coupling as a function of radical geometry for $\beta$-hydrogen atoms, is

$$B \cos^2 \theta, \qquad (1)$$

where $\theta$ is the angle between the C–H bond and the free radical 2p orbital, both projected on a plane perpendicular to the $\dot{C}$–$CH_3$ bond [5, 6, 9, 10]. In the present case this implies two disposable parameters, $B$ and $\theta_1$, where $\theta_1$ is the value of $\theta$ for $H_{(1)}$, the hydrogen with coupling $\beta_1$, provided the assumption is made that the methyl group has a regular shape so that $\theta_2 = \theta_1 \pm 120°$ and $\theta_3 = \theta_1 \mp 120°$. There are essentially three observations to be fitted, together with the value of the coupling for the rotating methyl group, 70 Mc/s [2]. The most satisfactory compromise appears to be $B = +138$ Mc/s, $\theta_1 = 18°$, which leads to the values of table 2. The agreement is reasonable. The positive sign to B is required on theoretical grounds [9, 10].

Another possible expression is

$$B_0 + B_2 \cos^2 \theta. \qquad (2)$$

With three parameters an exact fit can now be obtained, the required values being $B_0 = +9$ Mc/s, $B_2 = +122$ Mc/s and $\theta_1 = 18°$. A small value of $B_0$ is in accordance with observations on potassium glycollate [11] and lithium glycollate monohydrate [12], where $\beta$-hydrogens attached to oxygen atoms were shown

|                | $\beta_1$ | $\beta_2$ | $\beta_3$ | Rotating |
|----------------|-----------|-----------|-----------|----------|
| Observed       | 120       | 76        | 14        | 70       |
| Calculated (1) | +124      | +76       | + 6       | +69      |
| Calculated (2) | +119      | +76       | +14       | +70      |

Table 2. Comparison of observed couplings in Mc/s with those calculated from (1) with $B = +138$ Mc/s, $\theta_1 = 18°$ and from (2) with $B_0 = +9$ Mc/s, $B_2 = +122$ Mc/s and $\theta_1 = 18°$.

to have small couplings, 7 Mc/s in each case, even though it appeared that the hydrogen was exactly in the plane of the radical. It is interesting that the present treatment finds $B_0$ to be positive. Fessenden and Schuler [13] failed to find a coupling to two of the $\beta$-hydrogens in the cyclohexyl radical and presumed it to be less than the line width of 6 Mc/s. There is thus considerable evidence that the direction independent coupling constant is less than 10 Mc/s and, from the evidence of this paper, most probably positive. This is the sign to be expected if the spin in the radical p orbital polarizes the spins in the C–C bond to give a negative spin population at the adjacent carbon, which would in turn polarize the C–H bond in the free radical plane in the sense which gives a positive spin population on the hydrogen atom.

Neither expression (1) nor (2) distinguishes the four possible values of $\theta_1$ namely $\pm 18°$ or $\pm 162°$. $\theta_1 = +18°$ and $+162°$ correspond to the hydrogen near the plane being adjacent to the carboxyl group whereas with $\theta_1 = -18°$ or $-162°$ it is adjacent to the $\alpha$-hydrogen. The distinction between $+18°$ and $+162°$, and likewise between $-18°$ and $-162°$, is more subtle. In the crystal it is possible to distinguish between above and below the radical plane, a distinction which is not immediately apparent from figure 2. If the crystal structure were fully known so that neighbour molecules could be depicted the difference would be apparent; likewise if the oxygens of the –COOH group were out of the plane. In the absence of such information the approximate direction of the $a$ axis has been indicated as a feature which leads to a distinction between $\theta_1 = +18°$ and $+162°$.
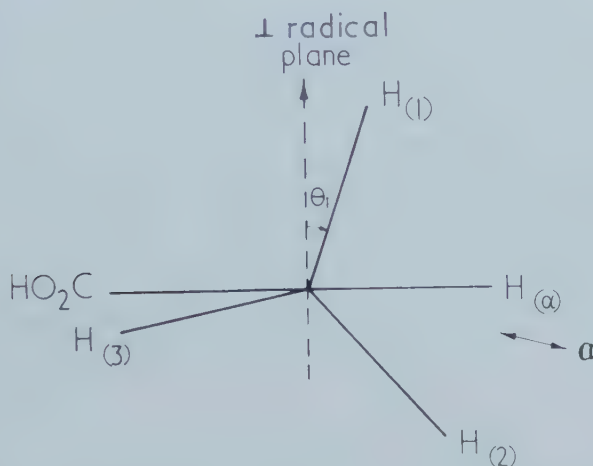


Figure 2. View of radical along $H_3C-\dot{C}$ bond showing definition of $\theta_1$.

There is experimental evidence which favours the $\theta_1 = +18°$ solution, although it rests on an assumption which is not rigorously justified and on the interpretation of the spectra when the magnetic field is not parallel to a crystal axis. From sets of such spectra it was deduced that the $H_{(3)}$ coupling tensor had its axis of largest coupling along the direction with direction cosines $(-0.22, 0.76, 0.61)$ in $a\,b\,c$ axes for radicals in the sites for which other elements have been given in table 1 of ref. [2]. Along this direction the coupling was $+21$ Mc/s and the tensor had almost exactly cylindrical symmetry with a perpendicular coupling of $+10$ Mc/s. If it could be assumed that the electron were concentrated at the free radical centre then the largest axis of the tensor would be parallel to the non-bonded direction $\dot{C} \ldots \ldots H_{(3)}$. If this assumption is still justified even though the electron is in a p orbital, then the angles between $\dot{C} \ldots \ldots H_{(3)}$ and other features can be calculated with the help of the information in [2]. These angles are given in the 'Observed' row of table 3, which also gives the expected values for the various possible values of $\theta_1$ if reasonable bond distances and angles are assumed. The agreement of the observed values with $\theta_1 = +18°$ is satisfactory considering the extended chain of measurements involved.

The skew equilibrium arrangement of the methyl group is probably dictated by the crystal structure and is not necessarily a property of an isolated radical. The barrier height also is probably a function of crystal structure, as other work has shown [14] that the methyl group of the radical $CH_3\dot{C}(COOH)_2$ in methyl malonic acid crystals is still rotating at $77°K$.

| | Angle of $\dot{C}$ . . . . . $H_{(3)}$ with | | | |
| --- | --- | --- | --- | --- |
| | (i) C–C | (ii) $\perp$ Radical | (iii) C–H$_{(\alpha)}$ | (iv) $\perp$ C–H$_{(\alpha)}$. |
| Observed | 18° | 100° | 136° | 49° |
| Calculated for $\theta_1 = +18°$ | 28 | 96 | 147 | 58 |
| $-18°$ | 28 | 96 | 92 | 6 |
| $+162°$ | 28 | 84 | 147 | 58 |
| $-162°$ | 28 | 84 | 92 | 6 |

Table 3.   Angle between the $\dot{C}$ . . . . . $H_{(3)}$ direction and (i) C–CH$_3$ bond direction; (ii) perpendicular to the radical plane in the upwards sense of figure 2; (iii) the C–H$_{(\alpha)}$ bond direction; (iv) the perpendicular to the C–H$_{(\alpha)}$ bond direction in the radical plane.  'Observed' results relate to $\dot{C}$ . . . . . $H_{(3)}$ along $(-0.22, 0.76, 0.61)$ and to directions (i)–(iv) given by the corresponding principal axes quoted in [2].  Calculated values assume $\dot{C}$–H$_{(3)}$ and $\dot{C}$–H$_{(\alpha)}$ 1·10 Å, C–$\dot{C}$ 1·54 Å, angle C–$\dot{C}$–H$_{(\alpha)}$ 120°, angle $\dot{C}$–C–H$_{(3)}$ 109·5° and the value of $\theta_1$ indicated.

## 4.2. *Rotational barrier*

The present experiments show that the rotation of the methyl group is fast compared to 100 Mc/s at $200°K$, but slower at $77°K$.  The barrier is expected to be three-fold, although the six-fold component may be large.  The lowest torsional energy levels have a three-fold degeneracy which may be lifted by the tunnel effect arising from a finite barrier height or by the hyperfine coupling itself.  The results show that the tunnelling rate is slower than $10^7$ per sec, since a faster rate than this would destroy the inequivalence of the hydrogens as observed above $200°K$.  Since the hyperfine coupling destroys the effects of the finite barrier height and the symmetry of the lowest set of levels, no influence of spin statistics is to be expected and a resolved spin can be associated with each individual hydrogen as assumed in the spectral analysis above.

The fact that rotation is more rapid than $10^8$ c/s at $200°K$ does not mean that most methyl groups have energies in excess of the barrier, but merely that the energy relaxation process in this degree of freedom is so rapid that each individual methyl group is excited to a state above or immediately below the barrier, at least once every $10^{-8}$ sec.

## References

[1] MIYAGAWA, I., and GORDY, W., 1960, *J. chem. Phys.*, **32**, 255.

[2] MORTON, J. R., and HORSFIELD, A., 1961, *J. chem. Phys.*, **35**, 1142.

[3] HORSFIELD, A., MORTON, J. R., and WHIFFEN, D. H., 1961, *Trans. Faraday Soc.*, **57**, 1657.

[4] INGRAM, D. J. E., 1958, *Free Radicals as studied by electron spin resonance* (Butterworths Scientific Publications), p. 53

[5] HELLER, C., and McCONNELL, H. M., 1960, *J. chem. Phys.*, **32**, 1535.

[6] POOLEY, D., and WHIFFEN, D. H., 1961, *Mol. Phys.*, **4**, 81.

[7] WHIFFEN, D. H., 1961, *Free Radicals in Biological Systems*, Ed. M. S. Blois (Academic Press), p. 227.

[8] HOLMBERG, R. W., LIVINGSTON, R., and SMITH, W. T., 1960, *J. chem. Phys.*, **33**, 541.

[9] McLACHLAN, A. D., 1958, *Mol. Phys.*, **1**, 233.

[10] LYKOS, P. G., 1960, *J. chem. Phys.*, **32**, 625.

[11] ATHERTON, N. M., and WHIFFEN, D. H., 1960, *Mol. Phys.*, **3**, 103.

[12] POOLEY, D., and WHIFFEN, D. H., 1961, *Trans. Faraday Soc.*, **57**, 1445.

[13] FESSENDEN, R. W., and SCHULER, R. H. (personal communication).

[14] POOLEY, D., HORSFIELD, A., MORTON, J. R., and WHIFFEN, D. H. (unpublished work).

# The repulsive energy in sodium chloride and potassium chloride crystals

by E. A. GUGGENHEIM, M. L. McGLASHAN, and J. E. PRUE

Department of Chemistry, The University, Reading

The repulsive energy in sodium chloride and potassium chloride crystals has been evaluated and related to the lattice constant. The accuracy aimed at was $\pm 0.2$ kcal mole$^{-1}$ but owing to some unidentified experimental error the accuracy claimed is only $\pm 0.6$ kcal mole$^{-1}$ as compared with previous analyses in which the uncertainty is about $\pm 2$ kcal mole$^{-1}$. The improvement has been achieved by critical evaluation of the experimental data, by the elimination of inaccuracies from the thermodynamic formulae and by carrying out the analysis at several specified temperatures.

## 1. Scope

The set of processes numbered (1) to (6), with M denoting an alkali metal,

$$\Delta H/\text{kcal mole}^{-1}$$

| | M = Na | M = K | |
|---|---|---|---|
| $MCl(s) \rightarrow M(s) + \frac{1}{2}Cl_2(g)$ | 98·23 | 104·18, | (1.1) |
| $M(s) \rightarrow M(g)$ | 25·86 | 21·49, | (1.2) |
| $\frac{1}{2}Cl_2(g) \rightarrow Cl(g)$ | 28·99 | 28·99, | (1.3) |
| $M(g) \rightarrow M^+(g) + e^-$ | 119·99 | 101·58, | (1.4) |
| $Cl(g) + e^- \rightarrow Cl^-(g)$ | $-87.33 - q$ | $-87.33 - q,$ | (1.5) |
| $M^+(g) + Cl^-(g) \rightarrow MCl(s)$ | $-185.74 + q$ | $-168.91 + q,$ | (1.6) |

adds up to zero. It was first studied by Born [1] and is called 'Born's cycle' for the alkali chloride MCl. The quoted values of the enthalpy increase all relate to 25°C and to negligible pressure. They will be discussed in §5. At the time of Born's pioneering papers on this subject experimental values of $\Delta H$ were available for the first four of the above processes but none for the last two. However, Born and Landé [2] estimated from a rough consideration of the compressibility of solid KCl that $\Delta H$ for process (6) differs from the calculable contribution from the Coulombic energy by only about 10 per cent and that the magnitude of the non-Coulombic interaction energy could be estimated to within about 30 per cent. Consequently they were able to estimate $\Delta H$ for process (6) to within about 5 kcal mole$^{-1}$. From this Born [1] predicted the value 119 kcal mole$^{-1}$ for process (5). Unfortunately the value of $\Delta H$ for process (3) was seriously wrong. Were it not for this, the value estimated for process (5) would have been $-91$ kcal mole$^{-1}$ as compared with the experimental value $-87$ kcal mole$^{-1}$ obtained [3] some twenty years later.

There have been several subsequent studies [4, 9, 10] of Born's cycle not only for alkali chlorides but for various other salts. These are all based on

approximate thermodynamic formulae due to Born and Mayer [5]. Owing
to approximations in these formulae and to experimental errors the accuracy
of the calculations is restricted to about $\pm 2$ kcal mole$^{-1}$. Such an uncertainty
is inevitable for most salts.

For sodium chloride and potassium chloride the experimental measurements
seemed sufficiently extensive and accurate to warrant the more refined analysis
undertaken here. This improved analysis has become possible through the
availability of low-pressure measurements of compressibility. It has necessi-
tated a more critical assessment of other experimental data and the use of exact
thermodynamic formulae in place of the approximate formulae of Born and
Mayer.

Our ultimate object is to obtain as detailed and accurate information as
possible concerning $E_r$ the repulsive (overlap) energy per mole in the crystal.
In contrast to previous authors we do not attempt an evaluation of what fraction
of $E_r$ is due to interaction between non-nearest neighbours. In our opinion any
such assignment is purely speculative since there is no experimental evidence
whatever on this. As a result of our different approach our analysis is more
straightforward, simpler and, we believe, more accurate than any previous
analysis.

In view of the high accuracy aimed at we shall specify in detail the sources
of all the data used. When better experimental measurements become available
it will thus be possible for anyone to revise the calculations with the minimum
expenditure of effort. Our calculations are restricted to the temperature
range 298°K to 100°K owing to the lack of experimental data, in particular for
the densities, outside this range.

## 2. Notation

The most important symbols to be used are the following:

| | |
|---|---|
| $n$ | the number of ions per conventional molecule ($n=2$ for an alkali halide); |
| $T$ | thermodynamic temperature; |
| $p$ | pressure; |
| $r$ | distance between a cation and an anion; |
| $R$ | equilibrium value of $r$ for nearest neighbours; |
| $V$ | volume per mole; |
| $L$ | Avogadro's constant; |
| $\alpha$ | coefficient of thermal expansion; |
| $\kappa$ | isothermal compressibility; |
| $\kappa_S$ | adiabatic compressibility; |
| $F$ | free energy (of Helmholtz) per mole; |
| $U$ | thermodynamic total energy per mole; |
| $S$ | entropy per mole; |
| $C_p$ | heat capacity at constant pressure per mole; |
| $\theta$ | characteristic temperature for acoustic modes; |

$x = \theta/T$;

$\phi(x)$      contribution of acoustic modes to $F/3n\mathbf{R}T$;

$E_p$      potential energy per mole;

$E_C$      Coulombic term in $E_p$;

$E_{dd}$      dipole–dipole dispersion energy term in $E_p$;

$E_{qd}$      quadrupole–dipole dispersion energy term in $E_p$;

$E_r$      repulsive (overlap) energy term in $E_p$.

### 3. Thermodynamics of a crystal

Since the exact detailed thermodynamic formulae relating to the acoustic modes of a crystal are, in contrast to inexact versions, not readily accessible, it is expedient to summarize the most important formulae. It will be assumed that the contribution of the acoustic modes to the molar free energy has the form

$$F_{ac}/3n\mathbf{R}T = \phi(\theta/T) = \phi(x), \tag{3.1}$$

where $\theta$ is a characteristic temperature, determined by the lattice constant $R$, and $x = \theta/T$. The form of the function $\phi$ depends on the model. Formula (1) includes as special cases the Einstein formula, the Nernst–Lindemann formula and the Debye formula. The molar free energy $F$ of the crystal has the form

$$F = E_p + F_{ac} = E_p(V) + 3n\mathbf{R}T\phi(x), \tag{3.2}$$

where $E_p$ denotes the potential energy when every atom is at rest on its lattice point and is determined by $V$ or $R$. Formula (2) is discussed in greater detail in the Appendix.

The following relations are derived from (2) by straightforward thermodynamics without making any further approximations whatever:

$$S = 3n\mathbf{R}(x\phi' - \phi), \tag{3.3}$$

$$E_p = U - 3n\mathbf{R}Tx\phi', \tag{3.4}$$

$$-pV = \frac{dE_p}{d \ln V} + 3n\mathbf{R}Tx\phi' \frac{d \ln \theta}{d \ln V}, \tag{3.5}$$

$$\frac{\alpha V}{\kappa} = \frac{\partial S}{\partial \ln V} = 3n\mathbf{R}x^2\phi'' \frac{d \ln \theta}{d \ln V} = \left(C_p - \frac{\alpha^2 TV}{\kappa}\right)\frac{d \ln \theta}{d \ln V}, \tag{3.6}$$

$$\frac{dE_p}{d \ln V} = -pV - \frac{TV}{\kappa} \frac{\phi'}{x\phi''}, \tag{3.7}$$

$$\frac{V}{\kappa} - pV = -\frac{\partial(pV)}{\partial \ln V} = \frac{d^2 E_p}{d(\ln V)^2} + 3n\mathbf{R}T(x\phi' + x^2\phi'')\left(\frac{d \ln \theta}{d \ln V}\right)^2$$
$$+ 3n\mathbf{R}Tx\phi' \frac{d^2 \ln \theta}{d(\ln V)^2}, \tag{3·8}$$

$$\frac{\alpha V}{\kappa} + \frac{V}{\kappa^2}\left(\frac{\partial \kappa}{\partial T}\right)_p + \frac{\alpha V}{\kappa^3}\left(\frac{\partial \kappa}{\partial p}\right)_T = 3n\mathbf{R}\frac{d^2 \ln \theta}{d(\ln V)^2} + 3n\mathbf{R}\frac{d(x^2\phi'')}{d \ln V}\frac{d \ln \theta}{d \ln V}, \tag{3.9}$$

$$\frac{d^2 E_p}{d(\ln V)^2} = -pV + \frac{V}{\kappa}\left\{1 - x\phi'\left(\alpha T + \frac{T}{\kappa}\frac{\partial \kappa}{\partial T} + \frac{\alpha T}{\kappa^2}\frac{\partial \kappa}{\partial p}\right)\right\}$$
$$- \frac{(x\phi' + x^2\phi'') - x\phi'(2x^2\phi'' + x^3\phi''')}{(x^2\phi'')^2}\frac{1}{3n\mathbf{R}T}\left(\frac{xTV}{\kappa}\right)^2. \tag{3.10}$$

In any of these formulae $d/d \ln V$ is equivalent to $\frac{1}{3} d/d \ln R$.

According to Einstein's approximation for the acoustic contributions

$$\phi = \ln (2 \sinh \tfrac{1}{2}x), \tag{3.11}$$

$$x\phi' = \tfrac{1}{2}x \coth \tfrac{1}{2}x, \tag{3.12}$$

$$x^2\phi'' = -(\tfrac{1}{2}x \operatorname{cosech} \tfrac{1}{2}x)^2. \tag{3.13}$$

According to Debye's approximation for the acoustic contributions

$$\phi = \int_0^x \ln (2 \sinh \tfrac{1}{2}\xi)\, \frac{3\xi^2}{x^3}\, d\xi, \tag{3.14}$$

$$x\phi' = \int_0^x (\tfrac{1}{2}\xi \coth \tfrac{1}{2}\xi)\, \frac{3\xi^2}{x^3}\, d\xi, \tag{3.15}$$

$$x^2\phi'' = -\int_0^x (\tfrac{1}{2}\xi \operatorname{cosech} \tfrac{1}{2}\xi)^2\, \frac{3\xi^2}{x^3}\, d\xi. \tag{3.16}$$

At sufficiently high temperature it makes no difference which of these approximations is used. We postpone until § 7 further discussion of which of these approximations we shall use, and with what justification.

## 4. High temperature formulae

At high temperatures when $x \ll 1$ the formulae of the previous section may be simplified by using the approximations

$$x\phi' = 1 + \tfrac{1}{12}x^2 \text{ (Einstein)}, \qquad x\phi' = 1 + \tfrac{1}{20}x^2 \text{ (Debye)}, \tag{4.1}$$

$$x^2\phi'' = -1 + \tfrac{1}{12}x^2 \text{ (Einstein)}, \qquad x^2\phi'' = -1 + \tfrac{1}{20}x^2 \text{ (Debye)}, \tag{4.2}$$

$$2x^2\phi'' + x^3\phi''' = O(x^4) \quad \text{(Einstein or Debye)}. \tag{4.3}$$

If the terms in $x^2$, as well as higher powers, are neglected formula (3.4) reduces to

$$E_p = U - 3n\boldsymbol{R}T \tag{4.4}$$

and formula (3.7) to

$$\frac{1}{3}\frac{dE_p}{d \ln R} = -pV + \frac{aTV}{\kappa} \tag{4.5}$$

and formula (3.10) to

$$\frac{1}{9}\frac{d^2E_p}{d (\ln R)^2} = -pV + \frac{V}{\kappa}\left\{1 - \alpha T - \frac{T}{\kappa}\left(\frac{\partial \kappa}{\partial T}\right)_p - \frac{\alpha T}{\kappa^2}\left(\frac{\partial \kappa}{\partial p}\right)_T\right\}. \tag{4.6}$$

Formulae (5) and (6) due to Born and Mayer [5] have been widely used. They imply that $x \ll 1$ and are therefore high-temperature formulae. They should therefore be used in conjunction with (4). In fact Born and Mayer used instead of (4) the zero-temperature approximation for $x\phi'$. This procedure has been copied by Mayer and Helmholz [6], by Huggins and Mayer [7], by Huggins [8], by Cubicciotti [9], and by Baughan [10].

## 5. Thermochemical and cognate data

We shall now specify the sources of all the data used. All the tabulated thermochemical data are expressed in kcal mole$^{-1}$ where the calorie is defined

as 4·184 J exactly and the mole is defined on the chemical scale, which differs inappreciably from the new unified scale.

The values of the enthalpy increases $\Delta H$ quoted in § 1 all relate to 25°C. The values for process (1.1), derived entirely from classical thermochemical measurements, were taken from the tables published by the Bureau of Standards [11]. The values for process (1.2) are those evaluated by Evans *et al.* [12] from the dependence on temperature of the vapour pressure of solid sodium and solid potassium. The value for process (1.3) was obtained by taking half the dissociation energy of the $Cl_2$ molecule obtained from the convergence limit of the continuous absorption spectrum [13], multiplying by $L$ and adding $(\frac{5}{2} - \frac{7}{4})RT = \frac{3}{4}RT$. The values for process (1.4) were obtained from the spectroscopic values [14] of the ionization energy of the sodium atom and of the potassium atom by multiplying by $L$ and adding $\frac{3}{2}RT$. The experimental values for process (1.5) have been reviewed by Pritchard [15]. We make a provisional estimate by subtracting $\frac{3}{2}RT$ from McCallum and Mayer's [3] experimental value $\Delta E_0$ of the electron affinity per mole. McCallum and Mayer claim an accuracy of only $\pm 1$ kcal mole$^{-1}$ for $\Delta E_0$, so that the value of $\Delta H$ is much less accurately known for process (1.5) than for any of the processes (1.1) to (1.4). We have therefore denoted the true but as yet unknown value of $\Delta H$ for process (1.5) by $\Delta E_0 - \frac{3}{2}RT - q$, as compared with the best experimental value of $\Delta E_0 - \frac{5}{2}RT$. We shall later determine the value of $q$ as accurately as possible and, provided McCallum and Mayer's estimate of their experimental uncertainty is correct, we shall find a value between $-1$ and $+1$ kcal mole$^{-1}$. For each salt the value of $\Delta H$ for process (1.6) is equal and opposite to the sum of the values for processes (1.1) to (1.5).

| (a) Sodium chloride | | | | |
|---|---|---|---|---|
| 1 | $T/°K$ | 298 | 200 | 100 |
| 2 | $\Delta H$/kcal mole$^{-1}$ | $-185·74+q$ | $-185·91+q$ | $-185·93+q$ |
| 3 | $S$/cal °K$^{-1}$ mole$^{-1}$ | 17·31 | 12·69 | 5·74 |
| 4 | $R$/Å | $2·820_0$ | — | — |
| 5 | $\rho$/g cm$^{-3}$ | — | 2·186 | 2·206 |
| 6 | $10^4\alpha/°K^{-1}$ | 1·21 ±0·01 | $1·06_5$±0·01 | 0·74 ±0·01 |
| 7 | $\kappa$/cm$^3$ kcal$^{-1}$ | 0·176±0·002 | 0·166±0·002 | 0·158±0·002 |
| 8 | $T(\partial\kappa/\partial T)$/cm$^3$ kcal$^{-1}$ | 0·030±0·003 | — | — |
| 9 | $-\kappa^{-2}(\partial\kappa/\partial p)$ | 4·5 ±0·25 | — | — |
| (b) Potassium chloride | | | | |
| 1 | $T/°K$ | 298 | 200 | 100 |
| 2 | $\Delta H$/kcal mole$^{-1}$ | $-168·91+q$ | $-169·11+q$ | $-169·19+q$ |
| 3 | $S$/cal °K$^{-1}$ mole$^{-1}$ | 19·74 | 14·98 | 7·61 |
| 4 | $R$/Å | $3·146_6$ | — | — |
| 5 | $\rho$/g cm$^{-3}$ | — | 2·006 | 2·026 |
| 6 | $10^4\alpha/°K^{-1}$ | 1·08 ±0·04 | 0·95 ±0·05 | 0·86 ±0·07 |
| 7 | $\kappa$/cm$^3$ kcal$^{-1}$ | 0·239±0·003 | 0·225±0·003 | 0·211±0·003 |
| 8 | $T(\partial\kappa/\partial T)$/cm$^3$ kcal$^{-1}$ | 0·050±0·005 | — | — |
| 9 | $-\kappa^{-2}(\partial\kappa/\partial p)$ | 3·71 ±0·10 | — | — |

Table 1. Primary experimental quantities.

## 6. EXPERIMENTAL DATA RELATING TO THE SOLIDS

The primary experimental quantities which we used in our calculations are given for the two salts in table 1 with estimates of the experimental uncertainty where these are important.

Values of $\Delta H$ for process (1.6) (see § 1) are given in row 2. They were calculated from

$$\Delta H(T) = \Delta H(298°\text{K}) + \int_{298°\text{K}}^{T} (C_p - 5R)dT, \qquad (6.1)$$

where $C_p$ is the molar heat capacity at constant pressure of the solid salt. The values of $\Delta H(298°\text{K})$ were those given in § 1, and we used the heat capacity measurements of Clusius *et al.* [16] for sodium chloride and of Berg and Morrison [17] for potassium chloride. Values of the entropy $S$ (relative to $S=0$ when $T=0$) are given in row 3. They were obtained by graphical integration of the same heat capacity measurements from

$$S = \int_0^T C_p \, d \ln T. \qquad (6.2)$$

Values of the nearest-neighbour distance $R$ and of the molar volume $V$ can be obtained either from x-ray measurements of $R$ or from measurements of the density $\rho$. We prefer values obtained from x-ray measurements but these are available only at room temperature. Values of $R$ at 298°K obtained from x-ray measurements [18] are given in row 4. Values of the density $\rho$ at 200°K and 100°K obtained by interpolation of a smooth curve drawn through the results of Henglein [19] are given in row 5. Values of the coefficient of thermal expansion $\alpha = V^{-1}\partial V/\partial T$ at vanishing pressure are given in row 6. Those for sodium chloride were interpolated from a smooth curve drawn through the direct measurements of Rubin *et al.* [20]. Those for potassium chloride were obtained by estimating slopes on a smooth curve drawn through the results of Henglein [19] at about 89, 194, and 273°K and of Baxter and Wallace [21] at about 273, 298, 323 and 343°K. The uncertainties in the values of $\alpha$ for potassium chloride are considerably greater than for sodium chloride. Values of the isothermal compressibility $\kappa = -V^{-1}\partial V/\partial p$ at vanishing pressure are given in row 7. In obtaining these values we have used the results of two types of measurements. Measurements of isothermal compression at high pressures lead by extrapolation to values of $\kappa$ at zero pressure. Measurements of the velocity of sound lead directly to values of the adiabatic compressibility $\kappa_s$ and thence by use of the formula

$$\kappa = \kappa_s + \alpha^2 TV/C_p \qquad (6.3)$$

to values of the isothermal compressibility $\kappa$. Of the values mentioned below all except those of Slater and of Bridgman were obtained from measurements of the velocity of sound by use of formula (3). For sodium chloride at 298°K our estimate covers the values of Slater [22], of Bridgman [23], and of Durand [24]. We rejected the values of Huntington [25] and Galt [26] which are obviously too high, and that of Spangenberg [27] which is obviously much too low, as well as older direct measurements made with large increments of pressure. At 200 and 100°K our values were obtained by interpolation of a smooth curve drawn through the results of Rose [28]. For potassium chloride at 298°K our

estimate covers the values of Slater [22], Durand (extrapolated from 280 K) [24], and Galt [26]. We rejected older direct measurements made with large increments of pressure. At 200 and 100 K our values were obtained by interpolation of a smooth curve drawn through the results of Durand [24].

Values of $T\,\partial\kappa/\partial T$ at vanishing pressure are given for 298°K only in row 8. They were obtained by estimating the slopes at 298 K of curves drawn through Durand's [24] values of $\kappa$. Values of $\kappa^{-2}\,\partial\kappa/\partial p$ at vanishing pressure are given for 298°K only in row 9. For sodium chloride our value covers the estimates of Slater [22] and of Bridgman [23]. For potassium chloride our value and the estimate of its uncertainty were taken directly from Slater [22] who claims that $\partial\kappa/\partial p$ is known with such accuracy only in the particular case of potassium chloride.

| | (a) Sodium chloride | | | |
|---|---|---|---|---|
| 1 | $T/°\mathrm{K}$ | 298 | 200 | 100 |
| 2 | $V/\mathrm{cm^3\ mole^{-1}}$ | 27·01 | 26·74 | 26·50 |
| 3 | $R/Å$ | $2·820_0$ | 2·810 | 2·802 |
| 4 | $U/\mathrm{kcal\ mole^{-1}}$ | $-182·78 + q$ | $-183·92 + q$ | $-184·94 + q$ |
| 5 | $(\alpha TV/\kappa)/\mathrm{kcal\ mole^{-1}}$ | $5·53 \pm 0·08$ | $3·43 \pm 0·05$ | $1·24 \pm 0·02$ |
| 6 | $(V/\kappa)/\mathrm{kcal\ mole^{-1}}$ | $153·_5 \pm 2$ | $161 \pm 2$ | $168 \pm 2$ |
| 7 | $\alpha T$ | $0·0361 \pm 0·0003$ | — | — |
| 8 | $T\kappa^{-1}(\partial\kappa/\partial T)$ | $0·170 \pm 0·017$ | — | — |
| 9 | $\alpha T\kappa^{-2}(\partial\kappa/\partial P)$ | $-0·16_2 \pm 0·01$ | — | — |
| 10 | $\alpha T + T\kappa^{-1}(\partial\kappa/\partial T) + \alpha T\kappa^{-2}(\partial\kappa/\partial P)$ | $0·044 \pm 0·02$ | — | — |
| 11 | $(6\mathbf{R}T)^{-1}(\alpha TV/\kappa)^2/\mathrm{kcal\ mole^{-1}}$ | $8·6 \pm 0·1$ | — | — |

| | (b) Potassium chloride | | | |
|---|---|---|---|---|
| 1 | $T/°\mathrm{K}$ | 298 | 200 | 100 |
| 2 | $V/\mathrm{cm^3\ mole^{-1}}$ | 37·53 | 37·17 | 36·80 |
| 3 | $R/Å$ | $3·146_6$ | 3·136 | 3·126 |
| 4 | $U/\mathrm{kcal\ mole^{-1}}$ | $-165·95 + q$ | $-167·12 + q$ | $-168·20 + q$ |
| 5 | $(\alpha TV/\kappa)/\mathrm{kcal\ mole^{-1}}$ | $5·05 \pm 0·20$ | $3·14 \pm 0·16$ | $1·50 \pm 0·12$ |
| 6 | $(V/\kappa)/\mathrm{kcal\ mole^{-1}}$ | $157 \pm 2$ | $165 \pm 2$ | $174 \pm 3$ |
| 7 | $\alpha T$ | $0·0322 \pm 0·0012$ | — | — |
| 8 | $T\kappa^{-1}(\partial\kappa/\partial T)$ | $0·209 \pm 0·021$ | — | — |
| 9 | $\alpha T\kappa^{-2}(\partial\kappa/\partial P)$ | $-0·11_9 \pm 0·00_6$ | — | — |
| 10 | $\alpha T + T\kappa^{-1}(\partial\kappa/\partial T) + \alpha T\kappa^{-2}(\partial\kappa/\partial P)$ | $0·122 \pm 0·02$ | — | — |
| 11 | $(6\mathbf{R}T)^{-1}(\alpha TV/\kappa)^2/\mathrm{kcal\ mole^{-1}}$ | $7·2 \pm 0·3$ | — | — |

Table 2. Derived experimental quantities.

In table 2 we give values of various derived experimental quantities which we shall need for our calculations. The values of the molar volume $V$ and of the distance $R$ between next-nearest neighbours were obtained at 298 K from the values of $R$ given in table 1, and at 200 K and 100 K from the values of $\rho$ given in table 1, according to the formula

$$V = 2LR^3 = M/\rho \tag{6.4}$$

with $L = 6·0230 \times 10^{23}\ \mathrm{mole^{-1}}$, $M = 58·448$ g mole$^{-1}$ for NaCl and $M = 74·557$ g mole$^{-1}$ for KCl. The values of the molar total energy (or molar enthalpy

at negligible pressure) $U$ of the solid relative to a state of zero energy defined as infinitely dispersed ions at rest were calculated from the values of $\Delta H$ in table 1 by use of the formula

$$U = \Delta H + 5RT. \tag{6.5}$$

The quantities in the other rows of table 2 were obtained by straightforward arithmetic from the quantities given in table 1.

## 7. ACOUSTIC CONTRIBUTIONS

Since the only contribution to the entropy is that of the vibrational degrees of freedom (acoustic modes) and since no other purely experimental quantity, except certain derivatives of the entropy, has this property, the entropy is the most useful quantity to provide information concerning the characteristic vibrational temperature. For any approximation such as Einstein's or Debye's we can therefore use the experimental values of $S$ to calculate values of $x = \theta/T$ and so of the functions $x\phi'$ which we need for use in formula (3.4), $\phi'/x\phi''$ which we need for use in formula (3.7), and $X$ defined by the relation

$$X = \{(x\phi' + x^2\phi'') - x\phi'(2x^2\phi'' + x^3\phi''')\}/(x^2\phi'')^2 \tag{7.1}$$

which we need for use in formula (3.10).

At sufficiently high temperatures Einstein's and Debye's approximations lead to identical conclusions. At lower temperatures we have confidence in *either* only when they lead to identical conclusions and, when they do, we are confident that any other reasonable approximation would also lead to identical conclusions.

Within the range of temperatures 298°K to 100°K Einstein's and Debye's approximations lead to identical conclusions. We shall describe our calculations

| (a) Sodium chloride | | | | | |
|---|---|---|---|---|---|
| 1 | $T/°$K | 298 | 200 | 100 | 100 |
| 2 | Approximation | E | E | E | D |
| 3 | $x$ | 0·648 | 0·975 | 1·937 | 2·778 |
| 4 | $\theta/°$K | 193·0 | 195·0 | 193·7 | 277·8 |
| 5 | $x\phi'$ | 1·035 | 1·078 | 1·295 | 1·355 |
| 6 | $-x^2\phi''$ | 0·966 | 0·925 | 0·738 | 0·700 |
| 7 | $-\phi'/x\phi''$ | 1·071 | 1·165 | 1·755 | 1·936 |
| 8 | $X$ | $5 \times 10^{-4}$ | — | — | — |
| (b) Potassium chloride | | | | | |
| 1 | $T/°$K | 298 | 200 | 100 | 100 |
| 2 | Approximation | E | E | E | D |
| 3 | $x$ | 0·525 | 0·794 | 1·585 | 2·253 |
| 4 | $\theta/°$K | 156·5 | 158·8 | 158·5 | 225·3 |
| 5 | $x\phi'$ | 1·023 | 1·052 | 1·201 | 1·240 |
| 6 | $-x^2\phi''$ | 0·977 | 0·949 | 0·815 | 0·786 |
| 7 | $-\phi'/x\phi''$ | 1·047 | 1·108 | 1·474 | 1·578 |
| 8 | $X$ | $2 \times 10^{-4}$ | — | — | — |

Table 3. Acoustic quantities.

in detail according to both approximations at 100°K at which temperature the discrepancies, if any, between the conclusions would be greatest, but to save space we have omitted details of Debye's approximation at the higher temperatures.

Values of $x$ obtained from the values of $S$ given in table 1 by the use of tables of Einstein [29] and Debye [30] functions are given in table 3, together with values of the derived quantities, $\theta$, $x\phi'$, $x^2\phi''$, and $\phi'_,x\phi''$ at 298°K, 200°K and 100°K for Einstein's (E) approximation, and at 100°K for Debye's (D) approximation. We also give in table 3 rough values at 298°K only (which is all we shall need) of $X$ which is given with sufficient accuracy by the formula

$$X = x^4/360 \text{ (Einstein)} \quad \text{or} \quad X = x^4/840 \text{ (Debye)}. \tag{7.2}$$

## 8. Decomposition of energy

The molar energy $U$ has the form

$$U = E_p + U_{ac}, \tag{8.1}$$

where $E_p$ denotes the molar potential energy when every atom is at rest at its equilibrium position and $U_{ac}$ is the contribution to the molar energy of the acoustic modes. According to formula (3.4)

$$U_{ac} = 6RTx\phi'. \tag{8.2}$$

Values of $U$, of $U_{ac}$ and of $E_p$ are given in rows 4, 5, and 6 respectively of table 4.

The potential energy $E_p$ is conveniently decomposed as follows

$$E_p = E_C + E_{dd} + E_{qd} + E_r. \tag{8.3}$$

We shall discuss each term on the right in turn.

By far the numerically largest and the most accurately known term in the crystal energy is $E_C$ the Coulombic energy of point charges. Using the value [4] 1·74756 for Madelung's constant we obtain for the Coulombic contribution $E_C$ to the molar energy

$$E_C = -\frac{6\cdot0230 \times 10^{23} \times 1\cdot74756 \times (4\cdot8029 \times 10^{-10})^2}{(R/\text{Å}) \times 10^{-8} \times 10^7 \times 4\cdot1840 \times 10^3} \text{ kcal mole}^{-1}$$

$$= -\frac{580\cdot31}{(R/\text{Å})} \text{ kcal mole}^{-1}. \tag{8.4}$$

Values of $E_C$ are given in row 7 of table 4.

We next consider the contribution of the dispersion energy. There are two terms, one $E_{dd}$ due to dipole dipole interaction, the other $E_{qd}$, much smaller, due to quadrupole–dipole interaction. We estimate these from the theoretical formulae of Mayer [31]

$$E_{dd} = -LCr^{-6}, \quad E_{qd} = -LDr^{-8} \tag{8.5}$$

with $C$ and $D$ for NaCl given by

$$\begin{aligned} C &= 180 \times 10^{-12} \text{ erg Å}^6, \quad LC = 2\cdot59 \times 10^3 \text{ kcal mole}^{-1} \text{ Å}^6, \\ D &= 180 \times 10^{-12} \text{ erg Å}^8, \quad LD = 2\cdot59 \times 10^3 \text{ kcal mole}^{-1} \text{ Å}^8, \end{aligned} \tag{8.6}$$

and for KCl by

$$\begin{aligned} C &= 452 \times 10^{-12} \text{ erg Å}^6, \quad LC = 6\cdot51 \times 10^3 \text{ kcal mole}^{-1} \text{ Å}^6, \\ D &= 560 \times 10^{-12} \text{ erg Å}^8, \quad LD = 8\cdot06 \times 10^3 \text{ kcal mole}^{-1} \text{ Å}^8. \end{aligned} \tag{8.7}$$

Values obtained by these formulae are given in rows 8 and 9 of table 4. Unfortunately we do not know how accurate are these theoretical coefficients, but we have verified that errors of as much as 10 per cent in $C$ and of 50 per cent in $D$ would not seriously affect our main conclusions. When we subtract $E_C$, $E_{dd}$ and $E_{qd}$ from $E_p$ we obtain the values of the repulsive (overlap) molar energy $E_r$ given in row 10 of table 4. These values of $E_r$ will be discussed in §11.

| | | (a) Sodium chloride | | | |
|---|---|---|---|---|---|
| 1 | $T/°\text{K}$ | 298 | 200 | 100 | 100 |
| 2 | $R/\text{Å}$ | $2\cdot820_0$ | $2\cdot810$ | $2\cdot802$ | $2\cdot802$ |
| 3 | Approximation | Einstein | Einstein | Einstein | Debye |
| 4 | $U$ | $-182\cdot78+q$ | $-183\cdot92+q$ | $-184\cdot94+q$ | $-184\cdot94+q$ |
| 5 | $U_{ac}$ | $3\cdot68$ | $2\cdot57$ | $1\cdot54$ | $1\cdot62$ |
| 6 | $-E_p$ | $186\cdot46-q$ | $186\cdot49-q$ | $186\cdot48-q$ | $186\cdot56-q$ |
| 7 | $E_C$ | $-205\cdot78$ | $-206\cdot52$ | $-207\cdot11$ | $-207\cdot11$ |
| 8 | $E_{dd}$ | $-5\cdot15$ | $-5\cdot26$ | $-5\cdot35$ | $-5\cdot35$ |
| 9 | $E_{qd}$ | $-0\cdot65$ | $-0\cdot67$ | $-0\cdot68$ | $-0\cdot68$ |
| 10 | $E_r$ | $25\cdot12+q$ | $25\cdot96+q$ | $26\cdot66+q$ | $26\cdot58+q$ |
| 11 | $-\partial E_p/\partial \ln R$ | $-17\cdot8\pm0\cdot3$ | $-12\cdot0\pm0\cdot2$ | $-6\cdot5\pm0\cdot1$ | $-7\cdot2\pm0\cdot1$ |
| 12 | $\partial E_C/\partial \ln R$ | $205\cdot8$ | $206\cdot5$ | $207\cdot1$ | $207\cdot1$ |
| 13 | $\partial E_{dd}/\partial \ln R$ | $30\cdot9$ | $31\cdot6$ | $32\cdot1$ | $32\cdot1$ |
| 14 | $\partial E_{qd}/\partial \ln R$ | $5\cdot2$ | $5\cdot4$ | $5\cdot4$ | $5\cdot4$ |
| 15 | $\partial E_r/\partial \ln R$ | $-224\cdot1\pm0\cdot3$ | $-231\cdot5\pm0\cdot2$ | $-238\cdot1\pm0\cdot1$ | $-237\cdot4\pm0\cdot1$ |
| 16 | $-\partial^2 E_p/\partial(\ln R)^2$ | $-1320\pm30$ | — | — | — |
| 17 | $\partial^2 E_C/\partial(\ln R)^2$ | $-206$ | — | — | — |
| 18 | $\partial^2 E_{dd}/\partial(\ln R)^2$ | $-185$ | — | — | — |
| 19 | $\partial^2 E_{qd}/\partial(\ln R)^2$ | $-42$ | — | — | — |
| 20 | $\partial^2 E_r/\partial(\ln R)^2$ | $1753\pm30$ | — | — | — |
| | | (b) Potassium chloride | | | |
| 1 | $T/°\text{K}$ | 298 | 200 | 100 | 100 |
| 2 | $R/\text{Å}$ | $3\cdot146_6$ | $3\cdot136$ | $3\cdot126$ | $3\cdot126$ |
| 3 | Approximation | Einstein | Einstein | Einstein | Debye |
| 4 | $U$ | $-165\cdot95+q$ | $-167\cdot12+q$ | $-168\cdot20+q$ | $-168\cdot20+q$ |
| 5 | $U_{ac}$ | $3\cdot63$ | $2\cdot51$ | $1\cdot43$ | $1\cdot48$ |
| 6 | $-E_p$ | $169\cdot58-q$ | $169\cdot63-q$ | $169\cdot63-q$ | $169\cdot68-q$ |
| 7 | $E_C$ | $-184\cdot42$ | $-185\cdot05$ | $-185\cdot64$ | $-185\cdot64$ |
| 8 | $E_{dd}$ | $-6\cdot71$ | $-6\cdot84$ | $-6\cdot98$ | $-6\cdot98$ |
| 9 | $E_{qd}$ | $-0\cdot84$ | $-0\cdot86$ | $-0\cdot88$ | $-0\cdot88$ |
| 10 | $E_r$ | $22\cdot39+q$ | $23\cdot12+q$ | $23\cdot87+q$ | $23\cdot82+q$ |
| 11 | $-\partial E_p/\partial \ln R$ | $-15\cdot9\pm0\cdot6$ | $-10\cdot4\pm0\cdot5$ | $-6\cdot6\pm0\cdot5$ | $-7\cdot1\pm0\cdot6$ |
| 12 | $\partial E_C/\partial \ln R$ | $184\cdot4$ | $185\cdot0$ | $185\cdot6$ | $185\cdot6$ |
| 13 | $\partial E_{dd}/\partial \ln R$ | $40\cdot3$ | $41\cdot0$ | $41\cdot9$ | $41\cdot9$ |
| 14 | $\partial E_{qd}/\partial \ln R$ | $6\cdot7$ | $6\cdot9$ | $7\cdot0$ | $7\cdot0$ |
| 15 | $\partial E_r/\partial \ln R$ | $-215\cdot5\pm0\cdot6$ | $-222\cdot5\pm0\cdot5$ | $-227\cdot9\pm0\cdot5$ | $-227\cdot4\pm0\cdot6$ |
| 16 | $-\partial^2 E_p/\partial(\ln R)^2$ | $-1237\pm30$ | — | — | — |
| 17 | $\partial^2 E_C/\partial(\ln R)^2$ | $-184$ | — | — | — |
| 18 | $\partial^2 E_{dd}/\partial(\ln R)^2$ | $-242$ | — | — | — |
| 19 | $\partial^2 E_{qd}/\partial(\ln R)^2$ | $-54$ | — | — | — |
| 20 | $\partial^2 E_r/\partial(\ln R)^2$ | $1717\pm30$ | — | — | — |

Table 4. All energies are given in kcal mole$^{-1}$.

## 9. EQUATION OF STATE

In the preceding section we evaluated $E_p$ and thence $E_r$ by use of formula (3.4). We shall now in a parallel way evaulate $dE_p$ $d \ln R$ and thence $dE_r/d \ln R$. At ordinary pressures $pV$ is negligible and so formula (3.7) becomes

$$\frac{dE_p}{d \ln R} = -\frac{3\alpha TV}{\kappa} \frac{\phi'}{x\phi''}. \tag{9.1}$$

Values thus obtained are given in row 11 of table 4. The quantities in rows 12, 13 and 14 were obtained simply from the relations

$$dE_c/d \ln R = -E_c, \tag{9.2}$$

$$dE_{dd}/d \ln R = -6E_{dd}, \tag{9.3}$$

$$dE_{qd}/d \ln R = -8E_{qd}. \tag{9.4}$$

By subtraction of the quantities in (2), (3) and (4) from that in (1) we obtain the values of $dE_r$ $d \ln R$ in row 15. These values will be discussed in § 11.

## 10. COMPRESSIBILITY

Having used formula (3.4) to evaluate $E_r$ and formula (3.7) to evaluate $dE_r$ $d \ln R$ we shall now use formula (3.10) to evaluate $d^2E_r/d(\ln R)^2$. At negligible pressure we may rewrite formula (3.10) as

$$\frac{d^2E_p}{d (\ln R)^2} = \frac{9V}{\kappa} \left\{ 1 - x\phi' \left( xT + \frac{T}{\kappa} \frac{\partial \kappa}{\partial T} + \frac{\alpha T}{\kappa^2} \frac{\partial \kappa}{\partial p} \right) \right\} - \frac{3X}{nRT} \left( \frac{\alpha TV}{\kappa} \right)^2 \tag{10.1}$$

where $X$ is defined by formula (7.1) and the term in $X$ is negligible.

It is only at room temperature that sufficiently accurate values of $\partial \kappa/\partial p$ at low pressure are available. For this reason our calculations are restricted to $298°$K. The values of $d^2E_p$ $d(\ln R)^2$ thus obtained are given in row 16 of table 4. The quantities in rows 17, 18 and 19 are obtained simply from the relations

$$d^2E_c/d(\ln R)^2 = E_c, \tag{10.2}$$

$$d^2E_{dd}/d(\ln R)^2 = 36E_{dd}, \tag{10.3}$$

$$d^2E_{qd}/d(\ln R)^2 = 64E_{qd}. \tag{10.4}$$

The values of $d^2E_r$ $d (\ln R)^2$ in row 20 are obtained by subtracting the values of (2), (3) and (4) from that of (1). These values will be discussed in § 11.

## 11. EMPIRICAL RELATION BETWEEN $E_r$ AND $R$. DETERMINATION OF $q$

If we assume for each salt an empirical relation between $E_r$ and $R$ of the form

$$E_r = B \exp (-AR), \tag{11.1}$$

with two adjustable parameters $A$ and $B$, we require two experimental data to determine these. The following experimental data are available for each salt. Firstly we have the values of $E_r$ for three values of $R$ obtained in § 8 but these contain the as yet undetermined additive constant $q$. Secondly we have values of $dE_r/d \ln R$ obtained in § 9 for three values of $R$. Thirdly we have the value of $d^2E_r/d (\ln R)^2$ obtained for one value of $R$ in § 10. Our most immediate

object is to determine as accurately as possible the value of the constant $q$ which we do as follows. From (1) we deduce

$$E_r = \frac{(dE_r/d \ln R)^2}{d^2E_r/d (\ln R)^2 - dE_r/d \ln R}. \tag{11.2}$$

Using the values of $dE_r/d \ln R$ in row 15 of table 4 and the values of $d^2E_r/d (\ln R)^2$ in row 20, we obtain for NaCl at $298°\text{K}$

$$E_r = 25 \cdot 4 \pm 0 \cdot 4 \text{ kcal mole}^{-1}, \tag{11.3}$$

and for KCl at $298°\text{K}$:

$$E_r = 24 \cdot 0 \pm 0 \cdot 4 \text{ kcal mole}^{-1}. \tag{11.4}$$

Comparison of these values with row 10 of table 4 gives

$$q = 0 \cdot 3 \pm 0 \cdot 4, \quad q = 1 \cdot 6 \pm 0 \cdot 4. \tag{11.5}$$

This discrepancy is a disappointment. It implies that there is somewhere an experimental error appreciably greater than assumed. The most likely sources of such an error are the measurements of $\partial \kappa / \partial p$ on sodium chloride and of $\alpha$ on potassium chloride. When we embarked on these calculations we hoped to determine $q$ to $\pm 0 \cdot 2$. Until this discrepancy is resolved we cannot do better than assume $q = 0 \cdot 6 \pm 0 \cdot 6$ as a compromise between (11.5) and the direct measurements of electron affinity which imply $q = 0 \pm 1 \cdot 0$.


## 12. Determination of $A$

We have in principle several ways of determining or checking the value of $A$. We may use either the relation

$$A = -\frac{dE_r/d \ln R}{RE_r} \tag{12.1}$$

at each of three temperatures, or the relation

$$A = \frac{d^2E_r/d(\ln R)^2 - dE_r/d \ln R}{-RdE_r/d \ln R} \tag{12.2}$$

at $298°\text{K}$. In view of the discrepancy disclosed in the previous section we cannot expect the value of $A$ obtained from (2) to be as accurate as we could wish. The use of (1) on the other hand implies the assumption of a value for $q$ to give the value of $E_r$. We have done the calculation for three values of $q$, namely 0, $0 \cdot 6$ and $1 \cdot 2$. The results are collected in table 5. Owing to the uncertainty in $q$ there is an uncertainty of about $\pm 2 \cdot 5$ per cent in $A$ for each salt. For each assumed value of $q$ there is agreement to within $\pm 0 \cdot 3$ per cent between the values of $A$ obtained at the three temperatures. It is moreover interesting to observe that, regardless of the value of $q$, the value of $A$ for sodium chloride is about 4 per cent greater than the value for potassium chloride. This is contrary to the customary assumption.

As a further check we compare in table 6 the experimental values of $E_r$ at $200°\text{K}$ and $100°\text{K}$ with values calculated from the experimental value of $E_r$ at $298°\text{K}$ according to formua (11.1) with $A = 3 \cdot 10$ Å$^{-1}$ for NaCl and $A = 2 \cdot 98$ Å$^{-1}$ for KCl. The agreement is impressive.

|  | (a) NaCl | | |
|---|---|---|---|
| Formula (2) at 298°K (q=0·3) | | 3·13 | |
| | q=0 | q=0·6 | q=1·2 |
| Formula (1) at 298°K | 3·16 | 3·09 | 3·02 |
| Formula (1) at 200°K | 3·17 | 3·10 | 3·03 |
| Formula (1) at 100°K | 3·19 | 3·12 | 3·05 |
| | (b) KCl | | |
| Formula (2) at 298°K (q=1·6) | | 2·85 | |
| | q=0 | q=0·6 | q=1·2 |
| Formula (1) at 298°K | 3·06 | 2·98 | 2·90 |
| Formula (1) at 200°K | 3·07 | 2·99 | 2·92 |
| Formula (1) at 100°K | 3·05 | 2·98 | 2·91 |

Table 5. Values of $A/\text{Å}^{-1}$.

Several authors [4, 9, 10] have made approximate estimates of $A$, or of the related parameter $a$ discussed in § 14, but none of them has attempted to verify whether the relation (11.1) is in fact accurate. This verification requires analysis of the experimental data at more than one temperature and this has not previously been attempted.

| $T/°K$ | 298 | 200 | 100 | 100 |
|---|---|---|---|---|
| Approximation | E | E | E | D |
| | | NaCl | | |
| $E_r$(expt., q=0·6) | 25·72 | 26·56 | 27·26 | 27·18 |
| $E_r$(calc., $A=3·10\text{ Å}^{-1}$) | (25·72) | 26·53 | 27·20 | 27·20 |
| | | KCl | | |
| $E_r$(expt., q=0·6) | 22·99 | 23·72 | 24·47 | 24·42 |
| $E_r$(calc., $A=2·98\text{ Å}^{-1}$) | (22·99) | 23·73 | 24·45 | 24·45 |

Table 6.

### 13. Comparison with quantum theory

So far as we know the only calculations from quantum theory of the repulsive energy with which to compare our values are those of Löwdin [38]. For values of $R$, in the neighbourhood of the equilibrium distance, the value of $E_r$ calculated by Löwdin for sodium chloride is 13 per cent lower than our estimate and for potassium chloride is 31 per cent lower. In view of the complicated nature of the theoretical problem this may perhaps be as good agreement as could reasonably be expected.

When Löwdin's values, in the neighbourhood of the equilibrium distance, are fitted by the empirical formula (11.1) the value of $A$ for sodium chloride is found to be $2 \cdot 7_0$ Å$^{-1}$ as compared with our estimate $3 \cdot 1_0$ Å$^{-1}$ and for potassium chloride $2 \cdot 8_0$ Å$^{-1}$ as compared with our estimate $2 \cdot 9_8$ Å$^{-1}$.

## 14. CONTRIBUTION OF NON-NEAREST NEIGHBOURS

This completes such analysis as we consider constructive. We must however explain why, in contrast to most previous authors, we have deliberately avoided any attempt to split the repulsive energy $E_r$ into a contribution from interactions between nearest neighbours and a much smaller contribution from interactions between non-nearest neighbours. It is generally accepted that the contribution from next nearest neighbours is roughly 5 per cent of that from nearest neighbours and that the contribution from more distant pairs is only about 0·05 per cent and so negligible. What we know factually about the contribution from non-nearest neighbours is little more than this. There is no experimental measurement which throws any light on the matter. The contribution from theory is almost entirely speculative. Under these circumstances the most reasonable attitude is to make the simplest possible assumptions which do not disagree with either experiment or theory.

All that theory tells us is that the repulsive energy between two atoms or ions is of the form $P(r) \exp(-ar)$ where $P(r)$ denotes a polynomial in $r$. It is customary to approximate to this by the form $b \exp(-ar)$, where $b$ is a constant. This is certainly a good approximation over any short range of $r$, but would not be accurate for changes in $r$ comparable with $r$ itself. It is general practice to assume for the repulsive energy between a pair of nearest-neighbour ions (of opposite sign)

$$E_{+-} = b \exp(-ar), \quad r \simeq R, \tag{14.1}$$

and for the repulsive energies between pairs of next-nearest neighbour ions (of same sign)

$$E_{++} = b_+ \exp(-ar), \quad r \simeq \sqrt{2}R, \tag{14.2}$$

$$E_{--} = b_- \exp(-ar), \quad r \simeq \sqrt{2}R. \tag{14.3}$$

These approximations imply two distinct assumptions (a) that the same value of $a$ may be used for all kinds of ion pairs and (b) that the same value of $a$ may be used for values of $r$ in the neighbourhood both of $R$ and of $\sqrt{2}R$. We admit that assumption (a) is plausible, but we know of no theoretical or experimental basis for (b). The only justification for this assumption is its simplicity.

Accepting these formulae for lack of anything better we have for the molar repulsive energy

$$E_r = 6L\{b \exp(-aR) + (b_+ + b_-) \exp(-\sqrt{2}aR)\}$$
$$= 6Lb \exp(-aR)\{1 + 2\lambda \exp(-[\sqrt{2}-1]aR)\}, \tag{14.4}$$

where $\lambda$ is defined by

$$\lambda = (b_+ + b_-)/2b. \tag{14.5}$$

Substituting from formula (1) of § 11 into (4), taking logarithms and differentiating with respect to $R$, we obtain

$$\frac{A}{a} = 1 + \frac{2(\sqrt{2}-1)\lambda}{\exp([\sqrt{2}-1]aR) + 2\lambda}. \tag{14.6}$$

In view of the crudeness of the assumption of a common value of $a$ in (1), (2) and (3) we can see no sense in making elaborate assumptions about $\lambda$. We shall tentatively assume $\lambda = 1$. Substituting numerical values of $R$ and $A$ into (6) we obtain by successive approximations

$$a/A = 0.979 \text{ for NaCl}, \quad a/A = 0.983 \text{ for KCl}, \tag{14.7}$$

so that the distinction between $a$ and $A$ is hardly significant. With these same assumptions the ratio $2\lambda \exp(-[\sqrt{2}-1]aR)$ of the contribution of next-nearest neighbours to that of nearest neighbours is $0.05_5$ for NaCl and $0.04_8$ for KCl.

Previous authors [4, 9] instead of setting $\lambda = 1$ have assumed

$$\lambda = \frac{15}{16} \frac{\bar{b}}{\boldsymbol{b}}, \tag{14.8}$$

where $\bar{b}$ denotes the arithmetic mean and $\boldsymbol{b}$ the geometric mean of $b_+$ and $b_-$. In the present context there is no case for such extraneous sophistication.

## 15. Previous work

There have been several previous analyses [4] of the crystal energy of alkali halides. In those prior to 1941 the use of the wrong value for the electronic charge led to an error between 1 and 2 kcal mole$^{-1}$ in $E_c$ with a consequent equal and opposite error in $E_r$. Recent analyses by Baughan [10] and by Cubicciotti [9] of the alkali halides are free from this error but contain other inaccuracies or uncertainties of comparable magnitude (over and above the loss of a factor 2 in Cubicciotti's values of the acoustic zero-temperature-energy†).

Baughan replaces the factor $\{\ldots\}$ in formula (10.1) by unity on the ground that the omitted terms " are small compared with unity and tend to cancel out ". This is Grüneisen's approximation (see Appendix, formulae (A 6)). It leads to an error in $A$ of 4 per cent for NaCl and of 9 per cent for KCl. Baughan thus finds that all alkali halides with the NaCl structure have values of $A$ the same within about $\pm 5$ per cent. He then assumes that they all have exactly the same value of $A$ and by correlating the lattice energies with the lattice spacings he obtains a best value $A = 3.07 \pm 0.04$ Å$^{-1}$. Our analysis shows that on the contrary the values of $A$ for NaCl and KCl differ by about 4 per cent. In fact Baughan uses the value of the potential energy at 0 K with the lattice spacing at room temperature but this leads to an error of only about 1 per cent in the value of $A$. On the other hand, Baughan refrains, as we have done, from attempting to split the repulsive energy into contributions from nearest and non-nearest neighbours.

Whereas we have put our faith in the determinations of $\kappa$ by Durand and we have rejected those of Spangenberg because they differ so violently from all other data, Cubicciotti has ignored the former and used the latter. It Spangenberg's measurements were right then those of Bridgman and of Slater would be so far wrong that we should have no information at all on $\partial\kappa/\partial p$.

† This has now been corrected: *J. Chem. Phys.*, 1961, **34**, 2189.

This would imply an uncertainty of about 15 per cent in $d^2E_r/d(\ln R)^2$ and consequently an uncertainty of about 3 kcal mole$^{-1}$ in $E_r$.

All previous authors, including Cubicciotti, have evaluated the potential energy terms $E_c$, $E_{dd}$ and $E_{qd}$ at 298°K or thereabouts but have used for $U_{ac}$ the zero-temperature-energy. Hence the value of the remaining term $E_r$ of the energy is a hybrid corresponding neither to the value of $R$ at 0°K nor to the value of $R$ at 298°K. Consequently there is an ambiguity of about $\pm 0.01$ Å in $R$ and a corresponding ambiguity of about $\pm 1$ kcal mole$^{-1}$ in $E_r$.

We have already in § 14 criticized attempts to decompose $E_r$ into a contribution from nearest neighbours and another much smaller contribution from non-nearest neighbours. We pointed out that such decomposition has no basis in either theory or experiment, but is dependent on assumptions as arbitrary as assigning 5 per cent to non-nearest neighbours. Such decomposition moreover leads to tediously complicated algebra, in particular the numerical solution of awkward simultaneous equations. But however arbitrary and awkward the analysis, the decomposition of $E_r$ into additive terms ought not to affect their sum which, as we have shown, is completely determinable from experiment. It so happens that Cubicciotti has carried out two distinct analyses [9, 33] differing in the assumptions concerning non-nearest neighbours. When we compare the resulting pairs of values for the total $E_r$ we find in most cases agreement to within about 0.2 kcal mole$^{-1}$, which we suppose to be the accuracy of solution of the awkward simultaneous equations. However, for NaF there is a discrepancy of 1.5 and for LiF of 2.9 kcal mole$^{-1}$. These discrepancies are a complete mystery.

Cubicciotti, following previous authors, has assumed that the value of $a$ is the same for all four alkali metals. We have shown that the values of $A$ for NaCl and KCl differ by about 4 per cent. There is no reason to suppose that the difference in the values of $a$ is any smaller.

In conclusion we would emphasize that these criticisms of Cubicciotti's analysis become irrelevant if an accuracy of about $\pm 2$ kcal mole$^{-1}$ is accepted.

<center>APPENDIX</center>

<center>*Grüneisen's formulae and approximations*</center>

The molar free energy $F$ of a crystal is given by

$$F = E_p(V) - 3nRT \int_0^\infty g(v) \ln \{2 \sinh (h v/2kT)\} \, dv, \qquad (A\ 1)$$

where $E_p$ denotes the potential energy when every atom is at rest in its equilibrium position and $3nNg(v)dv$ denotes the number of normal modes in a crystal of $nN$ atoms having frequencies in the range $v$ to $v + dv$ so that

$$\int_0^\infty g(v) \, dv = 1. \qquad (A\ 2)$$

Let $v_m$ denote the frequency at which $g(v)$ has its largest maximum. It is expedient to rewrite (1) as

$$F = E_p(V) - 3nRT \int_0^\infty j(v/v_m) \ln \{2 \sinh (h v/2kT)\} \, d(v/v_m). \qquad (A\ 3)$$

This formula is accurate. For it to become useful it is essential to make some approximation concerning the dependence of $j(v/v_m)$ on the molar volume $V$. The only proposed approximation sufficiently general, accurate and simple to be useful is that, when the volume varies, only $v_m$ changes while the form of $j(v/v_m)$ remains unchanged. Formula (3) then takes the form

$$F = E_p(V) + 3nRT\phi(\theta/T), \tag{A 4}$$

where $\theta = hv_m/k$. Formula (A 4) is due to Grüneisen [34] and is the same as formula (3.2) which is the basis of all our thermodynamic formulae.

Formula (A 4) says nothing about how $\theta$ varies with $V$. Grüneisen [34], in the absence of any theoretical or experimental information on this question, assumed as an approximation that $\ln \theta$ varied linearly with $\ln V$, that is to say

$$d^2 \ln \theta/d(\ln V)^2 = 0. \tag{A 5}$$

One consequence of this assumption is that at high temperatures where $X$, defined by formula (7.1) is effectively zero,

$$\alpha T + \frac{T}{\kappa} \frac{\partial \kappa}{\partial T} + \frac{\alpha T}{\kappa^2} \frac{\partial \kappa}{\partial p} = 0. \tag{A 6}$$

So far as we know, the validity of this relation has hitherto never been tested. From the data in row 10 of table 2 we see that the relation is not obeyed within the experimental accuracy. At the same time we observe from rows 7, 8, 9 of table 2 that the value of the expression on the left of (A 6) is considerably smaller than the largest of its three terms. Whether this partial cancellation is general or accidental we do not know.

Another test of Grüneisen's approximation is provided by formula (3.6), namely, whether the experimental quantity

$$\frac{\kappa C_p}{\alpha V} - \alpha T \tag{A 7}$$

is independent of temperature. Only for NaCl are the measurements of $\alpha$ sufficiently precise to afford a sensitive test. When the temperature changes from $298°$K to $100°$K the quantity in formula (7) changes from $0.64$ to $0.68$. We conclude that Grüneisen's approximation is not good enough for the degree of accuracy at which we are aiming.

## References

[1] BORN, M., 1919, *Verh. dtsch. phys. Ges.*, **21**, 19, 679.
[2] BORN, M., and LANDÉ, A., 1918, *Verh. dtsch. phys. Ges.*, **20**, 210.
[3] McCALLUM, K. J., and MAYER, J. E., 1943, *J. chem. Phys.*, **11**, 56.
[4] WADDINGTON, T. C., 1959, *Advances in Inorganic Chemistry and Radiochemistry*, Vol. 1 (New York: Academic Press), p. 158.
[5] BORN, M., and MAYER, J. E., 1932, *Z. Phys.*, **75**, 1.
[6] MAYER, J. E., and HELMHOLZ, W., 1932, *Z. Phys.*, **75**, 19.
[7] HUGGINS, M. L., and MAYER, J. E., 1933, *J. chem. Phys.*, **1**, 643.
[8] HUGGINS, M. L., 1937, *J. chem. Phys.*, **5**, 143; *Ibid.*, **15**, 212.
[9] CUBICCIOTTI, D., 1959, *J. chem. Phys.*, **31**, 1646.
[10] BAUGHAN, E. C., 1959, *Trans. Faraday Soc.*, **55**, 736.
[11] ROSSINI, F. D., *et al.*, 1952, *Circular 500*, U.S. Bureau of Standards.
[12] EVANS, W. H., JACOBSON, R., MUNSON, T. R., and WAGMAN, D. D., 1955, *J. Res. nat. Bur. Stand.*, **55**, 83.

[13] GAYDON, A. G., 1953, *Dissociation Energies* (London: Chapman and Hall), p. 223.

[14] MOORE, C. E., 1949, *Circular 467*, U.S. Bureau of Standards, Vol. 1, pp. 89, 227.

[15] PRITCHARD, H. O., 1953, *Chem. Rev.*, **52**, 529.

[16] CLUSIUS, K., GOLDMANN, J., and PERLICK, A., 1949, *Z. Naturf.* A, **4**, 424.

[17] BERG, W. T., and MORRISON, J. A., 1957, *Proc. roy. Soc.* A, **242**, 467.

[18] SWANSON, H. E., and TATGE, E., 1953, *Circular* 539, U.S. Bureau of Standards, Vol. 1, p. 65; SWANSON, H. E., and FUYAT, R. K., *Ibid.*, Vol. 2, p. 41.

[19] HENGLEIN, F. A., 1925, *Z. phys. Chem.*, **115**, 91.

[20] RUBIN, T., JOHNSTON, H. L., and ALTMAN, W. H., 1961, *J. phys. Chem.*, **65**, 65.

[21] BAXTER, G. P., and WALLACE, C. C., 1916, *J. Amer. chem. Soc.*, **38**, 259.

[22] SLATER, J. C., 1924, *Phys. Rev.*, **23**, 488; 1924, *Proc. Amer. Acad. Arts Sci.*, **61**, 135.

[23] BRIDGMAN, P. W., 1929, *Proc. Amer. Acad. Arts Sci.*, **64**, 19.

[24] DURAND, M. A., 1936, *Phys. Rev.*, **50**, 449.

[25] HUNTINGTON, H. B., 1947, *Phys. Rev.*, **72**, 321.

[26] GALT, J. K., 1948, *Phys. Rev.*, **73**, 1460.

[27] SPANGENBERG, K., 1956, *Naturwissenschaften*, **43**, 394; SPANGENBERG, K., and HAUSSÜHL, S., 1957, *Z. Kristallogr.*, **109**, 422.

[28] ROSE, F. C., 1936, *Phys. Rev.*, **49**, 50.

[29] SHERMAN, J., and EWELL, R. B., 1942, *J. phys. Chem.*, **46**, 641.

[30] BEATTIE, J. A., 1926, *J. Math. Phys.*, **5**, 1.

[31] MAYER, J. E., 1933, *J. chem. Phys.*, **1**, 270, 327.

[32] LÖWDIN, P., 1948, Thesis, Uppsala; 1956, *Advanc. Phys.*, **5**, 1.

[33] CUBICCIOTTI, D., 1960, *J. chem. Phys.*, **33**, 1579.

[34] GRÜNEISEN, E., 1926, *Handb. Phys.*, Vol. 10 (Berlin: Springer), p. 1.

# Environmental effects on atomic energy levels†

by J. JORTNER

Department of Physical Chemistry, Hebrew University of Jerusalem

and C. A. COULSON

Mathematical Institute, Oxford

This paper considers environmental effects both on the ground-state charge distribution and on the different energy levels of a hydrogen atom. The medium is represented by a continuous dielectric, and the effect of the polarization of this medium is computed, using both a simplified self-consistent-field variational treatment, and also a perturbation calculation. The dielectric effects of the medium are compared with similar results based on discrete molecular models, taking into account both dispersion and overlap-repulsion forces. The dielectric effects on the ground-state charge distribution are of the same order of magnitude as the effects due to dispersion forces. The dielectric effects on Rydberg-type electronic transitions lead to blue shifts. This conclusion is in agreement with some recent experimental results.

## 1. INTRODUCTION

The perturbation of the energy levels of an atom or a molecule by a compressed gas, a solvent or a solid can in certain cases by treated by the use of a continuous dielectric model for the surrounding medium [1, 2]. One condition for the adequacy of this treatment must be that the penetration of the charge of the trapped atom into the medium is sufficiently great as to make the bulk properties of the medium applicable. This approach, using bulk properties, is based on the assumption that the perturbing effect of the medium is mainly due to long-range interactions.

Several related phenomena are involved. Thus the presence of the surrounding medium affects the charge distribution of a trapped hydrogen atom—a situation that can be investigated experimentally by the use of electron-spin and nuclear magnetic resonance techniques [3, 4]. Further, a study of environmental effects on the energies of optical absorption frequencies yields information concerning the relative shifts of two distinct energy levels, when the nuclear configuration is always that of the ground state of the system. Finally, the dielectric medium model may be applicable for Rydberg-type transitions in the ultra-violet, when excitation of a bound electron causes a considerable change in the overlap of the charge-cloud with the medium. When it is realized that for a hydrogen atom the mean radius in a state of principal quantum number $n$ is almost proportional to $n^2$, it is clear that Rydberg transitions would be expected to show this effect in a pronounced manner.

In the present work we consider environmental effects on the charge distribution and excitation energy of a trapped atom, here taken to be hydrogen.

Application of the continuum model will involve a semi-empirical reduction of a complicated many-electron problem to a one-electron problem. We shall conclude with a comparison of the results predicted by a dielectric model with those due to dispersion and short-range repulsion forces.

## 2. Application of dielectric model to the ground state

To simplify the calculations we consider the environmental perturbation of the energy levels of atomic hydrogen. Our model (figure 1) is that of an $H$ atom located at the centre $O$ of a spherical cavity of radius $R_0$ in a continuous dielectric. The properties of this medium are specified by its static dielectric
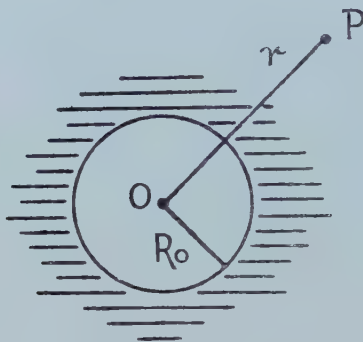


Figure 1.   Model of dielectric medium, shown shaded, with atom at centre of cavity of radius $R_0$.

constant $D_S$ and its optical dielectric constant $D_{op}$. This latter is the high-frequency dielectric constant, corresponding to frequencies higher than those of the nuclear vibrations. The problem of the interaction energy between an additional electron and a dielectric medium has already been treated in relation to electron trapping in the solid [5, 6, 7] and liquid states [8, 9].

We start with the interaction between the electron, the H nucleus, and the medium polarization. As a result of the polarization induced by the field of the moving electron, the unperturbed electron-nucleus interaction $v(r) = -1/r$ (in which we use atomic units of charge and mass and length) will be diminished by the medium. For $r > R_0$ the nuclear charge contributes $-1/D_S \, dv(r)/dr$ to the electrostatic field. Also the polarization field of the medium is $(1 - 1/D_S) q(r)/r^2$, where

$$q(r) = \int_0^r |\psi(r)|^2 \, d\tau \tag{1}$$

is the fraction of charge within a radius $r$, and $\psi(r)$ is the wave function of the valence electron in the ground state. Here and later we are assuming spherical symmetry.

Thus the total field acting on the electron in the 1s-state is derived from a potential $V_{1s}(r)$, where

$$-\operatorname{grad} V_{1s}(r) = -\frac{1}{D_S} \frac{dv(r)}{dr} + \alpha_S \frac{q(r)}{r^2} \tag{2}$$

with the abbreviation, which we shall frequently use:

$$\alpha_s = 1 - \frac{1}{D_s}. \tag{3}$$

Integrating (2) with the condition that $V_{1s}(\infty) = 0$, we have

$$V_{1s}(r) = -\frac{1}{D_s r} - \alpha_s \int_r^\infty q(r) r^{-2} \, dr. \tag{4}$$

Assuming continuity of $V_{1s}(r)$ at $r = R_0$, and setting

$$p(r) = 1 - q(r) = \int_r^\infty |\psi(r)|^2 \, dr, \tag{5}$$

we obtain the final expression

$$V_{1s}(r) = -\frac{1}{r} + \alpha_s \int_r^\infty p(r) r^{-2} \, dr, \quad r > R_0$$

$$= -\frac{1}{r} + \alpha_s \int_{R_0}^\infty p(r) r^{-2} \, dr, \quad r < R_0. \tag{6}$$

The Schrödinger equation may now be written down. It is an integro-differential equation since the potential energy function $V_{1s}(r)$ itself involves the wave function according to (5) and (6). This eigenvalue problem may be solved by a restricted form of variational self-consistent-field technique [1, 7]. If we begin with the one-parameter wave function

$$\psi_0(r) = \sqrt{\frac{\mu^3}{\pi}} \exp(-\mu r), \tag{7}$$

where $\mu$ is yet to be determined, we soon calculate from (5) that

$$p(r) = (1 + 2\mu r + 2\mu^2 r^2) \exp(-2\mu r). \tag{8}$$

Then, by use of (6), and dropping the suffix 1s for the moment,

$$V(\mu, r) = -\frac{1}{r} + \alpha_s \frac{(1 + \mu r) \exp(-2\mu r)}{r}, \quad r > R_0$$

$$= -\frac{1}{r} + \alpha_s \frac{(1 + \mu R_0) \exp(-2\mu R_0)}{R_0}, \quad r > R_0. \tag{9}$$

The wave equation is

$$\mathscr{H} \psi = E\psi,$$

where

$$\mathscr{H} = -\tfrac{1}{2}\nabla^2 + V(\mu, r). \tag{10}$$

We solve this equation variationally, putting

$$\psi = \psi_1(r) = \sqrt{\frac{\lambda^3}{\pi}} \exp(-\lambda r) \tag{11}$$

and choosing $\lambda$ so that

$$\frac{\partial}{\partial \lambda} \int \psi_1^* \mathscr{H} \psi_1 \, d\tau = 0. \tag{12}$$

Self-consistency is now achieved by choosing $\mu$ in (7) so that the corresponding value of $\lambda$ determined from (12) is such that $\lambda = \mu$. This gives the following equations to determine $\lambda$ and $E$:

$$\lambda = 1 - \alpha_s(\tfrac{11}{16} + \tfrac{11}{4}X + \tfrac{7}{2}X^2 + 2X^3) \exp(-4X), \tag{13}$$

$$E(\lambda) = \tfrac{1}{2}\lambda^2 - \lambda + \frac{\alpha_s}{R_0}\left\{(1+X)\exp(-2X) - (1 + \tfrac{21}{8}X + \tfrac{5}{2}X^2 + X^3)\exp(-4X)\right\} \quad (14)$$

in which $X = \lambda R_0$ and, as before, $\alpha_s = 1 - 1/D_s$.

More refined calculations could be made, choosing more complicated and flexible functions than the simple exponential (7). We have not made them, since although they would lead to a more accurate wave function and energy, it is most unlikely that they would significantly alter our main conclusions.

The special case of $R_0 = 0$ is of some interest. It corresponds to the 'interstitial ion' model, formerly treated using a somewhat different approach [7, 9]. Our present treatment leads to the results:

$$\lambda = 1 - \tfrac{11}{16}\alpha_s, \quad E(\lambda) = \tfrac{1}{2}\lambda^2 - \lambda + \tfrac{3}{8}\alpha_s\lambda. \quad (15)$$

The reference state in this system is a free electron located at infinite distance from the cavity, while the medium is polarized and produces the potential given by equation (6).

An alternative method of getting the same results as in (6)–(14) is to use the general expression for the total energy $W$ of the system consisting of dielectric medium plus trapped H atom.

$$W = \int \psi^*(r)\left\{-\tfrac{1}{2}\nabla^2 - \frac{1}{D_s r}\right\}\psi(r)d\tau - \frac{\alpha_s}{8\pi}\int \mathbf{D}_e^2 \, d\tau, \quad (16)$$

where the dielectric displacement vector $\mathbf{D}_e$ satisfies

$$\mathrm{div}\, \mathbf{D}_e = 4\pi \,|\,\psi(r)\,|^2, \quad (17)$$

and then solving the variational problem

$$\delta W = 0 \quad \text{for all} \quad \delta\psi \quad \text{such that} \quad \int \psi^*\psi \, d\tau = 1.$$

## 3. PERTURBATION OF THE GROUND-STATE ENERGY

Let us define the perturbation energy of the ground state due to the dielectric medium as the energy change

$$\Delta E(1s) = E_{\mathrm{H}}(1s) - E(\lambda), \quad (18)$$

where $E_{\mathrm{H}}(1s)$ is the energy of an isolated hydrogen atom in its ground state, and $E(\lambda)$ is given by (14) using the value of $\lambda$ given by (13).

The dependence of $\Delta E(1s)$ on the parameter $\alpha_s$ is shown in figure 2. Dielectric effects appear to decrease the binding energy. For the ground state this effect decreases sharply with increasing $R_0$, and obviously depends on the total amount of the valence electron charge-cloud that penetrates into the medium. This effect is qualitatively similar to the effect of short-range repulsion forces between two ground-state hydrogen atoms. A comparison of the two energies is of some interest. It is well known [10, 11] that the interaction energy of two H atoms with randomly oriented spins can be estimated by using the concept of pseudo-valence forces. This mutual energy $E(R)$, at separation $R$, is

$$E(R) = \tfrac{1}{4}\,{}^1E(R) + \tfrac{3}{4}\,{}^3E(R), \quad (19)$$

where ${}^1E(R)$ is the energy of the lowest ${}^1\Sigma_g$ state of the $H_2$ molecule, and ${}^3E(R)$ is the energy of the lowest ${}^3\Sigma_u$ state. The use of spectroscopic data [17] for these two states yields the values presented in table 1.

In order to obtain the total interaction energy by this means, the mutual pair energy shown in the table should be multiplied by the number of nearest

neighbour atoms $Z$. Thus in a face-centred cubic-solid there are three possible sites [3]: a substitutional site for which $Z=12$, an octahedral site for which $Z=6$, and a tetrahedral site for which $Z=4$. Other situations can be dealt with similarly.
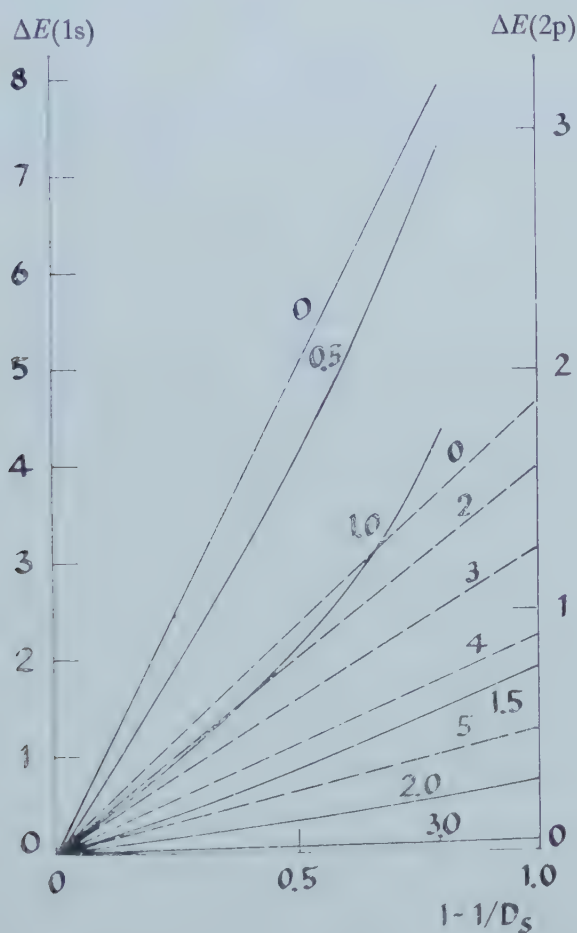


Figure 2. The dielectric effect on the energy levels of a hydrogen atom: Solid curves: the effect of the energy on the 1s ground state, calculated by the variation method; dashed curves: the effect on the energy of the 2p excited state, calculated by the perturbation method. Energies are in ev.

| $R$ and $2R_0$ $(a_0)$ | $E(R)$ (ev) | $\Delta E(1s)$ (ev) |
|---|---|---|
| 3 | 0·123 | 0·862 |
| 4 | 0·0268 | 0·326 |
| 6 | 0·000628 | 0·044 |
| 8 | −0·000395 | 0·006 |

Table 1. Interaction energies for the ground state of H, using spectroscopic data ($E(R)$) and the dielectric model ($\Delta E(1s)$) with $D_s=2$.

In comparing the values of $E(R)$ with the dielectric medium values $E(\lambda)$ the chief difficulties are (i) the number $Z$ of neighbours involved in $E(R)$, and (ii) the unambiguous determination of the relation between $R$, the distance of the neighbour atom from the central atom, and $R_0$ the cavity radius. It seems reasonable to identify $R_0$ with one half the distance between the nuclei, setting

$$R_0 \simeq \tfrac{1}{2}R. \tag{20}$$

This is the relationship adopted in table 1. It appears from this table that, when allowance is made for the factor $Z$, the perturbation energies resulting from the dielectric model treatment are of the same order of magnitude for small distances as the short-range repulsion forces; but for larger distances the dielectric model yields larger long-range repulsion forces.

### 4. CHARGE DISTRIBUTION IN GROUND STATE

We have already stated that the unpaired electron-spin density at the proton can be experimentally measured [3, 4]. Such data have recently been applied [3] to the theoretical evaluation of the interaction of ground-state H atoms with rare gas matrices [4]. It is of interest, therefore to see what density is predicted by our continuum model. As we shall show, the dielectric effect leads to expansion of the charge-cloud of the unpaired electron.

This latter follows from (11) and (13), since

$$|\psi(0)|^2 = \frac{\lambda^3}{\pi} \quad \text{and} \quad \lambda < 1. \tag{21}$$

The relative change in the unpaired electron density at the nucleus is defined by

$$\rho \equiv \rho_{\mathrm{d}} = \frac{|\psi(0)|^2 - |\psi_0(0)|^2}{|\psi_0(0)|^2} \tag{22}$$

where $|\psi_0(0)|^2 = 1/\pi$ is the unperturbed density. Thus the effect of the medium is to cause a relative change

$$\rho_{\mathrm{d}} = \lambda^3 - 1. \tag{23}$$

Since $\lambda < 1$, $\rho_{\mathrm{d}}$ is negative.

We must now compare this with the results of the discrete molecular model. If, as we shall suppose, the medium is non-polar, so that ionic effects need not be taken into account, we shall have to include both dispersion forces and overlap repulsion forces. An approximate expression for the perturbed wave function of the system of two interacting H atoms can be obtained from the general—and accurate—expression {see, e.g. reference [12]} for the perturbed wave function by inserting in it the Unsöld approximation. In this we replace all energy level differences by an approximate mean excitation energy $E_{\mathrm{H}}$. If the unperturbed wave function of the system is $\phi_0$ and if $\phi$ is the corresponding perturbed wave function, and $H'$ is the perturbation potential, then

$$\phi = \left\{ 1 + \frac{1}{2E_{\mathrm{H}}}[H' - (H')_{00}] + \frac{1}{4E_{\mathrm{H}}{}^2}[(H')^2 - (H'^2)_{00}] \right\}\phi_0. \tag{24}$$

For dispersion forces $(H')_{00}$, which is the mean-value of the perturbation potential in the ground state, vanishes identically.

Now the usual power-series expansion of $H'$ shows that we may treat it as zero on each hydrogen nucleus. Thus the unpaired spin density at either

nucleus is given by

$$|\psi(0)|^2 = \left\{ 1 - \frac{(H'^2)_{00}}{2E_H^2} \right\} |\psi_0(0)|^2 \qquad (25)$$

correct to terms of the fourth order in $H'$. But the van der Waals interaction energy is given by

$$E_V = \frac{(H'^2)_{00}}{2E_H} .$$

Thus equation (25) shows that the contribution of dispersion forces to the relative change in spin density at the nucleus is

$$\rho_V = Z\left( -\frac{E_V}{E_H} \right). \qquad (26)$$

It follows from (26) that the van der Waals forces cause a reduction in the charge density. Since the presence of these forces results in a partial excitation of the electron to higher energy levels, in which it is removed further from the nucleus, this reduction is not surprising. Our conclusions are similar to some results recently obtained by Adrian [4]. The main difficulties in relation both to the present treatment and that of Adrian, are (i) the doubt about the value of the coordination number $Z$, and (ii) the problem of the additivity of dispersion forces. These forces are additive in the approximation of second-order perturbation theory, which is as far as we have carried the analysis. But application of third-order perturbation theory does not lead to additive energies. It seems probable, however, that this error is not large in most cases of physical interest.

Short-range repulsion forces are caused by the overlap between the charge density of the trapped H atom and the charge distribution of the particles which constitute the medium. This effect can be approximately allowed for by ortho-gonalizing the wave function $\psi_0$ of the unpaired electron to the wave functions of all the other electrons $\phi_i$ of the medium. This is conveniently done by Schmidt's orthogonalization process. Thus, if $\psi^{or}$ is the orthogonalized wave function corresponding to $\psi_0$, then

$$\psi^{or} = \frac{\psi_0 - \sum_i S_i \phi_i}{\left( 1 - \sum_i S_i^2 \right)^{1/2}} \qquad (27)$$

in which $S_i$ is the overlap integral $\langle \psi_0 | \phi_i \rangle$. Equation (27) shows that $\psi^{or}$ mixes into $\psi_0$ small parts of the wave functions of all the electrons of the medium having the same spin. If the overlap integrals are small the contributions from the $\phi_i$ are additive.

Let us consider the interaction of the trapped H atom with a second H atom. Then for relatively large separations $R$, the change in electron density at the nucleus due to these exclusion forces is

$$\rho_e = S^2 - 2S \exp(-R). \qquad (28)$$

Since $\rho_e > 0$ for large $R$, this means that exclusion forces increase the charge density at the nucleus.

The various relative effects—$\rho_d$, $\rho_v$, $\rho_e$—are shown in table 2. In this table the dielectric value $\rho_d$ is calculated with $D_s = 2$.

The results in this table indicate that, just as in the energy changes of table 1, the dielectric contribution to $\rho$ is of the same order as that of the dispersion forces,

and rather smaller than that of the overlap forces.    But there are reasons for believing that our simple result (28) slightly over-emphasizes the exclusion

| $R$ (or $2R_0$) in $c_0$ | $\rho_d$ | $(1/Z)\rho_v$ | $(1/Z)\rho_e$ |
|---|---|---|---|
| 3 | $-0.081$ | $-0.0164$ | $0.0865$ |
| 4 | $-0.021$ | $-0.00296$ | $0.0287$ |
| 5 | — | $-0.000768$ | $0.00794$ |
| 6 | $-0.0027$ | $-0.000257$ | $0.00199$ |

Table 2.    Relative changes in spin density at the proton.

effect.    For in some practical applications [4] for rare gases and molecular matrices containing trapped H atoms, their contribution to $\rho_e$ is smaller than in table 2.

### 5. Optical excitation energies

Vertical electronic transitions are subject to the restrictions of the Franck–Condon principle.    This requires that immediately after the excitation the nuclear configuration of the medium is the same as in the ground state, whereas the core electrons of the medium have adjusted themselves to the new field resulting from the excited-state charge distribution of the trapped atom.    This latter is not spherically symmetrical, because allowed transitions will be of the form $1s \rightarrow np$.    We ought therefore to deal with an effective potential more general than (9).    This turns out to be rather complicated, so we shall make the assumption, entirely analogous to that usually made in atomic self-consistent field calculations, that the potential function $V_e$ in the excited state is entirely spherically symmetrical.    Without this simplification the problem of true self-consistence is almost insoluble.

So when calculating the wave function $\psi_p$ and energy $E_p$ in the excited state, we use the potential function (c.f. (4))

$$V_e(r) = -\frac{1}{D_s r} - \left(\frac{1}{D_{op}} - \frac{1}{D_s}\right) \int_r^\infty q_{1s}(r)\, r^{-2}\, dr$$

$$-\left(1 - \frac{1}{D_{op}}\right) \int_r^\infty q_p(r)\, r^{-2}\, dr, \quad r > R_0, \tag{29}$$

where the charge distribution $q_p$ in the excited state is given, as in (1), by

$$q_p(r) = \int_0^r |\psi_p|^2\, 4\pi r^2\, dr. \tag{30}$$

The second term in (29) arises from the nuclei of the medium, whose polarization is still determined by the ground-state electron density; but the third term comes from the electronic polarization associated with the excited-state electron density.

We may write (29) in the form

$$r > R_0, \quad V_e(r) = -\frac{1}{r} + (\alpha_s - \alpha_{op}) \int_r^\infty t^{-2}\, dt \int_t^\infty |\psi(1s)|^2\, d\tau$$

$$+ \alpha_{op} \int_r^\infty t^{-2}\, dt \int_t^\infty |\psi_e|^2\, d\tau,$$

$$r < R_0, \quad V_e(r) = -\frac{1}{r} + (\alpha_s - \alpha_{op}) \int_{R_0}^{\infty} t^{-2} \, dt \int_t^{\infty} |\psi(1s)|^2 \, d\tau$$

$$+ \alpha_{op} \int_{R_0}^{\infty} t^{-2} \, dt \int_t^{\infty} |\psi_e|^2 \, d\tau, \qquad (31)$$

with

$$\alpha_{op} = 1 - 1/D_{op}, \quad \alpha_s = 1 - 1/D_s.$$

We have made some calculations for the 1s →2p transition, employing the perturbation technique proposed by Coulson and Brown [1], who showed that if we write

$$V_e(r) = -\frac{1}{r} + V_{pert},$$

then we may calculate $V_{pert}$ on the supposition that in the integrations of (31) $\psi_e$ is given its unperturbed form, and then use $V_{pert}$ as a perturbation. For reasonable values of the cavity radius $R_0$ the resulting error was small, and almost certainly much smaller than that due to inadequacies in the whole model. We choose for $\psi_e$ the normalized one-parameter radial wave function

$$\psi_{2p} = \left( \frac{\nu^5}{3\pi} \right)^{1/2} r \exp(-\nu r) \quad \text{with} \quad \nu = \tfrac{1}{2}. \qquad (32)$$

The perturbation potential $V_{pert}$ due to the medium becomes

$$V_{pert}(r) = (\alpha_s - \alpha_{op}) \frac{1 + \lambda r}{r} \exp(-2\lambda r) + \alpha_{op} \frac{1 + \tfrac{3}{2}\nu r + \nu^2 r^2 + \tfrac{1}{3}\nu^3 r^3}{r} \exp(-2\nu r) \qquad (33)$$

for $r > R_0$. The value for $r < R_0$ is obtained from (33) by simply putting $r = R_0$ in the formula. Thus the perturbation energy is

$$\Delta E(2p) = \int_0^{R_0} |\psi_{2p}|^2 V_{pert}(R_0) \, d\tau + \int_{R_0}^{\infty} |\psi_{2p}|^2 V_{pert}(r) \, d\tau. \qquad (34)$$

Numerical calculations using this formula have been carried out for a non-polar medium, and are shown in figure 2 for various values of the cavity radius $R_0$ and for $1 - 1/D_s$ varying from 0 to 1 and with $D_{op} = D_s$. The environmental effect on the transition energy $\Delta E_{trans}$ is obtained from

$$\Delta E_{trans} = \Delta E(1s) - \Delta E(2p). \qquad (35)$$

The dependence of $\Delta E_{trans}$ on $R_0$ for $D_s = D_{op} = 2$ is given in figure 3. This shows that for relatively large $R_0$ the medium exerts a larger influence on the excited state than on the ground state. There is a blue shift for $R_0 > 1\cdot5a_0$.

## 6. HIGHER EXCITED STATES AND PHOTOIONIZATION

We have treated the problem of higher excited states by considering a non-polar medium for which $D_s = D_{op}$, and so $\alpha_s = \alpha_{op}$. In this case the second terms in (31) vanish identically, so that (31) is effectively the same as (6). This implies that, unlike the situation when $\alpha_s \neq \alpha_{op}$, there is no subsequent relaxation of the medium polarization, following the vertical excitation. We may therefore say that the energies of the vertical and equilibrium transitions are the same.

It is not easy to decide on suitable wave functions $\psi_e$ for the excited states, though we still adhere to the approximation of spherical symmetry. But probably good insight will be obtained if we adopt Slater-type atomic orbitals.

These are defined by

$$\psi_e = Nr^{n-1} \exp(-cr), \quad c = 1/n, \quad N^2 = \frac{(2/n)^{2n+1}}{4\pi(2n)!}. \tag{36}$$
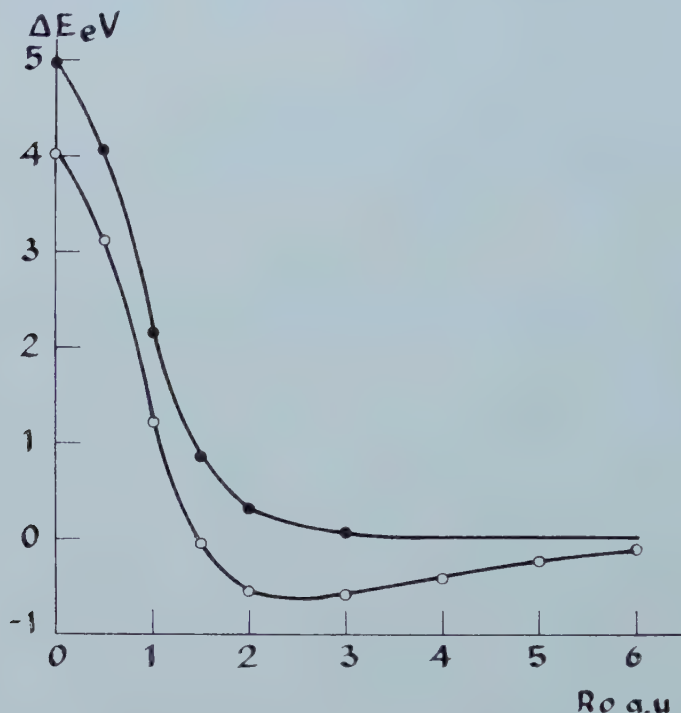


Figure 3.   The dielectric effect on optical transition energies when $D_s = D_{op} = 2$.   Open circles: transition $1s \rightarrow 2p$; full circles: photoionization process from the ground state.

This leads to

$$V_{np}(r) = -\frac{1}{r} + \alpha_{op} \int_r^\infty p(t)t^{-2}\,dt, \quad r > R_0 \tag{37}$$

with

$$p(t) = \exp(-2ct)\left\{1 + \sum_{j=1}^{2n-1} \frac{(2ct)^{2n-j}}{(2n-j)!}\right\}. \tag{38}$$

For $r < R_0$, the lower limit $r$ in the integral of (37) is replaced by $R_0$.   In the limiting case as $n \rightarrow \infty$, $p(t) \rightarrow 1$ and the potential function reduces to the simple form

$$V_{np}(r) = -\frac{1}{r} + \frac{\alpha_{op}}{R_0}, \quad r > R_0$$

$$= -\frac{1}{D_{op}r}, \quad r > R_0. \tag{39}$$

This particular potential function (39) has been used earlier by Reiss [13] to study the ionization processes of atoms trapped in silicon and germanium. If we adopt the first-order perturbation approximation, this potential (39) leads to an energy change $\Delta E$ given by

$$\Delta E = \frac{\alpha_{op}}{R_0}\left[1 - \exp(-2cR_0)\left\{1 + \sum_{j=1}^{2n-1} \frac{j(2cR_0)^{2n-j}}{2n.(2n-j)!}\right\}\right]. \tag{40}$$

We have made a comparison of the energy changes predicted by Reiss' model, using the approximate potential (39), and the complete dielectric treatment, in which the polarizing effect of the valence electron is taken into account. It is not worth while to report these calculations in detail. Their conclusion is that the approximate potential (39) seriously overestimates polarization effects in the medium when the atom is in its ground and first few excited states. Thus the use of a potential which does not incorporate the polarization of the dielectric by the central electron appears not to be justified.

Our treatment based on the dielectric model, and taking account of the polarization of the medium by the centrally bound electron, indicates that the energy of a vertically excited state is determined partly by the charge distribution in this excited state. But for the potential well which is represented by equation (37) when $n \to \infty$, the binding energy in the excited state is zero. Thus the changes in photoionization energy will depend upon the environment, through its influence on the ground state. This influence is shown graphically in figure 3.

## 7. Comparison with other effects on the excitation energy

We shall now return to a more complete discussion of the dispersion energy effect upon optical transitions. It is well known that dispersion forces usually lead to red spectral shifts [14, 15]. This is because the interaction energy between the trapped atom or molecule in its excited state and the medium is usually higher than in the ground state, leading to a displacement of the electronic transition energy to longer wavelengths. Unfortunately any accurate treatment of dispersion forces between an atom in a Rydberg-type excited state and another atom in its ground state is complicated by the fact that the interaction forces are not strictly spherically symmetrical. However, Margenau [21] has derived an appropriate expression for this interaction potential. He shows that it is positive if the mean excitation energy of the perturbing atom is smaller than the excitation energy of the trapped atom. In that case dispersion forces will lead to a blue shift.

An alternative to the use of Margenau's formula is to estimate the interaction energy using Buckingham's expression [16] for the dispersion force energy $E_v$ between two atoms A and B in any chosen states a distance $R$ apart. The formula is

$$E_v = -\frac{4a_0^2}{9R^6} \sum_{i=1}^{n_a} \sum_{j=1}^{n_b} \frac{\overline{(r_i^2)}^2 \overline{(r_j^2)}^2}{\overline{r_i^2} + \overline{r_j^2}}, \tag{41}$$

where $n_a$ and $n_b$ are the total numbers of electrons in the interacting atoms, and $r^2$ is the mean-square radius for an atomic orbital. For Slater orbitals (16)

$$\overline{r^2} = \tfrac{1}{4} n^2 (2n+1)(2n+2) a_0^2. \tag{42}$$

For the case of two hydrogen atoms however there is no difficulty in calculating the necessary polarizabilities to use in the conventional London expression. We show in table 3 a comparison between the spectral shift $\Delta E_d$ due to dielectric medium polarization (for the case of $D_{op} = D_s = 2$) and the dispersion shift $\Delta E_v$. This is given per neighbour, and so requires to be multiplied by the number of nearest-neighbour atoms to the trapped one. Red shifts are represented in this table by a positive sign, and blue shifts by a negative one

This table indicates that at relatively small distances (up to $6a_0$) the red shift due to van der Waals' forces is numerically of the same order of magnitude as the blue shift due to dielectric polarization. But at larger distances the dielectric effect is appreciably higher.

| $R$(or $2R_0$) ($a_0$) | $\Delta E_d$ (ev) | $\Delta E_v$ (ev) |
|---|---|---|
| 4 | −0·551 | −0·692 |
| 5 | −0·570 | 0·179 |
| 6 | −0·592 | 0·0619 |
| 8 | −0·443 | 0·0106 |
| 10 | −0·251 | 0·0028 |

Table 3.  Comparison of spectral shifts caused by dielectric effect ($\Delta E_d$) and dispersion forces ($\Delta E_v$) for a 1s→2p transition†.

The effects of overlap forces on the transition energy have been treated in some detail by Coulson and Polansky [2, 18] on the basis of a perturbation model. These results, which are as yet not fully published, predict a blue shift at relatively small distances (for which $R < 4a_0$).

### 8. Experimental evidence for long-range repulsion forces

It appears from the foregoing analysis that dielectric effects may lead to blue shifts caused by long-range interactions, and that these are too high to be attributed to short-range repulsion forces. Some experimental data seem to confirm this conclusion. Thus blue spectral shifts have been obtained for benzene and for the $^1L_b$ transition of naphthalene, when perturbed by helium at high pressures [19]. These effects could not be attributed to dispersion forces which are higher for the excited state of benzene than for the ground state, when it is interacting with helium. They were therefore assigned to long-range repulsive forces.

Blue shifts have also been observed [20, 22] for the $Hg\,^1S_0 \rightarrow\,^3P_1$ transition in the gas phase, when induced by He and by $H_2$ at high pressures. Originally [20] the low-density linear blue shift of the Hg absorption band in the presence of He was attributed to dispersion forces. It was then necessary to assume that these were higher for Hg in the ground state than in the excited state. However these assumptions now appear to be at variance with the calculations of Margenau [21] on the effect of such dispersion forces with Hg-rare gas interactions. More recently still, blue shifts have been reported for the same transition of Hg in rare gas matrices of A, Kr and Be at 4·2°K, and for the $^2S_{1/2} \rightarrow\,^2P_{1/2,\ 3/2}$ transitions of Na in an argon matrix at the same low temperature [22]. It is possible to provide an interpretation of these effects in terms of our dielectric effect, for the blue shifts due to the dielectric effect are usually superimposed on relatively large red shifts due to dispersion forces. We should therefore expect a net blue shift to be manifested in media of low polarizability,

† The calculations of $\Delta E_v$ in table 3 were made using Buckingham's expression [16] for the dispersion force. Alternative approximations, or—in this simple case—the use of exact polarizabilities, could introduce factors of the order of 2. But such factors are irrelevant for our present purposes.

and in transitions of low oscillator strength, when the effect of dispersion forces is relatively small. The latest experimental evidence is in agreement with this view. But of course it cannot yet be said to confirm in it detail.

## 9. Conclusions

We have given evidence in the preceding paragraphs to support the view that the energies of the ground and excited states of an atom are affected by the presence of a surrounding medium by virtue of three quite distinct factors. These are dispersion, overlap repulsion and medium polarization effects. So also is the charge density at the nucleus of the trapped atom. Simple calculations showed that in many cases the dielectric-medium contributions were of the same order of magnitude as the others, and ought not therefore to be excluded. These calculations were simple ones, involving merely a single hydrogen atom, but there is no reason to suppose that the situation would be very different if larger atoms and molecules, for which we have only much less accurate wave functions, were used instead. It is our opinion that these present calculations have shown the importance of the dielectric effect, and represent about as far as it is worth proceeding with such very general analysis. What is now needed is a more careful study of a limited number of particular cases, in which considerable effort would be available to improve substantially on the approximate treatments used in this paper. Only then would it become possible to state with certainty what is the relative importance of our three factors. Finally, we have neglected all exchange and charge-transfer effects. These may be important at small distances, but will be expected to be small at large ones. With molecules there will also be quadrupole forces, as is shown by the pressure-induced transitions of gaseous hydrogen.

## References

[1] Brown, R. D., and Coulson, C. A., 1958, *Calcul des Fonctions d'Onde Moléculaires* (Paris: Colloques Internationaux du Centre Nationale de la Recherche Scientifique, No. 82), pp. 311–327.
[2] Coulson, C. A., 1960, *Proc. roy. Soc.* A, **255**, 69.
[3] Foner, S. N., Cochran, E. L., Bowers, V. A., and Jen, C. K., 1960, *J. chem. Phys.*, **32**, 963.
[4] Adrian, F. J., 1960, *J. chem. Phys.*, **32**, 970.
[5] Landau, L., 1933, *Phys. Z. Sowjet.*, **3**, 664.
[6] Mott, N. F., and Gurney, R. W., 1940, *Electronic Processes in Ionic Crystals* (Oxford University Press).
[7] Simpson, J. H., 1949, *Proc. roy. Soc.* A, **197**, 269.
[8] Jortner, J., 1959, *J. chem. Phys.*, **29**, 837.
[9] Jortner, J., 1961, *J. chem. Phys.*, **34**, 678.
[10] Eyring, H., 1937, *J. Amer. chem. Soc.*, **54**, 3191.
[11] Coulson, C. A., and Stocker, D., 1959, *Mol. Phys.*, **2**, 397.
[12] Eyring, H., Walter, J., and Kimball, G. E., 1944, *Quantum Chemistry* (New York and London: Wiley).
[13] Reiss, H., 1956, *J. chem. Phys.*, **25**, 681.
[14] Longuet-Higgins, H. C., and Pople, J. A., 1957, *J. chem. Phys.*, **27**, 191.
[15] Ooshika, Y., 1954, *J. phys. Soc., Japan*, **9**, 594.
[16] Buckingham, R. A., 1937, *Proc. roy. Soc.* A, **160**, 94.
[17] Hirschfelder, J. O., Curtiss, C. F., and Bird, R. B., 1954, *Molecular Theory of Gases and Liquids* (New York: Wiley).

[18] POLANSKY, O. E., 1958, *Progress Report, Quantum Chemistry Group, Mathematical Institute, University of Oxford*, No. 4, 1957–58, p. 20.
[19] ROBERTSON, W. W., and KING, A. D., 1959, *J. chem. Phys.*, **31,** 473.
[20] MICHELS, A., and DE KLUIVER, H., 1956, *Physics*, **22,** 919.
[21] MARGENAU, H., 1932, *Phys. Rev.*, **40,** 397.
[22] ROBIN, J., BERGSON, R., GALATRY, L., and VODAR, B., 1956, *Disc. Faraday Soc.*, No. 22, 30.
[23] McCARTY, M., and ROBINSON, G. W., 1959, *Mol. Phys.*, **2,** 415.

# Systems of oscillators with statistical energy exchange in collisions

by MICHAEL HOARE

Max-Planck Institut für Physikalische Chemie, Göttingen
and Department of Chemistry, University of Washington

Classical transition probabilities are derived for the exchange of energy between sets of weakly coupled harmonic oscillators, subject to the assumption that energy is 'statistically redistributed' in all collisions. In the case of single oscillators the result is particularly simple and an explicit solution of the relaxation equation for such a system is derived. A 'mean first passage time' for the dissociation of truncated harmonic oscillators is also obtained using Widom's theory and the limiting case of equilibrium reaction is discussed.

The same approach is sketched briefly for the case of quantized systems in which statistical redistribution of energy is allowed.

Within the general scope of the model, these transition probabilities represent the most efficient conceivable coupling between system and heat bath.

## 1. INTRODUCTION

In recent years considerable interest has developed around the problem of the relaxation of systems of oscillators and its extension to the case of non-equilibrium chemical reaction [1–8]. Now that a satisfactory formal basis for these 'stochastic theories' has been laid, emphasis must be shifted to the problem of formulating physically reasonable transition probabilities in terms of which to derive the time development of systems. In the classical case, with which this paper is mainly concerned, the direct prediction of transition probabilities for systems of oscillators proves to be extraordinarily difficult and, while there is clearly no hope of approaching the four-body problem of colliding oscillators, even grossly simplified formulations lead to intractable equations of motion, due principally to the complication of 'multiple collisions'. At the same time there is little possibility of working backwards from experimental data to obtain transition probabilities, at least over the wide energy range of interest in chemical kinetics [9].

However, as will be shown here, a certain class of transition probabilities can be formulated under purely statistical assumptions about the collisional act, leaving aside its exact description. These consequently have a peculiarly fundamental character and express certain essential properties of the vibrational relaxation process which are not directly connected with the kinematics of collisions. In particular, this approach indicates an answer to the question: What is the nature of the most efficient possible coupling between heat-bath

2 G

and system? More elaborate formulations (allowing incomplete redistribution of energy in collisions) are useful as a means of avoiding a confrontation with the equations of motion whilst providing a precise basis for the employment of notions such as ' relaxation time for inter- or intramolecular energy transfer ', ' effective collision number ', etc. which are in common use in qualitative description.

A parallel treatment can be given for oscillators which are quantized, though free of specifically quantum restrictions on the redistribution of energy.

Physically, the fulfillment of ' statistical redistribution ' of energy in collisions seems to require the formation of a collision complex of lifetime reasonably long compared to the period of molecular vibrations. Though there is evidence for the occurrence of such ' sticky ' collisions in many systems of interest, the treatment presented here is directed more to the establishment of an important limiting case than to the description of a wide range of systems. Moreover, since reference to the ' flow ' of energy between oscillators is notoriously misleading, it will be preferable to regard the hypothesis of statistical redistribution simply as an assertion that all possible outcomes of a collision are equally probable. A similar hypothesis was introduced by Keck [10] in studying the three-body recombination of atoms.

## 2. FUNDAMENTAL TRANSITION PROBABILITIES FOR VIBRATIONAL EXCHANGE BETWEEN CLASSICAL OSCILLATORS

It will be assumed that the oscillators in question are dilutely dispersed in a heat bath composed likewise of oscillators. Assuming conservation of vibrational energy in all collisions we wish to calculate the classical transition probability distribution (transition kernel), $k(x, y)$, defined such that, for a given collision number per molecule, $Z$, $k(x, y)dy/Z$ is the probability that an oscillator with initial energy $x$ will undergo a transition to an element $dy$ at $y$ as a result of a heat bath collision. ($k(x, y)$ might perhaps be better described as a ' rate constant ' for the transition $x \to dy$ at $y$.)

All correctly formulated transition kernels must satisfy the conditions of detailed balance and completeness, which are respectively:

$$k(y, x)f(y) = k(x, y)f(x), \tag{2.1}$$

$$\int_0^\infty k(x, y)\, dy = Z, \tag{2.2}$$

where $f(x)$ is the equilibrium distribution. These two relations are together implied by the continuity equation:

$$\int_0^\infty f(y)k(y, x)dy - Zf(x) = 0. \tag{2.3}$$

It should be stressed that the condition (2.3) rules out, even as crude approximations, all models which require any kind of ' strict ' sharing of energy in collisions; these fail to preserve the equilibrium distribution.

Consider first the probability that an oscillator with energy $x$ will upon collision with a heat bath oscillator form a complex with total energy in $d\epsilon$ at $\epsilon$.

This is simply:

$$P(x, \epsilon)d\epsilon = f(\epsilon - x)\, d\epsilon; \quad \epsilon > x \atop = 0 \qquad\qquad ; \quad \epsilon < x, \right\} \tag{2.4}$$

where $f(\epsilon - x) = \beta \exp - \beta(\epsilon - x)$ is the Boltzmann distribution. $\beta = 1/kT$, $T$ being the heat bath temperature.

Assume now that the complex breaks up such that all possible distributions of energy are equally probable. The probability that when its total energy is $\epsilon$ the oscillator of interest has energy in $dy$ at $y$ is then just:

$$Q(\epsilon, y)dy = dy/\epsilon; \quad \epsilon > y \atop = 0 \qquad ; \quad \epsilon < y. \right\} \tag{2.5}$$

The desired transition kernel is then obtained by integrating these joint probabilities over all possible collisions and multiplying by the collision number:

$$k(x, y) = Z \int_0^\infty P(x, \epsilon) Q(\epsilon, y)\, d\epsilon; \tag{2.6}$$

or, with the restrictions in (2.4) and (2.5):

$$k(x, y) = Z\beta \exp(\beta x) \int_x^\infty \frac{1}{\epsilon} \exp(-\beta\epsilon)\, d\epsilon; \quad y < x \atop = Z\beta \exp(\beta x) \int_y^\infty \frac{1}{\epsilon} \exp(-\beta\epsilon)\, d\epsilon; \quad y > x. \right\} \tag{2.7}$$

This may be written more compactly in the form:

$$k(x, y) = Z\beta \exp(\beta x)\, ei[\beta \max(x, y)], \tag{2.8}$$

where $\max(x, y)$ is the larger of a given pair $(x, y)$ and $ei(x)$ is the exponential integral:

$$ei(x) = - Ei(-x) = \int_x^\infty \frac{1}{s} \exp(-s)\, ds.$$
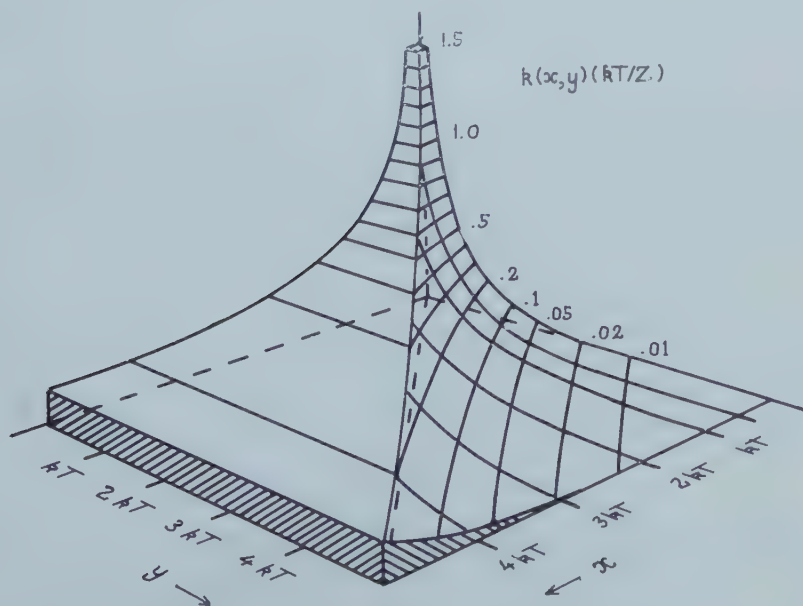


The fundamental transition kernel for single oscillators.

The completeness condition is readily demonstrated, being of course guaranteed by the method of formulation, while the detailed balance condition follows immediately from the symmetry of the expression (2.8).

It will be seen that an essential property of the fundamental transition kernel for single oscillators is that *from a given energy all down-transitions are equally probable*.

Using the assymptotic form: $ei(x) \sim (1/x) \exp(-x)$ it will be seen that for $x \gg y$; $k(x, y) \sim (1/\beta x)$, while for $y \gg x$; $k(x, y) \sim (1/\beta y) \exp(-\beta y)$. It is also apparent that the transition kernel has a singularity at $k(0, 0)$. The form of the complete function is shown in the figure.

### 3. Fundamental transition probabilities for systems of coupled oscillators

The above result is easily generalized to the case where the entity of interest is a molecule, represented by a system of weakly coupled oscillators, while the heat bath is composed of similar molecules, not necessarily with the same number of degrees of freedom. This case has direct importance in the theory of unimolecular reactions. Let the molecule of interest and the heat bath molecule be represented by $p$ and $q$ oscillators respectively. In this case there is a statistical weight factor governing the distribution of energy within the complex. By combinatorial arguments similar to those used by Kassel [11], it can be shown that if a complex of $(p+q)$ oscillators has energy $\epsilon$ then the probability that the chosen $p$ will have energy in $dy$ at $y$ is:

$$Q(\epsilon, y)dy = \frac{\Gamma(p+q)}{\Gamma(p)\Gamma(q)} \cdot \frac{(\epsilon-y)^{q-1} y^{p-1}}{\epsilon^{p+q-1}} dy. \qquad (3.1)$$

(As an informal proof it is sufficient to notice that the result is composed of three appropriate statistical weights of the form $t^{n-1}/\Gamma(n)$.)

Integration over the distribution function for the formation of complexes gives:

$$k(x, y) = ZA\beta^q \exp(\beta x) y^{p-1} \int_{\max(x, y)}^{\infty} \frac{(\epsilon-x)^{q-1}(\epsilon-y)^{q-1} \exp(-\beta\epsilon)}{\epsilon^{q+p-1}} d\epsilon, \qquad (3.2)$$

where $A = \Gamma(p+q)/\Gamma(p)[\Gamma(q)]^2$. This reduces to (2.7) of $p = q = 1$. $k(x, y)$ again has a singularity at $k(0, 0)$ but down-transitions from a given energy are no longer equally probable unless $q = 1$.

### 4. The fundamental relaxation of classical oscillators

Widom [8] has outlined the general theory of the relaxation of classical systems. The time-dependent distribution function $c(x, t)$ describing the relaxation is a solution of the following partial integro-differential equation expressing continuity of flux:

$$\left(\frac{\partial}{\partial t} + Z\right)c(x, t) = \int_0^{\infty} k(y, x) c(y, t) dy, \qquad (4.1)$$

$k(x, y)$ being the transition kernel as before. The solution of (4.1) was shown to be:

$$c(x, t) = \sum_{k=0}^{\infty} c_k \phi_k(x) \exp[-(Z-1/\lambda_k)t], \qquad (4.2)$$

where $\phi_k(x)$, $\lambda_k$ are the eigenfunctions and corresponding eigenvalues associated with the homogeneous equation:

$$\Phi(x) = \lambda \int_0^\infty k(y, x)\Phi(y) \, dy. \tag{4.3}$$

The $c_k$ are constants determined by the initial distribution $c(x, 0)$ and the orthogonality properties of the $\phi_k$, and the latter are normalized such that $\phi_0(x) = c(x, \infty) = f(x)$. Then, given the condition (2.3) it follows that $\lambda_0 = 1/Z$ and $c_0 = 1$, $c(x, t)$ relaxing to the equilibrium distribution as $t \to \infty$. The detailed balance condition (2.1) may be used to symmetrize $k(x, y)$ and facilitate the determination of eigenfunctions.

The eigenfunctions and eigenvalues corresponding to (4.3) with the statistical redistribution kernel (2.8) are readily found, since on differentiating twice it is seen to be equivalent to a modified Laguerre equation. In normalized form:

$$\phi_k(x) = \beta \exp(-\beta x)L_k(\beta x) \tag{4.4}$$

and
$$\lambda_k = (k+1)/Z; \quad k = 0, 1, 2 \ldots,$$

where $L_k(\beta x)$ are the Laguerre polynomials. The symmetrized form of $k(x, y)$ is in fact well known as the Green function corresponding to these. The final solution may thus be written:

$$c(x, t) = \beta \exp(-\beta x)\left\{1 + \sum_{k=1}^\infty c_k L_k(\beta x) \exp[-(k/k+1)Zt]\right\}. \tag{4.5}$$

Given the orthogonality relation:

$$\int_0^\infty \exp(-t)L_k(t)L_j(t) \, dt = \delta_{kj} \tag{4.6}$$

the constants $c_k$ are:

$$c_k = \int_0^\infty c(x, 0)L_k(\beta x) \, dx. \tag{4.7}$$

Since the relaxation of the system for small displacements from equilibrium is governed by the first term in the sum [8], we may recognize that the 'relaxation time' in the present case is simply $(2/Z)$ or twice the collision time.

Of special interest is the case where the initial distribution is a Boltzmann one, though at a temperature different from that of the heat bath. In this case we may write:

$$c(x, 0) = \beta(T/T_0) \exp[-(T/T_0)\beta x], \tag{4.8}$$

so that, using the relation:

$$\int_0^\infty \exp(-pt)L_k(t) \, dt = (p-1)^k/p^{k+1},$$

we find:

$$c_k = (1 - (T/T_0))^k, \tag{4.9}$$

where $T$, $T_0$ are the temperatures of heat bath and initial distribution respectively. It will be seen that the system does not relax through a continuous sequence of Boltzmann distributions and thus does not have a 'temperature' at intermediat times.

## 5. THE FUNDAMENTAL MEAN FIRST PASSAGE TIME FOR OSCILLATORS

In stochastic theories of chemical reaction the topic of interest is the time-development of a system in which molecules (oscillators), responding to heat bath collisions, undergo a modified random walk through the range of bound states and are eventually absorbed at one or more barriers corresponding to chemical reaction [1–7]. Here we shall confine attention to the case of single oscillators crossing a single absorbing barrier representing dissociation.

The general theory of this type of process has also been formulated by Widom [7]. If dissociation occurs at an energy $x^*$, the time-development of the system is described by a continuity equation similar to (4.1) but with a finite range to the integral:

$$\left(\frac{\partial}{\partial t}+Z\right)c(x,\ t)=\int_0^{x^*}k(y,\ x)c(y,\ t)\ dy. \tag{5.1}$$

A complete determination of the eigenfunctions corresponding to this equation appears to present considerable difficulty and so attention will be turned to the determination of the 'mean first passage time' for diffusion across the barrier, a quantity that can be obtained without explicit knowledge of the distribution function $c(x, t)$. We quote briefly the results of Widom [7].

If the total number of bound molecules at time $t$ is designated by:

$C(t)=\int_0^{x^*}c(x,\ t)\ dx$, where, for convenience we assume the initial distribution

normalized such that $C(0)=1$, then the distribution of passage times must be: $w(t)=-(d/dt)C(t)$ and its mean

$$=\int_0^\infty C(t)\ dt,$$

since $C(\infty)=0$. Defining a quantity

$$\tau(x)=\int_0^\infty c(x,\ t)\ dt,$$

the mean first passage time from a state $x$, it follows that:

$$\bar{t}=\int_0^{x^*}\tau(x)\ dx.$$

If both sides of equation (5.1) are integrated with respect to $\bar{t}$ from zero to infinity, then $\tau(x)$ and hence $\bar{t}$ are seen to be obtained by solution of the equation:

$$\tau(x)-c(x,\ 0)=\int_0^{x^*}k(y,\ x)\tau(y)\ dy. \tag{5.2}$$

On applying the kernel (2.8) and differentiating twice the following differential equation is obtained:

$$x\tau''(x)+(1+\beta x)\tau'(x)+\tau(x)=(1/Z)[xc''(x,\ 0)+(1+\beta x)c'(x,\ 0)], \tag{5.3}$$

where the primes stand for differentiation. Since $\exp(-\beta x)$ is a solution of the homogeneous equation, the complete solution is readily obtained. One of the constants of integration must be zero if the solution is to be finite and this in turn implies the condition: $c(0,\ 0)=0$. The second constant of integration is obtained by substitution back in the original integral equation and the result,

after integrating to obtain $\bar{t}$ is as follows:

$$\bar{t} = \frac{1}{Z}\left\{1 + \int_0^{x^*}\frac{1}{v}\left[\exp(\beta v) - 1\right]\right]\int_0^v c(w,0)\,dw\,dv + \left[\frac{ei(\beta x^*)[\exp(\beta x^* - 1)]}{\exp(-\beta x^*) + \beta x^* ei(\beta x^*)}\right]\right\}. \tag{5.4}$$

This will be seen to imply the following limiting conditions, which agree with expectation: (a) as $T \to \infty$, $(\beta \to 0)$, $\bar{t} \to 1/Z$, i.e. the reaction occurs on the first collision, while (b) as $x^* \to \infty$, $\bar{t} \to \infty$, the reaction becoming infinitely slow.

A more detailed investigation of the limiting behaviour of $\bar{t}$ discloses the relation of the expression (5.4) to the equilibrium hypothesis for chemical reaction. Consider first the hypothetical first-order rate constant which would correspond to this model if the equilibrium distribution were preserved during the course of the reaction. From the conventional definition:

$$k_{eq} = \frac{-1}{C(t)}\frac{dC(t)}{dt}$$

$$= \int_0^{x^*}\int_{x^*}^{\infty}\exp(-\beta x)\,k(x, y)\,dy\,dx \Big/ \int_0^{x^*}\exp(-\beta x)\,dx. \tag{5.5}$$

On evaluating this for the statistical redistribution kernel it is found that:

$$k_{eq} = Z\beta x^*\left[\frac{\exp(-\beta x^*) - \beta x^* ei(\beta x^*)}{1 - \exp(-\beta x^*)}\right]. \tag{5.6}$$

Using the asymptotic expression:

$$ei(x) \overset{x \to \infty}{\sim} \exp(-x)\left(\frac{1}{x} - \frac{1}{x^2}\right)$$

it may be seen that: $k_{eq} \to Z\exp(-\beta x^*) \to 0$ as $x^* \to \infty$. Thus at very high $x^*$ the rate constant is given by an 'Arrhenius equation' with pre-exponential factor equal to the collision number.

Consider now the rate at which oscillators with energy $x$ will make *down*-transitions. This is:

$$P_d(x) = \int_0^x k(x, y)\,dy = Z\beta x\exp(-\beta x)ei(\beta x). \tag{5.7}$$

In terms of (5.6) and (5.7) we now see that the mean first passage time can be written:

$$= \frac{1}{Z}\left\{1 + J[x^*; \ c(x, 0)] + \frac{P_d(x^*)}{k_{eq}}\right\}, \tag{5.8}$$

where $J$ is the transform appearing in (5.4). Now as $x^* \to \infty$, $P_d(x^*) \to Z$ and $J(x^*)$ grows with less than exponential order while $(1/k_{eq})$ grows exponentially, so that: $\bar{t} \to 1/k_{eq} \to \infty$, as $x^* \to \infty$. Thus in the limit of high dissociation energy, $\bar{t}$ becomes independent of the initial distribution and tends to the inverse of the equilibrium rate constant, as is the case under completely general conditions [2].

It is difficult to provide an informal explanation for the term $P_d(x^*)/k_{eq}$ in the above expression. One interesting though artificial consequence is that if $c(x, 0)$ is a $\delta$-function at $x^*$ then the mean first passage time is simply:

$$\bar{t} = \frac{1}{Z}\{1 + P_d(x^*)/k_{eq}\}. \tag{5.9}$$

In this the first term evidently represents the average time required for a first collision to take place, the second the eventual mean passage time for those oscillators that go down on the first collision.

It can be shown that by defining functions of the form:

$$\tau_n(x) = \int_0^\infty t^{n-1} \, c(x, t) \, dt \tag{5.10}$$

successively higher moments of the first passage time distribution can, in principle, be found. However, in the present case the second and higher moments are found to be infinite.

The condition that $c(0, 0)$ be zero in order that the mean first passage time be finite is clearly a consequence of the singularity at $k(0, 0)$ in the original transition kernel. The failure of $\bar{t}$ to be finite for an initial Boltzmann distribution evidently underlines a basic limitation to the validity of the classical approach. However, the mean first passage time is, at best, a rather indirect characterization of the evolution of the system and an explicit solution of (5.1) for the distribution function $c(x, t)$ would be required before the usefulness of the classical model could be satisfactorily evaluated.

## 6. Extensions to the model

Throughout the previous development it has been tacitly assumed that the collision number, $Z$, is in some way derivable from 'kinetic theory'. It is, of course, true that the specification of $Z$ is in itself a considerable problem and that only in a theory as superficial as this one is it really justifiable to treat it as a separate parameter unconnected with the central problem of describing collisions. However, to this order of validity, the present model may be extended to cover the case of 'incomplete statistical redistribution' of energy during collisions. When this is done it is found that nothing in the above results is changed except that the 'kinetic theory' collision number is replaced by an 'effective collision number'.

To illustrate this, suppose that all collisions have a characteristic duration $t_c$ and that there is a single 'relaxation time' for the intermolecular energy transfer, $\tau_c$. Then the incomplete redistribution of energy is described by a new transition kernel which, for purposes of integration, may be written:

$$k'(x, y) = (1 - \theta)k(x, y) + Z\theta \, \delta(x - y) \tag{6.1}$$

where $\theta = \exp(-t_c/\tau_c)$ and $\delta(x - y)$ is a delta-function at $x = y$. This tends to $k(x, y)$ as $t_c/\tau_c \to \infty$, while exchange of energy ceases as $t_c/\tau_c \to 0$. The completeness and detailed balance conditions hold over the entire range. If the kernel (6.1) is substituted into the continuity equations (4.1) and (5.1) then it is found that the derived relations are exactly as before except that the collision number $Z$ is replaced by an effective value given by:

$$Z' = Z(1 - \theta). \tag{6.2}$$

In principle this approach can be carried further through the introduction of a 'distribution of collision times', but it would be superfluous to develop such details here.

It is in the nature of the present formulation that, as long as the molecules of the system and heat bath behave simply as reservoirs for the transfer of internal energy, then the transition probabilities derived represent the most efficient

conceivable coupling between the two. Further, it is at least plausible that this upper limit retains its meaning even when the detailed kinematics of collisions is taken into account. Whether a statistical description or collisions can be reconciled with the demands of conservation laws and whether this can be accomplished short of a confrontation with the complete equations of motion, remain open questions.

## 7. Fundamental transition probabilities for a quantized system

Finally, we present a brief account of the transition probabilities governing the exchange of vibrational energy in systems of oscillators which, though quantized, are subject to no specifically quantum-mechanical restrictions preventing the statistical redistribution of energy.

In the case of single oscillators with a heat bath distribution:

$$n_i = a^i(1-a); \quad i = 0, 1, 2, \ldots;$$
$$(a = \exp(-h\nu/kT))$$

(7.1)

arguments similar to those of § 2 lead to the analogous result:

$$P_{ji} = Za^{-i}(1-a) \sum_{k=\max(i,j)}^{\infty} \frac{a^k}{k+1},$$

(7.2)

where $P_{ji}/Z$ is the probability that an oscillator in the $i$th level will make a transition to the $j$th level upon collision. The $P_{ji}$ satisfy the detailed balance and completeness conditions:

$$P_{ji} = P_{ij}a^{j-i}; \quad \sum_{j=0}^{\infty} P_{ji} = Z, \quad \text{for all } i.$$

(7.3)

If, in such a system, dissociation occurs at the $N+1$th level, then the equilibrium rate constant analogous to (5.5) is:

$$k_{eq} = Z\frac{(1-a)^2}{(1-a^{-(N+1)})} \sum_{i=0}^{N} \sum_{j=N+1}^{\infty} \sum_{k=\max(i,j)}^{\infty} \left(\frac{a^k}{k+1}\right).$$

(7.4)

In the same way the transition probabilities for exchange between molecules corresponding to $p$ degenerate oscillators and heat-bath molecules corresponding to $q$ are:

$$P_{ji} = Z(1-a)^q a^{-i} \left[ \frac{(p+j-1)!(p+q-1)!}{j!(p-1)![(q-1)!]^2} \right]$$
$$\sum_{k=\max(i,j)}^{\infty} \frac{a^k k!(q+k-j-1)!(q+k-i-1)!}{(k-j)!(k-i)!(p+q+k-1)!}.$$

(7.5)

This reduces to (7.2) if $p = q = 1$. The essence of this formula—the fluctuation of quanta within a collision complex of numerous degrees of freedom—was discussed by Kassel over thirty years ago, though at that time no explicit transition probabilities were derived [13].

## References

[1] Montroll, E. W., and Shuler, K. E., 1958, *Advanc. chem. Phys.*, **1**, 361.

[2] Shoon Kyung Kim, 1958, *J. chem. Phys.*, **28**, 1057.

[3] Wilson, D. J., 1960, *J. phys. Chem.*, **64**, 323.

[4] Nikitin, E. E., and Sokolov, N. D., 1959, *J. chem. Phys.*, **31**, 1371.

[5] Krieger, I. M., and Gans, P. J., 1960, *J. chem. Phys.*, **32**, 247.

[6] Gans, P. J., 1960, *J. chem. Phys.*, **33**, 691.

[7] Widom, B., 1959, *J. chem. Phys.*, **31**, 1387.

[8] Widom, B., 1960, *J. chem. Phys.*, **32**, 913.

[9] Harrington, R. E., Rabinovitch, B. S., and Hoare, M. R., 1960, *J. chem. Phys.*, **33**, 744.

[10] Keck, J. C., 1958, *J. chem. Phys.*, **29**, 410.

[11] Kassel, L. S., 1928, *J. phys. Chem.*, **32**, 1065.

[12] Kassel, L. S., 1928, *J. phys. Chem.*, **32**, 225.

[13] Kassel, L. S., 1932, *The Kinetics of Homogeneous Gas Reactions* (New York: Chemical Catalog Co.), Chap. V.

# Electron spin resonance and structure of the ionic radical, $\cdot PO_3^=$

by A. HORSFIELD, J. R. MORTON and D. H. WHIFFEN

Basic Physics Division, National Physical Laboratory, Teddington, Middlesex

It is shown that the ionic radical, $\cdot PO_3^=$, is formed by the action of $\gamma$-rays on disodium *ortho*-phosphite pentahydrate. The hyperfine coupling to the $^{31}P$ nucleus has principal values of 1967, 1514 and 1513 Mc/s and is consistent with a pyramidal ion having OPO angles of 110°.

## 1. Introduction

Numerous cases are known in which C–H bonds are broken by the action of high energy $\gamma$-rays on solids. One of the simplest is the loss of hydrogen from the formate ion, $HCO_2^-$, to give [1, 2, 3] the ionic radical $\cdot CO_2^-$. It seemed of interest to see if other negatively charged radicals could be formed similarly in irradiated inorganic materials. Consequently the electron resonance spectrum of irradiated disodium *ortho*-phosphite pentahydrate, $Na_2HPO_3 \cdot 5H_2O$, was investigated to see if hydrogen could be removed from the *ortho*-phosphite ion, $HPO_3^=$, to give the ionic radical $\cdot PO_3^=$, which is isoelectronic with the monomeric form of chlorine trioxide, $\cdot ClO_3$.

## 2. Experimental

Crystals of disodium *ortho*-phosphite pentahydrate were grown from aqueous solution and irradiated at room temperature by the Spent Fuel Irradiation Unit, A.E.R.E., Harwell, with $\gamma$-rays of mean energy 1·0 Mev. The appearance of the crystals and the electron resonance spectra indicated orthorhombic symmetry and this was confirmed by an x-ray investigation which gave unit cell dimensions $a = 6·4$, $b = 7·6$, and $c = 9·4$ Å, with two molecules of $Na_2HPO_3 \cdot 5H_2O$ per unit cell. The crystals tended to grow in hexagonal plates elongated along $b$ with $a$ perpendicular to the plates.

The spectra of single crystals were measured at 9000 Mc/s with a super-heterodyne spectrometer. The magnetic field was measured with a proton resonance magnetometer [4] and $g$ factors are based on the value 2·0036 for $\alpha,\alpha$-diphenyl $\beta$-picryl hydrazyl [5] recrystallized from carbon tetrachloride.

## 3. The spectra

A typical spectrum consisted of two strong single lines about 600 gauss apart whose centre was roughly in the position for $g = 2$ as in the figure (*a*). This is consistent with a pyramidal ionic radical $\cdot PO_3^=$ for which a strong hyperfine coupling to the $^{31}P$ nucleus ($I = \frac{1}{2}$) might be expected. The individual line widths varied with orientation in the range 8–16 Mc/s, and there was occasional evidence of weak hydrogen ' spin flip ' transitions [6]. There was

A. Horsfield *et al.*

no evidence of hyperfine coupling greater than 5 Mc/s to any $^{23}$Na nucleus or H nucleus in the radical or surrounding water molecules.
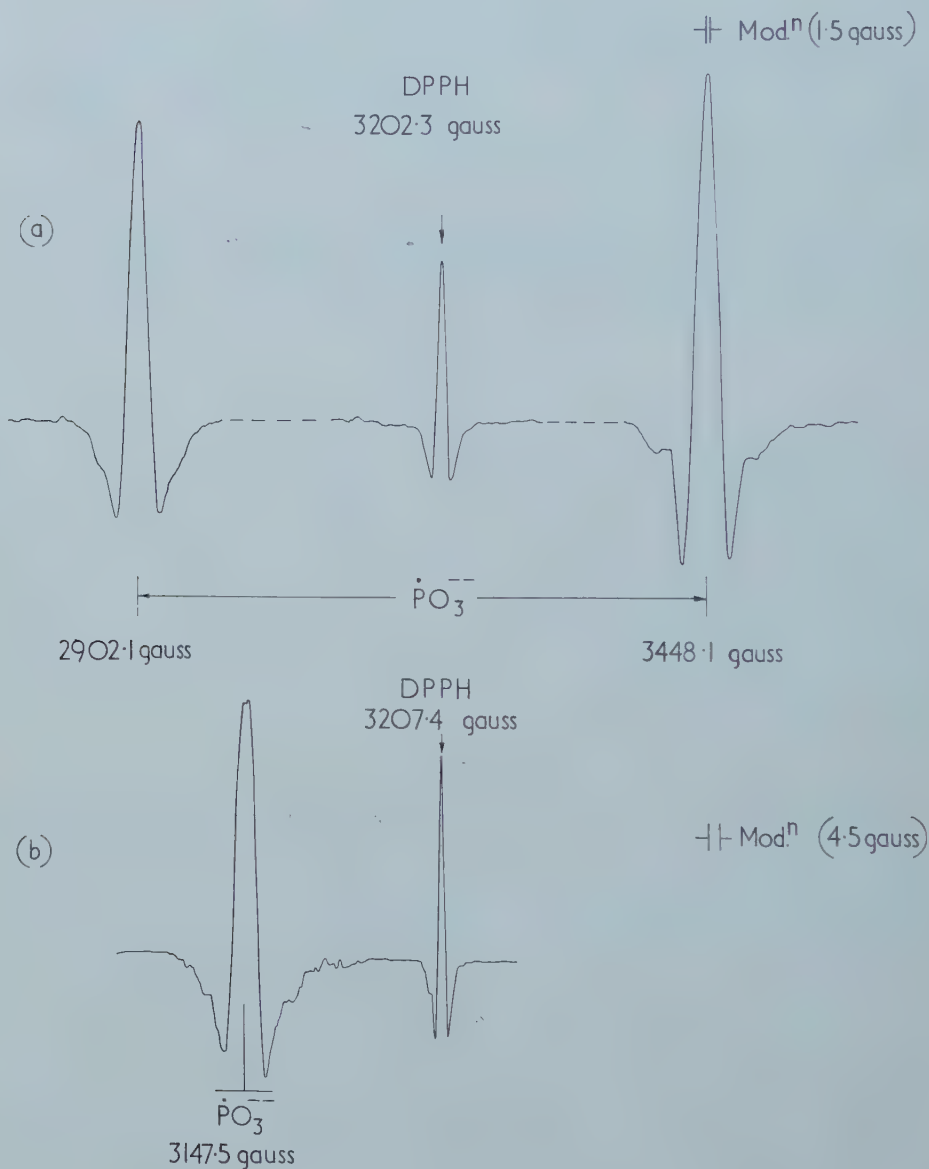


Second derivative of electron resonance spectrum of $\cdot PO_3^=$ in irradiated $Na_2HPO_3 . 5H_2O$. $H$ parallel to $b$; (a) $H_{r.f.}$ perpendicular to $H$, $\nu = 8980$ Mc/s, (b) $H_{r.f.}$ parallel to $H$ at crystal, perpendicular at DPPH, $\nu = 8995$ Mc/s.

Provided the magnetic field was lying in the *ab* or *bc* planes only two lines were observed, but when the field was in the *ac* plane each line split into two in a manner consistent with the $\cdot PO_3^=$ species occupying two magnetically

distinct sites. Since an orthorhombic cell contains four magnetically distinguish-able general sites, the $\cdot PO_3^=$ must occupy special sites and this indicates that the $HPO_3^=$ ions retain a plane of symmetry in the crystal, and this plane is perpendicular to the $b$ axis. The situation is wholly analogous to that of the glycollate ion in its potassium salt where a similar special position was revealed by an electron resonance study of the irradiated crystal [7].

The $HPO_3^-$ ion has a threefold symmetry axis [8] in the hexagonal crystal of $MgHPO_3 \cdot 6H_2O$. This symmetry cannot be strictly preserved in an ortho-rhombic lattice but the deviation is likely to be small. Both $HPO_3^=$ and $\cdot PO_3^=$ should possess a unique axis through the phosphorus and perpendicular to the plane of the oxygen atoms. The greatest hyperfine coupling of $PO_3^=$ is observed for one of the sites when the magnetic field lies in the $ac$ plane and makes an angle of $13°$ with $c$. The field will then lie along the axis of $\cdot PO_3^=$ and this is expected to be parallel to the P–H bonds of the undamaged host, so that it appears that the P–H bonds also lie in $ac$ at $\pm 13°$ from $c$.

## 4. The coupling constants

It is desirable to interpret the spectra in terms of the customary spin Hamiltonian, which for a doublet species with one nucleus of spin $\frac{1}{2}$ is

$$\mathscr{H} = \beta_0 \mathbf{S} \cdot g \cdot \mathbf{H} + \mathbf{S} \cdot T \cdot \mathbf{I} - \beta_N g_N \mathbf{I} \cdot \mathbf{H}.$$

For interpreting many electron resonance experiments, including most studies of organic radicals, approximate energy levels obtained by assuming that the first term greatly exceeds the second are satisfactory. However, in the present instance the high field approximation is insufficient and exact energies must be used. For a general magnetic field direction the secular equation is a quartic, but if the principal axes of the $g$ and $T$ tensors are parallel and the magnetic field direction is parallel to one of the axes, the equation factorizes into two quadratics. The $b$ crystallographic axis is necessarily a principal axis of $g$ and $T$ from the symmetry of the crystal and it is expected that the axis of the $\cdot PO_3^=$ will also be a principal axis of both tensors, in which case the two sets of tensor axes are coincident. It is convenient to refer to these three directions as $p$ (that is, parallel to the principal axis of largest coupling, which lies in the $ac$ plane at $13°$ from $c$), $q$ (coincident with $b$) and $r$ (in the $ac$ plane at $103°$ from $c$). The magnetic field can, of course, only be parallel to $p$ or $r$ for half the radicals simultaneously. If the magnetic field is along $p$ the Hamiltonian operator simplifies to

$$\mathscr{H} = \beta_0 H g_{pp} S_p + t_{pp} S_p I_p + t_{qq} S_q I_q + t_{rr} S_r I_r - \beta_N H g_N I_p,$$

where $t_{pp}$ is the $pp$ diagonal element of the hyperfine tensor and $S_p$ is the electron spin operator resolved along the $p$ direction, etc. It is convenient to choose a basic representation with $S_p$ and $I_p$ diagonal and basic spin wave functions of the form $|+ +\rangle$ where the first $+$ indicates that the eigen-value of $S_p$ is $+\frac{1}{2}$ and the second $+$ that the eigen-value of $I_p$ is also $+\frac{1}{2}$. The terms involving $S_q$, etc. can be written in terms of the usual raising and lowering operators. It will be found that there are no terms which mix levels such as $|+ +\rangle$ and $|+ -\rangle$ and the exact energy levels and wave functions of table 1 are obtained. The corresponding table for the magnetic field along $q$ or $r$ is obtained by permuting suffixes appropriately.

| Level | Energy | Wave function coefficients of | | | |
|---|---|---|---|---|---|
| | | $\lvert++\rangle$ | $\lvert--\rangle$ | $\lvert+-\rangle$ | $\lvert-+\rangle$ |
| i | $(U+t_{pp})/4$ | $\cos\phi$ | $\sin\phi$ | | |
| iii | $(-U+t_{pp})/4$ | $-\sin\phi$ | $\cos\phi$ | | |
| ii | $(W-t_{pp})/4$ | | | $\cos\theta$ | $\sin\theta$ |
| iv | $(-W+t_{pp})/4$ | | | $-\sin\theta$ | $\cos\theta$ |

$$U^2 = 4H^2(g_{pp}\beta_0 - g_N\beta_N)^2 + (t_{qq} - t_{rr})^2$$
$$W^2 = 4H^2(g_{pp}\beta_0 + g_N\beta_N)^2 + (t_{qq} + t_{rr})^2$$
$$\mathrm{Tan}\,2\phi = (t_{qq} - t_{rr})/2H\,(g_{pp}\beta_0 - g_N\beta_N)$$
$$\mathrm{Tan}\,2\theta = (t_{qq} + t_{rr})/2H\,(g_{pp}\beta_0 + g_N\beta_N)$$

Table 1.   Energy levels and wave functions when the field is parallel to a principal axis of $g$ and $T$.

The regular low field line—assuming all $t$ positive—is the i⟷iv transition and the high field line is ii⟷iii.   Since the position of each line depends on four unknowns, three $t$ and one $g$, the set of six lines obtained with the field consecutively along $p$, $q$ and $r$ must be considered together to obtain the six unknowns.   Fortunately each equation depends critically on only two parameters; for example the two transitions with the field parallel to $p$ are much more sensitive to $g_{pp}$ and $t_{pp}$ than to $t_{qq}$ and $t_{rr}$ and quite good values of the former may be found with only approximate values of the latter.   An iterative procedure then quickly leads to the self consistent set given in table 2.

| | $pp$ | $qq$ | $rr$ | Error |
|---|---|---|---|---|
| $H_+$  (gauss) | 3548 | 3448 | 3455 | $\pm 2$ |
| $H_-$ (gauss) | 2840 | 2902 | 2909 | $\pm 2$ |
| $\nu$ (Mc/s) | 9004 | 8980 | 8996 | $\pm 5$ |
| $t$ (Mc/s) | 1967 | 1514 | 1513 | $\pm 10$ |
| $g$ | 1·9994 | 2·0011 | 2·0004 | $\pm 0·0008$ |

Table 2.   Measured magnetic field for the high ($H_+$) and low ($H_-$) field resonances, microwave frequency ($\nu$) and principal values of the hyperfine and $g$-tensors for the radical $\cdot PO_3^=$.

The mixing of the electron-up and electron-down states also modifies the selection rules so that transitions i⟷iii and ii⟷iv are allowed when the microwave magnetic field is parallel to the static magnetic field.   These have intensity factors of $\sin^2 2\phi$ and $\sin^2 2\theta$ respectively instead of the $\cos^2(\theta+\phi)$ for normal lines.   Although $\phi$ is too small in the present instance for transitions i⟷iii to be observed, $\theta$ is considerably larger and transitions ii⟷iv, though weak, were easily observed as in the figure ($b$) when the microwave cavity was twisted so that the microwave and static fields were parallel.   The positions of these lines for the field parallel to $p$, $q$ and $r$ agreed with those calculated from the

values of table 2, being about 50 gauss downfield from the normal field for resonance with $g = 2 \cdot 00$. It must be admitted that the observed lines were consistently 2 gauss lower than their calculated field position. An unsuccessful search was made for the origin of this minor systematic discrepancy, which is the same size as the overall experimental errors. The errors are somewhat larger for these transitions as the signals due to the two distinguishable radicals are not fully resolved with the field parallel to $p$ and $r$ and the microwave and static fields parallel to each other. If any of the $t$ had been reversed in sign the observations would have been similar, although the observable transition would be i⟷iii in some instances. However, the calculated field for the transition would be increased by $2g_N\beta_N H/\beta_0 = 3$ gauss in these cases; the discrepancy would then be outside experimental error. There is thus experimental verification that all the principal values of $t$ are of the same sign.

## 5. The radical structure

It is clear from table 2 that $t_{qq} = t_{rr}$ within the experimental accuracy. This is to be expected for the ionic radical $\cdot PO_3^-$ which would have $C_{3v}$ symmetry in free space and is likely to be only very slightly disturbed by the lattice. It is clear that $p$ is the direction of the threefold axis and on any reasonable radical structure $t_{pp}$ must be the most positive principal hyperfine coupling and so all the $t$ should be taken positive. The $g$ tensor is nearly isotropic and $g_{qq} = g_{rr}$ within the experimental errors.

$AB_3$ type molecules with 25 valency electrons, as $\cdot PO_3^=$, have been discussed by Walsh [9] and are expected to be pyramidal. The wave function should be of $^2A_1$ character with the unpaired electron in an $a_1$ orbital involving 3s and 3p phosphorus character together with a contribution from the oxygens.

Mayers [10] has performed a SCF treatment for a neutral phosphorus atom in its $^4S$ ground configuration. For his wave function the 3s one electron orbital has $(8\pi/3)\psi^2(0) = 46 \cdot 93$ A.U. whence $(8\pi g\beta_0 g_N\beta_N/3h)\psi^2(0) = 10\ 100$ Mc/s which is therefore the hyperfine coupling to be expected for one electron in a 3s orbital of $^{31}P$. The observed isotropic coupling from table 2 is 1665 Mc/s so that the fractional occupancy of the 3s orbital by the unpaired electron is $0 \cdot 165$ provided polarization of the 1s and 2s shells can be neglected. Likewise Mayers' wave function gives $\langle r^{-3}\rangle_{\text{average}}$ for the 3p one-electron wave functions as $3 \cdot 34$ A.U. and so $(4g\beta_0 g_N\beta_N/5h)\langle r^{-3}\rangle_{\text{av}} = 574$ Mc/s. This corresponds to the anisotropic contribution for a pure 3p orbital along its axis and the observed 302 Mc/s corresponds to a 3p spin population of $0 \cdot 527$. These figures correspond to a phosphorus hybridization as $s^{0 \cdot 95}\ p^{3 \cdot 05}$ for the unpaired electron orbital and a spin population of $0 \cdot 103$ on each oxygen.

The wave function of the unpaired electron is predominantly located on the phosphorus atom and is analogous to a lone pair orbital. It is thus expected to be orthogonal to orbitals along the P–O bonds. Coulson [11] has shown how the directions of such orbitals can be obtained if the s/p hybridization ratio is known. Using the ratio given above, the orthogonal orbitals, assuming a pyramid of $C_{3v}$ symmetry, make angles of $110°$ with each other and this is therefore an estimate of the OPO angle. This may be compared with the value $110°$ found in the $HPO_3^=$ ion in its magnesium salt [8] and $109 \cdot 5°$ in $PO_4^\equiv$.

Although the hyperfine coupling in $\cdot PO_3^=$ is very large, exceeding even that of the hydrogen atom which is 1420 Mc/s, this is seen to be a consequence of the large value of $\psi(0)$ for a 3s phosphorus atom and not to any exceptional structure for the radical.

References

[1] OVENALL, D. W., and WHIFFEN, D. H., 1960, *Proc. chem. Soc.*, p. 420.
[2] BRIVATI, J. A., KEEN, N., SYMONS, M. C. R., and TREVALIAN, P. A., 1961, *Proc. chem. Soc.*, p. 66.
[3] OVENALL, D. W., and WHIFFEN, D. H., 1961, *Mol. Phys.*, **4**, 135.
[4] HORSFIELD, A., MORTON, J. R., and MOSS, D. G., 1961, *J. sci. Instrum.*, **38**, 322.
[5] HOLDEN, A. N., KITTEL, C., MERRITT, F. R., and YAGER, W. A., 1950, *Phys. Rev.*, **77**, 147.
[6] TRAMMELL, G. T., ZELDES, H., and LIVINGSTON, R., 1958, *Phys. Rev.*, **110**, 630.
[7] ATHERTON, N. M., and WHIFFEN, D. H., 1960, *Mol. Phys.*, **3**, 103.
[8] CORBRIDGE, D. E. C., 1956, *Acta cryst.*, **9**, 991.
[9] WALSH, A. D., 1953, *J. chem. Soc.*, p. 2301.
[10] MAYERS, D. F. (personal communication).
[11] COULSON, C. A., 1948, *Victor Henri Volume Commemoratif*, Contribution à l'étude de le Structure Moléculaire, p. 15.

# Regular models for solid hydrogen: I

by G. M. BELL and W. M. FAIRBAIRN

Mathematics Department, Faculty of Technology, University of Manchester

Unsymmetric regular models in which molecules on a lattice exist in two states with unequal degeneracies and unequal energies for pairs of like nearest neighbours are investigated. The lattice distribution probabilities are shown to be equal to those of the Ising model under a temperature dependent external field. However, where the energy of formation of a pair of unlike nearest neighbours is positive the model's behaviour is quite different from that of an Ising ferromagnet, since either the configurational specific heat is a continuous function of temperature or there is a first-order transition with latent heat evolved. An unsymmetric regular model is appropriate to solid orthohydrogen when the interactions are of quadrupole–quadrupole type. In general nearest-neighbour pair energies derived from the quadrupole–quadrupole interaction are found to be dependent on the orientation of the line joining the two sites, but for the simple and body-centred cubic lattices and certain quantization directions this dependence is not apparent. In these cases no transition is found.

## 1. Introduction

Hydrogen molecules are termed 'ortho' or 'para' according to whether their rotational wave functions are symmetrical or anti-symmetrical. The transformation of a para-molecule to an ortho-molecule, and the converse process, can occur but under normal conditions is such a rare event that a sample of hydrogen can be regarded as a mixture with constant proportions of the two species. In normal hydrogen the proportion of ortho-molecules is 75 per cent but for experimental purposes samples have been prepared in which this proportion varies from 0 to 91 per cent [1]. Hydrogen liquifies at 20 K and becomes solid at 14 K. Investigations of the curve of specific heat against temperature have disclosed anomalous behaviour below 2 K [2]. Hill and Ricketson interpreted this as a second-order transition for samples containing more than 60 per cent of ortho-hydrogen, but found no transition when the ortho-fraction was less than 60 per cent. Reif and Purcell [3] and Smith and Housley [1] obtained results of a similar nature in experiments using nuclear magnetic resonance; the latter authors investigated specimens with up to 86 per cent ortho-hydrogen.

Since the hydrogen molecules have small moments of inertia they can be considered at low temperatures to be in their lowest possible rotational states, $J = 0$ for para- and $J = 1$ for ortho-molecules. The $J = 1$ state is triply degenerate ($M = 0, \pm 1$) but this degeneracy can be removed by an electric field such as that which could be exerted on a molecule of solid hydrogen by the surrounding molecules. An axially symmetric field splits the level into two: one with $M = 0$, the other being degenerate with $M = \pm 1$. The transition in solid hydrogen is regarded as a consequence of such a splitting and the purpose of these papers will be to examine relevant theoretical models. Solid hydrogen has been discussed previously by Nakamura [4], who considered the specific heat in detail only for low ortho-concentrations, Babloyantz and Bellemans [5], who considered

2 H

temperatures higher than the transition range, and Tomita [6]. The present paper overlaps in places with Tomita's work but our methods and results are different.

Unfortunately the crystal structure of solid hydrogen is not known, except for pure para-hydrogen where it is hexagonal close-packed (h.c.p.) as might be expected for spherically symmetric $(J = 0)$ molecules. Since ortho-hydrogen molecules are not spherically symmetric a different crystal structure might be preferred for mixtures in which ortho-molecules predominate. Because of this we shall consider not only the h.c.p. structure but also some of the other regular crystal structures. It would be of great interest to have experimental evidence of the crystal structure of samples with a high proportion of ortho-molecules.

As the anomalous behaviour seems to depend on the ortho-molecules which are present, we shall consider first models relevant to pure ortho-hydrogen. The effect of the para-molecules in solid hydrogen is similar to that of non-magnetic atoms in a ferromagnetic material and will be considered in a later paper. In § 2 we introduce an 'unsymmetric regular model' of considerable intrinsic interest which resembles the well-known Ising model for cooperative assemblies in that the molecules on a crystal lattice have two possible states and nearest-neighbour interaction energies alone are considered. It differs, however, from the Ising model in that the two states are no longer 'symmetric' but may have different degeneracies and different energies for nearest-neighbour pairs with both members in the same state. Such a difference in degeneracies occurs for the two species $M = 0$, $M = \pm 1$ respectively of ortho-hydrogen when the original three-fold degeneracy is removed by an axially symmetric field and unequal like nearest-neighbour energies occur for the quadrupole–quadrupole interaction discussed in § 4. For this interaction it is necessary for many lattice structures to suppose, as we do formally in § 2, that the interaction energy depends on the orientation of the pair axis. In § 3 the particular 'isotropic' case where this dependence is not apparent is discussed and it is also supposed that the energy of formation of an unlike pair is positive (as in an Ising ferromagnet). It is then found that either a first order transition occurs or no transition at all, a conclusion quite different from that of Tomita. In § 5 the results of § 3 are applied to quadrupole–quadrupole interactions for lattices and quantization directions where these are isotropic and it is found that there is in fact no transition in these cases. In § 5 we discuss also the conclusions of Tomita for both the zeroth and first-order approximations which he used. In the conclusion (§ 6) we make some remarks on the possibility of obtaining a second-order transition in the non-isotropic unsymmetric model to be discussed in a second paper.

## 2. THE UNSYMMETRIC REGULAR MODEL

It is supposed that a molecule on the lattice can exist in either state $\lambda$, of degeneracy $g_\lambda$, or state $\mu$, of degeneracy $g_\mu$, and that $g_\mu > g_\lambda$. The number of molecules in the two states will be denoted by $N_\lambda$ and $N_\mu$ respectively and since each lattice site coincides with the centre of one molecule

$$N_\lambda + N_\mu = N, \qquad (2.1)$$

where $N$ is the total number of lattice sites. For later application to quadrupole–quadrupole interactions it must be supposed that the interaction energy of a nearest-neighbour pair of any given type depends on the angle made with the

crystal axis by the line joining the two sites of the pair. For the lattices discussed it is sufficient to allow this angle two possible values $\theta_0$ and $\theta_0'$ and to regard each site as having $z$ nearest-neighbour sites at angle $\theta_0$ and $z'$ at angle $\theta_0'$ to the axis. Then if $N_{\lambda\mu}$ and $N_{\lambda\mu}'$ denote the numbers of $\lambda$-$\mu$ nearest-neighbour site pairs with orientations $\theta_0$ and $\theta_0'$ respectively and if $N_{\lambda\lambda}$, $N_{\lambda\lambda}'$, $N_{\mu\mu}$ and $N_{\mu\mu}'$ are similarly defined,

$$
\left.
\begin{aligned}
N_{\lambda\mu} + 2N_{\lambda\lambda} &= zN_\lambda, & N_{\lambda\mu} + 2N_{\mu\mu} &= zN_\mu, \\
N_{\lambda\mu}' + 2N_{\lambda\lambda}' &= z'N_\lambda, & N_{\lambda\mu}' + 2N_{\mu\mu}' &= z'N_\mu,
\end{aligned}
\right\}
\tag{2.2}
$$

neglecting crystal boundary effects. If other than nearest-neighbour energies are negligible then the part of the energy depending on the lattice distribution is given by

$$
\begin{aligned}
E_C &= N_{\lambda\mu} w_{\lambda\mu} + N_{\lambda\mu}' w_{\lambda\mu}' + N_{\lambda\lambda} w_{\lambda\lambda} + N_{\lambda\lambda}' w_{\lambda\lambda}' + N_{\mu\mu} w_{\mu\mu} + N_{\mu\mu}' w_{\mu\mu}' \\
&= \tfrac{1}{4}(zw_{\mu\mu} + z'w_{\mu\mu}' + zw_{\lambda\lambda} + z'w_{\lambda\lambda}')N \\
&\quad - \tfrac{1}{4}(zw_{\mu\mu} + z'w_{\mu\mu}' - zw_{\lambda\lambda} - z'w_{\lambda\lambda}')(N_\lambda - N_\mu) \\
&\quad + wN_{\lambda\mu} + w'N_{\lambda\mu}',
\end{aligned}
\tag{2.3}
$$

where use is made of (2.1) and (2.2) in deriving the last expression and

$$
w = w_{\lambda\mu} - \tfrac{1}{2}(w_{\lambda\lambda} + w_{\mu\mu}), \qquad w' = w_{\lambda\mu}' - \tfrac{1}{2}(w_{\lambda\lambda}' + w_{\mu\mu}').
\tag{2.4}
$$

Here $w_{\lambda\mu}$, $w_{\lambda\mu}'$, etc. are the energies of nearest-neighbour pairs of the various types. The first term in the last expression of (2.3) is a constant, not dependent on the numbers or distribution of the $\lambda$ and $\mu$ types, and may be omitted. It is assumed that the partition function over the internal degrees of freedom is (apart from the degeneracy factors $g_\lambda$ and $g_\mu$) the same for species $\lambda$ and $\mu$ and it is denoted by $\Phi$. If $g(N_\lambda, N_\mu, N_{\lambda\mu}, N_{\lambda\mu}')$ is the number of ways in which $N_\lambda$ molecules of one type and $N_\mu$ of the other can be arranged on the lattice to give pair numbers $N_{\lambda\mu}$ and $N_{\lambda\mu}'$, then the partition function for the assembly is given by

$$
\Phi^N (g_\mu g_\lambda)^{N/2} \sum g(N_\lambda, N_\mu, N_{\lambda\mu}, N_{\lambda\mu}') \left(\frac{g_\mu}{g_\lambda}\right)^{(N_\mu - N_\lambda)/2} \exp(-E_C/kT),
\tag{2.5}
$$

where the summation is over all values of $N_\lambda$, $N_\mu$, $N_{\lambda\mu}$ and $N_{\lambda\mu}'$ compatible with the total number $N$ of lattice sites.

If in any given configuration each $\lambda$ is replaced by a $\mu$ and each $\mu$ by a $\lambda$ the values of $N_\lambda$ and $N_\mu$ are interchanged but $N_{\lambda\mu}$ and $N_{\lambda\mu}'$ are unaffected. Thus

$$
g(N_\lambda, N_\mu, N_{\lambda\mu}, N_{\lambda\mu}') = g(N_\mu, N_\lambda, N_{\lambda\mu}, N_{\lambda\mu}').
\tag{2.6}
$$

The Ising model at zero field is obtained from the more general model discussed here by putting $g_\lambda = g_\mu$, $w_{\lambda\lambda} = w_{\mu\mu}$ and $w_{\lambda\lambda}' = w_{\mu\mu}'$. It can then be seen, by (2.3) and (2.6), that an interchange of $\lambda$ and $\mu$ does not affect the magnitude of any term in the partition function. Thus if $\bar{N}_\lambda$ and $\bar{N}_\mu$ are respectively the average or equilibrium values of $N_\lambda$ and $N_\mu$ it follows that either $\bar{N}_\lambda = \bar{N}_\mu = \tfrac{1}{2}N$ or the equilibrium states exist in pairs for which the value of $\bar{N}_\lambda$ for one member is equal to that of $\bar{N}_\mu$ for the other. If, however, $g_\lambda \neq g_\mu$ or $w_{\lambda\lambda} \neq w_{\mu\mu}$ or $w_{\lambda\lambda}' \neq w_{\mu\mu}'$ this $\lambda$-$\mu$ symmetry characteristic of the zero-field Ising model no longer exists. However, let us denote the magnitude of an 'Ising dipole' by $d$ and then define an 'equivalent field' $H_e$ by the relation

$$
H_e d = \tfrac{1}{2}kT \ln\left(\frac{g_\mu}{g_\lambda}\right) - \tfrac{1}{4}(zw_{\mu\mu} + z'w_{\mu\mu}' - zw_{\lambda\lambda} - z'w_{\lambda\lambda}').
\tag{2.7}
$$

If we substitute (2.3) and (2.7) in (2.5) and omit the factors not dependent on the

2 H 2

numbers and distribution of $\lambda$ and $\mu$ then we have a configurational partition function given by

$$\sum g(N_\lambda, N_\mu, N_{\lambda\mu}, N_{\lambda\mu}') \exp\left\{-\frac{wN_{\lambda\mu}+w'N_{\lambda\mu}'+(N_\lambda-N_\mu)H_e d}{kT}\right\}. \qquad (2.8)$$

This is the configurational partition function of an 'anisotropic' (i.e. $w \neq w'$) Ising model in an external field $H_e$ and if $H_e$ is the temperature dependent function given by (2.7) the probabilities of the various states for the unsymmetric model and for this Ising model will be the same. It is convenient to denote the value of $T$ at which $H_e$ is zero by $T_0$ so that

$$T_0 = \tfrac{1}{2}(zw_{\mu\mu}+z'w_{\mu\mu}'-zw_{\lambda\lambda}-z'w_{\lambda\lambda}')/\{k\ln(g_\mu/g_\lambda)\}, \qquad (2.9)$$

$$H_e = \tfrac{1}{2}(k/d)(T-T_0)\ln(g_\mu/g_\lambda). \qquad (2.10)$$

### 3. Transitions in the isotropic case

The isotropic model where the angles of inclination to the crystal axis of all nearest-neighbour pairs of sites are equal will now be introduced by putting $z' = 0$ and it will also be supposed that $w > 0$. The model is now equivalent to the one proposed for solid ortho-hydrogen by Tomita. The configurational partition function is equal to that of an Ising model ferromagnet in an external field. The
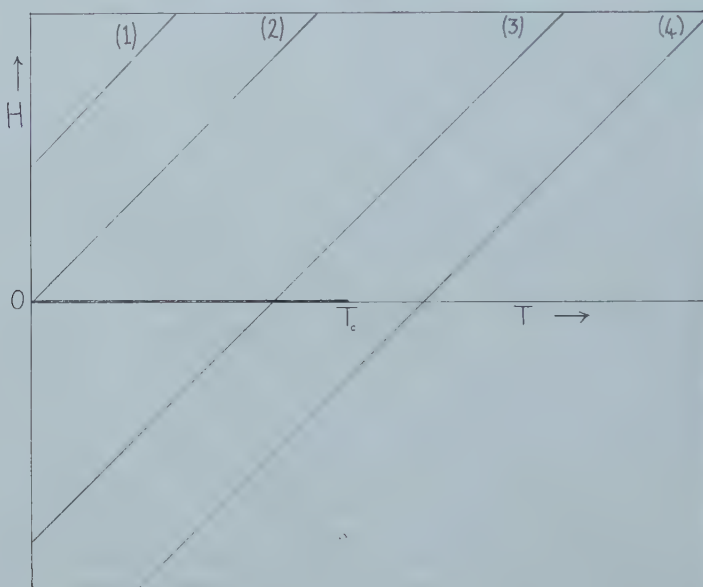


The effective field as a function of temperature.

latter was discussed by Domb [7] who concluded that if the state of the system is represented by a point on the $T$, $H$ plane (see figure) then all thermodynamic functions are continuous except on the segment $(0, T_c)$ of the $T$-axis, where $T_c$ is the critical temperature. If the field $H$ is taken as positive when $\mu$-molecules are directed along it and $\lambda$-molecules against it then on this segment of the $T$-axis there is a discontinuity

$$\Delta \bar{N}_\mu = \bar{N}_\mu(0+, T)-\bar{N}_\mu(0-, T) = -\Delta\bar{N}_\lambda > 0. \qquad (3.1)$$

Since the transition on the $T$-axis at $T = T_c$ is of the second order $\Delta\bar{N}_\mu \to 0$ as $T$ approaches $T_c$ from below. The Ising model has two independent state variables

$T$ and $H$; the unsymmetric model has only one and the point representing its state is confined to the line $H = H_c$, where $H_c$ is given by (2.10). Of the cases shown on the figure, in (1) when $w_{\mu\mu} < w_{\lambda\lambda}$, making $T_0 < 0$, in (2) where $w_{\mu\mu} = w_{\lambda\lambda}$, making $T_0 = 0$, and in (4) where $T_0 > T_c$ there is no transition at any finite temperature. There can only be a transition if $0 < T_0 \leqslant T_c$ so that the state line cuts the segment of discontinuity as in case (3) on the figure. The nature of the transition at $T_0$ derives from the fact that although their partition functions are the same the physical properties of the unsymmetric model and the Ising model at $H = H_c$ are different. For the Ising model $(\bar{N}_\lambda - \bar{N}_\mu)H_c d$ is entirely an energy term so that

$$E_c = w\bar{N}_{\lambda\mu} + (\bar{N}_\lambda - \bar{N}_\mu)H_c d. \tag{3.2}$$

while from equations (2.3) and (2.7) it can be seen that for the unsymmetric model $(\bar{N}_\lambda - \bar{N}_\mu)H_c d$ contains both energy and entropy contributions and that

$$E_c = w\bar{N}_{\lambda\mu} + (\bar{N}_\lambda - \bar{N}_\mu)H_c d - \tfrac{1}{2}(\bar{N}_\lambda - \bar{N}_\mu)kT \ln (g_\mu/g_\lambda). \tag{3.3}$$

From (2.6) and (2.8) there is no discontinuity in $\Delta\bar{N}_{\lambda\mu}$ as the state line crosses the $T$-axis and, since $H_c = 0$ at this point, there is no discontinuity in the energy of the Ising model. For the unsymmetric model on the other hand it can be seen at once from (3.3) that there is a latent heat or magnitude

$$\Delta E_c = - \tfrac{1}{2}\Delta(\bar{N}_\lambda - \bar{N}_\mu)kT_0 \ln (g_\mu/g_\lambda) = \Delta\bar{N}_\mu kT_0 \ln (g_\mu/g_\lambda) \tag{3.4}$$

due to the discontinuous increase $\Delta\bar{N}_\mu k \ln (g_\mu g_\lambda)$ in the entropy. The transition is thus of the first order, except possibly for the particular case $T_0 = T_c$. For $T_0 = T_c$ it is necessary, by (2.9) putting $z' = 0$, that

$$z(w_{\mu\mu} - w_{\lambda\lambda}) = 2kT_c \ln (g_\mu/g_\lambda). \tag{3.5}$$

As $T_c$ depends only on $w$ and the lattice structure and there is no connection between the energy constants and the degeneracies this case is not an important one. The result that there is either a first-order transition or no transition at all, except for the trivial case (3.5), is at variance with the conclusions of Tomita which will be discussed in § 5.

## 4. The interaction between two hydrogen molecules

For fixed $J$ the rotational wave function of a hydrogen molecule is of the form

$$\sum_{M=-J}^{+J} A_M Y_{JM}(\theta, \phi), \tag{4.1}$$

where the angles $\theta$ and $\phi$ define the orientation of the internuclear axis of the molecule with respect to some fixed axis of reference and $M$ is the component of $J$ along this axis. At such distances as occur in crystals of solid hydrogen the interaction between two molecules consists principally of valence forces, dispersion forces and the forces due to the electric quadrupole moment of the hydrogen molecule [9]. The potential function for this interaction can be written in the form

$$V_{\alpha\beta} = \sum_{l_1 l_2 m_1 m_2} A(l_1, l_2, m_1, m_2; \ r_0, \theta_0, \phi_0) \ Y_{l_1 m_1}(\theta_\alpha, \phi_\alpha) Y_{l_2 m_2}(\theta_\beta, \phi_\beta), \tag{4.2}$$

where $r_0$ is the length of the line joining the centres of the two molecules and the angles $\theta_0$ and $\phi_0$ define its orientation; the suffixes $\alpha$ and $\beta$ refer to the two molecules. The coefficients $A(l_1, l_2, m_1, m_2; \ r_0, \theta_0, \phi_0)$ can be determined from the known forms of the three interactions which have been mentioned previously, but we do not give these general results since we shall require only a few of the coefficients.

Using the rotational wave functions (4.1) and the potential (4.2) we can calculate the energy of interaction between two hydrogen molecules. If the para- and the ortho-molecules are in their ground states then the interaction energy of two para-molecules equals $A(0, 0, 0, 0; r_0, \theta_0, \phi_0), (4\pi)$, and is isotropic (independent of $\theta_0$ and $\phi_0$). The ortho–para energy contains terms with $l_1 = 0$, $l_2 = 2$, as well as the above term with $l_1 = l_2 = 0$: the ortho-ortho energy includes terms with $l_1 = l_2 = 2$ in addition to these.

The quadrupole quadrupole interaction occurs only in the terms in (4.2) for which $l_1 = l_2 = 2$ and, as has been shown by Nakamura [4], it gives the dominant contribution to these terms when $r_0 \sim 4$ Å. The contributions from the valence and the dispersion forces are of opposite sign and cancel approximately at these values of $r_0$. Thus, apart from the isotropic part, which is common to all pairs of hydrogen molecules, the energy of an ortho–ortho pair is predominantly that due to the interaction of two equal electric quadrupoles. Also to this approximation the anisotropic part of the energy of an ortho–para pair is zero.

If $M$ is a good quantum number the anisotropic part $w_{\alpha\beta}$ of the ortho–ortho pair energy is given by

$$w_{\alpha\beta} = \left(\frac{6e^2 \tilde{Q}^2}{25 r_0^5}\right) \gamma(M_\alpha) \gamma(M_\beta) P_4(\cos\theta_0), \qquad (4.3)$$

where $Q$ is the quadrupole moment of the hydrogen molecule and

$$\gamma(M) = \sqrt{(20\pi)} \int_0^\pi \sin\theta \, d\theta \int_0^{2\pi} d\phi \, Y_{1M}(\theta, \phi) Y_{20}(\theta, \phi) Y_{1M}^*(\theta, \phi)$$

$$= \begin{cases} 2, & \text{if } M = 0, \\ -1, & \text{if } M = \pm 1. \end{cases}$$

The energy (4.3) depends on $|M|$ and not on $M$. Thus the ortho-molecules can be divided into two sets which will be denoted by $\lambda$ and $\mu$: the set $\lambda$ contains those for which $M = 0$ and the set $\mu$ those for which $M = \pm 1$. With the notation used above

$$w_{\lambda\lambda} = 4x P_4(\cos\theta_0), \quad w_{\lambda\mu} = -2x P_4(\cos\theta_0), \quad w_{\mu\mu} = x P_4(\cos\theta_0), \qquad (4.4)$$

where $x = (6e^2 Q^2)/(25 r_0^5) = 2 \cdot 615 k$. These energies depend on the orientation of the intermolecular axis to the axis of quantization through the factor $P_4(\cos\theta_0)$.

## 5. THE ISOTROPIC (TOMITA) MODEL FOR SOLID HYDROGEN

The energies of pairs of ortho-hydrogen molecules given by (4.4) can be used to investigate the possibility of transitions in solid hydrogen. The results of §3 can be applied only to isotropic crystals and although the probable crystal structure of solid hydrogen is hexagonal close packed (to which we cannot apply the isotropic results) it is of interest to examine possible isotropic crystal structures.

Using the notation of (2.4), (2.9) and (4.4), with $z' = 0$ and $g_\mu = 2g_\lambda$, we have

$$kT_0 = -3zx P_4(\cos\theta_0)/2\ln 2 \quad \text{and} \quad w = -9x P_4(\cos\theta_0)/2. \qquad (5.1)$$

Thus $kT_0 = zw/3\ln 2$.

When $P_4(\cos\theta_0)$ is positive, both $T_0$ and $w$ are negative. The partition function is equal to that of an Ising antiferromagnet under a field $H_e$ which varies with temperature $T$ along a line similar to (1) in the figure. There is no transition point on the $T$-axis.

For the body-centred cubic lattice with axis of quantization parallel to one of the cube edges $\cos\theta_0 = \pm 1/\sqrt{3}$ and $P_4(\cos\theta_0) = -7/18$: thus both $T_0$ and $w$ are positive. On setting $z = 8$ in (5.1), $kT_0 = 3\cdot847w$. There will be a first-order transition if $kT_c$ is greater than $3\cdot847w$, but no transition if $kT_c$ is less than this value. A recent estimate by Domb and Sykes [8] using a high-temperature series approximation is that $2kT_c/zw$, in their notation $kT_c/qJ$, is equal to $0\cdot794$. This gives $kT_c = 3\cdot176w$. Using the less accurate Bethe approximation $kT_c = 3\cdot476w$, and with the still less accurate Bragg–Williams method $kT_c = \frac{1}{2}zw = 4w$. Thus there is no transition for this lattice, although the Bragg Williams approximation would give a spurious first-order transition.

For the simple cubic lattice with axis of quantization along a diagonal of the cube it is also true that $\cos\theta_0 = \pm\sqrt{\frac{1}{3}}$, but $z = 6$ and therefore (5.1) gives $kT_0 = 2\cdot885w$. In this case Domb and Sykes obtain $kT_c/qJ = 0\cdot752$, giving $kT_c = 2\cdot256w$: the Bethe method gives $kT_c = 2\cdot466w$, and the Bragg Williams method $kT_c = 3w$. As in the previous case there is no transition, although again the Bragg–Williams approximation gives a spurious first order transition.

The conclusions of §3 and of this section are at variance with those found by Tomita [6], whose model for solid hydrogen is equivalent to this isotropic model. It is of interest to investigate the reasons for the discrepancy.

Using the Bragg Williams method a parameter $s$, defined by $s = \frac{1}{2}(2N_\lambda - N_\mu)/N$ satisfies the equation

$$s = \{1 - \exp(-3sT_1/T)\}/\{1 + 2\exp(-3sT_1/T)\}, \qquad (5.2)$$

which is given by Tomita (p. 218, equation 10) where $T_1 = 4zw/9k$ in our notation. Tomita claims that (5.2) implies that there is a second-order transition at $T = T_1$. However, if one examines more closely the possible solutions of (5.2) it is found that a first-order transition has taken place at a higher temperature $T_0$, and that the second-order transition does not occur. It can be shown that

$$T_0 = 1\cdot082\,T_1 = 0\cdot962\,T_c,$$

as found using the Bragg Williams approximation for the two crystal lattices considered. Thus we see that the correct interpretation of (5.2) leads to the same conclusions as have been obtained using the concept of the effective field.

Using the Bethe approximation Tomita claims to have found a second-order transition under quite general conditions, but we have demonstrated in §3 that this is not so. The Bethe consistency conditions for the model are given by equations (17) and (18) of Tomita's paper, provided that on the right-hand side of (18) $z$ is replaced by $(z - 1)$ and on the left-hand side $\sigma$ is replaced by $\sigma^{1.2}$. Equivalent conditions could be obtained by substituting the first-order approximation for $g$ in the partition function (2.8) of this paper. A necessary condition for the occurrence of a transition is given by equation (19) of Tomita. Equations (17), (18) and (19) must be solved simultaneously to obtain the transition temperature, if it exists. However, Tomita considers only equations (17) and (19), and inserts a further condition instead of (18): this is that the ratio of $\lambda$-molecules to $\mu$-molecules remains constant from infinity (when it is $\frac{1}{2}$) down to the transition temperature. This is not true, and the transition temperature obtained by Tomita is inconsistent with the equilibrium condition (18). Thus no transition occurs. Also for equation (21') of Tomita to be equivalent, as claimed, to equation (21) the negative sign on $V$ must be omitted, as can be verified by substituting (15.1) and (15.2) in (21).

We have not investigated all possible solutions of (17), (18) and (19), but from our theory using the equivalent field these equations have no solution in the case of the quadrupole quadrupole interaction. Thus the isotropic model for solid ortho-hydrogen predicts no transitions, either first order or second order, although there might be a Schottky-type maximum in the specific heat curve.

## 6. Conclusion

Unsymmetric regular models in which the two species present have unequal statistical weights and unequal interaction energies for pairs of nearest neighbours of the same species have been investigated. When the energy of formation of an unlike pair is positive these models are found to have either a first-order transition with latent heat or no transition at all. Their behaviour is thus quite unlike an Ising ferromagnet although their distribution probabilities are shown to be equal to those of the Ising model under a temperature-dependent external field, termed the 'equivalent field'. We have, in particular, discussed nearest-neighbour pair energy ratios derived from the quadrupole–quadrupole interaction thought to be responsible for the lambda-point transitions in solid hydrogen. However, although this interaction energy is, in general, dependent on the orientation of the pair of sites we have confined ourselves to lattices and quantization directions for which the orientation dependence is not apparent; this has been termed the isotropic case and it has been found that no transitions occur although there will be a Schottky-type maximum in the specific heat.

The isotropic case is, however, probably not directly applicable to solid hydrogen since for lattices with coordination number 12 the quadrupole -quadrupole interaction energies do depend on the direction of the pair axis. However, from the results obtained it seems unlikely that changes in the proportions of molecules in the inequivalent $\lambda(M=0)$ and $\mu(M=\pm1)$ states are solely responsible for a second-order interaction. For the latter it seems necessary that the system should be able to exist in two equivalent states of maximum probability. These could arise either from the removal of the degeneracy of the $M=\pm1$ state which is unlikely in the relevant temperature range, or from spatial ordering on equivalent sub-lattices. In the next paper lattices for which the interaction energies are dependent on the orientation of the nearest-neighbour site pair will be discussed and it will be shown that with quadrupole–quadrupole interactions such spatial ordering can occur when $w$ and $w'$ (defined in § 2) are of opposite signs.

## References

[1] Smith, G. W., and Housley, R. M., 1960, *Phys. Rev.*, **117**, 732.
[2] Hill, R. W., and Ricketson, B. W. A., 1954, *Phil. Mag.*, **45**, 277.
[3] Reif, F., and Purcell, E. M., 1953, *Phys. Rev.*, **91**, 631.
[4] Nakamura, T., 1955, *Prog. theor. Phys.*, **14**, 135.
[5] Babloyantz, A., and Bellemans, A., 1959, *Mol. Phys.*, **2**, 169; 1960, *Ibid.*, **3**, 313.
[6] Tomita, K., 1955, *Proc. phys. Soc.* A, **68**, 214.
[7] Domb, C., 1949, *Proc. roy. Soc.* A, **199**, 199; 1960, *Advanc. Phys.*, **9**, 228.
[8] Domb, C., and Sykes, M. F., 1957, *Proc. roy. Soc.* A, **240**, 214.
[9] Margenau, H., 1943, *Phys. Rev.*, **63**, 385.

# The electric polarization of rod-like, charged macromolecules

by M. MANDEL

Laboratorium voor Physische Chemie, Rijksuniversiteit, Leiden, Netherlands

The polarizability in the longitudinal direction of rod-like, highly charged macromolecules has been evaluated. A simple model, emphasizing the discrete distribution of the fixed charges along the macromolecule, but neglecting interionic repulsion, has been used to calculate the statistical distribution of the counterions which gives rise to this polarization. For weak electric fields the expression obtained for the polarizability is analogous to that previously derived by Schwarz, although it contains less implicit information about the temperature dependence and the influence of the valency of the counterions. The possibility that saturation effects may appear with high electric fields is left open. An approximate formula for the relaxation time of the longitudinal polarization is also derived.

---

## 1. INTRODUCTION

In solutions of highly charged polyelectrolyte molecules, a certain fraction of the counterions is more or less firmly bound to the region occupied by the poly-ions. This has been shown, *inter alia*, by Wall and co-workers [1]. In the particular case of an elongated, uniformly charged particle (rigid rod-like molecule or nearly completely stretched polymer coil), theoretical calculation shows that, in the absence of added salt, the mean electric potential around the polyelectrolyte molecule decreases rapidly in the radial direction [2, 3]. The counterions which, according to a Boltzmann distribution, are attracted into the region of highest mean potential, are more or less trapped and form the fraction of the ' bound ' ions. Although radially fixed upon the polymer framework, these ions still have a certain freedom to move in the longitudinal direction of the molecule. Particular attention has been called upon this motion of ' bound ' ions by Schwarz [4, 5] who predicted, as a consequence, a large polarizability in an electric field for elongated, highly charged particles in solution.

The calculation by Schwarz for this polarizability of rod-like macromolecules [5] is, however, oversimplified in so far as he neglects the finite size of both fixed and longitudinally mobile charges, the mutual repulsion between the counterions and the discrete distribution of the fixed charges. (When calculating the variation of the electric potential in the radial direction, we may consider the regular distribution of fixed charges as a uniform one. But for a theoretical treatment of the longitudinal motion of ions at distances from the poly-ion which are of the same order of magnitude as the spacing between the fixed charges, this assumption is no longer true.) As a consequence of these approximations, for instance, the distribution function for the ' bound ' ions in the absence of an electric field, as derived by Schwarz, is Gaussian around the centre of the molecular rod. Such a distribution function cannot, however, be realistic because the strong repulsion between the like counterions will tend to flatten out the maximum.

In the present paper we will use, therefore, a different molecular model in order to derive the polarizability (and subsequently the relaxation time of the corresponding polarization) of rod-like, highly charged macromolecules in solution due to the longitudinal motion of 'bound' ions. This model will particularly emphasize the discrete distribution of the charges fixed upon the molecular rod and the steric hindrance between the polymer framework and the small, mobile ions. It neglects, as is done in Schwarz's calculations, the mutual repulsion between the ions.

## 2. The molecular model

Let us represent the macromolecule by a cylinder (or a very elongated prolate spheroid) with $N$ charged sites distributed regularly over its length $l$. Let us call $b$ the distance between two successive sites. Taking the axis of the cylinder as reference axis $x$, with its origin in the middle of the molecule, the coordinate of a certain site $k$ will be

$$x_k = kb, \qquad (1)$$

where $k$ is an integer ranging from $-(N-1)/2$ to $(N-1)/2$. (For simplicity's sake we have chosen $N$ as an odd number.) The site $k=0$ is at the origin of the $x$ axis. If we suppose that there is also a distance $b$ between each end of the molecule and the last charged site, the total length of the cylinder is

$$l = (N+1)b. \qquad (2)$$

For a highly charged macromolecule $N \gg 1$, so that for the spacing between the fixed charges we may write

$$b \simeq l/N. \qquad (3)$$

Each of these sites is supposed to bear a charge $\epsilon$. All 'bound' ions (also called mobile charges), which we consider to be identical, have a charge $-z\epsilon$. Let there be $n$ of such ions. The degree of association $\gamma$ of the counterions will be defined by

$$\gamma = zn/N. \qquad (4)$$

We admit that the 'bound' ions cannot leave the region close to the poly-ion, neither in radial nor in the longitudinal direction. We will calculate the distribution of those mobile charges on the $x$ axis only and not their location on the surface of the cylinder or spheroid. To do this, we introduce a potential energy $V$ for a mobile charge in the vicinity of the macromolecule. In the radial direction, $V$ will be nearly constant over a short distance and then rise sharply to values which are large with respect to $kT$. This forms a radial potential well which is consistent with the theoretical calculations [2, 3]. The exact shape of the function representing the variation of $V$ on the $x$ axis is not known. But it can be seen that it will be periodic, exhibiting a minimum near each charged site, due to the strong, electric attraction of the mobile ion by the fixed charge. The height of the potential barrier which separates two successive minima, however, does not only depend on the variation of the electric energy (which, in turn, depends on $b$ and the distance of closest approach of a 'bound' ion with respect to the polymer framework) but also on the steric repulsion between the ion carrying the mobile charge and the atoms or molecular groups situated near the charged site. As the structure of the macromolecule is assumed to be completely regular,

the potential energy curve of a 'bound' ion along the $x$ axis can be represented by a succession of equal minima, situated at or near the charged sites, separated by equally high barriers. In this picture, end-effects have been neglected, which is permissible if $N$ is sufficiently large.

Without a detailed calculation nothing can be said about the exact shape and height of the potential barriers in the $x$ direction. We therefore will use the most simple representation for the potential energy: a succession of square wells of width $a$ (minimum width to permit the introduction of a mobile charge into the well) and of height $h$. This value should be much smaller than the height of the potential barrier in the radial direction.

For simplicity, we locate the middle-point of the minima, characterized by a potential energy $V_0$, at the coordinates of the charged sites $x_k$ and the middle-points of the maxima at a new set of coordinates $x_j$, defined by

$$x_j = (j - \tfrac{1}{2})b, \tag{5}$$

where $j$ is an integer ranging from $-(N-1/2)$ to $+(N+1/2)$. At both ends of the macromolecule $x = \pm l/2$, we add an infinitely high potential barrier in order to account for the fact that the 'bound' ion cannot leave the polyelectrolyte molecule. The potential energy curve in the $x$ direction is represented by the figure.
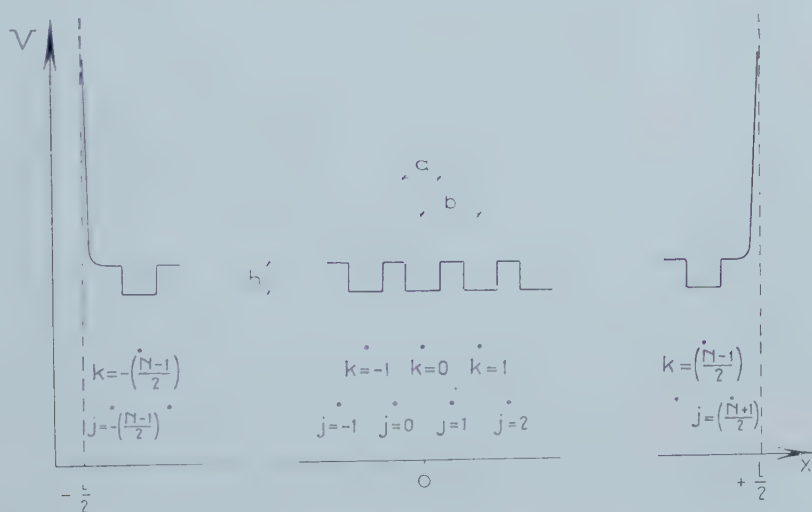


We thus obtain $N$ charged sites characterized by their coordinates $x_k$ and potential energy $V_0$ alternating with $(N+1)$ uncharged sites with coordinates $x_j$ and a potential energy $(V_0 + h)$.

The dipole moment in the longitudinal direction of the poly-ion, expressed with respect to the centre of gravity of the molecule (for reasons of symmetry situated at $x=0$) may be defined in the following way:

$$m_l = \left\{ \sum_k \epsilon x_k - \sum_{r=1}^{n} z\epsilon \left[ \sum_k p_r(x_k)x_k + \sum_j p_r(x_j)x_j \right] \right\}, \tag{6}$$

where $p_r(x)$ represents the probability that a mobile charge $r$ should be located at $x$. Taking into account the symmetrical distribution of the charged sites with

respect to the origin and the fact that all 'bound' ions are identical and that we neglect their interaction, $m_i$ can also be written:

$$m_l = -nze\left[\sum_k p_r(x_k)x_k + \sum_j p_r(x_j)x_j\right]. \tag{7}$$

In the absence of an electric field, the probability $p_r(x)$ will be given by:

$$p_r(x) = \frac{\exp\left[-\beta V(x)\right]}{\sum_{(\text{sites})} \exp\left[-\beta V'(x)\right]}, \tag{8}$$

where $\beta = (kT)^{-1}$ and the summation in the denominator is extended over all accessible sites $k$ and $j$. We thus can write the following expressions for $p_r(x_k)$ and $p_r(x_j)$ in the case where $N \gg 1$:

$$p_r(x_k) = \frac{\exp\left(-\beta V_0\right)}{N\exp\left(-\beta V_0\right) + (N+1)\exp\left(-\beta V_0 + \beta h\right)} \simeq \frac{1}{N[1+\exp\left(-\beta h\right)]}, \tag{9}$$

$$p_r(x_j) = \frac{\exp\left(-\beta V_0 - \beta h\right)}{N\exp\left(-\beta V_0\right) + (N+1)\exp\left(-\beta V_0 + \beta h\right)} \simeq \frac{\exp\left(-\beta h\right)}{N[1+\exp\left(-\beta h\right)]}. \tag{10}$$

Introducing (9) and (10) into (7) yields the longitudinal dipole moment due to the distribution of the mobile charges, which, in the absence of an electric field, is zero:

$$m_l = -\frac{nze}{N[1+\exp\left(-\beta h\right)]}\left[\sum_k x_k + \exp\left(-\beta h\right)\sum_j x_j\right] = 0. \tag{11}$$

## 3. THE POLARIZABILITY OF THE HIGHLY CHARGED MACROMOLECULE

With the molecular model described in the preceding section, we can evaluate the dipole moment induced by an external electric field and the corresponding polarizability $\alpha_l$ in the longitudinal direction.

Let us admit that in the presence of a constant external field, the component $E$ along the $x$ axis of the mean field inside the region occupied by the poly-ion is uniform. The potential energy of a 'bound' ion at a given site will now be modified by the electric potential energy due to this field. Putting the arbitrary origin of this electric potential energy at $x=0$ and assimilating the value of this energy at a given site to the value at the coordinate of its middle-point, we then can write for the probabilities $p_r(x_k)$ and $p_r(x_j)$ in the presence of an electric field:

$$p_r(x_k) = \frac{\exp\left(\beta z\epsilon Ex_k\right)}{\sum_k \exp\left(\beta z\epsilon Ex_k\right) + \sum_j \exp\left(-\beta h + \beta z\epsilon Ex_j\right)} = \frac{\exp\left(\beta qk\right)}{S}, \tag{12}$$

$$p_r(x_j) = \frac{\exp\left(-\beta h + \beta z\epsilon Ex_j\right)}{\sum_k \exp\left(\beta z\epsilon Ex_k\right) + \sum_j \exp\left(-\beta h + \beta z\epsilon Ex_j\right)} = \frac{\exp\left(-\beta h\right)\exp\left[\beta q(i-\frac{1}{2})\right]}{S} \tag{13}$$

Here we have made use of (1) and (5), introduced the parameter $q$

$$q = z\epsilon bE, \tag{14}$$

and written $S$ for the common denominator of (12) and (13):

$$S = \sum_{k=-\frac{1}{2}(N-1)}^{\frac{1}{2}(N-1)} \exp\left(\beta z\epsilon Ex_k\right) + \sum_{j=-\frac{1}{2}(N-1)}^{\frac{1}{2}(N+1)} \exp\left(-\beta h + \beta z\epsilon Ex_j\right). \tag{15}$$

With (12) and (13), (7) yields the expression for the dipole moment, due to the mobile charges, in the presence of an electric field:

$$m_l = - \frac{nz\epsilon b}{S} \left\{ \sum_k k \exp(\beta qk) + \exp(-\beta h) \sum_j (j - \tfrac{1}{2}) \exp[\beta q(j - \tfrac{1}{2})] \right\}$$

$$= - \frac{nz\epsilon b}{S\beta} \left( \frac{\delta S}{\delta q} \right). \tag{16}$$

The exact value of $S$ and also that of $m_l$ can be evaluated easily. We will, however, only be interested in those values of $m_l$ which are proportional to $E$. This may be expected with usual macroscopic fields. Therefore, if $q$ is sufficiently small, each exponential appearing in (15) and (16) will be replaced by the first terms of a series development. In the limit of large $N$ ($N \gg 1$) and taking into account the symmetrical distribution of the $k$ and $j$ sites with respect to the origin, $m_l$ may then be written, up to the first order in $E$:

$$m_l = - \frac{nz\epsilon \beta q b N^2}{12} = - \frac{nz^2\epsilon^2 b^2 N^2}{12kT} E. \tag{17}$$

Note that in this last expression (17), $h$ has disappeared. This is due to the fact that $m_l$ is established through the perturbation by the applied electric field, of the equilibrium distribution of the mobile charges. This perturbation depends only on the additional electric potential at each site and not on the absolute value of the total potential energy. The same value of $m_l$ would also have been obtained if the shape of the potential barrier in the molecular model had been chosen in such a way that the 'bound' ions can only be located at the charged $k$ sites.

The proportionality factor with respect to $-E$ in (17) represents the polarizability $\alpha_1$ of the polyelectrolyte ion in the longitudinal direction due to the mobile charges and is given by

$$\alpha_1 = \frac{nz^2\epsilon^2 b^2 N^2}{12kT} = \frac{\gamma z\epsilon^2 N l^2}{12kT}, \tag{18}$$

where use has been made of (3) and (4).

In the presence of an alternating electric field, equations (17) and (18) will still be valid as long as the frequency of the field is much smaller than $(2\pi\tau)^{-1}$, where $\tau$ is the relaxation time of the polarization of the poly-ion. An approximated expression for this relaxation time may be obtained by the following, simplified, reasoning.

For simplicity, we will consider the case where the mobile charges are distributed over $k$-sites only. In the absence of any electric field, all available sites have the same probability to be occupied [see equation (9), with $\exp(-\beta h) \leqslant 1$]. The average unidimensional ionic density $c$ (in ions per angstrom) will be given by

$$c = n/Nb', \tag{19}$$

where $b'$ is the distance expressed in angstroms. As long as $n$ is smaller than $N$, this average density will be much smaller than unity. We therefore can represent this situation by a regular distribution of the 'bound' ions over the total length of the polyelectrolyte molecule, each ion being free to move over a distance $l_r = \pm (2c)^{-1}$ around a mean position $\xi_r^0$. Those mean positions are regularly distributed over the axis of the poly-ion in such a way that $\sum_r \xi_r^0 = 0$.

In the presence of the electric field, this distribution of the mobile charge is altered and the dipole moment (17) is established. This may be interpreted again

by assuming that the 'bound' ions are slightly displaced from position $\xi_r{}^0$ into a new mean position $\xi_r$ such that

$$m_l = -z\epsilon \sum_{r=1}^{n} (\xi_r - \xi_r{}^0) = -nz\epsilon\overline{\Delta\xi}, \tag{20}$$

where $\overline{\Delta\xi}$ is the average displacement of the 'bound' ions under the influence of the applied field. From (17) and (20) it follows that

$$\overline{\Delta\xi} = \frac{z\epsilon b^2 N^2 E}{12kT}. \tag{21}$$

The mean velocity of the ions being equal to $\bar{v} = \bar{u}z\epsilon E$, where $\bar{u}$ is their mean mobility along the polymer framework, the mean time $\tau'$ necessary to establish the dipole moment

$$\tau' = \frac{\overline{\Delta\xi}}{\bar{v}} = \frac{b^2 \dot{N}^2}{12\bar{u}kT} = \frac{l^2}{12\bar{u}kT} = \frac{\alpha_1}{\bar{u}n(z\epsilon)^2}, \tag{22}$$

will be a measure of the order of magnitude for the relaxation time $\tau$. As $\bar{u}kT = D$, where $D$ is the mean diffusion constant of the counterions inside the radial potential well of the poly-ion, equation (22) may also be written

$$\tau' = \frac{b^2 N^2}{12D} = \frac{l^2}{12D}. \tag{23}$$

Note that, according to the molecular model which has been used, $\bar{u}$ and $\tau'$ will depend on the height $h$ of the potential barriers in the $x$ direction. As pointed out already, the calculation of $h$ is by no means a simple task.

## 4. Discussion

In the preceding section we have derived an expression for the polarizability of a rod-like poly-ion in terms of the longitudinal distribution of the 'bound' ions. The derivation was based upon an approximation which neglects the interaction of the counterions. It is difficult to estimate the perturbation introduced by the repulsive effect between these ions, but its influence will certainly become smaller and smaller when the value of $n$ decreases. In fact, in the absence of the electric field, the uniform ionic density which is characteristic for our model—as was shown at the end of the last section—will even be favoured by the repulsion between the like counterions.

From another point of view one may express some doubts about the utility of this model because most polyelectrolytes will not exhibit a rod-like structure even when in highly charged state [6]. They can rather be represented as a more or less stretched coil. The formulae of the preceding sections are still valid for these cases if we may assume that the molecule can be contained inside a prolate spheroid in such a way that the projections of the charged groups on the major axis of this spheroid are, on the average, distributed regularly along this axis.

In the case of a rod-like molecule the experimental determination of $\alpha_1$ (through dielectric measurements for instance) may give information about $\gamma$, provided the degree of polymerization ($N$) and the length ($l$) of the molecule are known. For coiled molecules it is generally much more difficult to determine $l$ independently so that $\alpha_1$ will only yield qualitative information.

For both types of molecule, however, the value of $b$ can be estimated with the help of molecular scale models. In the case of nearly fully ionized vinylic polymers

(such as polyacrylic or polymethacrylic acid) $b$ will be of the order of magnitude of some angstroms. This means that, for a molecule with a degree of polymerization 5000, fully ionized and at room temperature, $\alpha_1$ will be given by

$$\alpha_1 \simeq (\gamma z b'^2) 5 \times 10^{-12} \text{ cm}^3,$$

where $b'$ is distance $b$ expressed in angstrom units. Even for relatively small values of $\gamma$, the longitudinal polarizability will be exceptionally high. It is much more difficult to estimate the order of magnitude of $\tau'$ as nothing is known about the mean mobility $\bar{u}$ of the counterions inside the radial potential well near the poly-ion. From other experiments it has been concluded that the mobility of small ions should be much smaller inside an ionic atmosphere than in ordinary solution [7]. This will presumably also be the case for the ions in which we are interested here. The diffusion constant for ordinary small ions in aqueous solution at room temperature is of the order of magnitude of $10^{-5}$ cm$^2$ sec$^{-1}$. For the same poly-ion as used to estimate $\alpha_1$ we thus would have

$$\tau' \gg 2b'^2 \times 10^{-5} \text{ sec,}$$

which situates the critical frequency for the relaxation of the longitudinal polarization in an alternating field near $10^3$ cycles sec$^{-1}$.

As was pointed out already, (17) was derived using the first terms of a series development for the exponentials appearing in (15) and (16). This procedure was claimed to be valid with ordinary, macroscopic fields, $\beta q k$ (or $\beta q j$) being small with respect to unity. Using again a poly-ion with 5000 charged sites in a field of 1 volt cm$^{-1}$, putting $b$ arbitrarily equal to $3 \times 10^{-8}$ cm and $z$ to unity, the largest value of $\beta q k$ at room temperature will be of the order of magnitude of 0·005. This justifies our previous statement. Consequently, for ordinary macroscopic fields $\alpha_1$ will be independent of $E$. For large electric fields this will no longer be the case; the exact value of $S$ should be used and saturation effects will appear.

We finally want to compare the results of this calculation (18) and (22) with Schwarz's expressions for the longitudinal polarizability and relaxation time of a rod-like poly-ion [5]. For this comparison we will use the latter in the special case where the mobility of the poly-ion inside the radial potential well is neglected (i.e. $u_{11} = 0$ in Schwarz's notation). They read (using the notation of the present paper)

$$\alpha_1 = \frac{\gamma D_0 l^3}{8}, \tag{24}$$

$$\tau = \frac{D_0 l^3}{8\bar{u}Nz\epsilon^2} = \frac{\alpha_1}{\bar{u}n(z\epsilon)^2}, \tag{25}$$

where $D_0$ is the dielectric constant of the solvent inside the ionic atmosphere of the poly-ion. As $N$ is proportional to $l$, both calculations lead to analogous results with respect to the dependence on $l$ and $\gamma$. It may also be seen that the relation between $\alpha_1$ and $\tau$ is the same. The major difference resides in the temperature dependence of $\alpha_1$. In our expression (18) $T$ appears explicitly whereas (24) shows that the value of $\alpha_1$ given by Schwarz depends on the temperature only through $D_0$. It should be noted that the dielectric constant of the solvent near the poly-ion is neither well defined nor experimentally accessible. This is due to the fact that the structure of this part of the solvent may differ from that of the ordinary liquid and, furthermore, to dielectric

saturation which will probably occur in this region as a consequence of the numerous electric charges present. Therefore equation (24) contains one additional unknown parameter compared to our corresponding (18). Another difference between these two expressions for $\alpha_1$ is their dependence on the valency of the 'bound' ions, which is much more pronounced in (18) than in (20) where it appears only through $\gamma$. We may therefore state that the molecular model used in the present paper yields more information about the longitudinal polarizability than may be obtained from Schwarz's treatment.

Finally it should be noted that the dielectric properties of a solution of rod-like, charged macromolecules will not only depend on the polarizability of the solute molecules. Other effects may contribute as well to the overall dielectric behaviour of such solutions. We will consider this in a subsequent paper.

## References

[1] Huizenga, J. R., Grieger, P. F., and Wall, F. T., 1950, *J. Amer. chem. Soc.*, **72**, 2636.
[2] Fuoss, R., Katchalsky, A., and Lifson, S., 1951, *Proc. nat. Acad. Sci., Wash.*, **37**, 579.
[3] Alfrey, T., Berg, P., and Morawetz, H., 1951, *J. Polym. Sci.*, **7**, 543.
[4] Schwarz, G., 1956, *Z. Phys.*, **145**, 563.
[5] Schwarz, G., 1959, *Z. phys. Chem.*, **19**, 286.
[6] Lifson, S., 1957, *J. Polym. Sci.*, **23**, 431.
[7] Mandel, M., 1956, *Bull. Soc. chim. Belg.*, **65**, 308.

# The electron spin resonance spectra of the toluene, *p*-xylene and *m*-xylene anions

by J. R. BOLTON and A. CARRINGTON

Department of Theoretical Chemistry, University of Cambridge

The electron spin resonance (e.s.r.) spectra of the anions of toluene, *p*-xylene and *m*-xylene have been studied and the proton hyperfine coupling constants determined. These are in excellent agreement with the predictions of Hückel molecular orbital theory.

## 1. INTRODUCTION

The proton hyperfine coupling constants derived from the e.s.r. spectra of aromatic negative ions can be correlated with the distribution of the unpaired electron through the well known relationship proposed by McConnell [1]

$$a_H = Q\rho.$$

In this equation $a_H$ is the hyperfine splitting due to a proton attached to a carbon atom in an aromatic ring, and $\rho$ is the unpaired electron density at that carbon atom, $Q$ being a constant. For the benzene negative ion $Q$ has the value 22·5 gauss [2] and for larger molecules, the spin densities calculated from simple Hückel molecular orbital theory, together with values of $Q$ around 28 gauss, give adequate interpretations of the spectra [3].

In the case of benzene derivatives an additional complication arises because of orbital degeneracy. The benzene negative ion has a doubly-degenerate ground state and the introduction of a methyl group will remove this degeneracy in a manner which one might hope to predict. One object of the e.s.r. studies described in this paper is to determine the orbital of the unpaired electron. A further objective is to learn more about the possible participation of methyl groups in the conjugated system through hyperconjugation. It is commonly supposed that the observation of hyperfine structure from methyl protons attached to an aromatic system *proves* the importance of hyperconjugation. Unfortunately this is not the case since there are other mechanisms through which this splitting can arise. A detailed study of the methyl splittings in a range of simple radicals might give more information on this point.

In this paper we describe the e.s.r. spectra of the toluene, *p*-xylene and *m*-xylene anions and discuss the significance of the proton hyperfine coupling constants. These spectra have been described by previous authors [4, 5] but the resolution obtained was not sufficient to disclose the more interesting features.

## 2. ANALYSIS OF THE SPECTRA

The negative ions were prepared by the usual method [6] of reduction with sodium or potassium metal in dimethoxyethane *in vacuo* at −70°c. The e.s.r. spectra were obtained using a Varian 100 kc Spectrometer.

## 2.1. *Toluene*

The e.s.r. spectrum exhibits large splittings (approximately 5 gauss) due to the ortho and meta ring protons, together with small splittings (approximately 1 gauss) from the para ring proton and the methyl protons. Figure 1 shows the
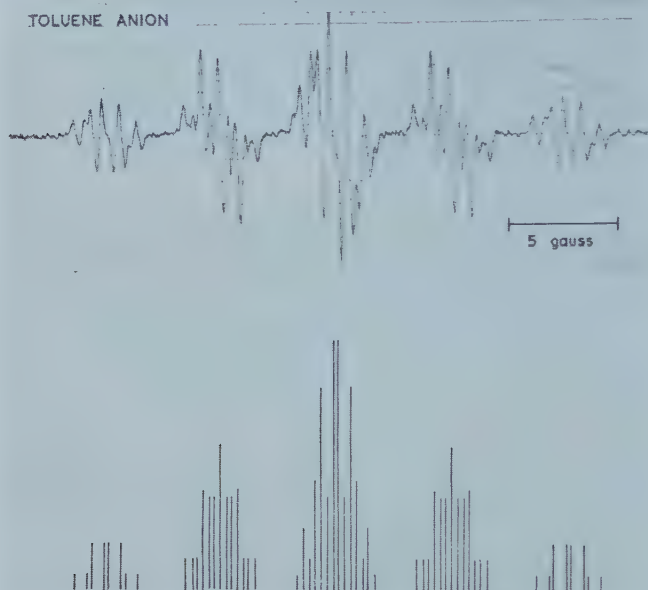


Figure 1. E.S.R. spectrum of the toluene anion.

spectrum obtained, together with a reconstruction based on the hyperfine coupling constants listed in table 1. The spectrum was analysed in the following manner. Five strong lines will arise from the ortho and meta protons and any

Toluene⁻ $a_1(a_{CH_3})$ $= 0.79$, $a_{2.6} = 5.12$, $a_{3.5} = 5.45$, $a_4 = 0.59$.
p-xylene⁻ $a_{1,4}(a_{CH_3})$ $= 0.10$, $a_{2,3,5,6} = 5.34$
m-xylene⁻ $a_{1,3}(a_{CH_3})$ $= 2.26$, $a_2 = 6.85$, $a_{4,6} = 1.46$, $a_5 = 7.72$.
p-xylene ¹³C splittings: $a_2 = 6.50$, $a_1 = 5.20$.

Table 1. Experimental hyperfine splitting constants (in gauss).

inequivalence of the two coupling constants will result in a splitting of the three central members of the quintet, but not of the outside members. Hence the observed splitting of the outside lines gives the para and methyl coupling constants. If these two constants are equal the outside group will consist of five lines with relative intensities 1 : 4 : 6 : 4 : 1 and this is clearly a close approximation to the truth. However, there is a further small splitting and from the distance between the extreme members of the group one can determine separate values for the two coupling constants. Knowing these values one can then determine the difference between the ortho and meta coupling constants from the widths of the three central groups in the spectrum, and finally reconstruct the details of the whole spectrum.

We have confirmed our assignment of the ortho and meta constants by studying the spectrum of the anion derived from *o*-deuterotoluene, in which the basic five line pattern obtained from toluene collapses to a four line pattern of relative intensities 1 : 3 : 3 : 1.

## 2.2. *p-xylene*

The e.s.r. spectrum of the *p*-xylene anion is shown in figure 2. It consists of a basic five line pattern arising from the four equivalent ring protons. However, we have also resolved the very small splitting of each line, due to the methyl
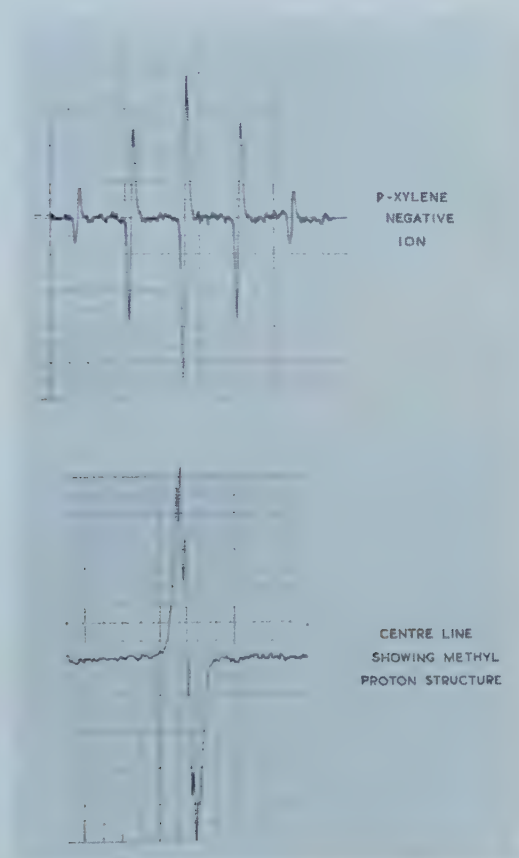


Figure 2. E.S.R. spectrum of the *p*-xylene anion, showing the proton hyperfine structure.

protons, and figure 2 shows the centre line of the spectrum under higher resolution.

Under higher amplification additional hyperfine lines due to $^{13}C$ are observed and two separate coupling constants have been obtained. The spectrum is shown in figure 3 and is discussed later.
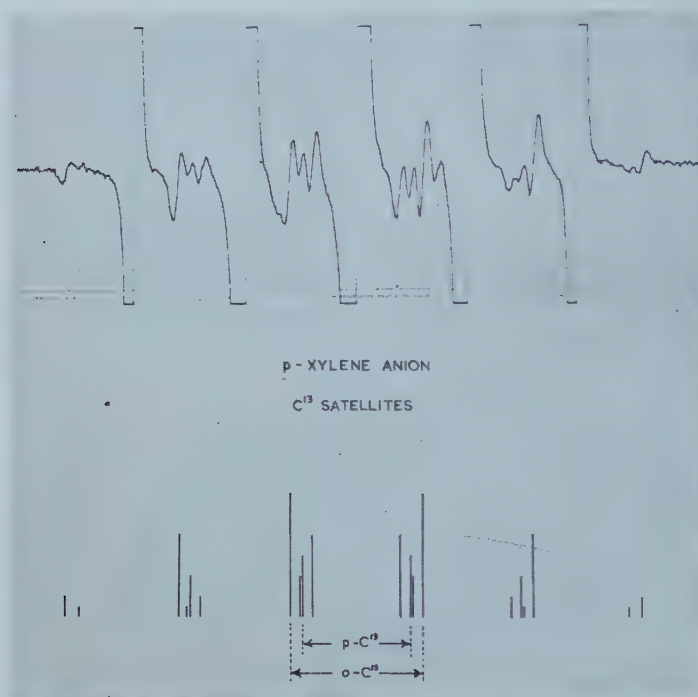
Figure 3.   E.S.R. spectrum of the *p*-xylene anion, showing the $^{13}$C hyperfine structure.
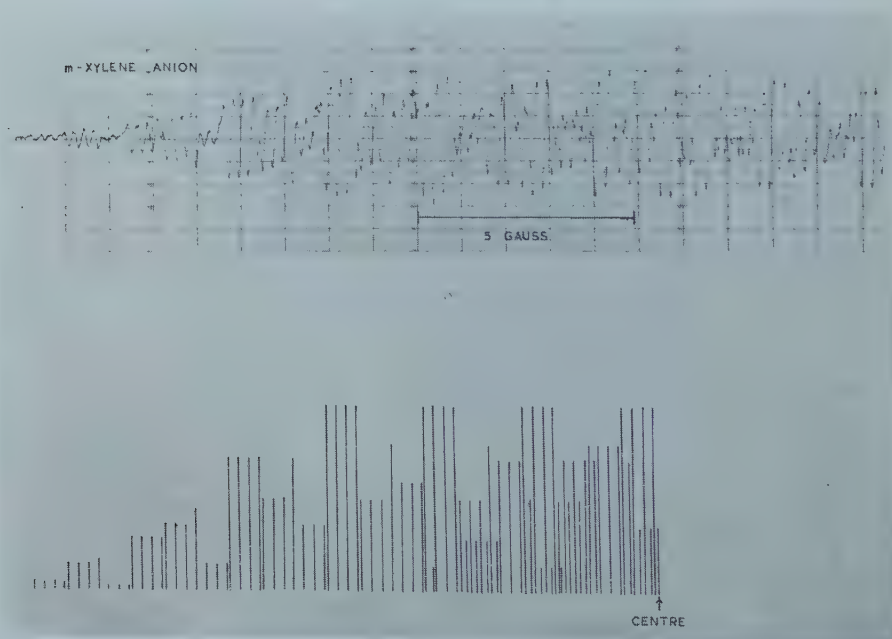


Figure 4.   E.S.R. spectrum of the *m*-xylene anion, with additional hyperfine structure
from $^{39}$K.

## 2.3. *m-xylene*

The spectrum of the *m*-xylene anion, shown in figure 4, is the most compli-cated we have obtained, owing to the fact that there are four different proton hyperfine constants and an additional quartet hyperfine structure arising from interaction of the anion with the potassium cation. The quartet splitting appears clearly at the ends of the spectrum, and the splitting due to the two equivalent ring protons and to the methyl protons is also obtained by close examination of the wings of the spectrum, where there is less overlapping of lines. We are then left with two doublet splittings which, for reasons outlined later, are expected to be approximately 7 gauss. They have been found by trial and error and the reconstruction shown in figure 4, based on the coupling constants listed in table 1, gives a very satisfactory account of the total spectrum. We have displayed half of the spectrum only, so that the details are more easily visible. The spectrum is, of course, symmetrical about its centre, so that all the required information can be obtained from half of it.

## 3. MOLECULAR ORBITAL THEORY

The benzene negative ion has a doubly degenerate ground state, the degenerate Hückel orbitals having the following probability distributions:



ANTISYMMETRIC                    SYMMETRIC
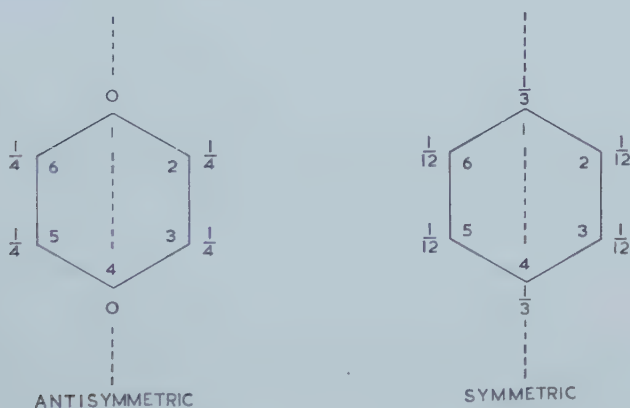
These orbitals are described as 'symmetric' or 'antisymmetric' according to their behaviour on reflection through a plane perpendicular to the ring and passing through atoms 1 and 4.

We now consider the way in which the degeneracy is removed by the intro-duction of methyl groups into the 1 and 4 positions. The methyl group is electron-repelling and we therefore expect the unpaired electron to occupy the antisymmetric orbital since, by so doing, it can avoid the atoms bearing the methyl groups. The e.s.r. spectrum is entirely consistent with this idea. Since in the benzene negative ion, in which the spin density must be $1/6$ at each carbon atom, the hyperfine splitting constant is 3·75 gauss, we expect the ring proton splitting in the *p*-xylene negative ion to be $3·75 \times 6/4 = 5·62$ gauss, which is indeed very close to the experimental value of 5·34 gauss. The methyl splitting indicates that there is only a very small amount of unpaired spin on atoms 1 and 4.

In the case of toluene the unpaired electron will again occupy the antisymmetric orbital and the splitting constants are in agreement with this prediction. We will have more to say about the difference between the ortho and meta coupling constants in due course. The further interesting feature is the much larger methyl proton splitting in toluene, compared with $p$-xylene. This is discussed in detail in a later paper.

The spectrum of the $m$-xylene anion shows quite clearly that here the unpaired electron occupies the symmetric orbital, in accord with our expectations. Taking the probability distribution given by Hückel theory, and a value of 22·5 for $Q$, we would expect two splitting constants to be close to 7·5 gauss, and the two equivalent ring protons to have a splitting in the region of 1·85 gauss.

It would be interesting to know the hyperfine constants for the $o$-xylene anion, in which the electron should again occupy the symmetric orbital. A seven line spectrum has been reported previously but we have found that the spectrum described [4, 5] actually arises from benzene, present as an impurity. We have not been able to obtain a spectrum from $o$-xylene up to the present.

As the above results show, the proton hyperfine constants are in good agreement with those predicted by the unmodified Hückel theory. It is tempting to see if the agreement between theory and experiment can be still further improved by taking the effect of the methyl group into account. Several methods of doing this have been suggested [7], most of which involve the methyl group in hyperconjugation with the ring system. However, we have found that the simplest interpretation of our results is to allow only for the inductive effect of the methyl group on the adjacent ring carbon atom, treating it as a slightly electropositive substituent. Therefore our only variable parameter in the molecular orbital theory is the Coulomb integral of the ring carbon bonded to the methyl group. The value which gives the best agreement with experiment is $\alpha - 0·13\beta$ where $\alpha$ is the Coulomb integral for all other ring carbon atoms and $\beta$ is the C–C resonance integral. The spectra of the $p$-xylene and toluene anions do not provide a test of this theory because of the symmetry restrictions on the orbitals, but the results of the calculation for $m$-xylene are shown in table 2. It might, at first sight,

|  | $a_2$ | $a_4$ | $a_5$ |
|---|---|---|---|
| Experimental | 6·85 | 1·46 | 7·72 |
| Unmodified Hückel | 7·50 | 1·88 | 7·50 |
| Hyperconjugative model | 7·01 | 2·00 | 7·74 |
| Inductive model | 6·91 | 2·05 | 7·87 |

Table 2. Comparison of experimental and theoretical ring proton splittings (in gauss) for the $m$-xylene anion, using $Q = 22·5$ gauss. The methyl groups are attached to atoms 1 and 3.

seem necessary to consider an inductive effect on the ring carbon atoms which are next-nearest neighbours to the methyl group, in order to account for the difference between the ortho and meta ring proton splitting constants in the toluene negative ion. One can certainly do this, but there are other effects which might account for the small difference observed.

It is difficult at this stage to draw any definite conclusions about hyperconjugation. It is not necessary to invoke this phenomenon in order to account for the ring proton splittings and it is perhaps not even necessary for an explanation of the methyl proton splittings. McLachlan [8] has shown, by valence

bond theory, that the methyl proton splitting could be due, at least in part, to spin exchange polarization. However, in the case of methyl-substituted aromatic positive ions, notably the positive ion of 9,10-dimethylanthracene, we have obtained strong evidence for the importance of hyperconjugation, which is discussed in a later paper [9].

The usual approach to hyperconjugation using molecular orbital theory is that outlined by Coulson and Crawford [10, 11], in which both the carbon atom and the hydrogen atoms of the methyl group contribute a $\pi$ electron to the aromatic system. We have carried out a somewhat simplified calculation of this type, neglecting overlap, and the results for *m*-xylene are shown in table 2. The calculated hyperfine constants are very similar to those calculated from the inductive model, and reasons for this are discussed elsewhere [9].

The theory of the hyperfine splitting due to $^{13}C$ in aromatic ions is now well understood [12, 13] and it has been shown that the splitting depends not only on the spin density on the carbon atom in question, but also on the spin density on neighbouring carbon atoms. The results we have obtained for the *p*-xylene anion give a direct demonstration of this effect. Two different splitting constants have been obtained, one of which arises from the four equivalent ring carbon atoms. The remaining lines are approximately half as intense and arise either from the ring carbon atoms bonded to the methyl groups, or less likely to the methyl group carbon atoms. In either case the carbon atoms are situated in positions where the orbital of the unpaired electron has a node, yet the two splitting constants are comparable.

## References

[1] McConnell, H. M., 1956, *J. chem. Phys.*, **24**, 764.

[2] Townsend, M. G., and Weissman, S. I., 1960, *J. chem. Phys.*, **32**, 309.

[3] Carrington, A., Dravnieks, F., and Symons, M. C. R., 1959, *J. chem. Soc.*, p. 947.

[4] Tuttle, T. R., and Weissman, S. I., 1958, *J. Amer. chem. Soc.*, **80**, 5342.

[5] Voevodskii, V. V., Solodovnikov, S. P., and Chibrikin, V. M., 1959, *Doklady Akad. Nauk SSSR.*, **129**, 1082.

[6] Paul, D. E., Lipkin, D., and Weissman, S. I., 1956, *J. Amer. chem. Soc.*, **78**, 116.

[7] Streitwieser, A., and Nair, P. M., 1959, *Tetrahedron*, **5**, 149.

[8] McLachlan, A. D., 1958, *Mol. Phys.*, **1**, 233.

[9] Bolton, J. R., Carrington, A., and McLachlan, A. D., 1962, *Mol. Phys.* (to be published).

[10] Coulson, C. A., and Crawford, V. A., 1953, *J. chem. Soc.*, p. 2052.

[11] Mulliken, R. S., Riecke, C. A., and Brown, W. G., 1941, *J. Amer. chem. Soc.*, **63**, 41.

[12] McLachlan, A. D., Dearman, H. H., and Lefebvre, R., 1960, *J. chem. Phys.*, **33**, 65.

[13] Karplus, M., and Fraenkel, G. K. (private communication).

# Mean energies of hybridized valence states

by U. ÖPIK

The J. J. Thomson Physical Laboratory, University of Reading, England

The concept of valence state is frequently used, and mean energies of valence states are needed, in semi-empirical studies of molecular structure. Tables of valence-state energies have been published only for unhybridized valence states; we mention those by Skinner and Pritchard [1], in which numerical values are given for a large number of important cases, and those by Moffitt [2], in which valence-state energies are expressed in terms of spectroscopic term energies. Energies of hybridized valence states have been calculated only in isolated instances, e.g. by Voge [3] and by Goldfarb and Jaffé [4], so that authors working on molecular structure have mostly had to rely for hybridized valence-state energies on rough guesses.

In this note we shall adopt Moffitt's definition [2] of a valence-state energy and give formulae by which one can quickly and easily calculate energies of hybridized valence states which involve s and p orbitals belonging to the same principal quantum number $n$. Energies calculated by this definition may or may not be more accurate than those calculated in the more usual way from the Slater–Condon parameters (see Goldfarb and Jaffé [4] for a list of references to the theory of this), but they are certainly more convenient to use.

Let $s$, $p_x$, $p_y$, $p_z$ denote the atomic s and p orbitals in the usual way. Let

$$t_i = s c_{si} + p_x c_{xi} + p_y c_{yi} + p_z c_{zi} \quad (i = 1, 2, 3, 4)$$

be the hybridized orbitals, where the coefficients $c_{\mu i}$ ($\mu = s, x, y, z$) are real and form an orthogonal matrix. We denote the valence states by $(t_1{}^{k_1} t_2{}^{k_2} t_3{}^{k_3} t_4{}^{k_4})$, $k_i$ being the number of electrons in the orbital $t_i$ ($k_i = 0$, 1 or 2); we shall omit to write $t_i{}^0$, write $t_i{}^1$ as $t_i$ and write $\lambda_i$ for $c_{si}{}^2$. When $k_i = 1$, the spin quantum number of the electron in $t_i$ may be $+\frac{1}{2}$ or $-\frac{1}{2}$, with equal probabilities. Thus a valence state is in general a mixed state whose component states are specified by the various possible choices of the spin quantum numbers of the electrons in singly filled orbitals. By expressing each component wave function as a linear combination of atomic stationary-state wave functions (ignoring the spin–orbit interaction), the mean energy of each component was obtained as a linear combination of spectroscopic term energies; the valence-state energy was then obtained by averaging over the component states.

In the table, each tabular entry is the coefficient with which the energy of the spectroscopic term stated on the left of the row occurs in the energy of the valence state stated at the top of the column. Energies of other valence states are obtained from those in the table by permuting the suffixes 1, 2, 3, 4. The recommended method of finding those spectroscopic term energies which are not known experimentally is extrapolation along isoelectronic sequences.

| Number of electrons | Spectroscopic term | $(t_1)$ |
|---|---|---|
| 1 | s — $^2S$ | $\lambda_1$ |
| | p — $^2P$ | $1-\lambda_1$ |

| Number of electrons | Spectroscopic term | $(t_1^2)$ | $(t_1 t_2)$ |
|---|---|---|---|
| 2 | $s^2$ — $^1S$ | $\lambda_1^2$ | $\tfrac{1}{2}\lambda_1\lambda_2$ |
| | sp — $^3P$ | $0$ | $\tfrac{3}{4}(\lambda_1+\lambda_2)$ |
| | sp — $^1P$ | $2\lambda_1(1-\lambda_1)$ | $\tfrac{1}{4}(\lambda_1+\lambda_2)-\lambda_1\lambda_2$ |
| | $p^2$ — $^3P$ | $0$ | $\tfrac{3}{4}(1-\lambda_1-\lambda_2)$ |
| | $p^2$ — $^1D$ | $\tfrac{2}{3}(1-\lambda_1)^2$ | $\tfrac{1}{4}(1-\lambda_1-\lambda_2)+\tfrac{1}{3}\lambda_1\lambda_2$ |
| | $p^2$ — $^1S$ | $\tfrac{1}{3}(1-\lambda_1)^2$ | $\tfrac{1}{6}\lambda_1\lambda_2$ |

| Number of electrons | Spectroscopic term | $(t_1^2 t_2)$ | $(t_1 t_2 t_3)$ (N.B. $\lambda_4=1-\lambda_1-\lambda_2-\lambda_3$) |
|---|---|---|---|
| 3 | $s^2p$ — $^2P$ | $\lambda_1(\lambda_1+\lambda_2)$ | $\tfrac{1}{4}\{(1-\lambda_4)^2-\lambda_1^2-\lambda_2^2-\lambda_3^2\}$ |
| | $sp^2$ — $^4P$ | $0$ | $\tfrac{1}{2}(\lambda_1+\lambda_2+\lambda_3)$ |
| | $sp^2$ — $^2D$ | $\tfrac{1}{2}\lambda_1(1-\lambda_1-\lambda_2)+\tfrac{2}{3}\lambda_2$ | $\tfrac{1}{8}(1+\lambda_1^2+\lambda_2^2+\lambda_3^2-\lambda_4^2)$ |
| | $sp^2$ — $^2P$ | $\tfrac{3}{2}\lambda_1(1-\lambda_1-\lambda_2)$ | $-\tfrac{1}{8}+\tfrac{1}{2}\lambda_4+\tfrac{3}{8}(\lambda_1^2+\lambda_2^2+\lambda_3^2-\lambda_4^2)$ |
| | $sp^2$ — $^2S$ | $\tfrac{1}{3}\lambda_2$ | $0$ |
| | $p^3$ — $^4S$ | $0$ | $\tfrac{1}{2}\lambda_4$ |
| | $p^3$ — $^2D$ | $\tfrac{1}{2}(1-\lambda_1)(1-\lambda_1-\lambda_2)$ | $\tfrac{1}{8}\{(1+\lambda_4)^2-\lambda_1^2-\lambda_2^2-\lambda_3^2\}$ |
| | $p^3$ — $^2P$ | $\tfrac{1}{2}(1-\lambda_1)(1-\lambda_1-\lambda_2)$ | $\tfrac{1}{8}\{(1-\lambda_4)^2-\lambda_1^2-\lambda_2^2-\lambda_3^2\}$ |

| Number of electrons | Spectroscopic term | $(t_1^2 t_2^2)$ | $(t_1^2 t_2 t_3)$ (N.B. $\lambda_4=1-\lambda_1-\lambda_2-\lambda_3$) | $(t_1 t_2 t_3 t_4)$ |
|---|---|---|---|---|
| 4 | $s^2p^2$ — $^3P$ | $0$ | $\tfrac{3}{4}\lambda_1(1-\lambda_4)$ | $\tfrac{3}{16}(1-\lambda_1^2-\lambda_2^2-\lambda_3^2-\lambda_4^2)$ |
| | $s^2p^2$ — $^1D$ | $\tfrac{2}{3}(\lambda_1+\lambda_2)^2$ | $\tfrac{1}{4}\lambda_1(1-\lambda_4)+\tfrac{1}{3}\lambda_2\lambda_3$ | $\tfrac{1}{16}(1-\lambda_1^2-\lambda_2^2-\lambda_3^2-\lambda_4^2)$ |
| | $s^2p^2$ — $^1S$ | $\tfrac{1}{3}(\lambda_1+\lambda_2)^2$ | $\tfrac{1}{6}\lambda_2\lambda_3$ | $0$ |

**Group 4**

| Config | Term | | | |
|---|---|---|---|---|
| $sp^3$ | $^5S$ | $0$ | $0$ | $\frac{5}{16}+\frac{1}{8}(\lambda_1^2+\lambda_2^2+\lambda_3^2+\lambda_4^2)$ |
| | $^3D$ | $0$ | $\frac{3}{8}(\lambda_2+\lambda_3)+\frac{1}{2}\lambda_1\lambda_4$ | $\frac{1}{4}+\frac{1}{8}(\lambda_1^2+\lambda_2^2+\lambda_3^2+\lambda_4^2)$ |
| | $^3P$ | $0$ | $\frac{3}{8}(\lambda_2+\lambda_3)$ | $0$ |
| | $^3S$ | $0$ | $\lambda_1\lambda_4$ | $-\frac{1}{16}+\frac{1}{4}(\lambda_1^2+\lambda_2^2+\lambda_3^2+\lambda_4^2)$ |
| | $^1D$ | $(\lambda_1+\lambda_2)(1-\lambda_1-\lambda_2)$ | $\frac{1}{2}(\lambda_1\lambda_4-\lambda_2\lambda_3)+\frac{1}{8}(\lambda_2+\lambda_3)$ | $\frac{1}{8}(\lambda_1^2+\lambda_2^2+\lambda_3^2+\lambda_4^2)$ |
| | $^1P$ | $(\lambda_1+\lambda_2)(1-\lambda_1-\lambda_2)$ | $\frac{1}{8}(\lambda_2+\lambda_3)-\frac{1}{2}\lambda_2\lambda_3$ | $0$ |
| $p^4$ | $^3P$ | $0$ | $0$ | $\frac{3}{16}(1-\lambda_1^2-\lambda_2^2-\lambda_3^2-\lambda_4^2)$ |
| | $^1D$ | $\frac{2}{3}(1-\lambda_1-\lambda_2)^2$ | $\frac{3}{4}(1-\lambda_1)\lambda_4$ | $\frac{1}{16}(1-\lambda_1^2-\lambda_2^2-\lambda_3^2-\lambda_4^2)$ |
| | $^1S$ | $\frac{1}{3}(1-\lambda_1-\lambda_2)^2$ | $\frac{1}{4}(1-\lambda_1)\lambda_4+\frac{1}{3}\lambda_2\lambda_3$ ; $\frac{1}{6}\lambda_2\lambda_3$ | $0$ |

**Group 5**  $(t_1^2t_2^2t_3)$ (N.B. $\lambda_4=1-\lambda_1-\lambda_2-\lambda_3$)  and  $(t_1^2t_2t_3t_4)$

| Config | Term | $(t_1^2t_2^2t_3)$ | $(t_1^2t_2t_3t_4)$ |
|---|---|---|---|
| $s^2p^3$ | $^4S$ | $0$ | $\frac{1}{2}\lambda_1$ |
| | $^2D$ | $\frac{1}{2}(\lambda_1+\lambda_2)(1-\lambda_4)$ | $\frac{1}{2}\{(1+\lambda_1)^2-\lambda_2^2-\lambda_3^2-\lambda_4^2\}$ |
| | $^2P$ | $\frac{1}{2}(\lambda_1+\lambda_2)(1-\lambda_4)$ | $\frac{1}{2}\{(1-\lambda_1)^2-\lambda_2^2-\lambda_3^2-\lambda_4^2\}$ |
| $sp^4$ | $^4P$ | $0$ | $\frac{1}{2}(1-\lambda_1)$ |
| | $^2D$ | $\frac{1}{3}(\lambda_1+\lambda_2)\lambda_4+\frac{2}{3}\lambda_3$ | $\frac{1}{3}(1-\lambda_1^2+\lambda_2^2+\lambda_3^2+\lambda_4^2)$ |
| | $^2P$ | $\frac{2}{3}(\lambda_1+\lambda_2)\lambda_4$ | $-\frac{1}{8}+\frac{1}{2}\lambda_1+\frac{1}{8}(-\lambda_1^2+\lambda_2^2+\lambda_3^2+\lambda_4^2)$ |
| | $^2S$ | $\frac{1}{3}\lambda_3$ | $0$ |
| $p^5$ | $^2P$ | $(\lambda_3+\lambda_4)\lambda_4$ | $\frac{1}{4}\{(1-\lambda_1)^2-\lambda_2^2-\lambda_3^2-\lambda_4^2\}$ |

**Group 6**  $(t_1^2t_2^2t_3^2)$ (N.B. $\lambda_4=1-\lambda_1-\lambda_2-\lambda_3$)  and  $(t_1^2t_2^2t_3t_4)$

| Config | Term | $(t_1^2t_2^2t_3^2)$ | $(t_1^2t_2^2t_3t_4)$ |
|---|---|---|---|
| $s^2p^4$ | $^3P$ | $0$ | $\frac{3}{8}(\lambda_1+\lambda_2)$ |
| | $^1D$ | $\frac{2}{3}(1-\lambda_4)^2$ | $\frac{1}{4}(\lambda_1+\lambda_2)+\frac{1}{3}\lambda_3\lambda_4$ |
| | $^1S$ | $\frac{1}{3}(1-\lambda_4)^2$ | $\frac{1}{6}\lambda_3\lambda_4$ |
| $sp^5$ | $^3P$ | $0$ | $\frac{3}{4}(\lambda_3+\lambda_4)$ |
| | $^1P$ | $2\lambda_4(1-\lambda_4)$ | $\frac{1}{4}(\lambda_3+\lambda_4)-\lambda_3\lambda_4$ |
| $p^6$ | $^1S$ | $\lambda_4^2$ | $\frac{1}{2}\lambda_3\lambda_4$ |

**Group 7**  $(t_1^2t_2^2t_3^2t_4)$   $(t_1^2t_2^2t_3^2t_4^2)$

| Config | Term | $(t_1^2t_2^2t_3^2t_4)$ |
|---|---|---|
| $s^2p^5$ | $^2P$ | $1-\lambda_4$ |
| $sp^6$ | $^2S$ | $\lambda_4$ |

Valence-state energies expressed as linear combinations of spectroscopic term energies.

REFERENCES

[1] SKINNER, H. A., and PRITCHARD, H. O., 1953, *Trans. Faraday Soc.*, **49,** 1254.
[2] MOFFITT, W., 1954, *Rep. Progr. Phys.*, **17,** 173.
[3] VOGE, H. H., 1936, *J. chem. Phys.*, **4,** 581.
[4] GOLDFARB, I. J., and JAFFÉ, H. H., 1959, *J. chem. Phys.*. **30,** 1622.

# ESR of aromatic ions in iodine

by J. KOMMANDEUR

Parma Research Laboratory, Union Carbide Corporation, Parma 30, Ohio†

(*Received* 28 *September* 1961)

The electron acceptor properties of iodine have been well established. A wide variety of its charge-transfer complexes is known [1, 2] and more recently a number of papers have appeared on the electronic conductivity of solid complexes of iodine with various organic donors, such as perylene, $p$-phenylene diamine, etc. [3, 4]. To explain the conductivity phenomena, it was suggested that the formation of aromatic ions might play a role [3]. The observed paramagnetism would then be due to these radical ions. Unfortunately, the spin system in these complexes is too concentrated to observe any details in the electron spin resonance signal, which might give some information on the nature of the paramagnetic species. By adding small amounts of organic donors to molten iodine we have now been able to obtain hyperfine structure. A 0·001 molar solution of perylene in molten iodine shows a signal with hyperfine structure, as indicated in the figure. It is compared to the signal exhibited by perylene in sulphuric acid, where the existence of the ion has been well established by Weissmann and other workers [5, 6]. It is obvious that some broadening of hyperfine components has occurred. To show the similarity of the spectra to greater advantage, a curve of perylene in sulphuric acid at lower temperatures ($-23^\circ$c) has been included, where the lack of rapid rotation also broadens the hyperfine spectrum.

Other electron donors gave similar results. Hyperfine spectra were obtained for the $p$-phenylene diamine [7] $\alpha$-naphthylamine, diamino-durene and diphenyl-$p$-phenylene diamine ions in molten iodine.

Many aromatic compounds give rise to an ESR signal in this system, but in the case of naphthalene, anthracene, tetracene, phenanthrene, and pyrene, only a wide structureless ESR line is observed. Analogous to perylene, it is suspected that these broad lines are also due to aromatic ions. The hyperfine structure could be broadened for the following reason: it was quantitatively established that with these compounds only a minor portion is ionized in the iodine melt, while in the cases of perylene and $p$-phenylene diamine almost all the molecules were accounted for by the intensity of the ESR signal. The lack of hyperfine structure in these hydrocarbons is probably due to this low degree of ionization and the resultant simultaneous presence of molecules and ions. Exchange of electrons could take place and the hyperfine interaction could be broadened out by this phenomenon. Weissmann [8] observed this effect at much higher concentrations of neutral molecules. In the present case, however, the possibility of transfer of the electron via iodine molecules—as indicated by

† Present address: Department of Physical Chemistry, University of Groningen, Groningen, The Netherlands.

the electronic conductivity—may considerably reduce the concentration of neutral molecules required for the effect. Electron exchange may also be responsible for the partial loss of hyperfine structure in perylene.
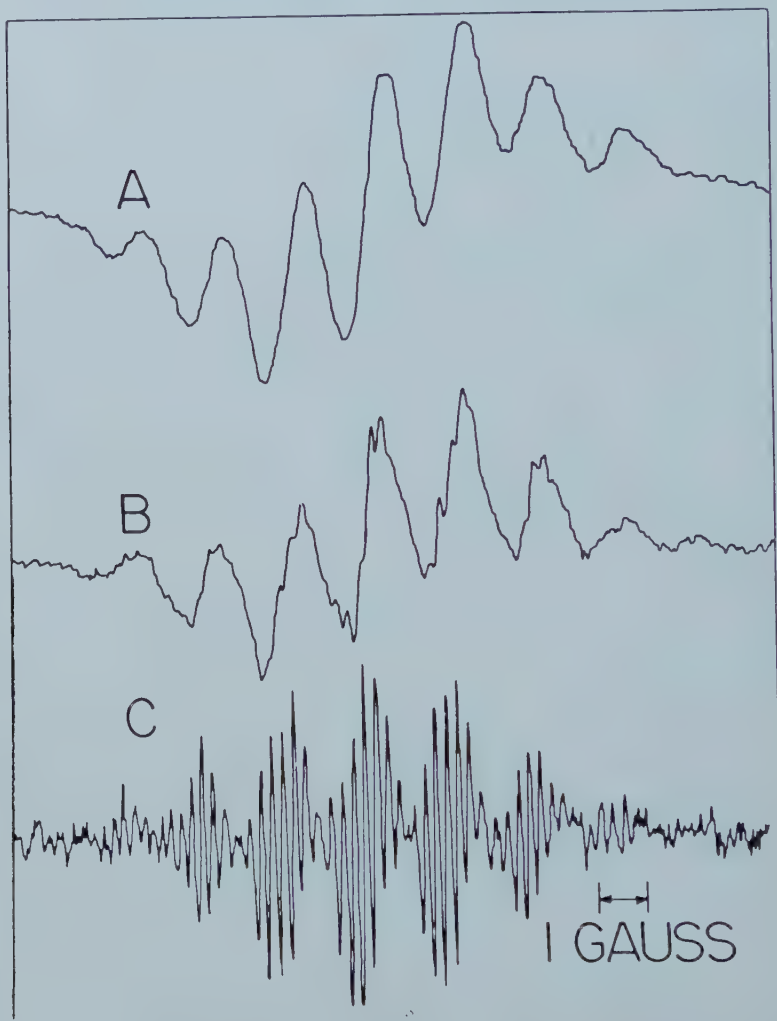


The ESR spectrum of the perylene positive ion.   A—in molten iodine at 120°c.   B—in concentrated $H_2SO_4$ at $-23°c$.   C—in concentrated $H_2SO_4$ at 25°c.

It is interesting to note that in the solidified melts broad ESR lines of widths corresponding to the over-all hyperfine splittings of the aromatic ions were observed, indicating that in the solid these ions are also present in molecular dispersion.   Single crystal studies on these systems may yield resolved hyperfine structure, and this is presently being investigated.

The experiments were carried out at 9500 Mc using magnetic-field modulation in the conventional way.   The sample cavity was the Varian variable temperature cavity, which allowed heating the closed sample tubes to at least 113°c, required to keep the iodine molten.

The author is indebted to Dr. L. S. Singer for the use of the ESR equipment and for many valuable discussions, and to Mr. S. A. Nowacki for his assistance in some of the measurements.

REFERENCES

[1] Mulliken, R. S., 1952, *J. Amer. chem. Soc.*, **74**, 811.
[2] Bhattacharya, R., and Basu, S., 1958, *Trans. Faraday Soc.*, **54**, 1286.
[3] Kommandeur, J., and Hall, F. R., 1961, *J. chem. Phys.*, **34**, 129.   Singer, L. S., and Kommandeur, J., 1961, *J. chem. Phys.*, **34**, 133.
[4] Buck, H. M., Lupinski, J. H., and Oosterhoff, L. J., 1958, *Mol. Phys.*, **1**, 196.
[5] Weissmann, S. I., de Boer, E., and Conradi, J. J., 1956, *J. chem. Phys.*, **26**, 963.
[6] Carrington, A., Dravnieks, F., and Symons, M. C. R., 1960, *J. chem. Soc.*, p. 947.
[7] Melchior, H. T., and Maki, A. H., 1961, *J. chem. Phys.*, **34**, 471.
[8] Ward, R. L., and Weissmann, S. I., 1954, *J. Amer. chem. Soc.*, **76**, 3612.

# INDEX OF AUTHORS (WITH THE TITLES OF PAPERS)